PROCEEDINGS

THE UCLA INTERNATIONAL CONFERENCE ON RADIATION AND REMOTE PROBING OF THE ATMOSPHERE

AUGUST 28-30, 1973

Department of Meteorology
University of California
Los Angeles, California

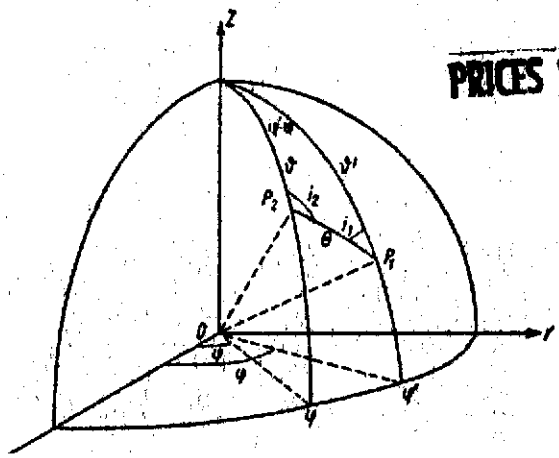

Jacob G. Kuriyan Editor

Sponsored by:
U.S. DEPARTMENT OF TRANSPORTATION — C.I.A.P.
NATIONAL AERONAUTICS AND SPACE ADMINISTRATION
T.R.W. SYSTEMS INC.
U.S. ARMY RESEARCH OFFICE
U.C.L.A.

PROCEEDINGS

THE UCLA INTERNATIONAL CONFERENCE ON RADIATION AND REMOTE PROBING OF THE ATMOSPHERE

AUGUST 28-30, 1973

Department of Meteorology
University of California
Los Angeles, California

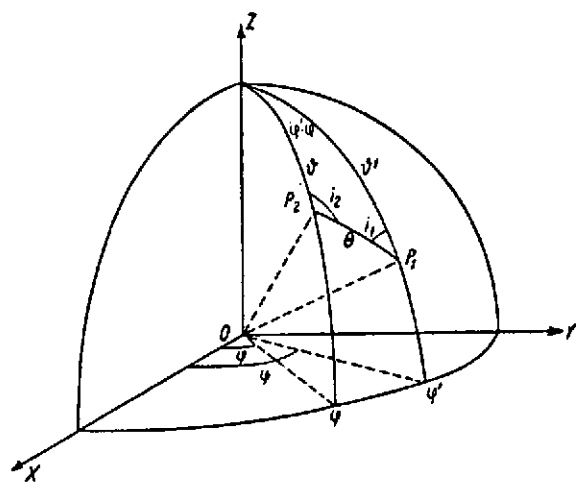

Jacob G. Kuriyan Editor

Sponsored by:
U.S. DEPARTMENT OF
TRANSPORTATION — C.I.A.P.
NATIONAL AERONAUTICS AND
SPACE ADMINISTRATION
T.R.W. SYSTEMS INC.
U.S. ARMY RESEARCH OFFICE
DEPARTMENT OF METEOROLOGY, U.C.L.A.

Additional copies may be obtained

from

Western Periodicals Company

13000 Raymer Street

North Hollywood, California 91605

Override - NASA Funded 11/12-74

THE UCLA INTERNATIONAL CONFERENCE ON RADIATION AND REMOTE PROBING OF THE ATMOSPHERE

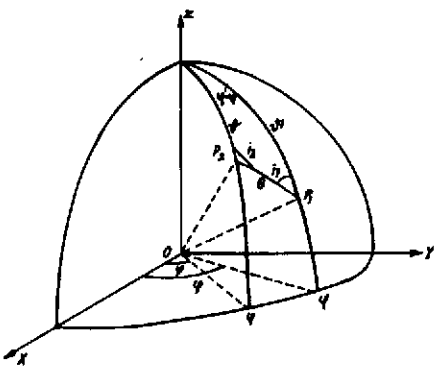

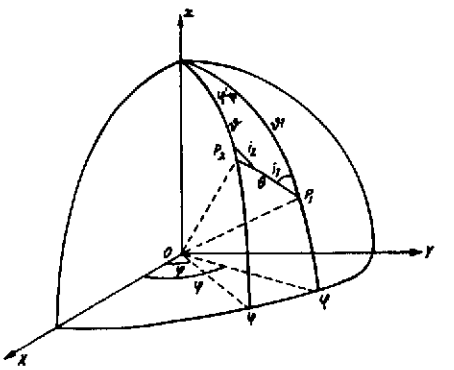

AUGUST 28-30, 1973
UNIVERSITY OF CALIFORNIA
LOS ANGELES

Sponsored by:
TRW SYSTEMS
DEPARTMENT OF TRANSPORTATION
NASA
U.S. ARMY RESEARCH OFFICE

CONFERENCE CHAIRMAN

Jacob G. Kuriyan
University of California, Los Angeles

ARRANGEMENTS CHAIRMAN

Len Speltz
TRW Systems

CONFERENCE SECRETARY

N. Sundararaman
California State University (Northridge)

PROGRAM CONSULTANTS

M. T. Chahine
JPL Caltech

D. Deirmendjian
Rand

C. R. N. Rao
University of California, Los Angeles

S. V. Venkateswaran
University of California, Los Angeles

M. G. Wurtele
University of California, Los Angeles

PROGRAMME

Tuesday, August 28, 1973

Morning:

9:00	Welcome Address	
	Memorial —	Tribute to Professor Z. Sekera M. G. Wurtele, W. F. Libby and D. S. Saxon
9:30	Speaker:	S. Chandrasekhar University of Chicago
	Topic:	"Polarization of a Sunlit Sky"
	Chairman:	D. S. Saxon University of California, Los Angeles
10:45	Coffee Break	
11:00	Speaker:	G. Yamamoto Tohoku University Sendai, Japan
	Topic:	"Radiative Transfer of Visible Radiation in Turbid Atmospheres"
	Chairman:	J. Bjerknes University of California, Los Angeles
12:15	Lunch Break	

Afternoon:

1:30	Speaker:	R. T. H. Collis Stanford Research Institute
	Topic:	Lidar Observations of Atmospheric Particulate Content
	Chairman:	J. D. Lawrence NASA-Langley Research Center
2:30	Speaker:	J. G. Kuriyan University of California, Los Angeles
	Topic:	"Particulate Sizes from Polarization Measurements"
	Chairman:	J. D. Lawrence NASA-Langley Research Center
3:30	Coffee Break	
3:45	Panel Discussion:	"Remote Sensing"
	Chairman:	M. Tepper NASA Headquarters

This page is reproduced at the back of the report by a different reproduction method to provide better detail.

Dedicated to the Late Professor Zdenek Sekera, 1905-1973.

Wednesday, August 29, 1973

Morning:

9:00	Speaker:	H. C. van de Hulst Sterrewacht te Leiden Leiden, Netherlands
	Topic:	"Visible Radiation in Cloud Layers"
	Chairman:	A. J. Grobecker U. S. Department of Transportation
10:15	Coffee Break	
10:30	Speaker:	J. C. Gille National Center for Atmospheric Research Boulder, Colorado
	Topic:	"Method of Calculating Infrared Transfer in the Atmosphere — A Review"
	Chairman:	W. R. Bandeen NASA-Goddard Space Flight Center
12:00	Lunch Break	

Afternoon:

1:30	Speaker:	I. Kuscer (Jointly with N. J. McCormick) Univerza v Ljubljana Ljubljana, Yugoslavia
	Topic:	"Some Analytical Results in Radiative Transfer"
	Chairman:	S. V. Venkateswaran University of California, Los Angeles
2:30	Speaker:	R. A. McClatchey Air Force Cambridge Research Laboratories
	Topic:	"Molecular Absorption Parameters in Atmospheric Modelling"
	Chairman:	C. R. N. Rao University of California, Los Angeles
3:30	Coffee Break	
3:45	Speaker:	W. M. Irvine (Jointly with J. Lenoble) University of Massachusetts
	Topic:	"Solving Multiple Scattering Problems in Planetary Atmospheres"
	Chairman:	S. Ueno University of Southern California

Thursday, August 30, 1973

Morning:

9:00	Speaker:	V. E. Suomi University of Wisconsin
	Topic:	"Infrared Radiation"
	Chairman:	J. G. Kuriyan University of California, Los Angeles
10:15	Coffee Break	
10:30	Speaker:	C. D. Rodgers Clarendon Laboratory Oxford, England
	Topic:	"Infrared Remote Sensing"
	Chairman:	M. T. Chahine Jet Propulsion Laboratories Pasadena
12:00	Lunch Break	

Afternoon:

1:30	Speaker:	K. S. Bullrich Johannes Gutenberg-Universität Mainz, West Germany
	Topic:	"Scattering and Absorption from Polydispersed Aerosols"
	Chairman:	D. Deirmendjian Rand Corporation Santa Monica
2:30	Panel Discussion:	"Unsolved Problems in Atmospheric Radiation"
	Chairman:	J. London University of Colorado
3:30	Coffee Break	
3:45	Panel Discussion:	"Environmental Problems and Atmospheric Radiation"
	Chairman:	F. Singer University of Virginia

PREFACE

The death of Zdenek Sekera on January 1, 1973 deprived Meteorology and Geophysics of a distinguished pioneer in atmospheric optics.

It was perhaps his early association with Linke and the tabulations he made of Chandrasekhar's solution to the transfer problem in a multiple scattering atmosphere that prepared him to grasp the significance of such research to remote sensing. During the intense activity in space research that followed the launch of the Sputnik, Sekera was one of the strongest proponents of the meteorological applications of satellites.

While Sekera had an obvious bias for theoretical research, he recognized that there would be no substitute for experimental observations. The dearth of experimentalists in his area of scientific interest dictated that he begin an experimental programme at UCLA which, over the last twenty years, has produced some of the outstanding scientists in experimental atmospheric optics.

The systematic measurements of skylight polarization by Sekera and his associates, under varied atmospheric conditions indicated, without doubt, measurable deviations from Chandrasekhar's predictions. These he attributed to the presence of particles in the atmosphere which invalidated the assumption of a molecular atmosphere. Thus began his long and arduous endeavor to solve the 'inverse problem', that is, to determine the optical characteristics of atmospheric particles from remote measurements of skylight polarization. This problem is best defined in his 1967 paper*, where he illustrated the inverse solution to the Rayleigh atmosphere that is afforded by the tabulations of Chandrasekhar's results. He observed that such a solution in a turbid atmosphere will have to incorporate a non-Lambertian ground reflector, and a proper parameterization of the phase matrix for aerosol scattering.

Having identified the problem he dedicated his considerable scientific resources to solving it. Evidence of his single-minded zeal and his meticulous investigative abilities can be found in his numerous reports and papers on the transfer of radiation through planetary atmospheres. While each report addressed itself to a narrow problem, his reports, taken in their entirety, convey the perseverance with which he strove, unremittingly, ignoring scientific fads and fashions, to reach his goal.

The examination of Sekera's scientific pursuit, and the obstacles that he had to overcome, suggests that such adventures, in the existing framework of funding for science, are a rarity. On the one hand, the pioneering spirit is epitomized by the youthful mind, unfettered by the bonds of tradition, and to have "dreams that others do not have and ask, why not?" On the other hand, it takes a considerable scientific reputation, a quality often equated to age, to win the support of funding agencies, so as to be able to conduct these long term investigations of a speculative nature. It is gratifying that Sekera had the correct blend of talents to launch and sustain such a research effort until it reached fruition.

*Icarus, 6, 348, 1967.

It was Professor Sekera's intention to devote his first years of retirement to writing a monograph, to review the developments in the field of atmospheric optics and remote sensing of pollutants. It seemed desirable therefore, to organize a conference, dedicated to his memory to bring together his outstanding colleagues, for an in-depth review and discussion of the progress achieved in the various aspects of the field.

The management of TRW Systems, Inc. appreciated the need for such a conference and offered to support, financially, our endeavor. Soon after, the National Aeronautics and Space Administration, the United States Department of Transportation and the United States Army Research Office joined in this venture to enable us to bring the foremost scientists in the field to discuss and summarize the state of the art in the transfer of radiation through planetary atmospheres, a problem of paramount importance to remote sensing.

The area of remote sensing involves the scientist, the engineer and the governmental agencies. Unfortunately, this field exhibits an unhealthy preoccupation with the development of hardware, perhaps due to the immediate commercial value and glamour associated with gadgetry, and a general neglect of basic scientific research. This imbalance reflects in the appearance of sophisticated instruments whose measurements are interpreted not on the basis of theoretical analysis, but on algorithms and numerical empiricisms. A finite, albeit small, investment in basic research is essential in order to assure maximal utilization of resources.

This conference exposed the users of remote sensing (the government agencies such as the National Aeronautics and Space Administration and the United States Department of Transportation) and the industries that develop the hardware (such as TRW Systems, Inc.) to the pioneering scientists whose fundamental investigations have proved to be a cornerstone to remote sensing. That Chandrasekhar's solution of the Rayleigh scattering problem, or van de Hulst's meticulous investigations of the Mie scattering, were not motivated by the relevance of their work to user agencies, did not diminish the importance of their contributions to applied research. It may even be argued that mission-oriented research would mould thinking along guidelines that stifle creativity and prove, in the long run, to be counter productive.

If this conference brought out the importance of basic theoretical and experimental research to the field of remote sensing, then it would have been an appropriate tribute to the late Professor Sekera. If, in addition, it revived, in some small measure, an interest in such investigations, it would have pleased Professor Sekera.

Jacob G. Kuriyan

ACKNOWLEDGEMENTS

When it was proposed that an International Conference on Atmospheric Radiation, dedicated to the late Professor Z. Sekera be held at U.C.L.A., the endorsement and support of the idea by Mr. Hugh Brady and Mr. A. E. Sabroff of TRW Systems Inc. encouraged me to expand the list of invited speakers and solicit assistance from other agencies. The additional contributions of Dr. M. Tepper, and Dr. W. R. Bandeen of the National Aeronautics and Space Administration, Dr. A. J. Grobecker of the U.S. Department of Transportation, and Dr. A.V. Dodd of the U.S. Army Research Office made it possible for us to hold the conference.

The administrative support from the chairman of our department, Professor M. G. Wurtele and the executive Vice Chancellor of our university, Professor David S. Saxon launched the operation and during various phases, my colleagues Dr. M. T. Chahine, Dr. D. Deirmendjian, Dr. C. R. N. Rao, Dr. N. Sundararaman and Professor S.V. Venkateswaran, the members of our staff, Mr. Dan Dibble, Mr. Ted Doty, Mrs. Dotti Deutsch and Mrs. Betty Shieh, and my student D.H. Phillips provided invaluable assistance. Mr. L. Speltz of TRW Systems, Inc. was largely responsible for bringing some semblance of order into an otherwise chaotic and informal organization. The announcements and the attractive programme brochures are but a few fruits of his toil.

That Professor F. Singer's talk at the conference was reported in the Asahi Times (Japan, September 10, 1974) or that Professor S. Chandrasekhar was heard on the V.O.A. shortwave broadcasts around the world or that Dr. A.J. Grobecker and Professor H.C. van de Hulst appeared on TV or that numerous papers carried the Associated Press interview of Dr. M. Tepper, were not just accidents of circumstance but the result of a dedicated effort to inform the public by Mr. Tom Tugend of UCLA (public relations) and Mr. Don Bane of TRW Systems, Inc.

The many students of the Department of Meteorology who volunteered their services selflessly, to drive the visiting scientists to and from the hotel, to help meet the audio visual requirements of the speakers etc. and Dr. N. Sundararaman who orchestrated their efforts, contributed to the relaxed and pleasant atmosphere. Most of the participants noticed, and were appreciative of, the diversion provided by the camera person of the UCLA Media Center and we are thankful to them for the video tape record of the proceedings that will be a permanent source of inspiration for our future students.

The excellent typing of Mrs. Betty Shieh and Mrs. Juliette Holcomb, and the drafting of Mrs. Beverly Gladstone contributed greatly to the aesthetic appearance of this monograph.

The success of this conference rests on the interest and support of the many friends and colleagues of the late Professor Z. Sekera, who, at short notice, graciously rearranged their schedule to be with us, and to them, I am most grateful.

Jacob G. Kuriyan
Editor and
Conference Chairman

TABLE OF CONTENTS

INTRODUCTORY NOTES

This conference dealt with the transfer of visible and infrared radiation and its relevance to remote sensing.

The scientific sessions began with the talk of Professor S. Chandrasekhar on the "Polarization of a Sunlit Sky". His eloquence and clarity of presentation belied the fact that this was, apart from one lecture a few years ago at Oxford, a short visit to his field, after a complete break of over twenty years. Since his lecture is not included in the proceedings I shall dwell upon those points in his lecture that are of a historical nature and are, therefore, absent in his treatise on Radiative Transfer.

In the mid 1940's when Chandrasekhar was studying the transfer equation there arose the question of the inclusion of the polarization of the radiation field. Finding his eminent physicist-colleagues equally unaware and the textbooks on optics of no great assistance, he scoured the library and found the trace of a clue, an obscure reference to a paper by G. G. Stokes in a book by Walker entitled the "Analytical Theory of Light". It then seemed logical to Chandrasekhar, that a matter as important could not have escaped the attention of the old masters and hence, he proceeded to examine the collected papers of Lord Rayleigh, Lord Kelvin, and Sir G.G. Stokes. The discovery, by Chandrasekhar, of the relevant paper, after over 90 years of obscurity, brought about a revival of the Stokes formalism that has immortalized Stokes. Indeed, the name is even emblazoned in neon at the Jodrell Bank Observatory.

Chandrasekhar marched into the field of radiative transfer armed with a technique for solving the relevant equation, not fully aware of its power or versatility. Progressively he attempted to solve problems representing more difficult and realistic situations and the problems yielded, before the method failed. It was indeed an intellectual adventure and, therefore, it is not surprising that he described it as his "happiest years of research". The enormous application that his research has found in the field of remote sensing ought to dispel the myth that useful results come only from mission-oriented research and add substance to the theory that fundamental thinking requires a mind free to soar at will.

An amusing anecdote that illustrates the mysterious path that leads to scientific discovery was in the success he had persuading a young astronomer, W. A. Hiltner, to study eclipsing binary stars, to confirm the 11% polarization that his calculations predicted. The first measurements, taken during an eclipse, detected the polarization and was greeted with elation. But, contrary to expectation, the polarization persisted even in the following days. This was subsequently identified as the first experimental detection of another phenomenon, interstellar polarization.

The section on the transfer of visible radiation begins with the article by W. M. Irvine and J. Lenoble, that assumes little prior knowledge of the field on the part of the reader and presents, in a critical fashion, various analytical approximations and exact numerical solutions to the transfer problem. They conclude by identifying some of the outstanding unsolved questions.

Most of the methods used in the solution of the transfer problem assume that the medium is plane parallel and ignore effects of sphericity. The Monte Carlo method is free of such assumptions and its underlying mathematical framework is described in the paper contributed to the proceedings by G. I. Marchuk and G. A. Mikhailov. The principal criticism levelled at the Monte Carlo method seems to be the inordinate amount of computing time that is required if the results are to have a great degree of precision.

G. Yamamoto, under whose leadership the group in Japan has made fundamental contributions to the field of atmospheric radiation, presents, in a paper with M. Tanaka, detailed analyses of the exact methods that are currently in use to solve the transfer problem viz: the doubling method and the closely related matrix method, the iterative method, Chandrasekhar's method of discrete ordinates and the Monte Carlo method. In order to consider the transport of radiation through a turbid atmosphere it is necessary to develop a model of the atmosphere and characterize the aeorsols by parameters. For some assumed values of these parameters Yamamoto and Tanaka evaluate the effects of the aerosols on the heat budget and on the atmospheric temperature profile. They point out the crucial role played by the complex index of refraction of the aerosols in these calculations.

The wealth of information obtained by the concerted research effort of the Mainz group is reported in the paper by K. Bullrich, R. Eiden, G. Eschelbach, K. Fischer, G. Hänel, and J. Heintzenberg. The extensive experiments with the aid of in-situ sampling techniques help them to arrive at representative values of the aerosol parameters which are used to compute the radiation field and, hence, infer the heating rate due to aerosols. K. Bullrich et al. conclude that the heating rate due to aerosols could be of the same order as that due to water vapor.

These numerical experiments on the radiative effects of aerosols suggest the need for their inclusion in the climatic studies and in the numerical simulation of atmospheric circulation. The independent investigations of K. Ya. Kondratyev's group in the USSR summarized in his latest book echo the conclusions of Bullrich and Yamamoto. While these results dispel all doubts as to the adequacy of the theoretical methods to calculate radiative effects of aerosols, they also emphasize the importance and the desirability of experimental determination of the relevant aerosol parameters on a global basis so as to arrive at realistic estimates of heating and cooling.

Perhaps the overriding and common feature of van de Hulst's numerous publications are the sound physical principles he uses to arrive at approximate solutions to complicated scattering problems. It seems desirable that a first estimate of the effect of aerosols on the heat budget should be generalizations of the many approximate expressions derived by van de Hulst and compiled in his treatise on the "Light Scattering by Small Particles". In his paper he investigates the scattering in cloud layers, a problem that has received scant attention primarily because of its intrinsic difficulty. In the research world of the atmospheric sciences mathematical analysis often takes a back seat to numerical experiments with computers. van de Hulst points out the importance of tailoring a calculation to the specific problem and the possibility of an overkill. In his words "...it does not always require a professional furniture maker to prevent a four legged table from rocking. If the sole purpose is to avoid spilling coffee, a folded paper under it may be equally satisfactory."

Under certain idealized situations it is still possible to use analytical methods to solve the transfer problem. These may provide useful clues to obtain approximate solutions under more realistic conditions. I. Kuščer and N. J. McCormick describe the singular eigenmode expansions to study the transport of radiation through thick atmospheres.

In the study of the transfer problem in the absence of scattering the approximations of Schuster, Schwarzschild, Eddington and Milne have played a central role, facilitating physical interpretation of unusual phenomena. In the presence of scattering, the Mie solution, in the form of an infinite series, complicates the problem. In a set of lectures delivered at the Department of Meteorology, UCLA at the request of Professor Sekera, D. S. Saxon described the Mie solution and obtained the Born-Rayleigh-Gans, the Frauhofer and the Wentzel-Kramers-Brillouin-Jeffreys approximations. That the reciprocity principle was a consequence of the time reversal invariance of the Maxwell's equations was also established. The integral and phase shift formalisms were explored, and the geometrical optics and the Rayleigh-Gans limit to the scattering cross sections derived. This unpublished set of lecture notes are included in this monograph.

In remote sensing from space probes the signal that is detected has been transported through an intervening medium and, therefore, carries information pertaining to the source as well as the constituents of the medium. For instance, infrared image of land surfaces will be contaminated by atmospheric effects and there is a need to factor out this interference. K. Ya. Kondratyev, A. A. Buznikov, O. B. Vasilyev and O. I. Smokty discuss the method of transfer functions that enable the elimination of atmospheric effects from spectral photometric data measured from a spacecraft. The fascinating experimental data gathered by the Soviet spacecraft Soyuz 7, Soyuz 9 and SALYUT show that the Soviet scientists continue to enjoy the lead in the field of theoretical and experimental atmospheric radiation and insert a note of urgency for international collaboration, to derive the benefit of these investigations.

The next paper deals with the use of a ground based polarimeter to derive equivalent optical characteristics of the medium. The importance of such a determination and the inherent non-uniqueness in model calculations are discussed. These optical parameters can be used in a program such as those described by Yamamoto and Bullrich to derive the radiative effects of aerosols. A ship-based polarimeter will be used to infer the particulate characteristics in the forthcoming GARP Atlantic Tropical Experiment, off the coast of Senegal. The heat budget estimates from this experiment, it is envisaged, will complement the direct measurement of radiant flux. Helicopter-borne polarimeter measurements of upwelling radiation have also been interpreted using similar methods. However, there has not been statistically significant amount of data to warrant a definitive statement.

The other remote sensing device that is based on these theoretical developments is the lidar. The Stanford Research Institute is one of the foremost centers of Lidar research and the use of lidars to measure atmospheric particulates is described by R. T. H. Collis, P. B. Russell, E. E. Uthe and W. Viezee. While the location of the scattering layer is uniquely determined, the inference of the characteristics of the aerosol particles from the intensity of the signal involves other assumptions. A careful assesment of the success and the limitations of the method is provided by Collis et al.

The section on infrared radiation included the talk by Professor V.E. Suomi on the role of radiation in the general circulation of the atmosphere. This was a highly entertaining and informative discourse liberally illustrated with color slides. He pointed out that the general circulation models were plagued with truncation errors, problems of boundary conditions and finite differencing schemes and, therefore, on the time scale of a few days, radiation was ignored. He predicted that this situation would change dramatically in the next year or two when radiation will become an integral part of the model calculations.

The article by J. C. Gille reviews the methods used in the transfer of infrared radiation. High precision radiation measurements are shown to agree with calculations using line-by-line integrations. The advantages of using the various types of band models to obtain approximate results are also discussed. The paper includes the transmittance, fluxes and the heating rate calculations in an inhomogeneous atmosphere.

Line-by-line calculations require the specification of molecular parameters. R. A. McClatchey gives the most recent calculations of specific parameters for H_2O, CO_2, N_2O, CO, CH_4 and O_2. The random model is then used to calculate transmittance spectra. The systematic and thorough tables produced by McClatchey et al. have proved to be of great value to the research scientist.

The use of satellites for the remote sounding of the earth's atmosphere is discussed by C. D. Rodgers. The radiation that is detected has information on the temperature and composition of the atmosphere as well as the emissivity of the surface. The underlying theory of the retrieval of this information from radiation field measurements is given. The types of instruments that are in use on space probes for infrared remote sounding of planetary atmospheres and their uses are also described.

The panel on "Unsolved Problems" in atmospheric radiation was chaired by Professor J. London and included Professors V. E. Suomi, H. C. van de Hulst, S. Twomey and Dr. D. Deirmendjian. Professor London initiated the discussion by enumerating the outstanding unsolved problems published in the Bulletin of the American Meteorological Society in 1971. Professor Suomi urged that radiation experiments be performed in concert with one another, as in the Soviet Union, so that intercomparisons and correlations can be studied. It is interesting and perhaps not a coincidence, since Professor Suomi was one of the architects of GARP, that the forthcoming GARP Atlantic Tropical Experiment will include such complete radiation experiments. Professor van de Hulst suggested that infrared band model absorption could probably be systematized along the lines of his early contributions. As for multiple scattering calculations the theory is adequate and to quote him "I feel like a waiter in a restaurant. In the beginning when everyone is hungry and thirsty you pour some water and coffee and give some bread, because that is what they will ask for anyhow. But this is more or less the end of the dinner and they are all saturated. So we have to ask "Do you want anything else, Sir?"

Professor Twomey pointed out that assumptions of spherical particles and uniform refractive index in aerosol calculations are inherently unrealistic and hence, render the results to be of questionable value. Dr. Deirmendjian stressed the usefulness of the concept of equivalent description of the atmosphere in terms of spherical scattering. It has been stressed elsewhere in this monograph that the determination of the parameters of an equivalent description of the atmospheric scattering can be used,

as explained by Bullrich and Yamamoto, to calculate heating rates. The knowledge of the parameters is only the intermediate step of the calculation and it is a non-unique result. This, however, leads to the inference of the entire radiation field and hence, heating rates. If, for instance, the inferred size distribution is to be used to deduce the cloud nucleation abilities, clearly the results will go awry, since the model is only one member of an equivalence class. The alternative method of treating scattering as due to a medium with a coordinate-dependent refractive index is used by radioscientists. At present no great advantage is envisioned by these methods unless experiments can be designed to determine the relevant probability distribution function. It is perhaps useful to recall Sekera's justification for the use of a spherical scatterer with uniform refractive index. In his "Advances of Geophysics" review article he observed that it is likely that most aerosols have a water coating and, therefore, assume a spherical shape. Further Kerker proved a theorem that a spherical object "with a thin coating scatters light as if the inner core were not present provided that the outer shell has a moderate refractive index", and hence the assumption of a uniform refractive index.

The panel on Remote Sensing consisting of Dr. W.R. Bandeen, Dr. J.D. Lawrence, Jr. of NASA, Dr. C.B. Farmer of JPL, and Mr. P.G. White of TRW, was chaired by Dr. M. Tepper of NASA. Drs. Bandeen, Lawrence, and Tepper described the Earth Observation Program carried out by NASA, including the various meteorological satellites and the satellites to survey earth resources and monitor environmental quality. Some of the typical instrument packages on them and the proposed experiments were discussed. Mr. P. G. White described the use of a multichannel ocean color sensor to monitor the chlorophyll content in the oceans from radiative field measurements. Dr. C. B. Farmer discussed the radiometric and spectroscopic remote sensing techniques used at JPL. The modification of Chahine's algorithm that was used to determine the temperature profile on Mars and the study of the 4.7 μ band in the Jovian atmosphere using a Michelson interferometer that detected the presence of Deuterated Methane were two of the examples of remote sensing of planetary atmospheres. Dr. Farmer concluded his talk with a description of his high speed Michelson interferometer, designed to detect trace gases, that has been flown on the Concord and the Good Year Blimp.

The conference ended on a note of cautious optimism when Professor Fred Singer argued that the evidence available indicated no increase in global particulate levels during the last decade. He pointed out that man's activities perturb the atmosphere in a local fashion and hence local observations must be interpreted with care.

Apart from minor corrections of spelling and misprints, the texts reproduced here are those submitted by the authors.

Jacob G. Kuriyan
Editor

SOLVING MULTIPLE SCATTERING PROBLEMS IN PLANETARY ATMOSPHERES†

William M. Irvine
Department of Physics and Astronomy
University of Massachusetts
Amherst, Massachusetts 01002

and

J. Lenoble
Laboratoire d'Optique Atmospherique
Universite des Sciences et Techniques de Lille
59-Villeneuve d'Asco, France

1. INTRODUCTION

Radiative transfer problems in planetary atmospheres within the extended visible portion of the spectrum may conveniently be referred to as multiple scattering problems, to distinguish them from transfer problems at longer wavelengths where thermal emission by the atmosphere is important. We shall begin this paper by recalling several earlier reviews on this topic. Eleven years ago, van de Hulst and Irvine (1962) discussed just this question and stressed the necessity for considering anisotropic, forward-directed single scattering within the multiple scattering problem. Almost all computations prior to that time had been made for nearly isotropic scattering, a situation which rarely applies in an actual planetary atmosphere (although the results obtained for isotropic scattering may be used to interpret observations of more realistic atmospheres; see below). Methods for attacking such problems were proposed in that paper and by van de Hulst (1963), and the review was updated by Irvine (1968). During the following decade, very considerable progress was made in computational methods, in large part as a result of improved electronic computers. These computational techniques were the subject of a recent review by Hunt (1971), which contains extensive references. The extension of computed results outside of their original domain of validity has been the subject of extensive work by van de Hulst (e.g., 1971) through the use of asymptotic expansions, "similarity relations" for transforming the results from one set of atmospheric parameters to another, and the computation of a large number of "test cases" of atmospheric scattering with the aid of easily parameterized phase functions. An up-to-date discussion of the theoretical, analytic approach to radiative transfer theory in the visible spectrum is the subject of a recent book by V. V. Sobolev (1972), which is being prepared for English translation by Pergamon Press. This text brings together in one place a comprehensive account of

† Contribution from the Five College Observatories Number 171.

radiative transfer theory for atmospheres with highly anisotropic scattering, and includes a discussion of approximate methods and also the problems associated with multiple scattering in inhomogeneous and spherical atmospheres.

The recent reviews tend, however, to be either directed toward research workers within the field, or to be not yet generally available. In the present paper, we shall take a somewhat different point of view, and shall orient the discussion toward the scientist with little or no prior experience in radiative transfer theory who finds himself confronted with such a problem during the course of his research. We shall thus begin in quite an elementary manner, shall try to bring together in a coherent picture available results and procedures, and shall rely heavily on earlier reviews for both lists of references and the basis of the following discussion.

The standard English language textbook on radiative transfer theory (not limited to planetary atmospheres) is that of Chandrasekhar (1950), whose terminology we shall generally follow. Other important general references include the books by Sobolev (1956) and Busbridge (1960).

2. ANSWERS DESIRED FROM THE THEORY

The degree of complexity in a multiple scattering problem depends to a large extent upon the answer desired for a particular application. Because the identical transfer problems have been considered within the contexts of astrophysics, atmospheric optics, and neutron transport theory, there is a rather confusing wealth of nomenclature, and it would be well to begin with a set of definitions.

The basic physical quantity entering both the theory and observation is the specific intensity of radiation I (radiance in atmospheric optics, angular neutron flux in neutron transport theory). It is defined as the energy per unit area, time, frequency interval, and solid angle, crossing a small test surface which is oriented normal to the direction of propagation. The monochromatic flux H (radiation flux, energy dependent neutron current) is the radiant energy per unit area, time and frequency interval crossing a small test surface, measured positive from one side and negative from the other. It is a vector quantity, with direction determined by the normal to the surface under consideration, and is obtained by integrating I over solid angle and taking account of the projected area for non-normal incidence:

$$H = \int_{4\pi} d\Omega \cos\theta \, I(\Omega) \tag{1}$$

where the direction of propagation is specified by polar and azimuthal angles $(\theta,\phi) \equiv \Omega$ defined with respect to the surface normal and $d\Omega$ is an element of solid angle. The flux incident upon a surface from one side only is known as the illumination (irradiance); the illumination due to direct solar radiation is called the insolation.

The conceptually simplest property of a planet or an atmosphere which may be desired in a particular application is the albedo, defined as the ratio of the total flux reflected by the atmosphere (which equals the illumination of the upper atmospheric boundary from below) to the incident solar flux. If the atmosphere overlies a planetary surface, then the planetary albedo is the ratio of the total reflected flux to the incident flux. The usual definitions apply to the case of parallel radiation incident on the atmosphere. We may then distinguish between 1) the case of a plane atmosphere, which

applies to a situation at a particular point on a planetary disk and leads to the definition of the plane albedo as

$$A(\mu_0) = \int_{2\pi,\ up} d\Omega\ \mu\ I(\text{at top of atm.})/\pi F\ \mu_0 \tag{2}$$

where θ_0 is the angle of incidence, πF is the solar flux at the position of the planet through a surface perpendicular to the direction of insolation, so that $\pi F\ \mu_0$ is the flux through the upper atmospheric boundary, and we have set $\mu = \cos\theta$, $\mu_0 = \cos\theta_0$. The plane albedo may depend significantly upon angle of incidence θ_0. This is not the case for the spherical or Bond albedo, which is the corresponding ratio of reflected to incident flux for parallel solar radiation incident on a spherical planet. Integrating over the planetary disk, we obtain

$$A_s = \frac{\int_0^{2\pi} d\gamma \int_0^R dr\ r\ A[\mu_0(r,\gamma)]}{\pi R^2} \tag{3}$$

where γ and r are polar coordinates on the (plane) disk of the planet of radius R. Thus, the spherical albedo may be found once the plane albedo is known as a function of position on the disk. The albedo is of paramount importance in determining the total solar energy absorbed by an atmosphere and is thus fundamental in computations of thermal balance. It may also serve as a measure of the expected relative surface brightness for a series of objects for which the directional distribution of reflected intensity does not vary greatly.

Some problems require knowledge of the surface illumination. We may define the ratio of this illumination to the insolation at the top of the atmosphere as a quantity $V(\mu_0,\tau_0)$:

$$V(\mu_0,\tau_0) = \int_{2\pi,\ down} d\Omega\ \mu\ I(\text{at bottom of atm.})/\pi F\ \mu_0 \quad . \tag{4}$$

In many instances, it is of course desirable to know the angular distribution of radiant energy reflected, transmitted, or within an atmosphere; that is, the intensity I. Measurements of the brightness versus position on a planetary disk ("limb darkening") or the brightness distribution across the terrestrial sky are observations of the intensity. In addition, knowledge of I as a function of angle is required for accurate computations of planetary phase curves and accurate computations of albedos. If polarization may be neglected (see below), the intensity will satisfy the equation of radiative transfer (74), whose solution is discussed in subsequent sections (4-6).

If only the radiation emerging from an atmosphere is desired, then one may seek the reflection and transmission functions which may be defined as

$$\begin{aligned} R(\Omega,\Omega_0) &= I(\text{at top going up})/F\ \mu_0 \\ T(\Omega,\Omega_0) &= I(\text{at bottom going down})/F\ \mu_0 \end{aligned} \tag{5}$$

and which may be found without the necessity for obtaining the entire radiation field within the medium. R and T are the reflected and transmitted intensities for incident solar flux π through a surface oriented perpendicular to the solar direction, so that the reflected and transmitted intensities for unit incident flux through the top of the atmosphere are clearly R/π and T/π, respectively. Other definitions of analogous quantities are sometimes employed, such as the scattering and transmission functions $S_c = 4\mu\,\mu_0\,R$ and $T_c = 4\mu\,\mu_0\,T$ (Chandrasekhar, 1950).

The most detailed diagnostic information concerning the composition and state of a planetary atmosphere is frequently obtained from observations of polarization. Since we shall not consider problems of the propagation of coherent radiation for which phase relations may be important (as potentially with laser probes), the radiation field including polarization may be characterized by the four Stokes parameters (see Chandrasekhar, 1950). Up to the present time, almost all observations have been of the linear polarization

$$P = (I_\perp - I_{\parallel})/(I_\perp + I_{\parallel}) \quad , \tag{6}$$

where $I_\perp$ and $I_{\parallel}$ are the radiation intensities with electric vector perpendicular to and parallel to the plane defined by the angles of incidence and reflection on the planetary atmosphere. Measurement and interpretation of the linear polarization versus phase angle and wavelength for Venus have provided stringent limitations on the properties of the cloud particles for that planet (Hansen and Arking, 1971). The circular polarization for radiation reflected by a planet is generally very small, but some measurements are now becoming available (e.g., Swedlund et al., 1972). The polarization may be obtained by solving a vector transfer equation in which the components of vector I are the four Stokes parameters.

Because the scattering within a planetary atmosphere is to a good approximation elastic (or, in a different use of the word from above, "coherent"), each of the quantities considered above may refer either to radiation of a particular frequency (e.g., I_ν) or to the corresponding quantity integrated over wavelength ($I = \int d\nu\, I_\nu$). See, however, the comments under frequency in the following section.

3. DEFINING CHARACTERISTICS OF THE PROBLEM

Almost all theoretical and computational work on multiple scattering problems to date has attacked the direct problem; that is, the physical parameters characterizing the atmosphere (see below) are taken as given, certain boundary conditions are assumed for the sources of radiation, and the radiation field in the atmosphere is sought. The inverse problem, in which the radiation field is assumed known, and it is desired to infer the parameters characterizing the atmosphere, is of course usually more appropriate for the interpretation of observations. Because of the multitude of parameters needed to characterize an actual atmosphere (and perhaps underlying surface), however, there has not as yet been developed any reliable and consistent procedure for solving the inverse problem (some steps have been taken by Twomey, 1963; Herman and Yarger, 1969; Bellman et al., 1965; Fymat and Kalaba, 1973). The usual procedure is to assume a set of values for the atmospheric parameters which are being sought and compute the expected intensity (or albedo, or other measured characteristic of the radiation field) for that particular model atmosphere. Comparison of results obtained for a set of models will then hopefully allow one to define the properties of the atmosphere. In the present review, we shall assume that the latter procedure is being followed, so that we shall discuss solution of the direct problem. It is then necessary to specify those characteristics of the atmosphere which will determine the radiation field for a particular model.

Of fundamental importance in this regard are the scattering and absorbing properties of an elemental volume of the atmosphere. The extinction coefficient α (more correctly called the volume extinction coefficient) determines the attenuation of a beam that is normally incident on a plane layer of geometric thickness ds according to

$$dI/I = -\alpha\, ds \quad , \tag{7}$$

which of course leads to the usual law of exponential attenuation. The extinction coefficient thus describes the attenuation per unit length suffered by a beam, and may also be thought of as the effective interaction cross section per unit volume of the medium. For a monodisperse medium consisting of n particles per unit volume each with an extinction cross section C, we would have $\alpha = nC$, which is of course the reciprocal of the mean free path. For a distribution of particle sizes or properties, the appropriate average must be performed. In the study of stellar atmospheres, but not ordinarily planetary atmospheres, the mass extinction coefficient is employed. It is related to the volume extinction coefficient by $\alpha_\rho = \alpha/\rho$, where ρ is the mass density.

The extinction coefficient consists of two parts, a scattering coefficient σ and an absorption coefficient κ, each with dimensions and definitions parallel to that for the total extinction coefficent. Some workers apply the term "absorption coefficient" to α, in which case κ is referred to as the coefficient of true absorption. In any case, κ defines that portion of the energy removed from a beam which is converted into other forms of energy (or into radiation with a frequency outside the range being considered), while σ describes the radiation which is scattered from one direction into another without such change of frequency. It is important to emphasize that each of these coefficients is a macroscopic quantity characterizing the average properties of a volume element of the atmosphere, so that it makes no difference whether the scattering or absorption is produced by a gas, aerosol particles, or some combination.

Fortunately, the solution of most multiple scattering problems requires only the specification of the ratio

$$\sigma/\alpha = \tilde{\omega}_0 \quad , \tag{8}$$

which is known as the single scattering albedo. It clearly represents the probability that, if a photon interacts within an element of volume, it will be scattered rather than truly absorbed. It will be identical with the average particle albedo of the aerosols in the atmosphere provided that the scattering and absorption by atmospheric gases are negligible.

The directional distribution of radiation scattered by an element of volume is described by the phase function p, which is sometimes referred to as the scattering diagram (indicatrix of scattering in Russian work, normalized scattering kernel in neutron transport theory). It is normalized such that

$$\frac{1}{4\pi}\int_{4\pi} d\Omega\; p(\cos\gamma) = 1 \tag{9}$$

where γ is the angle of scattering. Thus $p(\cos\gamma)\, d\Omega/4\pi$ is the probability that radiation which is scattered will be deviated through an angle γ into an element of solid angle $d\Omega$.

As was mentioned in the introduction, a principal complicating factor in the solution of planetary scattering problems is the marked anisotropy of $p(\gamma)$ in practical applications. This property is often characterized by

$$g = \langle \cos \gamma \rangle = \frac{1}{2} \int_{-1}^{1} d(\cos \gamma) \cos \gamma \, p(\cos \gamma) \quad , \tag{10}$$

the asymmetry factor, which equals the weighted mean cosine of the scattered radiation. Clearly $g = 0$ for isotropic scattering and approaches 1 for the more and more forward-elongated phase functions which are typical of scattering by aerosol particles with dimensions comparable to or larger than the wavelength (cf. Irvine, 1965). Small metallic particles or large rough particles may have $g < 0$ (predominance of backward over forward scattering). The determination of $p(\cos \gamma)$ requires some assumptions concerning the ratio of molecules to aerosol particles and concerning the particle size, shape, and composition in the atmosphere. Only spherical particles have been considered in detail, for which Mie theory applies. Problems involved in the specification of $p(\cos \gamma)$ have been considered in the books by van de Hulst (1957) and Shifrin (1951) and for spheres by Deirmendjian (1969); numerical problems are reviewed by Hunt (1971); Greenberg (1968) has compared the scattering on spherical to nonspherical particles.

The atmospheres must also be characterized by its optical thickness τ_0 . The element of optical path $d\tau = \alpha ds$, so that $\tau_0 = \int ds \alpha$ along the vertical path through the atmosphere.

The quantities underlined above in this section are sufficient to define the porperties of a homogeneous, plane-parallel atmosphere. To complete the specification of a particular problem for such an atmosphere, we must give the boundary conditions including the specification of the radiation sources and the properties of any underlying surface. Normally in the consideration of visible radiation in planetary atmospheres the only source of radiation is incident sunlight. It is almost always possible to neglect the finite size of the solar disk, so that this radiation incident at the top of the atmosphere may be taken as parallel and hence defined by

$$I_0 = \delta(\mu - \mu_0) \, \delta(\phi - \phi_0) \, \pi F \tag{11}$$

where the corresponding flux normal to the beam has been taken equal to πF as above.

The properties of the planetary surface may be much more difficult to characterize. Up to the present time, only isotropically scattering ("Lambert") surfaces and specularly reflecting surfaces have been considered in any detail, although the analytical procedure to be used with a more complicated law of reflection is known (see Sobolev, 1972).

For a particular application it may, of course, not be permissible to assume that the atmosphere is homogeneous and plane-parallel. The introduction of the possible inhomogeneity of the atmosphere may significantly complicate attempts to model the problem, although study of such situations offers the opportunity to potentially determine the altitude profile of such basic atmospheric properties as temperature and pressure. Some of the computational approaches to multiple scattering problems remain virtually unchanged for atmospheres which are vertically inhomogeneous, as has been emphasized by Hunt (1971). In that case the difficulty occurs in knowing how to limit the models to be considered

from an infinitude possible with the abandonment of homogeneity. Analytical results are more limited in extent, although a beginning has been made in this direction (cf. Sobolev, 1972; Kanal, 1973; Yanovitskii, 1972; Ueno, 1960; Bellman, Kalaba, and Ueno, 1963; Chamberlain and McElroy, 1966; Fymat and Abhyankar, 1970).

Horizontal inhomogeneity is much more difficult to handle, and useable results have been obtained to date only by quite approximate methods or by Monte Carlo techniques (Van Blerkom, 1971); see Section 7 below. A somewhat more tractable problem, at least theoretically, concerns the illumination of a homogeneous atmosphere by a horizontally inhomogeneous external source such as a searchlight beam. Initial results with this problem were obtained by Chandrasekhar (1958), and more recently it has been investigated by Rybicki (1971) and Romanova (1971, 1973).

The necessity for considering the sphericity of an atmosphere arises for certain problems such as the examination of twilight phenomena or the illumination over a planetary disk near inferior conjunction. The most attention to these effects seems to have been given by the Soviet group, and results are summarized by Sobolev (1972) (cf. also Sobolev, 1973; Ueno, 1973). Fortunately, for most applications the plane-parallel approximation is sufficient, since the thickness of the atmosphere is very much less than the radius of curvature of the planet.

Infrequently one may be interested in the time response of an atmosphere to an impulsive source of radiation. The velocity of light insures that the propagation of radiation through an atmosphere occurs much more rapidly than temporal changes of atmospheric properties, except perhaps in such instances as a solar eclipse. In the optical probing of an atmosphere the temporal return may be important, however, and an approach such as that used by Romanova (1969) or Minin (1971) might be utilized.

As we have stated above, radiation at separate frequencies may normally be considered separately in solving multiple scattering problems for visible light in planetary atmospheres. It is also generally possible to uncouple the visible transfer problems from those in the thermal infrared, because the overlap between the black body curves for the sun and for a planet is quite small. Recently, however, the possible importance of incoherent (in the frequency domain) scattering such as Raman scattering has been pointed out for the reflection from Uranus and Neptune (Wallace, 1972). Rigorously, problems of this sort would require simultaneous solution of transfer problems at a set of frequencies. In practice approximate methods based on a monochromatic solution may be adequate for at least some applications.

A more usual frequency-related problem concerns the computation of the shape of absorption lines formed by reflection of solar radiation from a planetary atmosphere containing a gaseous absorber. Since the atmosphere is "cold" (relative to the radiation temperature of the incident sunlight), each frequency in the line or band may be treated separately, so that the problem reduces to a series of monochromatic transfer problems. The difficulty arises in the number of such parallel problems that must be solved to define a line shape with sufficient precision; see the discussion in Section 7.

The multiple scattering theory which we are considering assumes that the scattering centers in the atmosphere are far enough apart so that each particle is in the far field of the scattered radiation from any other particle (according to van de Hulst, 1957, this will be satisfied if the inter-particle distance is greater than about three times the particle radius, unless the particles are very large indeed with respect to the wavelength of radiation). As a result, the particles effectively cast no

shadows. This situation would seem to apply to all conceivable atmospheric situations, including multiple scattering by large rain drops. There are, however, other situations where the scattering centers are large enough and their volume density is great enough that mutual shadowing may occur. This effect is thought to produce the "opposition effect" observed as a sharp increase in brightness in the back-scattered direction for observations of Saturn's rings, the surface of the moon and certain asteroids (cf. Bobrov, 1970; Veverka, 1970). The usual multiple scattering theory may in some cases be modified to include such effects (Irvine, 1966); see also Section 7 below.

4. RAPID, APPROXIMATE ANSWERS

In the present section, we shall examine the possibility of finding the answer to a particular multiple scattering problem without the necessity for performing detailed calculations. More explicitly, the methods and results presented in this section require no programming of electronic computers for their application to the problem at hand. When such an approach will be useful depends, of course, on both the quantity being sought (Section 2 above) and upon the accuracy desired. We shall initially limit the discussion to homogeneous, plane-parallel, coherently scattering atmospheres illuminated in a steady state by parallel solar radiation.

Precise formulas will be given where this is possible. In many cases, however, we must resort to approximate procedures. Two of the most useful are described below:

Similarity Relations. It would be a great simplification in planetary scattering problems if the solution for a given anisotropic phase function could be reduced to the known solution for isotropic scattering. We would expect that such a transformation might exist provided that the radiation field has been "smoothed" by a large percentage of multiple scattering and/or by integration over angle. Such "smoothing" is necessary to remove the sharp maxima and minima which are present in the primary scattered radiation if the phase function is highly anisotropic. Obviously no information concerning the azimuthal dependence of the radiation field can be obtained from such a comparison, since for isotropic scattering the intensity is independent of azimuth.

Such "similarity relations" have been used for some time in neutron transport theory (cf. Davison, 1957; Sobolev, 1972). It may be shown that the solution to a given transport problem for a single scattering albedo $\tilde{\omega}_0$ and optical thickness τ_0 will be "similar" (may be approximated by) the solution to the same problem for isotropic scattering and an albedo $\tilde{\omega}_0^*$ and optical thickness τ_0^*, where

$$\tilde{\omega}_0^* = \frac{(1 - g)\omega_0}{1 - g\tilde{\omega}_0} \quad , \tag{12}$$

$$\tau_0^* = (1 - g\tilde{\omega}_0)\, \tau_0 \, . \tag{13}$$

More recently, van de Hulst has pointed out that essentially the same "similarity relation" may be expressed as

$$k^* \tau_0^* = k\tau_0 \tag{14}$$

$$\frac{1 - \tilde{\omega}_0^*}{k^*} = \frac{1 - \tilde{\omega}_0}{k} \tag{15}$$

where k is the inverse diffusion length in the atmosphere (see A.1. below). For the most interesting case of $(1 - \tilde{\omega}_0) \ll 1$, Equations (14) and (15) reduce to Equations (12) and (13) (cf. Figure 1 and Sobolev, 1972, Ch. VIII).

The validity of the relations (14) and (15) for determining the profile of absorption lines formed in a scattering and absorbing atmosphere has been studied by Hansen (1969), who finds good agreement with the exact theoretical results except for large angles of incidence of the solar radiation. The validity for integrated quantities such as the albedo is even more striking (van de Hulst and Grossman, 1968).

Eddington and other Approximations. Approximate values of the flux H may be obtained without rigorously solving the transfer equation by procedures developed for use in stellar atmospheric problems by Eddington, Schuster, Schwarzschild and others [some historical background is given in Sobolev (1956) and Beasley et al. (1967)]. These approximations have different realms of validity.

When the radiation field consists largely of multiply scattered light, so that sharp maxima and minima resulting from the shape of the phase function are smoothed out, the Eddington approximation will provide useful answers. This will be particularly true for quantities integrated over angle, such as the albedo or transmitted flux. This condition applies to thick atmospheres with nearly conservative scattering $(\tau_0 \gg 1, \ (1 - \tilde{\omega}_0) \ll 1)$, but the useful range of parameters is quite large.

An alternative approach, with a similar range of applicability, is the "modified two-stream" approximation proposed by Sagan and Pollack (1967).

When single scattering predominates, as will occur for a thin layer or for a semi-infinite medium if the absorption is large $(\tilde{\omega}_0 \ll 1)$, it is preferable to use the standard two-stream approximation (see below).

We now proceed to the computation of physical quantities, using approximately the ordered sketched in Section 2.

A. Albedos

1. Semi-infinite atmospheres

In this case the properties of any underlying surface can be ignored. It is important to point out, however, under what conditions an actual atmosphere may be considered to be semi-infinite. If the atmosphere is weakly absorbing, in the sense that $[3(1 - \tilde{\omega}_0)(1 - g)]^{1/2} \tau_0 \ll 1$, the atmospheric

reflection will be identical to that of a semi-infinite atmosphere to $O([3(1 - g)\tau_0]^{-1})$. In contrast, when $k\tau >> 1$, the departure from the semi-infinite condition is $O(\exp - 2k\tau_0)$, where k is the inverse diffusion length.

The parameter k is determined by solving the "characteristic equation" for a given phase function. It is the smallest discrete eigenvalue of the transfer equation, so that deep within a homogeneous absorbing medium the radiation field decays as $e^{-k\tau}$. For isotropic scattering

$$\frac{\tilde{\omega}_0}{2k} \ln\left(\frac{1 + k}{1 - k}\right) = 1 \quad , \tag{16}$$

while Figure 1 presents curves relating $\tilde{\omega}_0$, k, and g for the case of the Henyey-Greenstein phase function

$$p(\cos \gamma) = (1 - g^2)/(1 + g^2 - 2g \cos \gamma)^{3/2} \tag{17}$$

for which g is the asymmetry factor $\langle \cos \gamma \rangle$. Equation (17) is a convenient phase function formany purposes, since it may be varied from purely forward scattering (g = 1) to purely backward scattering (g = -1) by changing just the one parameter g. The "similarity principles" (see above) suggest that the curves in Figure 1 will apply quite closely to any phase function with the same $g = \langle \cos \gamma \rangle$.

The plane and spherical albedos are rigorously given for any phase function by

$$A(\mu_0) = 1 - \phi_1^0(\mu_0)/\mu_0 \quad , \tag{18}$$

and

$$A_s = 1 - 2\alpha_1^0 \quad , \tag{19}$$

where the auxiliary function $\phi_1^0(\mu_0)$ and its zeroth moment

$$\alpha_1^0 = \int_0^1 d\mu_0 \, \phi_1^0(\mu_0) \tag{20}$$

are defined in Section 6. A list of available tables is given in Table 1. In the case of isotropic scattering equations (18) and (20) reduce to

$$\begin{aligned} A(\mu_0) &= 1 - H(\mu_0)(1 - \tilde{\omega}_0)^{1/2} \\ A_s &= 1 - 2(1 - \tilde{\omega}_0)^{1/2} h_1 \end{aligned} \tag{21}$$

where $H(\mu) \equiv H^0(\mu)$ is the familiar Chandrasekhar H-function (see Table 1) and h_1 is its first moment $\int d\mu \, \mu \, H(\mu)$. Note that ϕ_1^0 and H are functions of $\tilde{\omega}_0$, although this is often not explicitly indicated.

For general anisotropic scattering with an asymmetry $|g| \gtrsim 0.33$ appropriate tables will not be available. Unless the numerical solution of an integral equation is undertaken to obtain $\phi_1^0(\mu_0)$, we must then proceed in an approximate fashion, or make use of asymptotic expressions that apply in certain limiting cases.

Setting $\tau_0 = \infty$ in Equation (37) below, we obtain for the albedo of a semi-infinite atmosphere in the Eddington approximation

$$A(\mu_0) = \frac{\tilde{\omega}_0}{2}\left[\frac{2 - 3b\mu_0 + 3g(1 - \tilde{\omega}_0)\,\mu_0\,(2\mu_0 - b)}{(1 + b)(1 - k^2\mu_0^2)}\right] \quad \text{for } \tilde{\omega}_0 \neq 1 \,. \tag{22}$$

where $b = 2k(1 - g\tilde{\omega}_0)^{-1}/3$, $k^2 = 3(1 - \tilde{\omega}_0)(1 - \tilde{\omega}_0 g)$, and g is given by Equation (10). A comparison of results obtained from this approximation with the exact solution to the transfer problem is illustrated in Figure 2 and Figure 3. Note the good agreement between the exact and approximate results over a wide range of values of the parameters $\tilde{\omega}_0$, g, and μ_0. Figure 4 illustrates the spherical albedo for a semi-infinite atmosphere as computed from Equation (21).

The albedo for the "modifed two-stream approximation" is given by

$$A = (r - s)/(r + s) \qquad \tilde{\omega}_0 \neq 1 \tag{23}$$

where

$$\begin{aligned} r &= 1 - \tilde{\omega}_0 f_1 + \tilde{\omega}_0 b_1 \\ s &= [(1 - \tilde{\omega}_0 f_1)^2 - \tilde{\omega}_0^2 b_1^2]^{1/2} \\ f_1 &= (1 + g)/2 \\ b_1 &= 1 - f_1 \end{aligned} \tag{24}$$

and g has been defined in Equation (10). When τ_0 or $\tilde{\omega}_0$ are small, it is preferable to use the standard two-stream approximation. The equations are the same as (23) to (24) except that

$$f_1 = \frac{1}{2}\int_0^1 d\mu\; p(\mu) \quad . \tag{25}$$

2. Finite atmospheres

If the atmospheric optical thickness is not semi-infinite, we must in general take account of the reflecting properties of the planetary surface. Detailed results have been obtained only for isotropic (Lambert Law) surface reflection and specular reflection. We shall confine ourselves to the former case, referring the reader to Sobolev (1972, Ch. IV, §5), and Casti, Kalaba, and Ueno (1969) for a discussion of the latter.

In this case, the probability that a photon incident at an angle arccos μ_0 to the surface normal will be reflected at an angle arccos μ into an element of solid angle $d\Omega$ will be

$$2\, a\, \mu\, d\Omega/2\pi \tag{26}$$

where a is the albedo of the surface. The incident intensity I_0 is then related to the reflected intensity I by

$$\begin{aligned} I\mu &= (2\, a\, \mu)\, I_0\mu_0/2\pi \quad , \\ I &= a\, I_0\mu_0\, /\pi \quad . \end{aligned} \tag{27}$$

We may now express the albedo in the presence of a planetary surface in terms of quantities characterizing the atmosphere in the absence of such a surface (i.e., for $a = 0$). Designating the former quantities with a superposed bar, we have (e.g., Sobolev, 1972, Ch. IV)

$$\bar{A}(\mu_0,\tau_0) = A(\mu_0,\tau_0) + \frac{a\, V_s(\tau_0)}{1 - a\, A_s(\tau_0)}\, V(\mu_0,\tau_0) \tag{28}$$

where the surface illumination $V(\mu_0,\tau_0)$ is defined by Equation (4) and, in analogy to the definition of A_s,

$$V_s(\tau_0) = 2\int_0^1 d\mu_0\, \mu_0\, V(\mu_0,\tau_0) \quad . \tag{29}$$

The problem is thus reduced to finding the reflected and transmitted flux in the absence of an underlying surface.

In terms of the auxiliary functions defined in Section 6, the <u>exact expressions</u> are

$$A(\mu_0,\tau_0) = 1 - \phi_1^0(\mu_0,\tau_0)/\mu_0 \tag{30}$$

and

$$V(\mu_0,\tau_0) = \psi_1^0(\mu_0,\tau_0)/\mu_0 \quad . \tag{31}$$

The corresponding spherical albedo and surface illumination are

$$A_s(\tau_0) = 1 - 2\int_0^1 d\mu_0 \, \phi_1^0(\mu_0,\tau_0) \tag{32}$$

and

$$V_s(\tau_0) = 2\int_0^1 d\mu_0 \, \psi_1^0(\mu,\tau_0) \quad . \tag{33}$$

We emphasize again that the functions ϕ_1^0 and ψ_1^0 are their moments, as well as the X- and Y-functions introduced below, are functions of $\tilde{\omega}_0$.

For values of $\tau_0 \gtrsim 3$, one may frequently avoid the necessity of detailed computation, even if quite precise results are desired, by using asymptotic formulae to interpolate between known results for $\tau_0 = \infty$ and numerically obtained anwers at moderate τ_0 . Van de Hulst (1968) has described this procedure in detail.

For isotropic scattering we have in terms of the familiar X- and Y-functions (suppressing the dependence upon τ_0)

$$\phi_1^0(\mu) = \frac{2\mu(1 - \tilde{\omega}_0)[(2 - \tilde{\omega}_0\alpha_0)\, X(\mu) + \tilde{\omega}_0\beta_0\, Y(\mu)]}{(2 - \tilde{\omega}_0\alpha_0)^2 - (\tilde{\omega}_0\beta_0)^2} \tag{34}$$

$$\psi_1^0(\mu) = \frac{2\mu(1 - \tilde{\omega}_0)[\tilde{\omega}_0\beta_0\, X(\mu) + (2 - \tilde{\omega}_0\alpha_0)\, Y(\mu)]}{(2 - \tilde{\omega}_0\alpha_0)^2 - (\tilde{\omega}_0\beta_0)^2} \tag{35}$$

where

$$\alpha_0 = \int_0^1 d\mu \, X(\mu) \quad , \qquad \beta_0 = \int_0^1 d\mu \, Y(\mu) \quad . \tag{36}$$

Tables of X and Y are referenced in Table 1. With their aid, we may use the similarity relations [Equations (12) - (15)] to relate a given problem to the corresponding solution for isotropic scattering. The steps in this procedure would thus be 1) relate the known values of $\tilde{\omega}_0$, g, and τ_0 to the "similar" values for isotropic scattering; 2) solve the appropriate isotropic problem for A, A_s, V, and V_s for the case of no surface reflection (a = 0) by using tables of X and Y functions; 3) find the desired albedo for $a \neq 0$ from Equation (28).

The Eddington approximation when $\tau_0 < \infty$ takes the more complicated form

$$A(\mu_0,\tau_0) = 2(C_1 + C_2 + D) \tag{37}$$

where

$$C_1 = F[T_1 e^{k\tau_0}(1 + b) + T_2 e^{-\tau_0/\mu_0}(1 - b)] \tag{38}$$

$$C_2 = -F[T_1 e^{-k\tau_0}(1 - b) + T_2 e^{-\tau_0/\mu_0}(1 + b)] \tag{39}$$

$$F = \frac{\tilde{\omega}_0}{4} \frac{1}{(1 - k^2\mu_0^2)\,[e^{k\tau_0}(1 + b)^2 - e^{-k\tau_0}(1 - b)^2]} \tag{40}$$

$$D = \frac{-3}{4} \frac{[1 + (1 - \tilde{\omega}_0)g]}{(1 - k^2\mu_0^2)} \mu_0\tilde{\omega}_0 \tag{41}$$

$$k^2 = 3(1 - \tilde{\omega}_0)\,(1 - \tilde{\omega}_0 g) \tag{42}$$

$$T_1 = 2 + 3\mu_0 + 3(1 - \tilde{\omega}_0)\, g\, \mu_0(1 + 2\mu_0) \tag{43}$$

$$T_2 = 2 - 3\mu_0 - 3(1 - \tilde{\omega}_0)\, g\, \mu_0(1 - 2\mu_0) \tag{44}$$

$$b = \frac{2k}{3(1 - \tilde{\omega}_0 g)} \tag{45}$$

As in the semi-infinite case, it will be most precise for thick layers with small absorption, but in such cases it can be quite precise even for quite anisotropic phase functions (cf. Kawata and Irvine, 1970). For a purely scattering atmosphere $\tilde{\omega}_0 = 1$ and these equations simplify to

$$A(\mu_0,\tau_0) = 1 - \frac{2\,R\,(\mu_0,\tau_0)}{4 + 3(1 - g)\tau_0}$$

$$R(\mu_0,\tau_0) = 1 + \frac{3\mu_0}{2} + (1 - \frac{3\mu_0}{2})\, e^{-\tau_0/\mu_0} \quad . \tag{46}$$

The corresponding expressions for the modified two-stream approximation have the same general realm of applicability, and take the form

$$A = \frac{G[1 - \exp(-2\, s\, \tau_0/\mu_0)]}{1 - G^2 \exp(-2\, s\, \tau_0/\mu_0)} \tag{47}$$

where s is defined in Equation (24) and $G = (r - s)(r + s)^{-1}$ with r given by Equation (24). For $\tilde{\omega}_0 = 1$, we have the limit

$$A = \frac{b_1\, \tau_0/\mu_0}{1 + b_1\, \tau_0/\mu_0} \tag{48}$$

with $b_1 = 1 - f_1$ and $f_1 = (1 + g)/2$.

When single scattering predominates, the two-stream approximation may be used. We may then use Equations (47) or (48) with $b_1 = 1 - f_1$ and f_1 defined by (25).

In addition to the reference quoted above, comparison of exact and approximate expressions of this form has been carried out by Irvine (1968; but note the error corrected in Kawata and Irvine, 1970) and Lyzenga (1973). Additional results are presented in Figures 5 and 6. It appears that for a conservative atmosphere ($\tilde{\omega}_0 = 1$), both the modified two-stream and the Eddington approximation give agreement with exact results to better than about 5% for quite anisotropic scattering (at least to $g \lesssim 0.8$) for values of $\tau_0 \gtrsim 5$ and angles not too close to grazing incidence. For $\tilde{\omega}_0 < 1$, the situation is more complex, the accuracy of the approximate methods depending upon whether reflection or transmission (see next sub-section) is being sought, as well as on $\tilde{\omega}_0$, g, and τ_0. As has been stated above, the Eddington approximation and the modified two-stream approximation have the same general realm of validity; from the evidence to date, it appears that within this realm the Eddington approximation is preferable. When low order scattering predominates, the usual two-stream approximation is preferable. Note that for a given atmosphere (fixed τ_0, $\tilde{\omega}_0$, g, μ_0) it may be appropriate to use an Eddington-type approximation for the transmitted radiation (which has a high component of multiple scattering if τ_0 is large) and the two-stream approximation for the reflected flux (if $(1 - g) \ll 1$ and $\tilde{\omega}_0$ is not too close to unity, low order scattering will then predominate).

An interesting possibility is to combine the Eddington approximation and the similarity principles; i.e., use the Eddington approximation for $g = 0$ and values of $\tilde{\omega}_0$ and τ_0 related to the actual g, $\tilde{\omega}_0$, and τ_0 by Equations (12) - (13). In the trial cases shown, this procedure and the standard Eddington approximation bracketed the exact values (see Figure 5).

B. Surface Illumination (Finite Atmosphere)

It is sometimes important to know the flux incident on the surface of a planet, either to estimate sky brightness or to compute heat deposition. In relative units, this illumination is defined by the function $V(\mu_0,\tau_0)$ introduced by Equation (4). If the surface reflects isotropically with an albedo a (Lambertian reflection), the actual surface illumination $\bar{V}$ is related to that for the same

atmosphere but with $a = 0$ by

$$\overline{V}(\mu_0,\tau_0) = \frac{V(\mu_0,\tau_0)}{1 - a\, A_s(\tau_0)} \tag{49}$$

where A_s is the spherical albedo of the atmospheres for $a = 0$.

The exact expression for $V(\mu_0,\tau_0)$ has been given above [Equation (31)]. It is also obvious from energy conservation that if $\tilde{\omega}_0 = 1$,

$$A(\mu_0,\tau_0) + V(\mu_0,\tau_0) = 1 \quad . \tag{50}$$

When $\tilde{\omega}_0 = 1$ (conservative scattering), we may bound $V(\mu_0,\tau_0)$ by

$$\frac{\mu_0}{(1 - g)\tau_0 + 1} < V(\mu_0,\tau_0) < \frac{1 + \mu_0}{(1 - g)\tau_0 + 1} \tag{51}$$

which provides the useful approximation (Sobolev, 1972, Ch. VIII)

$$V(\mu_0,\tau_0) \simeq \frac{1/2 + \mu_0}{(1 - g)\tau_0 + 1} \qquad \tilde{\omega}_0 = 1 \tag{52}$$

for which the maximum error may be determined from (51).

Turning again to the Eddington approximation, we have

$$V(\mu_0,\tau_0) = 2(C_1 e^{-k\tau_0} + C_2 e^{k\tau_0} + D e^{-\tau_0/\mu_0}) + e^{-\tau_0/\mu_0} \qquad \tilde{\omega}_0 \neq 1 \tag{53}$$

where C_1, C_2, and D are determined by Equations (38) - (41) above, or

$$V(\mu_0,\tau_0) = \frac{2R(\mu_0,\tau_0)}{4 + 3(1 - g)\tau_0} \qquad \tilde{\omega}_0 = 1 \tag{53a}$$

where $R(\mu_0,\tau_0)$ is given by the second of Equations (46).

Some new results are presented in Figure 6, where we have plotted the diffuse contribution to $V(\mu_0,\tau_0)$; that is, the total surface illumination minus the unscattered contribution. The exact curves were computed using the doubling method as described below, while the approximate results were obtained from the equations given above. Observe that at least for $\tilde{\omega}_0 \gtrsim 0.98$ and $\tau_0 \gtrsim 5$, the Eddington approximation gives accuracy of a few percent in the transmitted flux, even for quite anisotropic scattering. Note the comments in the previous section concerning realms of validity and concerning the combined Eddington-similarity approximation.

When the transmitted radiation results primarily from low order scattering, we may use the two-stream approximation to obtain

$$V(\mu_0,\tau_0) = \frac{e^{-2\,s\,\tau_0/\mu_0}(1 - G^2)}{(1 - G^2 e^{-2\,s\,\tau_0/\mu_0})} \qquad \tilde{\omega}_0 \neq 1$$

$$V(\mu_0,\tau_0) = 1 - A(\mu_0,\tau_0) \qquad \tilde{\omega}_0 = 1 \quad . \tag{54}$$

with s and G determined as in Equation (47) except that f_1 is given by (25).

The similarity principles may be used as described at the beginning of this section to approximately reduce the problem for a general anisotropic phase function to one with isotropic scattering. Thus, when $V(\mu_0,\tau_0)$ is not dominated by low order scattering, we relate the values of $\tilde{\omega}_0$, g, and τ_0 to the corresponding "similar" values for isotropic ($g = 0$) scattering with Equations (12) - (13) or (14) - (15), find V and A_s from Equations (31), (32), (34), (35), and the relevant tables for isotropic scattering, and then use Equation (49).

C. Energy Deposition in the Atmosphere

Determination of the atmospheric temperature profile may require knowledge of the solar energy absorbed as a function of altitude. The temperature profile may be needed for dynamic computations or to calculate the atmospheric thermal emission. The rate at which energy is absorbed by the atmosphere per unit of verticle optical depth per cm^2 will be given by the derivative of the net flux $\Delta = -dH/d\tau$ (cf. Fouquart, 1971).

If the single scattering albedo and the optical thickness are not too small, we may usefully apply the Eddington approximation to obtain

$$\Delta = \pi F(1 - \tilde{\omega}_0)[4\mu_0(C_1 e^{-k\tau} + C_2 e^{k\tau} + D e^{-\tau/\mu_0}) + e^{-\tau/\mu_0}] \tag{55}$$

where the constants C_1, C_2, and D have been defined previously [Equations (38) - (41)].

D. Intensity

As we have pointed out, most planetary atmospheres most of the time contain a sufficient number of aerosol particles to make the phase function quite anisotropic. Nonetheless, comparison with the results for more nearly isotropic scattering is sometimes useful; clear days of exceptional visibility do occur for the Earth, and otherplanets may have nearly aerosol-free layers in their atmospheres (cf. the discussion of Uranus by Belton et al., 1971). In addition, use of the similarity relations allow us in many instances to relate the solution of a more complex scattering problem to the simple solution for isotropic or nearly isotropic scattering.

Table I presents a "Tables of Tables" of functions providing the exact solutions for the reflection and transmission of light from homogeneous atmospheres scattering according to the phase functions listed. Extensive results are available only for isotropic scattering and Rayleigh scattering. The authors may use somewhat different notations, and the reader should read the articles to ensure that he uses the appropriate formula relating the computed functions and the desired intensity. Note particularly that, in writing an expression for (say) the reflected intensity, different authors may take the incident solar flux normal to the solar direction as πF, π, 1, $\pi F\mu_0^{-1}$, μ_0^{-1}, etc.

There is an annoying tendency for tables to exclude those particular parameter values that are important for the application you have in mind. In this connection, asymptotic expressions relating solutions for $\tau_0 = \infty$ to solutions for $\tau_0 >> 1$ are often very helpful. Van de Hulst (e.g., 1968) has emphasized this approach, which of course, can be used with numerically computed values corresponding to arbitrary phase functions, as well as when tables are available. He has emphasized that by an appropriate choice of abscissa it is often possible to interpolate accurately between $\tau_0 = \infty$ and values as small as $\tau_0 \tilde{>} 3$. As examples of such formulas, we may cite the azimuth independent portion of the reflection R and transmission T functions, which are related to the corresponding quantities in the semi-infinite case by

$$R(\mu,\mu_0,\tau_0) = R_\infty(\mu,\mu_0) - \frac{M N e^{-2k\tau_0}}{1 - N^2 e^{-2k\tau_0}} u(\mu) u(\mu_0) \tag{56a}$$

$$T(\mu,\mu_0,\tau_0) = \frac{M e^{-k\tau_0}}{1 - N^2 e^{-k\tau_0}} u(\mu) u(\mu_0) \tag{56b}$$

where k is the inverse diffusion length illustrated in Figure 1 (cf. also van de Hulst, 1970b), M and N are constants defined by

$$N = 2\int_0^1 d\mu_0\, \mu_0\, u(\mu_0)\, i(-\mu_0) \quad ,$$
$$M = 2\int_{-1}^1 d\mu\, \mu\, i^2(\mu) \quad . \tag{57}$$

The quantity $u(\mu)$ is the "escape function" describing the relative angular distribution of radiation emerging from an atmosphere for which the radiation sources are at great depths (or, equivalently, the transmission through a very thick atmosphere), and $i(\mu)$ describes the relative angular distribution of intensity within the deep layers of a thick atmosphere. They are normalized such that

$$\frac{\tilde{\omega}_0}{2}\int_0^1 d\mu\ i(\mu) = 1$$

$$2\int_0^1 d\mu\ \mu\ i(\mu)\ u(\mu) = 1 \qquad (58)$$

In practice, $u(\mu)$ may be found from the tabular or computed values of transmitted intensity for sufficiently large τ_0, while the constants M and N may be obtained by solving Equation (56a) or (56b) at two values of τ_0 in the asymptotic regime (given that R or T is known at those τ_0).

Note that $u(\mu)$ depends only weakly on the phase function asymmetry g (see van de Hulst and Grossman, 1968). Sobolev (1972, Ch. VIII) has shown that in the case $\tilde{\omega}_0 = 1$, $u_0(\mu) \equiv u(\tilde{\omega}_0 = 1, \mu)$ may be approximately represented in linear fashion as

$$u_0(\mu) = (1 + \beta\mu)(1 + 2\beta/3)^{-1} \qquad (\tilde{\omega}_0 = 1) \qquad (59)$$

where

$$\beta^{-1} = \frac{1}{\pi}\int_0^\pi d\theta\ \sin^2\theta\ p(\cos\theta) \quad . \qquad (60)$$

Figure 7 illustrates this approximation for a quite forward-directed phase function (g = 0.75). According to a strict application of the similarity principles, $R(\mu,\mu_0)$ should be identical for all phase functions when $\tilde{\omega}_0 = 1$. This does not give particularly good results in the present case.

Various simplifications are possible in Equation (56) in certain cases. If absorption is small ($1 - \tilde{\omega} \ll 1$, so that $k \ll 1$)

$$R(\mu,\mu_0,\tau_0) = R_\infty(\mu,\mu_0) - h(\tau_0)\ u_0(\mu)\ u_0(\mu_0)$$

$$T(\mu,\mu_0,\tau_0) = e^{-k\tau_0}\ f(\tau_0)\ u_0(\mu)\ u_0(\mu_0) \qquad (61)$$

where

$$h(\tau_0) = \frac{4k}{3(1 - g)} + f(\tau_0) \quad ,$$

$$f(\tau_0) = \frac{8k}{3(1 - g)(e^{2k\tau_0} - 1) + 6\delta k} \quad , \qquad (62)$$

$$\delta = 4\int_0^1 d\mu\ \mu^2\ u_0(\mu) \quad ,$$

and $u_0(\mu)$ and $R_\infty(\mu,\mu_0)$ refer to the case $\tilde{\omega}_0 = 1$.

In the conservative case ($\tilde{\omega}_0 = 1$) or more generally if $k\tau_0 << 1$, Equation (61) takes the particularly simple form

$$R(\mu,\mu_0,\tau_0) = R_\infty(\mu,\mu_0) - 4\,\frac{u_0(\mu)\,u_0(\mu_0)}{3(1-g)\,\tau_0 + 3\delta} \tag{63}$$

$$T(\mu,\mu_0,\tau_0) = \frac{4\,u_0(\mu)\,u_0(\mu_0)}{3(1-g)\,\tau_0 + 3\delta} \tag{64}$$

Other particular cases, such as $k\tau_0 >> 1$, may be easily deduced from (56).

Perhaps the most convenient and rapid approximation to use if the angular dependence of the radiation field is desired is a combination of exact first order scattering plus higher order scattering computed for the appropriate isotropic case from the similarity principles. Thus, if we take the incident solar flux through a surface normal to the solar direction as πF, we find (suppressing the dependence upon τ_0)

$$R(\Omega,\Omega_0) = \frac{\tilde{\omega}_0 F}{4}\left[\frac{X(\mu)\,X(\mu_0) - Y(\mu)\,Y(\mu_0) + [p(\Omega,\Omega_0) - 1][1 - \exp(-\tau_0(\mu^{-1} + \mu_0^{-1})]}{\mu + \mu_0}\right] \tag{65}$$

for the reflected intensity, and

$$T(\Omega,\Omega_0,\tau_0) = \frac{\tilde{\omega}_0 F}{4}\left[\frac{X(\mu_0)\,Y(\mu) - X(\mu)\,Y(\mu_0) + (p(\Omega,\Omega_0) - 1)(e^{-\tau_0/\mu} - e^{-\tau_0/\mu_0})}{\mu - \mu_0}\right] \tag{66}$$

for the transmitted intensity, where $X(\mu)$ and $Y(\mu)$ are given for isotropic scattering in the tables listed in Table 1. We have allowed for azimuthal dependence (ϕ) in Equations (65) and (66) by writing R and T as functions of $\Omega \equiv (\theta,\phi)$ and $\Omega_0 \equiv (\theta_0,\phi_0 = 0)$.

Alternatively, we might compute the higher order scattering using the tabulated functions available for scattering according to the phase function $p(\mu) = 1 + \tilde{\omega}_1\mu$, as suggested by Sobolev (1956, 1972). This amounts to finding the source function for the radiation field in an Eddington approximation. A comparison of such an approximation with exact values for the reflection from a semi-infinite atmosphere is shown in Figure 8.

Other approximate methods are available which are particularly useful if the phase function is very forward directed, such as the expansion of I in a Taylor series in angle about the direction of incidence (Sobolev, 1972, §7, Ch. VIII), but the availability of modern computers makes it essentially as easy to obtain an "exact" solution to the actual transfer equation (see next section).

E. Polarization

Quite precise polarization data are becoming available for the planets, and their interpretation requires a correspondingly precise solution of transfer problems. A "quick look" estimate of polarization can be obtained, however, using a procedure originally suggested by Lyot (see Kuiper, 1947).

The linear polarization of radiation reflected from an atmosphere arises in large part (but not entirely) from the singly scattered light. A reasonable estimate is therefore to compute the intensity difference due to primary scattering $(I_\perp^{(1)} - I_\parallel^{(1)})$, where $I_\perp$ and $I_\parallel$ represent the intensities with electric vector perpendicular and parallel to the scattering plane (the plane containing the directions of incidence and emergence), respectively; and divide this quantity by the total intensity, either computed theoretically in the absence of polarization (i.e., from the scalar transfer equation or an approximation as in the previous section) or derived from observation. The percentage of linear polarization is then

$$p \simeq \frac{(I_\perp^{(1)} - I_\parallel^{(1)})}{I} \tag{67}$$

which will be a function of angles of incidence and reflection, as well as the parameters characterizing the atmosphere $(\tilde{\omega}_0, \tau_0$, phase function).

Computation of the first order intensities in each polarization requires that a form be assumed for the phase matrix. For very small particles, Rayleigh scattering may be used. For spheres of any diameter, Mie theory is appropriate (e.g., van de Hulst, 1957). Radially inhomogeneous spheres lead to a modification of Mie's original theory (see Olaofe and Levine, 1967). Tabular material, as well as a description of the integration over particle size distribution which is normally required, is given by Deirmendjian (1969).

If the particles have dimensions on the order of the wavelength or larger and have typical crystalline forms, no general theory exists for computing the phase matrix.

5. PRECISE NUMERICAL METHODS

In this section, we shall consider methods for solving multiple scattering problems which may be made arbitrarily precise by choosing a sufficient number of, say, Gaussian integration points in a necessary numerical integration. Such methods are necessary to obtain precise solutions when the phase function is highly anisotropic, as will normally be the case in planetary atmospheres. Those methods which carry analytical procedures as far as possible will be considered in the next section; they also ultimately require numerical methods, such as the solution of an integral equation.

It is possible to combine any of the methods in this section with a procedure to "separate off" the extreme forward diffraction peak in the radiation field that occurs in low order scattering by particles large compared with the wavelength. This may be done either by re-defining the phase function to exclude this peak (and appropriately renormalizing $\tilde{\omega}_0$ and τ_0; cf. van de Hulst, 1971a; Hansen, 1969) or by separating the radiation field into two parts with the aid of a "small angle" approximation such as that employed by Romanova (cf. Malkova, 1972; Irvine, 1968).

The different methods discussed below each have certain advantages and disadvantages, and the choice will depend to some extent upon the particular problem being solved. They all require access to an electronic computer of at least moderate size. We shall limit the present discussion to finding intensities averaged over azimuth, since each component of an expansion of the intensity in a Fourier series in azimuth may be found in the same manner, and the zeroth order term is numerically the most difficult to compute (see next section; Dave and Gazdag, 1970; and van de Hulst, 1971).

A. Adding or Doubling Method

The antecedants of this procedure apparently go back to Stokes (1862), who considered the transmission and reflection by a stack of glass plates. The principle is simply stated: if we know the complete reflection and transmission properties $R(\mu,\mu_0)$ and $T(\mu,\mu_0)$ of each of two layers, we may find the reflection and transmission from the combined layer by computing the successive reflections back and forth (and the corresponding loss to transmission) between the two layers. The infinite series comprising the reflection or transmission in fact converges quite rapidly to a geometric series, so that the required sum is quickly obtained (van de Hulst and Grossman, 1968). A detailed numerical procedure is described by Hansen (1969). It consists essentially of repeated numerical integration over angle to obtain each successive reflection and transmission. The same method was developed independently by Twomey et al. (1966).

What is in essence this method has been developed independently by several authors in different fields. A helpful historical summary is given by Plass et al. (1973). Because the calculation of the series is equivalent to inverting a matrix, the method has received a variety of applications, including matrix operator theory (cf. Kattawar et al., 1973) and discrete space theory (Preisendorfer, 1965; Grant and Hunt, 1969). The most detailed study of the precision, error propagation, and application to inhomogeneous atmospheres has been given by Grant and Hunt (cf. Hunt, 1971), who also showed that the procedure can be used to obtain the internal radiation field (including the case with a distribution of internal energy sources).

In the limit in which all layers to be added are infinitesimally thin, the equations lead to the invariant imbedding theory used extensively by Bellman, Kalaba, Ueno, and others (e.g., Bellman, 1969). The Grant and Hunt algorithm to obtain the internal radiation field leads in the same limit to the Riccati transformation equations of Rybicki and Usher (1966).

Given a reliable integration scheme, the difficulty is only in obtaining $R(\mu,\mu_0)$ and $T(\mu,\mu_0)$ for the constituents layers. We may distinguish two cases. If the atmosphere is homogeneous, we begin with a layer of known properties and successively double its thickness. Conceptually the simplest procedure is to begin with layers sufficiently thin ($\tau_0 \ll 1$) that only single scattering is important. Hansen (1969) takes initial values of $\tau_0 = 2^{-25}$, while Irvine (1968) has obtained at least one per cent accuracy by choosing $\tau_0 = 2^{-9}$. A layer of optical thickness $\tau_0 = 32$ (for many purposes semi-infinite) is obtained following thirty or fourteen doublings, respectively. It may be possible to take a coarser angular grid if the initial layer is chosen somewhat thicker ($\tau_0 \approx 1/2$), in which case the first R and T must be found from another method, such as successive scattering (see below and van de Hulst and Grossman, 1968).

If the atmosphere is inhomogeneous, layers of different reflection and transmission characteristics are added at each step. If each layer may be taken to have a finite width, the procedure is essentially the same as before, with a little added bookkeeping to construct each layer and then add them together. This will frequently be the case in practice, since our knowledge of the gradient of (for example) $\tilde{\omega}_0$ in an atmosphere will normally not be sufficiently accurate to warrant a more detailed procedure.

If, however, we wish to compute a model with continuously varying optical properties, the speed of the adding method is largely lost, and it may not have an advantage over method (C) below.

This method has a number of advantages:

1) the numerical procedure is straight forward, involving only integrations over angle;

2) a physical interpretation of the results is available at each step;

3) there is no difference in principle in the program for isotropic and for highly anisotropic scattering, although in practice more Gaussian points must be used in the integrations when the phase function is anisotropic;

4) results are obtained for a range of angles of incidence (those used in the integration scheme);

5) results are obtained for a range of optical thicknesses between the final value and the starting value.

Drawbacks of the method are:

1) a complete new computation must be performed if the single scattering albedo $\tilde{\omega}_0$ is changed (as will occur as a function of frequency within an absorption line or band);

2) the method must begin with extremely thin layers or with results obtained from another method;

3) if only one angle of incidence is required in a given application, the method may be less economical for a layer of relatively small thickness ($\tau_0 \lesssim 1$) than other methods in which μ_0 is given as a parameter.

B. Successive Scattering

Like the previous method, the physical reasoning behind the method of successive scattering is very simple: compute the intensity by adding the contributions due to photons which have been scattered once, twice, etc.:

$$I(\tau,\Omega) = \sum_n \omega_0^n \, I_n(\tau,\Omega) \tag{68}$$

where $I_n(\tau,\Omega)$ is the intensity due to n-times scattered photons in the conservative case ($\tilde{\omega}_0 = 1$).

Mathematically, this procedure corresponds to finding the Neumann series solution to the integral equation for the source function.

In addition to physical simplicity, the great attraction of the method lies in the ability to relate the solution to a problem for arbitrary $\tilde{\omega}_0$ to the solution for $\tilde{\omega}_0 = 1$ and the same optical thickness τ_0. This means that in a set of models within which the ratio of scattering to absorption (i.e., $\tilde{\omega}_0$) is changing, while the optical thickness remains constant, only one radiative transfer problem need be solved (to obtain the I_n for $\tilde{\omega}_0 = 1$). In the case of absorption line formation, this situation will apply to semi-infinite atmospheres (for which $\tau_0 = \infty$ in both the continuum and the line).

It has long been recognized that the series (68) converges extremely slowly for $\tau_0 \gtrsim 1$ unless $\tilde{\omega}_0 \ll 1$. Van de Hulst and Irvine (1962) have pointed out, however, that the ratio of successive terms I_n/I_{n-1} approaches a constant value as n increases, so that the sum in Equation (68) may be truncated and the remainder replaced by a geometric series. The approach to this situation is slow, however, for $\tau_0 \lesssim 1$.

Of perhaps greater significance is the discovery (Uesugi and Irvine, 1970) that even for $\tau_0 = \infty$, I_n approaches an asymptotic form as $n \to \infty$. In practice, this enables the method to be used even for extremely thick atmospheres (cf. van de Hulst, 1970). The appropriate asymptotic expressions for $1 \ll \tau_0 < \infty$ have not been worked out, however.

The necessary equations to be used in a numerical computation are presented in van de Hulst (1948) for the case of isotropic scattering, in Irvine (1964) for the case of an arbitrary phase function with $\tau_0 < \infty$, and in Uesugi et al. (1970) for $\tau_0 = \infty$. Successive numerical integrations over angle and optical depth are required unless $\tau_0 = \infty$. The usual procedure has been to use Gaussian integration (or some variant such as Radau integration) for the former and a Simpson rule approach to the latter (evenly spaced points are desirable in the τ-integration because the value of the integral is needed at all intermediate values of τ).

Of considerable importance is the immediate applicability of the method for finite τ_0 to vertically inhomogeneous atmospheres, which requires no substantive change in the procedure. Another advantage of the procedure (applicable to small τ_0) occurs if only one angle of incidence is important in a particular abpplication. The method gives an answer for that value, without wasting computer time determining the intensity for all other values of the parameter θ_0.

Disadvantages of the successive scattering method remain slow convergence for $(1 - \tilde{\omega}_0) \ll 1$ and $\tau_0 \gtrsim 1$; and, if the intensity is desired as a function of μ_0, the necessity to solve a new problem for each such value to be considered.

C. Invariant Imbedding

As we have mentioned above, if the layers being added in the adding method are very thin, the procedure reduces to the method referred to as invariant imbedding. The origin of this method in radiative transfer theory lies with the "principles of invariance" introduced by Ambartsumyan (1943) and extended and generalized by Chandrasekhar (e.g., 1950). The invariant imbedding equations form an initial value (at $\tau_0 = 0$) problem for the determination of the radiation field. Its practicality for use as a

numerical method has been demonstrated by Bellman and his colleagues (e.g., 1963). Because a thick layer is built up only slowly, however, the method would seem to have been superseded by Method A.

D. Spherical Harmonics and Discrete Ordinates

The spherical harmonics procedure was used in a low order of approximation in neutron transport theory, but generally discarded with the advent of larger computers. Recently, however, adaptation of the method to such machines has given promising results (e.g., Devaux and Herman, 1971).

Since the spherical harmonics form a complete set, it is natural to approximate the m-th azimuthal component of the intensity (see Section 6) at an optical depth τ by an expression of the form

$$I^m(\tau,\mu) = \sum_{n=m}^{L} (2n + 1)\, A_m^n(\tau)\, P_m^n(\mu) \quad . \tag{69}$$

In the p-th order of approximation, $L = 2p - 1 + m > N$, where N is the number of terms retained in a Legendre expansion of the phase function. Substitution of (69) into the equation of transfer leads to a system of first order, linear differential equations for the coefficients $A_m^n(\tau)$. The boundary conditions that no diffuse radiation be incident on the atmosphere from outside cannot be satisfied for all μ by an expression like (69). Instead one may choose, for example,

$$\int_0^1 d\mu\; I^m(0,\mu)\; P_m^{m+2j-1}(\mu) = 0 \tag{70}$$

for $j = 1, 2, \ldots, p$.

If the atmosphere is homogeneous, the solution to the coupled differential equations takes the form

$$A_m^n(\tau) = \sum_{i=-p}^{p} k_m^i\, g_m^n\, (\nu_m^i)\, e^{-\nu_m^i \tau} + h_m^n\, e^{\tau/\mu_0} \tag{71}$$

where the g_m^n are defined by a system of $2p$ linear homogeneous algebraic equations, the k_m^i are specified by the boundary conditions, and the h_m^n are defined by another system of algebraic equations. The constants ν_m^i are the roots of the characteristic equation obtained from the condition that the equation system for the g_m^n have a nontrivial solution. The only numerical difficulty in this procedure is the solution for the ν_m^i, which, however, is simplified by the fact that the values in the (p-1)-st approximation provide a good approximation to the (p-1) smaller roots in the p-th approximation. In the limit as $p \to \infty$, this solution leads to the exact eigenfunction solution obtained by Case and co-workers (see sub-section E below).

If the atmosphere is inhomogeneous, the equation for the A_m^n may be solved by finite differences. Suitable linear transformations eliminate possible instabilities.

The spherical harmonic method for $m = 0$ leads to equations identical to those obtained by the method of discrete ordinates, proposed by Wick (1943) and developed by Chandrasekhar (1950). The approach here is to replace the integral term in the transfer equation (74) by a Gaussian quadrature

sum, so that we obtain a system of linear, differential equations for the $2p$ functions $I^m(\tau,\mu_j)$, where the discrete values μ_j are (for the strict Gauss formula) the roots of $P_{2p}(\mu)$. When $m \neq 0$, the equations differ slightly from those obtained by the spherical harmonic method, but the method of solution remains the same.

The method has the advantage that the formulae have been worked out in detail for the homogeneous case (Chandrasekhar, 1950); increasing the number of directions for a given choice of p does not appreciably change the computation time; if the atmosphere is homogeneous the computation time is independent of τ_0; and the angle of incidence appears only in the last stage of the computation, so that several values of μ_0 may be treated without a large expense of computer time.

The principle drawbacks of the method seem to be that it is difficult to obtain an a priori idea of the accuracy of a given order of approximation; the computation time increases with increasing anisotropy of the phase function (increasing number of terms N in a Legendre expansion); and numerical difficulties occur in the solution of the characteristic equation for ν when $N \gtrsim 30$.

E. Eigenfunction Expansion

This elegant procedure will be discussed at this symposium by Professor Kuščer (cf. also Case and Zweifel, 1967; Pahor and Zweifel, 1969), so that I will not dwell upon it here. It provides a complete, rigorous, mathematical solution once the eigenfunctions have been obtained for a particular problem. Much analytical work has been done, but the final expressions are relatively complicated. There has not yet been much in the way of numerical results for the case of anisotropic scattering of most interest to this paper.

F. Gauss-Seidel Method

The method of successive scattering can be looked upon as a way of iterating an initial estimate of the solution (first order scattering) to obtain a final solution. The speed of convergence of such an iterative procedure can be considerably enhanced by using the Gauss-Seidel procedure, as has been demonstrated by Herman (e.g., Herman and Browning, 1965). The procedure, like the successive scattering approach, is essentially unaltered if the atmosphere is vertically inhomogeneous, and it is easily modified to include polarization.

The principal drawback of this approach is its apparent limitation to relatively thin atmospheres ($\tau \lesssim 5$), and the necessity to re-solve the problem each time the single scattering albedo is changed in a homogeneous atmosphere (unlike the successive scattering approach).

G. Monte Carlo Method

Given enough computer time, there is probably no radiation transfer problem in planetary atmospheres that cannot be solved by means of the Monte Carlo method. Basically, a Monte Carlo computation follows one photon at a time on a three-dimensional traversal of an atmosphere. The interaction of the photon with the atmospheric constituents is described by defining suitable probability distributions.

Consider, for example, a Rayleigh scattering atmosphere. The scattering phase function is

$$p(\mu) = \frac{3}{4}(1 + \mu^2) \tag{72}$$

so that the probability that a photon is scattered through an angle θ is given by the probability distribution

$$P(\cos\theta) = \int_{-1}^{\cos\theta} p(\mu)\, d\mu \Big/ \int_{-1}^{1} p(\mu)\, d\mu \quad . \tag{73}$$

In a Monte Carlo calculation of the process, a random number uniformly distributed between 0 and 1 is generated and equated to $P(\cos\theta)$, which thus determines $\cos\theta$. Distances between collisions and reflections off surfaces may be handled in the same manner. For most applications, where reflected or transmitted intensities are desired, the photon is followed until it emerges from the atmosphere, when its direction is recorded.

It is obvious that very many photons must be followed for the method to have any value. Since Monte Carlo programs can use up huge amounts of computer time, most of the mathematical sophistication goes not into setting up the problem, but in finding ways to make it run more economically. Programs may involve upwards of 10^6 photons and take hours to run, so it seems prudent that Monte Carlo calculations be avoided if there is any other method available to solve the problem at hand.

The ability of the Monte Carlo method to treat radiation transfer in the terrestrial atmosphere is shown in a long series of papers by Plass and Kattawar. Of these, specific reference is made to Plass and Kattawar (1968) where the Monte Carlo program is described and to Kattawar and Plass (1968) where polarization is included. Danielson, Moore, and van de Hulst (1969) describe a Monte Carlo program for plane-parallel atmospheres with a Henyey-Greenstein phase function. Sanford and Pauls (1973) used an "inverse" Monte Carlo technique in studying circumstellar dust shells. This method follows photons backwards from the detector and gives improved statistics.

This method may be the only practical approach for difficult geometries (see below), but it should probably be avoided if other methods are available. Another possible application is in obtaining the distribution of path lengths traveled by photons, which can be used to solve spectral line problems (see Section 7 below).

6. ANALYTICAL SOLUTIONS

Considerable progress has been made since the time of earlier reviews (van de Hulst and Irvine, 1962; Busbridge, 1960; Kuščer, 1958) in the rigorous analysis of radiative transfer for general anisotropic scattering. The approach of Case and others was mentioned in Section 5(E) above. An alternative (but related) approach is the expression of the solution in terms of functions of one variable which may be determined from appropriate integral equations. This method is associated with the classical H, X and Y functions. The necessary functions may be specified either by non-linear integral equations plus necessary constraints to insure uniqueness, or by linear singular integral equations with corresponding constraints. It has been shown in recent years that the solution for any phase function expressible in a Legendre expansion can be obtained in this way. As the auxiliary functions which arise in this process are often referred to in the literature, and the terminology can be confusing, it seemed advisable to present the solution here. Note that it is not clear that in the final numerical computation this method is superior to the others described in the preceding section.

The complex of algebra required for quite anisotropic scattering has thus far prevented the development of a general algorithm using this method, and very little is available in numerical results for such cases. Nonetheless, it is useful to have the analytic form of the solution available for an arbitrary phase function, approximate and asymptotic formulas can be obtained rigorously, and it may in the future be possible to successfully program such a procedure for machine computation. Note, however, that the method has thus far been developed almost entirely for homogeneous atmospheres (however, see Sobolev, 1972, Ch. III).

We shall treat the general problem of an azimuthally dependent radiation field, since this will be frequently encountered in practice. Consider, then a homogeneous, plane-parallel layer characterized by a phase function $p(\cos\gamma)$, a single scattering albedo $\tilde{\omega}_0$, and an optical thickness τ_0. We use coordinates such that θ is the polar angle with respect to the downward normal in the atmosphere, ϕ is the corresponding azimuthal angle, and we set $\mu = \cos\theta$, $\Omega \equiv (\theta,\phi)$. Let parallel radiation be incident in a direction $\Omega_0 = (\theta_0, \phi = 0)$ with a flux πF through a surface oriented perpendicular to the radiation. We measure the optical thickness τ downwards from the top of the atmosphere.

The diffuse intensity $I(\tau,\Omega,\Omega_0) \equiv I(\tau,\mu,\mu_0,\phi,\phi_0 = 0)$ satisfies the equation of radiative transfer:

$$\mu \frac{dI}{d\tau} = - I + B \quad , \tag{74}$$

where the source function $B(\tau,\Omega,\Omega_0)$ is given by

$$B(\tau,\Omega,\Omega_0) = \frac{\tilde{\omega}_0}{4\pi}\int_0^{2\pi} d\theta \int_{-1}^{1} d\mu'\ p(\Omega,\Omega')\ I(\tau,\Omega',\Omega_0) + \frac{\tilde{\omega}_0}{4} F\, e^{-\tau/\mu_0}\, p(\Omega,\Omega_0) \quad . \tag{75}$$

We shall expand the phase function as

$$p(\cos\gamma) = 1 + \sum_{n=1}^{N} \tilde{\omega}_n P_n(\cos\gamma) \tag{76}$$

with

$$\frac{1}{4\pi}\int_{-1}^{1} d(\cos\gamma)\ p(\cos\gamma) = 1 \tag{77}$$

so that

$$p(\Omega,\Omega') = p^0(\mu,\mu') + 2\sum_{m=1}^{N} p^m(\mu,\mu')\cos m(\phi - \phi') \tag{78}$$

with

$$p^m(\mu,\mu') = \sum_{i=m}^{N} c_i^m \, P_i^m(\mu) \, P_i^m(\mu') \tag{79}$$

and

$$c_i^m = \tilde{\omega}_i \, \frac{(i-m)!}{(i+m)!} \quad ,$$

$$\cos\gamma = \mu\,\mu' + \sqrt{1-\mu^2}\,\sqrt{1-\mu'^2}\,\cos(\phi-\phi') \quad .$$

In Equations (76) and (79), $P_n(\mu)$ and $P_n^m(\mu)$ are the Legendre and the associated Legendre polynomials, respectively. We may then expand the intensity in a cosine series in azimuth, so that

$$\begin{aligned} I(\tau,\mu,\mu_0,\phi) &= I^0(\tau,\mu,\mu_0) + 2\sum_{m=1}^{N} I^m(\tau,\mu,\mu_0)\cos m\phi \quad , \\ B(\tau,\mu,\mu_0,\phi) &= B^0(\tau,\mu,\mu_0) + 2\sum_{m=1}^{N} B^m(\tau,\mu,\mu_0)\cos m\phi \quad . \end{aligned} \tag{80}$$

Substitution of (80) into the transfer equation shows that each azimuthal component I^m satisfies a separate transfer equation with a source function B^m. If the B^m are known, we may integrate these equations to obtain

$$\begin{aligned} I^m(\tau,\mu,\mu_0) &= \int_0^{\tau} \frac{d\tau'}{\mu} B^m(\tau',\mu,\mu_0)\, e^{-(\tau-\tau')/\mu} \qquad \mu > 0 \\ I^m(\tau,\mu,\mu_0) &= -\int_{\tau}^{\tau_0} \frac{d\tau'}{\mu} B^m(\tau',\mu,\mu_0)\, e^{-(\tau-\tau')/\mu} \qquad \mu < 0 \end{aligned} \tag{81}$$

The radiation field is thus determined if we can find the $B^m(\tau,\mu,\mu_0)$.

If the internal radiation field is desired, we may set

$$B^m(\tau,\mu,\mu_0) = \sum_{i=m}^{N} c_m^i \, P_i^m(\mu) \, B_i^m(\tau,\mu_0) \quad . \tag{82}$$

The B_i^m are in turn determined from an integral equation whose solution may be expressed in terms of functions $H^m(\mu)$ if the atmosphere is semi-infinite, or $X^m(\mu)$ and $Y^m(\mu)$ if the atmosphere is finite. For details, see Sobolev (1972).

We shall limit the further discussion to the radiation emerging from the atmosphere.

A. Semi-Infinite Atmospheres

The reflection function $R(\mu,\mu_0,\phi) = I(\tau = 0, -\mu, \mu_0, \phi)/F$ in this case may be expanded in the corresponding azimuthal series as

$$R(\mu,\mu_0,\phi) = R^0(\mu,\mu_0) + 2 \sum_{m=1}^{N} R^m(\mu,\mu_0) \cos m\phi \quad . \quad \mu > 0 \tag{83}$$

Each azimuthal component may be expressed in terms of auxiliary functions $\phi_i^m(\mu)$ as

$$R^m(\mu,\mu_0) = \frac{\tilde{\omega}_0}{4} \sum_{i=m}^{N} c_m^i (-1)^{i+m} \frac{\phi_i^m(\mu)\, \phi_i^m(\mu_0)}{\mu + \mu_0} \tag{83a}$$

Each $\phi_i^m(\mu)$ may in turn be expressed by means of an H-function H^m:

$$\phi_i^m(\mu) = q_i^m(\mu)\, P_m^m(\mu)\, H^m(\mu) \tag{84}$$

where the q_i^m are polynomials which must be determined by solving a system of linear algebraic equations. One form of this system is

$$q_i^m(\mu) = R_{im}{}^m(\mu) + \sum_{k=m+1}^{N} [q_k{}^m(\mu) + \frac{k+m-1}{k-m} q_{k-2}^m(\mu)] \times \int_0^1 d\mu\, H^m(\mu)\, g_{ik}^m(\mu) \tag{85}$$

where the $R_{ik}^m(\mu)$ may be found from the recurrence relation

$$(i - m+1)\, R_{i+1,k}^m(\mu) + (i + m)\, R_{i-1,k}^m(\mu) = (2i+1 - \tilde{\omega}_0\tilde{\omega}_i)\mu\, R_{ik}^m(\mu) \tag{86}$$

with $R_{kk}^m(\mu) = 1$ and $R_{ik}^m(\mu) = 0$ for $i < k$, and the g_{ik}^m are defined by

$$\begin{aligned} g_{ik}^m(\mu) &= \Psi_m^m(\mu)\, R_{ik}^m(\mu) - \Psi_k^m(\mu)\, R_{im}^m(\mu) \\ \Psi_k^m(\mu) &= \frac{\tilde{\omega}_0}{2} P_m^m(\mu) \sum_{i=k}^{N} c_i^m\, R_{ik}^m(\mu)\, P_i^m(\mu) \quad . \end{aligned} \tag{87}$$

A further discussion of the determination of these quantities is given by van de Hulst (1970c).

The appropriate H-function for the m-th azimuthal component satisfies the non-linear integral equation

$$H^m(\mu) = 1 + \mu\, H^m(\mu) \int_0^1 d\mu' \, \frac{\Psi^m(\mu')}{\mu + \mu'} H^m(\mu') \tag{88}$$

where $\Psi^m(\mu) \equiv \Psi_m^m(\mu)$ is the characteristic function for the given phase function (79). Equation (88) is usually solved numerically by iteration. Alternatively, H^m may be found from the non-linear integral equation

$$H^m(\mu)\, T^m(\mu) = 1 + \mu \int_0^1 \frac{d\mu'\, \Psi^m(\mu')\, H^m(\mu')}{\mu' - \mu} \tag{89}$$

which may be solved explicitly if the function

$$T^m(\mu) = 1 + \mu \int_{-1}^1 \frac{d\mu'\, \Psi^m(\mu')}{\mu' - \mu} \tag{90}$$

is not too perverse (cf. Mullikin, 1964, who has also examined in detail the uniqueness of solutions to (88) and (89), a question further investigated by Pahor and Kuscer, 1966).

B. Finite Atmospheres

The functions R, T, ϕ_i^m, ψ_i^m, X^m, and Y^m will all be functions of $\tilde{\omega}_0$ and τ_0, but for simplicity we shall not indicate this dependence explicitly. We then find that the reflection function can still be expressed in the series (83), while the transmission function has the corresponding expansion

$$T(\mu,\mu_0,\phi) = T^0(\mu,\mu_0) + 2 \sum_{m=1}^{N} T^m(\mu,\mu_0) \cos m\phi \quad . \tag{91}$$

The expansion components are expressed in terms of auxiliary functions by

$$\begin{aligned} R^m(\mu,\mu_0) &= \frac{\tilde{\omega}_0}{4} \sum_{i=m}^{N} c_i^m (-1)^{i+m} \, \frac{\phi_i^m(\mu)\, \phi_i^m(\mu_0) - \psi_i^m(\mu)\, \psi_i^m(\mu_0)}{\mu + \mu_0} \\ T^m(\mu,\mu_0) &= \frac{\tilde{\omega}_0}{4} \sum_{i=m}^{N} c_i^m \, \frac{\phi_i^m(\mu_0)\, \psi_i^m(\mu) - \phi_i^m(\mu)\, \psi_i^m(\mu_0)}{\mu - \mu_0} \end{aligned} \tag{92}$$

where the auxiliary functions may be expressed in terms of X- and Y-functions:

$$\phi_i^m(\mu) = [X^m(\mu)\, r_i^m(\mu) + (-1)^{i+m}\, Y^m(\mu)\, s_i^m(-\mu)]\, P_m^m(\mu)$$

$$\psi_i^m(\mu) = [X^m(\mu)\, s_i^m(\mu) + (-1)^{i+m}\, Y^m(\mu)\, r_i^m(-\mu)]\, P_m^m(\mu) \quad . \tag{93}$$

The $r_i^m(\mu)$ and $s_i^m(\mu)$ are polynomials to be determined from an appropriate set of linear algebraic equations similar to (85) (Sobolev, 1972).

The X^m and Y^m are determined either from non-linear equations of the form studied by Chandrasekhar (1950) and Busbridge (1960):

$$X^m(\mu) = 1 + \mu \int_0^1 d\mu' \, \frac{\Psi^m(\mu')}{\mu + \mu'} \, [X^m(\mu')\, X^m(\mu) - Y^m(\mu)\, Y^m(\mu')]$$

$$Y^m(\mu) = e^{-\tau_0/\mu} + \mu \int_0^1 d\mu' \, \frac{\Psi^m(\mu')}{\mu - \mu'} \, [Y^m(\mu)\, X^m(\mu') - Y^m(\mu')\, X^m(\mu)] \tag{94}$$

or from linear singular equations (cf. Leonard and Mullikin, 1964; Carlstedt and Mullikin, 1966). In each case, appropriate constraints are necessary.

7. FURTHER COMPLEXITY

The theoretical models which form the basis for the methods and results described in the last three sections are sometimes too simplified to elucidate actual physical situations. We shall now comment briefly on the extension of the theory into more complex situations.

A. Horizontal Inhomogeneity

Anyone who has flown above a cloud deck must have observed the striking departures from the idealized plane-parallel state which frequently occur. Humps and troughs, towers and valleys, rifts and gaps are present. What will their effect be on the angular distribution of reflected intensity? On the strength of absorption lines as a function of position on a planetary disk? On the polarization? These questions have hardly been posed, let alone answered.

The only approach for planetary atmospheres used heretofore in this situation seems to be the Monte Carlo method. The results suggest that the presence of deep towers and troughs, such as might be expected for cumulus clouds on Earth and perhaps on a planet with violent convective regions such as Jupiter (cf. Squires, 1957), can profoundly influence the form of the radiation field emerging from the atmosphere. The difference from the plane-parallel case is particularly marked when absorption is present ($\tilde{\omega}_0 < 1$; cf. Van Blerkom, 1971). In addition, the presence of horizontal striations will of course introduce an azimuthal dependence in the radiation field, even if the phase function is isotropic.

Figure 9 has been kindly supplied by Appleby (private communication) and shows the center to limb variation of the equivalent width for a weak line observed in a planetary spectrum at opposition. A simple square line shape was used, and a square wave cloud profile with maxima (and minima) running normal to the scan direction has been assumed. The resulting curves are qualitatively similar to those obtained by Hunt (1971) for a vertically inhomogeneous atmosphere, and show the possible pitfalls of interpreting observational data with an oversimplified model (even though Hunt's models are themselves the most sophisticated yet applied to the Jovian atmosphere!).

In my opinion, investigation of this problem should have a top priority within present multiple scattering theory.

B. Shadowing and Surface Reflection

If the constituent scatterers making up a particulate medium are sufficiently close together that the wavelength

$$\lambda \ll \rho^2/\Delta \quad , \tag{95}$$

where ρ is the particle radius and Δ is the mean free photon path (or the slant thickness of the layer, if that is smaller), they will cast shadows on each other (see the last paragraph of Section 3). If such a medium is viewed from the direction of incident radiation (scattering angle $\gamma = \pi$), no shadows can be seen. This phenomenon can be observed around an airplane shadow when flying over a rough ground, around one's own shadow cast upon dewy grass, apparently also in the "opposition effect" or anomalous brightening at small phase angles observed for a number of astronomical objects (including the Moon, Mars, Saturn's rings, and certain asteroids), and also for powdered surfaces in the laboratory (Oetking, 1966). Analysis of the effect may be viewed as part of another largely untouched theoretical problem, the nature of the reflection from natural surfaces.

If the "surface particles" may be taken to be randomly distributed in three dimensions, the problem may be reduced to the computation of a correction to the usual multiple scattering theory, at least in so far as diffraction of light into the shadow behind each particle may be neglected (Irvine, 1966). The environment within Saturn's rings probably approximates such random conditions, but the necessity for particle support in the vertical direction means that it cannot strictly apply to a surface. Nonetheless, Veverka (1970; and private communication) has obtained good agreement with the observed reflectivity of the Moon and of powdered surfaces using the Irvine (1966) procedure.

Further comparison of theory and experiment is clearly needed. The case of partially transparent particles $(1 - \tilde{\omega}_0 \ll 1)$ is particularly important. In this case, multiple scattering will predominate and it is important to determine if the opposition peak will be washed out. There is as yet insufficient laboratory data available for comparison with theory. Both observational and theoretical investigations of additional types of surface are of fundamental importance in many radiation problems, including the reflection from planetary atmospheres adjoining such surfaces. It is interesting in this regard that even small objects in the solar system seem to have a low density regolith (e.g., Phobos and Deimos).

C. Computation of Spectra

Absorption spectra formed by diffuse reflection or transmission of solar radiation through a partially absorbing planetary atmospheres call for special attention. Both the line shape

$$r_\nu = \frac{I_\nu}{I_c} \tag{96}$$

and the equivalent width

$$W = \int d\nu \, (1 - r_\nu) \tag{97}$$

are of interest, where I_c is the intensity in the continuous spectrum adjacent to the line and I_ν is the intensity in the line.

To obtain a precision comparable with that obtainable by modern observational procedures, a theoretician must evaluate I_ν at a large number of frequencies within the absorption band. At any given frequency, if the assumptions referred to in Section 3 in this connection are valid, any of the methods described in Sections 4-6 may be used. The requirement of multiple calculations may, however, change the computing economics involved in choosing the optimum procedure.

It is possible, provided $p(\cos \gamma)$ is independent of frequency within the limited frequency range of the absorption feature and that the atmosphere is homogeneous, to reduce this problem to the solution of a single transfer problem in the continuum plus the performance of a quadrature or sum. This procedure requires a knowledge of either the probability distribution of photon path lengths travelled by the reflected light (Appleby and Irvine, 1973; Kargin, Krasnokutskya, and Feigel'son, 1972) or the intensity corresponding to successive orders of scattering (Uesugi, Irvine, and Kawata, 1971). Both these procedures also provide some physical insight into the nature of the line formation process. Results at present are limited to homogeneous atmospheres, but with this restriction the method looks promising. Because of the smoothing character of the integration process which specifies the intensity, it would seem that great accuracy is not needed in the determination of the probability distribution, and approximate or numerical results have been obtained by van de Hulst (this Symposium) and Romanova (1965) as well as by the authors cited previously.

The alternative approach, through successive scattering, is limited at present to homogeneous, semi-infinite atmospheres. The procedure is straightforward, and the asymptotic theory developed by van de Hulst (1970) may simplify the computations.

D. Polarization

Strictly speaking, all multiple scattering problems should be solved taking polarization into account, since the electromagnetic field is a vector field. The approach to such problems is conceptually quite simple; it consists of replacing the scalar equation of transfer (74) by a vector equation of exactly the same form except that $I \to \underline{I}$, a vector whose four components are the Stokes parameters, and $p \to \underline{p}$, the phase matrix which specifies the polarization produced in a single act of scattering and whose sixteen components generally satisfy a number of equalities.

Precise numerical methods such as the adding method may be generalized to include polarization, and the results indicate that if only the total intensity (or flux) is desired, computations made with scalar equations will normally be accurate to a few per cent. Computation of the polarization, of

course, requires use of the vector equations. We shall not discuss this question further, but refer the reader to the recent review by Coffeen and Hansen (1973: cf. also Hansen, 1971).

Analytical work on the polarization of multiply scattered light for anisotropic phase functions is largely absent (cf., however, the symmetry relations discussed by Hovenier, 1969). This is another field where further research is very desirable. Considerable insight into both computational methods and physical results has been gained from the extensive work of Hansen and Herman (cf. Coffeen and Hansen, 1973; Herman et al., 1970).

ACKNOWLEDGEMENTS

We are very grateful to the members of the ad hoc Committee on "Standard Procedures to Compute Atmospheric Radiative Transfer in a Scattering Atmosphere" of the Radiation Commission of the I.A.M.A.P. for their contributions to the report of that Committee, upon which we have drawn in writing this review. Our particular thanks go to H. C. van de Hulst, D. Van Blerkom, J. F. Appleby, Y. Kawata, and A. P. Lane for supplying us with materials for computations; and to a large number of authors who have answered our request for reprints of their recent work. This research was supported in part by NASA Grant NGL 22-010-023 and NSF Grant GP 22742.

REFERENCES

1. V. A. Ambartsumyan, 1943: Dokl. Akad. Nauk. USSR 38, 257.

1a. J. F. Appleby and W. M. Irvine, 1973: "Path Length Distributions of Photons Diffusely Reflected from a Semi-Infinite Atmosphere," Ap. J. 183, 337.

2. J. K. Beasley, J. T. Apkins, and F. W. Billmeyer, 1967: "Scattering and Absorption of Light in Turbid Media," in Electromagnetic Scattering, ed. R. L. Rowell and R. S. Stein, Gordon and Breach Pub.

3. R. E. Bellman, 1969: "Invariant Imbedding and Computational Methods in Radiative Transfer," in Transport Theory, American Mathematical Society, Providence, RI.

4. R. E. Bellman, R. Kalaba, and S. Ueno, 1963: "Invariant Imbedding and Diffuse Reflection from a Two-Dimensional Flat Layer," Icarus 1, No. 4.

5. R. E. Bellman, R. Kalaba, and M. C. Prestrud, 1963: Invariant Imbedding and Radiative Transfer in Slabs of Finite Thickness, American Elsevier Pub. Co., New York.

6. R. E. Bellman, H. Kagiwada, R. Kalaba, and S. Ueno, 1965: "Inverse Problems in Radiative Transfer: Layered Media," Icarus 4, 119.

7. M. J. S. Belton, M. B. McElroy, and M. J. Price, 1971: "The Atmosphere of Uranus," A.J. 164, 191.

8. M. S. Bobrov, 1970: "Physical Properties of Saturn's Rings," Solar System Research 4, 127.

9. I. W. Busbridge, 1960: The Mathematics of Radiative Transfer, Cambridge University Press.

10. J. L. Carlstedt and T. W. Mullikin, 1966: "Chandrasekhar's X and Y Functions," Ap. J. Suppl. 12, No. 113.

11. K. M. Case and P. F. Zweifel, 1967: Linear Transport Theory, Addison-Wesley Pub. Co., Reading, MA.

12. J. L. Castie, R. Kalaba, and S. Ueno, 1969: "Reflection and Transmission Functions for Finite Isotropically Scattering Atmospheres with Specular Reflectors," J. Quant. Spect. Rad. Trans. 9, 537.

13. J. W. Chamberlain and M. D. McElroy, 1966: "Diffuse Reflection by an Inhomogeneous Planetary Atmosphere," Ap. J. 144, 1148.

14. S. Chandrasekhar, 1950: Radiative Transfer, Oxford University Press.

15. S. Chandrasekhar, 1958: "On the Diffuse Reflection of a Pencil of Radiation by a Plane-Parallel Atmosphere," Proc. Nat. Acad. Sci. USA 44, 933.

16. D. L. Coffeen and J. E. Hansen, 1973: "Polarization Studies of Planetary Atmospheres," in Planets, Stars and Nebulae with Photopolarimetry, ed. T. Gehrels, University of Arizona Press.

17. R. E. Danielson, D. R. Moore, and H. C. van de Hulst, 1969: J. Atmos. Sci. 26, 1078.

18. J. V. Dave and J. Gazdag, 1970: "A Modified Fourier Transform Method for Multiple Scattering Calculations in a Plane-Parallel Mie Atmosphere," Appl. Optics 9, 1457.

19. B. Davison, 1957: Neutron Transport Theory, Oxford University Press.

20. D. Deirmendjian, 1969: Electromagnetic Scattering on Spherical Polydispersions, American Elsevier Pub. Co., New York.

21. C. Devaux and M. Herman, 1971: C. R. Acad. Sc. Paris 273, 849.

22. Y. Fouquart, 1971: "Effects of Scattering on the Heating Rates Due to Absorption of Solar Radiation," J. Quant. Spect. Rad. Trans. 11, 709.

23. A. L. Fymat and K. D. Abhyankar, 1969: "Theory of Radiative Transfer in Inhomogeneous Atmospheres. I. Perturbation Method," Ap. J. 158, 315.

24. A. L. Fymat and K. D. Abhankar, 1970: "Theory of Radiative Transfer in Inhomogeneous Atmospheres. IV. Application of the Matrix Perturbation Method to a Semi-Infinite Atmosphere," Ap. J. 159, 1019.

25. A. L. Fymat and R. E. Kalaba, 1973: "On Horak's and Sobolev's Interpretations of the Visual Phase Curve," Ap. J., in press.

25a. I. P. Grant and G. E. Hunt, 1969: Proc. Roy. Soc. A313, 183.

26. J. M. Greenberg, 1968: in Interstellar Grains in Nebulae and Interstellar Matter, ed. B. M. Middlehurst and L. Aller, University of Chicago Press.

27. J. E. Hansen, 1969: "Exact and Approximate Solutions for Multiple Scattering by Cloudy and Hazy Planetary Atmospheres," J. Atmos. Sci. 26, 478.

28. J. E. Hansen, 1969: "Radiative Transfer by Doubling Very Thin Layers," Ap. J. 155, 565.

29. J. E. Hansen, 1969: "Absorption Line Formation in a Scattering Planetary Atmosphere: A Test of van de Hulst's Similarity Relations," Ap. J. 158, 337.

30. J. E. Hansen, 1971: "Multiple Scattering of Polarized Light in Planetary Atmospheres: II. Sunlight Reflected by Terrestrial Water Clouds," J. Atmos. Sci. 28, 1400.

31. J. E. Hansen and A. Arking, 1971: "Clouds of Venus: Evidence for Their Nature," Science 171, 669.

31a. B. M. Herman and D. N. Yarger, 1969: "Estimating the Vertical Atmospheric Ozone Distribution by Inverting the Radiative Transfer Equation for Pure Molecular Scattering," J. Atmos. Sci. 26, 153.

32. B. M. Herman and S. R. Browning, 1965: "A Numerical Solution of the Equation of Radiative Transfer," J. Atmos. Sci. 22, 559.

32a. B. M. Herman, S. R. Browning, and R. J. Curran, 1970: "The Effect of Atmospheric Aerosols on Scattered Sunlight," J. Atmos. Sci. 28, 419.

32b. G. E. Hunt, 1973: "Formation of Spectral Lines in Planetary Atmosphere IV. Theoretical Evidence for Structure of the Jovian Clouds from Spectroscopic Observations of Methane and Hydrogen Quadrupole Lines," Icarus 18, 637.

33. G. E. Hunt, 1971: "A Review of Computational Techniques for Analyzing the Transfer of Radiation through a Model Cloudy Atmosphere," J. Quant. Spect. of Rad. Trans. 11, 655.

34. G. E. Hunt and I. P. Grant, 1969: "Discrete Space Theory of Radiative Transfer and Its Application to Problems in Radiative Transfer," J. Atmos. Sci. 26, 963.

35. W. M. Irvine, 1964: "The Formation of Absorption Bands and the Distribution of Photon Optical Paths in a Scattering Atmosphere," Bull. Astron. Inst. Netherlands 17, 266.

36. W. M. Irvine, 1965: "Light Scattering by Spherical Particles: Radiation Pressure, Asymmetry Factor and Extinction Cross Section," J. Opt. Soc. Amer. 55, 16.

37. W. M. Irvine, 1966: "The Shadowing Effects in Diffuse Reflection," J. Geophys. Res. 71, 2931.

38. W. M. Irvine, 1968: "Multiple Scattering by Large Particles. II. Optically Thick Layers," Ap. J. 152, 823.

39. W. M. Irvine, 1968: "Diffuse Reflection and Transmission by Cloud and Dust Layers," J. Quant. Spect. Rad. Trans. 8, 71.

40. M. Kanal, 1973: "Multiple Scattering Theory of Radiative Transfer in Inhomogeneous Atmospheres," J. Math. Phys. 14, 888.

41. B. A. Kargin, L. D. Krasnokutskaya, and E. M. Feigel'son, 1972: "Reflection and Absorption of Solar Energy in Cloud Layers," Fiz. Atmosfer. Okean. 8, 505.

42. G. W. Kattawar and G. N. Plass, 1968: "Radiance and Polarization of Multiple Scattered Light from Haze and Clouds," Appl. Optics 7, 1519.

43. G. W. Kattawar, G. N. Plass, and F. E. Ketchings, 1973: "Matrix Operator Theory of Radiative Transfer Theory. II: Scattering from Maritime Haze," Appl. Optics 12, 1071.

44. Y. Kawata and W. M. Irvine, 1970: "The Eddington Approximation for Planetary Atmospheres," Ap. J. 160, 787.

45. G. P. Kuiper, 1947: The Atmospheres of the Earth and Planets, University of Chicago Press.

46. I. Kuščer, 1958: "Diffuse Reflection of Light from a Semi-Infinite Scattering Medium," J. Math. Phys. 37, 52.

47. A. Leonard and T. W. Mullikin, 1964: "Spectral Analysis of the Anisotropic Neutron Transport Kernel in Slab Geometry with Applications," J. Math. Phys. 5, 399.

48. D. R. Lyzenga, 1973: "Note on the Modified Two Stream Approximation of Sagan and Pollack," Icarus 19, 240.

49. V. S. Malkova, 1972: "Limits of Applicability of the Small Angle Approximation in Clouds," Fiz. Atmosfer. Okean. 8, 1100.

50. I. N. Minin, 1971: "Nonsteady-State Emission of a One-Dimensional Medium of Finite Optical Thickness," Sov. Astron. - A. J. 15, 260.

50a. T. W. Mullikin, 1964: "Radiative Transfer in Finite Homogeneous Atmospheres with Anisotropic Scattering. I. The Uniqueness Problem for Chandraskhar's ψ and ϕ Equations," Ap. J. 139, 1267.

51. G. O. Olaofe and S. Levine, 1967: "Electromagnetic Scattering by a Spherically Symmetric Inhomogeneous Particle," in Electromagnetic Scattering, ed. R. L. Rowell and R. F. Stein, Gordon and Breach Pub.

51a. S. Pahor and I. Kuščer, 1966: "On the Non-Uniqueness of Solutions of Chandrasekhar's S-Equation in Radiative Transfer," Ap. J. 143, 888.

52. G. N. Plass and G. W. Kattawar, 1968: "Monte Carlo Calculations of Light Scattering from Clouds," Appl. Optics 7, 415.

53. G. N. Plass, G. W. Kattawar, and F. E. Ketchings, 1973: "Matrix Operator Theory of Radiative Transfer. I: Rayleigh Scattering," Appl. Optics 12, 314.

54. R. W. Preisendorfer, 1965: Radiative Transfer on Discrete Spaces, Pergamon Press, Oxford.

55. L. M. Romanova, 1969: Fiz. Atmosfer. Okean. 5, 463.

55a. L. M. Romanova, 1965: Fiz. Atmosfer. Okean. 1, 599.

56. L. M. Romanova, 1971: "Some Characteristics of the Light Field in Clouds and Fogs for a Point, Collimated, Stationary Source," Fiz. Atmosfer. Okean. 7, 1153.

57. L. M. Romanova, 1973: "Reflection and Transmission of a Narrow Pencil of Light by a Thick Layer of a Turbid Medium for Isotropic Scattering and Absorption," Fiz. Atmosfer. Okean. 9, 198.

58. G. B. Rybicki and P. D. Usher, 1966: "The Generalized Riccati Transformation as a Simple Alternative to Invariant Imbedding," Ap. J. 146, 871.

59. G. B. Rybicki, 1971: "A Seachlight Problem with Isotropic Scattering," J. Quant. Spect. Rad. Trans. 11, 827.

60. C. Sagan and J. Pollack, 1967: "Anisotropic Nonconservative Scattering in the Clouds of Venus," J. Geophys. Res. 72, 469.

61. M. T. Sandford and T. A. Pauls, 1973: "Monte Carlo Radiative Transfer Solutions for Cool Stellar Photospheres," Ap. J. 179, 875.

62. K. S. Shifrin, 1951: Light Scattering in Turbid Media, Gostekhizdat, U.S.S.R.

63. V. V. Sobolev, 1956: Transfer of Radiant Energy in the Atmospheres of Stars and Planets, Gos. Izd. Tekh. - Teor. Literatur, Moscow.

64. V. V. Sobolev, 1972: Light Scattering in Planetary Atmospheres, Izd. Nauka, Moscow.

65. V. V. Sobolev, 1973: "Scattering of Light in a Homogeneous Sphere," Astrofizika 8, No. 2.

66. P. Squires, 1957: "The Equatorial Clouds of Jupiter," Ap. J. 126, 185.

67. G. G. Stokes, 1862: Proc. Roy. Soc. 11, 545.

68. J. B. Swedlund, J. C. Kemp, and R. D. Wolstencroft, 1972: "Circular Polarization of Saturn," Ap. J. 178, 257.

68a. S. Twomey, 1963: "On the Numerical Solution of Fredholm Integral Equations of the First Kind," J. Assoc. Comp. Mach. 10, 97.

69. S. Twomey, H. Jacobowitz, and H. B. Howell, 1966: J. Atmos. Sci. 23, 289.

70. S. Ueno, 1960: "The Probabilistic Method for Problems of Radiative Transfer: X. Diffuse Reflection and Transmission in a Finite Inhomogeneous Atmosphere," Ap. J. 132, 729.

71. S. Ueno, 1973: "On the Resolvent of Milne's Integral Equation for a Spherical Isotropically Scattering Medium," J. Quant. Spect. Rad. Trans., in press.

72. A. Uesugi and W. M. Irvine, 1970: "Multiple Scattering in a Plane-Parallel Atmosphere. II. Curves of Growth for Reflection Spectra," Ap. J. 161, 243.

72a. A. Uesugi, W. M. Irvine, and Y. Kawata, 1971: "Formation of Absorption Spectra by Diffuse Reflection from a Semi-Infinite Planetary Atmosphere," J. Quant. Spec. Rad. Trans. 11, 797.

73. D. Van Blerkom, 1971: "Diffuse Reflection from Clouds with Horizontal Inhomogeneities," Ap. J. 166, 235.

74. H. C. van de Hulst, 1948: "Scattering in a Planetary Atmosphere," Ap. J. 107, 220.

75. H. C. van de Hulst, 1957: Light Scattering by Small Particles, John Wiley & Sons, New York.

76. H. C. van de Hulst and W. M. Irvine, 1962: "General Report on Radiation Transfer in Planets: Scattering in Model Planetary Atmospheres," Mem. Soc. Roy. Sci. Liege, 15th Series, Vol. 7, 78.

77. H. C. van de Hulst, 1963: "A New Look at Multiple Scattering," NASA Institute for Space Studies.

78. H. C. van de Hulst 1968: "Asymptotic Fitting, A Method for Solving Anisotropic Transfer Problems in Thick Layers," J. Comp. Phys. 3, 291.

79. H. C. van de Hulst and K. Grossman, 1968: "Multiple Light Scattering in Planetary Atmospheres," in The Atmospheres of Venus and Mars, ed. J. C. Brandt and M. B. McElroy, Gordon and Breach, Science Pub.

80. H. C. van de Hulst, 1970: "High Order Scattering in Diffuse Reflection from a Semi-Infinite Atmospheres," Astron. and Astrophys. 9, 374.

81. H. C. van de Hulst, 1970b: "The Spectrum of the Anisotropic Transfer Equation," Astron. and Astrophys. 9, 366.

82. H. C. van de Hulst, 1970c: "Reduction to H Functions in Radiative Transfer with a General Anisotropic Phase Function," Astron. and Astrophys. 9, 359.

83. H. C. van de Hulst, 1971: "Multiple Scattering in Planetary Atmospheres," J. Quant. Spect. Rad. Trans. 11, 785.

84. H. C. van de Hulst, 1971a: "Some Problems of Anisotropic Scattering in Planetary Atmospheres," in Planetary Atmospheres, ed. C. Sagan et al., D. Reidel Pub. Co., Holland.

85. J. Veverka, 1970: Thesis, Harvard University.

86. L. Wallace, 1972: "Rayleigh and Raman Scattering by H_2 in a Planetary Atmosphere," Ap. J. 176, 249.

87. G. C. Wick, 1943: Zeits. F. Physik 120, 702.

88. E. G. Yanovitskii, 1972: "The Albedo and Surface Illumination of a Planet Surrounded by a Purely Scattering Inhomogeneous Atmosphere," Fiz. Atmosfer. Okean. 8, 518.

TABLE I

I. Semi-Infinite Atmospheres (H-functions)

A. Isotropic Scattering

1. D. W. N. Stibbs and R. E. Weir (1959)
   $0 \le \tilde{\omega}_0 \le 1$; $\mu = 0(0.05)1$
   Interpolating polynomials given

B. Linearly Anisotropic ($p = \tilde{\omega}_0(1 + x \cos\theta)$)

1. Chandrasekhar (1950) paragraphs 46-47
   $\mu = 0(0.05)1$
   $\tilde{\omega}_0 = 0.1(0.1)0.9(0.025)0.975$ for $x = 1$
   $x = -1.0(0.2)1.0$ for $\tilde{\omega}_0 = 1$

2. D. L. Harris (1957)
   $\mu = 0(0.05)1$ $x = -1(0.2)1$
   $\tilde{\omega}_0 = 0.975$

3. V. V. Sobolev (1956), Tables 6 - 8
   $\mu = 0(0.1)1$ $\tilde{\omega}_0 = 0.4(0.1)1$
   $x = 1$
   More extensive tables are contained in Minin et al. (1963)

C. Rayleigh Phase Matrix

1. K. D. Abhyankar and A. L. Fymat (1971)
   $\tilde{\omega}_0 = 0(0.1)0.6(0.05)0.8(0.025)0.9(0.01)0.98(0.005)0.995(0.001)0.999$
   $\mu = 0(0.01)1$

2. J. Lenoble (1970)
   $\tilde{\omega}_0 = 0.2(0.2)0.6(0.1)0.9(0.025)0.95(0.01)0.99$
   $\mu = 0(0.05)1$

3. S. Chandrasekhar (1950), paragraph 70
   $\tilde{\omega}_0 = 1$, $\mu = 0(0.05)1$

D. Rayleigh Phase Function ($p = \frac{3\tilde{\omega}_0}{4}(1 + \cos^2\theta)$)

1. J. Lenoble (1970)
   $\tilde{\omega}_0 = 0.2(0.2)0.6(0.1)0.9, 0.925, 0.95(0.01)0.99$
   $\mu = 0(0.05)1$

2. Chandrasekhar (1950), Table 21
   $\tilde{\omega}_0 = 1$ $\mu = 0(0.05)1$

E. Other

1. A. K. Kolesov and I. O. Smotkii (1972)

$p = 1 + \Sigma\, x_i\, P_i(\mu) \qquad i = 1, \ldots, 3$

$\tilde{\omega}_0 = 1 \qquad \mu = 0(0.1)1$

selected x_i

2. V. V. Sobolev (1972), Chapter VII

$p = 1 + \Sigma\, x_i\, P_i(\mu) \qquad i = 1, \ldots, 2$

$\tilde{\omega}_0 = 1 \qquad \mu = 0(0.1)1$

$(x_1, x_2) = (1, 1)$ and $(3/2, 1)$

cf. A. K. Kolesov and V. V. Sobolev (1969) for more detailed tables

3. A. K. Kolesov (1972)

Henyey-Greenstein phase functions

4. Fymat (1971)

Rayleigh-Cabannes phase matrix (linear combination of Rayleigh and isotropic scattering)

$\tilde{\omega}_0 = 0(0.1)0.6(0.05)0.8(0.025)0.9(0.01)0.98(0.005)0.995(0.001)0.999$

$\mu = 0(0.01)1$

q = depolarization factor = 0.4(0.5)0.95

II. Finite Atmospheres (X and Y Functions)

A. Isotropic Scattering

1. J. L. Carlstedt and T. W. Mullikin (1966)

$\mu = 0(0.01)1.0 \qquad \tilde{\omega}_0 = 0.3(0.1)0.9,\ 0.95(0.01)1.0$

$\tau_0 = 0.2(0.2)3.0,\ 3.5$

asymptotic formulae for $\tau \gtrsim 3.5$

2. J. Caldwell (1971)

$\mu = 0(0.2)1 \qquad \tilde{\omega}_0 = 1$

$\tau_0 = 0.5(0.5)4.5$

3. Y. Sobouti (1963)

$\mu = 0(0.02)1.20(0.05)2(0.1)3(0.2)5(0.5)10(1)20$

$\tau_0 = 0.1(0.1)0.6(0.2)1.0(0.5)3$

$\tilde{\omega}_0 = 0.1(0.1)0.8(0.05)1$

Values for $\mu > 1$ useful for certain problems

4. R. Bellman et al. (1966)
   $\tilde{\omega}_0^2 = 0.4$ $[\tau_0 = 0(0.1)3]$
   $\tilde{\omega}_0^2 = 0.9$ $[\tau_0 = 0(0.1)6]$
   $\tilde{\omega}_0^2 = 0.975$ $[\tau_0 = 0(0.1)10]$
   $\tilde{\omega}_0^2 = 1.0$ $[\tau_0 = 0(0.1)20]$
   7 angles from Gaussian quadrature

5. D. F. Mayers (1962)
   $\mu = 0(0.025)1$
   $0.05 \leq \tau_0 \leq 10$
   $\tilde{\omega}_0^2 = 0.5, 0.8, 0.9, 0.95, 1$

B. Linearly Anisotropic
   1. ?

C. Rayleigh Phase Matrix
   1. Z. Sekera and A. B. Kahle (1966)
      $\tau_0 = 0.15, 0.25, 0.5, 0.7, 1, 2, 4, 8, 16, 100$
      $\tilde{\omega}_0^2 = 1$ $\mu = 0(0.02)1$

   2. S. Chandrasekhar and D. Elbert (1954)
      $\tau_0 = 0.05(0.05)0.25, 0.5, 1$
      $\mu = 0(0.02)1$ $\tilde{\omega}_0 = 1$

   3. K. L. Coulson, J. V. Dave, and Z. Sekera (1960)
      $\tau_0 = 0.02, 0.05, 0.10, 0.15, 0.25, 0.50, 1$
      $\tilde{\omega}_0^2 = 1$
      Intensity and polarization, but not X and Y functions

D. Rayleigh Phase Function
   1. A. V. Seigart (1970)
      $\tilde{\omega}_0^2 = 0.3(0.2)0.7(0.1)0.9, 0.95, 0.98, 0.99, 0.995, 0.999, 1$
      $\tau_0 = 0.2(0.2)1.0(0.5)3(1)5, 10, 20, \infty$
      20 Gaussian points for μ

BIBLIOGRAPHY FOR TABLE

1. K. D. Abhyankar and A. L. Fymat, 1971: "Tables of Auxiliary Functions for the Non-Conservative Rayleigh Phase Matrix in Semi-Infinite Atmospheres," Ap. J. Suppl. 23, 35.

2. R. Bellman, et al., 1966: "Numerical Results for Chandrasekhar's X and Y Functions of Radiative Transfer," J. Quant. Spect. Rad. Trans. 6, 479.

3. J. Caldwell, 1971: "The X- and Y-Functions of Chandrasekhar," Ap. J. 163, 111.

4. J. L. Carlstedt and T. W. Mullikin, 1966: "Chandrasekhar's X- and Y-Functions, Ap. J. Suppl. 12, No. 113, 449.

5. S. Chandrasekhar, 1950: Radiative Transfer, Oxford.

6. S. Chandrasekhar and D. Elbert, 1954: Trans. Amer. Phil. Soc. 44, 643.

7. K. L. Coulson, J. V. Dave, and Z. Sekera, 1960: Tables Related to Radiation Emerging from a Planetary Atmosphere with Rayleigh Scattering, Univ. of Calif. Press.

7a. A. L. Fymat, 1971: Tables of Auxiliary Functions for Polarized Anisotropic Molecular Scattering and Resonance Fluorescence Line Scattering in Semi-Infinite Atmospheres, Jet Propulsion Lab.

8. D. L. Harris, 1957: "Diffuse Reflection from Planetary Atmospheres," Ap. J. 126, 408.

9. A. K. Kolesov, 1972: "Reflection and Transmission of Light by a Semi-Infinite Atmosphere for Anisotropic Scattering," Trudy Astron. Obs. Leningrad Gos. Univ. 29.

10. A. K. Kolesov and O. I. Smoktii, 1972: "Diffuse Reflection and Transmission of Light by a Semi-Infinite Atmosphere with a Four-Term Scattering Indicatrix," Sov. Ast. - A. J. 15, 802.

11. A. K. Kolesov and V. V. Sobolev, 1969: Trudy Astron. Obs. Leningrad Gos. Univ. 26.

12. J. Lenoble, 1970: "Importance de la Polarisation dans le Rayonnement Diffuse par une Atmosphere Planetaire," J. Quant. Spect. Rad. Trans. 10, 533.

13. D. F. Mayers, 1962: "Calculation of Chandrasekhar's X- and Y-Functions for Isotropic Scattering," M. N. 123, 471.

14. Z. Sekera and A. B. Kahle, 1966: "Scattering Functions for Rayleigh Atmospheres of Arbitrary Thickness," Rand Report R-452-PR.

15. V. V. Sobolev, 1956: Perenos Luchistoi Energii v Atmosferakh Zvezd i Planet, Gos. Izd. Tekh-Teor. Lit., Moscow.

16. V. V. Sobolev, 1972: Rasseyanie Sveta v Atmosferakh Planet, Izd. "Nauka", Moscow.

17. Y. Sobouti, 1963: "Chandrasekhar's X-, Y-, and Related Functions, Ap. J. Suppl. 7, No. 72, 411.

18. D. W. N. Stibbs and R. E. Weir, 1959: "On the H-Functions for Isotropic Scattering," M. N. 119, 512.

19. A. V. Seigart, 1970: "Radiative Transfer in Atmospheres Scattering According to the Rayleigh Phase Function with Absorption," Ap. J. Suppl. 22, 1.

FIGURE CAPTIONS

FIGURE 1: Inverse diffusion length k as a function of single scattering albedo $\tilde{\omega}_0$ for a Henyey-Greenstein phase function (17) with four choices of the asymmetry factor g = <cos γ>.

FIGURE 2: Albedo of a semi-infinite atmosphere for isotropic scattering (p(cos γ) = 1) as a function of single scattering albedo $\tilde{\omega}_0$ and angle of incidence μ_0. Crosses (μ_0 = 1) from the Eddington approximation (Equation 22), curves from the exact solution (Equation 21).

FIGURE 3: Albedo of a semi-infinite atmosphere versus angle of incidence μ_0 for the phase function $p(\cos\gamma) = 1 + 1.5\cos\gamma + P_2(\cos\gamma)$, where P_2 is the Legendre polynomial of second order. Exact results (solid line) from Equation (21) compared with the Eddington approximation (open circles, Equation (22)), for three choices of single scattering albedo $\tilde{\omega}_0$.

FIGURE 4: Spherical albedo A_s of an isotropically scattering semi-infinite atmosphere as a function of single scattering albedo $\tilde{\omega}_0$.

FIGURE 5: Plane albedo A(1) versus optical thickness τ_0 for normal incidence on a homogeneous atmosphere with a single scattering albedo $\tilde{\omega}_0$. The phase function is computed from Mie scattering theory for spherical particles with an index of refraction m = 1.33 (corresponding to water droplets in the visible spectrum) and a size parameter 2 (radius)/(wavelength) = 20. The corresponding asymmetry factor g = 0.76. Approximate methods are described in the text, exact results computed from the adding method (Section 5.A). Results shown for two values of $\tilde{\omega}_0$.

FIGURE 6: Diffuse surface illumination as a function of optical thickness τ_0 for normal incidence and the same phase function as in Figure 5. Results shown for three values of the single scattering albedo $\tilde{\omega}_0$.

FIGURE 7: Escape function $u_0(\mu)$ for conservative scattering ($\tilde{\omega}_0$ = 1) with a Henyey-Greenstein phase function (Equation 17) and an asymmetry factor g= 0.75. Straight line is the approximation given by Equations (59) and (60).

FIGURE 8: Reflection function for a conservative ($\tilde{\omega}_0$ = 1) semi-infinite atmosphere with a phase function characteristic of maritime haze (phase function A, g = 0.7861, from Irvine, 1968) for normal incidence. Exact results (adding method; Section 5.A) compared with intensity obtained for a source function found using the Eddington approximation. Exact results for isotropic scattering shown for comparison.

FIGURE 9: Center to limb variation of the equivalent width W of a weak line computed for a planet at opposition. Reflecting layer model (absorbing gas overlying perfectly reflecting cloud)compared with "cumulus tower" structure as shown. R = radius of planet, r = radius vector of observed point on (plane) disk of planet.

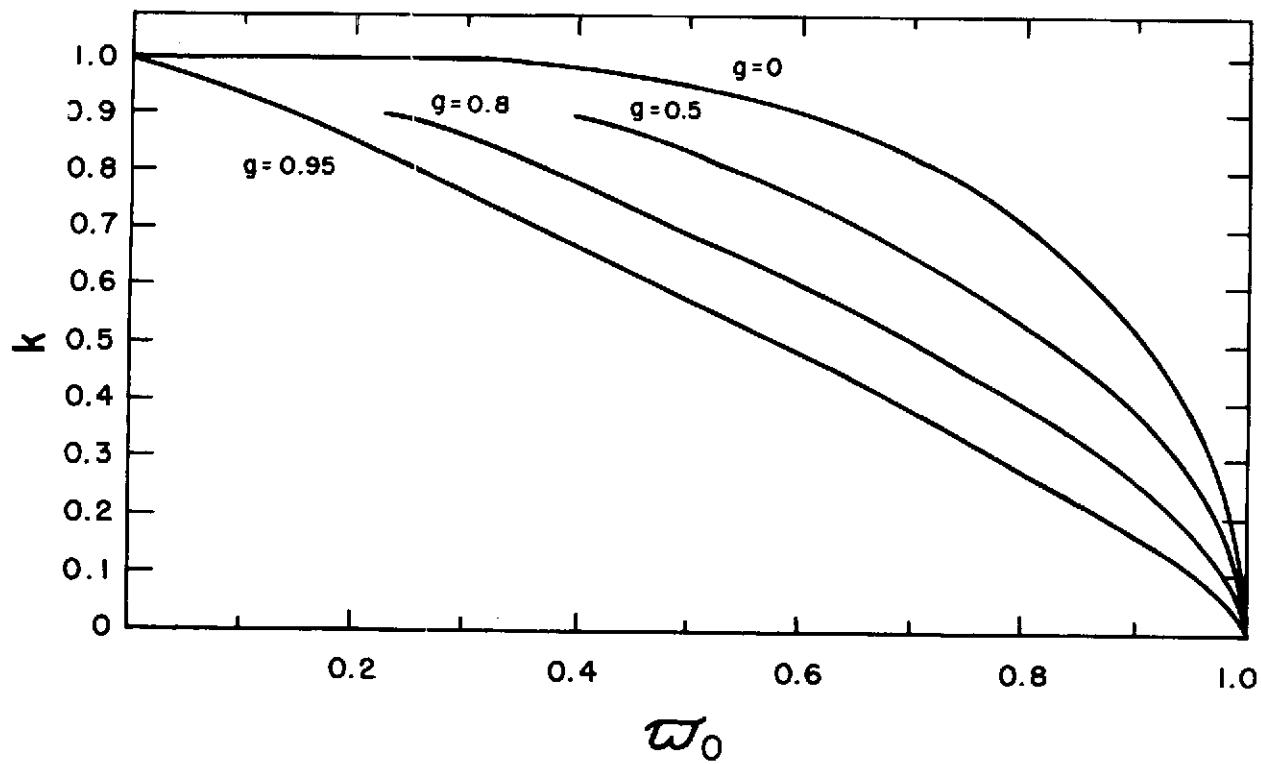
1.0
0.9
0.8
0.7
0.6
0.5
0.4
0.3
0.2
0.1
0
k
g=0
g=0.8
g=0.5
g=0.95
0.2
0.4
0.6
0.8
1.0
ϖ_0

FIGURE 1

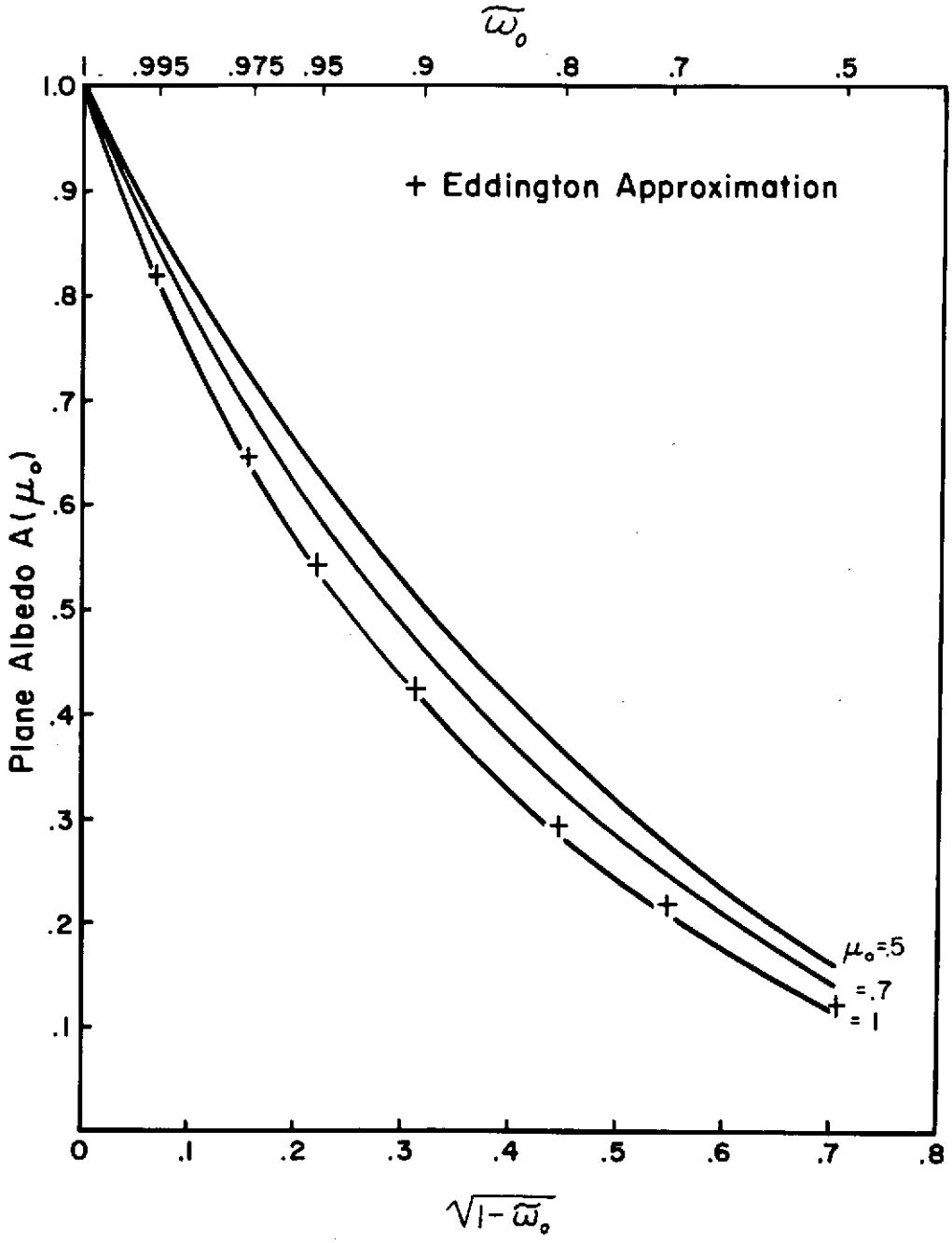
$\tilde{\omega}_o$
1
.995
.975
.95
.9
.8
.7
.5
1.0
.9
.8
.7
.6
.5
.4
.3
.2
.1
0
.1
.2
.3
.4
.5
.6
.7
.8
+ Eddington Approximation
Plane Albedo $A(\mu_o)$
μ_o=.5
=.7
=1
$\sqrt{1-\tilde{\omega}_o}$

FIGURE 2

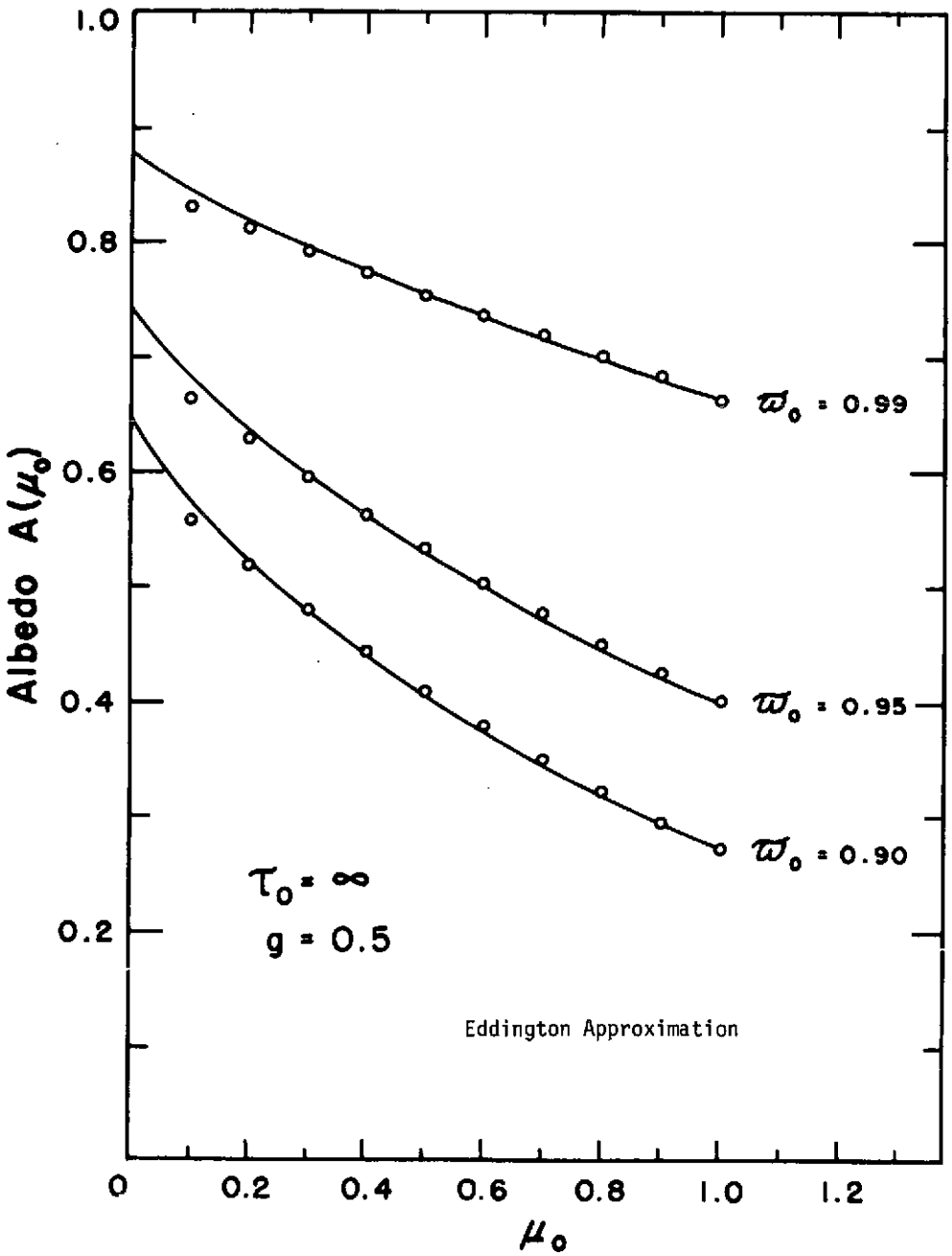
1.0
0.8
0.6
0.4
0.2
Albedo $A(\mu_0)$
$\varpi_0 = 0.99$
$\varpi_0 = 0.95$
$\varpi_0 = 0.90$
$\tau_0 = \infty$
$g = 0.5$
Eddington Approximation
0
0.2
0.4
0.6
0.8
1.0
1.2
μ_0

FIGURE 3

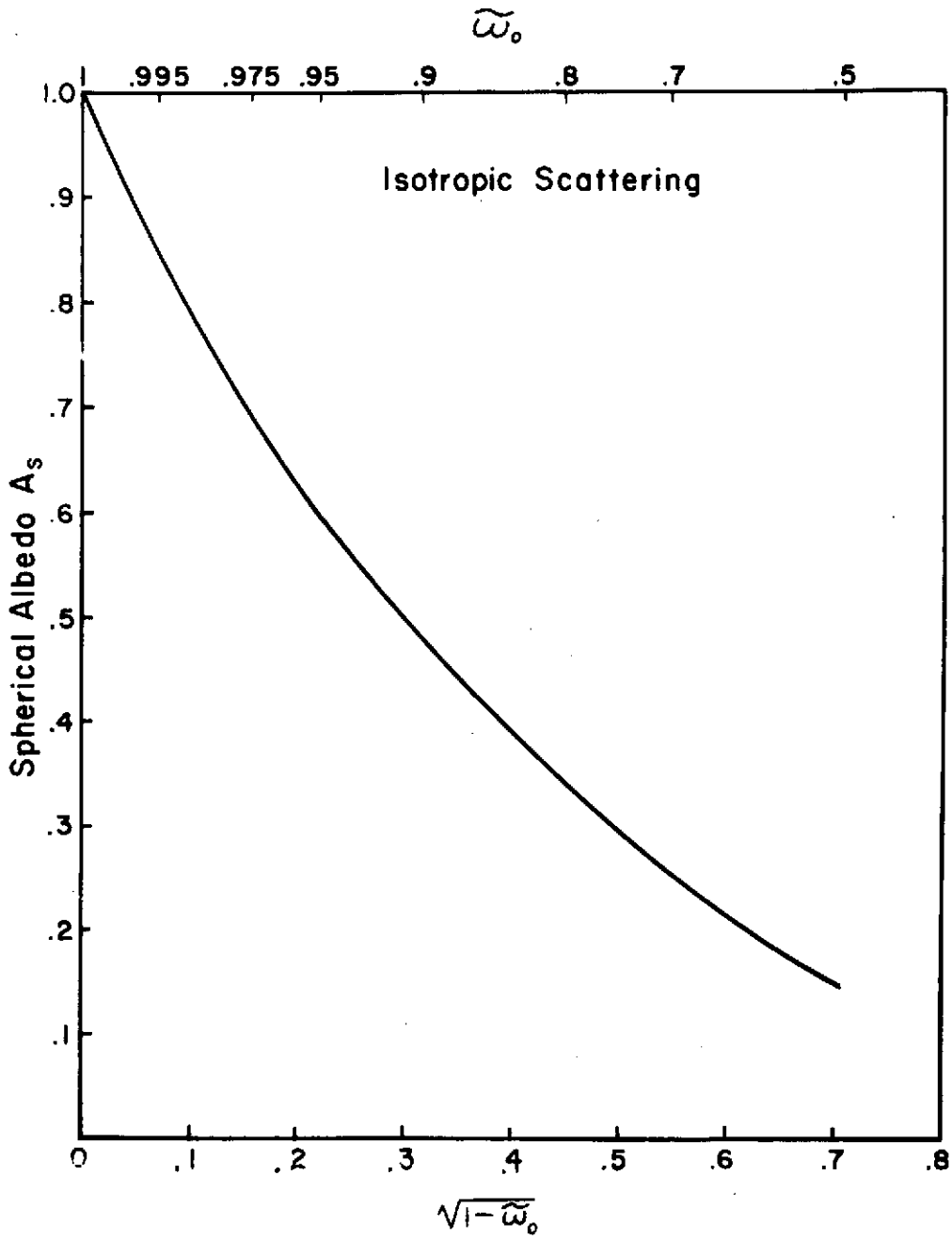
$\tilde{\omega}_o$
1
.995
.975
.95
.9
.8
.7
.5
Isotropic Scattering
Spherical Albedo A_s
1.0
.9
.8
.7
.6
.5
.4
.3
.2
.1
0
.1
.2
.3
.4
.5
.6
.7
.8
$\sqrt{1-\tilde{\omega}_o}$

FIGURE 4

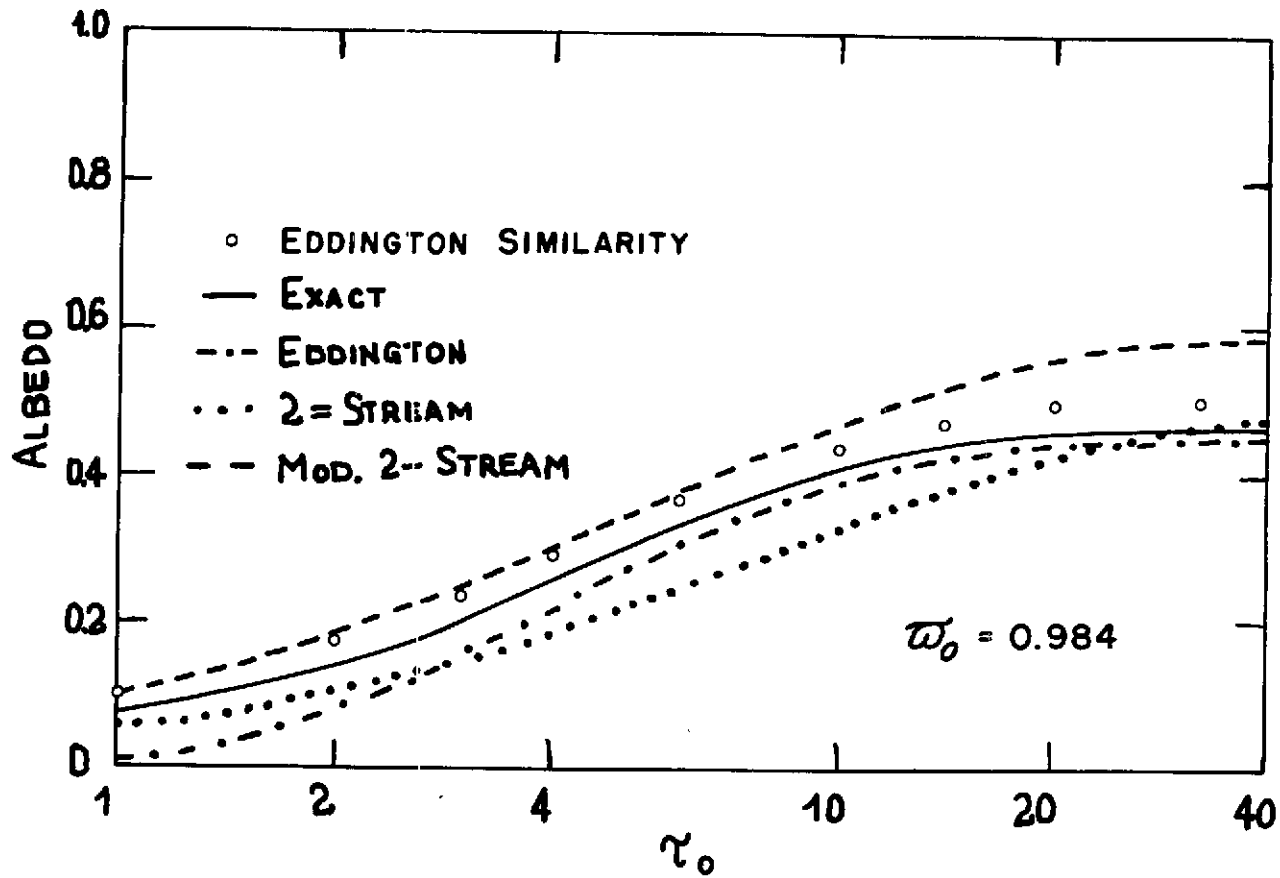
1.0
0.8
0.6
0.4
0.2
0
ALBEDO
EDDINGTON SIMILARITY
EXACT
EDDINGTON
2 = STREAM
MOD. 2-- STREAM
ϖ_o = 0.984
1
2
4
10
20
40
τ_o

FIGURE 5a

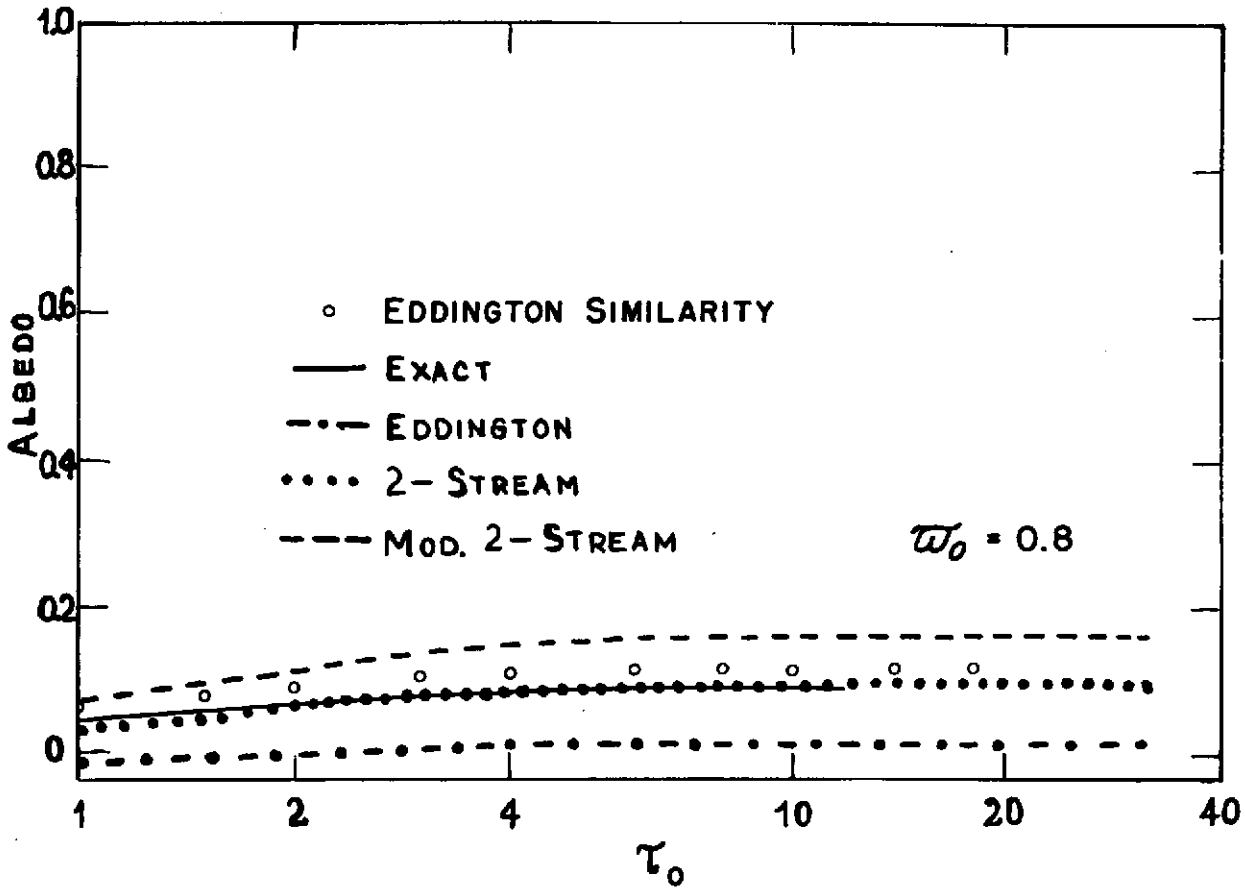
1.0
0.8
0.6
0.4
0.2
0
ALBEDO
EDDINGTON SIMILARITY
EXACT
EDDINGTON
2-STREAM
MOD. 2-STREAM
ω_0 = 0.8
1
2
4
10
20
40
τ_0

FIGURE 5b

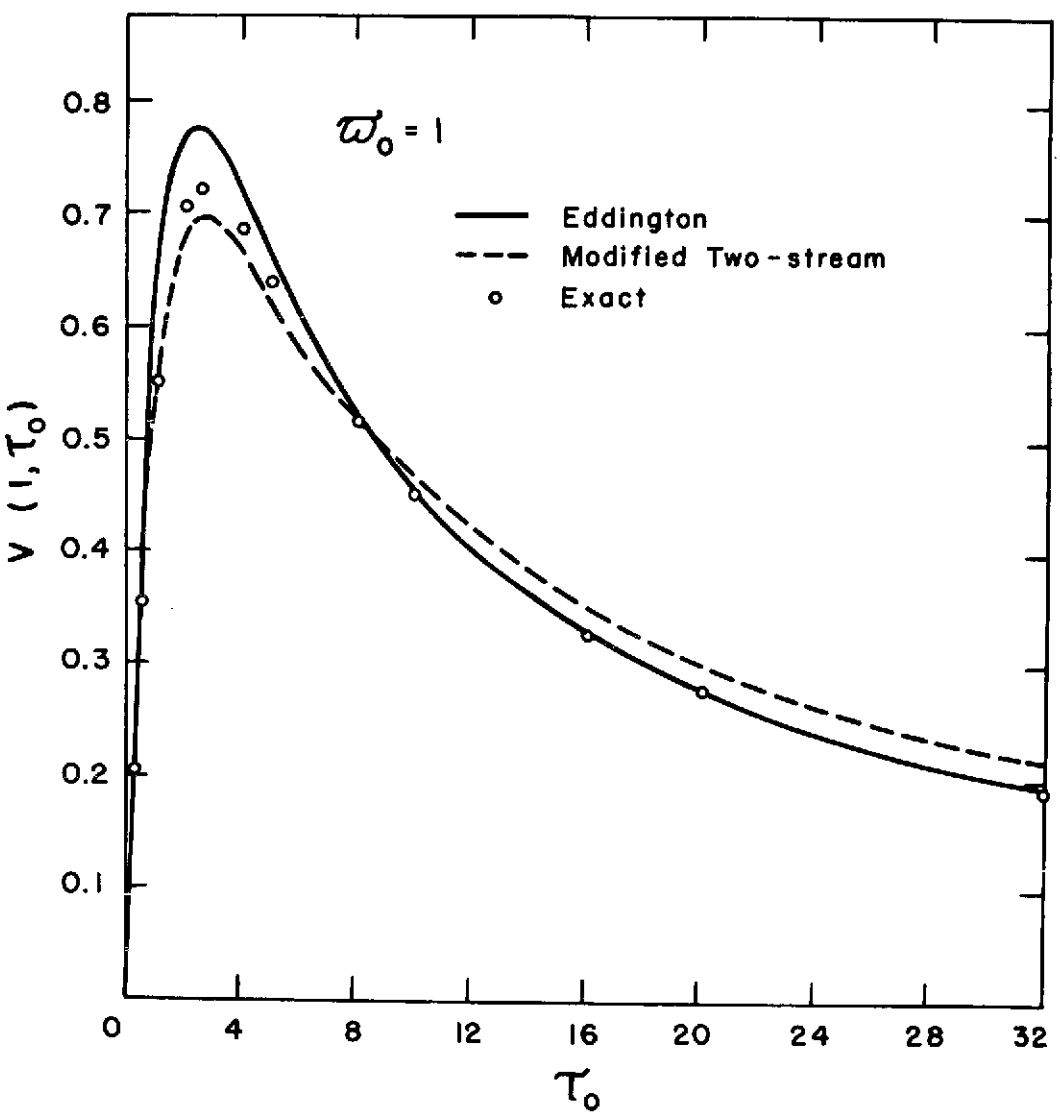
$\varpi_0 = 1$
Eddington
Modified Two-stream
Exact
$V(1,\tau_0)$
0.8
0.7
0.6
0.5
0.4
0.3
0.2
0.1
0
4
8
12
16
20
24
28
32
τ_0

FIGURE 6a

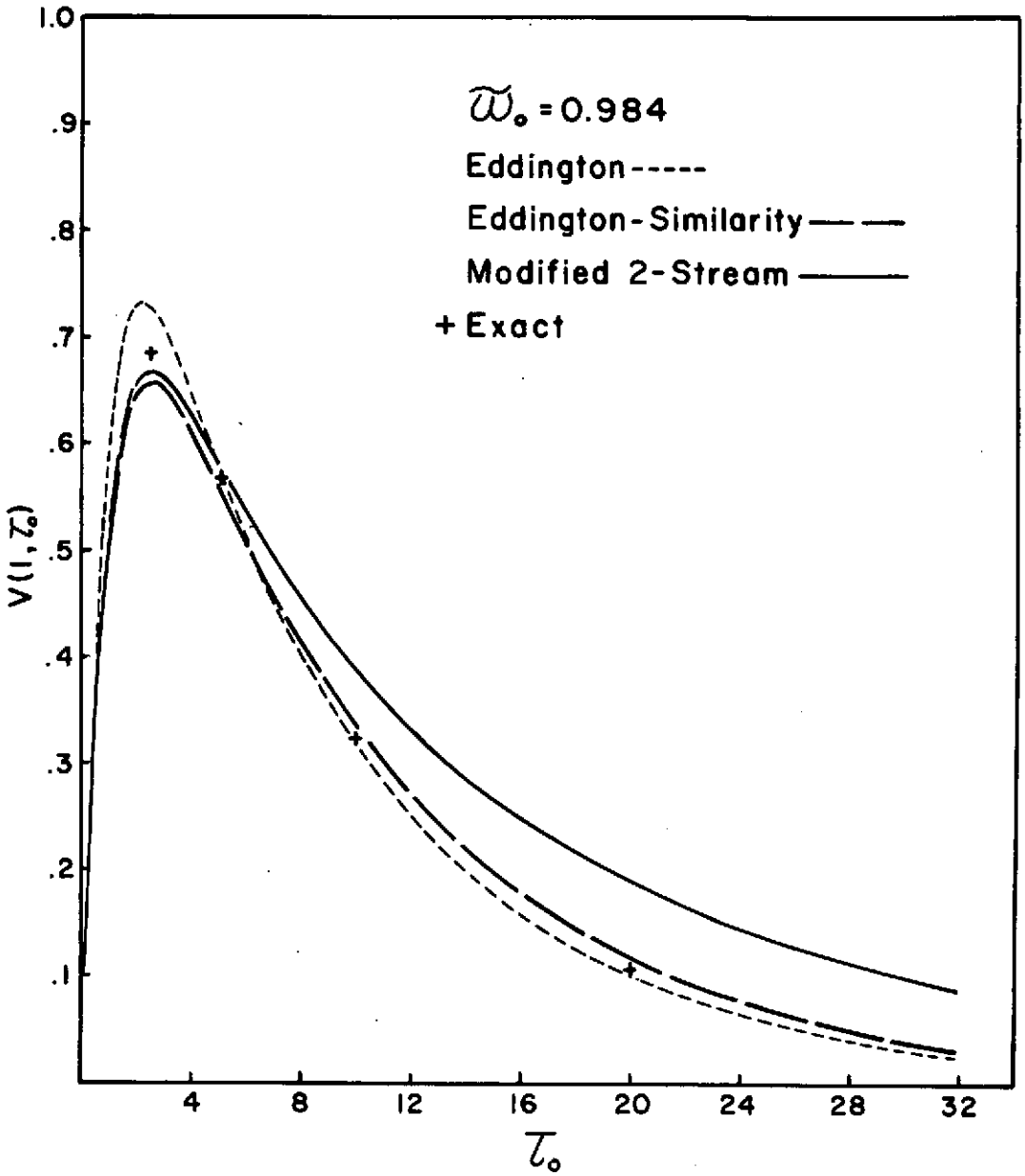
$\varpi_o = 0.984$
Eddington-----
Eddington-Similarity— —
Modified 2-Stream ———
+ Exact
V(1, τ_o)
τ_o
1.0
.9
.8
.7
.6
.5
.4
.3
.2
.1
4
8
12
16
20
24
28
32

FIGURE 6b

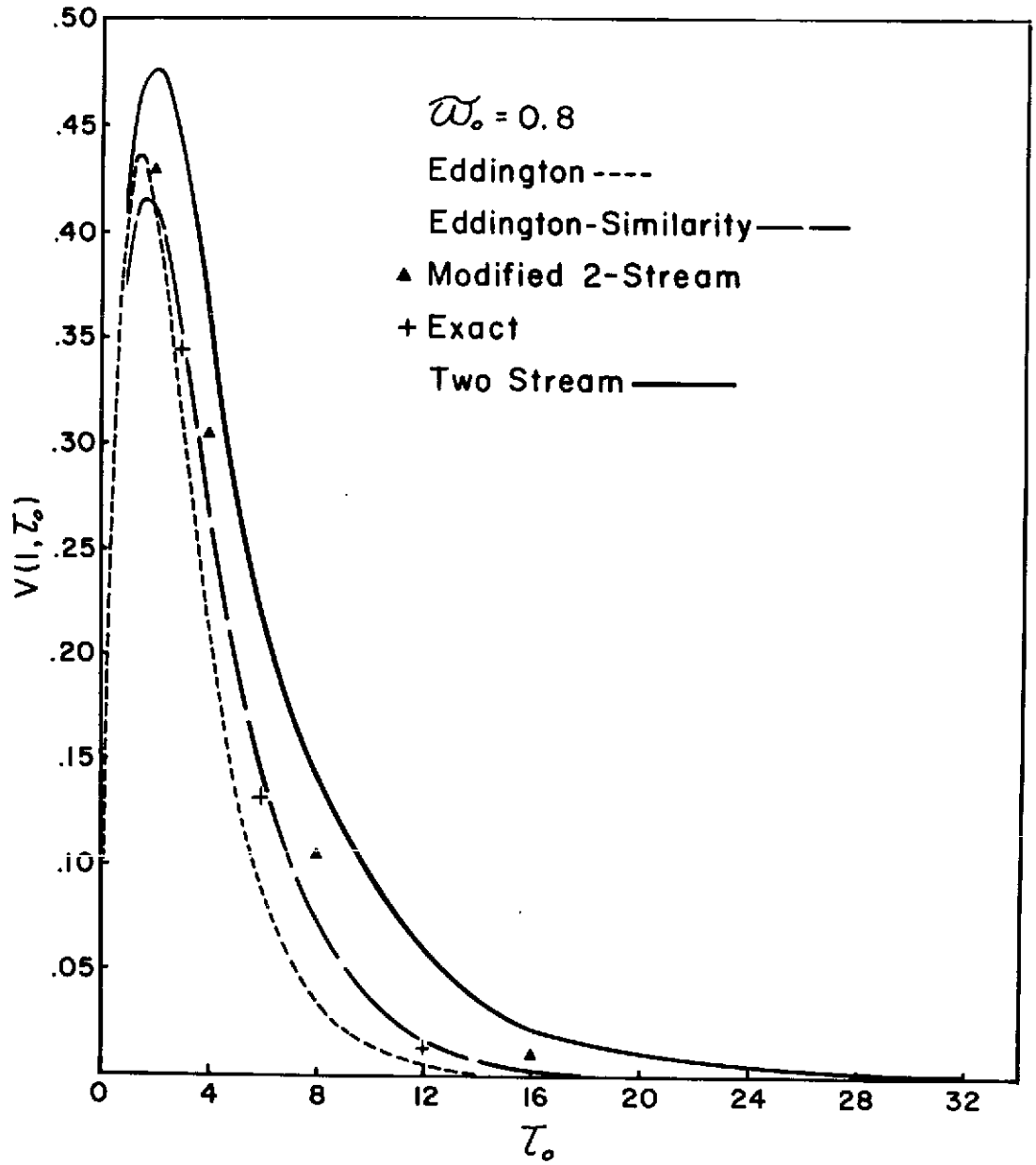
.50
.45
.40
.35
.30
.25
.20
.15
.10
.05
V(1, τ₀)
0
4
8
12
16
20
24
28
32
τ₀
ω₀ = 0.8
Eddington ----
Eddington-Similarity — —
▲ Modified 2-Stream
+ Exact
Two Stream ———

FIGURE 6c

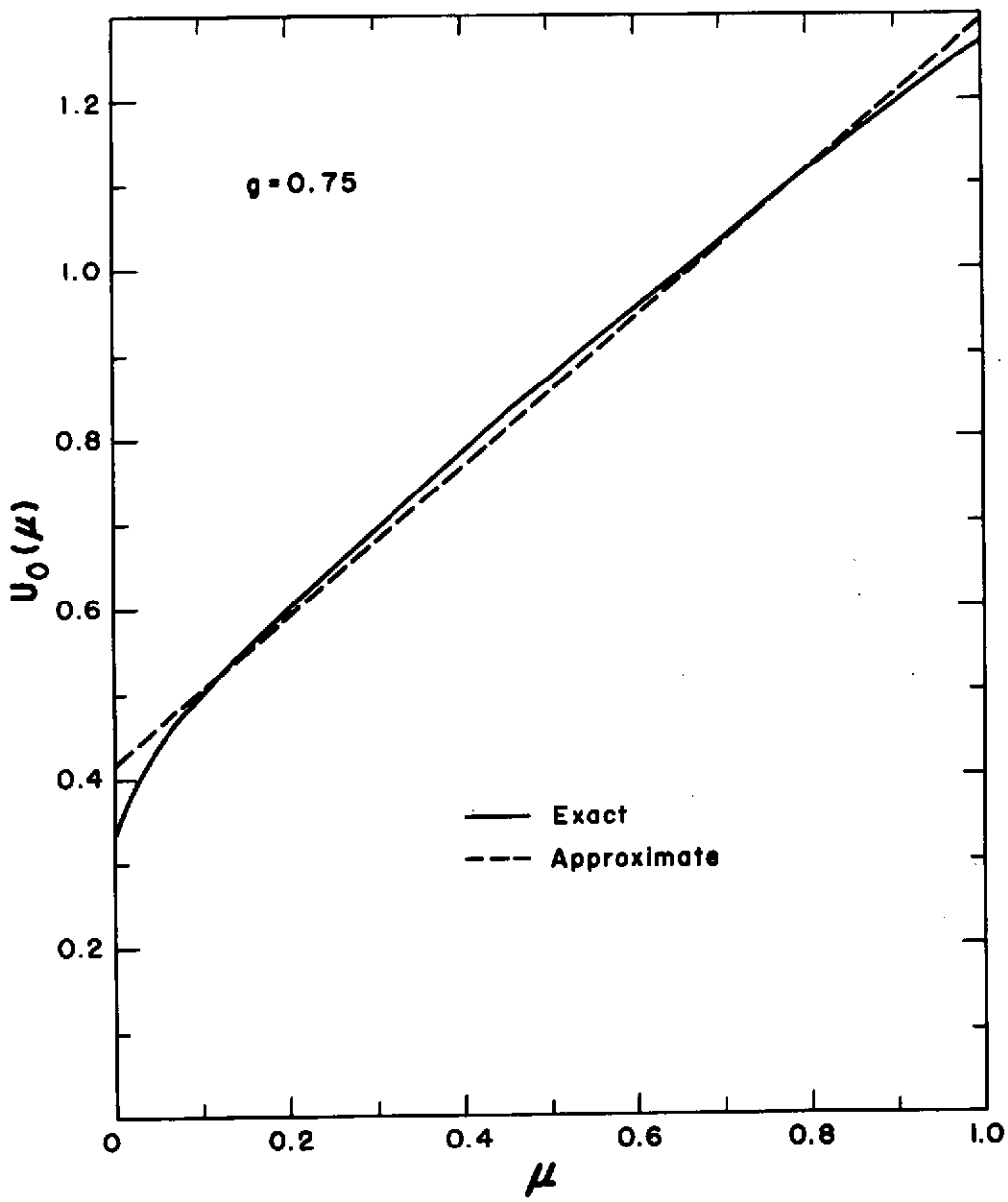

FIGURE 7

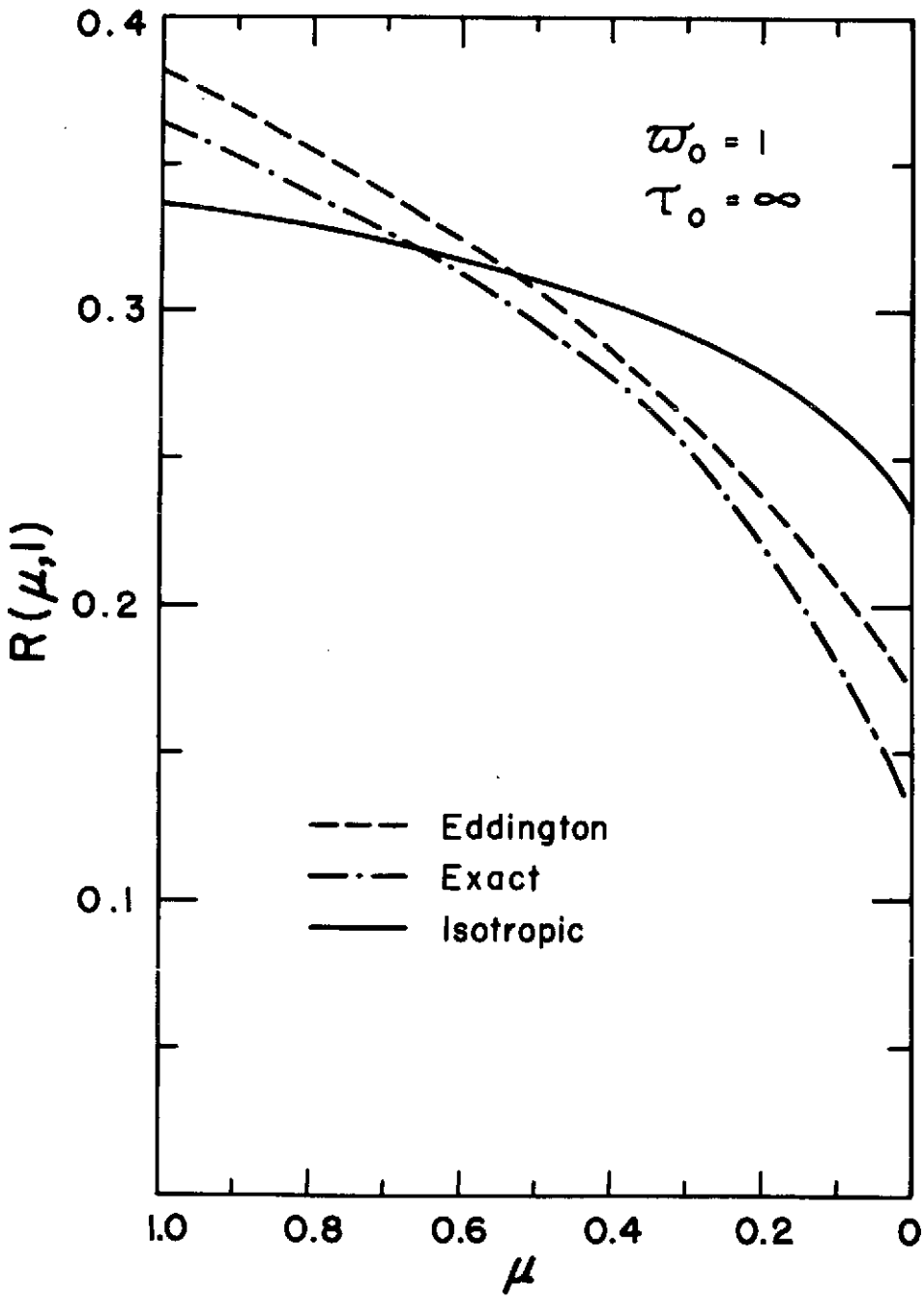
0.4
0.3
0.2
0.1
R(μ,1)
ϖ0 = 1
τ0 = ∞
Eddington
Exact
Isotropic
1.0
0.8
0.6
0.4
0.2
0
μ

FIGURE 8

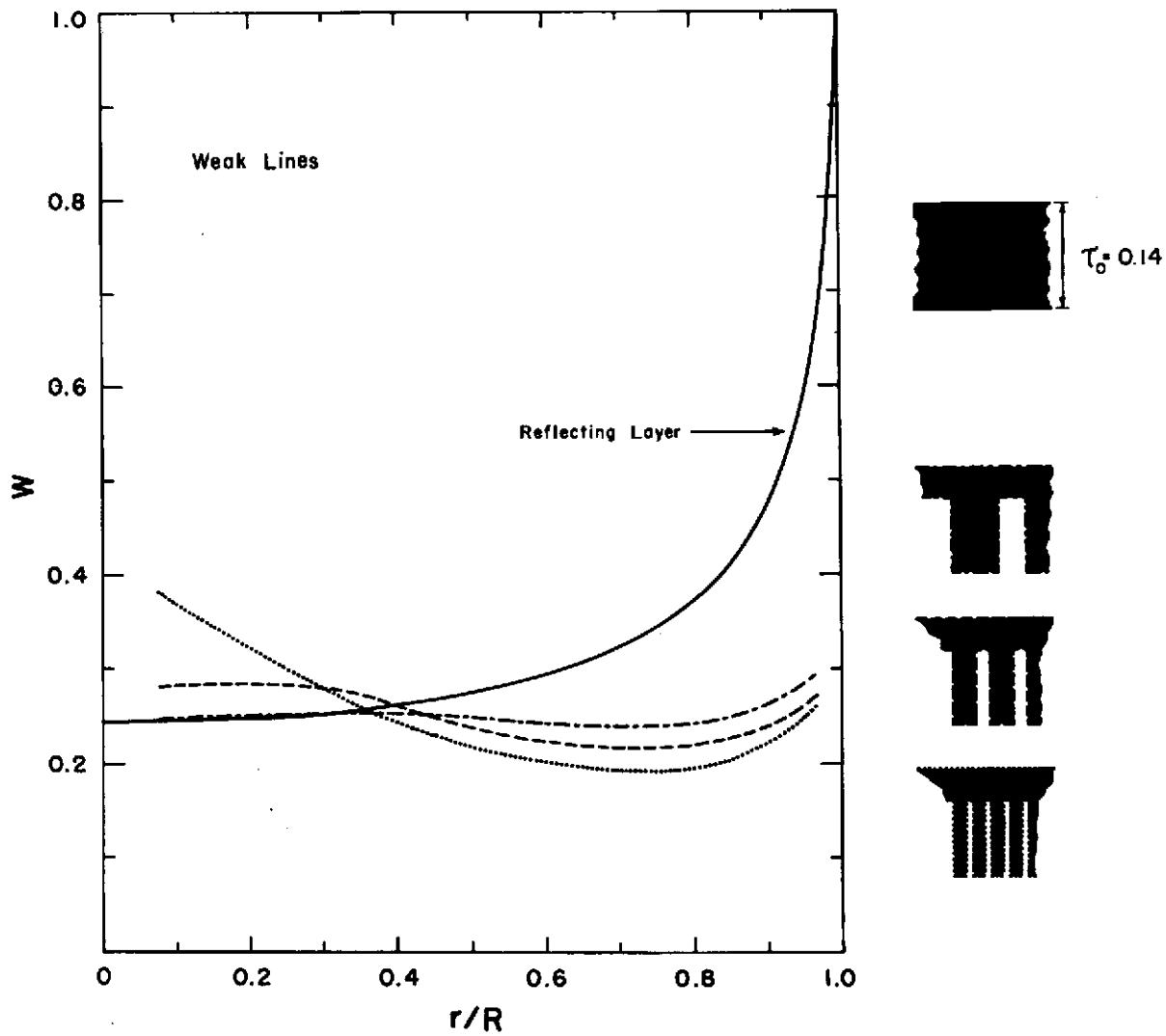
1.0
0.8
0.6
0.4
0.2
W
Weak Lines
Reflecting Layer
0
0.2
0.4
0.6
0.8
1.0
r/R
τ_0= 0.14

FIGURE 9

SOLUTION OF THE RADIATIVE TRANSFER THEORY PROBLEMS BY THE MONTE CARLO METHOD

G.I. Marchuk and G.A. Mikhailov
Computer Center, Siberian Branch
U.S.S.R. Academy of Sciences
Novosibirsk, Siberia, U.S.S.R.

There are a number of physical problems that require the exact calculation of radiative transfer that includes multiple scattering and the detailed radiative model of the medium. First there are problems of interpretation of optical observations from meteorological satellites in the short-wave part of the spectrum. In some cases it is necessary to consider the sphericity of the atmosphere, the propagation function and the polarization of the light. This problem is related to the satellite orientation problem, which demands exact calculations of the spectral brightness of the atmosphere within the horizon line. The second important class of problems deal with the theory of the spreading of narrow beams of light. As a rule in these problems it is necessary to determine such subtle characteristics of the radiation field as the time-dependence of the intensity for a localized collimating receiver with a slight divergence of the source, the perturbation of observed intensity due to insertion of some object in the medium, etc. The latter problem is connected with the development of optical location method and method for transferring information with the help of optical quantum generator.

In the approximation of ray optics as a rule such problems are described by the integral - differential transfer equation with the corresponding boundary conditions. It is practically impossible to solve this equation by means of classical methods of numerical mathematics (finite difference methods, spherical harmonics, etc.), if real indicatrixes, non-homogeneity of the medium and polarization are considered and if it is necessary to estimate local and temporal characteristics of the radiation field. When the propagation function is used for calculating the scattered radiation field in the case of non-homogeneous medium, the problem cannot be described by integral - differential equation and it must be solved by the sequential calculation of the intensity of multiply scattered light following the increase of multiplicity. In many cases this can be practically realized only by the Monte Carlo methods: the process of light diffusion can be considered as a random Markov chain of photon collisions with a substance, which lead either to scattering or to absorption of photons. The Monte Carlo method is based on the simulation of trajectories of this chain by computers and the construction of the statistical estimate of the desired functionals.

The construction of random trajectories for the physical model of the process is called direct simulation. The mathematical aspect of direct simulation is in finding the optimal methods for simulating random variables by means of a computer. As a matter of fact the direct simulation of photon trajectories does not differ from the neutron trajectories simulation or gamma-quanta, which is used for the solution of complicated problems of nuclear physics. A number of methods for decreasing the probable error of the algorithm are developed. As a rule these methods are, in effect, to carry out the simulation on the modified model and to compensate for the resulting shift by introducing special "weights" and by analytical averaging. The effectiveness of the application of different methods of reducing the variance depends to a large extent upon the specifics of the problem. As a rule the consideration of a new class of problems requires special investigation of the exactness of various combinations of the well-known algorithms and the development of new modifications. In particular work of this kind has been done for the solution of the problem of narrow beam scattering (together with Kargin and Krekov) and for radiative transfer in a spherical atmosphere (together with Nazaraliev and Darbinian). Different aspects of theory and practice of the Monte-Carlo methods as applied to light scattering theory are considered in [2-6] and [18-20].

Direct simulation of light scattering and the mathematical form of medium radiation model representation. As it has already been pointed out the radiative transfer process in the approximation of ray optics represents a homogeneous Markov chain, realizations of which are particle trajectories in phase space $X = R \times \Omega$ of coordinates $r \in R$ and directions $\vec{\omega} \in \Omega$. As i-th "state" of the chain let us consider point $x_i \in X$ immediately before i-th particle collisions. Let the distribution of the initial collisions χ_0 with the density $\psi(\chi)$ be given. Random transfer from χ_i into χ_{i+1} can be divided into three elementary random events: (1) "the choice" of the scattering type (for example molecular or aerosol) or absorption, (2) "the choice" of the dispersion direction, (3) "the choice" of the distance to the next collision. While solving the problems by the Monte Carlo method these random events are consecutively simulated on the computer. If the absorption function is considered, then this function argument (for example, effective mass of water vapour along the particle trajectory) is calculated, and the estimate of the result is multiplied by the absorption function corresponding to the value of the argument. If polarization is considered, the Stokes vector after simulation of the scattering is transformed by a scattering matrix.Its components are the direction function before and after scattering (see [7,8]). The simulation of the polarization becomes slightly more complicated if the "dispersion" matrix (analogue of scattering coefficient [7]) is not scalar. In this case it is already necessary to use "weight" multipliers which take into account the attenuation of the Stokes vector components along the path of the particle. For estimating the temporal distribution of the intensity the time of particle motion along the trajectory is also calculated.

Before the methods of simulating basic random trajectory elements are considered we shall say several words about the mathematical form of the representation of the characteristics of the radiative model of the medium. The experience of Monte Carlo method calculations shows that the scattering coefficient and the density of the absorbing substance for a non-homogeneous medium can be specified most conveniently in terms of piecewise constants, i.e. to divide the medium into domains with constant values of these characteristics. Scattering indices and absorption functions can be specified in terms of tables with linear interpolation between points.

The forms of model representation described above are apparently most appropriate for universal calculation programs. But other analytical methods of representation permitting the simulation of the path and the scattering direction can be used as well.

Now let us pass to the consideration of the random values that define the particle trajectory - the dispersion direction and free path. Random values are usually simulated by the transformations of one or more independent random numbers, uniformly distributed in the interval [0,1]. We shall denote these standard random numbers by the symbol α with different indices. There exist different ways of generating random numbers and among them the method of recurrent correlations which produces a sequence of pseudo-random numbers is most commonly used. These sequences are quite determined, but the method of the conversion from the previous number to the consequent one is arithmetically so complicated that in totality the numbers obtained in this way possess many "random" characteristics. The method of residues is most commonly used, for example in such a form (for computer BESM-6):

$$u_0 = 1, \quad u_n \equiv u_{n-1} \cdot 5^{17} \pmod{2^{40}}, \qquad \alpha_n = u_n \cdot 2^{-40}$$

Different methods of random values simulation on the basis of distribution laws are described in [9-11]. Let the probability density $f(x)$ be given and let $F(x)$ - be the corresponding distribution function. It is well known, that the random value

$$\xi = F^{-1}(\alpha) \tag{1}$$

is distributed in accordance with the density $f(x)$. In cases when the function $F^{-1}(\alpha)$ is not expressed in terms of elementary functions, the simulation with the help of formula (1) may be found too difficult. In references[10,11] the question is studied on the determination of the suitable numerical simulation formulae of the form:

$$\xi = g(\alpha_1, \alpha_2, \ldots, \alpha_k) \quad .$$

In particular in [11] the most economical formula for the simulation of the Rayleigh law for the cosine of the angle of photon molecular dispersion in the atmosphere is determined in terms of the density

$$f(x) = \frac{3}{8}(1+x^2), \quad -1 \leq x \leq +1.$$

Let $\alpha, \alpha_1, \alpha_2, \alpha_3$ be independent and distributed uniformly in (0,1). Then the Rayleigh law can be simulated by means of the formula

$$\xi = \begin{cases} \frac{8}{3}\alpha - 1, \; 0 \leq \alpha \leq \frac{3}{4} \quad , \\ \\ \text{sign}\left(\alpha - \frac{7}{8}\right) \max(\alpha_1, \alpha_2, \alpha_3), \; \frac{3}{4} < \alpha \leq 1 \; . \end{cases}$$

It is obvious that for $0 \le \alpha \le 3/4$ random numbers $\alpha_1, \alpha_2, \alpha_3$ may not be selected.

Photon dispersion indices for aerosols are usually given by the tables. Let us consider a corresponding simulation algorithm, obtained with the help of formula (1). Let the probability density be linear in each interval : $x_k < x \le x_{k+1}$, $k = 0, 1, \ldots, n$, $f(x_k) = y_k$. Denote

$$\Delta x_k = x_k - x_{k-1} < 0, \quad s_k = -\frac{y_{k-1} + y_k}{2} \Delta x_k .$$

Evidently $\sum_{k=1}^{n} s_k = 1$. Let $M = \alpha - \sum_{k=1}^{m} s_k \le 0$, $M + s_m > 0$.

Then

$$\xi = x_m - \frac{y_m \Delta x_m + \sqrt{y_m^2 (\Delta x_m)^2 - 2\Delta x_m (y_m - y_{m-1}) M}}{y_m - y_{m-1}}$$

There is a certain interest in the most economical formulae for recalculating the particle path direction coordinates at the collision, as obtained by Chentzov. Let Θ be the latitude angle and ϕ the azimuth angle of the new direction with respect to the previous one.

$$\mu = \cos \Theta , \quad \delta_1 = \sqrt{1 - \mu^2} \cos \phi, \quad \delta_2 = \sqrt{1 - \mu^2} \sin \phi,$$

a,b,c - are coordinates of the previous direction,

$$a^2 + b^2 + c^2 = 1, \quad a\delta_1 - b\delta_2 = A ,$$

and a', b', c', are coordinates of the new direction.

Then a', b', c' can be calculated by the formulae:

$$a' = a \left(\mu - \frac{A}{1 + |c|}\right) + \delta_1, \quad b' = b\left(\mu - \frac{A}{1 + |c|}\right) - \delta_2 ,$$

$$c' = c\,\mu - A \operatorname{sign} c.$$

Since the angle ϕ is isotropic, δ_1 and δ_2 can be calculated with the help of the following algorithm:

a) independent α_1 α_2 are chosen and

$x = 1 - 2\alpha_1$, $y = 1 - 2\alpha_2$ are calculated;

b) if $m = x^2 + y^2 \le 1$, we assume

$$\delta_1 = x\sqrt{\frac{1 - \mu^2}{m}} , \quad \delta_2 = y\sqrt{\frac{1 - \mu^2}{m}} ;$$

if $x^2 + y^2 > 1$ then the condition "a" is realized again, etc. Let us consider now the simulation of the free path l of the particle. Let $\sigma(\vec{r})$ be a total coefficient of attenuation at the point $\vec{r}$ of the space. Then the "natural" distribution function of the variable l is expressed by the formula:

$$F(x) = 1 - \exp(-\int_0^x \sigma(\vec{r}_0 + t\vec{\omega})dt), \quad x \geq 0,$$

where $\vec{r}_0$ is the initial point of the particle path, and $\vec{\omega}$ is a unit vector of the path direction. Formula (1) states that for obtaining the "sample" value of l it is necessary to solve the equation

$$F(l) = \alpha, \quad \alpha \in [0, 1],$$

which is equivalent to the following:

$$\int_0^l \sigma(\vec{r}_0 + t\vec{\omega})\, dt = -\ln\alpha \quad . \tag{2}$$

The latter equation can be easily solved, if σ is piecewise constant and $\{\rho_i\}$ distances are calculated up to the boundaries of the constancy domains σ along the path directions. The algorithm for the calculation of the distances $\{\rho_i\}$ for the spherical geometry is described in [4]. In [13] the most economical but complicated algorithm for calculating $\{\rho_i\}$ is developed for practically arbitrary geometrical configurations of the medium.

Lately a rather simple method for simulating the free path has been developed, and it may help to effectively solve some problems of radiative transfer in a medium with an arbitrary dependance of $\sigma(\vec{r})$ by the Monte Carlo method. In [12] this method is described in the following way. It is supposed that $\sigma(\vec{r}) \leq \sigma_m = \text{const}$. For the simulation of l two sequences of independent "sampling" values are constructed: $\xi_1, \ldots, \xi_n$ - with the density $\sigma_m \exp(-\sigma_m x)$; $\alpha_1, \ldots \ldots \alpha_n$ for a distribution uniform in [0,1];

$$\zeta_n = \sum_{k=1}^{n} \xi_k$$

Let it be

$$N = \min \{ n : \alpha_n \leq \sigma(r + \xi_n \vec{\omega})/ \sigma_m \} .$$

Then $l = \zeta_n$. It is obvious, that this way permits us to radically simplify calculations based on the Monte Carlo method for many complicated problems. In [12] there is an awkward and complicated proof of the indicated method of simulating l.

Let us consider a very simple proof which makes the meaning of the method clear and permits us to generalize it to a certain extent. To both parts of the transfer equation

$$(\vec{\omega}, \text{grad } I) + \sigma(\vec{r})\, I(\vec{r}, \vec{\omega}) = \int I(\vec{r}, \vec{\omega}')\, \sigma_s(\vec{r})\, g(\vec{\omega}' \to \vec{\omega}) d\vec{\omega}' + I_0(\vec{r}, \vec{\omega}) \tag{3}$$

we shall add corresponding parts of the equality

$$[\sigma_m - \sigma(\vec{r})]\, I(\vec{r}, \vec{\omega}) = \int I(\vec{r}, \vec{\omega}')[\sigma_m - \sigma(\vec{r})]\, \delta(\vec{\omega}' - \vec{\omega})d\vec{\omega}'$$

and combine the integral on the right hand side. The ordinary method of simulating l, corresponding to the obtained equation, obviously, coincide with the method considered above. The proof given here shows how to apply this method only within the limits of certain medium domains. It also becomes obvious how to combine such a simulation of l with "weight" methods of calculation, which will be considered below. It is known, that the average number of "physical" collisions is equal to

$$(\sigma, I) = \iint \sigma(\vec{r})\, I(\vec{r}, \vec{\omega})d\vec{r}\, d\vec{\omega}.$$

Hence the average number of collisions in case of the simulation of kinetic equation is equal to (σ_m, I). These arguments may help in the case of the selection of the method of the particle path simulation for the concrete problem.

Now let us consider the question of the evaluation of radiation intensity $I(\vec{r}, \vec{\omega})$ by the direct simulation. Only integrals of function I can be directly estimated within some domains of phase space, using the fact that the term

$$\int_D \sigma(x)I(x)dx, \qquad \text{where } x = (\vec{r}, \vec{\omega}),\ D \subset X = R \times \Omega,$$

represents the average number of collisions in the domain D, and the surface integral

$$\int_S ds \int_{\Omega_k} (\vec{\omega}, \vec{n})\, I(\vec{r}, \vec{\omega})d\vec{\omega},$$

(where $\vec{n}$ - normal to the surface S at the point $\vec{r}$), is equal to the number of the particles crossing the surface in the directions $\vec{\omega} \in \vec{\Omega}_k \subset \vec{\Omega}$. Hence we can estimate the average integral values of the intensity by calculating the particle collisions or the intersections on some surfaces. Thus in fact the estimate of the distributions of the intensity can be obtained from the histogram.

In [14] another method for estimating the distribution density is suggested, based on the mean square approximation of the desired density with the help of systems of orthogonal functions. Let $f(x)$ be the distribution density and $\{p_i(x)\}$, $i = 1,2,\ldots,m$ - the system of functions, orthonormalized with the weight $\rho(x)$. The best mean square approximation of the function $f(x)$ can be expressed in terms of linear combinations of the function $p_i(x)$ with the following coefficients:

$$a_i = \int f(x)\rho(x)p_i(x)dx = M.O.\rho(\xi)p_i(\xi).$$

Let the sampling sequence $x_1, \ldots, x_n$ be obtained. Then the value

$$a_i^* = \frac{\sum_{k=1}^{n} \rho(x_k) p_i(x_k)}{n}$$

may serve as a statistical estimate for a_i and for the function $f(x)$ the function

$$f^*(x) = \sum_{i=1}^{m} a^*_i p_i(x).$$

This method is particularly convenient for estimating "smooth" distributions, when one may a priori suggest that the distribution density is well approximated with the help of a small number of coefficients.

As a practical rule for the choice of the number of coefficients one may choose to consider only those coefficients whose absolute value essentially exceeds the value of their statistical error.

There exists a group of methods under the general title of "local calculation methods" for estimating the intensity directly at the point. These methods are beyond the limits of direct simulation and will be considered later.

It should be noted that in the Monte Carlo calculations one may, together with mean calculations, simultaneously estimate their meansquare error which defines the accuracy of the calculations.

The Monte Carlo method and the general integral transfer equation. The process of shortwave radiative transfer with the wavelength λ may be considered as a homogeneous Markov chain where the states of this chain are the "positions" of the particles in the phase space $X = R \times \Omega$ with the coordinates $\vec{r} \in R$ and the directions $\vec{\omega} \in \Omega$ immediately before the collisions. The transport density $k(x', x)dx$ is the collision probability in $(x, x + dx)$, and the variable

$$p(x') = 1 - \int_X k(x', x)dx$$

is the probability of the "death" (i.e. absorption or escape) of the particle immediately after collision at point x'. Taking into account the representation $x = (\vec{r}, \vec{\omega})$, where $\vec{r} \in R$, $\vec{\omega} \in \Omega$, one may write

$$k(x', x) = \frac{\sigma_s(\vec{r}')e^{-\tau(\vec{r}', \vec{r})}g(\mu)\delta(\omega - \omega_0)[\sigma_s(\vec{r}) + \sigma_c(\vec{r})]}{2\pi[\sigma_s(\vec{r}') + \sigma_c(\vec{r}')]|\vec{r}-\vec{r}'|^2}, \qquad (4)$$

where σ_s and σ_c are the total coefficients of dispersion and absorption respectively; $\tau(\vec{r}', \vec{r})$ is the optical length of the segment $(\vec{r}', \vec{r})$; $\mu = (\vec{\omega}', \vec{\omega})$; $g(\mu)$ is the dispersion index and $\vec{\omega}_0$ is determined by the relation

$$\vec{\omega}_o = \frac{\vec{r} - \vec{r}'}{|\vec{r} - \vec{r}'|} \quad .$$

The general principles for constructing the most economical modification of the Monte Carlo method for solving radiative transfer problems can be obtained by considering the transfer integral equation.

$$f(x) = \int_X k(x', x)f(x')dx' + \psi(x), \tag{5}$$

or

$$f = Kf + \psi.$$

Here $f(x)$ is the collision density at the point $x \in X$, $\psi(x)$ is the "initial" collision density, which can be conventionally considered to be situated in the field of the physical source. It is supposed, that the solution of the equation (5) can be represented in the form of Neumann series:

$$f = \sum_{n=0}^{\infty} K^n\psi, \quad K^o\psi = \psi \ .$$

The function $K^n\psi$ represents the n-th order collision density from the "source" with the density ψ. Different integral characteristics of the transfer process, as a rule, can be represented in the form of linear functionals of the solution of equation (5).

$$I_\phi = (f, \phi) = \int_X f(x)\phi(x)dx = \sum_{n=0}^{\infty}(K^n\psi, \phi).$$

From here it is obvious that

$$I_\phi = M\xi, \qquad \xi = \sum_{n=0}^{N}\phi(x_n),$$

where $\{x_n\}$ is the particle collisions chain and N is the number of the last collision. The latter formula shows that for estimating the functional I_ϕ by the Monte Carlo method it is necessary to simulate the chain of the trajectories $\{x_n\}$ by means of the computer and to average the sums of the values $\phi(x)$ for the different order collisions.

Let us also consider the equation conjugated with (5) with respect to the function $\phi(x)$

$$f^*(x) = \int_X k(x, x')f^*(x')dx' + \phi(x). \qquad (6)$$

It is easy to show that

$$I_\phi = (\psi, f^*).$$

Hence supposing $\psi(x) = \delta(x - x_0)$, we obtain $f^*(x_0) = \phi(x_0) + M \sum_{n=1}^{N} \phi(x_n)$.

The latter correlation may be used for approximately estimating the "value function" $f^*(x)$ in the case of simulation of particle trajectories.

The "value" function plays an exclusively important role in the mathematical representation of inverse problems of atmospheric optics [15].

The local calculation method and its modifications. The local calculation method is based on the estimation of the particle flux at the location of the receiver. In reference [16] it is shown that for obtaining an estimate of the total particle flux at the point $x^* = (\vec{r}^*, \vec{\omega}^*)$ it is necessary to average the expressions in the following form for all the collisions:

$$F = \frac{\exp(-\tau(\vec{r}, \vec{r}^*))\, g(\mu^*)}{2\pi |\vec{r} - \vec{r}^*|^2} \qquad (7)$$

where $\tau(\vec{r}, \vec{r}^*)$ is the optical length of the segment $(\vec{r}, \vec{r}^*)$, $\mu^* = \cos\theta^*$, θ^* is the angle between the particle direction before the collision and vector $\vec{r}^* - \vec{r}$, and $g(\mu^*)$ is the scattering index. This statement can be proved in the following way. If we assume $\phi = \delta(x - x^*)$, we shall obtain

$$I_\phi = (f, \phi) = f(x^*).$$

the expression

$$(f, \phi) = (Kf + \psi, \phi) = (\psi, \phi) + (f, K^*\phi)$$

shows that for estimating the functional I_ϕ one may use the function $K^*\phi$. But

$$[K^*\phi](x) = \int_X k(x, x')\delta(x' - x^*)dx' = k(x, x^*).$$

The variable $k(x, x^*)$ is determined by the expression (4). Integrating this expression over angles we obtain a variable that differs from (7) by the multiplier $\sigma(\vec{r})$. This can be explained by the fact, that the flux density $I(x)$ and the collision density $f(x)$ are connected by the relation

$$f(x) = I(x)\sigma(x), \quad x = (\vec{r}, \vec{\omega}).$$

Due to the multiplier $|\vec{r}^* - \vec{r}|^2$ in the denominator of the expression (7), the local estimate of the particle flux has infinite dispersion. It is known, that the probability convergence of this estimate is equal to $1/\sqrt[3]{N}$ (where N is the trajectory number instead of $1/\sqrt{N}$ in the case of finite dispersion. Therefore in different ways one tries to obtain modifications of this method with finite dispersion (see for example [4]) exploiting the properties of the symmetry of the system.

For estimating the angular flux distribution at the point $\vec{r}^*$ it is necessary to average values $F\Delta_i$, where Δ_i is the characteristic function of the angle interval Ω_i , e.g.

$$\Delta_i = \begin{cases} 1, & \dfrac{\vec{r}^* - \vec{r}}{|\vec{r}^* - \vec{r}|} \in \Omega_i \\ 0, & \dfrac{\vec{r}^* - \vec{r}}{|\vec{r}^* - \vec{r}|} \notin \Omega_i \end{cases} .$$

In order to get a similar estimate averaged in the domain of the detector D , the point $\vec{r}^* \in D$ should be chosen randomly according to the known density $p(\vec{r}^*)$, and the estimate of the flux (7) should be multiplied by the variable $|D| / p(\vec{r}^*)$. Under this condition one may deal with the choice of density $p(\vec{r}^*)$ to get an estimate of the intensity integral with finite dispersion [6].

It is obvious that the estimate of the form of $F\Delta_i$ is not efficient, if Ω_i is a small angular interval. This occurs for example when it is necessary to estimate the readings of the collimating detector. In such cases the "double" local calculation method with random sampling at an intermediate dispersion point in the domain, corresponding to the interval Ω_i can give a satisfactory result [20].

Modification of the simulation using information on the "value" function. The method developed here includes algorithms for simulating based on "value" [16] which use approximate information on the solution of the conjugate equation (6). Let $g^*(x) \geq 0$. Let us consider the homogenous Markov chain $\{x_n\}$ with the density of transfer probabilities

$$p(x', x) = \frac{k(x', x)\, g^*(x)}{[K^* g^*](x')} \tag{8}$$

and with the initial density $r(x) = \psi(x)g(x) / (\psi, g)$. Beginning with the transition $x_m \to x_{m+1}$, let us also introduce the "cut-off" probability (or "absorption") of the trajectories $\varepsilon_p(x) \leq \delta_p < 1$.

Furthermore let N be the random number of the last (before the "cut-off") condition of the chain and

$$Q_0^{(o)} = \frac{(\psi, g^*)}{g^*(x_0)}, \quad Q_n^{(o)} = \frac{(\psi, g^*)}{g^*(x_0)} \prod_{i=1}^{n} \frac{[K^* g^*](x_{i-1})}{g^*(x_i)},$$

$$Q_n \begin{cases} Q_n^{(o)}, & n \le m, \\ Q_n^{(o)} \cdot \prod_{i=m}^{n-1} \frac{1}{1 - \varepsilon_p(x_i)}, & m < n \le N, \\ 0, & n > N, \end{cases}$$

$$\xi = \sum_{n=0}^{\infty} Q_n \phi(x_n).$$

If $g^*(x) > 0$, then

$$M(Q_n \phi(x_n)) = (K^n \psi, \phi) \quad \text{and} \quad M\xi = \sum_{n=0}^{\infty} (K^n \psi, \phi) = I_\phi .$$

The condition $g^* > 0$ can be changed for a weaker one; $g^* > 0$ at $f^* > 0$, because on the strength of equation (6) and relation $I_\varphi = (\psi, f^*)$ the points where $f^* = 0$, can be excluded from the space X. In [17] it is proved that in the case of $g^* = f^*$ and $\delta_p = 0$ the dispersion of the random variable ξ is equal to 0. The estimate of the variable $D\xi$ can be given under the following conditions:

$$g^* = \text{const}(1 + \varepsilon) f^*, \quad |\varepsilon(x)| \le \delta < 1, \tag{9}$$

$$\|K\| \frac{1 + \delta}{(1 - \delta)(1 - \delta_p)} < 1.$$

Let us notice that the condition (9) is fulfilled if

$$0 < M_1 \le \frac{g^*(x)}{f^*(x)} \le M_2 < +\infty .$$

Supposing $c = 2 / (M_1 + M_2)$, we have

$$cg^* = (1 + \varepsilon)f^*, \quad |\varepsilon(x)| \leq \frac{M_2 - M_1}{M_2 + M_1} < 1 .$$

The lack of dependence upon the constant in expression (9) is a rather useful property of the method considered here, e.g. it is sufficient to have information on the function proportional to f^*. It is well known, that the efficiency of the Monte Carlo method algorithms can be determined by the variable $S = tD\xi$, where t is average computing time for getting one "sampling" value of ξ. We note that m is the simulated collision number without absorption.

From the estimate for $D\xi$ it follows that if $\varepsilon_p(x) = O(\delta)$ and $m \simeq |\ln \delta|$, then $\lim_{\delta \to 0} S = 0$. The relations given here show that the Monte Carlo method Algorithms for the arbitrary $0 < \phi(x) \in L^*$ can be improved by using approximate information on f^*. In this connection it is appropriate to select large values of m in the cases where "good" approximation of the "value" function is used.

The density (8) simulation in real problems is carried out by the simulation of the corresponding distributions of the "elementary" random variables: initial coordinates x_o, the free path l and the particle velocity direction $\vec{\omega}$. It can be demonstrated that if trajectory simulation is obtained by multiplying the conditional probability densities of the variables x_o, l and $\vec{\omega}$ by the "values" of the points in phase space, then the probabilistic error of the functional estimate will be equal to 0. In this connection the exact simulation based "on value" [7] is attained. Thus using <u>a priori</u> information on the relative "value" of x_o, l, $\vec{\omega}$, one may construct the algorithm corresponding to the method considered here.

It is necessary to make a remark about the value function f_o^*, appropriate for the calculation of several functionals I.

Let the function $\phi(x)$ in addition depend upon a certain parameter t ($t = 1, 2, \ldots, S$) and the demands upon the exactness of the estimate of the variables $I(t) = (f, \phi_t)$, where $\phi_t = \phi(x, t)$, are determined by the weight $\mu(t) \geq 0$, and also $\sum_{t=1}^{S} \mu(t) = 1$. It is necessary, by means of selection of the modifying function g^*, to minimize the variable

$$D_1 = \sum_{t=1}^{S} D\xi(t)\mu(t),$$

where $\xi(t) = \sum_{n=0}^{N} Q_n \phi(x_n, t)$ and $M\xi(t) = I(t)$. Let us determine the functions ϕ_o and f_o^* by the relations $\phi_0(x) = \left(\sum_{t=1}^{S} \phi^2(x, t) \times \mu(t) \right)^{1/2}$, $f_o^* = Kf_o^* + \phi_o$, and let $I_o = (f, \phi_o)$. Calculating directly the variable D_1 and using the Helder inequality it is not difficult to show, that if $g^* = f_o^*$ then

$$D_1 \leq I_o^2 - \sum_{t=1}^{S} I^2(t)\mu(t).$$

The latter inequality is the reason for using approximate information about f_0^* in the Monte Carlo calculations.

With the help of a priori estimates of the "value" function, effective algorithms were obtained for solving problems of the theory of radiative transfer in a spherical atmosphere [4].

On the basis of the above discussion, the use of the asymptotic solution of the Milne problem has been developed to improve the radiation transfer calculations through the layer of a thick substance in the Computer Center of the Siberian Branch of the USSR Academy of Sciences.

The dependent tests method, the estimate of the derivatives and the solution of the inverse problems. The dependent tests method for the solution of the transfer theory problems is based on the fact that particle trajectories simulation in different systems is carried out in terms of one and the same random numbers. One may, in particular, estimate the functional for different values of the parameter of the system on the basis of exactly the same trajectories, eliminating the resulting shift with the help of special weight factors. Let λ be a system parameter e.g.

$$k(x, x') = k(x, x', \lambda) \text{ and } \phi(x) = \phi(x, \lambda) = \phi_\lambda.$$

Then

$$I_\phi(\lambda) = \sum_{n=0}^{\infty} (K_\lambda^n \psi, \phi_\lambda).$$

Let us consider the relation

$$(K_\lambda^n \psi, \phi_\lambda) = \underbrace{\int\int \ldots \int}_{n+1} \psi(x^{(o)})\, k(x^{(o)}, x^{(1)}, \lambda) \ldots$$

$$\times\, k(x^{(n)}, x, \lambda)\, \phi(x, \lambda) dx^{(o)}\, dx^{(1)} \ldots dx^{(n)}\, dx$$

$$= \underbrace{\int\int \ldots \int}_{n+1} \psi(x^{(o)})\, k(x^{(o)}, x^{(1)}, \lambda_o) \ldots k(x^{(n)}, x, \lambda_o)$$

$$\times \frac{k(x^{(o)}, x^{(1)}, \lambda)}{k(x^{(o)}, x^{(1)}, \lambda_o)} \cdots \frac{k(x^{(n)}, x, \lambda)}{k(x^{(n)}, x, \lambda_o)}\, \phi(x, \lambda) dx^{(o)} \ldots dx^{(n)} dx,$$

from which we can see that the trajectories, constructed for $\lambda = \lambda_o$, can be used to estimate $I_\phi(\lambda)$, if after each transition $x' \to x$ the auxiliary "weight" of the particle is multiplied by the variable

$$\frac{k(x', x, \lambda)}{k(x', x, \lambda_0)}$$

It is supposed, that there do not exist points x, x', in which $k(x', x, \lambda) \neq 0$, and $k(x', x, \lambda_0) = 0$.

In practice $k(x', x, \lambda)$ is represented in the form of the bundle of the conditional probability densities of the elementary random variables (the path of the particle and the cosine of the scattering angle) and after each elementary "sampling" the auxiliary "weight" of the particle is multiplied by the relation between the corresponding probability densities for the values λ and λ_0.

So, after the selection of the next path l "the weight" should be multiplied by

$$\frac{\sigma(l, \lambda)e^{-\tau(l, \lambda)}}{\sigma(l, \lambda_0)e^{-\tau(l, \lambda_0)}} = \frac{\sigma(l, \lambda)}{\sigma(l, \lambda_0)} e^{-[\tau(l, \lambda) - \tau(l, \lambda_0)]},$$

$$Q(\lambda) = Q'(\lambda) \frac{\sigma(l, \lambda)}{\sigma(l, \lambda_0)} e^{-[\tau(l, \lambda) - \tau(l, \lambda_0)]},$$

and after the selection of the μ, i.e. cosine of the scattering angle:

$$Q(\lambda) = Q'(\lambda) \frac{g(\mu, \lambda)}{g(\mu, \lambda_0)}.$$

On the basis of the dependent tests method one may estimate the change in the radiation field due to small changes in the aerosol dispersion coefficient, albedo or indicatrix.

It is also appropriate to use the dependent tests method for the simultaneous calculation of radiative transfer involving different wavelengths.

Now let us consider the case, when the dispersion coefficients σ_i, $i = 1,\ldots,m$, are parameters in m fixed spheres and the variables

$$I_k(\sigma_i) = M \sum_{n=0}^{N} Q_n(\sigma_i) \phi_k(x_n, \sigma_i), \tag{10}$$

are calculated, where the averaging is carried out over a certain definite distribution of particle trajectories. In [4] the expression of the form

$$\frac{\partial I_k}{\partial \sigma_i} = M \sum_{n=0}^{N} Q_n \phi_k^{(n)} \left[\frac{\partial \ln Q_n}{\partial \sigma_i} + \frac{\partial \ln \phi_k^{(n)}}{\partial \sigma_i} \right]$$

is shown and the algorithm for its calculation is given. Thus, simultaneously with the estimation of variables I_k by the Monte Carlo method one may calculate the matrix of the derivatives $\partial I_k / \partial \sigma_i$. This gives the possibility of solving inverse problems, that are stated in [15]. Let the meanings of $\tilde{I}_k$ be experimentally measured, and the initial approximation for the desired dispersion coefficients $\sigma_1^{(o)}, \ldots, \sigma_m^{(o)}$ is known. We find the next approximation, obtained by means of the solution of the linear system of equations, is of the form:

$$\sum_{i=1}^{m} \frac{\partial I_k}{\partial \sigma_i} (\sigma_i - \sigma_i^{(0)}) = \tilde{I}_k - I_k^{(0)} .$$

In the case of overdetermination of the latter system it should be solved by means of the least squares method, using auxiliary weights for "regularization" of the algorithm. The example of the solution of the inverse problem by this method is given in [4]. Calculations by the Monte Carlo method can be used to search for mostly "informative" systems of functionals.

The methods described here can obviously be applied for the effective averaging of the characteristics of the radiation model of the medium, when the least change of the main functionals in the sense of the least squares method occurs.

In conclusion it should be noted, that the results of the calculations of different problems of radiation transfer theory by the Monte Carlo method are given in the works [3, 4].

REFERENCES

1. Z. Sekera, 1956: Advances in Geophys. 3, No. 4, 43.

2. G. I. Marchuk, G. A. Michailov, 1967: Izv. AN SSSR, seria "Fizika atmosfery i okeana". 3, No. 3, (in Russian).

3. G. I. Marchuk, G. A. Michailov, 1967: Izv. AN SSSR, seria "Fizika atmosfery i okeana". 3, No. 4, (in Russian).

4. G. I. Marchuk, G. A. Michailov, M. A. Nazaraliev, R. A. Darbinian, 1968: "Solution of direct and some inverse problems of atmospheric optics by Monte-Carlo method". Novosibirsk, (in Russian).

5. B. M. Golubitzki, M. V. Tantashev, A. R. Zakirova, 1966: Izv AN SSSR, seria "Fizika atm. i okeana". 2, No. II.

6. G. M. Krekov, G. A. Michailov, B. A. Kargin, 1968: Izv. vuzov, fizika. No. 4, 5, (in Russian).

7. G. V. Rozenberg, 1955: UFN, 56, vyp. I, (in Russian).

8. S. Chandrasekhar,1953: "Transfer of ray energy". Moscow, (in Russian).

9. D. I. Golenko, 1965: "Simulation and statistical analyses of pseudo-random numbers by computers". Moscow, (in Russian).

10. G. A. Michailov, 1965: "Probability theory and its application". 10, No. 4, (in Russian).

11. G. A. Michailov, "Zhurn. Vych. matem. i mat. fizika", 6, No. 6, (in Russian).

12. W. A. Coleman, 1968: Nucl. Sci. and Eng., 32, No. I.

13. E. S. Kuropatenko, V. N. Ogibin, 1968: "Zhurn vych matem. i mat. fizika", 8, No. I, (in Russian).

14. N. N. Chentzov, 1962: DAN SSSR, 147, No. I, (in Russian).

15. G. I. Marchuk, 1964: Kosmicheskiye issledovaniya, 2, vyp. 3, (in Russian).

16. V. G. Zolotukhin, S. M. Ermakov, 1963: in the book "Voprosy fizika zashchity reaktorov", Moscow, (in Russian).

17. G. A. Michailov, 1968: "Zhurn. vych. matem. i mat. fizika", 8, No. 5, (in Russian).

18. G. A. Kattawar, G. N. Plass, 1968: "Radiation and polarization of multiple scattered light from haze and clouds". Applied optics, 7, 8.

19. G. A. Michailov, M. A. Nazaraliev, 1971: "Calculation of the light polarization in spherical atmosphere by the Monte Carlo method". Izv. AN SSSR, seria "Fizika atm i okeana", 7, 4, (in Russian).

20. V. S. Antufeev, G. A. Michailov, M. A. Nazaraliev, 1971: "Modifications of the local estimates considering axial symmetry in the problems of atmospheric optics". In the book, "Probability methods of the solution of the problems of mathematical physics", Computer Center, SO AN SSSR, Novosibirsk, (in Russian).

RADIATIVE TRANSFER OF VISIBLE RADIATION IN TURBID ATMOSPHERES

Giichi Yamamoto and Masayuki Tanaka
Geophysical Institute
Tohoku University
Sendai, Japan

1. INTRODUCTION

The progress and popularization of the high speed electronic computer have caused a marked improvement in techniques of obtaining numerical solutions to equation of radiative transfer which deals with the multiple scattering and absorption processes of solar radiation in the atmosphere. Main objectives of recent investigations in this field are to clarify quantitatively the radiative transfer processes in turbid atmospheres as well as in clouds and their thermal and optical effects. In order to do so, most of the recent studies take into account the effect of multiple scattering and accompanying polarization effect as strictly as possible, based on realistic model atmospheres. At the same time, usefulness of radiation observations for obtaining informations on aerosols and clouds, such as their size distributions and optical properties, has come to be recognized and the methods are going to be developed.

Among these problems, recent advancement in the study of radiative transfer of visible radiation in turbid atmospheres is reviewed in this paper, in which particular emphasis is laid on its thermal effect. In the following second section, several representative methods of solving equation of radiative transfer are reviewed. Section 3 describes the relation between atmospheric turbidity and reflectivity of the turbid atmosphere and accordingly the heat budget of the earth. Section 4 describes the flux divergence of solar radiation inside the turbid atmosphere, which naturally occurs due to the absorptive property of aerosols. Section 5 reviews the problems of the intensity distribution of diffuse radiation and its state of polarization.

2. EQUATION OF RADIATIVE TRANSFER

Recently the trend of study of radiative transfer is changing from obtaining analytical solutions for simplified atmospheric models to obtaining numerical solutions for realistic ones. In this respect, many numerical methods have been proposed recently that a working group was established as the Radiation Commission of the IAMAP for the purpose of examining merit and demerit of various methods. Generally speaking, selection of the methods depends upon the model atmospheres to be used and upon the nature of the required informations. In addition, reseacher's subjective point of view or taste inevitably comes into selecting the methods. Therefore, in this paper we shall describe several representative methods and merit and demerit of them from our subjective point of view.

Now we shall consider the diffuse radiation field in a plane-parallel atmosphere illuminated by the sun at μ_0, ϕ_0, where $\mu_0 = \cos\theta_0$, θ_0 being the zenith angle, and ϕ_0 is the azimuthal angle. The flux of the solar radiation at the top of the atmosphere is assumed to be πF. The equation of radiative transfer is then given by Chandrasekhar (1950)

$$\mu \frac{d\, I(\tau,\mu,\phi)}{d\tau} = I(\tau,\mu,\phi) - \frac{1}{4\pi}\int_{-1}^{+1}\int_{0}^{2\pi} p(\tau,\mu,\phi;\mu',\phi')\, I(\tau,\mu',\phi')\, d\mu'\, d\phi' - \frac{F}{4} e^{-\tau/\mu_0}\, p(\tau,\mu,\phi;-\mu_0,\phi_0) \quad , \tag{1}$$

where I is the intensity of the diffuse radiation, p is the phase function which represents the angular distribution of the scattered light due to single scattering, τ is the optical thickness measured from the top of the atmosphere, and μ and ϕ designate the direction of light, where $\mu = \cos\theta$ (θ being the polar angle) and ϕ is the azimuthal angle. We can draw a line between an inhomogeneous and a homogeneous atmosphere according as the phase function p depends upon the optical thickness τ or not. From the principle of energy conservation, the following normalization condition for p is derived:

$$\frac{1}{4\pi\omega}\int_{-1}^{+1}\int_{0}^{2\pi} p(\tau,\mu,\phi;\mu',\phi')\, d\mu'\, d\phi' = 1 \tag{2}$$

where ω is the albedo for single scattering of the medium at level τ, which is defined by the ratio of the volume scattering coefficient, $\beta^{(s)}$, to the volume extinction coefficient, $\beta^{(e)}$, i.e.

$$\omega = \beta^{(s)}(\tau)/\beta^{(e)}(\tau) \quad . \tag{3}$$

When the atmosphere is composed of different kinds of scatterers, p is expressed as

$$p(\tau,\mu,\phi;\mu',\phi') = \frac{1}{\beta^{(e)}}\sum_i \beta_i^{(s)}\, p_i(\tau,\mu,\phi;\mu',\phi') \quad , \tag{4}$$

where $\beta_i^{(s)}$ and p_i are respectively the volume scattering coefficient and phase function of the i-th component. The boundary conditions are given by

$$I(0,-\mu,\phi) = 0 \quad , \tag{5}$$

and

$$I(\tau_s,+\mu,\phi) = I_g(+\mu,\phi) \quad , \tag{6}$$

where $I_g(+\mu,\phi)$ is intensity of the reflected light, which depends upon both reflection characteristics of the underlying surface and incoming radiation to the surface. The problem of radiative transfer without consideration of the surface reflection (i.e., $I_g = 0$) is called the standard problem and that with consideration of the surface reflection is called the planetary one.

So far the polarization of the radiation field is disregarded. In case of considering polarization, the radiation field is expressed, instead of the scalar intensity I, by the one column matrix (or vector) $\mathbf{I}$ which is composed of four Stokes parameters. Correspondingly the law of single scattering is expressed by the phase matrix $\mathbf{p}$ (4x4) instead of the phase function p. The equation of radiative transfer appropriate to this case is obtained by replacing I and p in Eq. (1) by $\mathbf{I}$ and $\mathbf{p}$, respectively.

The problem of obtaining the diffusely reflected radiation at the top of the atmosphere, $I(0,+\mu,\phi)$, and the diffusely transmitted radiation at the bottom of the atmosphere, $I(\tau_s,-\mu,\phi)$, by solving equation of radiative transfer (1) under boundary conditions (5) and (6), is called the problem of diffuse reflection and transmission.

In order to solve this problem, Chandrasekhar (1950) has introduced the scattering function, S, and the transmission function, T, and has derived simultaneous non-linear integral equations for these functions, S and T, by means of the principle of invariance. Then by expanding the phase function p in a series of Legendre polynomials, and accordingly, expanding the functions S and T in Fourier cosine series in azimuthal angles, he has separated the integral equations for S and T into a set of integral equations for a pair of expansion coefficients, S^m and T^m, of respective degrees. The solutions of these integral equations are then given in the form of tabulated functions, such as X- and Y-functions.

This method has succeeded in cases of isotropic and Rayleigh scatterings. The most comprehensive tables for Rayleigh scattering have been published by Sekera and his collaborators (1960). In addition, Sekera (1963), Chamberlain and McElroy (1966) and Fymat and Abhyankar (1969) have extended this method to inhomogenous atmospheres. However, this method is not necessarily profitable in the case of highly anisotropic scattering. It is due to the reasons that the expansion of the phase function for anisotropic scattering generally needs many terms, particularly when the forward scattering predominates, and accordingly computing time in obtaining numerical solutions of X- and Y-functions corresponding to each term becomes enormous.

Recently several methods, by which the problem of diffuse reflection and transmission can be solved with less amount of computation than the classical method of Chandrasekhar, have been developed.

2.1 Doubling Method

van de Hulst (1963) has shown that if the problem of diffuse reflection and transmission can be solved for a layer of small thickness τ_0, then starting from this solution it can also be solved for layers of thickness $2\tau_0$, $4\tau_0$, etc., with relatively easy calculation, and thus the computing time in obtaining the solution for any thick layer can considerably be saved. The method is called the doubling method, and effectiveness of this method has been shown numerically by van de Hulst and Grossman (1968). They obtained the solution for the initial layer by the Neumann series method (iteration in orders of scattering). Irvine (1968) has also obtained the solution for an elongated phase function by the combination of the Neumann series method and doubling method. On the other hand, Hansen (1969) has proposed to save labor of obtaining the solution for the initial layer by starting

from an extremely thin layer. In this case, the initial layer can be considered as a single scattering layer and the corresponding scattering and transmission functions can be given by the phase function. We shall describe an outline of this method in the following:

Let us assume that the intensity of the incident radiation at the top of the layer of thickness τ_0 to be $I_{inc}(\mu',\phi')$. The diffusely reflected radiation, $I(0,+\mu,\phi)$, and diffusely transmitted radiation, $I(\tau_0,-\mu,\phi)$, respectively are expressed by using the scattering function S and transmission function T as follows (Chandrasekhar, 1950):

$$I(0,+\mu,\phi) = \frac{1}{4\pi\mu}\int_0^1\int_0^{2\pi} S(\tau_0;\mu,\phi;\mu',\phi')\, I_{inc}(\mu',\phi')\, d\mu'\, d\phi' \quad , \tag{7}$$

and

$$I(\tau_0,-\mu,\phi) = \frac{1}{4\pi\mu}\int_0^1\int_0^{2\pi} T(\tau_0;\mu,\phi;\mu',\phi')\, I_{inc}(\mu',\phi')\, d\mu'\, d\phi' \quad . \tag{8}$$

When the incident radiation is the parallel beam of the net flux πF per unit area perpendicular to the incident direction, we have

$$I_{inc}(\mu',\phi') = \pi F\, \delta(\mu' - \mu_0)\, \delta(\phi' - \phi_0) \quad , \tag{9}$$

where δ is Dirac's δ-function and (μ_0, ϕ_0) is the direction of the incident beam. Inserting (9) into (7) and (8), we have

$$I(0,+\mu,\phi) = \frac{1}{4\mu} S(\tau_0;\mu,\phi;\mu_0,\phi_0)\, F \quad , \tag{10}$$

$$I(\tau_0;-\mu,\phi) = \frac{1}{4\mu} T(\tau_0;\mu,\phi;\mu_0,\phi_0)\, F \quad . \tag{11}$$

Now we shall assume that the second layer with the same thickness is added below the first. The component $\frac{1}{4\mu} S(\tau_0;\mu,\phi;\mu_0,\phi_0)\, F$ is unaffected by this addition, but the diffusely transmitted radiation $\frac{1}{4\mu} T(\tau_0;\mu,\phi;\mu_0,\phi_0)\, F$ and directly transmitted radiation $\pi F\, \delta(\mu - \mu_0)\, \delta(\phi - \phi_0)\, e^{-\tau_0/\mu_0}$ are partly transmitted through the second layer and partly reflected by it to become an additional radiation incident upon the first layer from below. As shown in Fig. 1, succession of the processes is repeated endlessly. Since the combination of the initial and second layers must be equivalent to a single layer of thickness $2\tau_0$, one can write the relationships between the function $S(\tau_0;\mu,\phi;\mu_0,\phi_0)$ [or $T(2\tau_0;\mu,\phi;\mu_0,\phi_0)$] for the combined layer and the functions $S(\tau_0;\mu,\phi;\mu_0,\phi_0)$ and $T(\tau_0;\mu,\phi;\mu_0,\phi_0)$ for respective layers, as follows:

$$S(2\tau_0;\mu,\phi;\mu_0,\phi_0) = S(\tau_0;\mu,\phi;\mu_0,\phi_0)$$

$$+ e^{-\tau_0/\mu} \sum_0 (\tau_0;\mu,\phi;\mu_0,\phi_0)\, e^{-\tau_0/\mu_0}$$

$$+ \frac{e^{-\tau_0/\mu_0}}{4\pi} \int_0^1\int_0^{2\pi} T(\tau_0;\mu,\phi;\mu',\phi') \sum_0 (\tau_0;\mu',\phi';\mu_0,\phi_0) \frac{d\mu'}{\mu'} d\phi'$$

$$+ \frac{e^{-\tau_0/\mu}}{4\pi} \int_0^1\int_0^{2\pi} \sum_0 (\tau_0;\mu,\phi;\mu',\phi')\, T(\tau_0;\mu',\phi';\mu_0,\phi_0) \frac{d\mu'}{\mu'} d\phi'$$

$$+ \frac{1}{16\pi^2} \int_0^1\int_0^{2\pi}\int_0^1\int_0^{2\pi} T(\tau_0;\mu,\phi;\mu'',\phi'') \sum_0 (\tau_0;\mu'',\phi'';\mu',\phi')$$

$$\times T(\tau_0;\mu',\phi';\mu_0,\phi_0) \frac{d\mu'}{\mu'} d\phi' \frac{d\mu''}{\mu''} d\phi'' \quad , \tag{12}$$

and

$$T(2\tau_0;\mu,\phi;\mu_0,\phi_0) = T(\tau_0;\mu,\phi;\mu_0,\phi_0)\, e^{-\tau_0/\mu_0} + e^{-\tau_0/\mu}\, T(\tau_0;\mu,\phi;\mu_0,\phi_0)$$

$$+ e^{-\tau_0/\mu} \sum_e (\tau_0;\mu,\phi;\mu_0,\phi_0)\, e^{-\tau_0/\mu_0}$$

$$+ \frac{1}{4\pi} \int_0^1\int_0^{2\pi} T(\tau_0;\mu,\phi;\mu',\phi')\, T(\tau_0;\mu',\phi';\mu_0,\phi_0) \frac{d\mu'}{\mu'} d\phi'$$

$$+ \frac{e^{-\tau_0/\mu_0}}{4\pi} \int_0^1\int_0^{2\pi} T(\tau_0;\mu,\phi;\mu',\phi') \sum_e (\tau_0;\mu',\phi';\mu_0,\phi_0) \frac{d\mu'}{\mu'} d\phi'$$

$$+ \frac{e^{-\tau_0/\mu}}{4\pi} \int_0^1\int_0^{2\pi} \sum_e (\tau_0;\mu,\phi;\mu',\phi')\, T(\tau_0;\mu',\phi';\mu_0,\phi_0) \frac{d\mu'}{\mu'} d\phi'$$

$$+ \frac{1}{16\pi^2} \int_0^1\int_0^{2\pi}\int_0^1\int_0^{2\pi} T(\tau_0;\mu,\phi;\mu'',\phi'') \sum_e (\tau_0;\mu'',\phi'';\mu',\phi')$$

$$\times T(\tau_0;\mu',\phi';\mu_0,\phi_0) \frac{d\mu'}{\mu'} d\phi' \frac{d\mu''}{\mu''} d\phi'' \quad , \tag{13}$$

where

$$\sum_0 (\tau_0;\mu,\phi;\mu_0,\phi_0) = \sum_{n=1,3,\ldots}^{\infty} S_n(\tau_0;\mu,\phi;\mu_0,\phi_0) \quad , \tag{14}$$

$$\sum_e (\tau_0;\mu,\phi;\mu_0,\phi_0) = \sum_{n=2,4,\ldots}^{\infty} S_n(\tau_0;\mu,\phi;\mu_0,\phi_0) \quad , \tag{15}$$

$$S_1 (\tau_0;\mu,\phi;\mu_0,\phi_0) = S(\tau_0;\mu,\phi;\mu_0,\phi_0) \quad , \tag{16}$$

and

$$S_n(\tau_0;\mu,\phi;\mu_0,\phi_0) = \frac{1}{4\pi} \int_0^1 \int_0^{2\pi} S(\tau_0;\mu,\phi;\mu',\phi') S_{n-1}(\tau_0;\mu',\phi';\mu_0,\phi_0) \frac{d\mu'}{\mu'} d\phi' \tag{17}$$

Thus, if the scattering and transmission functions for the initial layer are known, those for $2\tau_0$, $4\tau_0$, etc. are successively derived from (12) and (13). If we take the value of τ_0 to be sufficiently small, the initial layer can be considered as a single scattering layer, whose scattering and transmission functions are given by

$$S(\tau_0;\mu,\phi;\mu_0,\phi_0) = (\frac{1}{\mu} + \frac{1}{\mu_0})^{-1} \left\{1 - e^{-\tau_0(1/\mu+1/\mu_0)}\right\} p(\mu,\phi;-\mu_0,\phi_0) \quad , \tag{18}$$

$$T(\tau_0;\mu,\phi;\mu_0,\phi_0) = (\frac{1}{\mu} + \frac{1}{\mu_0})^{-1} \left\{e^{-\tau_0/\mu_0} - e^{-\tau_0/\mu}\right\} p(-\mu,\phi;-\mu_0,\phi_0) \quad . \tag{19}$$

In practical computation considerable advantage is gained in computing time and computer storage if the azimuth dependent functions, such as p, S and T, are expanded in Fourier series in $(\phi - \phi_0)$. Generally the phase function $p(\mu,\phi;\mu',\phi')$ can be expanded in cosine series in $(\phi' - \phi)$ as follows:

$$p(\mu,\phi;\mu',\phi') = \sum_{m=0}^{\infty} p^m(\mu,\mu') \cos m(\phi' - \phi) \quad , \tag{20}$$

where

$$p^m(\mu,\mu') = \frac{1}{(1+\delta_{0,m})\pi}\int_0^{2\pi} p(\mu,\phi;\mu',\phi')\cos m(\phi'-\phi)\,d\phi' \tag{21}$$

$$\delta_{0,m} = 0 \quad \text{if} \quad m \neq 0 \quad \text{and} \quad = 1 \quad \text{if} \quad m = 0 \ .$$

Correspondingly the functions S and T are expanded as follows:

$$S(\tau;\mu,\phi;\mu',\phi') = \sum_{m=0}^{\infty} S^m(\tau;\mu,\mu')\cos m(\phi'-\phi) \quad , \tag{22}$$

and

$$T(\tau;\mu,\phi;\mu',\phi') = \sum_{m=0}^{\infty} T^m(\tau;\mu,\mu')\cos m(\phi'-\phi) \quad . \tag{23}$$

Inserting (20), (22) and (23) into (12) we have relation for the expansion coefficients of m-th degree as follows:

$$\begin{aligned} S^m(2\tau_0;\mu,\mu_0) = {} & S^m(\tau_0;\mu,\mu_0) + e^{-\tau_0/\mu}\sum_0^m(\tau_0;\mu,\mu_0)\,e^{-\tau_0/\mu} \\ & + e^{-\tau_0/\mu_0}\,\frac{1}{(4-2\delta_{0,m})}\int_0^1 T^m(\tau_0;\mu,\mu')\sum_0^m(\tau_0;\mu',\mu_0)\,\frac{d\mu'}{\mu'} \\ & + e^{-\tau_0/\mu}\,\frac{1}{(4-2\delta_{0,m})}\int_0^1 \sum_0^m(\tau_0;\mu,\mu')\,T^m(\tau_0;\mu',\mu_0)\,\frac{d\mu'}{\mu'} \\ & + \frac{1}{(4-2\delta_{0,m})^2}\int_0^1\int_0^1 T^m(\tau_0;\mu,\mu'')\sum_0^m(\tau_0;\mu'',\mu')\,T^m(\tau_0;\mu',\mu_0)\,\frac{d\mu'}{\mu'}\,\frac{d\mu''}{\mu''} \quad , \end{aligned} \tag{24}$$

where

$$\sum_0^m (\tau_0;\mu,\mu_0) = \sum_{n=1,3,\ldots}^{\infty} S_n^m(\tau_0;\mu,\mu_0) \quad , \tag{25}$$

$$S_1^m(\tau_0;\mu,\mu_0) = S^m(\tau_0;\mu,\mu_0) \quad , \tag{26}$$

and

$$S_n^m(\tau_0;\mu,\mu_0) = \frac{1}{(4 - 2\delta_{0,m})} \int_0^1 S^m(\tau_0;\mu,\mu') \, S_{n-1}^m(\tau_0;\mu',\mu_0) \, \frac{d\mu'}{\mu'} \quad . \tag{27}$$

Similar relations can be derived for T^m . The succeeding computation is simply to replace the integrals involved in equations for S^m and T^m by sums through Gauss quadrature. Therefore it is straightforward. It is apparent that $S^m(2^p\tau_0)$ and $T^m(2^p\tau_0)$ are generated in p cycles starting with $S^m(\tau_0)$ and $T^m(\tau_0)$ rather than 2^p cycles of the simply additive procedure.

According to Hansen (1968) necessary computing time is remarkably short except for strongly peaked phase functions. For aerosol phase functions varying three orders of magnitude from their peak to their lowest value (requiring about 50 terms in the cos $m\phi$ expansion) the total computing time is 4 minutes on the IBM 360/95 for the scattering and transmission functions (and derived quantities) for every τ-multiple of 2 from 2^{-25} to 2^7 for 20 values of μ, 20 values of μ_0, and any reasonable number of values of $\phi - \phi_0$. As can be seen from this example the doubling method is very effective in obtaining numerical solutions of the problem of diffuse reflection and transmission for homogeneous atmospheres. However, for inhomogeneous atmospheres the doubling procedure can no longer be applied, since the functions for the second layer are different from that of the first. In this case only additive procedure is applicable, so that the above merit is greatly diminished.

Hansen (1971a) has also applied this method to the case in which polarization is taken into account. In this case formulation of the problem can be made with use of Chandrasekhar's $\mathbf{S}$ and $\mathbf{T}$ matrices instead of the functions S and T . The definition of $\mathbf{S}$ and $\mathbf{T}$ is analogous to that of S and T. The different point is that, even if the atmosphere is homogeneous, the scattering and transmission matrices for the case, in which the top of the layer is illuminated by the incident radiation, should be distinguished from those for the case, in which the bottom of the layer is illuminated by the incident radiation, (Hovenier, 1969). Therefore, if we designate the incident radiation fields at the top and bottom of the layer by $\mathbf{I}_{inc}(\mu',\phi')$ and $\mathbf{I}^*_{inc}(\mu',\phi')$ respectively, it is necessary to consider the matrices, $\mathbf{S}$, $\mathbf{T}$, $\mathbf{S}^*$ and $\mathbf{T}^*$ defined followingly:

$$\left.\begin{aligned} \mathbf{I}(0,+\mu,\phi) &= \frac{1}{4\pi\mu} \int_0^1 \int_0^{2\pi} \mathbf{S}(\tau_1;\mu,\phi;\mu',\phi') \, \mathbf{I}_{inc}(\mu',\phi') \, d\mu' \, d\phi' \quad , \\ \mathbf{I}(\tau_1;-\mu,\phi) &= \frac{1}{4\pi\mu} \int_0^1 \int_0^{2\pi} \mathbf{T}(\tau_1;\mu,\phi;\mu',\phi') \, \mathbf{I}_{inc}(\mu',\phi') \, d\mu' \, d\phi' \quad , \end{aligned}\right\} \tag{28}$$

$$\left.\begin{aligned} \mathbf{I}^*(\tau_1;-\mu,\phi) &= \frac{1}{4\pi\mu}\int_0^1\int_0^{2\pi} \mathbf{S}^*(\tau_1;\mu,\phi;\mu',\phi')\,\mathbf{I}^*_{inc}(\mu',\phi')\,d\mu'\,d\phi' \quad , \\ \mathbf{I}^*(0;+\mu,\phi) &= \frac{1}{4\pi\mu}\int_0^1\int_0^{2\pi} \mathbf{T}^*(\tau_1;\mu,\phi;\mu',\phi')\,\mathbf{I}^*_{inc}(\mu',\phi')\,d\mu'\,d\phi' \quad . \end{aligned}\right\} \tag{29}$$

If we take such distinction into consideration, the matrix $\mathbf{S}$ for the layer of thickness $2\tau_0$ can be obtained referring to the doubling equation (12) as follows:

$$\begin{aligned} \mathbf{S}(2\tau_0;\mu,\phi;\mu_0,\phi_0) &= \mathbf{S}(\tau_0;\mu,\phi;\mu_0,\phi_0) + e^{-\tau_0/\mu}\,\boldsymbol{\Sigma}_0(\tau_0;\mu,\phi;\mu_0,\phi_0)\,e^{-\tau_0/\mu_0} \\ &+ \frac{e^{-\tau_0/\mu_0}}{4\pi}\int_0^1\int_0^{2\pi} \mathbf{T}^*(\tau_0;\mu,\phi;\mu',\phi')\;\boldsymbol{\Sigma}_0(\tau_0;\mu',\phi';\mu_0,\phi_0)\,\frac{d\mu'}{\mu'}\,d\phi' \\ &+ \frac{e^{-\tau_0/\mu}}{4\pi}\int_0^1\int_0^{2\pi} \boldsymbol{\Sigma}_0(\tau_0;\mu,\phi;\mu',\phi')\,\mathbf{T}(\tau_0;\mu',\phi';\mu_0,\phi_0)\,\frac{d\mu'}{\mu'}\,d\phi' \\ &+ \frac{1}{16\pi^2}\int_0^1\int_0^{2\pi}\int_0^1\int_0^{2\pi} \mathbf{T}^*(\tau_0;\mu,\phi;\mu'',\phi'')\;\boldsymbol{\Sigma}_0(\tau_0;\mu'',\phi'';\mu',\phi')\,\mathbf{T}(\tau_0;\mu',\phi';\mu_0,\phi_0) \\ &\cdot \frac{d\mu'}{\mu'}\,d\phi'\,\frac{d\mu''}{\mu''}\,d\phi'' \quad . \end{aligned} \tag{30}$$

Similarly the matrix $\mathbf{T}(2\tau_0)$ can be obtained by changing the functions $\mathbf{T}$ and $\boldsymbol{\Sigma}_e$ in equation (13) to $\mathbf{T}$ and $\boldsymbol{\Sigma}_e$ respectively. Here we should note that

$$\boldsymbol{\Sigma}_0(\tau_0;\mu,\phi;\mu_0,\phi_0) = \sum_{n=1,3,\ldots}^{\infty} \mathbf{S}_n(\tau_0;\mu,\phi;\mu_0,\phi_0) \quad , \tag{31}$$

$$\mathbf{S}_1(\tau_0;\mu,\phi;\mu_0,\phi_0) = \mathbf{S}(\tau_0;\mu,\phi;\mu_0,\phi_0) \quad , \tag{32}$$

$$\mathbf{S}_n(\tau_0;\mu,\phi;\mu_0,\phi_0) = \frac{1}{4\pi}\int_0^1\int_0^{2\pi} \mathbf{S}(\tau_0;\mu,\phi;\mu',\phi')\,\mathbf{S}_{n-1}(\tau_0;\mu',\phi';\mu_0,\phi_0)\,\frac{d\mu'}{\mu'}\,d\phi' \quad ,$$

if n is odd, (33)

and

$$\mathbf{S}_n(\tau_0;\mu,\phi;\mu_0,\phi_0) = \frac{1}{4\pi}\int_0^1\int_0^{2\pi} \mathbf{S}^*(\tau_0;\mu,\phi;\mu',\phi')\,\mathbf{S}_{n-1}(\tau_0;\mu',\phi';\mu_0,\phi_0)\,\frac{d\mu'}{\mu'}\,d\phi' \quad ,$$

if n is even. (34)

Similar doubling equations for $\mathbf{S}^*$ and $\mathbf{T}^*$ can also be obtained. However, in the case of a homogeneous atmosphere the following simple relations hold:

$$\mathbf{S}(\tau_0;\mu,\phi;\mu_0,\phi_0) = \mathbf{S}^*(\tau_0;\mu,\phi_0;\mu_0,\phi) \quad , \tag{35}$$

and

$$\mathbf{T}(\tau_0;\mu,\phi;\mu_0,\phi_0) = \mathbf{T}^*(\tau_0;\mu,\phi_0;\mu_0,\phi) \quad , \tag{36}$$

so that the doubling equations for $\mathbf{S}^*$ and $\mathbf{T}^*$ are needless.

The matrices $\mathbf{S}$ and $\mathbf{T}$ for the initial layer can be obtained respectively from (18) and (19) by replacing the phase function p in these equations by the phase matrix $\mathbf{p}$. As in the case of the scalar equations, by means of the Fourier expansion of the matrices concerned with respect to $(\phi_0 - \phi)$, we can separate the doubling equation for $\mathbf{S}$ (or $\mathbf{T}$) into a set of equation corresponding to the coefficient matrices of respective degrees. The expansion of the elements of the matrices concerned is shown in general form as follows:

$$M_{ij}(\tau_0;\mu,\phi;\mu_0,\phi_0) = M_{ij}^m(\tau_0;\mu,\mu_0)\cos m(\phi_0 - \phi) \quad , \tag{37}$$

for $i = 1,2;\ j = 1,2$ or $i = 3,4;\ j = 3,4$,

$$M_{ij}(\tau_0;\mu,\phi;\mu_0,\phi_0) = M_{ij}^m(\tau_0;\mu,\mu_0)\sin m(\phi_0 - \phi) \quad , \tag{38}$$

for $i = 1,2;\ j = 3,4$ or $i = 3,4;\ j = 1,2$,

where the matrix $\mathbf{M} = (M_{ij})$ represents any matrix concerned.

Inserting (37) and (38) into (30), we have

$$\mathbb{S}^m(2\tau_0;\mu,\mu_0) = \mathbb{S}^m(\tau_0;\mu,\mu_0) + e^{-\tau_0/\mu} \sum_0^m (\tau_0;\mu,\mu_0)\, e^{-\tau_0/\mu_0}$$

$$+ e^{-\tau_0/\mu_0} \frac{1}{(4 - 2\delta_{0,m})} \int_0^1 \mathbb{T}^{*m}(\tau_0;\mu,\mu') \left| \sum_0^m (\tau_0;\mu',\mu_0) \frac{d\mu'}{\mu'} \right.$$

$$+ e^{-\tau_0/\mu} \frac{1}{(4 - 2\delta_{0,m})} \int_0^1 \left. \sum_0^m (\tau_0;\mu,\mu') \right| \mathbb{T}^m(\tau_0;\mu',\mu_0) \frac{d\mu'}{\mu'}$$

$$+ \frac{1}{16\pi^2} \int_0^1 \int_0^1 \mathbb{T}^{*m}(\tau_0;\mu,\mu'') \left| \sum_0^m (\tau_0;\mu'',\mu') \right| \mathbb{T}^m(\tau_0,\mu',\mu_0) \frac{d\mu'}{\mu'} \frac{d\mu''}{\mu''} \quad , \tag{39}$$

where $\mathbb{M}^m = (M_{ij}^m)$, and the operation $\mathbb{C} = \mathbb{A}/\mathbb{B}$ is defined as follows:

$$C_{ij} = A_{i1} B_{ij} + A_{i2} B_{2j} - A_{i3} B_{3j} - A_{i4} B_{4j} \quad , \tag{40}$$

for $i = 1,2;\ j = 1,2$ or $i = 3,4;\ j = 3,4$,

and

$$C_{ij} = A_{i1} B_{1j} + A_{i2} B_{2j} + A_{i3} B_{3j} + A_{i4} B_{4j} \quad , \tag{41}$$

for $i = 1,2;\ j = 3,4$ or $i = 3,4;\ j = 1,2$.

Effectiveness of this method has been shown by Hansen (1971b) in evaluating the intensity and degree of polarization of the near infrared radiation diffusely reflected by water clouds.

2.2 Matrix Method

Twomey et al. (1966) have shown that if the radiation field is approximated by a discrete distribution at points or a latitude circles on the unit sphere, matrix relationships can be written between the incident and reflected or transmitted radiation fields, and that the reflection and transmission matrices thus defined satisfy algebraic equations which can be used to compute the optical properties of thick layers by building up thick layers from thinner sub-layers.

More recently, this method has been extended by Tanaka (1971a) and by Jacobowitz and Howell (1971) for the case in which polarization is taken into account. However, the matrix method and doubling method can be considered to be essentially equivalent. For instance, starting from the doubling equation (24), we can derive the matrix equation as follows:

If we introduce

$$\tilde{M}(\tau_0;\mu,\mu_0) = \frac{1}{(4 - 2\delta_{0,m})\mu} M^m(\tau_0;\mu,\mu_0) \quad , \tag{42}$$

$$M^m \equiv (S^m, T^m, \Sigma_0^m) \quad , \tag{43}$$

equation (24) can be written as

$$\begin{aligned}\tilde{S}^m(2\tau_0;\mu,\mu_0) = {} & \tilde{S}^m(\tau_0;\mu,\mu_0) + e^{-\tau_0/\mu} \tilde{\Sigma}_0^m(\tau_0;\mu,\mu_0) e^{-\tau_0/\mu_0} \\ & + e^{-\tau_0/\mu_0} \int_0^1 \tilde{T}^m(\tau_0;\mu,\mu') \tilde{\Sigma}_0^m(\tau_0;\mu',\mu_0) d\mu' \\ & + e^{-\tau_0/\mu} \int_0^1 \tilde{\Sigma}_0^m(\tau_0;\mu,\mu') \tilde{T}^m(\tau_0;\mu',\mu_0) d\mu' \\ & + \int_0^1\int_0^1 \tilde{T}^m(\tau_0;\mu,\mu'') \tilde{\Sigma}_0^m(\tau_0;\mu'',\mu') \tilde{T}^m(\tau_0;\mu',\mu_0) d\mu' d\mu''\end{aligned} \tag{44}$$

Now we shall approximate the radiation field by discrete distribution and introduce the $N \times N$ matrix $\tilde{\mathbb{M}}^m$ ($\equiv \tilde{\mathbb{S}}^m, \tilde{\mathbb{T}}^m, \tilde{\mathbb{\Sigma}}_0^m$) whose elements are given by

$$\tilde{M}_{ij}^m(\tau_0) = \tilde{M}^m(\tau_0;\mu_i,\mu_j) w_i \quad , \tag{45}$$

$$(i,j = 1,2,\ldots,N) \ ,$$

where w_i represents the quadrature weight at the division $\mu = \mu_i$. By use of (45), equation (44) can be written as

$$\begin{aligned}\tilde{\mathbb{S}}^m(2\tau_0) = {} & \tilde{\mathbb{S}}^m(\tau_0) + \mathbb{E}(\tau_0) \tilde{\mathbb{\Sigma}}_0^m(\tau_0) \mathbb{E}(\tau_0) \\ & + \tilde{\mathbb{T}}^m(\tau_0) \tilde{\mathbb{\Sigma}}_0^m(\tau_0) \mathbb{E}(\tau_0) + \mathbb{E}(\tau_0) \tilde{\mathbb{\Sigma}}_0^m(\tau_0) \tilde{\mathbb{T}}^m(\tau_0) \\ & + \tilde{\mathbb{T}}^m(\tau_0) \tilde{\mathbb{\Sigma}}_0^m(\tau_0) \tilde{\mathbb{T}}^m(\tau_0) \quad ,\end{aligned} \tag{46}$$

where $\mathbb{E}(\tau_0)$ is the diagonal matrix whose elements are given by

$$E_{ij} = e^{-\tau_0/\mu_i} \quad , \quad \text{if } i = j \quad ,$$
$$= 0 \quad , \quad \text{if } i \neq j \quad , \tag{47}$$

and

$$\bar{\Sigma}^m_0(\tau_0) = \sum_{n=1,3,\ldots}^{\infty} \mathbb{S}^m_n(\tau_0) \quad , \tag{48}$$

$$\mathbb{S}^m_1(\tau_0) = \mathbb{S}^m(\tau_0) \quad ,$$
$$\mathbb{S}^m_n(\tau_0) = \mathbb{S}^m(\tau_0)\, \mathbb{S}^m_{n-1}(\tau_0) \quad . \tag{49}$$

Inserting (47), (48) and (49) into (46), we have the following alternative form of (46):

$$\begin{aligned} \mathbb{S}^m(2\tau_0) &= \mathbb{S}^m(\tau_0) + (\tilde{\mathbb{T}}^m(\tau_0) + \mathbb{E}(\tau_0))\, \mathbb{S}^m(\tau_0) \\ &\quad \times (\mathbf{1} + [\mathbb{S}^m(\tau_0)]^2 + [\mathbb{S}^m(\tau_0)]^4 + \cdots)\, (\tilde{\mathbb{T}}^m(\tau_0) + \mathbb{E}(\tau_0)) \\ &= \mathbb{S}^m(\tau_0) + (\tilde{\mathbb{T}}^m(\tau_0) + \mathbb{E}(\tau_0))\, (\mathbf{1} - [\mathbb{S}^m(\tau_0)]^2)^{-1}\, (\tilde{\mathbb{T}}^m(\tau_0) + \mathbb{E}(\tau_0)) \quad , \end{aligned} \tag{50}$$

where $\mathbf{1}$ is the identity matrix. Similarly, from the doubling equation for $T^m(2\,\tau_0;\,,\,\tau_0)$ we can derive

$$\begin{aligned} \tilde{\mathbb{T}}^m(2\tau_0) + \mathbb{E}(2\tau_0) &= (\tilde{\mathbb{T}}^m(\tau_0) + \mathbb{E}(\tau_0)) \\ &\quad \times (\mathbf{1} + [\mathbb{S}^m(\tau_0)]^2 + [\mathbb{S}^m(\tau_0)]^4 + \cdots)\, (\tilde{\mathbb{T}}^m(\tau_0) + \mathbb{E}(\tau_0)) \\ &= (\tilde{\mathbb{T}}^m(\tau_0) + \mathbb{E}(\tau_0))\, (\mathbf{1} - [\mathbb{S}^m(\tau_0)]^2)^{-1}\, (\tilde{\mathbb{T}}^m(\tau_0) + \mathbb{E}(\tau_0)) \quad . \end{aligned} \tag{51}$$

Equations (50) and (51) are equivalent to the matrix relations derived by Twomey et al. (1966) for the case in which the thicknesses of the initial and second layers are made to be equal ($\tau_1 = \tau_2 = \tau_0$).

Tanaka (1971a) has extended the matrix method for a more general case in which polarization of the radiation field and inhomogeneity of the atmosphere are taken into account. In this case, the matrix method is expressed by simultaneous algebraic relations with regard to four matrices which correspond to $\mathbf{S}$, $\mathbf{T}$, $\mathbf{S}^*$ and $\mathbf{T}^*$. By use of the interaction principle, which has been introduced by Preisendorfer (1965) and which is the extension of the principle of invariance introduced by Ambartsumian (1943) and Chandrasekhar (1950), Hunt and Grant (1969) have made a more general formulation of the matrix method which involves evaluation of not only reflected and transmitted fields but also internal fields.

Effectiveness of the matrix method is of the same order as that of the doubling method. Both methods are effective for a homogeneous atmosphere even if it is thick, and not so effective for a thick inhomogeneous atmosphere. However, both methods are effectively applicable to the earth's atmosphere, because its optical thickness is not so thick ($\tau \leq 1$), although it is inhomogeneous and turbid.

2.3 Iterative Method

The method of solving equation of radiative transfer by successive iteration has been adopted by many researchers. In this sense it is one of the most popular methods. The Neumann series method which has extensively used by Irvine (1965, 1968) consists of expanding the radiation field by orders of scattering and of determining successively higher order terms of scattering, starting from lower order terms. Herman and Browning (1965) have proposed to solve the formal solution for the specific intensity of equation of transfer, by means of the iterative procedure using the Gauss-Seidel technique. Herman et al. (1971) have applied this method to the turbid atmospheres. So we shall describe briefly on this method.

The equation of transfer appropriate to the case in which polarization is considered can be obtained by changing I, p, and F in (1) to $\mathbf{I}$, $\mathbf{p}$, and $\mathbf{F}$ respectively, where $\mathbf{I}$ and $\mathbf{F}$ are the Stokes representations of the field intensity and incident solar flux, respectively, and $\mathbf{p}$ is the phase matrix. The formal solutions of this equation can be written as

$$\mathbf{I}(\tau_n;+\mu,\phi) = \mathbf{I}(\tau_{n+1},+\mu,\phi)\, e^{-(\tau_{n+1} - \tau_n)/\mu} + \int_{\tau_n}^{\tau_{n+1}} \mathbf{J}(t;+\mu,\phi)\, e^{-(t - \tau_n)/\mu}\, \frac{dt}{\mu} \quad , \tag{52}$$

$$\mathbf{I}(\tau_n;-\mu,\phi) = \mathbf{I}(\tau_{n-1},-\mu,\phi)\, e^{-(\tau_n - \tau_{n-1})/\mu} + \int_{\tau_{n-1}}^{\tau_n} \boldsymbol{\mathcal{J}}(t;+\mu,\phi)\, e^{-(\tau_n - t)/\mu} \frac{dt}{\mu} \quad , \tag{53}$$

where $0 = \tau_0 < \tau_{n-1} < \tau_n < \tau_{n+1} < \tau_N = \tau_S$, and $\boldsymbol{\mathcal{J}}$ is the source vector given by

$$\boldsymbol{\mathcal{J}}(t;\pm\mu,\phi) = \frac{1}{4\pi} \int_0^{2\pi} \int_{-1}^{+1} \mathbf{P}(\pm\mu,\phi;\mu',\phi')\, \mathbf{I}(t,\pm\mu',\phi')\, d\phi'\, d\mu' + \frac{1}{4} \mathbf{P}(\pm\mu,\phi;\, -\mu_0,\phi_0)\, \mathbf{F}\, e^{-t/\mu_0} \tag{54}$$

Here it is assumed that the atmosphere is homogeneous and $\mathbf{P}$ is independent of τ . If we consider the p-th Stokes parameter I_p , equation (53) becomes

$$I_p(\tau_n,-\mu,\phi) = I_p(\tau_{n-1},-\mu,\phi)\, e^{-(\tau_n - \tau_{n-1})/\mu} + \int_{\tau_{n-1}}^{\tau_n} \mathcal{J}_p(t;-\mu,\phi)\, e^{-(\tau_n - t)/\mu} \frac{dt}{\mu} \quad , \tag{55}$$

and

$$\mathcal{J}_p(t;-\mu,\phi) = \frac{1}{4\pi} \sum_{q=1}^{4} \int_0^{2\pi} \int_{-1}^{+1} P_{pq}(-\mu,\phi;\pm\mu',\phi')\, I_q(t;\pm\mu',\phi')\, d\mu'\, d\phi' + \frac{1}{4} \sum_{q=1}^{4} P_{pq}(-\mu,\phi;-\mu_0,\phi_0)\, F_q\, e^{-t/\mu_0} \quad , \tag{56}$$

where $\mathcal{J}_p$ is the p-th element of the source vector $\boldsymbol{\mathcal{J}}$ and P_{pq} is the (p,q) element of the phase matrix $\mathbf{P}$. Equation for $I_p(\tau_n,+\mu,\phi)$ can also be obtained similarly. The problem to solve these equations under certain boundary conditions, e.g., $I_p(0,-\mu,\phi) = 0$ and $I_p(\tau_s,+\mu,\phi) = 0$, is a so-called two-point boundary value problem, and its numerical solution can be obtained by the Gauss-Seidel iterative technique.

Now let us denote $I_p(\tau_n,-\mu,\phi)$ by $I_p^{(n)}(-\mu,\phi)$ and $\tau_n - \tau_{n-1}$ by $\Delta\tau$, then equation (55) can be written as

$$I_p^{(n)}(-\mu,\phi) = I_p^{(n-1)}(-\mu,\phi)\, e^{-\Delta\tau/\mu} + \mathcal{J}_p(-\mu,\phi)\,(1 - e^{-\Delta\tau/\mu}) \quad , \tag{57}$$

where $\bar{\mathcal{J}}_p(-\mu,\phi)$ is the average value of $\mathcal{J}_p$ defined by

$$\bar{\mathcal{J}}_p(-\mu,\phi) = \int_{\tau_{n-1}}^{\tau_n} \mathcal{J}_p(t;-\mu,\phi)\, e^{-(\tau_n - t)/\mu}\, \frac{dt}{\mu} \Big/ (1 - e^{-\Delta\tau/\mu}) \quad . \tag{58}$$

If $\Delta\tau$ is small, $\bar{\mathcal{J}}_p$ is approximated by the value of $\mathcal{J}_p(t;-\mu,\phi)$ at $t = \tau_{n-1/2} = \tau_n - \Delta\tau/2$. Namely from (56), we have

$$\begin{aligned} \bar{\mathcal{J}}_p(-\mu,\phi) \simeq\ & \mathcal{J}_p^{(n-1/2)}(-\mu,\phi) \\ & + \frac{1}{4\pi} \sum_{q=1}^{4} \int_{-1}^{+1} \int_{0}^{2\pi} P_{pq}(-\mu,\phi;\pm\mu',\phi')\, I_q^{(n-1/2)}(\pm\mu',\phi')\, d\mu'\, d\phi' \\ & + \frac{1}{4} \sum_{q=1}^{4} P_{pq}(-\mu,\phi;-\mu_0,\phi_0)\, F_q^{(n-1/2)} \quad , \end{aligned} \tag{59}$$

where $F_q^{(n-1/2)} = F_q\, e^{-(\tau_n - \Delta\tau/2)/\mu_0}$. In practical computation the evaluation of the integral $\int_{-1}^{+1}\int_{0}^{2\pi}$ ------ $d\mu'\, d\phi'$ is made by use of the quadrature formula.

Inserting (59) into (57), and rewriting it with respect to levels n, n-1, n-2, instead of levels n, n-1/2, and n-1, we have

$$\left.\begin{aligned} I_p^{(1)}(-\mu,\phi) &= \mathcal{J}_p^{(0)}(-\mu,\phi)\,(1 - e^{-\Delta\tau/\mu}) \quad , \\ I_p^{(n)}(-\mu,\phi) &= I_p^{(n-2)}(-\mu,\phi)\, e^{-2\Delta\tau/\mu} + \mathcal{J}_p^{(n-1)}(-\mu,\phi)\,(1 - e^{-2\Delta\tau/\mu}) \quad . \end{aligned}\right\} \tag{60}$$

$(n \geq 2)$

The only non-zero parameters at the level $\tau = 0$ are those associated with the outward directed intensities for which $\mu > 0$ (i.e., the reflected radiation) and the incident parallel flux represented by $F_q^{(0)}$. However, the outward directed intensities are unknown initially, and thus, for the purpose of getting the solution started, they are assumed to be zero. This gives the first approximation to the parameter $I_p^{(1)}$. The second equation in (60) is then used to compute the parameters at the second and succeeding levels, for $\mu < 0$. Parameters for $\mu > 0$ are assumed to be zero for all of these initial calculations. At the bottom of the medium ($\tau = \tau_s$) initial calculations for all $I_p^{(n)}(-\mu,\phi)$ have been made.

Starting with (52) and utilizing the boundary condition, $I_p(\tau_s;+\mu,\phi) = 0$, a pair of computing equations analogous to (60) may be derived for the Stokes parameters for $\mu > 0$. Using the equations so obtained, these parameters are computed starting with the first level above the bottom and working back up to the level $\tau = 0$. However, now values for Stokes parameters for $\mu < 0$ have already been computed, and these values are used in the numerical evaluation of the source term. When the level $\tau = 0$ is reached, initial values for all of the unknowns have been computed, and the same process is now repeated, utilizing the previously calculated values for all unknowns appearing on the right hand side of the set of equations, until successive values of the same variable agree to within some specified tolerance.

In the above approach, double integrals with respect to the polar and azimuthal angles are directly involved, so that it is not necessarily advantageous in saving computing time as well as computer storage. In this respect, Dave and Gazdag (1970) have suggested an approach in which the phase function (and related function) are expanded as a Fourier cosine series whose total number of terms varies with the angle of incidence and reflection.

There are various kinds of the iterative method other than shown above. The merit of the above iterative method is that in addition to the solution to the problem of diffuse reflection and transmission, that for the internal field can also be obtained by it, and that no special difficulty arises in solving the problem for an inhomogeneous atmosphere. The disadvantage of this method is that it becomes time consuming when the optical thickness increases. It is due to simple addition of thin layers by this method, contrary to the doubling method.

2.4 Method of Discrete Ordinates

Chandrasekhar (1946, 1950) has developed a method to replace the equation of transfer (1) by the system of $2n$ linear differential equations, by approximating the continuous radiation field with the $2n$ discrete streams of radiation. Recently this method is not so widely used as before, except by Samuelson (1965, 1969) and Yamamoto et al. (1971) for the study of transfer of thermal radiation inside the clouds. One of the reasons will be due to somewhat insufficient explanation in Chandrasekhar's statement in obtaining the roots of the characteristic equation, and due to difficulty of determining the constants of integration for optically thick, but finite layers. As can be seen below these difficulties can be avoided, so that the method of discrete ordinates still has wide applicability. We shall review the method following Chandrasekhar.

The phase function $p(\mu,\phi;\mu',\phi')$ is expanded by the Legendre polynomials, P_ℓ, in the form

$$p(\mu,\phi;\mu',\phi') = p(\cos\Theta) = \sum_{\ell=0}^{N} \tilde{\omega}_\ell P_\ell(\cos\Theta) \quad , \tag{61}$$

where $\tilde{\omega}_0$ is albedo for single scattering, $\tilde{\omega}_\ell$'s $(\ell = 1, ---, N)$ are constants independent of Θ Θ being the angle of scattering, and $\cos\Theta = \mu\mu' + (1 - \mu^2)^{1/2} (1 - \mu'^2)^{1/2} \cos(\phi' - \phi)$. Therefore we have

$$P_\ell(\cos\Theta) = P_\ell[\mu\mu' + (1 - \mu^2)^{1/2} (1 - \mu'^2)^{1/2} \cos(\phi' - \phi)] \quad . \tag{62}$$

By use of the addition theorem of spherical harmonics for (62), we have

$$P_\ell(\cos\Theta) = P_\ell(\mu) P_\ell(\mu') + 2 \sum_{m=1}^{\ell} \frac{(\ell - m)!}{(\ell + m)!}$$

$$\times P_\ell^m(\mu) P_\ell^m(\mu') \cos m(\phi' - \phi) \quad . \tag{63}$$

Corresponding to the above expansion of the phase function, the intensity of radiation is also expanded as follows:

$$I(\tau,\mu,\phi) = I^{(0)}(\tau,\mu) + \sum_{m=1}^{N} I^{(m)}(\tau,\mu) \cos m(\phi_0 - \phi) \quad . \tag{64}$$

Inserting (61), (63) and (64) into equation (1), it can be separated into $(N + 1)$ independent equations with respect to $I^{(m)}$ as follows:

$$\mu \frac{dI^{(m)}(\tau,\mu)}{d\tau} = I^{(m)}(\tau,\mu) - \frac{1}{2} \sum_{\ell=m}^{N} \frac{(\ell - m)!}{(\ell + m)!} \tilde{\omega}_\ell P_\ell^m(\mu) \int P_\ell^{(m)}(\mu') I^{(m)}(\tau,\mu') d\mu'$$

$$- \left(\frac{2 - \delta_{0,m}}{4}\right) F e^{-\tau/\mu_0} \sum_{\ell=m}^{N} (-1)^{\ell+m} \frac{(\ell - m)!}{(\ell + m)!} \tilde{\omega}_\ell P_\ell^m(\mu) P_\ell^m(\mu_0) \quad , \tag{65}$$

$$(m = 0, 1, 2, ---, N) \quad .$$

In the method of discrete ordinates the integral involved in (65) is replaced by sums according to Gauss's quadrature formula, and each of the $(N + 1)$ equations is replaced by an equivalent system of linear equations of order $2n$. Solutions must be sought in approximations n such that

$$4n - 1 > 2N \quad . \tag{66}$$

The $2n(N+1)$ linear inhomogeneous differential equations which replace the $(N+1)$ linear inhomogeneous integro-differential equations given by (65) are

$$\mu_i \frac{dI^{(m)}(\tau,\mu_i)}{d\tau} = I^{(m)}(\tau,\mu_i) - \frac{1}{2} \sum_{\ell=m}^{N} \frac{(\ell-m)!}{(\ell+m)!} \tilde{\omega}_\ell P_\ell^m(\mu_i) \sum_j a_j P_\ell^m(\mu_j) I^{(m)}(\tau,\mu_j)$$

$$- \left(\frac{2-\delta_{0,m}}{4}\right) F e^{-\tau/\mu_0} \sum_{\ell=m}^{N} (-1)^{\ell+m} \frac{(\ell-m)!}{(\ell+m)!} \tilde{\omega}_\ell P_\ell^m(\mu_i) P_\ell^m(\mu_0) \tag{67}$$

$$(i = \pm 1, ---, \pm n; \quad j = \pm 1, ---, \pm n; \quad 0 \le m \le N) \quad ,$$

where a_j's are the weights appropriate to the Gauss's quadrature formula based on the division μ_i of the interval $(-1, +1)$.

The complete solution of the system of equations given by (67) involves $2n(N+1)$ constants of integration, which are to be determined from the following boundary conditions;

$$\left.\begin{aligned} I^{(m)}(0,-\mu_i) &= 0 \ , \\ I^{(m)}(\tau_1,+\mu_i) &= 0 \ , \end{aligned}\right\} \quad (i = 1, ---, n; \quad m = 0, 1, ---, N) \quad . \tag{68}$$

The solution for (67) can be obtained by an entirely analogous method for every m so that we shall here describe the method of obtaining the solution for $m = 0$, i.e., the azimuthally independent case. The general solution for the homogeneous part of (67) is given by

$$I_G^{(0)}(\tau,\mu_i) = \sum_{\alpha=1}^{n} \frac{L_\alpha e^{-k_\alpha \tau}}{1+\mu_i k_\alpha} \left[\sum_{\ell=0}^{N} \tilde{\omega}_\ell \xi_\ell(+k_\alpha) P_\ell(\mu_i) \right]$$

$$+ \sum_{\alpha=1}^{n} \frac{L_{-\alpha} e^{+k_\alpha \tau}}{1-\mu_i k_\alpha} \left[\sum_{\ell=0}^{N} \tilde{\omega}_\ell \xi_\ell(-k_\alpha) P_\ell(\mu_i) \right] \ , \tag{69}$$

$$(i = \pm 1, ---, \pm n) \quad ,$$

where $L_{\pm\alpha}$ are the $2n$ constants of integration, and k_α's are the roots of the following system of characteristic equations;

$$\xi_\ell(k) = \frac{1}{2} \sum_{j=-n}^{n} \frac{a_j P_\ell(\mu_j)}{1+\mu_j k} \sum_{\alpha=0}^{N} \tilde{\omega}_\lambda \xi_\lambda(k) P_\lambda(\mu_j) \quad , \tag{70}$$

$$(\ell = 0, 1, ---, N) \quad .$$

In order to evaluate $k_{\pm\alpha}$, Chandrasekhar (1950) and Samuelson (1965) have used a single equation obtained from (70) by setting $\ell = 0$, i.e.,

$$1 = \frac{1}{2} \sum_{j=-n}^{n} \frac{a_j}{1 + \mu_j k} \sum_{\alpha=0}^{N} \tilde{\omega}_\lambda \, \xi_\lambda(k) \, P_\lambda(\mu_j) \quad , \tag{71}$$

and they stated that this equation is of order n in k^2 and involves $2n$ distinct nonvanishing roots occurring in pairs as $\pm k_\alpha (k_{-\alpha} = -k_\alpha)$ for the case of non-conservative scattering. Since the function $\xi_\ell(k)$ is even (or odd) with respect to k when ℓ is even (or odd), it is true that the roots occur in pairs. The order of equation (70) in k , however, is given for the case with $0 < \tilde{\omega}_0 < 1$ as follows:

$$\left.\begin{array}{ll} (2n + N) \ , & \text{for } N = \text{even and } \ell = \text{even} \ , \\ (2n + N - 2) \ , & \text{for } N = \text{even and } \ell = \text{odd} \ , \\ (2n + N - 1) \ , & \text{for } N = \text{odd and } \ell = \text{even and odd} \ . \end{array}\right\} \tag{72}$$

Thus it is evident that any equation in (70) including (71) has in general more than $2n$ roots. It is true that in the conservative case treated by Chandrasekhar, in which the phase function is expanded till the second order of Legendre polynomials, equation (70) has $2n$ roots. However, in more general cases as treated by Samuelson and also by Yamamoto et al., it can be shown by numerical calculation that any equation in (70) has more than $2n$ real roots. Therefore the $2n$ values of $k_{\pm\alpha}$ should be determined as the common roots of the system (70). [Yamamoto, Tanaka and Asano, 1971].

In order to complete the solution, a particular integral must be found which, when added to equation (69), satisfies equation (67). This particular integral is given in the form

$$I_p^{(0)}(\tau, \mu_i, \mu_0) = \frac{1}{4} F \frac{\gamma_0 \, e^{-\tau/\mu_0}}{1 + \mu_i/\mu_0} \left[\sum_{\ell=0}^{N} \tilde{\omega}_\ell \, \xi_\ell\left(\frac{1}{\mu_0}\right) P_\ell(\mu_i) \right] \quad , \qquad (i = \pm 1, \text{---}, \pm n) \ , \tag{73}$$

where

$$\gamma_0 = H(\mu_0) \, H(-\mu_0) \quad , \tag{74}$$

and

$$H(x) = \frac{1}{\mu_1 \cdots \mu_n} \frac{\prod_{j=1}^{n} (x + \mu_j)}{\prod_{\alpha=1}^{n} (1 + k_\alpha x)} \tag{75}$$

The integral given by equation (73), when added to the general solution in equation (69), comprises the complete solution to equation (67), and this is

$$I^{(0)}(\tau,\mu_i) = \sum_{\alpha=1}^{n} \frac{L_\alpha e^{-k_\alpha \tau}}{1 + \mu_i k_\alpha} \left[\sum_{\ell=0}^{N} \tilde{\omega}_\ell \, \xi_\ell(+k_\alpha) \, P_\ell(\mu_i) \right]$$

$$+ \sum_{\alpha=1}^{n} \frac{L_{-\alpha} e^{+k_\alpha \tau}}{1 - \mu_i k_\alpha} \left[\sum_{\ell=0}^{N} \tilde{\omega}_\ell \, \xi_\ell(-k_\alpha) \, P_\ell(\mu_i) \right]$$

$$+ \frac{1}{4} F \frac{\gamma_0 e^{-\tau/\mu_0}}{1 + \mu_i/\mu_0} \left[\sum_{\ell=0}^{N} \tilde{\omega}_\ell \, \xi_\ell\left(\frac{1}{\mu_0}\right) P_\ell(\mu_i) \right] , \qquad (76)$$

$$(i = \pm 1, \text{---}, \pm n) \ .$$

Now, the $2n$ constants of integration $L_{\pm\alpha}$ $(\alpha = 1, \text{---}, n)$ have to be determined by the following boundary conditions:

$$I^{(0)}(0,-\mu_j) = \sum_{\alpha=1}^{n} \frac{L_\alpha}{1 - \mu_i k_\alpha} \left[\sum_{\ell=0}^{N} \tilde{\omega}_\ell \, \xi_\ell(+k_\alpha) \, P_\ell(-\mu_j) \right]$$

$$+ \sum_{\alpha=1}^{n} \frac{L_{-\alpha}}{1 + \mu_j k_\alpha} \left[\sum_{\ell=0}^{N} \tilde{\omega}_\ell \, \xi_\ell(-k_\alpha) \, P_\ell(-\mu_j) \right]$$

$$+ \frac{1}{4} F \frac{\gamma_0}{1 - \mu_j/\mu_0} \left[\sum_{\ell=0}^{N} \tilde{\omega}_\ell \, \xi_\ell\left(\frac{1}{\mu_0}\right) P_\ell(-\mu_j) \right] , \qquad (77)$$

$$(j = 1, \text{---}, n) \ ,$$

and

$$I^{(0)}(\tau_1,+\mu_j) = \sum_{\alpha=1}^{n} \frac{L_\alpha e^{-k_\alpha \tau_1}}{1+\mu_j k_\alpha} \left[\sum_{\ell=0}^{N} \tilde{\omega}_\ell \xi_\ell(+k_\alpha) P_\ell(\mu_j) \right]$$

$$+ \sum_{\alpha=1}^{n} \frac{L_{-\alpha} e^{+k_\alpha \tau_1}}{1-\mu_j k} \left[\sum_{\ell=0}^{N} \tilde{\omega}_\ell \xi_\ell(-k_\alpha) P_\ell(\mu_j) \right]$$

$$+ \frac{1}{4} F \frac{\gamma_0 e^{-\tau/\mu_0}}{1+\mu_j/\mu_0} \left[\sum_{\ell=0}^{N} \tilde{\omega}_\ell \xi_\ell\left(\frac{1}{\mu_0}\right) P_\ell(\mu_j) \right] \qquad (78)$$

$$(j = 1, ---, n) \quad .$$

Samuelson (1969) stated that the method of discrete ordinates is not very amenable to studies involving the optical range $\tau > 1$ because of instabilities that are inherent in the method for the intermediate optical thickness, and that these instabilities arise as a result of the great disparity in magnitude of the coefficients, $e^{\pm k_\alpha \tau}$, in (76). Thus the direct application of the boundary conditions (77) and (78) to determine the constants $L_{\pm\alpha}$ leads to highly unstable solution when the magnitude of the exponent pairs, $\pm k_\alpha \tau$, differ greatly. To avoid this difficulty Yamamoto et al. (1971) have proposed to use, instead of (77) and (78), the following equations derived respectively from [(77) + (78)] and [(77) - (78)]:

$$\sum_{\alpha=1}^{n} M_\alpha \left[\frac{1}{1-\mu_j k_\alpha} \sum_{\ell=0}^{N} (-1)^\ell \tilde{\omega}_\ell \xi_\ell(k_\alpha) P_\ell(\mu_j) + \frac{e^{-k_\alpha \tau_1}}{1+\mu_j k_\alpha} \sum_{\ell=0}^{N} \tilde{\omega}_\ell \xi_\ell(k_\alpha) P_\ell(\mu_j) \right]$$

$$= I^{(0)}(0,-\mu_j) + I^{(0)}(\tau_1,+\mu_j) - I_p^{(0)}(0,-\mu_j,\mu_0) - I_p^{(0)}(\tau_1,\mu_j,\mu_0) \quad , \qquad (79)$$

$$(j = 1, ---, n) \quad ,$$

$$\sum_{\alpha=1}^{n} N_\alpha \left[\frac{1}{1 - \mu_j k_\alpha} \sum_{\ell=0}^{N} (-1)^\ell \tilde{\omega}_\ell \xi_\ell(k_\alpha) P_\ell(\mu_j) - \frac{e^{-k_\alpha \tau_1}}{1 + \mu_j k_\alpha} \sum_{\ell=0}^{N} \tilde{\omega}_\ell \xi_\ell(k_\alpha) P_\ell(\mu_j) \right]$$

$$= I^{(0)}(0,-\mu_j) - I^{(0)}(\tau_1,+\mu_j) - I_p^{(0)}(0,-\mu_j,\mu_0) + I_p^{(0)}(\tau_1,\mu_j,\mu_0) \quad , \qquad (80)$$

$$(j = 1, ---, n) \quad ,$$

where

$$\left.\begin{aligned} M_\alpha &= L_\alpha + L_{-\alpha} e^{+k_\alpha \tau_1} \\ N_\alpha &= L_\alpha - L_{-\alpha} e^{+k_\alpha \tau_1} \end{aligned}\right\} \quad (\alpha = 1, ---, n) \quad . \qquad (81)$$

The coefficients $L_{\pm\alpha}$ are directly obtained by the following relations:

$$\left.\begin{aligned} L_\alpha &= (M_\alpha + N_\alpha)/2 \quad , \\ L_{-\alpha} &= (M_\alpha - N_\alpha) e^{-k_\alpha \tau_1}/2 \quad , \end{aligned}\right\} \quad (\alpha = 1, ---, n) \quad , \qquad (82)$$

where M_α and N_α $(\alpha = 1, ---, n)$ are solutions of $2n$ simulataneous equations (79) and (80).

Equations (79) and (80) give stable solutions even for intermediate values of $k_\alpha \tau_1$. When its values becomes very large, $L_{\pm\alpha}$ obtained by (79), (80) and (82) tend to solutions identical to those for semi-infinitely thick atmosphere. It is thus shown that the method of discrete ordinates is useful for any optical thickness.

The method of discrete ordinates can be applicable in evaluating not only the reflected and transmitted lights at the boundaries of the atmosphere but also the internal radiation field. It can be applicable to layers of any thickness with a relatively short computing time. Most of the computing time in this method is consumed for the expansion of the phase function and the determination of the roots of the characteristic equations. When the forward peak of the phase function predominates, many terms are necessary for the expansion of it. As the double expansion of the phase function with respect to m and ℓ is used in this method, difficulty arising from strongly peaked phase function is more serious than in other methods. In this respect, the "truncated peak" approximation (see Potter, 1970 and Hansen, 1969a), which tends to decrease the anisotropy of the phase function by including some portion of the forward peak into the incident radiation, seems worth noticing in combined use with the method of discrete ordinates.

2.5 Monte Carlo Method

During the recent ten years many attempts have been carried out to apply the Monte Carlo method to the problems of multiple scattering of radiation in the atmosphere. In this method the solution is obtained by a series of statistical analyses, performed by applying mathematical operators to random numbers. The problem of the time-dependent scattering of the pulsed point source due to the cloud layer is solved by this method by Skumanich and Bhattachajie (1961), and then extensive applications of this method to the problem of radiative transfer have been made by Collins and Wells (1965). Later, they modified their code to include the effects of water vapor and carbon dioxide absorption (Collins et al. 1967) and to allow for molecular and aerosol polarization (Collins, 1968). Plass and Kattawar (1968) have also developed a similar computer code to that of Collins and Wells (1968), and solved the problem of diffuse reflection and transmission for clouds. Starting with this study they have carried out a series of reseaches taking into account effects of polarization, inhomogeneous stratification, absorption of gaseous constituents for realistic models of various systems, such as turbid atmospheres, clouds, and atmosphere-ocean systems. Danielson et al. (1969) have also applied the Monte Carlo method for the problem of transfer of visible radiation in the clouds.

One of the merits of the Monte Carlo method is that it can be applicable not only to a plane-parallel atmosphere but also to atmospheres of any geometry. Most interesting one for us is the spherical-shell atmosphere. Marchuk and Mikhailov (1967), Kattawar et al. (1971) and Collins et al. (1972) have attacked this case. Marchuk et al. have evaluated the intensity of diffusely reflected light as observed from the position of satellite. Kattawar et al. have evaluated the flux and polarization of the reflected light from the Venus atmosphere assuming several models for it. Collins et al. have studied the intensity and degree of polarization of the reflected and transmitted radiations on both Rayleigh and turbid atmospheres, taking into account scattering by molecules and aerosols as well as absorpition by gaseous constituents. Collins et al. (1972) have also developed a new code which is capable of estimating the Stokes parameters for discrete directions at the receiver position, by utilizing the backward Monte Carlo procedure.

Another merit of the Monte Carlo method is that no particular difficulties arise due to anisotropy of the phase function, complexity of the optical stratification and reflection characteristics of the underlying surface.

On the other hand, the disadvantage of the Monte Carlo method is that the standard deviations of the results obtained are roughly inversely proportional to the square root of the computing times. Therefore the method may not be suitable when high accuracy is required.

So far we have reviewed briefly methods of numerical solution of equation of radiative transfer from the point of view of application to realistic model atmospheres. The difficulty which arises, when the degree of anisotropy of the phase function is large, is more or less common in most of the methods. According to the doubling method or matrix method the reflected and transmitted lights can easily be evaluated however thick the layer is, provided that it be homogeneous. If the layer is inhomogeneous, it becomes difficult to treat a thick layer by these methods. The iterative method is effective in obtaining solutions for the reflected and transmitted radiations as well as for the internal field. However, it is unsuitable for a thick layer, irrespective of whether it be homogeneous or not. The method of discrete ordinates can be applicable to a layer of any thickness and leads

to the solutions for the reflected and transmitted radiation as well as the internal field. However, the difficulty due to anisotropy of the phase function is more serious than in other methods. The Monte Carlo method is more flexible than other methods in the point that it can be applicable to, for instance, the spherical-shell atmosphere. However, it is time consuming when high accuracy of computation is required. In conclusion, it will be difficult to say which method is effective in general. Anyway, because of the fact that the earth's atmosphere, even if it is turbid, is not so thick optically, can be considered approximately homogeneous, most of the problems in this field are now soluble, so far as the earth's atmosphere is concerned.

There are still other methods. For instance, Bellman and his collaborators (1966) have developed the method to transform the integro-differential equation of transfer into a system of simultaneous differential equations of the initial value type by the invariant imbedding technique. However, because of the reason that at present this method treats idealized models, we omitted its explanation

3. EFFECT OF AEROSOLS ON THE THERMAL REGIME OF THE EARTH

Recently, increase of man's activity, particularly of his industrial activity, has been changing his environment. Increase of aerosols in the atmosphere is one of the noticeable changes. This increase will affect the radiation field in the atmosphere and will result in the change in the heat budget of the earth-atmosphere system. Most of the up-to-date studies with respect to the turbid atmosphere were concentrated to clarify its optical side, such as the intensity of skylight and its state of polarization. However, it will become important to investigate its thermal effect. Recently, Rasool and Schneider (1971) have evaluated the change of the earth surface temperature due to increase of aerosols by use of the two-stream approximation in solving equation of radiative transfer. Yamamoto and Tanaka (1972) have solved the same problem utilizing the matrix method, and evaluated the change of the global albedo due to increase of aerosols and the resulting change in the heat budget of the earth. Their results will be shown below.

With regard to the vertical distribution of aerosols, that compiled by Elterman (Fig. 2) is used in their model atmospheres. As to the size distribution of aerosols, the "haze C" model proposed by Deirmendjian (1964) is used. This model simulates the size distribution in the continental air masses fairly well, and is given by

$$n(r) = \begin{cases} C \times 10^{4}, & \text{for } 0.03\mu \le r \le 0.1\mu \\ Cr^{-4}, & \text{for } 0.1\mu \le r \le 10\mu \end{cases},$$

where C is a constant and $n(r)dr$ is the number concentration of aerosols of radii between r and $r + dr$, included in the whole air column.

The optical thickness due to aerosols, τ_M, is then given by

$$\tau_M = \int_0^\infty \pi r^2 Q(\alpha,m)\, n(r)\, dr \quad , \tag{83}$$

where $\alpha = 2\pi r/\lambda$, and $Q(\alpha,m)$ is the efficiency factor of the Mie scattering. Because of the optical ineffectiveness of small particles (say, $r < 0.1\mu$) , and of the scarcity of large particles (say, $r > 10\mu$) , $n(r)$ in (83) can be replaced by Cr^{-4} over the whole range of the integral. Then we have

$$\tau_M = \beta \lambda^{-1} \tag{84}$$

where

$$\beta = 2\pi^2 C \int_0^\infty Q(\alpha,m)\, \alpha^{-2}\, d\alpha \quad . \tag{85}$$

In this study β is taken, instead of the aerosol amount, as a parameter representing the turbidity of the atmosphere. This quantity β has a meaning similar to that of the turbidity coefficient of Ångstrom, β_A , which is defined by $\tau_M = \beta_A \lambda^{-1.3}$.

As the value of the real part of refractive index of aerosols, $n_r = 1.50$ is assumed, and for its imaginary part, $n_i = 0$, 0.005, 0.01, 0.02, 0.05, and 0.1 are assumed, in order to cover inaccuracy involved in the determination of this quantity at present. Such quantities as the phase function, albedo for single scattering, extinction coefficient, etc., which are necessary for computation, are evaluated based on the Mie theory. The surface reflection is assumed to follow the Lambert law of reflection, and average reflectivity for sea and land surfaces is assumed to be $A_s = 0.05$ and $A_s = 0.15$ respectively. The values of turbidity are changed from $\beta = 0$ (the pure Rayleigh atmosphere) to $\beta = 0.4$ (corresponding to the atmosphere over large cities).

As the effect of polarization on the flux of radiation is small (e.g. Tanaka, 1971b), it is neglected. Also as we assume the horizontally homogeneous, plane-parallel atmosphere, we need to consider only the azimuthally independent part of the radiation field. Then equation of radiative transfer (1) becomes

$$\mu \frac{dI^{(0)}(\tau,\mu)}{d\tau} = I^{(0)}(\tau,\mu) - \frac{1}{2}\int_{-1}^{+1} p^{(0)}(\tau;\mu,\mu')\, I^{(0)}(\tau,\mu')\, d\mu'$$

$$- \frac{1}{4} F e^{-\tau/\mu_0} p^{(0)}(\tau;\mu,-\mu_0) \quad , \tag{86}$$

and the boundary conditions are given by

$$\left.\begin{aligned} I^{(0)}(0,-\mu) &= 0 \quad , \\ I^{(0)}(\tau_s,+\mu) &= I_g(+\mu) \quad , \end{aligned}\right\} \tag{87}$$

where τ_s is the optical thickness corresponding to the whole air column, and I_g is the intensity of the reflected radiation from the Lambert surface.

Yamamoto et al. have evaluated $I^{(0)}(0,+\mu)$ and $I^{(0)}(\tau_s,-\mu)$ as a function of λ and β. Here, as the atmosphere is inhomogeneous, the mixing ratio of aerosols varies with height, and accordingly the ratios $\beta_R^{(s)}/\beta^{(e)}$ and $\beta_M^{(s)}/\beta^{(e)}$ are functions of τ, where $\beta_R^{(s)}$ and $\beta_M^{(s)}$ are the volume scattering coefficient of molecules and aerosols respectively. To compute the properties of the whole layer by building up the whole layer from thinner sublayers, they first divide the atmosphere into sufficient number of parts with same optical thickness and assume that each part is optically homogeneous. They then divide each part into several sublayers whose thickness are given by $\Delta\tau_1 = \tau_0$ and $\Delta\tau_n = 2^{n-2}\tau_0$ $(n \geq 2)$, where $\Delta\tau_n$ is the optical thickness of the n-th sublayer. An example of this dividing scheme is illustrated in Fig. 3. Steps of computation are also shown in the figure. Clearly, this combined scheme economizes computing time considerable in comparison to simply additive scheme.

If $I^{(0)}(0,+\mu)$ and $I^{(0)}(\tau_s,-\mu)$ are evaluated, the corresponding fluxes are given by

$$\left.\begin{aligned} R(\mu_0) &= 2\pi \int_0^1 I^{(0)}(0,+\mu)\mu \, d\mu \quad , \\ T(\mu_0) &= 2\pi \int_0^1 I^{(0)}(\tau_s,-\mu)\mu \, d\mu \quad . \end{aligned}\right\} \tag{88}$$

It is evident that these quantities are dependent upon μ_0, although μ_0 is not explicitly involved in $I^{(0)}(0,+\mu)$ and $I^{(0)}(\tau_s,-\mu)$. The flux of the incident solar radiation referred to the horizontal top surface of the atmosphere is given by $\pi F\mu_0$. Therefore, the diffuse reflectivity $\mathcal{R}(\mu_0)$ and transmissivity $J(\mu_0)$ referred to $\pi F\mu_0$ are given by

$$\left.\begin{aligned} \mathcal{R}(\mu_0) &= R(\mu_0)/\pi F\mu_0 \\ J(\mu_0) &= T(\mu_0)/\pi F\mu_0 \quad . \end{aligned}\right\} \tag{89}$$

An average reflectivity $\overline{R}$ and transmissivity $\overline{J}$ over the sunlit hemisphere are then given by

$$\left.\begin{aligned} \overline{R} &= 2\int_0^1 R(\mu_0)\, d\mu_0/\pi F \quad , \\ \overline{J} &= 2\int_0^1 T(\mu_0)\, d\mu_0/\pi F \quad . \end{aligned}\right\} \tag{90}$$

Of course, the contribution of the direct solar radiation is not included in $T(\mu_0)$, $J(\mu_0)$ and $\bar{J}$. The transmitted flux and transmissivity of the direct solar radiation at $\tau = \tau_s$ are given by $\pi F \mu_0 e^{-\tau_s/\mu_0}$ and $e^{-\tau_s/\mu_0}$, respectively, and the average transmissivity of the direct solar radiation over the sunlit hemisphere is given by

$$2\int_0^1 e^{-\tau_s/\mu_0}\,\mu_0\,d\mu_0 = 2\,E_3(\tau_s) \quad , \tag{91}$$

where $E_3(\tau_s)$ is the exponential integral of the third order. Solutions of the equation of transfer were obtained for the spectral region from 0.3 to 2.3μ. Although values of R and J (or $\bar{R}$ and $\bar{J}$) are obtained as functions of λ, μ_0, β, A_s and n_i (or λ, β, A_s and n_i), it is not the purpose of the present paper to explain such detail.

The average value of $\bar{R}$ over wavelength, which is nothing but the global albedo A_0, is now given by

$$A_0 = \int_{0.3\mu}^{2.3\mu} \pi F(\lambda)\,\bar{R}(\lambda)\,d\lambda \Big/ \int_{0.3\mu}^{2.3\mu} \pi F(\lambda)\,d\lambda \quad . \tag{92}$$

It should be noticed that the effect of absorption by atmospheric absorption bands is not taken into account in A_0. Fig. 4 shows A_0 as a function of β and n_i for two cases of $A_s = 0.05$ and $A_s = 0.15$. An interesting feature is that when n_i is small, A_0 increases with increase of β, while for very large values of n_i, A_0 decreases with increase of β.

In the above calculations we assumed cloudless atmospheres. Actually, however, about half of the earth surface is covered by clouds. Because of the large optical thickness of normal clouds, which is about two orders of magnitude greater than that of a cloudless atmosphere, the effect of aerosols will be reduced in a cloudy atmosphere.

If we designate the global albedo of the real atmosphere by A, then we have

$$A = nA_c + (1 - n)\,A_0 \quad , \tag{93}$$

where n is the global average cloud amount, and A_c is its average albedo. Based on the estimation by Robinson (1966) and Budyko (1969), we shall adopt the values $n = 0.05$ and $A_c = 0.5$. If we assume that the overall area ratio of ocean to land, 0.71: 0.29 is applicable to each latitudinal belt, appropriate values of A_0 for given β and n_i values can easily be obtained from the curves of A_0 in Fig. 4. Accordingly, we can estimate the values of A, which are also shown in Fig. 4. It is seen that the effect on A due to changes in β and n_i has been significantly reduced due to the existence of clouds. Still it can be seen that A decreases with increase of β for a very large value of n_i ($n_i = 0.1$).

Based on the above estimation of A we shall next discuss the effect of increase of aerosols on the thermal regime of the earth by use of a simple global model.

An equivalent blackbody temperature T_e (°K) of the earth-atmosphere system, which corresponds to the net incident solar energy, is given by

$$\pi R^2 S(1 - A) = 4\pi R^2 \sigma T_e^4 \quad , \tag{94}$$

where R is the radius of the earth, S is the solar constant, and σ is the Stefan-Boltzmann constants. Taking the value of $T_e = 254.1$ K for the molecular atmosphere ($\beta = 0$) as a reference, the value of ΔT_e is shown in Fig. 5 as a function of β, with n_i as a parameter. It can be seen from the figure that for small values of n_i, ΔT_e decreases with increase of β, whereas for $n_i = 0.05$ no appreciable change of ΔT_e vs. β is seen; for values of n_i larger than 0.05, ΔT_e increase with increase of β.

A similar estimation of global average temperature near the earth surface, T_s can be made as follows: If we let the global average outgoing longwave flux from the top if the atmosphere be I, then

$$\pi R^2 S(1 - A) = 4\pi R^2 I \quad . \tag{95}$$

According to Budyko (1969), I is expressed empirically as a function of T_s as

$$I = a + bT_s - (a_1 + b_1 T_s)n \tag{96}$$

where n is the global clouds amount, and a, b, a_1, and b_1 are numerical constants. If I is expressed by kcal cm^{-2} $month^{-1}$, $a = 14.0$, $b = 0.14$, $a_1 = 3.0$ and $b_1 = 0.10$ are the values evaluated by Budyko. Again taking the value of $T_s = 292.0$ K as a reference for a molecular atmosphere ($\beta = 0$), the form of the functional variation of ΔT_s with β and n_i, shown in Fig. 6, is seen to be similar to that of ΔT_e given in Fig. 5. It is noticed, however, that the overall changes of ΔT_s are larger than those of ΔT_e. It is shown that the results obtained by Yamamoto and Tanaka agree fairly well with that obtained by Rasool and Schneider, though the latter being restricted to the case of small n_i.

Corresponding to the behavior of A_0, the transmissivity averaged over the sunlit hemisphere and wavelength is shown in Fig. 7. This figure shows that the average transmissivity of diffuse radiation increases with increase of β, but it decreases with increase of n_i. The average transmissivity of the direct solar radiation versus β is also shown in the figure as a single curve irrespective of the value of β. Curves indicated by (DIRECT + DIFFUSE) mean the total transmissivity on the earth surface. Because of the predominant contribution of direct solar radiation, it decreases with increase of β and n_i. The important point shown in this figure is that transmissivity and accordingly the intensity of transmitted radiation depends strongly upon n_i. This fact suggests us the possibility of determining the value of n_i from the field observations of the direct solar and sky radiations and the careful analysis of the observed results.

Fig. 8 presents the heating rate (°C day^{-1}) due to absorption of solar radiation by aerosols averaged over the globe and whole air column. It shows that the heating rate evidently increases with the increase of β, n_i, and A_s.

In conclusion, the effect of air pollution on the heat budget of the earth depends greatly upon the value of n_i. Namely, we are led to quite contrary conclusions depending upon where the true value of n_i is larger than 0.05 or not. Therefore a more accurate determination of n_i is badly needed.

It should be noticed that in the above computation, the effect of absorption of solar radiation in the near infrared region by water vapor and carbon dioxide is not taken into account. According to our recent evaluation (unpublished), if we take into account the absorption due to gaseous constituents, the value of the albedo A_0 decreases slightly from that shown in Fig. 4. However, the variation of A_0 due to increase of β is almost similar as the result shown in Fig. 4.

Of course, in a more accurate evaluation of the fluxes of radiation over the whole range of solar spectrum, it will be necessary to consider scattering and absorption by aerosols and absorption by gaseous constituents simultaneously. In this case, new difficulty arises in the absorption band region in evaluating multiple scattering process due to the fact that, in contrast to a smoothly varying property of n_i with regard to wavelength, absorption by gaseous constituents varies intensely with wavelength due to the line structure of the absorption band. It is extremely time consuming to follow this change directly.

In treating the above non-gray absorption problem, Yamamoto et al. (1970, 1971) and Hunt and Grant (1969) have used the mean transmission function for a spectral interval $\Delta\nu$ in the form of a finite sum of exponential terms, i.e.,

$$\frac{1}{\Delta\nu}\int_{\Delta\nu} e^{-k_\nu u}\, d\nu = \frac{1}{M}\sum_{i=1}^{M} e^{-a_i u} \quad , \tag{97}$$

where ν is the wavenumber, and k_ν and u are the volume absorption coefficient and the effective amount of absorbing gas, respectively. Since no interaction between radiation of different wavenumbers occurs in the radiative transfer process which we are considering, it is possible to adopt a new independent variable such that the absorption coefficient increase (or decrease) monotonously with increase or decrease of the new variable. Then a_i in the equation (97) is interpreted as the mean absorption coefficient in the i-th subinterval in the new wavenumber coordinate system.

The equation of radiative transfer (86), for instance, is then transformed to the following equation in the new wavenumber coordinate system:

$$\mu \frac{dI_i^{(0)}(\tau_i,\mu)}{d\tau_i} = I_i^{(0)}(\tau_i,\mu) - \frac{\tilde{\omega}_i}{2}\int_{-1}^{+1} p^{(0)}(\mu,\mu')\, I_i^{(0)}(\tau_i,\mu')\, d\mu'$$

$$- \frac{\tilde{\omega}_i}{4} F e^{-\tau_i/\mu_0} p^{(0)}(\mu,-\mu_0) \quad , \tag{98}$$

where $\tilde{\omega}_i$ is the albedo for single scattering, i.e., $\tilde{\omega}_i = \beta^{(s)}/(\beta^{(e)} + a_i)$, $\beta^{(s)}$ and $\beta^{(e)}$ being the volume scattering and extinction coefficients of aerosols, respectively, τ_i is the optical thickness for i-th subinterval and $P^{(0)}$ is the normalized phase function. Using the solution of equation (98), the solution of (86) averaged over a spectral interval $\Delta\nu$ is given in the form,

$$\overline{I_\nu^{(0)}}(x,\mu) = \frac{1}{\Delta\nu}\int_{\Delta\nu} I_\nu^{(0)}(\tau_\nu,\mu)\, d\nu = \frac{1}{M}\sum_{i=1}^{M} I_i^{(0)}(\tau_i,\mu) \quad , \tag{99}$$

where x is the geometrical thickness defined by

$$x = \tau_i/(\beta^{(e)} + a_i) = \tau_i/\beta_i \tag{100}$$

Evidently, this method is applicable to all methods of solving transfer equation described in Section 2.

4. HEATING OF THE LOWER ATMOSPHERE DUE TO ABSORPTION OF SOLAR RADIATION BY AEROSOLS

In the preceeding section, we have evaluated the rate of heating due to aerosol absorption averaged over the globe and whole air column. In this section, we shall clarify the vertical distribution of the heating rate within the air column (Yamamoto et al., 1973). The model atmospheres used are same as used in the preceeding section. The method of calculation used is similar to the Neumann series method by Irvine (1965).

The alternative form of equation of transfer is given by

$$\mu \frac{dI^{(0)}(\tau,\mu)}{d\tau} = I(\tau,\mu) - \mathcal{S}(\tau,\mu) \quad , \tag{101}$$

where $\mathcal{S}$ is the source function defined by

$$\mathcal{S}(\tau,\mu) = \frac{1}{2}\int_{-1}^{+1} P^{(0)}(\tau;\mu,\mu')\, I^{(0)}(\tau,\mu')\, d\mu'$$

$$+ \frac{1}{4} F\, e^{-\tau/\mu_0}\, P^{(0)}(\tau;\mu,-\mu_0) \quad . \tag{102}$$

If we use the boundary conditions given by (87), the formal solution of (101) is given by

$$I^{(0)}(\tau,+\mu) = I_g\, e^{-(\tau_s-\tau)/\mu} + \int_\tau^{\tau_s} \mathcal{S}(t,+\mu)\, e^{-(t-\tau)/\mu}\, \frac{dt}{\mu} \quad , \tag{103}$$

$$I^{(0)}(\tau,-\mu) = \int_0^{\tau} \mathcal{J}(t,-\mu)\, e^{-(\tau-t)/\mu}\, \frac{dt}{\mu} \quad . \tag{104}$$

Inserting (103) and (104) into (102), we have the integral equation for $\mathcal{J}$ as follows:

$$\begin{aligned}\mathcal{J}(\tau,\pm\mu) = {} & \frac{1}{4} F e^{-\tau/\mu_0} p^{(0)}(\tau;\pm\mu,-\mu_0) + \frac{1}{2}\int_0^1 p^{(0)}(\tau;\pm\mu,+\mu')\, I_g\, e^{-(\tau_s-\tau)/\mu'}\, d\mu' \\ & + \frac{1}{2}\int_0^1 p^{(0)}(\tau;\pm\mu,+\mu') \left[\int_{\tau}^{\tau_s} \mathcal{J}(t,+\mu')\, e^{-(t-\tau)/\mu'}\, dt\right] \frac{d\mu'}{\mu'} \\ & + \frac{1}{2}\int_0^1 p^{(0)}(\tau;\pm\mu,-\mu') \left[\int_0^{\tau} \mathcal{J}(t,-\mu')\, e^{-(\tau-t)/\mu'}\, dt\right] \frac{d\mu'}{\mu'}\end{aligned} \tag{105}$$

If we put $I_g = 0$ in equation (105) we have the equation for the standard problem. Namely, denoting the source function for it by $\mathcal{J}_s$, we have

$$\begin{aligned}\mathcal{J}_s(\tau,\pm\mu) = {} & \frac{1}{4} F e^{-\tau/\mu_0} p^{(0)}(\tau;\pm\mu,-\mu_0) \\ & + \frac{1}{2}\int_0^1 p^{(0)}(\tau;\pm\mu,+\mu') \left[\int_{\tau}^{\tau_s} \mathcal{J}_s(t,+\mu')\, e^{-(t-\tau)/\mu'}\, dt\right] \frac{d\mu'}{\mu'} \\ & + \frac{1}{2}\int_0^1 p^{(0)}(\tau;\pm\mu,-\mu') \left[\int_0^{\tau} \mathcal{J}_s(t,-\mu')\, e^{-(\tau-t)/\mu'}\, dt\right] \frac{d\mu'}{\mu'}\end{aligned} \tag{106}$$

The solution of equation (106) can be obtained by the iterative method. We shall define $\mathcal{J}_s^{(n)}$ as follows:

$$\mathcal{J}_s^{(1)}(\tau,\pm\mu) = \frac{1}{4} F e^{-\tau/\mu_0} p^{(0)}(\tau;\pm\mu,-\mu_0) \quad , \tag{107}$$

$$\mathcal{J}_s^{(n)}(\tau,\pm\mu) = \frac{1}{4} F e^{-\tau/\mu_0} p^{(0)}(\tau;\pm\mu,-\mu_0)$$

$$+ \frac{1}{2}\int_0^1 p^{(0)}(\tau;\pm\mu,+\mu') \left[\int_\tau^{\tau_s} \mathcal{J}_s^{(n-1)}(t,+\mu') e^{-(t-\tau)/\mu'} dt\right] \frac{d\mu'}{\mu'}$$

$$+ \frac{1}{2}\int_0^1 p^{(0)}(\tau;\pm\mu,-\mu') \left[\int_0^{\tau} \mathcal{J}_s^{(n-1)}(t,-\mu') e^{-(\tau-t)/\mu'} dt\right] \frac{d\mu'}{\mu'}$$

$$(n \geq 2) \quad . \tag{108}$$

Evidently, $\mathcal{J}_s^{(n)}$ represents the radiation scattered up to n times. Then the function $\mathcal{J}_s$ can be obtained by iterating (108) until the following condition is satisfied for any value of τ and μ :

$$\frac{\left|\mathcal{J}_s^{(n)}(\tau,\pm\mu) - \mathcal{J}_s^{(n-1)}(\tau;\pm\mu)\right|}{\left|\mathcal{J}_s^{(n-1)}(\tau,\pm\mu)\right|} \leq \varepsilon \quad , \tag{109}$$

where ε is a small value corresponding to the required accuracy.

Next, we shall proceed to obtain the solution of the planetary problem, or of equation (105). The intensity of the reflected radiation, I_g, can be expressed, utilizing the solution of the standard problem to be (Chandrasekhar, 1950)

$$I_g = \frac{A_s F \{\mu_0 e^{-\tau_s/\mu_0} + t(\mu_0)\}}{1 - \bar{\mathcal{J}} A_s} \quad , \tag{110}$$

and

$$\bar{\mathcal{J}} = \frac{4}{F}\int_0^1 d\mu_0 \int_o^{\tau_s} dt \int_0^1 \mathcal{J}_s(t,+\mu) e^{-t/\mu} d\mu \quad , \tag{111}$$

$$t(\mu_0) = \frac{2}{F}\int_0^{\tau_s} dt \int_0^1 \mathcal{J}_s(t,-\mu) e^{-(\tau_s-t)/\mu} d\mu \quad , \tag{112}$$

where A_s is the reflectivity of the Lambert surface. Then we shall express $\mathcal{J}$ as follows:

$$\mathcal{J}(\tau,\pm\mu) = \mathcal{J}_s(\tau,\pm\mu) + \mathcal{J}_\Delta(\tau,\pm\mu) \quad . \tag{113}$$

From (105) and (106), we have the following equation for $\mathcal{J}_\Delta$:

$$\begin{aligned}\mathcal{J}_\Delta(\tau,\pm\mu) = {} & \frac{1}{2} I_g \int_0^1 P^{(0)}(\tau;\pm\mu,+\mu') \, e^{-(\tau_s-\tau)/\mu'} \, d\mu' \\ & + \frac{1}{2}\int_0^1 P^{(0)}(\tau;\pm\mu,+\mu') \left[\int_\tau^{\tau_s} \mathcal{J}_\Delta(t,+\mu') \, e^{-(t-\tau)/\mu'} \, dt\right] \frac{d\mu'}{\mu'} \\ & + \frac{1}{2}\int_0^1 P^{(0)}(\tau;\pm\mu,-\mu') \left[\int_0^{\tau} \mathcal{J}_\Delta(t,-\mu') \, e^{-(\tau-t)/\mu'} \, dt\right] \frac{d\mu'}{\mu'}\end{aligned} \tag{114}$$

Further we shall put

$$I_g = f(A_s,\mu_0) \, I_g^* \quad , \tag{115}$$

where from (110)

$$f(A_s,\mu_0) = A_s F/(1 - \bar{\alpha} A_s) \quad , \tag{116}$$

and

$$I_g^* = \mu_0 \, e^{-\tau_s/\mu_0} + t(\mu_0) \quad . \tag{117}$$

Correspondingly we shall write $\mathcal{J}_\Delta$ as follows:

$$\mathcal{J}_\Delta(\tau,\pm\mu) = f(A_s,\mu_0) \, \mathcal{J}_\Delta^*(\tau,\pm\mu) \quad . \tag{118}$$

Inserting (115) and (118) into (114), we have the following equation for $\mathcal{J}^*_\Delta$:

$$\mathcal{J}^*_\Delta(\tau,\pm\mu) = \frac{1}{2} I^*_g \int_0^1 P^{(0)}(\tau;\pm\mu,+\mu')\, e^{-(\tau_s-\tau)/\mu'}\, d\mu'$$

$$+ \frac{1}{2}\int_0^1 P^{(0)}(\tau;\pm\mu,+\mu') \left[\int_\tau^{\tau_s} \mathcal{J}^*_\Delta(t,+\mu')\, e^{-(t-\tau)/\mu'}\, dt\right] \frac{d\mu'}{\mu'}$$

$$+ \frac{1}{2}\int_0^1 P^{(0)}(\tau;\pm\mu,-\mu') \left[\int_0^{\tau} \mathcal{J}^*_\Delta(t,-\mu')\, e^{-(\tau-t)/\mu'}\, dt\right] \frac{d\mu'}{\mu'} \quad . \tag{119}$$

Equations (114) and (119) take a similar form. However, as the surface reflectivity A_s is not included in (119), if its solution is once obtained, the solution for any value of A_s can be obtained from (118). The solution of (119) can be obtained by solving the following equation by the iterative procedure as in the case of the standard problem:

$$\mathcal{J}^{*(1)}_\Delta(\tau,\pm\mu) = \frac{1}{2} I^*_g \int_0^1 P^{(0)}(\tau;\pm\mu,+\mu')\, e^{-(\tau_s-\tau)/\mu'}\, d\mu' \quad , \tag{120}$$

$$\mathcal{J}^{*(n)}_\Delta(\tau,\pm\mu) = \frac{1}{2} I^*_g \int_0^1 P^{(0)}(\tau;\pm\mu,+\mu')\, e^{-(\tau_s-\tau)/\mu'}\, d\mu'$$

$$+ \frac{1}{2}\int_0^1 P^{(0)}(\tau;\pm\mu,+\mu') \left[\int_\tau^{\tau_s} \mathcal{J}^{*(n-1)}_\Delta(t,+\mu')\, e^{-(t-\tau)/\mu'}\, dt\right] \frac{d\mu'}{\mu'}$$

$$+ \frac{1}{2}\int_0^1 P^{(0)}(\tau;\pm\mu,-\mu') \left[\int_0^{\tau} \mathcal{J}^{*(n-1)}_\Delta(t,-\mu')\, e^{-(\tau-t)/\mu'}\, dt\right] \frac{d\mu'}{\mu'} \quad , \tag{121}$$

until the condition,

$$\frac{\left| \mathcal{J}^{*(n)}_\Delta(\tau,\pm\mu) - \mathcal{J}^{*(n-1)}_\Delta(\tau,\pm\mu) \right|}{\left| \mathcal{J}^{*(n-1)}_\Delta(\tau,\pm\mu) \right|} \leq \varepsilon \quad , \tag{122}$$

is satisfied. If $\mathcal{S}_s$ and $\mathcal{S}^*_\Delta$ are obtained the downward and upward fluxes, D and U respectively, of the diffuse radiation are given by

$$D = \int_0^{2\pi} d\phi \int_0^1 I^{(0)}(\tau,-\mu)\mu \, d\mu$$

$$= 2\pi \int_0^1 \int_0^\tau \mathcal{S}_s(t,-\mu)\, e^{-(\tau-t)/\mu} \, d\mu \, dt + f(A_s,\mu_0)\, 2\pi \int_0^1 \int_0^\tau \mathcal{S}^*_\Delta(t,-\mu)\, e^{-(\tau-t)/\mu} \, d\mu \, dt \, , \tag{123}$$

and

$$U = \int_0^{2\pi} d\phi \int_0^1 I^{(0)}(\tau,+\mu)\mu \, d\mu$$

$$= 2\pi \, I_g \int_0^1 e^{-(\tau_s-\tau)/\mu} \mu \, d\mu + 2\pi \int_0^1 \int_\tau^{\tau_s} \mathcal{S}_s(t,+\mu)\, e^{-(t-\tau)/\mu} \, d\mu \, dt$$

$$+ f(A_s,\mu_0)\, 2\pi \int_0^1 \int_\tau^{\tau_s} \mathcal{S}^*_\Delta(t,+\mu)\, e^{-(t-\tau)/\mu} \, d\mu \, dt \quad . \tag{124}$$

The total net flux, N , is then given by

$$N = D(\tau) + \pi F \mu_0 \, e^{-\tau/\mu_0} - U(\tau) \quad , \tag{125}$$

where $\pi F \mu_0 \, e^{-\tau/\mu_0}$ represents the flux of the direct solar radiation.

The results of the computation is shown below. Fig. 9 shows the vertical distribution of the net flux $\lambda = 0.45\mu$, $n_i = 0.03$, and $A_s = 0.05$ taking μ_0 and β as parameters. The solid line represents the case for $\beta = 0.15$ and the broken line, for $\beta = 0.30$. It can be seen in the figure that the net flux increases with increase of μ_0 and that it decreases appreciably below 5 km, while it is almost constant above 5 km.

Fig. 10 shows the vertical distribution of the net flux for $\lambda = 0.45\mu$, $\mu_0 = 0.75$, and $A_s = 0.15$ taking β and n_i as parameters. If $n_i = 0$, the net flux is independent of height, as it ought to be, and it decreases with increase of β , corresponding to increased diffuse reflection. In the cases of $n_i = 0.03$ and 0.1 , the net flux decreases rapidly with decrease of height, and the rate

of decrease is larger for larger n_i and β . A noticeable point in the case of $n_i = 0.03$ and particularly of $n_i = 0.1$ is that the net flux increases with increase of β , contrary to the case of $n_i = 0$. The explanation of this result is that, if n_i is large, the upward reflected radiation from the earth surface and lower atmosphere is absorbed by aerosols more strongly when aerosols are more abundant, causing the net flux to increase with β . Therefore, this effect is more evident when the surface reflectivity A_s is large, although it is not shown in the figure.

The heating rate ($^\circ C\ day^{-1}$) for each height is then obtained by integrating the net flux with regard to wavelength and further taking average of it with respect to the sun's altitude. It should be noted here that the present computation of the heating rate is due to absorption of solar radiation by aerosols from 0.3μ to 0.8μ , and absorption of solar radiation in the near infrared region by water vapor and carbon dioxide as well as aerosols is not taken into account. Fig. 11 indicates an example of the result for the case of $\beta = 0.075$, $n_i = 0.03$, and $A_s = 0.15$, showing the latitude-altitude variation of the heating rate. Fig. 12 indicates another example for same values of n_i and A_s , but for $\beta = 0.15$. The turbidity value of $\beta = 0.075$ will not be so far from the global average value of it, and $\beta = 0.15$ corresponds to the value over rural districts of Japan at present. Figs. 11 and 12 indicate that the heating rate is greater in the lower atmosphere of the low latitude region, and that in the case of $\beta = 0.15$, the heating rate in the lower troposphere is comparable to that due to absorption of solar radiation by water vapor and carbon dioxide. However, the heating rate is very sensitive to n_i . For instance in the case of $n_i = 0.01$, the overall heating rate diminishes to about 2/5 of that for $n_i = 0.03$. This again suggests to us the importance of a more accurate determination of n_i . In this respect, the results shown in Figs. 9 and 10 indicate another possibility of determining n_i from field observations, utilizing an airplane or balloon, of the vertical distribution of the flux.

5. INTENSITY AND POLARIZATION OF RADIATION REFLECTED AND TRANSMITTED BY TURBID ATMOSPHERES

The problem of diffuse reflection and transmission of the solar radiation by turbid atmospheres is one of the main topics in the atmospheric optics and its study has been making rapid progress in recent years. Extensive investigations have been carried out by Feigelson et al. (1960a,b) in which the effect of inhomogeneity of atmosphere has been taken into account by considering a two-layer model. An interesting point in their investigations is that they specify the scattering properties of atmosphere basing on the directly observed phase function, but no account has been made by them on the effect of polarization of the radiation field.

Series of calculations and observations of the transmitted solar radiation field (intensity and polarization) have been presented by Bullrich et al. (1967, 1968, 1969) and de Bary et al. (1965). Their calculations were based upon an approximation which added the singly-scattered radiation by aerosols to the multiple-scattered radiation by the molecular atmosphere. Since this approximation do not correctly allow for higher order scattering by aerosols nor for any interaction between scattering due to the two components, aerosols and molecules, it gives results of varying degrees of accuracy, depending upon the optical depth of the aerosol components.

Recently, series of investigations have been made by Plass and Kattawar (1968, 1970, 1971) taking into account the effects of polarization, vertical distribution of aerosol and ozone absorption. In these studies, they used the Monte Carlo method and avoided all the mathematical difficulties involved. The only difficulty of the Monte Carlo method is its enormous computations required to achieve sufficient accuracy and resolution of the angular distribution (see Section 2.5). In fact, the resolution of their results with respect to the azimuthal angle is too low to enable one to draw a picture of the angular distribution of the intensity and state of polarization of the emergent radiation.

Herman et al. (1971) and Tanaka (1971b,c) have investigated the intensity and polarization of radiation emerging from turbid atmospheres. Herman et al. have used the iterative method which is described in Section 2.3, and computed the intensity and polarization of the diffusely transmitted sunlight for atmospheres containing various distributions of aerosols, as well as normal molecular constituents. Comparing the theoretical results with observations of their own, they have shown that inclusion of aerosols in the theoretical models results in considerably better agreement between the observation and theory than can be achieved by assuming a pure molecular atmosphere for the theoretical computations. Tanaka has adopted the matrix method originally developed by Twomey et al. (1966) and generalized by himself to be applicable to the inhomogeneously stratified medium and also to the case of polarized light. He has shown that general tendency of the diffusely transmitted radiation thus obtained is in good agreement with the results of classical observations.

We shall briefly review Tanaka's results which give detailed information about the angular distributions of the intensity and polarization of the skylight and their dependence on atmospheric parameters.

As to the size distribution of aerosols, he assumed a continental type of aerosols compiled by Manson (1965), but with the largest size of 3.0μ in radius. The refractive index of aerosols was assumed to be 1.33. The phase matrix for this distribution of spherical particles is calculated from the Mie theory for wavelengths of 0.45μ and 0.7μ.

In order to study the effects of changes of aerosol amount, computations were carried out for the following cases:

(1) a pure Rayleigh atmosphere ($\beta = 0$);

(2) (1) plus a conceivable normal aerosol amount ($\beta = 0.1$);

(3) (1) plus twice the normal aerosol amount ($\beta = 0.2$) .

In all these cases the same relative vertical distribution of aerosols are given by Elterman (1964) was used.

Fig. 13 shows a result of comparison between measured and computed phase functions. The broken line in the figure indicates the computed phase function, $p = 1/2(P_1 + P_2)$, where P_1 and P_2 are components of the phase matrix, for the aerosols alone at $\lambda = 0.45\mu$ and the solid line that for the lowest layer of the turbid atmosphere with $\beta = 0.1$. The measured values by Foitzick and

Zschaeck (1952) and Reeger and Seidentopf (1946), which are concerned with a white light, are cited from Feigelson et al.'s monograph (1960a). These measurements were made in a layer near the earth surface under conditions with the visibility range of about 20 km which is roughly compatible with the turbidity condition of $\beta = 0.1$ for $\lambda = 0.45\mu$. Agreement between measured and computed phase functions as shown in Fig. 13, therefore, implies that the model of aerosols used by Tanaka's study is reasonable, at least with regard to the angular distribution of scattered light.

Fig. 14 shows an example of the calculated angular distribution of intensities of the diffusely reflected (the left half of the figure) and transmitted (the right half of the figure) radiation at $\lambda = 0.45\mu$ for the case of $\beta = 0.1$ ($T = T_1$ according to the notation of the orginal paper), $A = 0.25$ and $\theta_0 = 33°$, where A and θ_0 are the surface albedo and solar zenith angle, respectively. This figure shows that as for the diffusely transmitted radiation (or skylight), there is a bright aureole around the sun and a dark zone stretching from antisolar sky sideways to the part of the sky below the sun. This general tendency of the figure coincides with the results by Feigelson et al. (1960a,b) and follows fairly well the observed distribution of sky brightness. As for the diffusely reflected radiation, it can be seen that the distribution of brightness is more uniform than that of the skylight. In this case, a darker area appears around the image point of the sun and it tends to brighten toward the horizon. Again, this general tendency agrees well with Feigelson et al.'s results.

Fig. 15 shows the angular dependence of the degree of polarization of both the diffusely reflected (the right half) and transmitted (the left half) radiation for the same case as Fig. 14. From the figure, it can be seen as for the diffusely transmitted radiation that there is a region with minimum polarization in the sky around the sun and region with maximum polarization in the antisolar sky. As for the diffusely reflected radiation, we can see that a region with minimum polarization generally appears on the opposite side ($\phi = 180°$) of the solar image and that a region with maximum polarization is stretching sideways from the solarside ($\phi = 0°$) to the horizon near $\phi = 90°$ where the polarization of the reflected radiation is most pronounced.

Corresponding distribution of the direction of polarization plane is shown in Fig. 16. As can be seen, the diffusely reflected and transmitted radiation fields are nearly symmetric in this case. It should be noted that the direction of polarization plane is not remarkably affected by the existence of aerosols, in accordance with Bullrich's (1964) suggestion. This is especially true for the diffusely reflected radiation.

By reviewing Tanaka's results in more detail, it is pointed out that his results agree qualitatively well with observations, but quantitatively some discrepancy remains. An example of comparisons between observed (Coulson, 1971) and calculated results (Kano, 1964; Plass and Kattawar, 1970; Tanaka, 1971) is shown in Fig. 17 on the degree of polarization at the maximum for various wavelengths as a function of sun elevation. Plass and Kattawar's results correspond to the model atmosphere with refractive index of aerosols $m = 1.55\text{-}0.0i$, surface reflectivity $A = 0.0$ and turbidity coefficient $\beta = 0.09$, whereas Tanaka's results correspond to the model atmosphere with $m = 1.33\text{-}0.0i$, $A = 0.25$, $\beta = 0.1$ (broken lines) and that with $m = 1.33\text{-}0.0i$, $A = 0.25$, $\beta = 0.2$ (solid lines), respectively. As shown in the figure, Tanaka's results can explain observed dependence of maximum polarization on the sun elevation better than that of Kano and Plass and Kattawar. But his choice of the value of

refractive index is less realistic than Plass and Kattawar's. A more detailed comparison between observed and calculated polarizations in Fig. 17 reveals that the wavelength dependence of the observed polarization can not be explained by theoretical calculations. This fact suggests that the refractive index of aerosols may depend upon the wavelength. A more detailed knowledge on optical properties of aerosols is needed to explain polarization phenomena.

REFERENCES

Ambartsumian, V. A., 1942: Diffusion of light by planetary atmospheres. Astron. Zh., 19, No. 5.

Astroshenko, V. S., E. M. Feigelson, K. S. Glazova, and M. S. Malkevich, 1960b: Calculation of the brightness of light in the case of anisotropic scattering (II). Transaction (Trudy) of the Institute of Atmospheric Physics No. 3, Consulatant Bureau, Inc., New York, 226 pp.

Bellman, R. E., H. H. Kagiwada, and R. E. Kalaba, 1966: Invariant imbedding and a reformulation of the internal intensity problem in radiative transfer theory. Mon. Not. R. Astr. Soc., 132, 183-191.

Budyko, M. I., 1969: The effect of solar radiation variations on the climate of the earth. Tellus, 21, 611-619.

Bullrich, K., 1964: Scattered radiation in the atmosphere and the natural aerosol. Advances in Geophysics, 10, 99-260.

Bullrich, K., E. de Bary, W. Blattner, R. Eiden, G. Hanel, and W. Nowak, 1967: Research on atmospheric optical radiation transmission. Final Rept., Contract AF61(052)-595, Meteorologisch-Geophysikalisch Institute der Johanes Gutenberg-Universitat, Mainz, Germany, 68 pp.

Bullrich, K., W. Blattner, T. Conley, R. Eiden, G. Hanel, K. Heger, and W. Nowak, 1968: Research on atmospheric optical radiation transmission. Sci. Rept. No. 6, Contract F61052 67C 0046, Meteorologisch-Geophysikalisches Institute der Johanes Gutenberg-Universitat, Mainz, Germany, 83 pp.

Bullrich, K., R. Eiden, G. Eschelbach, K. Fischer, G. Hanel, K. Hereg, H. Schollmayer, and G. Steinhorst, 1969: Research on atmospheric optical radiation. Sci. Rept. No. 7, Contract F61052 67C 0046, Institut fur Meteorologie der Johanes Gutenberg-Universtat, Mainz, Germany, 111 pp.

Chamberlain, J. W., and M. B. McElroy, 1966: Diffuse reflection by an inhomogeneous planetary atmosphere. Ap. J., 144, 1148-1158.

Chandrasekhar, S., 1946: On the radiative equilibrium of a stellar atmosphere. XII, Ap. J., 104, 191-202.

Chandrasekhar, S., 1950: Radiative Transfer. Oxford, England, Clarendon Press, 393 pp.

Collins, D. G., and M. B. Wells, 1965: Monte Carlo codes for study of light transport in the atmosphere, Report RRA-T54 (Radiation Research Associates, Inc., Fort Worth, Texas) Vols. 1 and 2.

Collins, D. G., K. Cunninghan, and M. B. Wells, 1967: Monte Carlo studies of light transport, Report RRA-T74 (Radiation Research Associates, Inc., Fort Worth, Texas).

Collins, D. G., 1968: Report RRA-T86 (Radiation Research Associates, Inc., Fort Worth, Texas).

Collins, D. G., W. G. Blattner, M. B. Wells and H. G. Horak, 1972: Backward Monte Carlo calculations of the polarization characteristics of the radiation emerging from spherical-shell atmospheres. Appl. Opt., 11, 2684-2696.

Coulson, K. L., J. V. Dave, and Z. Sekera, 1960: Tables relating to radiation emerging from a planetary atmosphere with Rayleigh scattering. Berkeley, University of California Press, 548 pp.

Coulson, K. L., 1971: On the solar radiation field in a polluted atmosphere. J. Quant. Spectrosc. Radiat. Transfer, 11, 739-755.

Danielson, R. E., D. R. Moore, and H. C. van de Hulst, 1969: The transfer of visible radiation through clouds. J. Atmos. Sci., 26, 1078-1086.

Dave, J. V., and J. Gazdag, 1970: A modified Fourier transform method for multiple scattering calculations in a plane parallel Mie atmosphere. Appl. Opt., 9, 1457-1466.

de Bary, E., B. Braun, and K. Bullrich, 1965: Tables related to light scattering in a turbid atmosphere. Vol. 3, Air Force Cambridge Research Laboratories, Contract AF61(052)-595, Bedford, Mass., 581-831.

Deirmendjian, D., 1964: Scattering and polarization properties of water clouds and hazes in the visible and infrared. Appl. Opt., 3, 187-196.

Elterman, L., 1964: Rayleigh and extinction coefficients to 50 km for the region 0.27μ to 0.55μ . Appl. Opt., 3, 1139-1147; also in Handbook of Geophysics and Space Environments, McGraw-Hill Books Company, Inc., New York.

Feigelson, E. M., M. S. Malkevich, S. Ya Kogan, T. D. Koronatova, K. S. Glazova and M. A. Kuznetova, 1960a: Calculation of the brightness of light in the case of anisotropic scattering (I). Transactions (Trudy) of the Institute of Atmospheric Physics No. 1, Consultant Bureau, Inc., New York, 104 pp.

Feigelson, E. M., 1960b: See Astroshenko, V.S. et al 1960b.

Foitzik, and Zschaeck, 1952: Messungen der spectralen Zerstreuungsfunktion bodenaher Luft bei guter Sicht, Dunst, und Nebel. Zeitschr. f. Met., 7, 1-9.

Fymat, A. L., and K. D. Abhyankar, 1969: Theory of radiative transfer in inhomogeneous atmospheres. I. Perturbation Method. Ap. J., 158, 315-324.

Hansen, J. E., 1969a: Exact and approximate solutions for multiple scattering by cloudy and hazy planetary atmospheres. J. Atmos. Sci., 26, 478-487.

Hansen, J. E., 1969: Radiative transfer by doubling very thin layers. Ap. J., 155, 565-573.

Hansen, J. E., 1971a: Multiple scattering of polarized light in planetary atmospheres. Part I. The doubling method. J. Atmos. Sci., 28, 120-125.

Hansen, J. E., 1971b: Multiple scattering of polarized light in planetary atmospheres. Part II. Sunlight reflected by terrestrial clouds. J. Atmos. Sci., 28, 1400-1426.

Herman, B. M., and S. R. Browning, 1965: A numerical solution to the equation of radiative transfer. J. Atmos. Sci., 22, 559-566.

Herman, B. M., S. R. Browning and R. J. Curran, 1971: The effect of atmospheric aerosols on scattered sunlight. J. Atmos. Sci., 28, 419-428.

Hovenier, J. W., 1969: Symmetry relationships for scattering of polarized light in a slab of randomly oriented particles. J. Atmos. Sci., 26, 488-499.

Hunt, G. E., and I. P. Grant, 1969: Discrete space theory of radiative transfer and its application to problem in planetary atmospheres. J. Atmos. Sci., 26, 963-972.

Irvine, W.M.,1965:Multiple scattering by large particles. Ap. J., 142, 1563-1575.

Irvine,W.M.,1968: Multiple scattering by large particles. II. Optically thick layers. Ap. J. 152, 823-834.

Jacobowitz, H., and H. B. Howell, 1971: On the matrix method applied to the multiple scattering of polarized light. J. Atmos. Sci., 28, 1301-1303.

Kano, M., 1964: Effect of a turbid layer on radiation emerging from a planetary atmosphere. Doctral Dissertation, University of California, Los Angeles.

Kattawar, G. W., and G. N. Plass, 1968a: Radiance and polarization of multiple scattered light from haze and clouds. Appl. Opt., 7, 1519-1527.

Kattawar, G. W., G. N. Plass, and C. N. Adams, 1971: Flux and polarization calculations of the radiation reflected from the clouds of Venus. Ap. J., 170, 371-386.

Manson, J. E., 1965: in Handbook of Geophysics and Space Environments, McGraw-Hill Book Company, Inc., New York.

Marchuk, G. E., and G. A Mikhailov, 1967: The solution of problems of atmospheric optics by a Monte-Carlo method. IZVESTIYA Atmos. Oceanic Phys., 3, 147-155.

Plass, G. N., and G. W. Kattawar, 1968a: Influence of single scattering albedo on reflected and transmitted light from clouds. Appl. Opt., 7, 361-367.

Plass, G. N., and G. W. Kattawar, 1970: Polarization of the radiation reflected and transmitted by the earth's atmosphere. Appl. Opt., 9, 1122-1130.

Plass, G. N., and G. W. Kattawar, 1971: Radiance and polarization of the earth's atmosphere with maze and clouds. J. Atmos. Sci., 28, 1187-1198.

Potter, J. F., 1970: The delta function approximation in radiative transfer theory. J. Atmos. Sci., 27, 945-951.

Preisendorfer, R. W., 1965: Radiative transfer in discrete spaces. Oxford, Pergamon Press.

Rasool, S. I., and S. H. Schneider, 1971: Atmospheric carbon dioxide and aerosols--effects of large increases on global climate. Science, 173, 138-141.

Reeger, E., and H. Seidentopf, 1946: Die Streufunktion des atmospharischen Dunst mach Scheinwerfermessungen. Optik, 1, 15-41.

Robinson, N., 1966: Solar Radiation. Amsterdam, Elsevier, 347 pp.

Samuelson, R. E., 1965: Radiative transfer in a cloudy atmosphere. NASA Technical Report R-215, 87 pp.

Samuelson, R. E., 1969: The thermal radiation field emitted by anisotropically scattering cloudy atmospheres. Icarus, 10, 258-273.

Sekera, Z., 1963: Radiative transfer in a planetary atmosphere with imperfect scattering, RAND Pub. R-452-PR, RAND Corp., Santa Monica, Calif., 64 pp.

Skumanich, A., and K. Bhattacharji , 1961: Monte Carlo study of time-dependent scattering in a plane parallel cloud. J. Opt. Soc. Am., 51, 484.

Tanaka, M., 1971a: Radiative transfer in turbid atmospheres. I. Matrix analysis for the problem of diffuse reflection and transmission. J. Meteor. Soc. Japan, 49, 296-312.

Tanaka, M., 1971b: Radiative transfer in turbid atmospheres. II. Angular distribution of intensity of the solar radiation diffusely reflected and transmitted by turbid atmospheres. J. Meteor. Soc. Japan, 49, 321-332.

Tanaka, M., 1971c: Radiative transfer in turbid atmospheres. III. Degree of polarization of the solar radiation reflected and transmitted by turbid atmospheres. J. Meteor. Soc. Japan, 49, 333-342.

Twomey, S., H. Jacobowitz, and H. B. Howell, 1966: Matrix method for multiple scattering problems. J. Atmos. Sci., 23, 289-296.

van de Hulst, H. C., 1963: A new look at multiple scattering, New York, NASA Goddard Space Flight Center, 81 pp.

van de Hulst, H. C. and K. Grossmann, 1968: in The Atmosphere of Venus and Mars, Gordon and Breach, New York, 35-36.

Yamamoto, G., M. Tanaka and S. Asano, 1970: Radiative transfer in water clouds in the infrared region. J. Atmos. Sci., 27, 282-292.

Yamamoto G., M. Tanaka and S. Asano, 1971: Radiative Heat Transfer in water clouds by infrared radiation. J. Quant. Spect. Rad. Tr.11 697-708.

Yamamoto, G., and M. Tanaka, 1972: Increase of global albedo due to air pollution. J. Atmos. Sci., 29, 1405-1412.

Yamamoto, G., M. Tanaka and S. Ohta, 1973: Heating of lower atmosphere due to absorption of solar radiation by aerosols. To be published.

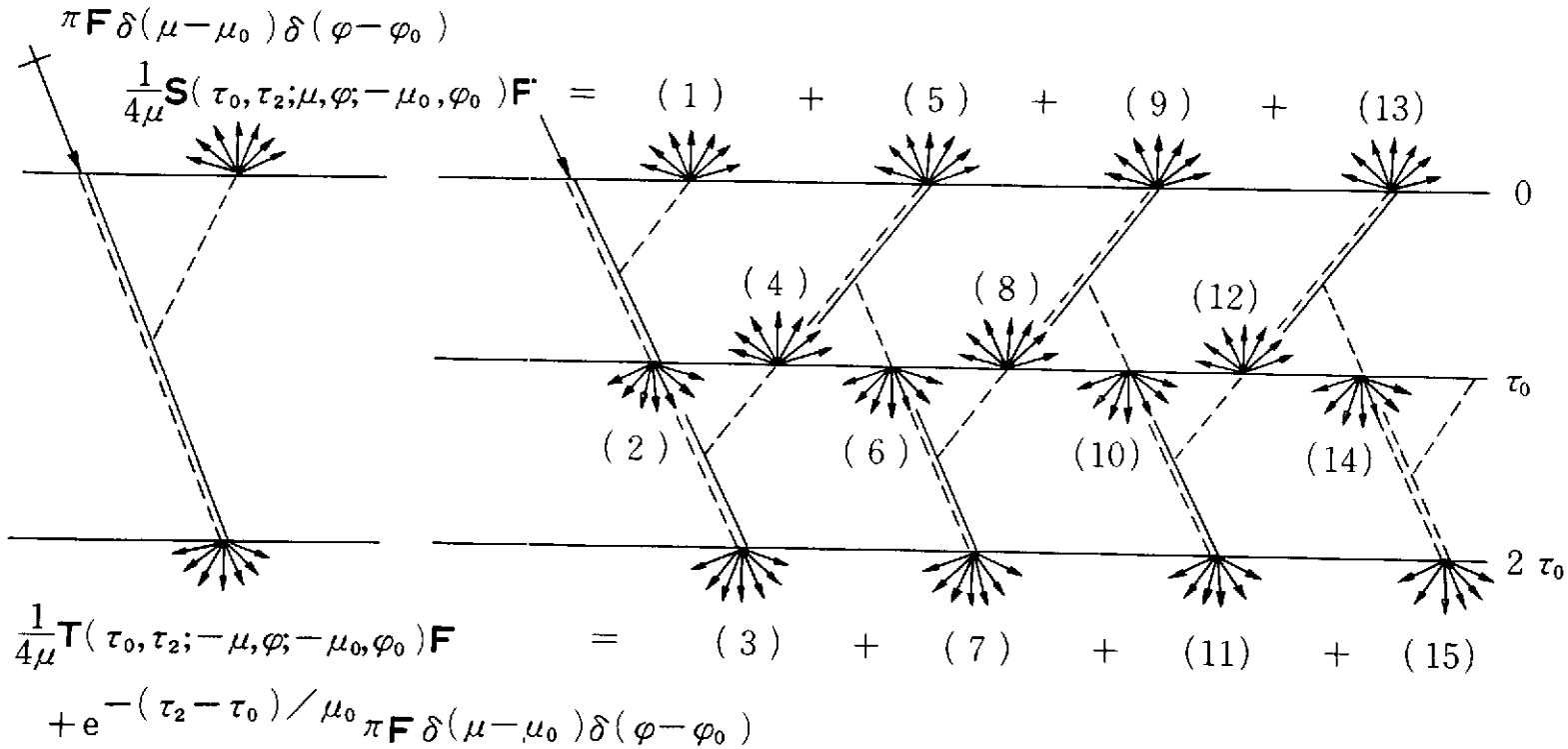

Fig. 1 Schematic diagram of the individual contribution making up the whole reflected and transmitted radiation. Solid line segments indicate direct transmission and broken line segments, diffuse reflection and transmission.

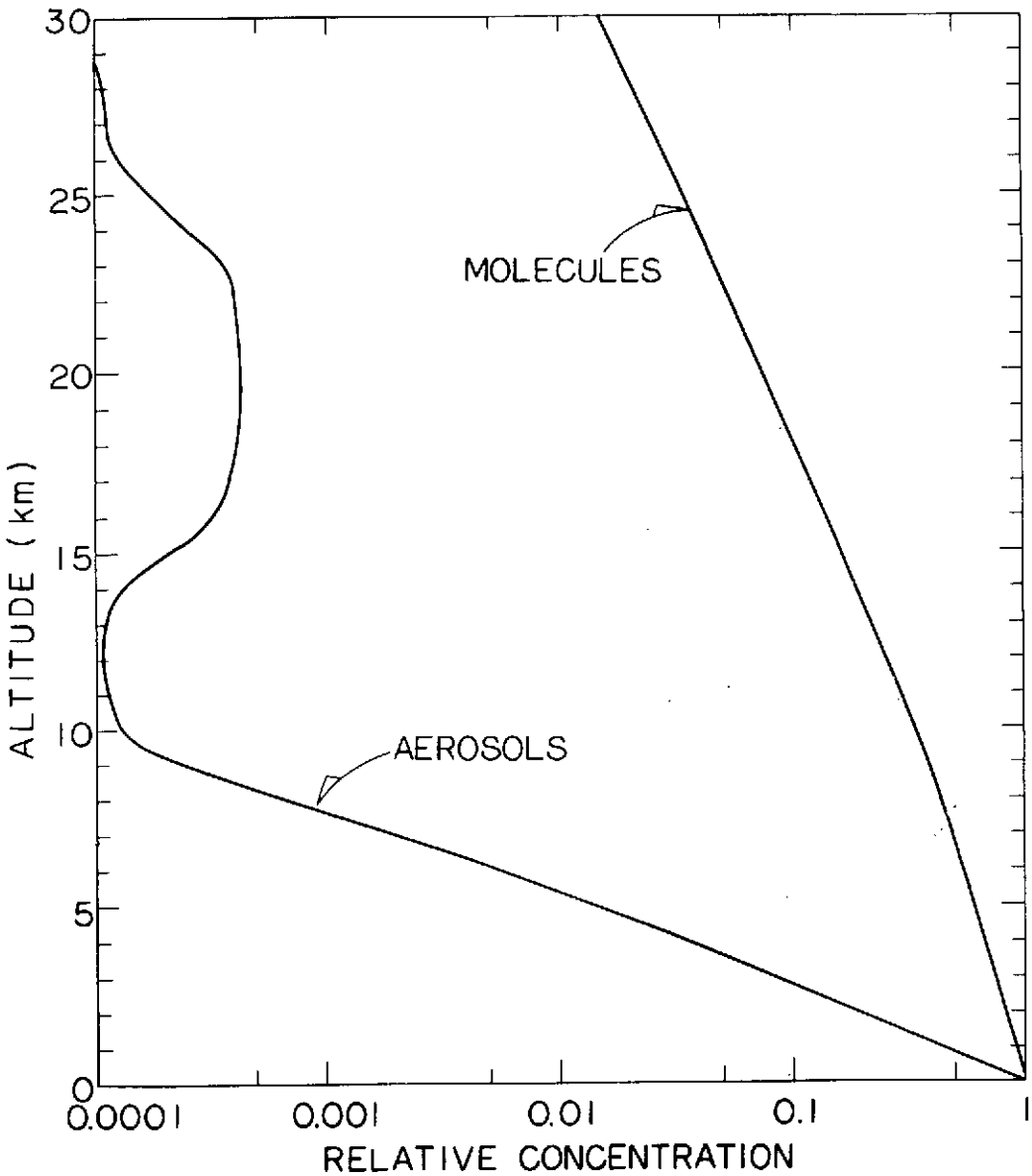

Fig. 2 Vertical distribution of the relative concentration of particles and air molecules.

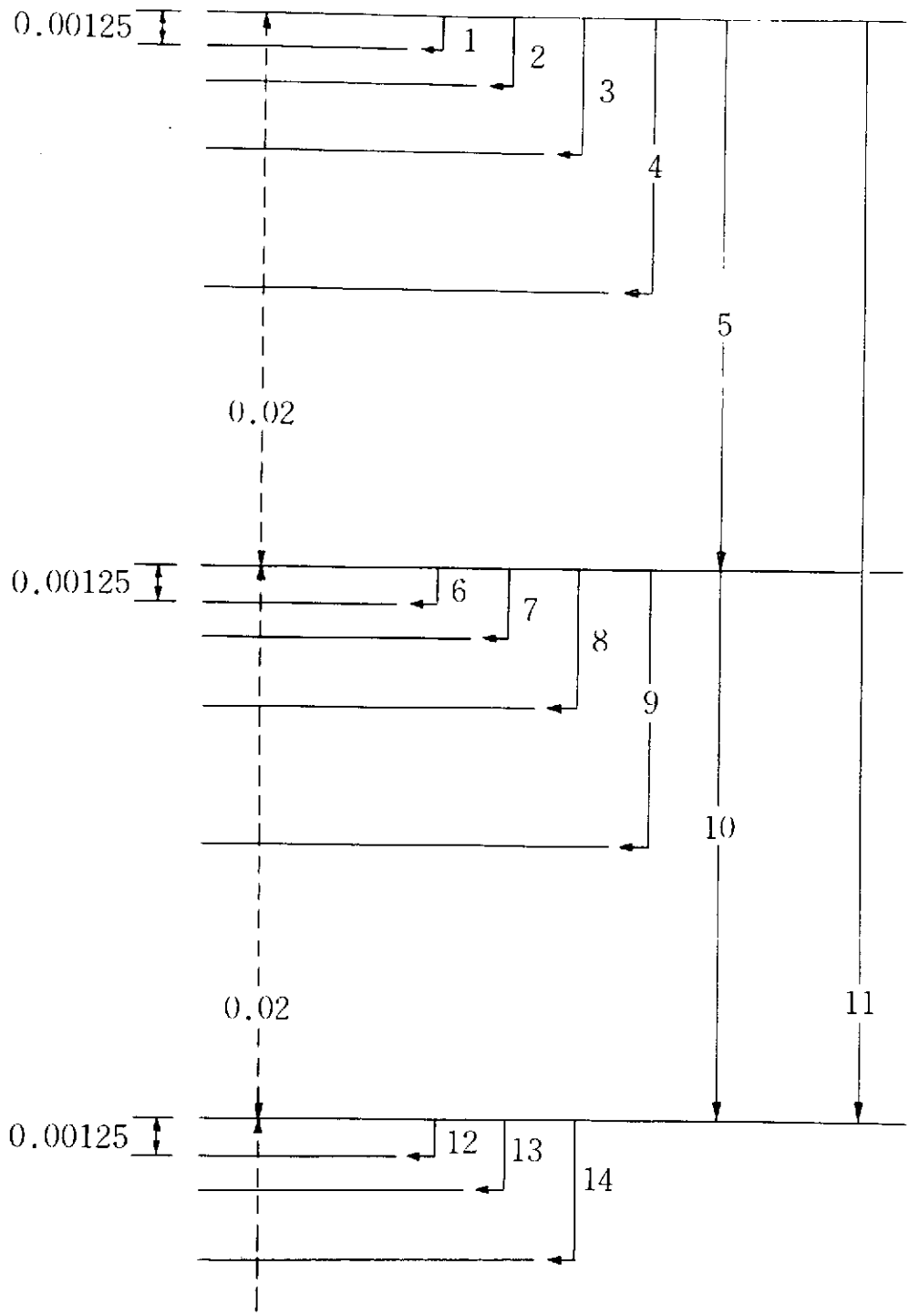

Fig. 3 Division of the whole atmospheric layer into a number of thinner sub-layers. The scheme used for $\lambda = 0.45\ \mu$ and $\beta = 0.1$ is shown as an example.

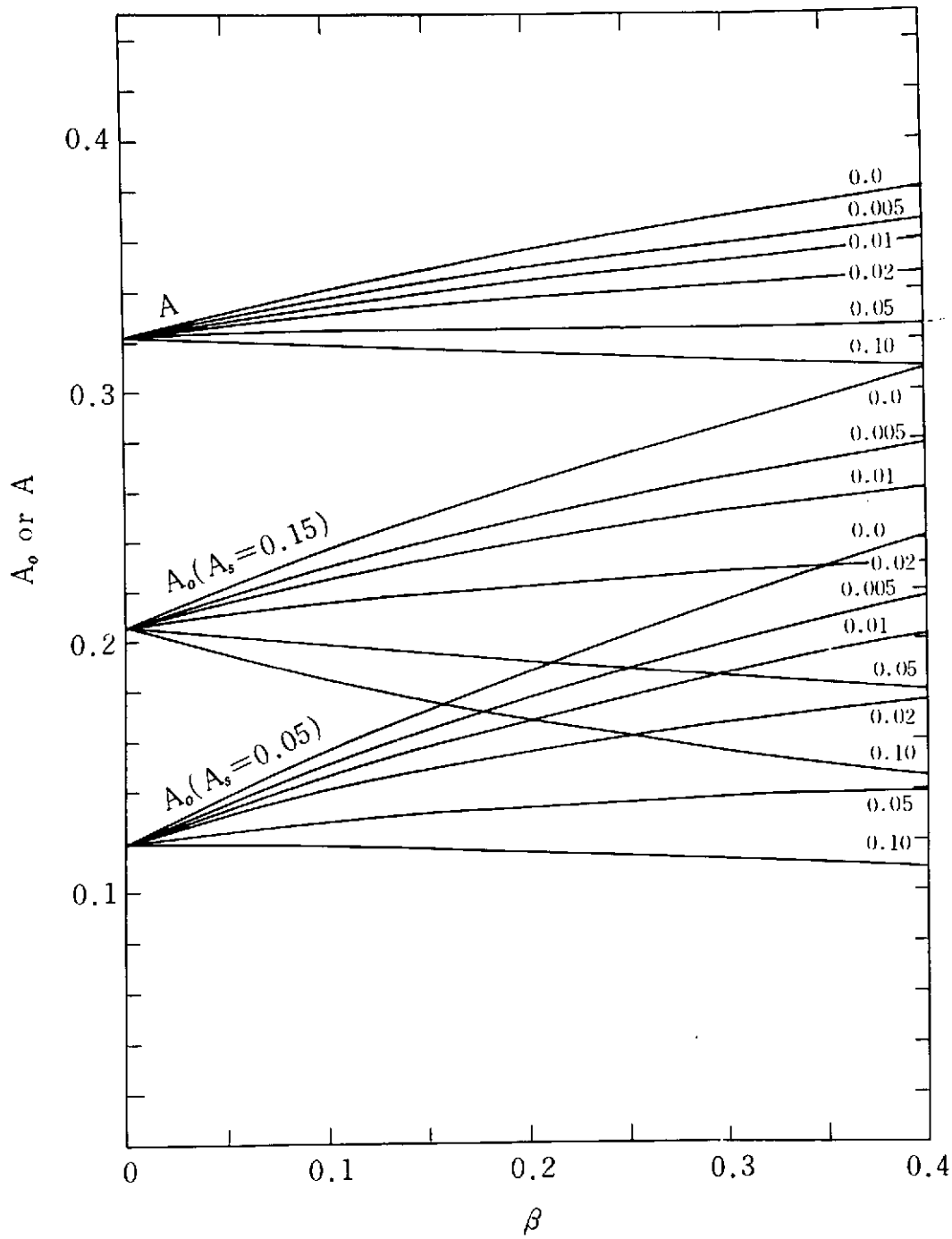

Fig. 4 Albedo of the earth as a function of β for different n_i values. A_0 indicates albedo for cloudless atmospheres, and A albedo which takes into account existence of clouds.

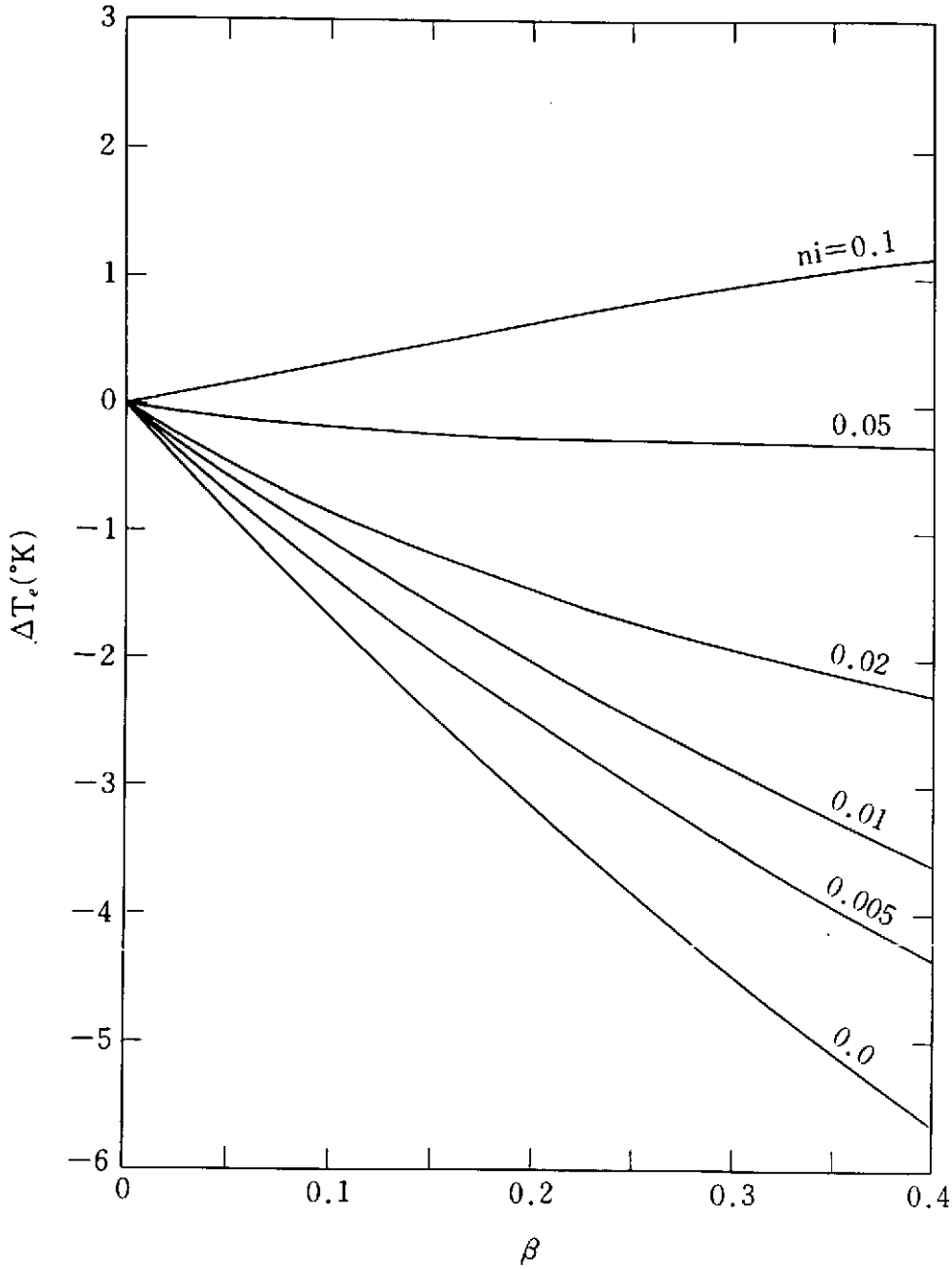

Fig. 5 Effective blackbody temperature, ΔT_e, as a function of β for different n_i values.

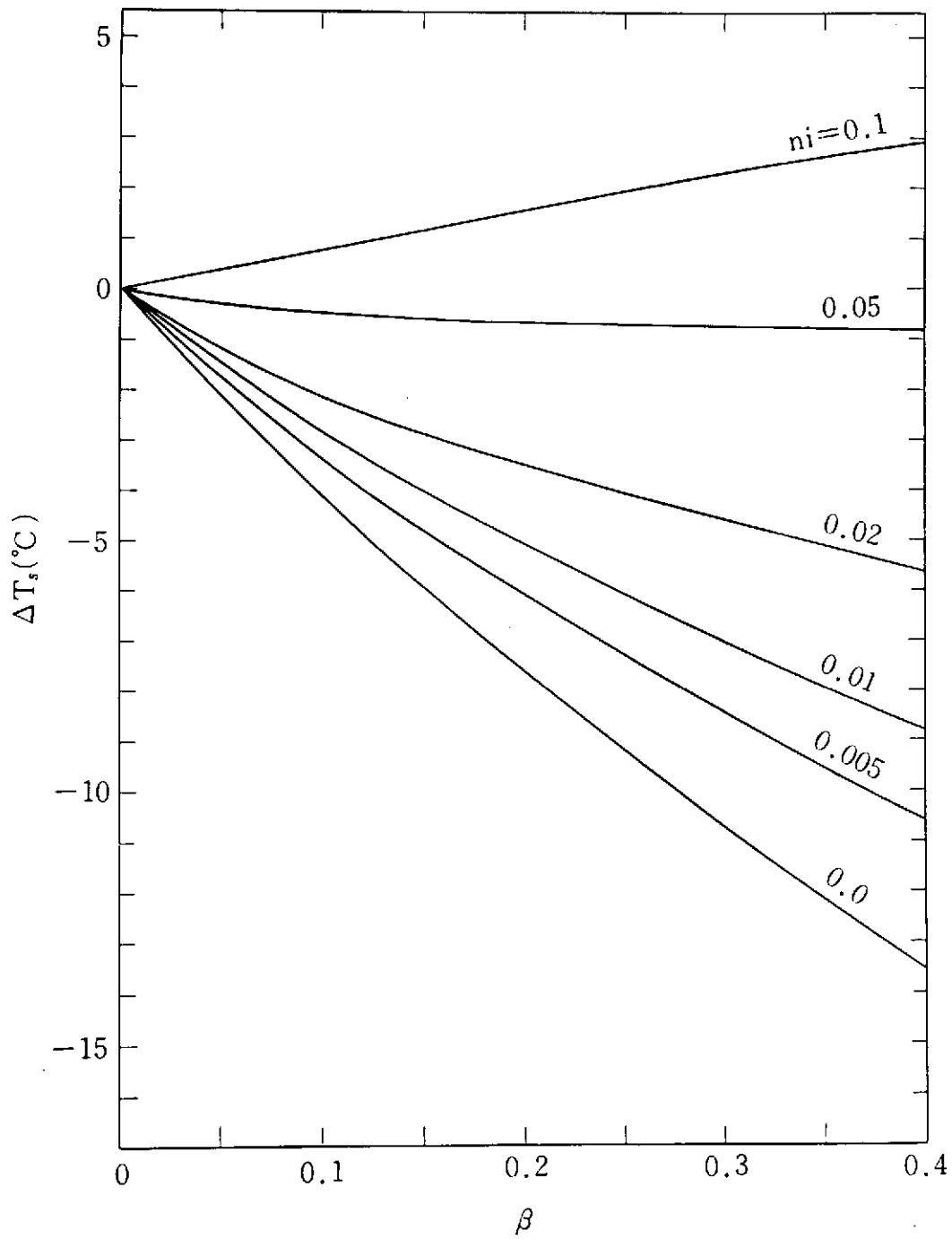

Fig. 6 Surface temperature, ΔT_s , as a function of β for different n_i values.

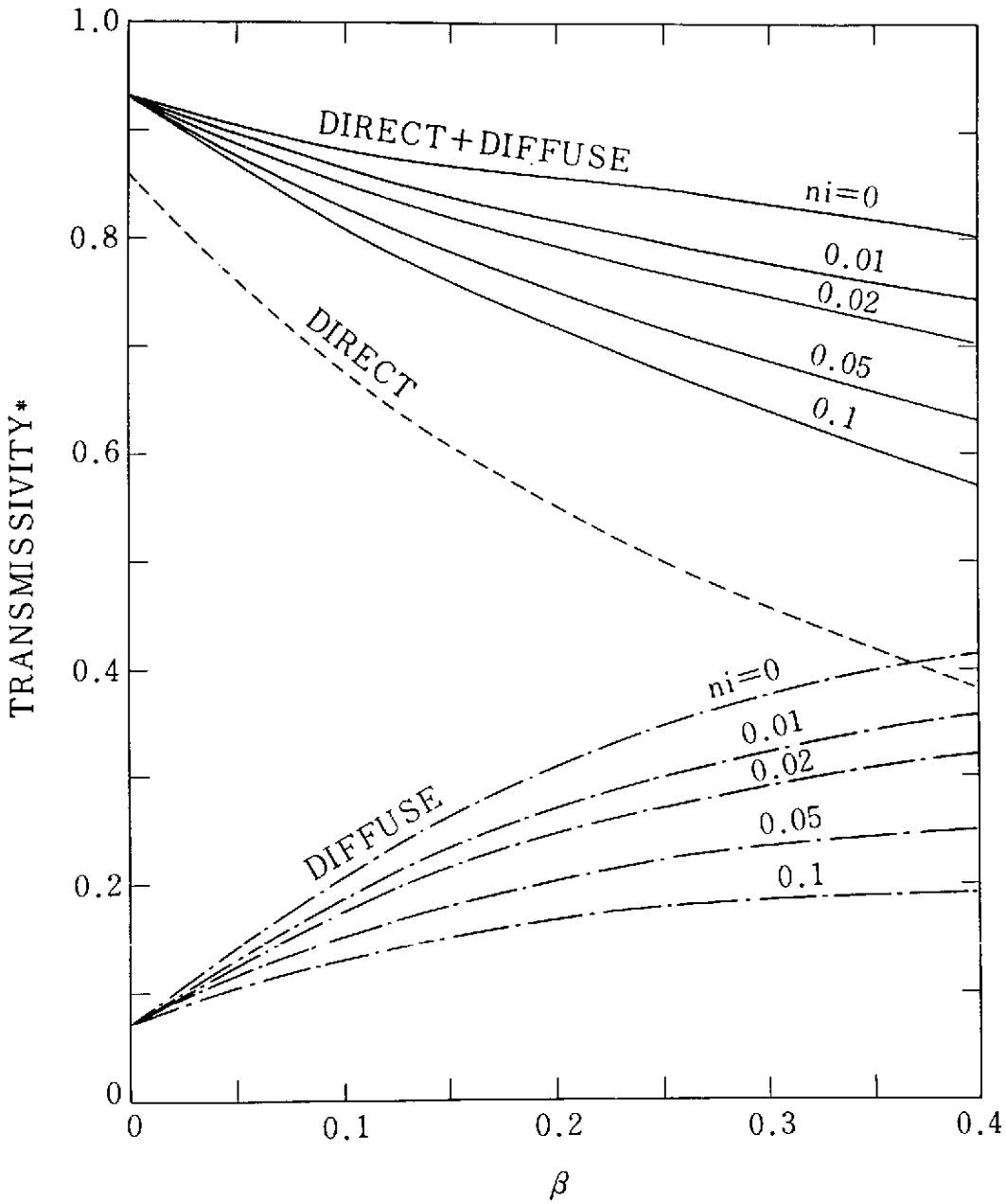

Fig. 7 Transmissivity averaged over the sunlit hemisphere and wavelength as a function of β . Curves denoted DIRECT, DIFFUSE, and DIRECT + DIFFUSE show transmissivity for direct, diffuse, and total components, respectively.

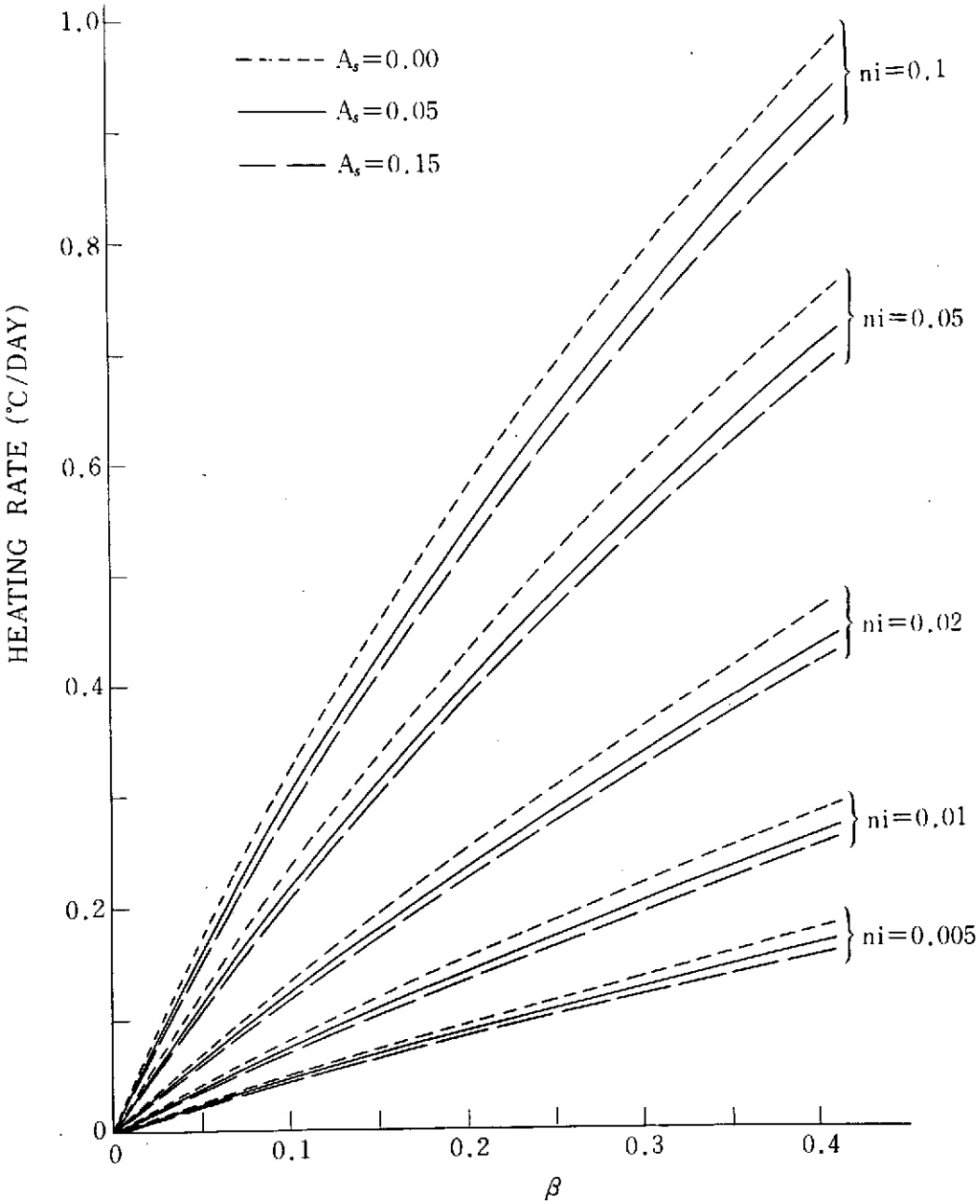

Fig. 8 Average heating rate of the earth's atmosphere as a function of β for different n_i values.

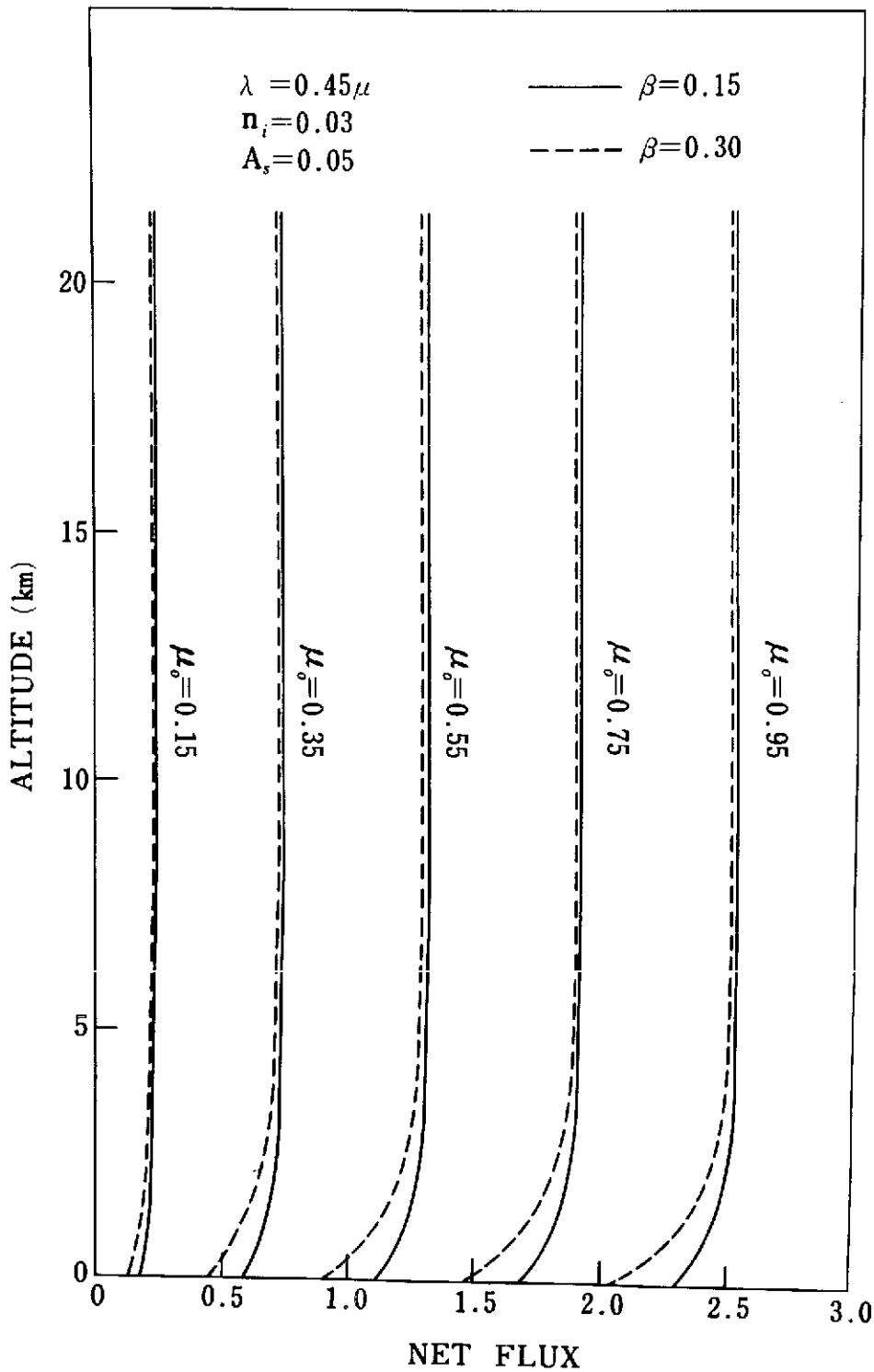

Fig. 9 Net downward flux versus altitude for $\lambda = 0.45\ \mu$, $n_i = 0.03$ and $A_s = 0.05$ taking β and μ_0 as parameters. Solid and broken lines correspond to $\beta = 0.15$ and $\beta = 0.30$ respectively.

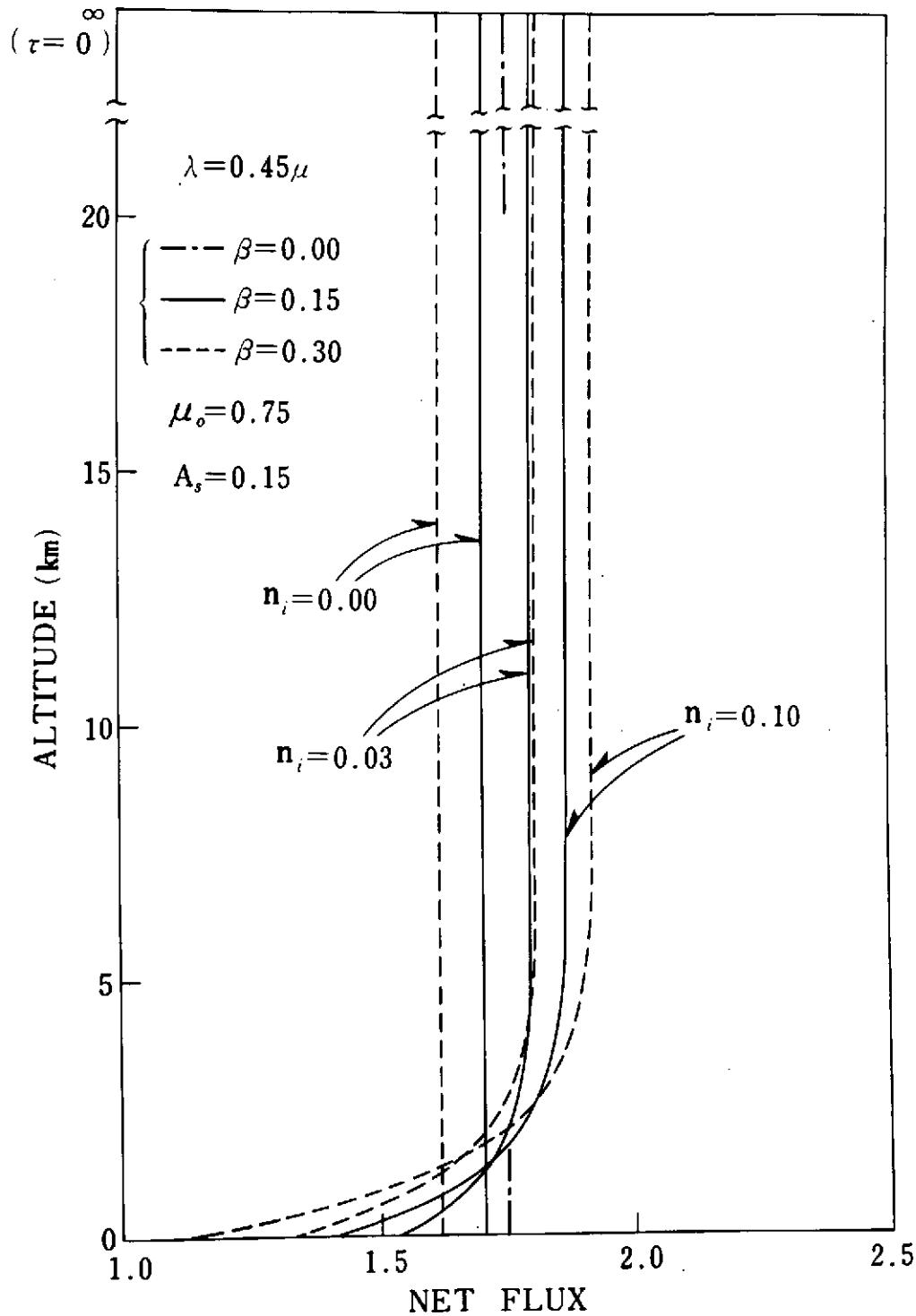

Fig. 10 Net downward flux versus altitude for $\lambda = 0.45\ \mu$, $A_s = 0.15$, and $\mu_0 = 0.75$ taking β and n_i as parameters.

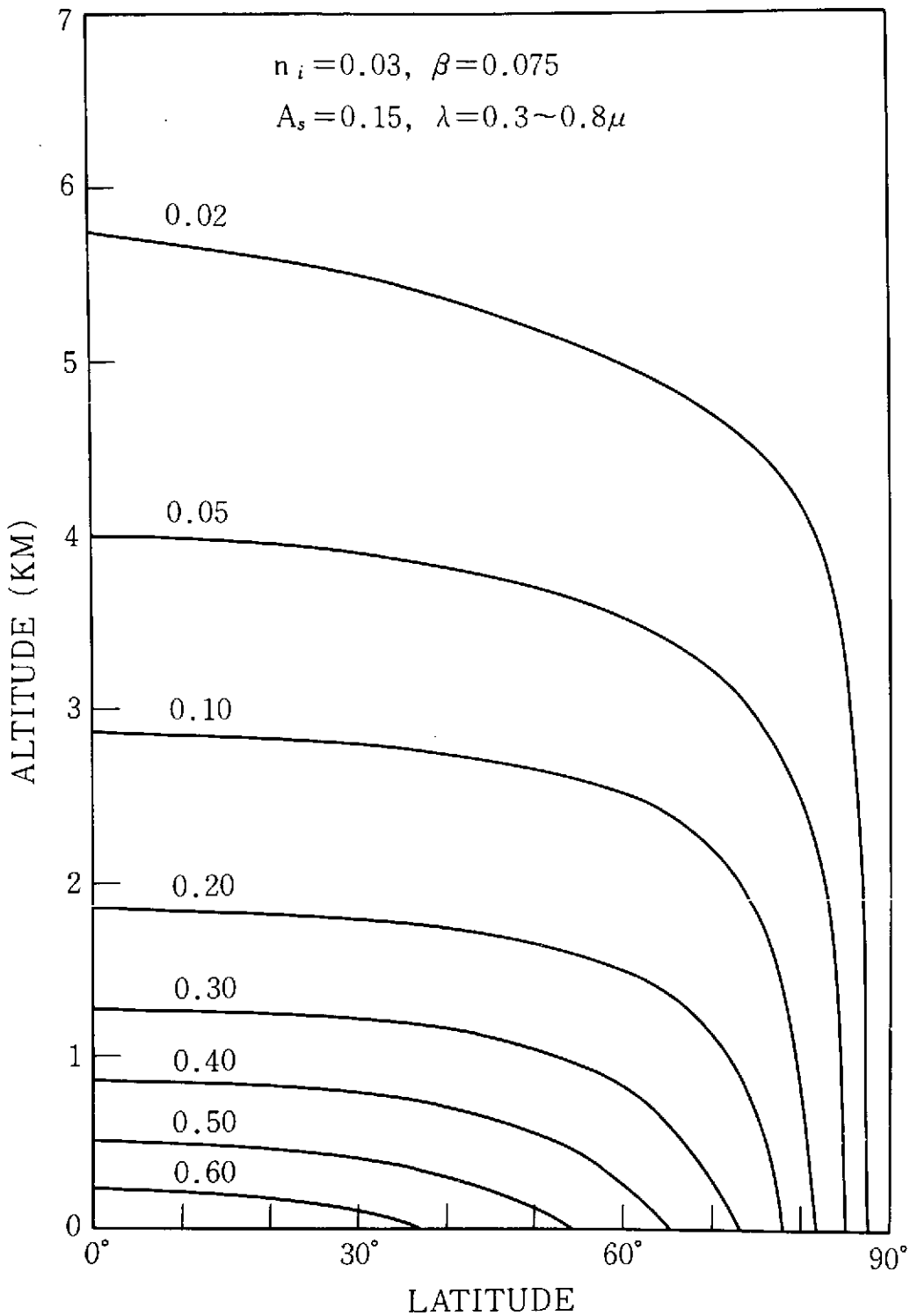

Fig. 11 Latitude-altitude variation of heating rate (°C/day) due to absorption of the visible radiation by aerosols for $\beta = 0.075$, $n_i = 0.03$ and $A_s = 0.15$.

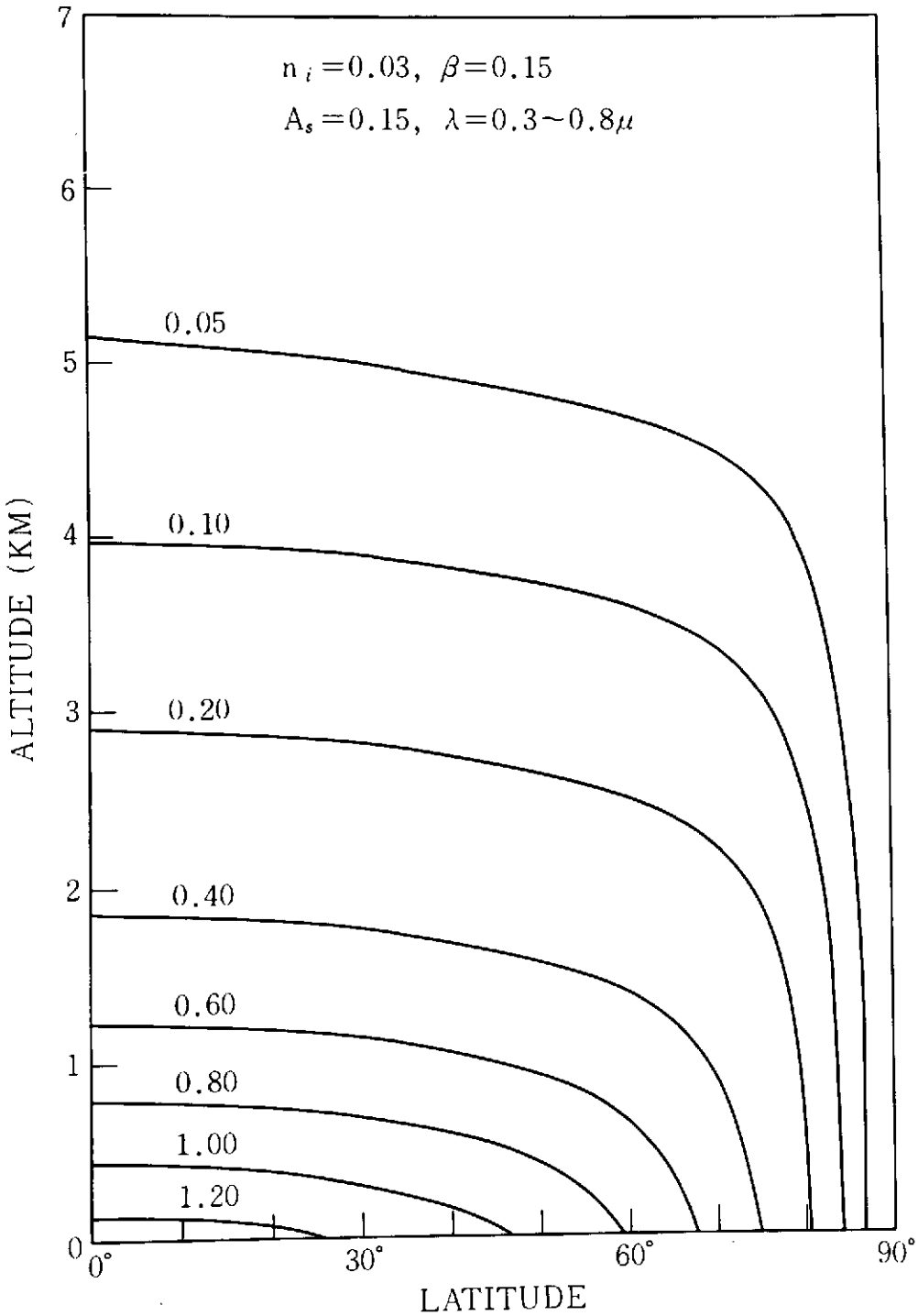

Fig. 12 Same as Fig. 11 but for $\beta = 0.15$.

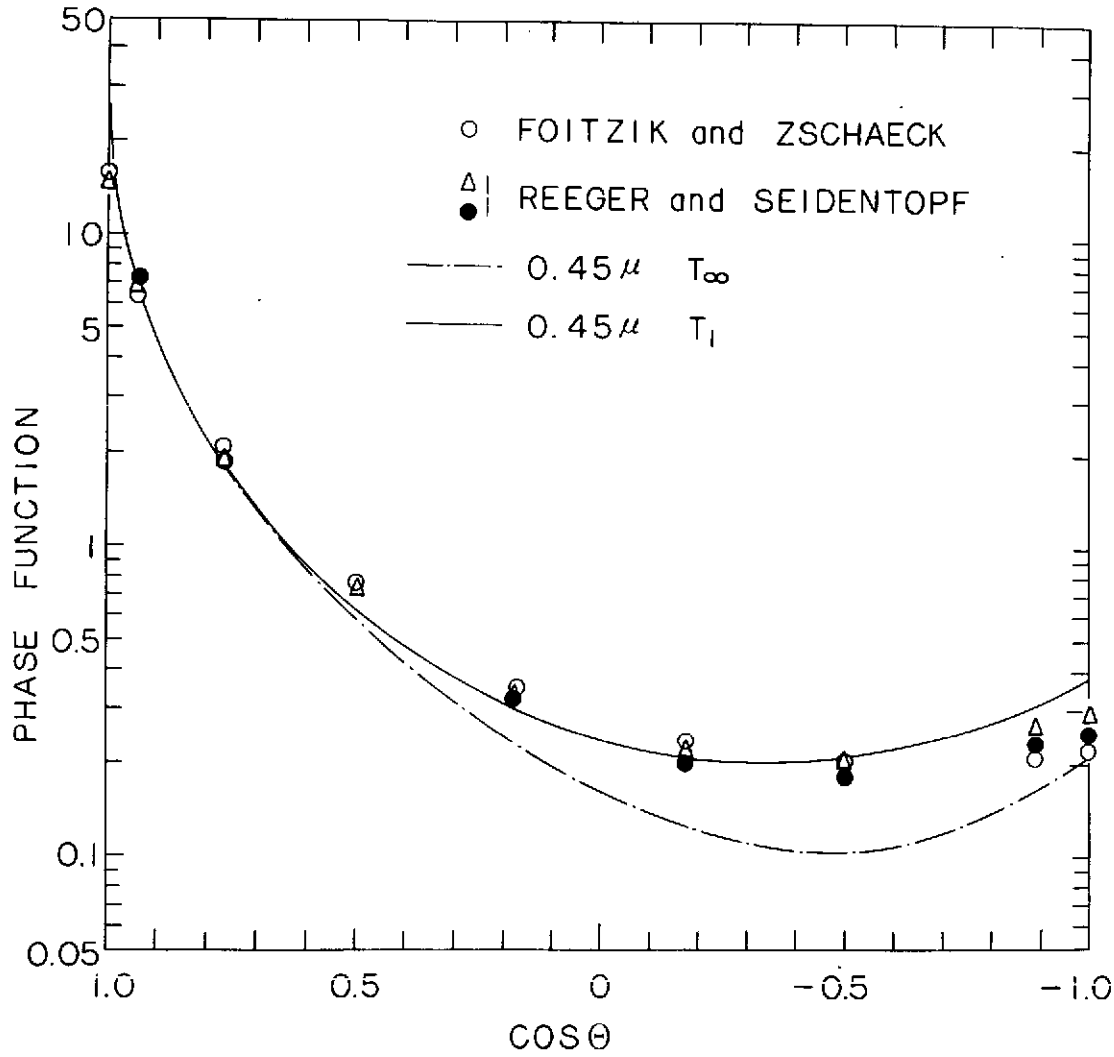

Fig. 13 Comparison between measured and computed phase functions. Broken line shows the computed phase function, $(P_1 + P_2)/2$, for pure aerosols and solid line, that for the real atmosphere containing both aerosols and air molecules. White circles indicate measurements by Foitzick and Zshaeck and triangles and black circles, measurements by Reeger and Seidentopf.

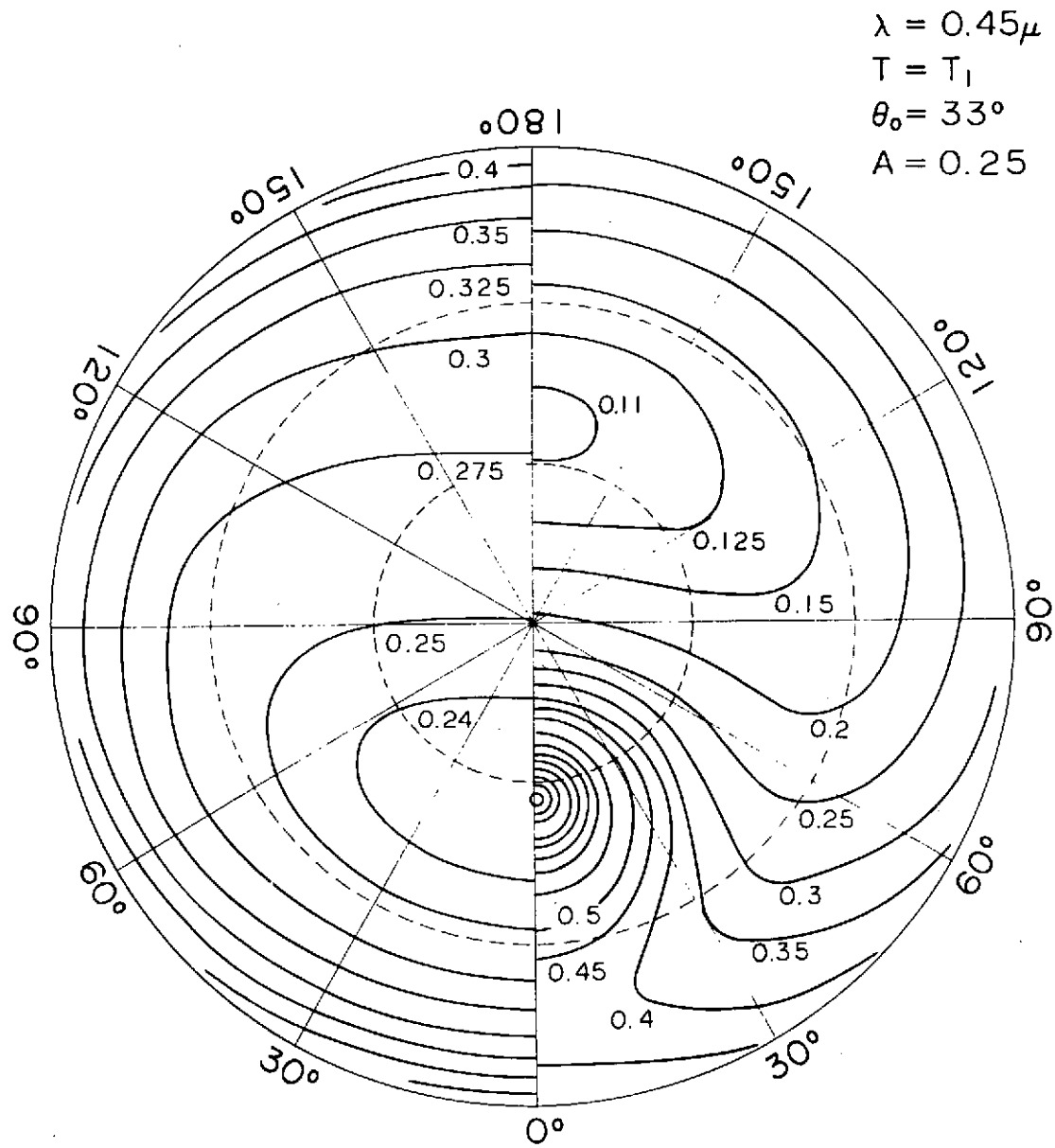

Fig. 14 Distribution of intensities of the diffusely reflected and transmitted radiation for $\lambda = 0.45\ \mu$, $\theta_0 = 33°$, $\beta = 0.1$ $(T = T_1)$ and $A = 0.25$. The right half of the figure shows transmitted radiation and the left half, reflected radiation.

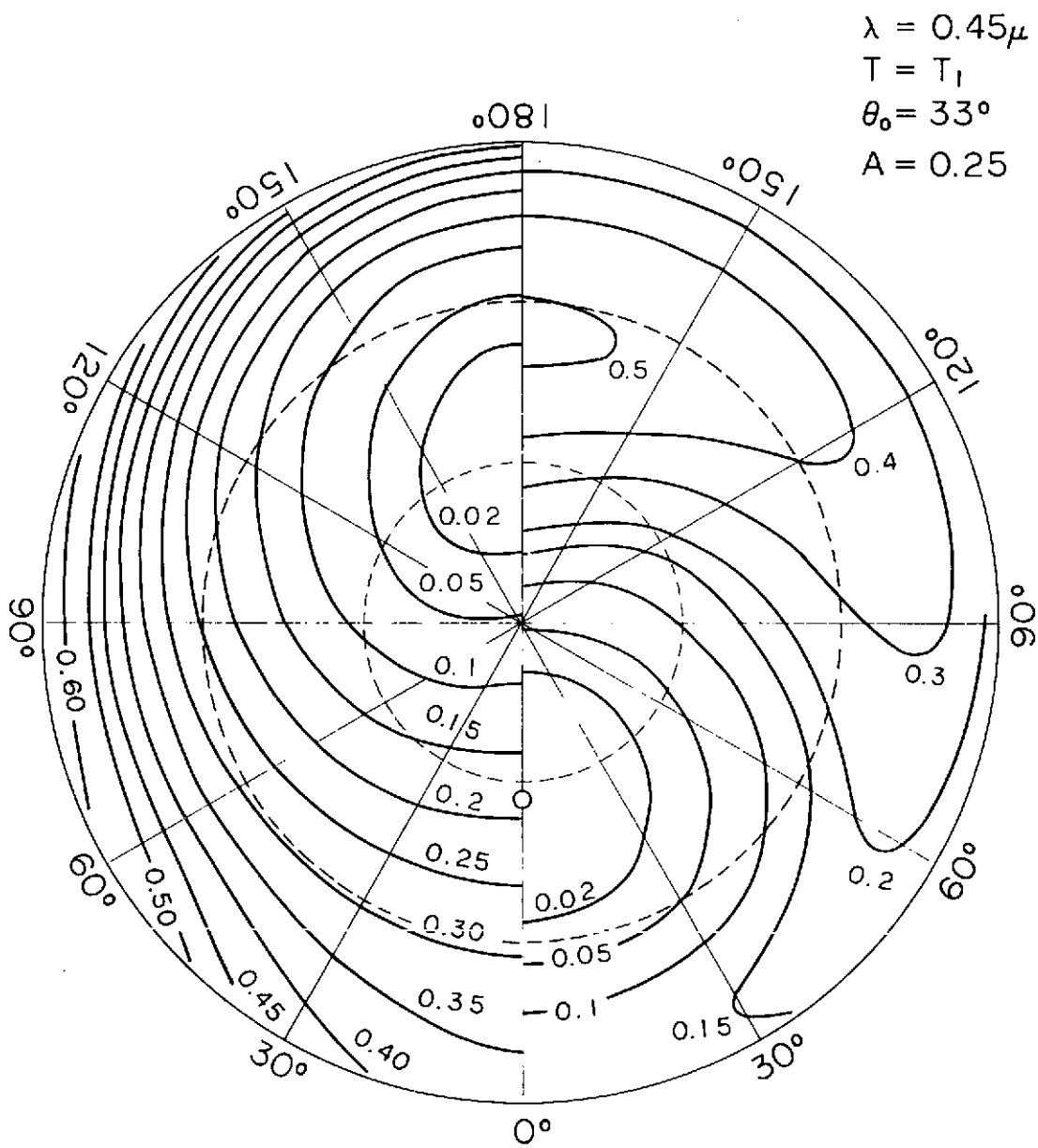

Fig. 15 Distribution of the degree of polarization of the diffusely reflected (the left half) and transmitted (the right half) radiation for the same case as Fig. 14.

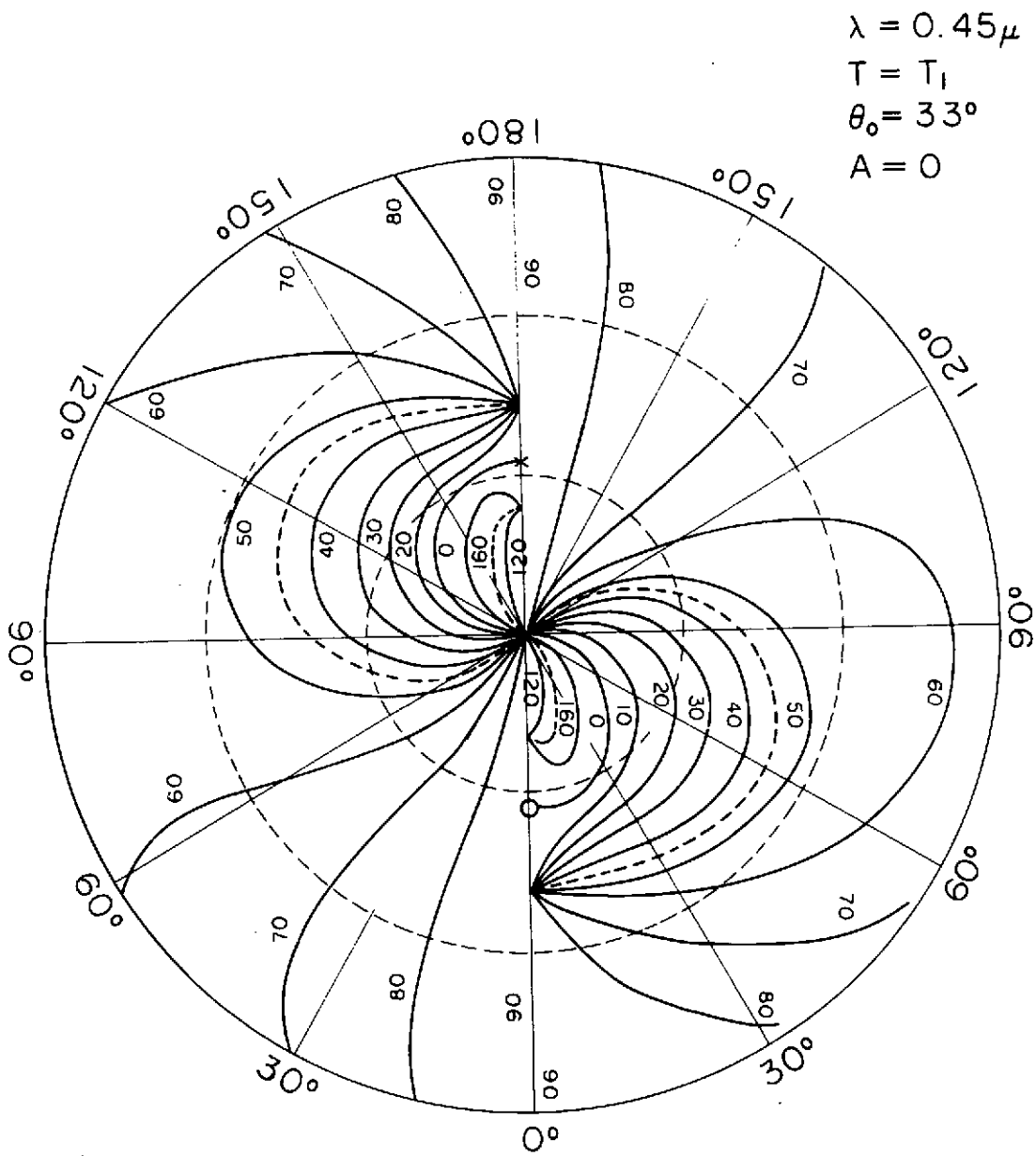

Fig. 16 Distribution of the direction of polarization plane of the diffusely reflected (the left half) and transmitted (the right half) radiation for the same case as Fig. 14 but for A = 0.0.

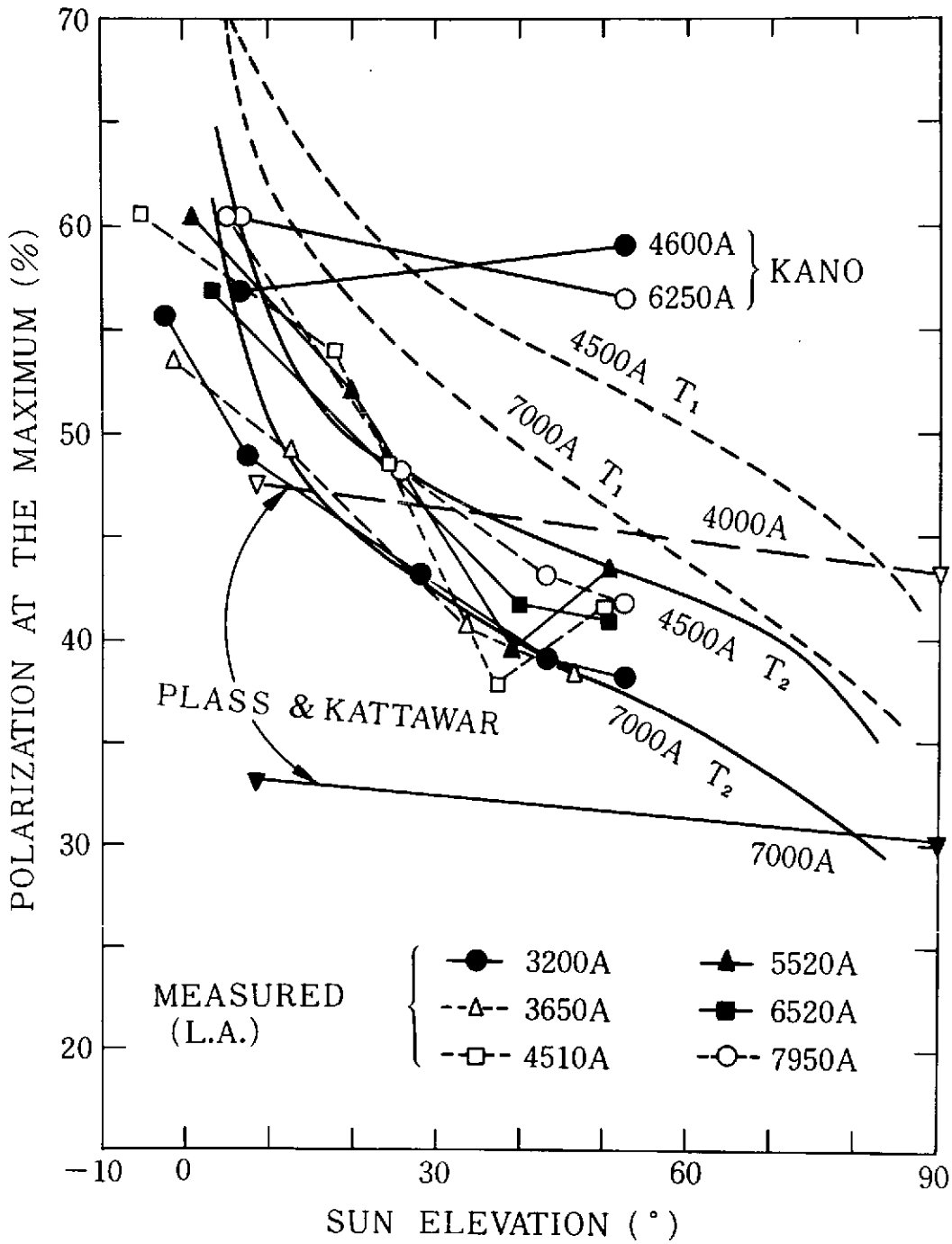

Fig. 17 Degree of polarization at the maximum versus sun elevation as measured by Coulson, compared with the theoretical values obtained by Kano, Plass and Kattawar, and Tanaka.

SCATTERING AND ABSORPTION FROM POLY-DISPERSED AEROSOLS

K. Bullrich, R. Eiden, G. Eschelbach, K. Fischer,
G. Hänel, and J. Heintzenberg
Johannes Gutenberg-Universitat
Mainz, Germany

Abstract

In the present study, results from numerical computations of the diffuse sky radiances and degree of polarization are given. These results were obtained by solving the equation of radiative transfer in the formulation of Eschelbach. In these computations, multiple scattering and absorption by aerosol particles were considered. In addition, results from experimental measurements of the complex refractive index of aerosol samples at different relative humidities are presented. From the radiation flux divergences which were computed based on the determined properties of atmospheric aerosol particles, atmospheric heating rates were derived which were found to be comparable to the heating rates by water vapor. In how far these heating rates are compensated due to cooling as a result of infrared emission of the aerosol particles has not yet been investigated.

1. INTRODUCTION

The knowledge of the heat balance of the atmosphere is of paramount importance in meteorology. The heat balance is highly controlled by the radiation balance. Thus, its evaluation comprises--among other calculations--the computation of the radiant fluxes in the visible and their divergences. The computation of these divergences at different heights of the atmosphere necessitates to meet two requirements:

1) the equation of radiative transfer must be solved by taking into account multiple scattering in a turbid atmosphere;

2) the properties of extinctive material in the atmosphere, that affects multiple scattering and absorption of radiative transfer.

The fulfillment of both these conditions requires expert knowledge in the field of mathematics as well as in the field of physics and chemistry.

2. RESULTS

I. Computations with the Help of the Equation of Radiative Transfer

The equation of radiative transfer is an integrodifferential equation describing the radiation field in an extinctive medium by taking into account the multiple scattering. The solution yields the four Stokes' parameters of the atmospheric radiation field. The vertical radiant flux is obtained by integrating the vertical components of the radiance over all directions. To solve our problems, the equation of radiative transfer must be transformed into a system of linear algebraic equations by discretion of the coordinates of space and angle for obtaining a numerical solution. The basic features of this technique have been described by Herman et al. (1971). Eschelbach et al. (1969) published as a modification for adjusting this technique to the complexity of the scattering properties of the atmospheric aerosol. Under the assumption of the atmosphere being plane parallel, infinite in extent and homogeneous in a horizontal plane, the spatial functional relationship of the radiation is reduced to a mere height dependence. This technique gives the radiation field also inside of the atmosphere. Thus, it is suitable for determining divergences. Since this procedure has been published, it is appropriate to concentrate on the results obtained. Of course, only some exemplary computational results can be given here. They are based upon specific assumptions on the properties of the atmospheric aerosol particles which will be commented upon in the second part of this paper.

On the other hand, we hasten to mention that several authors reported on other methods to solve the equation of radiative transfer which all have their merit if applied to the range of problems they chose to investigate. [W. G. Blättner et al.(1971); S. Chandrasekhar (1969); C. Devaux et Lenoble (1972); J. E. Hansen (1971); K. Heger (1971); A. C. Holland et al. (1970); J. W. Hovenier (1971); H. C. van de Hulst (1963); W. M. Irvine (1968); G. W. Kattawar and G. N. Plass (1968); I. Kuscer and M. Ribaric (1959); G. S. Livshitz (1973); H. Quenzel (1971); E. Raschke (1972); M. Tanaka (1971); G. Yamamoto et al (1972)].

a) Sky Radiance

The first example gives the computed regional distribution of sky radiance sighted from the surface of the earth, for the green wavelength $\lambda = 0.55\ \mu$ at the solar zenith distance of 37°, (See Figure 1, left).

The isolines of sky radiance have been plotted as functions of the zenith angle ϑ and the azimuth angle φ in polar coordinates. ϑ is the radial and φ angular component. It has been assumed that the turbidity factor was $T = 4$, the real part of the complex refractive index of the aerosol particles was $m = 1.5$ and the albedo of the surface of the earth was $A = 0.25$. The computation has been based upon Junge's model of aerosol particle size distribution $dN/d \log r = \text{const}\ r^{-\nu^*}$, with $\nu^* = 3$ which will be commented upon later. N denotes the number of aerosol particles per cm^3, r the particle radius, and A is the ratio of the amount of radiation reflected by the surface of the earth to the amount incident upon it.

The values refer to a normalized extraterrestrial solar irradiance being $S_{0\lambda} = \pi$. These values include the multiple scattering on air molecules and aerosol particles. Though the computation has taken multiple scattering into account, the computed values in most cases show characteristic deviations from the measured ones. This is due to absorption of radiation by the atmospheric aerosol

particles. This absorption can be accounted for by adjusting the imaginary part of the complex refractive index, which is written $m = n - ki$, with n being the real and k the imaginary part of the complex refractive index. It will be pointed out later that the assumption of $m = 1.5 - 0.02i$ is realistic for continental atmospheric aerosol particles.

The influence of aerosol absorption shown in Figure 1, right, has been evaluated under the above assumption of refractive index. The isolines represent the ratio I/I_{abs}, i.e. I denotes the sky radiance without and I_{abs} with aerosol absorption. The assigned parameters and the way of presentation have been chosen the same as in the previous Figure 1, left. It is obvious that the regional distribution of sky radiance is greatly influenced by aerosol absorption: The values including absorption are increased by 10% to 50%.

It is noteworthy that in those regions of the sky which are far from the sun, the fraction of multiple scattering can be double or more that of primary scattering; no sooner than in the immediate surroundings of the sun, it becomes negligible in comparison with primary scattering.

Figure 2 shows an example of the influence of the scattering of higher order for the case of albedo $A = 0$. There can be seen the ratio of the sky radiance I in the sun's vertical and the counter-vertical for multiple scattering to that for primary I_{PS}. If absorption is considered (values represented by dashed lines), the effect becomes smaller.

b) Divergences of Radiant Flux and Heating Rates

The above computations can be conducted for any heights above the ground. The integration of the radiances taken over all directions yields the radiant flux which can be computed for both vertical directions, downward and upward. The differentiation of the vertical radiant fluxes F in relation to the height z yields the radiant divergences dF/dz which are needed for determining the heating rates with respect to time for the visible:

$$dT/dt = \frac{1}{\rho c_p} \int_{\lambda_1}^{\lambda_2} (dF/dz)\, d\lambda \quad ,$$

with T denoting the temperature; t, the time; ρ, the air density; c_p, the specific heat at constant pressure p, λ, the wavelength; F, the radiant flux; and z, the height above MSL.

Figure 3 shows the daily heating rates in the lower troposphere for the zenith distances of 37° and 66°; the three albedo values of the surface $A = 0$, $A = 0.25$, and $A = 0.8$; and for the spectral range, $0.45\ \mu \leq \lambda \leq 0.85\ \mu$ under the assumption that the decrease of aerosol particles with the height z follows the relation $N(z) = e^{-(z/H_D)}$ with $H_D = 1.25$ km denoting the vertical extent of the homogeneous turbid atmosphere and under the further assumptions that again $m = 1.25 - 0.02i$ and $T = 4$. The decrease of the heating rates with increasing height had to be expected, because the decrease of the absorbent aerosol particles acts in the same direction. The influence of the surface albedo can be clearly seen. Since the amount of turbidity factor, $T = 4$, applies for central Europe, the results presented here imply that at least near the ground the influence of the aerosol in the short-wave portion of the spectrum is equal to or even greater than that of the vapor pressure if the mean value of vapor pressure is assumed to amount to 2 grams per cm^2 according to Roach (1961). (Of course, these heating rates are counterbalanced by cooling rates of the same order of magnitude due to outgoing radiation in the infrared as has been shown by Grassl in 1973).

These introductory remarks were meant to point out which important conclusions on the energy balance of the planet, earth, could be drawn if the equation of radiative transfer could be solved under realistic boundary conditions which apply to the atmospheric conditions.

c) Degree of Polarization of the Sky Radiance

Some supplementary examples of the degree of polarization of sky radiation are given which have been obtained by way of theory as well of experiment. It is well known that Sekera and his collaborators have made comprehensive studies on this subject with regard to the molecular atmosphere. Today, it is possible to account for the multiple scattering on molecules and aerosol particles; this results in a remarkably good agreement between theory and experiment. It is the polarization of sky radiation which is such a sensitive indicator for the addition of aerosol particles in the conservative hypothetical atmosphere consisting of gas molecules only.

Figure 4 gives an example out of the numerous measuring series of sky radiation polarization which have been carried out at first at Mainz and then at various places of the globe; this example gives the results obtained at Mainz. To the left, there are the results of the measurements taken by Nowak (1970); to the right, there are the results of the computations conducted by Eschelbach (1973).

On Figure 5, one can see the difference $P_{PS} - P$ (%) between the sky light polarization for primary scattering (P_{PS}) and that for multiple (P) in the sun's vertical and counter vertical (calculations). The strong influence of higher order scattering is remarkable, particularly if no absorption is assumed.

In this context, the elliptical polarization of the sky radiation has a bearing, too. Already in 1955, Sekera had furnished proof that elliptical polarization cannot occur in a mere molecular atmosphere, whereas R. Eiden in his measurements of the distribution of sky radiation in 1970 had found characteristic features of this elliptical polarization.

Figure 6 gives an example of the results of measurements taken at Mainz. The ellipticity $\tan \beta$ is plotted as a function of the azimuth angle α. (The elliptical polarization is characterized by $\tan \beta$; β is the ratio of the greater to the smaller axis of the ellipse which is traced by the electrical vector). A maximum is located in between the azimuth angles 40° and 90°; it amounts to $\tan \beta = 0.1$ or less, depending on turbidity and elevation h of the observation in the sky. It is the highest for large elevation above the horizon. In both directions to the sun's vertical, the ellipticity decreases continuously and goes sometimes to negative values. $\tan \beta$ being negative means lefthanded elliptical polarization. What is the explanation for these measurement results? Already Mie had proved that only linear polarization of the natural light can be expected when it is scattered on aerosol particles and gas molecules. Thus the production of elliptically polarized skylight due to primary scattering is not possible. But in case of higher-order scattering processes, the light which is subject to another scattering process is already at least partly linearly polarized. From these processes, we can expect elliptical polarized light from the sky. Furthermore, the position of the plane of polarization with regard to the reference plane plays an important role. If the plane of polarization of the incidient light is parallel or normal to the reference plane, the scattered light cannot show anything but linear polarization; for instance, the plane of polarization in the sun's vertical is parallel to the reference plane. Therefore, no elliptical polarization can be found here. Thus, Arago looked for elliptical polarization here in vain. Fesenkov (1961) could not find any elliptical polarization in the sky because the atmosphere at Alma Ata was too clean.

Figure 7 represents results from computations. The measured data only are understandable if absorption is assumed.

II. The Atmospheric Aerosol

Over the past few years, increasing attention has been focused to possible global temperature changes due to absorption by particulate matter in the atmosphere. Only minimal data, for instance, on the absorbing properties of natural atmospheric particles are available as yet.

The examples given here furnished proof that the variations of sky radiance and its degree of polarization can be simulated by computations if the equation of radiative transfer is solved by accounting for multiple scattering in the turbid atmosphere as well as absorption by the aerosol particles. This requires the making of specific assumptions on the constitution of the atmospheric aerosol particles. On the other hand, quite a contrary approach has been tried by drawing conclusions on the physical properties of the aerosol particles from physical experiments in the way of radiation measurements. However, we do not go into detail here because the interpretation is always somewhat equivocal.

It is rather deemed necessary to discuss the question whether the assumptions on the size distribution and the physical properties of the aerosol particles are realistic. Recently, some basic experiments have been made for answering this question. They covered the complex influence of the relative humidity on the aerosol particle size distribution and the refractive index of the particles.

a) Aerosol Particle Size Distributions

Figure 8 shows a variety of mean aerosol particle size distributions derived from recent measurements which were based on different measuring techniques at various locations of the globe by Junge in 1971. The graph shows a schematic size distribution of tropospheric aerosol particles: the curve No. 1 denotes the background distribution; No. 2, the continental; No. 3, the maritime (background plus seasalt component); No. 4, the Sahara dust component. These are the basic models of aerosol particle size distribution which have the tendency of turning up again and again. There are individual exceptions from this rule, e.g. in the neighborhood of aerosol sources. And in the higher troposphere and in the stratosphere, the radius range is less wide resembling a logarithmic Gaussian distribution.

The immediate response of the degree of polarization to the aerosol particle size distributions had been demonstrated by Eiden's computations in 1971 which are are shown in Figure 9. The aerosol particle size distributions have been assumed to follow logarithmic Gaussian distributions, the most frequent radius of which is called R_0. Linear polarization has been attributed to the incident radiation; thus, its degree of polarization (ordinate) at the scattering angle $\phi = 0°$ (ϕ is the abscissa) is 100%. The upper part of Figure 9 shows the angular dependent polarization for water droplets; the lower part, for coal particles for various wavelengths. The differences in the refractive indices result in considerable deviations of the values.

b) Real and Imaginary Parts of the Complex Refractive Indices of Atmospheric Aerosol Particles Obtained From Sample Measurements

It is not sufficient to know the size distribution of the aerosol particles. Their physical and chemical properties must also be known for determining their influence on the attenuation of radiation due to scattering and absorption processes in the atmosphere. These properties are characterized by the complex refractive index, $m = n - ik$, with n denoting the real part and k, the imaginary part. The complex structure of the aerosol particles precludes the direct measurement of the real as well as the imaginary part. Certainly, most of the individual chemical constituents--water soluble or insoluble--suspended in the atmospheric aerosol are rather well known. However, it is the mixed structure of the individual particles that forbids any straightforward statement on the refractive index. Therefore, Hänel, in 1966, developed a measuring method for determining the real part of the complex refractive index of aerosol particle samples. He found values ranging between 1.33 for water and 1.77 for dry matter following the influence of the given relative humidity as mentioned previously.

Now, let us concentrate on recent investigations into the imaginary part of the refractive index carried out by K. Fischer in 1973. The measurements have been performed on films of aerosol particles collected by an automatic jet impactor at several urban and remote sites. Details of the measuring method will be published later. We want to place the emphasis on some examples of the results obtained.

The imaginary part, k, of the complex refractive index is called the absorptive index; $K = \frac{4\pi}{\lambda} k$ is called the absorption coefficient; k/ρ, the mass absorptive index with ρ being the density of the aerosol particles; and K/ρ, the mass absorption coefficient. K/ρ is specified by the energy which is absorbed in an infinitesimal wavelength interval and indicates the relevance of the selectivities of the light absorption in the atmosphere.

Figure 10 shows the mass absorption coefficient, K/ρ, in the wavelength range between 0.4 and 2.4 μ. The aerosol samples were taken at four different places. The result from Mainz is an example of urban air particles of medium absorptivity. The samples from Tsumeb, South Africa, and Jungfraujoch, high mountains, Switzerland, were collected at remote sites with low aerosol particle concentrations. Mace Head (Ireland) represents collections at a remote site on the western coast of Ireland.

It should be noted that the values of the clean air sample from Tsumeb in Southwest Africa are similar to that of Mainz (urban origin) which contains soot and further carbon mixed polymerides of polluted air. The absorption coefficients of carbon containing residues of combustion mainly range between 0.3 and 0.8. Thus the absorption of a sample is essentially determined by relatively small contributions of such strongly absorbent constituents like carbon compounds. The South Africa Tsumeb particles are originated by bush burning during the seasonal dry spell. These particles are removed by abrasion if dry blades of grass and leaves are ribboning each other. These particles consist of organic matter, i.e. carbonic compounds, which affect the values like those of polluted air samples taken at Mainz.

Also relatively few carbon compounds are contained in the collections of the high altitude Jungfraujoch aerosol particles.

The mass absorption coefficient measured from samples collected at Mace Head, Ireland, shows lower values. The wind from the north brought air directly from the Atlantic Ocean which is not contaminated by any human activity.

Bands of liquid water are found in the absorption spectra of the investigated aerosol particles. The measurements were performed at a relative humidity of air of 35%. In spite of this relative low relative humidity, water vapor of environmental air is condensed and absorbed on the aerosol substance (Winkler, et al. 1972; Hänel, 1972) thus increasing the absorption additionally. The density of the particles varies with the relative humidity as well as the amount of additional absorption caused by the bands of liquid water in the IR.

On the other side, it is to be seen that between the wavelengths 0.4 and 2.4 μ that the absorption of the investigated aerosol particles as a dry substance may be labeled as grey to a good approximation. That means a continuous attenuation of solar radiation at every process of scattering in the aerosol layer over industrial regions as well as over those with uncontaminated air. The values of the mass absorptive index range from 10^{-3} to 10^{-2} cm^3/g.

Figure 11 shows results of measurements of the mass absorption index, k/ρ, in the wavelength range 2-17 micron from samples taken at Mainz and Jungfraujoch. The peak at 3 micron is originated by water in the atmosphere. The maxima at 7 and 9 microns is caused by $(NH_4)_2\ SO_4$. The absolute amount of absorption depends upon soot and other carbon admixtures. See also Volz (1972, 1973).

Figure 12 represents results from the west coast of Ireland at westerly winds from the ocean (dashed line) and easterly winds (full line) from the continent.

c) The Density of the Atmospheric Aerosol Particles

The measured values of the mass absorptive index k/ρ and the mass absorption coefficient yield the density ρ of the aerosol particles. In order to determine the density Hänel* in 1972 developed special techniques for measuring the mass and the volume of aerosol particles. Mean densities of several types of aerosol particles at the relative humidity of 35% have been found as follows in Table 1.

d) The Change of Light Extinction, Scattering, and Absorption Due to Atmospheric Aerosol Particles as a Function of the Relative Humidity

As mentioned in the beginning, the relative humidity modifies the radius of the aerosol particles--and thus also their size distribution as well as their complex refractive index. In this way, the attenuation of radiation and the angular dependent scattered radiation become remarkably dependent upon the mositure.

There are two basic ways of determining the variation of these radiation parameters as functions of the relative humidity: (a) The radiation parameter under investigation is being measured on particles in an air volume under different relative humidities. (b) The changes in the radiation parameters are being calculated with the help of Mie's theory by basing the computation upon direct measurements of the essential aerosol parameters, namely the size distribution, density, mass and complex refractive index at various relative humidities. The latter method has been applied for obtaining the results discussed here. This method had been developed by Hänel in 1972 under the assumption that during the moisture change the aerosol particles do not coagulate and that they are in thermodynamical equilibrium with the surrounding air. The latter condition is practically always fulfilled at relative humidities less than

* Ph.D. Thesis, University of Mainz

95%; whereas at relative humidities equal to or greater than 95%, it is fulfilled only if the moisture changes are going on rather slowly. Furthermore, it is assumed that the chemical composition and the structure of the particles in dry state are independent of the size of the particles, i.e. that differences in size are only due to differences in mass of the particles. The investigation covered three continental and one maritime type of aerosol.

Figure 13 refers to two aerosol particle size distributions called Model 6 and Model 3 here. The change in size distribution due to a change in relative humidity has been demonstrated. The abscissa is the radius r in cm; the ordinate is $dN/d \log r$ per cm^3; and N is the total number of particles per cm^3.

The "Model 6" characterizes an aerosol particle size distribution in clean air (see also Figure 8). The samples of which have been collected on top of the Hohenpeissenberg in southern Germany at a height of 1,000 m above MSL.

The "Model 3" represents an aerosol particle size distribution which in April 1969 had been measured by Jaenicke on board the research vessel "Meteor" on the central Atlantic. These aerosol samples represnt a typical maritime aerosol (Junge and Jaenicke, 1971).

Table 2 shows the change in the mean values of the density, of the real, and of the imaginary parts of the complex refractive index of aerosol particle samples; and the ratio of the volume of the humid aerosol sample to that of the dry as a function of the relative humidity. The samples were taken on board the "Meteor" on the North Atlantic. The values are valid for the wavelength $\lambda = 0.59\ \mu$.

Figure 14, which is valid for the wavelength $\lambda = 0.55\ \mu$, shows the functional relationship between the relative humidity f and the changes of the extinction coefficient $\sigma_E(f)$, the scattering coefficient $\sigma_S(f)$, the absorption coefficient $\sigma_A(f)$, and the total geometrical cross-section $Q(f)$. The ratios $\sigma_A(f)/\sigma_0$ are the abscissa, whereas the ordinate represents $1 - f$ in its lower part and f in its upper part. (f) denotes the moist state at the relative humidity f; the index 0 denotes the dry state at the relative humidity $f = 0$.

Obviously, three conclusions can be drawn:

(1) The extinction coefficient $\sigma_E(f)$ and the total geometrical cross section $Q(f)$ are closely related. Both these quantities have almost the same rate of growth with increasing relative humidity. The differences do not surpass 20% to 30%.

(2) The scattering coefficient shows a greater rate of growth with increasing relative humidity than the extinction coefficient.

(3) The absorption coefficient shows only little variation with the relative humidity.

The physical explanation for these effects can be seen from Figure 15. The ordinate represents the efficiency factors σ/Q. The abscissa represents the generalized size parameters (R. Penndorf, 1962; H. C. van de Hulst, 1957; D. Deirmendjian, 1969; G. Hänel, 1971)

$$\alpha^* = \frac{2\pi r}{\lambda} \sqrt{(n-1)^2 + k} \quad .$$

The solid lines refer to $f = 0$. The dashed lines are valid for large values of f. The black color means extinction, red means scattering, and blue means absorption.

It can be seen that the efficiency factors related with high relative humidities oscillate around the efficiency factors related with low relative humidities, i.e. the mean value almost remains the same. This explains the close relationship between the extinction and the total geometrical cross section of all particle sizes.

The efficiency factors scattering at $f = 0$ are very well lower than the efficiency factors extinction. At high relative humidities, the imaginary part of the complex refractive index is diminished. This raises the efficiency factors scattering so that they come close to the values of the efficiency factors extinction. This means that their mean value increases with increasing relative humidity. Consequently, the scattering coefficient shows a higher rate of growth with increasing relative humidity than the extinction coefficient whereas the efficiency factors absorption considerably decrease with increasing relative humidity. Correspondingly, the absorption coefficients can only slightly increase with increasing relative humidity.

The conclusions drawn from Figure 14 also apply to the wavelength $\lambda = 1.0\ \mu$. At $f = 97\%$, the extinction and scattering coefficients show a 20% to 30% higher rate of growth than those in Figure 14. The absorption coefficient shows only a slightly higher rate of growth with increasing relative humidity at $\lambda = 1.0\ \mu$ than at $\lambda = 0.55\ \mu$. Deviations occur if the aerosol particle size distributions differ from those of the Models 3 and 6. The investigation of a mixed aerosol, e.g. a maritime aerosol mixed with Saharian aerosol (see Figure 8), yields a lesser rate of growth with increasing relative humidity at a wavelength $\lambda = 1.0\ \mu$ than at $\lambda = 0.55\ \mu$. This is due to the special type of aerosol particle size distribution and the small imaginary part of the complex refractive index.

Figure 16 shows the variation of the scattering function as a function of the relative humidity on account of the previously mentioned measurements of the refractive index and the aerosol particle density. The scattering angle ϕ is the abscissa. The radiation intensity is the ordinate. The results in Figure 16 refer to an aerosol particle size distribution for continental aerosol (see Figure 8) as it has been measured at Mainz, Germany. It is obvious that an increase in the relative humidity affects an increase in the angular dependent scattering within the range of small scattering angles, i.e. in the range of forward scattering, whereas it affects a strong decrease of scattering intensity at scattering angles > 30°. A similar functional relationship with the relative humidity exists for the angular dependent degree of polarization or the elliptical polarization respectively,

e) Measurements of the Wavelength Dependent Extinction Over the North Atlantic

Finally, extinction measurements taken over the North Atlantic shall demonstrate the great variations of the spectral extinction coefficient upon quick changes in air mass of different source regions. The self-recording of spectral extinction coefficients which is presented in Figure 17 has been obtained on the Atlantic on board the research vessel "Meteor". The ordinate represents the extinction coefficient σ_λ; the abscissa the time elapsed on the 17th of April 1969 from 01 until 24 o'clock. The different curves refer to six wavelengths within the range from 0.475 μ up to 0.924 μ. The values have been recorded with an integrating nephelometer in an open scattering volume. From 01 up to about 08 o'clock in the morning, almost grey extinction prevailed in the SE trade wind, the corresponding

standard visibility amounting to about 100 km. On Figure 18, it can be seen how the extinction depends upon the wavelength. The ordinate is the extinction coefficient without Rayleigh scattering. The abscissa is the wavelength. Both are in the logarithmic scale. After 8 o'clock in the morning, the extinction strongly increases and it is stronger in the near infrared than in the short wave range--the corresponding standard visibility being only about 20 km. The change in the behaviour of the extinction coefficient can be explained with: (a) a change in the aerosol particle size distribution due to the transport of Saharian dust by the NE trade wind (the maximum in the aerosol particle size distribution is shifted towards greater radii (see Figure 8); (b) the air in the NE trade wind is drier than the air in the SE trade wind; (c) the refractive index is influenced by the quartz component of the Saharian dust.

f) The Influence of the Relative Humidity on the Volume Extinction of an Artificial KCl Aerosol

The influence of relative humidity is pointed out by a laboratory experiment with an artificial potassium chlorate aerosol. In Figure 19, the ordinate shows the extinction coefficient in logarithmic scale; the abscissa shows the elapsed time in linear scale and the relative humidity in an arbitrary non-linear scale. The four curves are valid for the four wavelengths they are labeled with each. Obviously, the difference in extinction between the blue and the green spectrum is smaller than that between the red and the infrared spectrum. The simultaneous measurements of the aerosol particle size distribution yielded a Gaussian distribution with the maximum radius being $r = 0.15\ \mu$.

At the relative humidity of 80%, potassium chlorate dissolves; the particle grow strongly. Consequently, the maximum radius of the particles is shifted towards greater radii resulting in anomalous extinction, i.e. the extinction in the blue spectrum does not differ from that in the green spectrum. With the further increase in relative humidity, the maximum of extinction is shifted from its initial position at $\lambda = 0.475\ \mu$ towards $\lambda = 0.875\ \mu$ -- this affects the blue sun or the blue moon, respectively. (Covert, Charlson and Ahlquist, 1972; Ahlquist, Covert and Heintzenberg, 1972).

REFERENCES

Ahlquist, N. C., D. S. Covert, and J. Heintzenberg: Labor measurements performed at Mainz, December 1972 (Private Communication).

de Bary, E. and G. Eschelback, 1973: The ratio of primary scattering to total scattering of sky radiance. Tellus, submitted for publication.

Blättner, W. G., D. G. Collins, and M. B. Wells, 1971: Monte Carlo calculations in spherical shell atmospheres. Rad. Res. Ass., Sci. Rept. 2, BRA-T 7104 (AFCRC-71-0382).

Chandrasekhar, S., 1950: Radiative Transfer, Clarendon Press, Oxford.

Chandrasekhar, S., 1969: Exact and approximate solutions for multiple scattering by clouds and hazy planetary atmospheres. J. Atm. Sci. 26, 478.

Covert, D. S., R. J. Charlson, and N. C. Ahlquist, 1972: A study of the relationship of chemical composition and humidity to light scattering by aerosols. J. Appl. Meteorol. 11, 968.

Deirmendjian, D., 1969: Electromagnetic scattering on spherical polydispersions. American Elsevier Publications, Co., Inc., New York.

Devaux, C. et J. Lenoble, 1972: Etude du Rayonnement dans les nuages. Univ. des Sciences et Techniques de Lille. Contract No. 6600201, Comite de Recherches Atmospheriques.

Eiden, R., 1970: Influence of the atmospheric aerosol on the elliptical polarization of the skylight. Proceedings of the WMO/IUGG Symposium held in Bergen, August 1968, WMO No. 248 TP. 136, Technical Note No. 104.

Eiden, R., 1971: Determination of the complex index of refraction of spherical aerosol particles. Appl. Optics 10, 749.

Eiden, R. und G. Eschelbach, 1973: Das atmospharische Aerosol und seine Bedeutung fur den Energiehaushalt der Atmosphare. (The atmospheric aerosol and its influence on the energy budget of the atmosphere. Zeitschr. f. Geophysik 9, 189.

Eschelbach, G., K. Bullrich, et al 1969: Research on atmospheric optical radiation transmission. AFCRL Contract F-61052-67-C-0046, No. 7, p. 54.

Eschelbach, G., 1973: Computations of the influence of aerosols on the atmospheric radiation balance in the visible spectrum. Beitr. Phys. d. Atm., 46, 249.

Eschelbach, G., 1973: Calculs numeriques concernant la luminance, le teaux polarisation et les divergences du flux energetique dans l'atmosphere trouble tenant compte de le diffusion multiple. Ann. de Geophysique, in press.

Fischer, K., 1970: Bestimmung der Absorption von sichtbarer Strahlung durch Aerosolpartikel. (Measurements of absorption of visible radiation by aerosol particles) Beitr. Phys. d. Atm., 43, 244.

Fischer, K. und G. Hänel, 1972: Bestimmung physikalischer Eigenschaften atmospharischer Aerosolteilchen uber dem Atlantik. "Meteor" Forsch.-Erg. Reihe B.

Fischer, K., 1973: Infrared mass absorption index of natural atmospheric aerosols. (Unpublished)

Fischer, K., 1973: Mass absorption coefficient of natural aerosol particles in the 0.4 - 2.4 micron wavelength interval. Beitr. Phys. d. Atm., in press.

Fesenkov, V. G., 1961: Presence of elliptical polarization in the light of day sky. Soviet Astron. A. Y. 4 (5), New York, 741.

Grassl, H., 1973: Aerosol influence on radiative cooling. Tellus, 25.

Hänel, G., 1971: Die Grosse atmospharischer Aerosolteilchen als Funktion der relativen Luftfeuchtigkeit. (The size of atmospheric aerosol particles as a function of the relative humidity) Beitr. Phys. d. Atm. 43, 119.

Hänel, G., 1971: New results concerning the dependence of visibility on relative humidity. Beitr. Phys. d. Atm. 44, 137.

Hänel, G., 1972a: Computation of the extinction of visible radiation by atmospheric aerosol particles as a function of the relative humidity, based upon measured properties. Aerosol Sci., 3, 377.

Hänel, G., 1972b: The ratio of the extinction coefficient to the mass of atmospheric aerosol particles as a function of the relative humidity. Aerosol Sci. 3, 455.

Hansen, J. E., 1971: Multiple scattering of polarized light in planetary atmospheres. J. Atm. Sci. 28, 120.

Heger, K., 1971: Einfach-Zweifach- und Dreifachstreuung der Sonnenstrahlung in der truben Atmosphare. Beitr. Phys. d. Atm. 44, 201.

Herman, M. B., S. R. Browning, and R. J. Curran, 1971: The effect of atmospheric aerosols on scattered sunlight. J. Atm. Sci. 28, 419.

Holland, A. C., and G. Gagne, 1970: The scattering of polarized light by polydisperse systems of irregular particles. Appl. Optics 9, 1113.

Hovenier, J. W., 1971: Multiple scattering of polarized light in planetary atmospheres. Astron. Astrophys. 13, 7.

van de Hulst, H. C., 1957: Light Scattering by Small Particles. John Wiley and Sons, Inc., New York.

van de Hulst, H. C., 1963: A new look at multiple scattering. Mimeographed Report, NASA, Inst. for Space Studies, New York.

Irvine, W. M., 1968: Multiple scattering by large particles. II: Opically thick layers. Astrophys. J. 152, 823.

Junge, Chr., 1971: Der Stoffkreislauf der Atmosphare. Jahrbuch der Max Planck-Gesellschaft, 149.

Junge, C. and R. Jaenicke, 1971: New results in background aerosols studies from the Atlantic expedition of the R. V. Meteor. Spring 1969. Aerosol Sci., 2, 305.

Kattawar, G. W. and G. N. Plass, 1968: Radiance and polarization of multiple scattered light from haze and clouds. Appl. Optics 7, 1519.

Kuščer, I and M. Ribaric, 1959: Matrix formation in the theory of diffusion of light. Optica Acta 6, 42.

Livshitz, G. Sh., 1973: The scattered light of the daily sky. Alma Ata.

Nowak, W., 1970: Zur spektralen Verteilung der Himmelslicht-polarisation. Optik, 32, 22.

Penndorf, R. B., 1962: Scattering and extinction coefficients for small absorbing and non-absorbing aerosols. J. O. S. A., 52, 896.

Quenzel, H., 1971: Das atmospharische Strahlungsfeld im Spektralbereich der Sonnenstrahlung. Wiss. Mitt. des Meteorol. Inst. Univ. München.

Raschke, E., 1972: Multiple scattering calculation of the transfer of solar radiation in an atmosphere-Ocean System. Beitr. Phys. d. Atm. 45, 1.

Roach, W. T., 1961: The absorption of solar radiation by water vapor and CO_2 in a cloudless atmosphere. Q. J. Roy. Met. Soc. 87, 364.

Sekera, Z., 1955: Investigation of polarization of skylight. Final Rep., Contr. No. AF 19 (122), 239.

Tanaka, M., 1971: Radiative transfer in turbid atmospheres I. J. of the Meteorol. Soc. Japan, 49, 296.

Tanaka, M., 1971: Radiative transfer in turbid atmospheres II. J. of the Meteorol. Soc. Japan, 49, 321.

Volz, F. E., 1972: Infrared absorption by atmospheric aerosol substances. J. Geoph. Res. 77, 1017.

Volz, F. E., 1972: Infrared refractive index of atmospheric aerosol substances. Appl. Optics, 11, 755.

Volz, F. E., 1973: Infrared optical constants of ammonium sulfate, sahara dust, volcanic pumice, and flyash. Appl. Optics, 12, 564.

Winkler, P. and Chr. Junge, 1972: The growth of atmospheric aerosol particles as a function of the relative humidity. J. de Recherches Atmospheriques, 6, 617.

Yamamoto, G. and M. Tanaka, 1972: Increase of global albedo due to air pollution. J. Atm. Sci. 29, 1405.

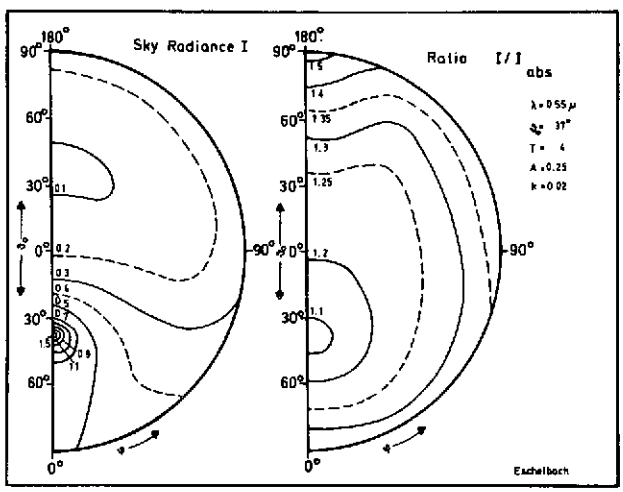

Figure 1: Left: Isolines of the sky radiance I on polar coordinates. Zenith distance of the sun ϑ_o = 37°, wavelength λ = 0.55 micron, turbidity factor T = 4, albedo of the surface A = 0.25. Power law of the aerosol size distribution with exponent 3, real part of the refractive index m = 1.5, no absorption.

Right: I/I_{abs} where I is the sky radiance without absorption and I_{abs} is that with absorption; imaginary part of the refractive index k = 0.02. (G. Eschelbach, 1973)

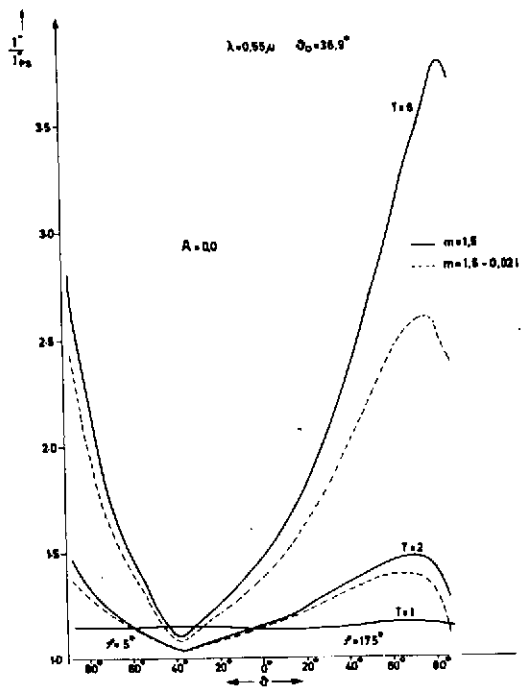

Figure 2: Ratio of the sky radiance I (ordinate) in sun's vertical and counter vertical (abscissa) for multiple scattering to that for primary scattering Ips. Azimuth angle α = 5° respectively 175° zenith distance of the sun ϑ_o = 37°; wavelength λ = 0.55 micron, turbidity factors T = 1, T = 2, T = 6; albedo A = 0. Full lines: no absorption (real part of the refractive index m = 1.5); dashed lines: with absorption (imaginary part of the refractive index k = 0.02). Aerosol model as Figure 1 (G. Eschelbach, 1973).

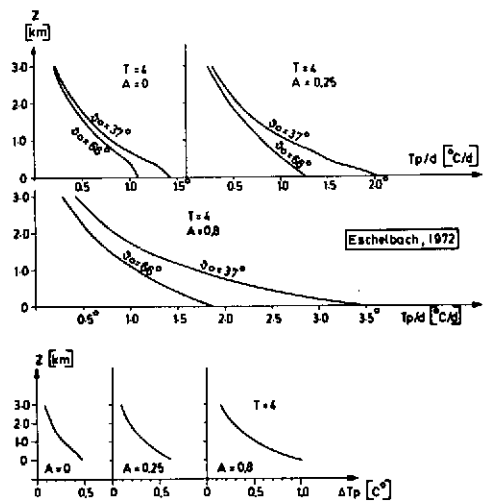

Figure 3: Upper: Heating in °C per day (abscissa) due to the aerosol absorption versus height z (ordinate) for the zenith distances of the sun ϑ_o = 37°, 66° and albedo A = 0, 0.25, 0.8. Wavelength range 0.45 - 0.85 micron.

Lower: Same conditions as in upper figure, but heating in °C for a day during the last third of April or second third of August at 50° north (G. Eschelbach, 1973).

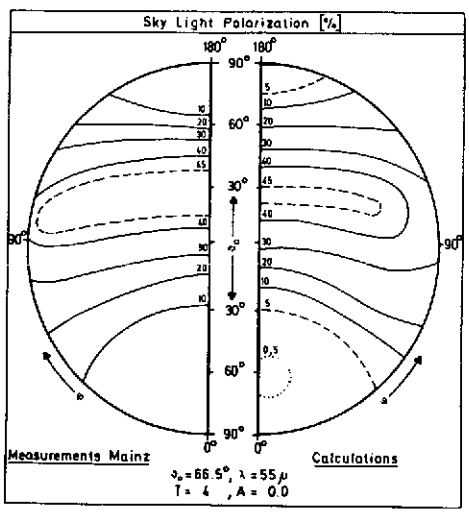

Figure 4: Isolines of skylight polarization P (%) on polar coordinates. Zenith distance of the sun ϑ_0 = 66.5°, wavelength λ = 0.55 micron, turbidity factor T = 4, albedo A = 0.

Left: measurement performed at Mainz (W. Nowak, 1970).

Right: calculations (G. Eschelbach, 1973).

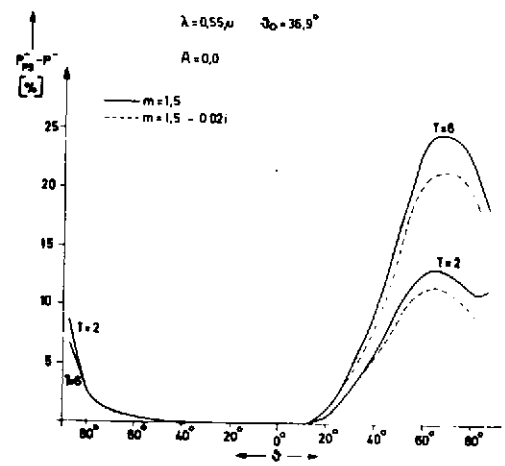

Figure 5: Difference P_{PS} - P (%) between the skylight polarization for primary scattering (P_{PS}) and that for multiple scattering (P) [ordinate] in sun's vertical and counter vertical [abscissa]. Zenith distance of the sun ϑ_0 = 37°, wavelength λ = 0.55 micron, albedo A = 0, turbidity factors T = 2, T = 6. Full lines: no absorption; dashed lines: with absorption. (G. Eschelbach, 1973).

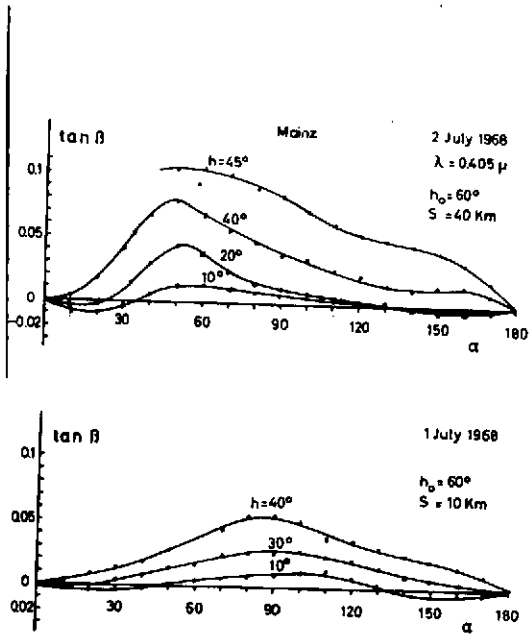

Figure 6: Elliptical polarization of skylight. Results of measurements performed at Mainz. Ordinate: tan β (β = a/b; a major, b minor axis of the ellipse traced by the electrical vector); abscissa: azimuth angle α, h elevation of the observation. Sun's altitude H_0 = 60°, wavelength λ = 0.405 micron.

Upper: visual range S = 40 km.

Lower: visual range S = 10 km.

(R. Eiden, 1970).

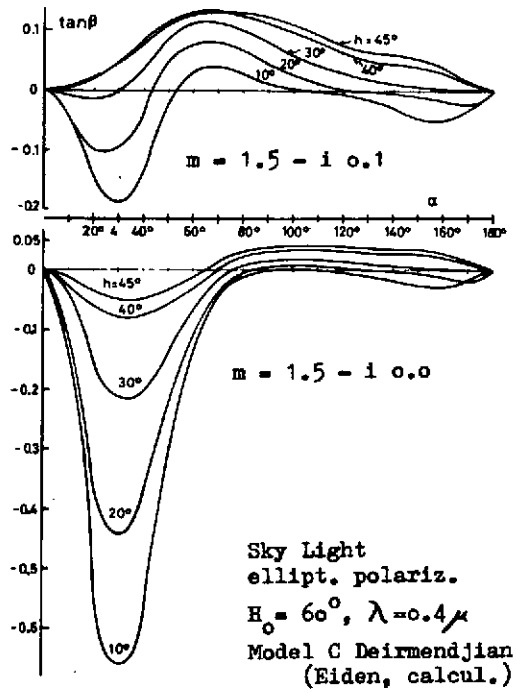

Figure 7: Same conditions as in Figure 6. However, results are from computations.

Upper: with absorption (imaginary part of the refractive index k = 0.1).

Lower: without absorption.

Power law of the size distribution with exponent 3: r = 0.1 - 10 micron; exponent 0: r = 0.04 - 0.1 micron.

(R. Eiden, 1970).

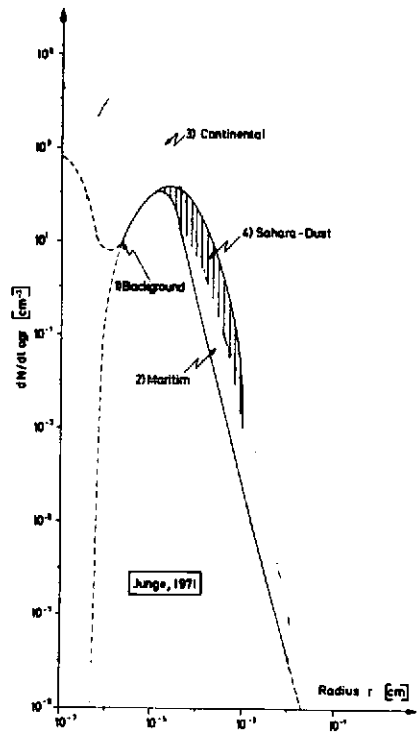

Figure 8: Schematic size distribution of tropospheric aerosol particles. 1) background; 2) continental; 3) background plus seasalt component (maritime); and 4) Sahara dust component. (C. Junge, 1971).

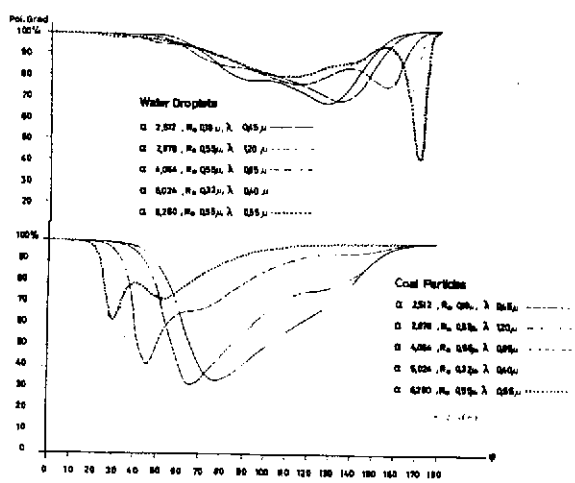

Figure 9: Degree of polarization of scattered radiation by water droplets and coal particles (ordinate) versus scattering angle (abscissa). Size parameter $\alpha = 2\pi r/\lambda$; λ wavelength, r radius of the particles, R_0 radius pertaining to the maximum of a particular Gaussian size distribution. (R. Eiden, 1973).

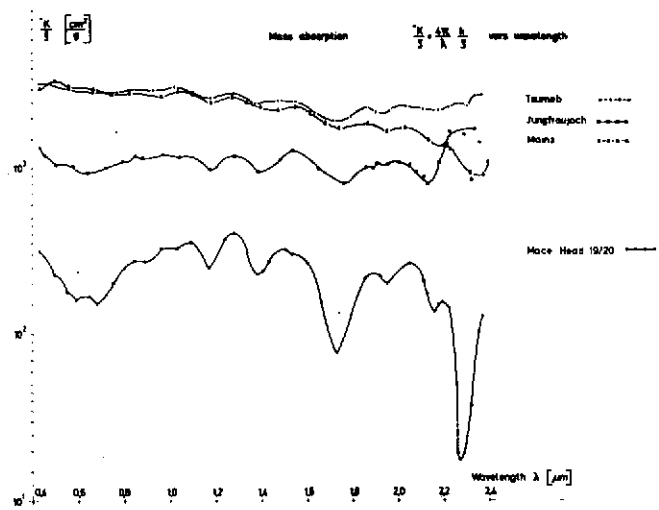

Figure 10: Mass absorption constant K/ρ cm^2/g, (ordinate) versus wavelength (0.4 - 2.5 micron, abscissa). Aerosol samples taken at Mainz (ΔΔΔ), Tsumeb (Southwest Africa +++), Jungfraujoch (high mountain 000), Mace Head (Ireland ...). (K. Fischer, 1973).

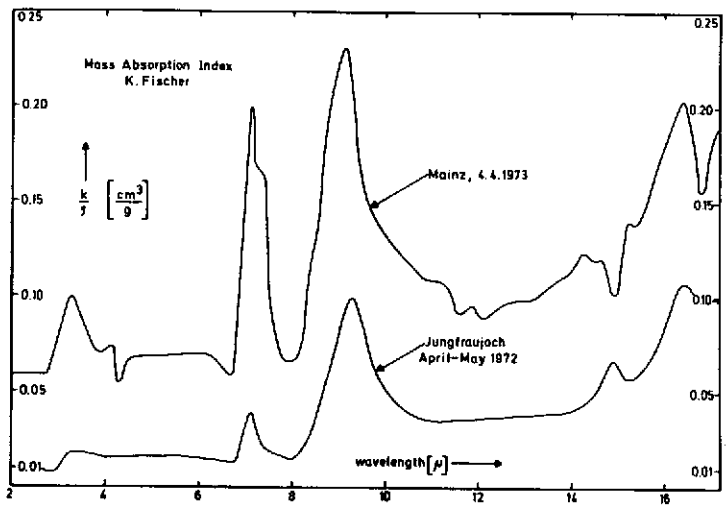

Figure 11: Mass absorption index k/ρ cm^3/g (ordinate) versus wavelength (2 - 17 micron, abscissa). Aerosol samples from Mainz and Jungfraujoch. (K. Fischer, 1973).

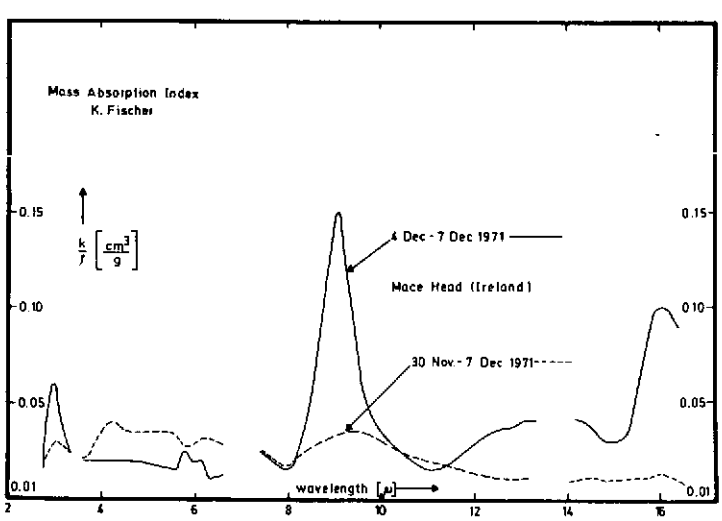

Figure 12: Same as Figure 11, but samples are from the west coast of Ireland (Mace Head). Full lines: westerly winds, dashed lines: easterly winds.

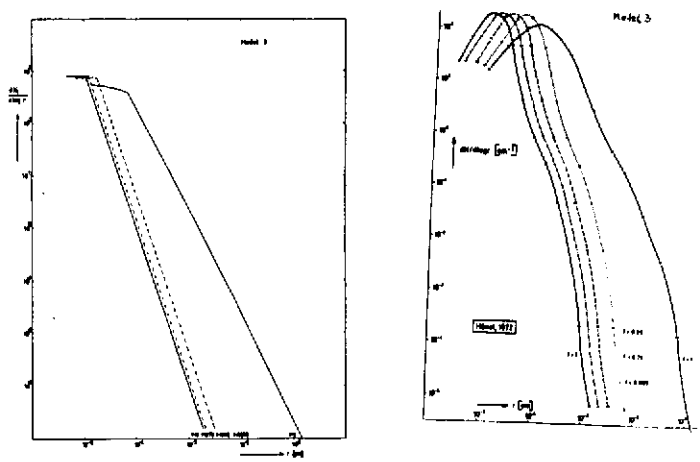

Figure 13: Variation of the size distribution of tropospheric aerosol particles with relative humidity of the air f (f = 0; dry, f = 1.0; 100%).

Left: aerosol samples taken in clean continental air at Hohenpeissenberg, 1000 m NN.

Right: samples from Central North Atlantic, sea-salt aerosol.

(G. Hänel, 1972).

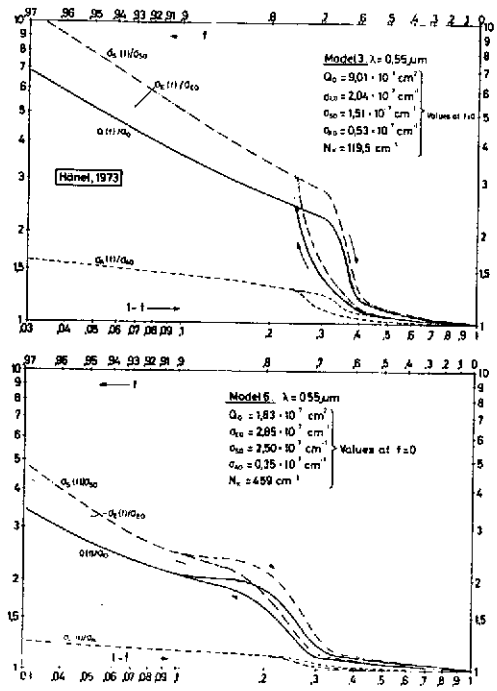

Figure 14: Ratio of $\frac{\sigma_S(f)}{\sigma_{S_0}}$; $\frac{\sigma_E(f)}{\sigma_{E_0}}$; $\frac{\sigma_A(f)}{\sigma_{A_0}}$; $\frac{Q(f)}{Q_0}$

(ordinate) versus relative humidity of the air f upper abscissa; 1 - f lower abscissa. σ_S scattering coefficient; σ_E extinction; σ_A absorption; Q total geometrical cross-section of the aerosol particles; f relative humidity. Subscript 0 pertains to f = 0. Wavelength λ = 0.55 micron; N_K total number of particles. Size distribution of aerosol particles according to Models 3 and 6 given in Figure 13. (G. Hänel, 1972).

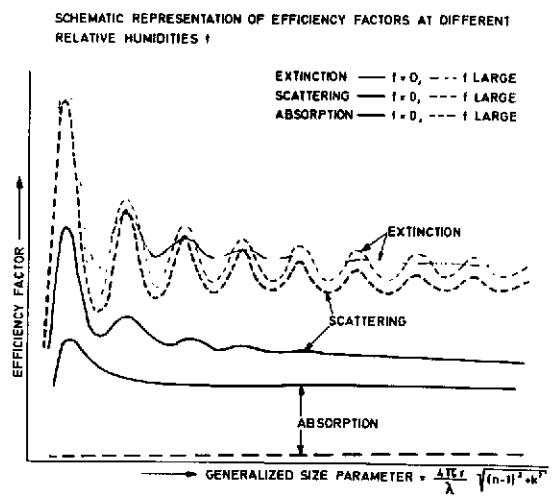

Figure 15: Efficiency factor (ordinate) for scattering, absorption and extinction at different relative humidities f versus generalized size parameter

$$\alpha^* = \frac{4\pi r}{\lambda} \sqrt{(n-1)^2 + k^2} \quad ;$$

n is real and k is imaginary part of the refractive index (abscissa). Full lines: f = 0; dashed lines: f large.
(G. Hänel, 1971).

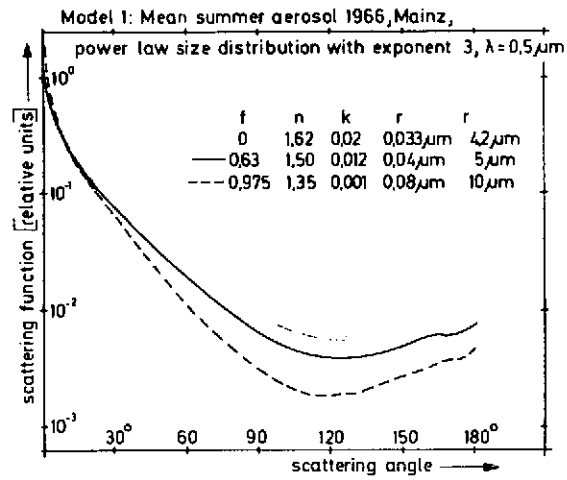

Figure 16: Scattered intensities as function of the scattering angle ϕ for three relative humidities; i.e. three real and imaginary parts of the refractive index (n, k) and three boundary radii r_1, r_2 for a typical summer aerosol size distribution measured at Mainz following a power law with exponent 3. Wavelength λ = 0.5 micron. Full line: f = 0.63, n = 1.5, k = 0.012, r_1 = 0.04 micron, and r_2 = 5 micron. Dash-dot line: f = 0, n = 1.62, k^2 = 0.02, r_1 = 0.033 micron, and r_2 = 4.2 micron. Dashed line: f = 0.975, n = 1.35, k^2 = 0.001, r_1 = 0.08 micron, and r_2 = 10 micron. (G. Hänel, 1973--unpublished).

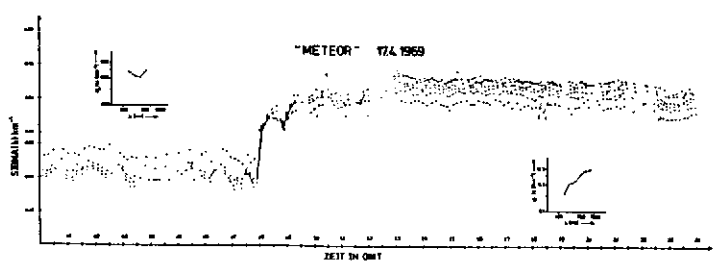

Figure 17: Measured volume extinction coefficient σ [km^{-1}] (ordinate) as a function of time (abscissa) during April 17, 1969, on board the "Meteor" on the North Atlantic for different wavelengths ranging between 0.475 - 0.924 micron. From noon on results influenced by Sahara dust. (J. Heintzenberg, 1970--unpublished).

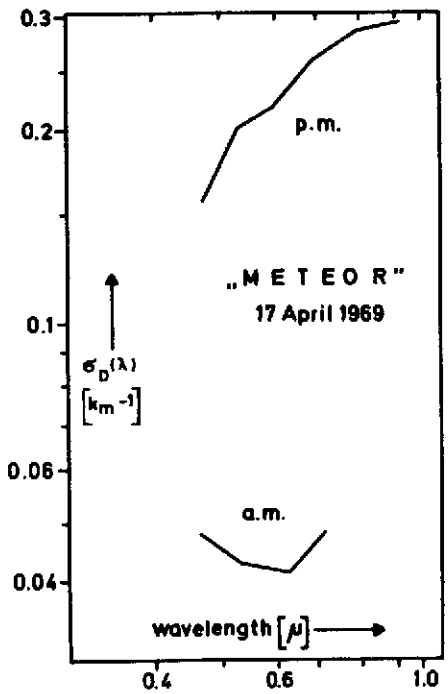

Figure 18: Measured volume extinction coefficient $\sigma_D(\lambda)$ as a function of wavelength on board the "Meteor" on the North Atlantic during morning (a.m.) and afternoon (p.m.) on April 17, 1969. Rayleigh scattering subtracted. (J. Heintzenberg).

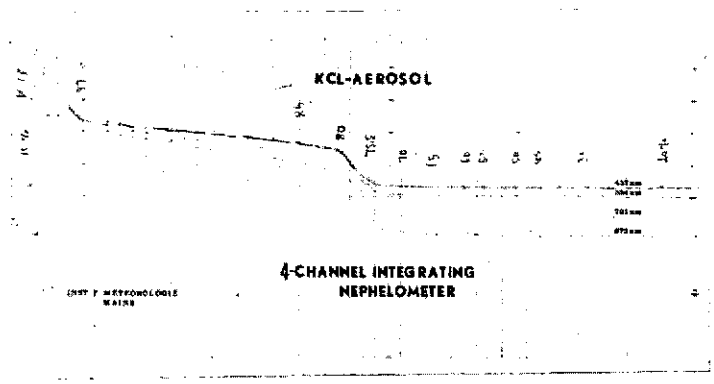

Figure 19: The influence of the relative humdity on the volume extinction, illustrated with an experiment with an artificial KCl aerosol. Ordinate: spectral extinction coefficient (log. scale). Abscissa: elapse time (linear) and the relative humidity (non-linear).

Table 1: Mean density g/cm^3 of different types of aerosol particles. Relative humidity 35%. (Hänel, 1972a).

	Urban (Mainz)	Mountain (Hohen-peissenberg)	Maritime (Atlantic)	Maritime--Continental (Sahara dust over Atlantic)
Increasing humidity	2.77		2.41	2.59
		1.81		
Decreasing humidity	2.68		2.35	2.53

Table 2: Example of results of measurements in April, 1969, on board the "Meteor" on the North Atlantic. (K. Fischer and G. Hänel, 1972).

Increasing Rel. Humidity					Decreasing Rel. Humidity				
f	ρ	n	k	V/V_0	f	ρ	n	k	V/V_0
0.000	2.45	1.55	0.047	1.00	0.835	1.28	1.37	0.009	5.22
0.305	2.41	1.54	0.046	1.03	0.701	1.42	1.40	0.014	3.46
0.497	2.35	1.53	0.044	1.07	0.599	2.11	1.50	0.036	1.31
0.604	2.25	1.52	0.041	1.16	0.516	2.22	1.51	0.040	1.19
0.676	1.98	1.48	0.032	1.48	0.400	2.33	1.53	0.043	1.09
0.722	1.36	1.39	0.012	4.06	0.317	2.38	1.54	0.045	1.05
0.900	1.20	1.36	0.006	7.50	0.202	2.40	1.54	0.045	1.04
0.962	1.09	1.35	0.003	15.00	0.000	2.45	1.55	0.047	1.00

Mean bulk density, real part n and imaginary part k of the mean refractive index at the wavelength of light = 0.589 micron as well as the ratio V/V_0 of the volume of the humid aerosol sample to that of the dry one as functions of relative humidity f.

MULTIPLE SCATTERING IN CLOUD LAYERS; SOME RESULTS

H. C. van de Hulst
Leiden Observatory
Sterrewacht
Leiden 2401, Netherlands

1. INTRODUCTION

Radiative transfer, for the purpose of this lecture, is the art of calculating how the light in a cloud layer or in a turbid air layer may bounce once, or several, or many times in succession against cloud droplets, aerosol particles and air molecules. This once was a formidable subject but by now most problems are solved in principle and many questions have a ready answer in the published literature. But the answer may be hard to find and it is too often disguised in difficult mathematical terms. Therefore, in this talk I shall mostly present to you a variety of slides to show what is now available in the way of accurately computed models.

I fully understand that this is only one side of a wide set of problems. Professor Sekera knew both sides: the first and major side is to assess under what circumstances and with what specifications meteorological problems require the inclusion of a diffuse radiation field set up by multiple scattering or radiative transfer. The second minor problem is to perform with good accuracy the calculation once such a model problem is set up. I shall address myself in this talk only to such models and say little more of the real world.

At one frequency of visible light the properties of a small volume of air (including all its constituents) are characterized mainly by the individual scattering albedo a and the "asymmetry factor" of the single scattering pattern g . An albedo smaller than 1 means that some light at the frequency gets lost, i.e. absorbed, in addition to the scattering process. The energy does not get lost but reappears in heating and eventually in infrared emission but this part is not under discussion now. The cloud layer, or the total atmosphere, is characterized by its total optical thickness b and a level within the atmosphere may be identified by the optical depth τ from the top down. Unidirectional incidence (e.g. from the Sun shining on the atmosphere) is noted by the cosine μ_0 of the angle between the normal and the direction of incidence. The direction of emergence μ is defined similarly. You will notice in the slides that I found it useful to introduce separate symbols for the most often occurring integrals over μ_0 or μ , the symbol U standing for $\int_0^1 \ldots 2\mu_0 \, d\mu_0$ or $\int_0^1 \ldots 2\mu d\mu$ and the symbol N standing for those same integrals without the factor $2\mu_0$ or 2μ . Both have the character of weighted averages and both correspond to simple physical situations. When applied to μ_0 the U means uniform illumination and N the illumination by a narrow layer of

isotropic sources. When applied to μ the U defines the emergent flux and the N the density of the emergent radiation, all with proper normalization.

The range of parameters we have to cover thus becomes

$$\begin{aligned} a &: \quad 0 \ldots 1 \\ g &: \quad -1 \ldots 1 \\ b &: \quad 0 \ldots \infty \\ \tau &: \quad 0 \ldots b \\ \mu_0 &: \quad 0 \ldots 1, \ U, \ N \\ \mu &: \quad 0 \ldots 1, \ U, \ N \end{aligned}$$

I shall say very little about methods because other speakers at this conference have covered that subject. But as a word of general warning, I may remark that it does not always require a professional furniture maker to prevent a four-legged table from rocking. If the sole purpose is to avoid spilling coffee, a folded paper under one leg may be equally satisfactory. Similarly practical solutions exist for some problems in multiple scattering. A lot depends on the required precision in the particular problem at hand. For instance, since nearly 50 years observations of the planet Venus have given the degree of polarization of the light reflected under various angles from its cloud layers with an accuracy of 0.1 per cent. Clearly, their explanation requires calculations which can claim at least that accuracy, a job which has been cleared only recently. In many other situations only a rough estimate is needed and a 1 per cent, or even 10 per cent, error is acceptable. Most sample computations I describe below have been performed to 5-figure accuracy. They are taken from a reference book in preparation.

I shall not give many references. Review papers from an earlier symposium (Hunt, 1971; van de Hulst, 1971) as well as several papers at this symposium (Kuščer and McCormick, 1974; Irvine, 1974) give a good lead into the extensive literature.

2. INTERNAL RADIATION FIELD IN A SLAB

For convenience the illustrations in this section and the next one are from isotropic scattering. This is not essential. The theory for anisotropic scattering is equally well developed but numerical results are less readily available.

Figure 1 shows the full internal radiation field $I(\overset{\circ}{1},\tau)$ (up and down) for an atmosphere with $b = 1$, $a = 1$, perpendicular incidence $\mu_0 = 1$, and backed by a soil with albedo 0.20 and uniform diffuse reflection by Lambert's law. Note the discontinuities at $\overset{\circ}{1} = 0$ for $\tau = 0$ (top) and $\tau = b$ (bottom). The transition from these discontinuities to smooth curves for any τ close to top or bottom makes the mathematics annoying in numerical and analytical methods alike.

In further illustrations, we omit the ground surface. Figure 2 shows the radiation density or source function (expressed as a "gain") as a function of τ. For $b = 0.1$ the gain remains close to 1, which means that the influence of the atmosphere is hardly felt. At larger b ($b = 1$ or 2) it bulges into a curve. At $b = 10$ we see that a "diffusion domain" has developed, in which the dependence on τ is linear. This is always so if $a = 1$ because a constant net flux has to be transported. At the bottom ($\tau = 10$) it edges slightly off in exactly the same form as has been studied for approximately 80 years now. This is the famous Hopf solution of the Milne problem, which is shown separately

as a graph of $\tau + q(\tau)$ in Figure 3.

3. VERY THIN AND VERY THICK SLABS

Obviously there must be simple limiting forms for small b and for large b. But how small is small and how large is large? Let the facts speak in Figure 4, which shows in the domain $a = 0 \ldots 1$, $b = 10^{-3} \ldots 10^{3}$ where deviations from simple forms become 1 per cent or 5 per cent. The curves have been accurately constructed for the function $1RU$ (= reflected flux for perpendicular incidence) in isotropic scattering. But this limitation is not essential. Any other example would show a very similar pattern. At small a there is overlap and, hence, never a computing problem. At large a, a fairly wide gap is seen between the extreme curves at both sides, i.e., "single-scattering" and "$b = \infty$." This gap is narrowed down to 6 doubling steps (less than 2 decades) in b if we take at both sides the next better and still very simple approximation and thus go from "single + double scattering" to "asymptotic formulae."

A few comments on the appropriate methods for both domains may be in order.

Small b. The method of successive orders, of which single scattering and double scattering form the first terms, is simple to grasp and easy to perform. Unless $b = \infty$ and $a = 1$, the sum of all orders converges as a geometric series because the ratio between successive terms tends to a constant. This constant, the eigenvalue, is well known for all b and for a variety of phase functions. The corresponding eigenfunctions may be easily computed.

A method which may have merits for numerical work in isotropic scattering for $b \leq 2$ is to expand the Milne operator systematically in these eigenfunctions. Some tests show that a few terms suffice, fewer than in successive scattering.

Large b. The key is the existence of a diffusion domain, which is any domain of τ far from boundaries and sources. The theory is conceptually simplest for non-conservative scattering. Then a diffusion stream down consists of the basic "mode"

$$I(\tau,\Theta) = P(\cos\Theta)\, e^{-k\tau}$$

and, similarly, up with reversed signs of τ and $\cos\Theta$. This is symbolically illustrated in Figure 5. Near each boundary a transition domain occurs, which involves other modes. These modes are spelled out precisely in the method of singular eigenmode expansions (= Case Method) which will be explained by Professor Kuščer. However, if our sole purpose is to derive the asymptotic equations for large b, we don't have to do that but can simply postulate the existence of an injection and escape function. Near any boundary the diffusion stream suffers negative reflection by a coefficient $\ell = e^{-2kq} < 1$, which also can be interpreted as reflection against a point at an optical depth q beyond the boundary.

My preferred derivation of these concepts (van de Hulst, 1968a) goes via some simple fictitious experiments. The results are straightforward and precise and this basis is as solid as the basis for writing the equation of radiative transfer. Yet my more mathematical friends, conditioned by a century-old tradition, persist in referring to this approach as "heuristic" or "handwaving."

In order to make this less abstract, let us look at actual examples. Figure 6 shows the values of J (source function) for a = 0.90 as function of τ for various b. The diffusion domain shows again as a straight line because now the J-scale is logarithmic. In this example, the albedo is sufficiently different from 1 to cause fairly strong damping, k = 0.5254. As a consequence, only the downwards diffusion stream shows. The counter stream with negative strength running upwards is numerically insignificant.

It gets more interesting if the upstream also counts, which is always true when a is close to 1. Figure 7 shows 1RU in the entire a, b domain. The linear ordinates chosen for this graph are $(b + 1)^{-1}$ and $\sqrt{1 - a}$ so that the entire physical range of the parameters is mapped on a square. Full 100 per cent reflection occurs only in the upper right corner, a = 1, b = ∞. There is a strong suggestion that all curves become geometrically similar near this corner. This is indeed confirmed by the asymptotic equations. Taking an arbitrary direction of incidence μ_0 and observing that the non-reflected flux must be lost either in the atmosphere or in the ground (here assumed black) we have for an arbitrary phase function:

$$\left.\begin{array}{l}\text{Loss in atmosphere } L_{at}\\ \text{Loss in ground } L_{gr}\\ \text{Combined loss } L_{at} + L_{gr}\end{array}\right\} = \frac{4K(1,\mu_0)}{\sqrt{3(1-g)}} \left\{\begin{array}{l} t\,\frac{1-f}{1+f}\\ t\,\frac{2f}{1-f^2}\\ t\,\frac{1+f^2}{1-f^2}\end{array}\right.$$

$$\text{Ratio } L_{at}/L_{gr} = (1 - f)^2/2f$$

With incident flux = 1,

$$t = \sqrt{(1-a)}\,, \quad t << 1$$

$$s = (b+2q)^{-1}, \quad s << 1$$

q = extrapolation length

$K(1, \mu_0)$ = interjection function for a = 1, b = ∞

g = asymmetry factor of phase function

$$f = e^{-\frac{t}{s}\sqrt{3(1-g)}}$$

Values of the quantity q and the function $K(1,\mu_0)$ can be found for a range of assumptions in the literature (van de Hulst, 1968b).

An enlarged and more accurately constructed portion of Figure 7 near the upper right corner is shown in Figure 8 together with some exact ratio curves loss in atmosphere/loss in ground. The labeling has been changed to show the lost flux, rather than its complement, the reflected flux. It is seen that the combined loss curves become similar and the ratio curves approach straight lines, all in exact correspondence with the formulae reproduced above. The physical basis of the similarity is that the losses due to a slight deviation from conservative scattering ($1-a \ll 1$, losses in atmosphere) and those due to a large but finite depth ($1/b \ll 1$, losses in underlying soil) both act as "deep" sinks. Therefore, they have the same dependence on angle of incidence.

Note also that they are by no means additive (which would correspond to straight-line connections between the intersections of the axes in Fig. 8). For, the losses due to a minute absorption per scattering event need a very deep atmosphere to work out fully and the losses due to seeping of the radiation through a very thick atmosphere require an albedo close to 1 in order to materialize at all.

4. REPRESENTATION OF THE PHASE FUNCTION

All of the preceding problems should be redone, in principle, for any new assumption about the phase function. The most important parameter besides the albedo a is the asymmetry factor g, but even in the absence of polarization a complete presentation in the traditional form

$$\Phi(\cos\alpha) = \sum_{n=0}^{\infty} \omega_n P_n(\cos\alpha)$$

where P_n are the Legendre functions, requires the set of coefficients $\omega_0 = a$, $\omega_1 = 3ga$, ω_2, ω_3, etc.

Figure 9 based on the work of a number of authors, shows how g varies for Mie particles from small to large, nonabsorbing and absorbing. We cannot dwell on all interesting details shown in this figure. An important fact is that typical values for water drops in clouds are $g = 0.75$ to 0.9. This makes it necessary to pay attention to very highly asymmetric phase functions.

Instead of dutifully performing a new and lengthy calculation every time that a new phase function is proposed, it is tempting to economize. There are indeed several good reasons for doing so:

a. economy or convenience

b. details corresponding to higher ω_n tend to be washed out in polydisperse clouds

c. influence of any coefficient besides ω_1 vigorously vanishes in the diffusion domain if scattering is conservative $(\omega_0 = 1)$

d. numerical similarity tests show that influence of ω_2 etcetera is weak, except in first-order scattering.

Sometimes the fraction f scattered into the forward hemisphere has been used as a distinctive parameter instead of g. Figure 10 shows in an f, g plot many phase functions that have been used as practicing examples. The Henyey-Greenstein phase functions defined by $\omega_n = (2n+1)a\, g^n$, which I have used in most of my examples, form a good middle-of-the-road choice.

Figure 11 shows by one example out of many, how strongly the value of g influences the result. The atmosphere is semi-infinite ($b = \infty$). The plotted function is URU, which is the reflected flux for uniformly distributed incidence but also equals the Bond albedo of a planet covered by such an atmosphere. At $g = 0.85$ a drop in a from 1 to 0.99 causes a drop in URU from 1 to 0.56.

5. SIMILARITY CHECKS

There are certain similarity rules by which it is possible to transform a, b, and g to a new set in such a way that the results, e.g., reflection pattern, transmission pattern, absorbed flux, etc., come out approximately the same. These rules permit us with fair confidence to use tables that happen to be available. Often this may be a table for isotropic scattering, $g = 0$, but many other applications are possible. For instance, in dealing with a variety of assumptions about composition and size distribution of aerosols, all of which lead to a strongly forward directed phase function, it would be "safer" to reduce all results by means of the similarity rules to a standard phase function with $g = 0.75$ than to isotropic scattering with $g = 0$.

The similarity rules may be summarized as follows:

Nonconservative: transform a, b, g so that

$$kb = \text{constant}$$
$$(1-a)/k = \text{constant}$$
$$\text{with } k(a,g) = \text{diffusion exponent}$$

Conservative: transform b, g so that

$$b(1-g) = \text{constant}$$

Strict forward scattering is no scattering at all. Hence, addition or subtraction of a mathematically sharp forward peak leads to <u>exactly</u> the same results. It may be verified that this artifact falls within the similarity rules.

Note that $b = \infty$ remains $b = \infty$ and $a = 1$ remains $a = 1$. Hence, full similarity should exist for any phase function if $b = \infty$, $a = 1$. Figure 12 provides a striking illustration. The extrapolation length q for widely varying phase functions is always between 0.71 and 0.72 with minute differences in the next decimals depending on ω_2 and ω_3. An illustration of the similarity rule for conservative scattering is shown in Figure 13. It gives the function URU for Henyey-Greenstein function S over the full range $g = -1$ to $g = +1$. Strangely enough, I have never yet found the exact limit at $g = 1$.

We may also check similarity with g = constant. Three functions with $g = 0$ are shown in Figure 14. For convenience we denote by "unit forward peak" a hypothetical conservative phase function in which all energy is scattered in the forward direction. This phase function has $\omega_n = 2n + 1$. Similarly, a "unit backward peak" has $\omega_n = (2n+1)(-1)^n$. With this notation, the specification of the three functions shown in Fig. 14 is:

	ω_0	ω_1	ω_2	ω_3	ω_4
isotropic $\Phi(\cos\alpha) = 1$	1	0	0	0	0
Rayleigh function $\Phi(\cos\alpha) = 3/4(1+\cos^2\alpha)$	1	0	0.5	0	0
1/2 "unit forward peak" + 1/2 "unit backward peak"	1	0	5	0	9

Note that the value of ω_2 in the second example is exactly one tenth of that in the third example. This suggests an interpolation method to do even a little better than simple similarity. Take the result for isotropic scattering and the equivalent result for the double peak function. Divide the difference in parts 1:9 and the result should be (about) that for the Rayleigh phase function. Tests show that it works.

There have been statements in the literature that the results obtained with full Rayleigh scattering (including polarization) and those for the Rayleigh phase function (without polarization) should be about the same in total intensity. This statement is only half correct. The differences are small but also the differences with isotropic scattering are small, as expected from similarity. This is numerically illustrated in Figure 15. The same graphs serve to illustrate another point. Similarity is most useful if the details of the single scattering are washed out, i.e., for thick layers and for quantities involving integrations over μ or μ_0. Indeed, the "deviations from similarity" are of the order of 10^{-2} in the reflection function itself, 10^{-3} in the moment UR, and 10^{-4} in the bi-moment URU.

A test with gratifying results has also been made with six phase functions with $g = 1/3$. All phase functions shown in Table 1 have been selected to have $a = 0.9$, $g = 1/3$ and they have been arranged in the order of growing ω_2. The symbol HG(g) stands shorthand for "conservative Henyey-Greenstein function with asymmetry factor g". The reflected flux for perpendicular incidence against a semi-infinite layer has been exactly computed for each of these assumptions and is shown in the last column. There is indeed a slow progression (because of similarity) and the results rise smoothly with ω_2 (suggesting that ω_3 etc. hardly count).

Figure 16 shows sketches (on scale) of each of these phase functions. Figure 17 shows the dependence on ω_2. Since the first-order scattering pattern never can be changed and, therefore, escapes any similarity transformation, it is useful to know what fraction of the reflected radiation arises from first-order scattering. This is shown in Figure 18 for $a = 1$, all b, HG phase functions with all positive g, referring to the reflected flux for perpendicular incidence.

A final example, Figure 19, typical for a case in which I do not recommend using similarity is the absorbed fraction of the incident flux in a layer with $b = 1$, perpendicular incidence. For $a = 0$, the absorption is $1 - e^{-1}$; and for $a = 1$, it is zero, so anisotropy makes no difference in these end points. But at intermediate values, near $a = 0.6$ or 0.8, anisotropy ($g = 0.75$) <u>increases</u> the

absorbed fraction by 3 per cent for grazing incidence but decreases this fraction by 4 per cent for perpendicular incidence.

6. POLARIZATION

I shall say nothing much about polarization, because Rayleigh scattering has been treated in Professor Chandrasekhar's lecture (Chandrasekhar, 1974) and I have no additions to make to what I presented at an earlier symposium (van de Hulst, 1971).

Yet I wish to show two slides. Figure 20 shows the degree of polarization reflected back from a semi-infinite Rayleigh atmosphere for all angles of incidence and angles of view in the normal plane (azimuth difference 0° or 180°). Figure 21 shows the cross-section of this figure for a planet viewed at phase angle 10°. Both figures show a striking "near-reciprocity". This is understandable on physical grounds: the first-order scattering contributions are strictly reciprocal, hence it must show the same degree of polarization. The contributions from higher-order scattering lead to quite different functions in the exact solutions but to rather similar results in the precise numbers.

Likewise, the asymptotic forms of the reflection and transmission by thick slabs with Rayleigh scattering can be readily found from general thick layer theory, which makes it often possible to avoid the lengthy exact expressions derived by Mullikin (1966).

7. EMISSION BY INTERNAL SOURCES

Any problem in which we find the absorption at an internal point for a given direction of incidence can by reciprocity be inverted into a problem in which we have an internal isotropic source and wish to find the patterns of the emerging radiation.

Although such a problem will find more application in infrared radiation, it may be useful to show in Figure 22 an example for isotropic scattering, $b = 1$, μ and a variable. In this example, the sources were homogeneously distributed over all depths $\tau = 0$ to 1. The resulting curves of emergent radiation cannot easily be guessed but are readily derived from the reciprocal problem.

8. PATH LENGTH DISTRIBUTIONS

Spectral absorption lines still form one of the most important sources of information on planetary atmospheres. The information contained in these lines is useful only in connection with a model of the atmosphere and a theory of absorption lines in diffuse reflection by multiple scattering. Obviously we have all we need if we know the probability distribution $p(\lambda)$ of the optical path length λ.

At first sight, this seems to pose an entirely new problem. Fortunately, this is not true for we can define certain strict equivalence rules. Some such rules are indicated, but not spelled out, in Figure 23. The exact solution of a problem posed in an area corresponding to one of the four levels in this diagram can often be transposed to yield the exact solution to an equivalent problem in the next higher or next lower level. The principle of the transposition is contained in the keyword of the first column.

We shall here discuss only the transition from the second to the third level and this not in the most general case to keep things simple. The appropriate formulae are brought together in Table 2.

It is seen that determination of the path length distribution requires an inverse Laplace transform and determination of the mean path length $\langle\lambda\rangle$ requires a simple differentiation. This method can be extended at will. For instance, the dispersion σ^2 about the mean path length requires a second-order differentiation. The relations of Table 2 are exact and the results are precise, provided the formulae or tables of $R(a,b)$ from which we start are precise. Once $p(\lambda)$ is known, the road towards a discussion of line profiles, curves of growth, etc., is open although this is still a complicated affair.

Two numerical examples, both for isotropic scattering, may illustrate this method. Figure 24 shows $p_n(\lambda)$ for n-th order reflection from a slab with $b = 1$, $\mu = \mu_0 = 1$. The curves for $n = 1$ and 2 have been exactly computed by Irvine (1964). Note the kink in the $n = 2$ curve. It is possible to fit any two-parameter standard curve to the exact $\langle\lambda\rangle$ and σ^2. I recommend the choice of a Poisson curve defined by

$$p(\lambda) = \frac{m}{\Gamma(k)} (m\lambda)^{k-1} e^{-m\lambda}$$

with $m = \langle\lambda\rangle/\sigma^2$, $k = m\langle\lambda\rangle = m^2\sigma^2$. This corresponds to a skew curve with the maximum at $\langle\lambda\rangle - 1/m$. The dotted curve in Fig. 24 shows that already at $n = 2$, a fair approach to the exact path length distribution is reached. For $n = 5$, we give only this fitted Poisson curve. It is quite likely that the exact curve (which is not available) would show only minute differences. Figure 25 shows what happens to the average path length $\langle\lambda\rangle$ if $a = 1$ and b goes to infinity. Irvine (1964) made the conjecture that it would diverge as $1.7b$. The actual ratio $\langle\lambda\rangle/b$ varies (for $\mu = \mu_0 = 1$) from 1.5 at $b = 0$ to 2 at $b = \infty$.

REFERENCES

Chandrasekhar, S.	1974	This symposium.
Hunt, G. E.	1971	J. Quant. Spectrosc. Rad. Transf. 11, 655.
Irvine, W. M.	1964	Bull. Astr. Inst. Netherlands 17, 266.
Irvine, W. M.	1974	This symposium.
Kuscer, I. and McCormick, N. J.	1974	This symposium
Mullikin, T. W.	1966	Astrophys. J. 145, 866.
van de Hulst, H. C.	1968a	Bull. Astr. Inst. Netherlands 20, 77.
van de Hulst, H. C.	1968b	J. Computational Physics 3, 291.
van de Hulst, H. C.	1971	J. Quant. Spectrosc. Rad. Transf. 11, 785.

TABLE 1: Similarity test for six phase functions all with $a = 0.9$, $g = 1/3$. The computed function is 1RU = reflected fraction of flux for perpendicular incidence against a semi-infinite medium.

Phase Function	ω_0	ω_1	ω_2	ω_3	1RU
(a) linearly anisotropic 0.9 (1 + cos α)	0.9	0.9	0	0	0.327
(b) 1.2 HG(1/2) - 0.3 forward peak	0.9	0.9	0	-1.05	0.326
(c) 0.9 HG(1/3)	0.9	0.9	0.50	0.27	0.332
(d) 0.8 HG(1/4) + 0.1 forward peak	0.9	0.9	0.75	0.79	0.336
(e) 0.6 isotropic + 0.3 forward peak	0.9	0.9	1.50	2.10	0.349
(f) 0.6 forward peak + 0.3 backward peak	0.9	0.9	4.50	2.10	0.451

TABLE 2: General recipe to find path length distribution and mean path length in diffuse reflection.

Preparation:

Find $R(a,b)$ by any acceptable method.

Choose values of unwritten parameters μ_0, μ, g

Notation for inverse Laplace transform:

$F(\lambda) = L^{-1}\{f(\gamma)\}$ defines the function satisfying $f(\gamma) = \int_0^\infty F(\lambda)\, e^{-\gamma\lambda} d\lambda$

Full reflection function:

$$p(a,b,\lambda) = \frac{1}{R(a,b)} L^{-1}\left\{R\left[\frac{a}{1+\gamma},\ b(1+\gamma)\right]\right\}$$

$$\langle\lambda(a,b)\rangle = \frac{\partial\ \ell n\ R(a,b)}{\partial\ \ell n\ a} - \frac{\partial\ \ell n\ R(a,b)}{\partial\ \ell n\ b}$$

Separate scattering orders:

$$p_n(b,\lambda) = \frac{1}{R_n(b)}\ L^{-1}\left\{\frac{R_n[b(1+\gamma)]}{(1+\gamma)^n}\right\}$$

$$\langle\lambda_n(b)\rangle = n - \frac{d\ \ell n\ R_n(b)}{d\ \ell n\ b}$$

for $b \to \infty$: $\quad p_n(\infty,\lambda) = \frac{\lambda^{n-1}\, e^{-\lambda}}{(n-1)!}$, $\quad \langle\lambda_n(\infty)\rangle = n$

Checks:

$$R(a,b) = \sum_{n=1}^{\infty} a^n\, R_n(b)$$

$$p(a,b,\lambda)\ R(a,b) = \sum_{n=1}^{\infty} p_n(b,\lambda)\ a^n\ R_n(b)$$

$$\langle\lambda(a,b)\rangle\ R(a,b) = \sum_{n=1}^{\infty} \langle\lambda_n(b)\rangle\ a^n\ R_n(b)$$

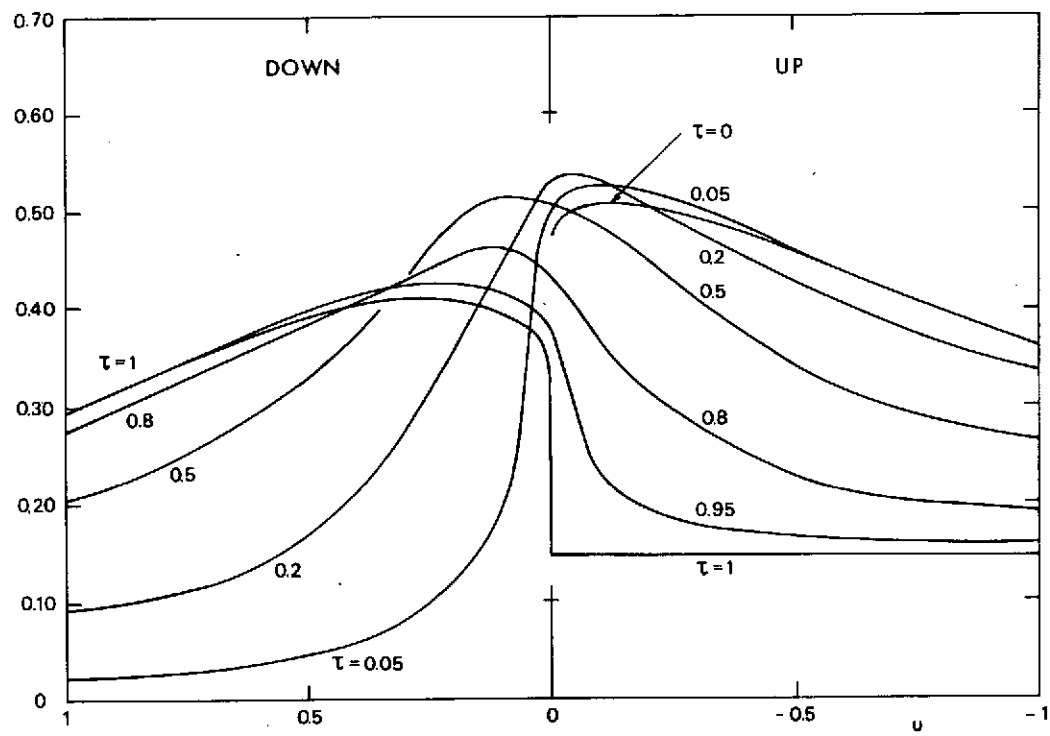

Fig. 1 Radiation field, expressed as intensity versus cosine of angle with normal (u) in an atmosphere of total optical depth, 1, with conservative isotropic scattering if radiation enters perpendicularly from above and if the soil has Lambert scattering with albedo 0.20. Curves for seven values of optical depth, τ, are shown. Unit incident flux (here and in other figures).

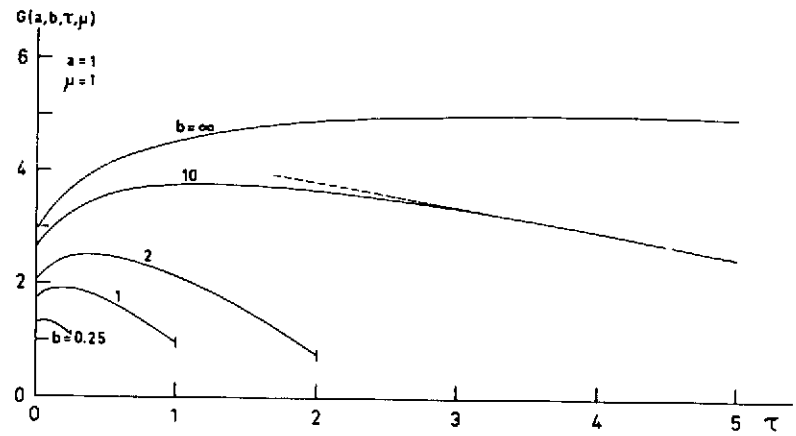

Fig. 2 Radiation density as a function of optical depth τ in an atmosphere with five assumptions about the optical thickness b. In all examples, the scattering is isotropic and conservative and radiation incident perpendicularly from the top ($\tau = 0$). The radiation density is expressed as a gain, i.e., divided by the radiation density existing in the incident beam in the absence of an atmosphere.

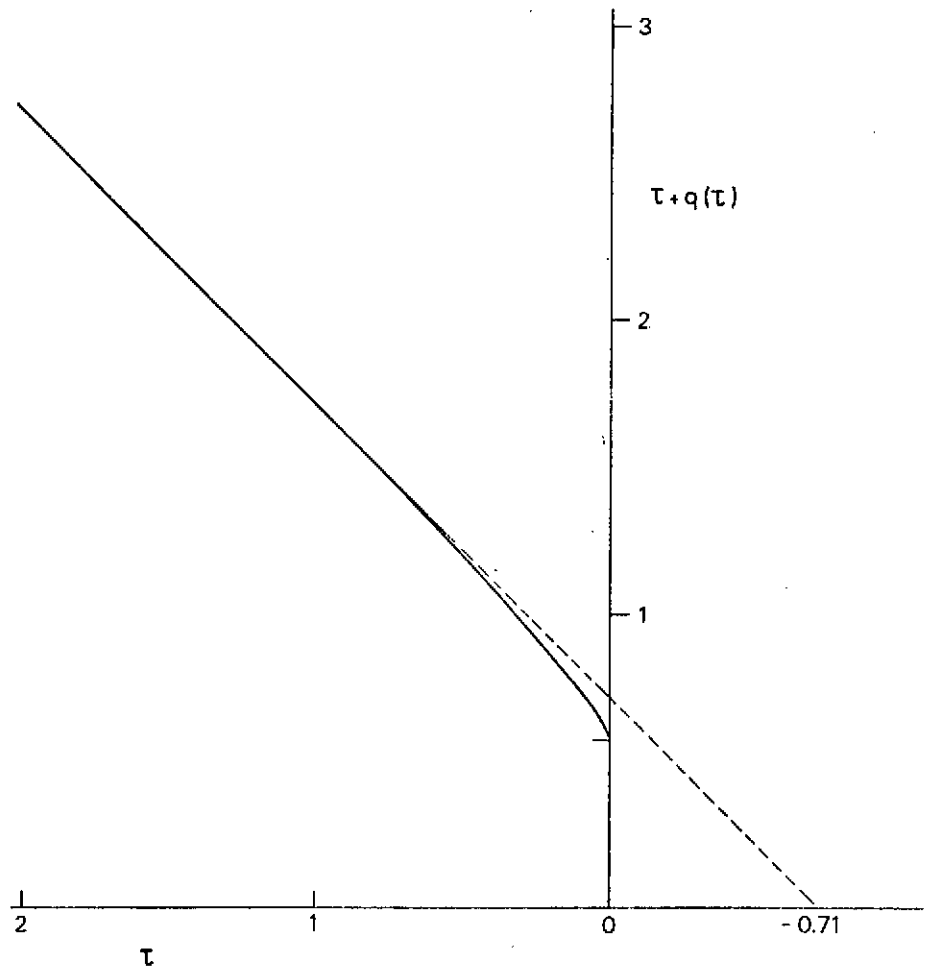

Fig. 3 Hopf solution for radiation density near the boundary where a constant net flux of radiation emerges from a conservative isotropically scattering atmosphere.

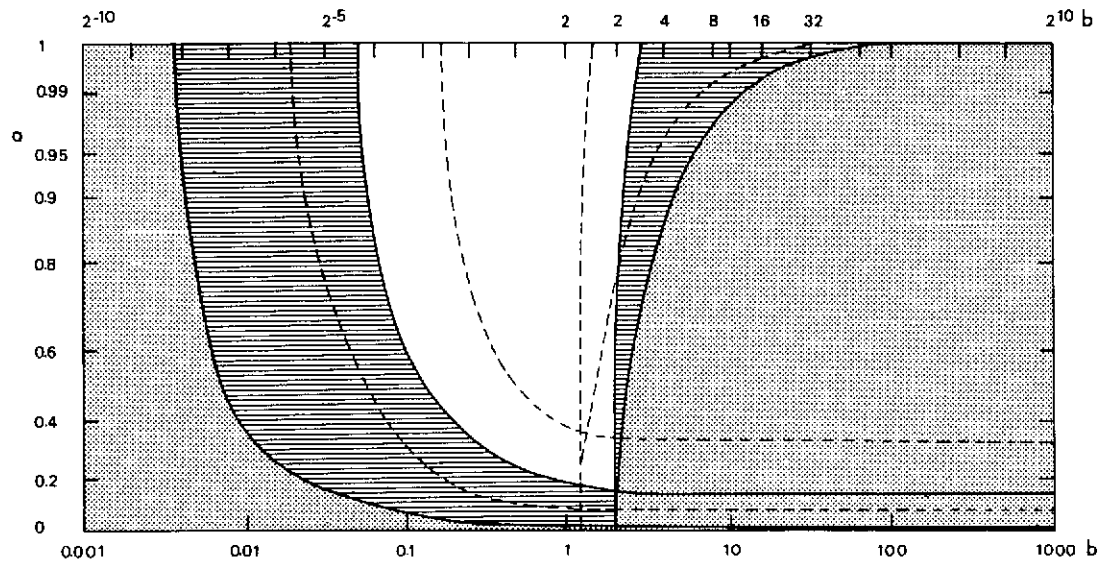

Fig. 4

Limits of 1 per cent error (drawn) and 5 per cent error (dashed) for certain approximations in in one example for isotropic scattering. The approximations are from left to right:

1. (small b) single scattering only
2. (small b) single and double scattering combined
3. (large b) asymptotic formulae
4. (large b) formulae for $b = \infty$

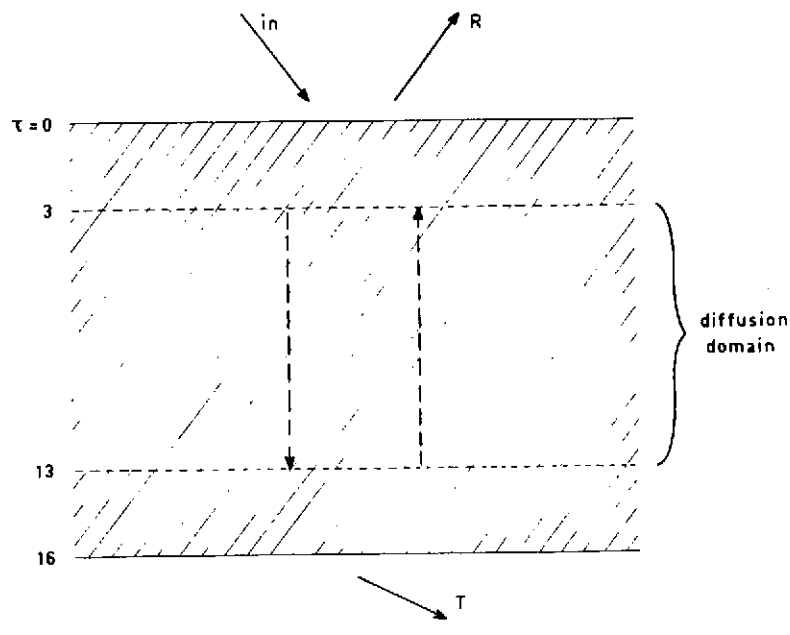

Fig. 5 A diffusion domain is a region of optical depth well away from any boundaries or internal source layers.

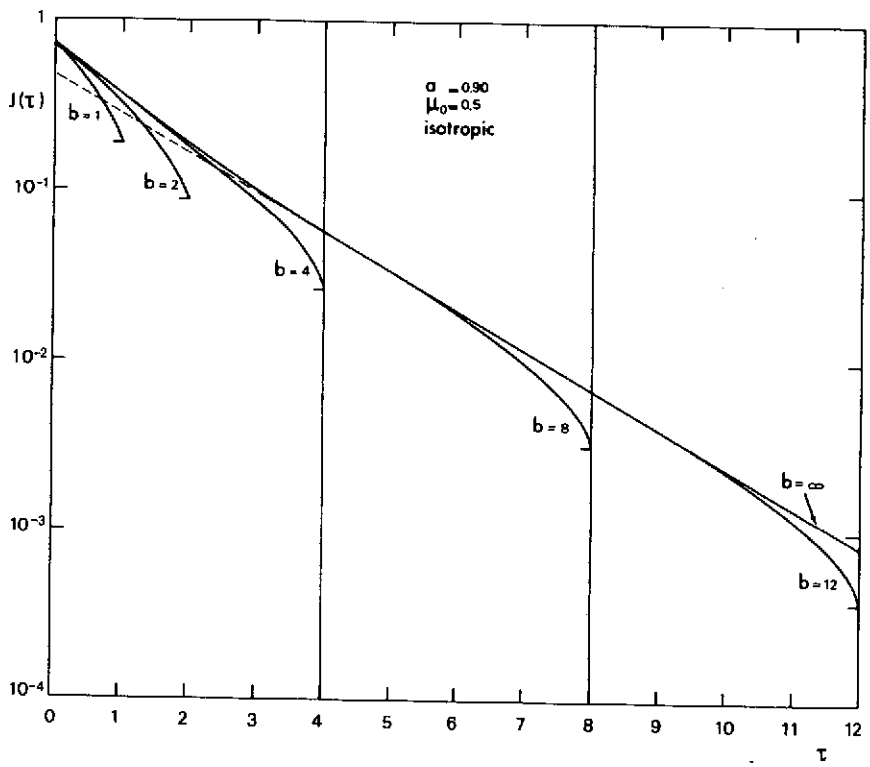

Fig. 6 Source function in a non-conservative atmosphere. If the total depth is large enough, a diffusion domain develops.

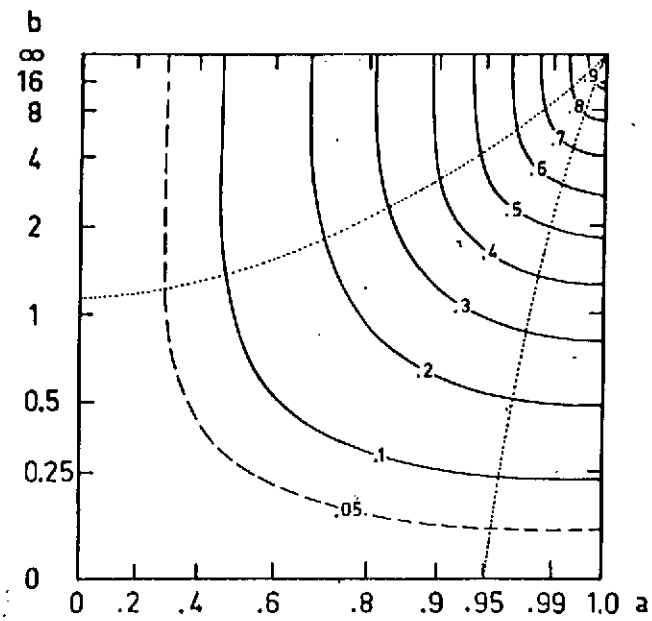

Fig. 7 Reflected flux for perpendicular incidence for all values of a and b, isotropic scattering. Linear scales of $\sqrt{1-a}$ and $(1+b)^{-1}$.

C-3

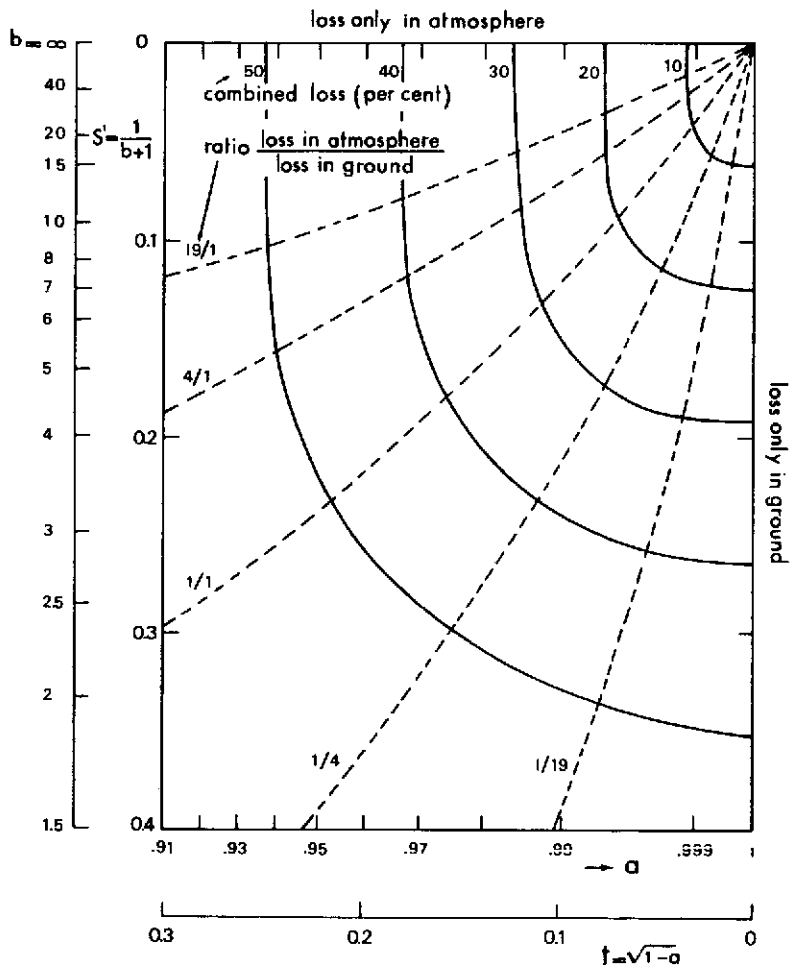

Fig. 8 Enlarged portion of Fig. 7 in upper right corner, where losses are small, together with curves showing where these losses occur.

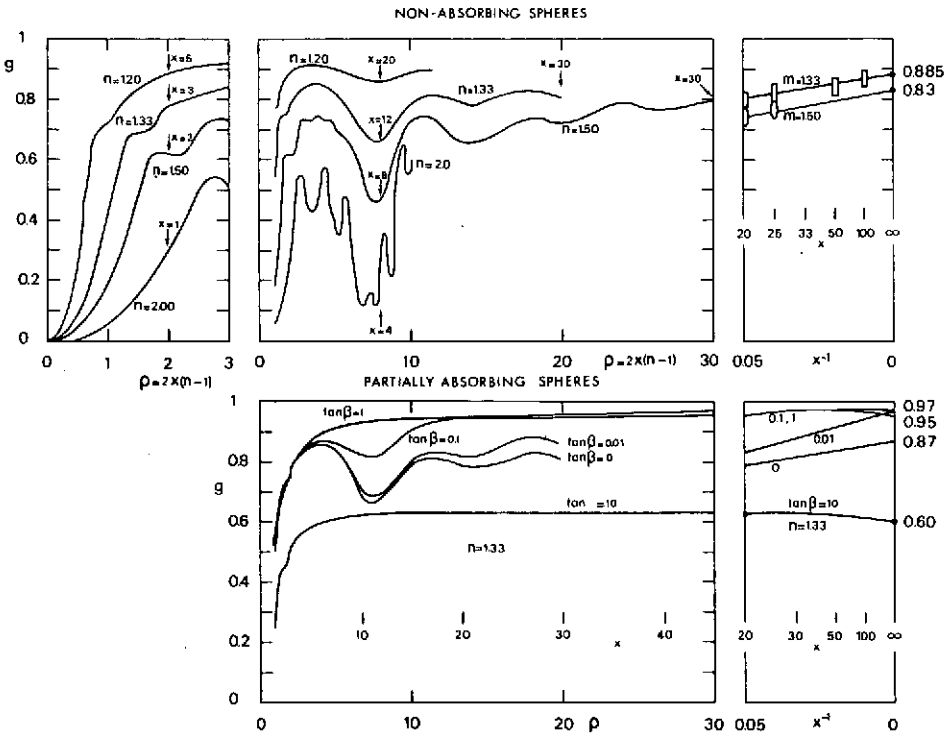

Fig. 9 Asymmetry factor of the phase function of spherical scatterers according to the Mie theory. The curves are based on the work of many authors. A full explanation is not presented in this lecture.

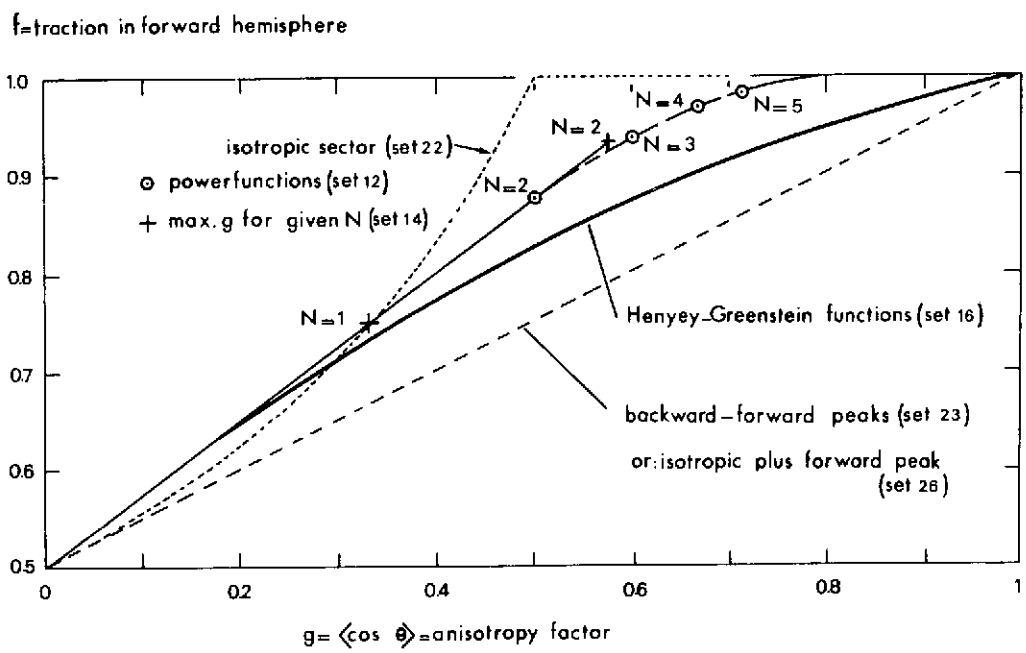

Fig. 10

Various phase functions commonly used as practicing examples have been plotted in a diagram of f (= fraction scattered into forward hemisphere) against g (= asymmetry factor).

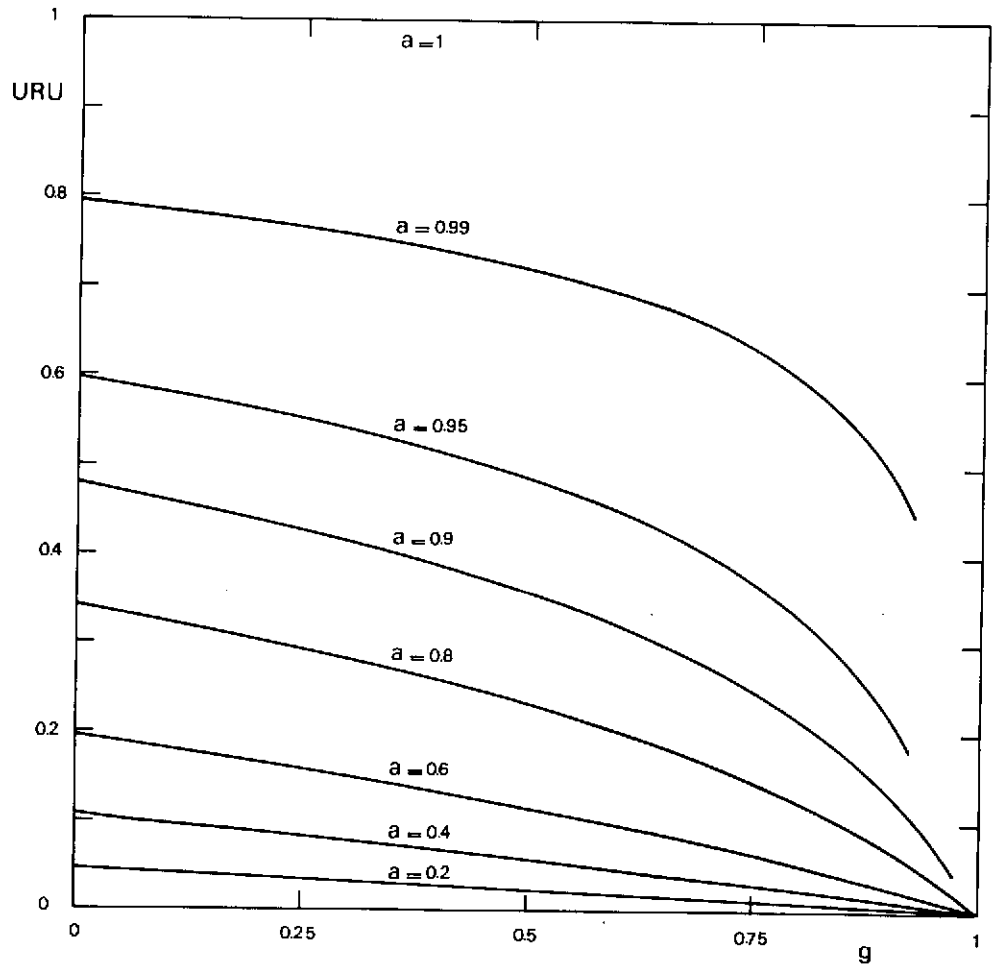

Fig. 11 The Bond albedo URU of a planet covered with a semi-infinite atmosphere depends strongly on the asymmetry factor g of the phase function if the albedo a for single scattering is kept constant. Henyey-Greenstein phase functions.

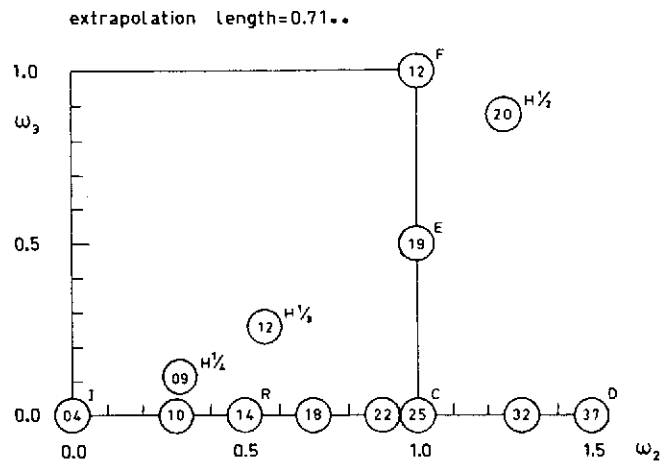

Fig. 12

The extrapolation length q' in conservative scattering is 0.71 for almost any phase function. The diagram shows that the third and fourth decimals depend systematically on ω_2 and ω_3.

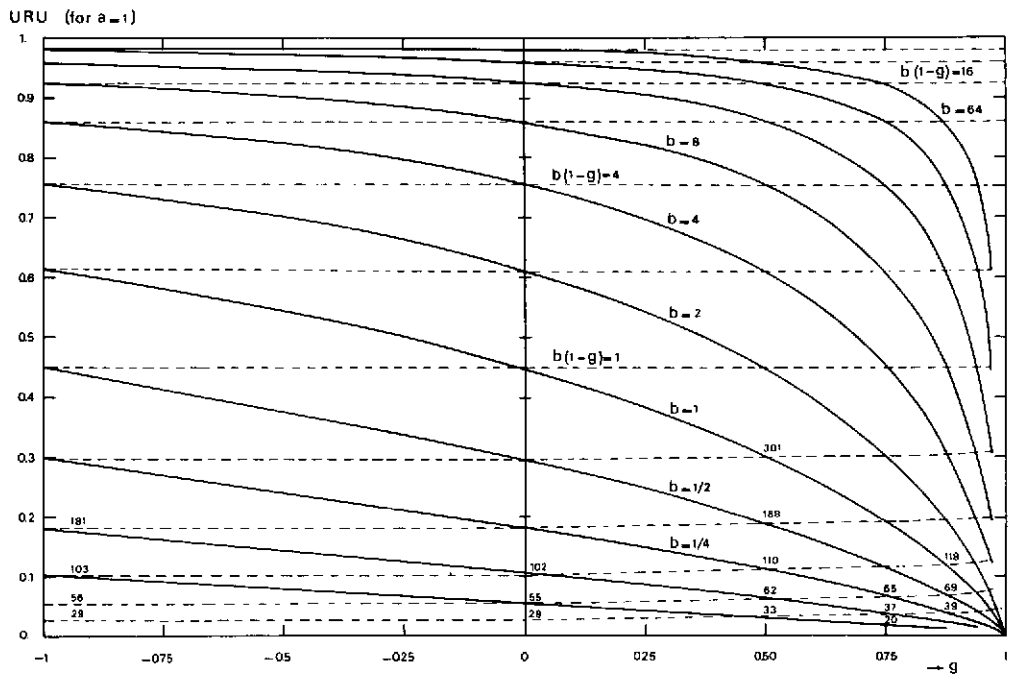

Fig. 13 The similarity rule for conservative scattering is illustrated by means of the bimoment of the reflection function, URU. Dotted curves connecting similar situations are about horizontal.

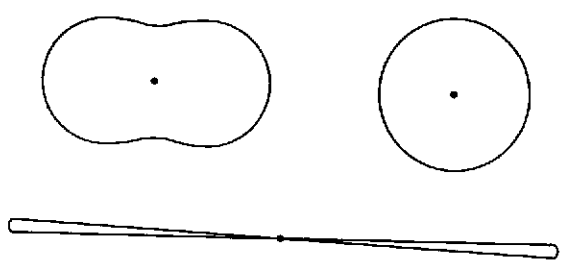

Fig. 14 Three phase functions with $g = 0$ used in similarity tests are isotropic scattering, Rayleigh phase function, and double-peak function. (The last one cannot be drawn on scale since a very narrow peak with a very large intensity is meant).

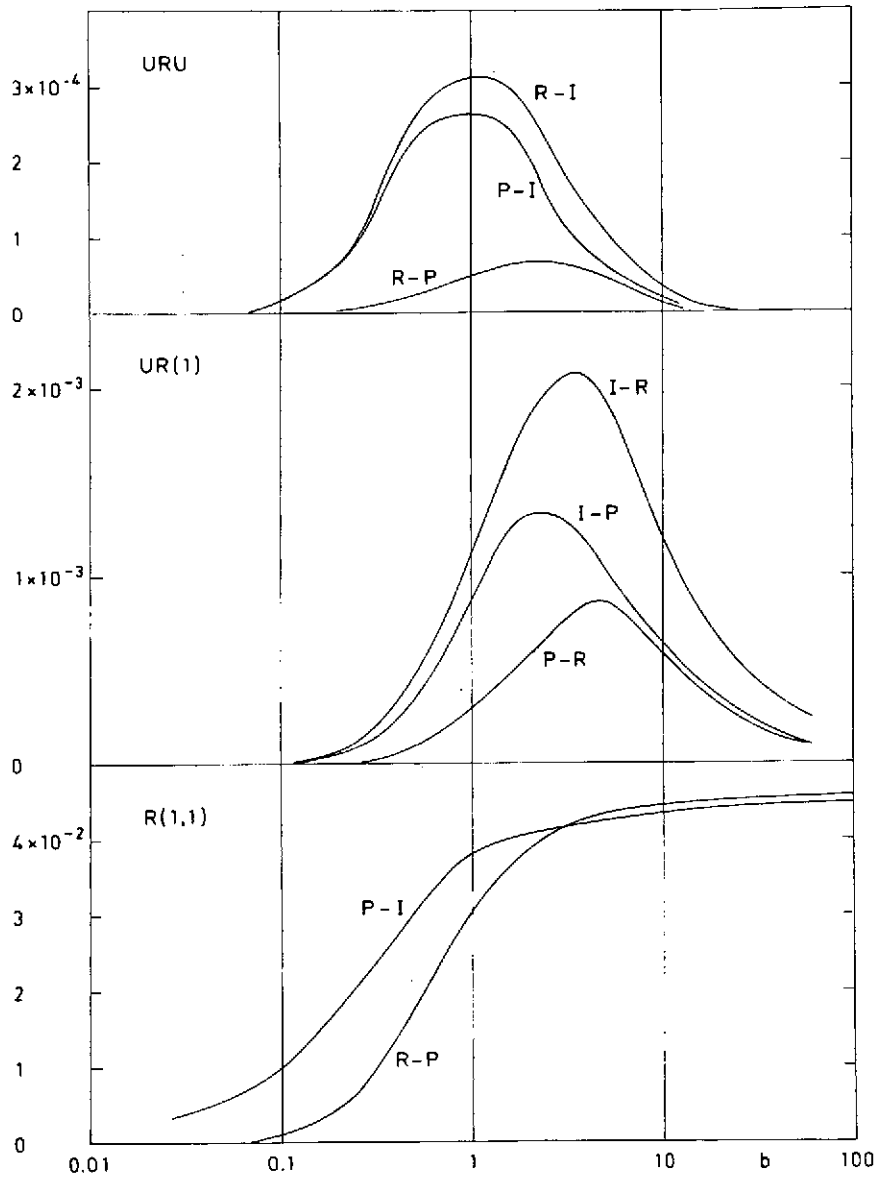

Fig. 15 Mutual differences in reflection function, its moment 1RU, and its bimoment URU, among three assumed conservative scattering laws. The Rayleigh phase function (P) shows differences with correct Rayleigh scattering (R) of the same order as with isotropic scattering (I). Abscissa is optical thickness b.

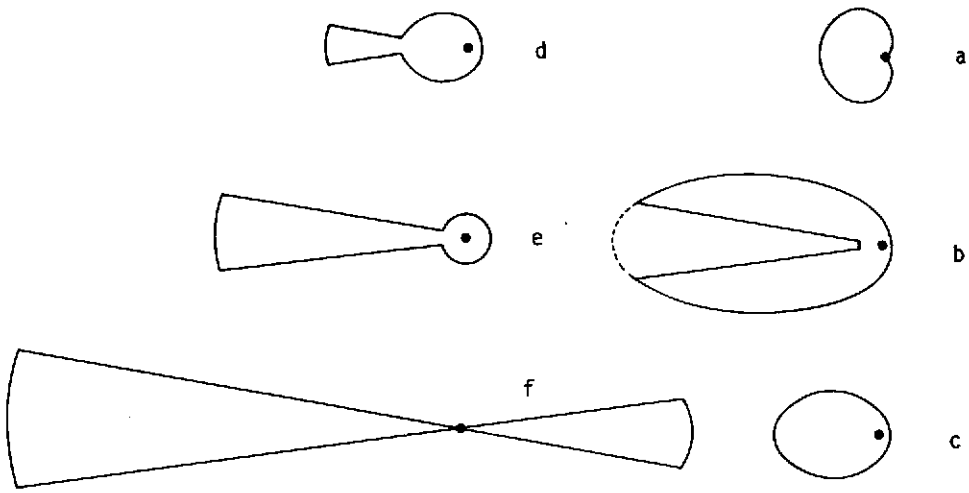

Fig. 16 Six non-conservative phase functions with a = 0.9, g = 1/3 as specified in Table 1. In order to give a somewhat realistic impression, the cone of the added or subtracted forward peaks has been widened to 15° (total width) but the lengths of the peaks corresponding to this width should be ten times stronger than shown.

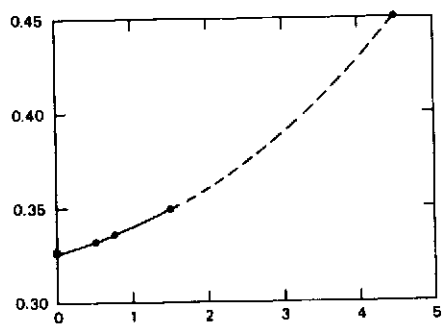

Fig. 17 Reflected flux for perpendicular incidence against a semi-infinite atmosphere for the six non-conservative phase functions of Fig. 16.

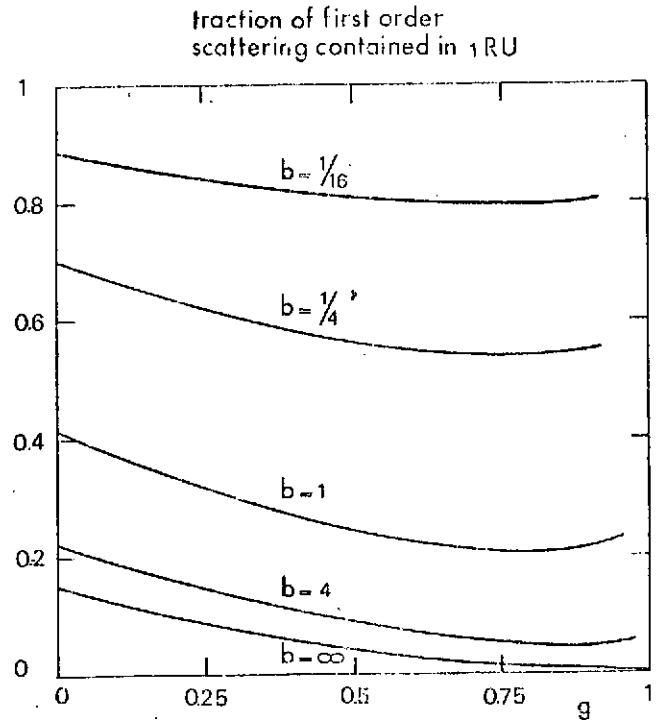

Fig. 18 A numerical example showing how in reflection the fraction due to single scattering depends on the asymmetry factor g and the depth b. A conservative Henyey-Greenstein phase function is assumed.

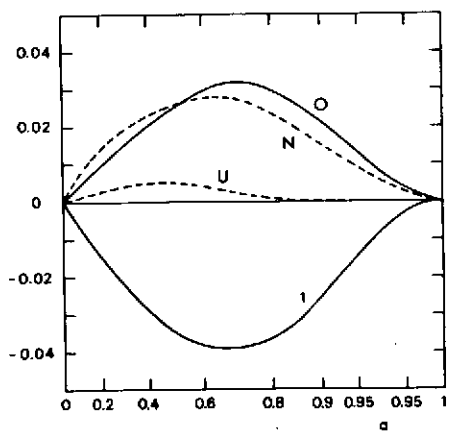

Fig. 19 The effect of a drastic asymmetry on the absorbed fraction of the incident flux may have different signs depending on the direction of incidence.

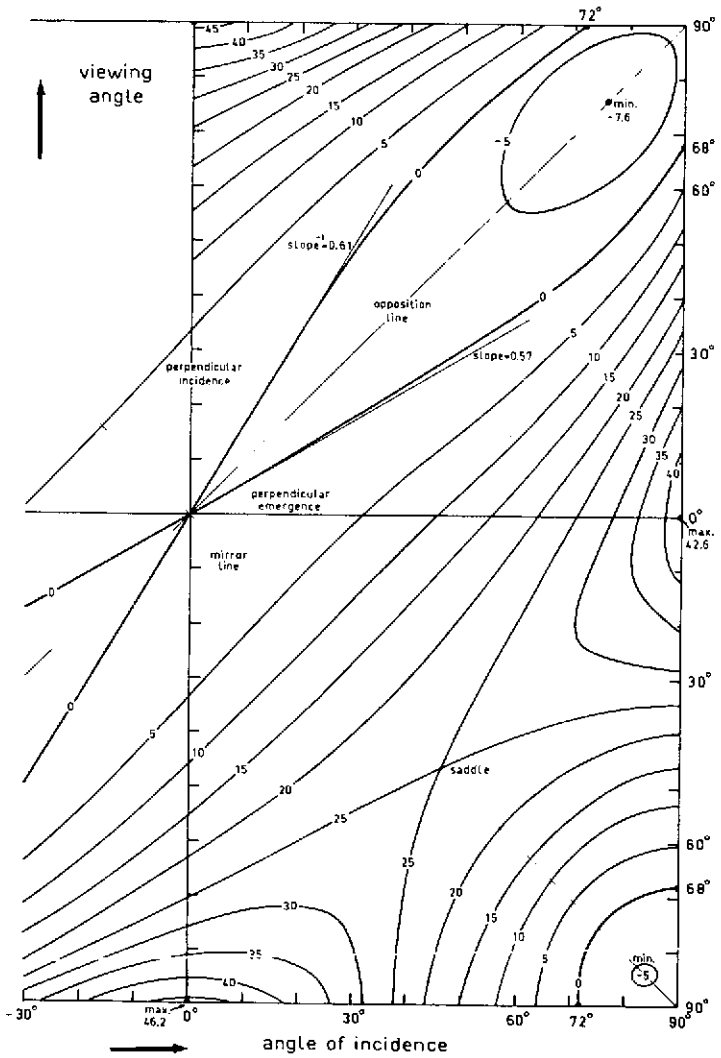

Fig. 20 When direction of view (earth) and direction of illumination (Sun) are chosen in a plane containing the normal, the polarization of the radiation diffusely reflected from an infinitely deep Rayleigh scattering atmosphere may be read from this graph. The curves were computed from available exact solutions. The symmetry about the two diagonals is only approximate.

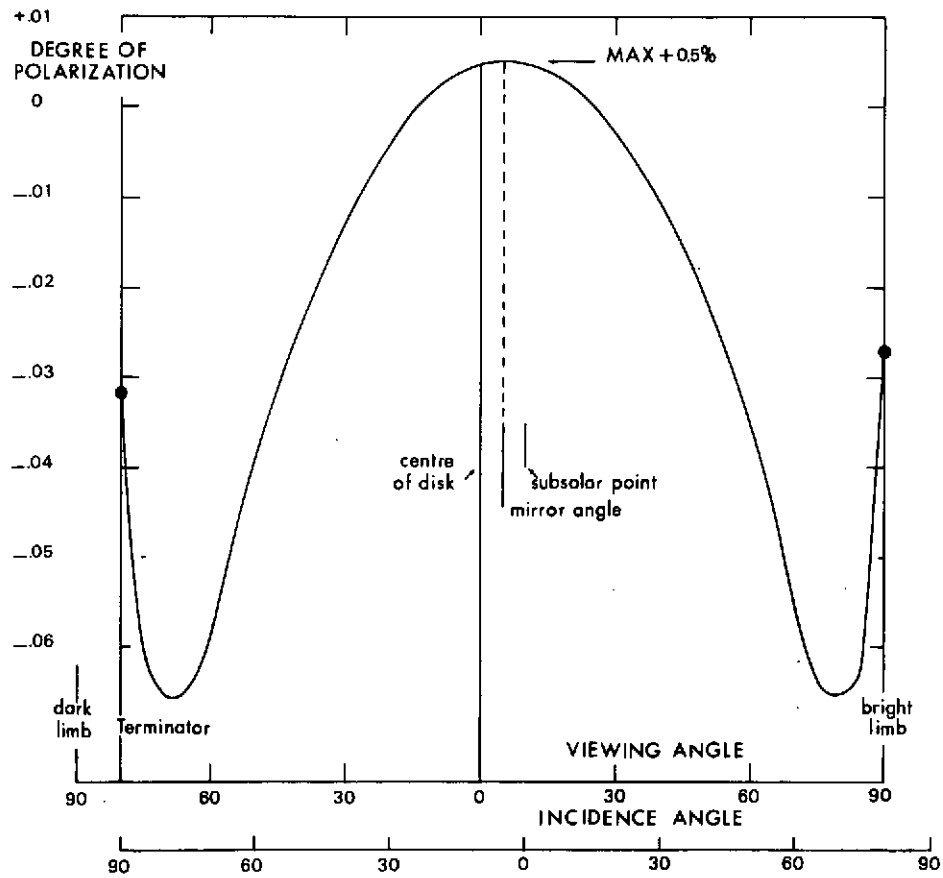

Fig. 21 Cross-section through the preceding figure corresponding to a planet seen with phase angle 10°. The curve shows the degree of polarization along the great circle of the planet which contains the sub-earth and sub-sun point.

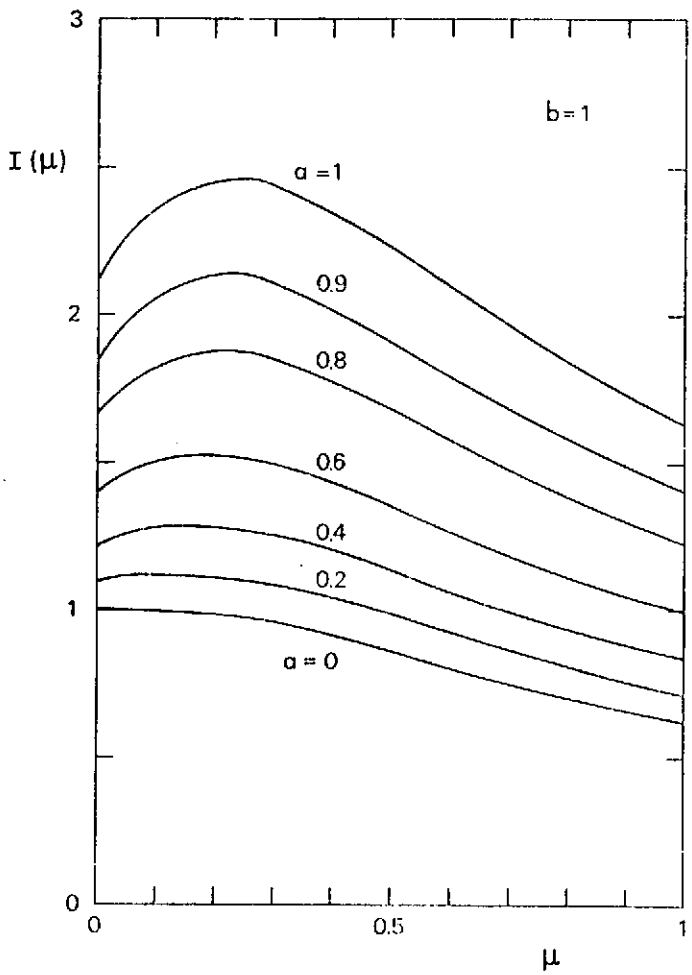

Fig. 22 Intensity emerging under various angles (cosine = μ) from a layer with optical thickness 1, homogeneously filled with emitting sources. The scattering is assumed isotropic with albedo a.

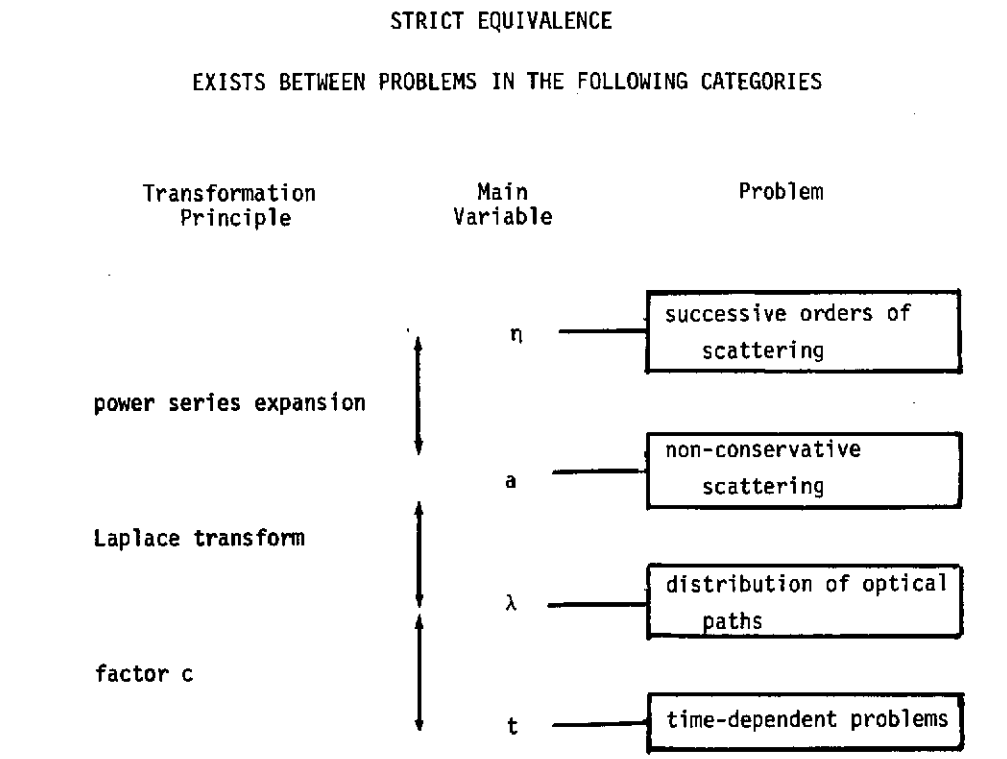

Fig. 23 Principles on which certain strict equivalence rules can be formulated.

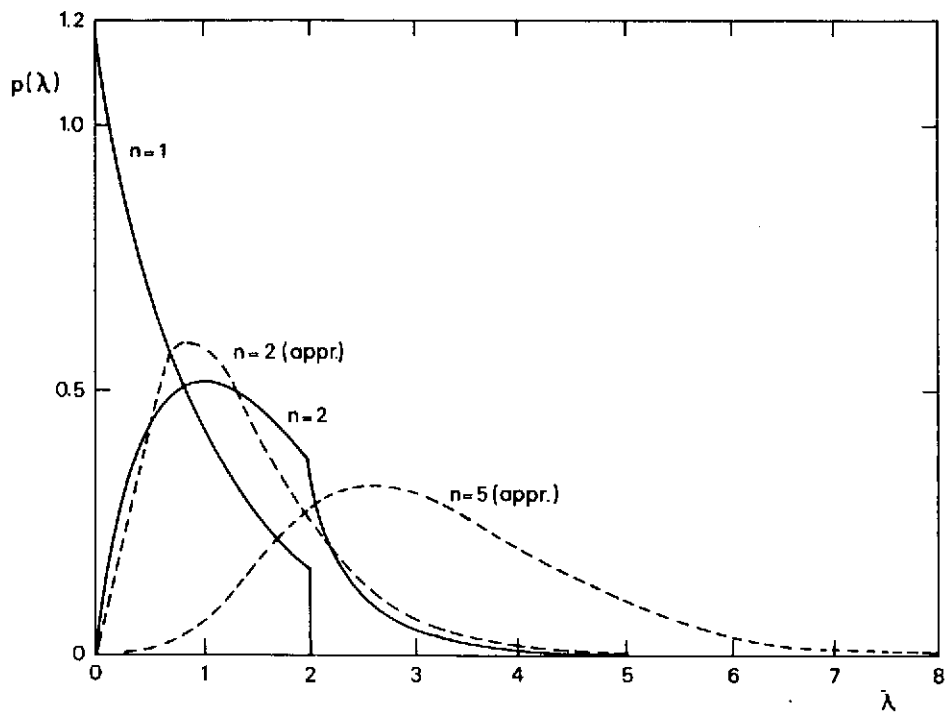

Fig. 24 Path length distribution of n-th order refection from an isotropically scattering layer with total depth 1, perpendicular incidence and emergence. Exact curves for n = 1, 2; Asymptotic approximation for n = 2, 5.

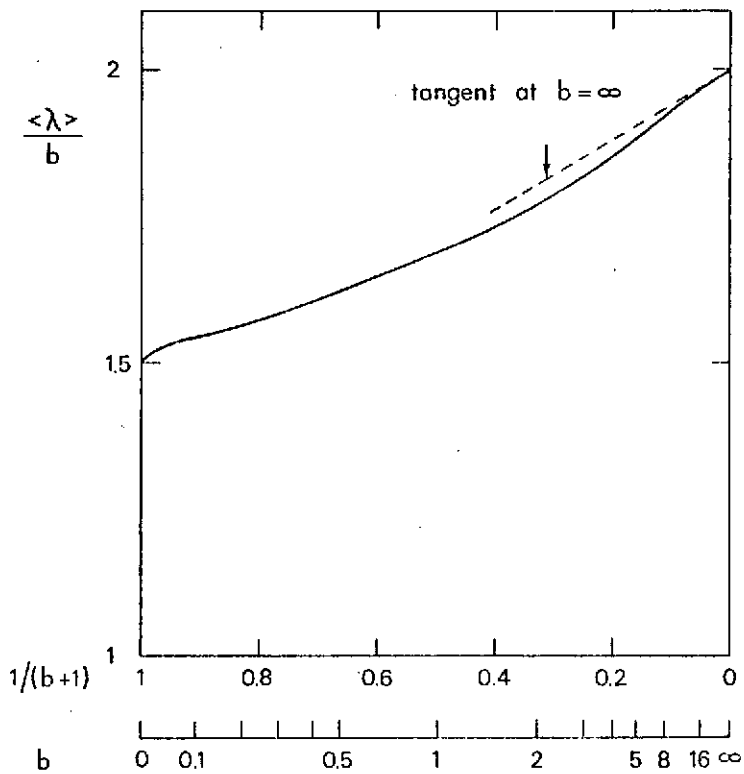

Fig. 25 The average path length for reflection against a slab with conservative isotropic scattering grows approximately as the optical thickness b, but the ratio climbs slowly from 1.5 to 2.

SOME ANALYTICAL RESULTS FOR RADIATIVE TRANSFER IN THICK ATMOSPHERES

I. Kuščer and N. J. McCormick*
Department of Physics
University of Ljubljana
Ljubljana, Yugoslavia

Abstract

Singular eigenmode expansions are a convenient analytical tool with which to study problems of monochromatic radiative transfer in thick or semi-infinite atmospheres. Some closed-form solutions are presented for anisotropic scattering, with the neglect of polarization effects.

A basic ingredient for applications to the semi-infinite medium is Chandrasekhar's H-function, which is best defined through the Wiener-Hopf factorization $[\Lambda(z)]^{-1} = H(z)H(-z)$. Herein $H(z)$ is required to be regular in the right-half of the complex plane, while $\Lambda(z)$ is the dispersion function whose zeros are the discrete relaxation lengths. Use of the Busbridge polynomials $q_\ell(z)$, along with $H(z)$, permits the construction of adjoint eigenmodes. A biorthogonality relation follows which may be used to determine the coefficients in eigenmode expansions.

Attention is given to the solutions of the Milne and albedo problems in order that the method of matched asymptotic approximations may be used to describe the solution for a thick atmosphere adjacent to a diffusely reflecting ground. Expressions for the emerging distributions are quoted. A possible extension of the general scheme to problems involving polarization is indicated.

1. INTRODUCTION

The equation of transfer, which may be regarded as a specialized form of the Boltzmann equation, rarely permits closed-form analytic solutions. Most often these refer either to an infinite or semi-infinite medium of uniform composition, with no exchange of energy in scattering. However, since problems of this type are of basic importance for the optics of turbid atmospheres, a discussion of some of the analytic methods and results appears justified.

The two leading analytic methods are the Fourier-transform technique (the Wiener-Hopf technique in the case of a semi-infinite medium[1]), and the method of singular eigenmode expansions.[2-5] They differ more in appearance than in substance, so that an exposition of the latter method will suffice. We are going to concentrate upon problems for semi-infinite atmospheres with anisotropic scattering. Such

* Present address: Department of Nuclear Engineering, University of Washington, Seattle, Washington.

problems have been extensively studied in the monographs of Chandrasekhar,[5] Sobolev,[7] Busbridge,[8] and Case and Zweifel,[3] as well as in papers by Mullikin,[9] Maslennikov,[10] and many others. Thus genuinely new and meaningful results can hardly be expected. Yet we trust that the use of singular eigenfunctions can expose new mathematical aspects of the problems and we believe it leads to a condensed presentation.

If the intensity depends only upon one coordinate (τ), on the cosine of the polar angle with respect to the positive τ-axis (μ), and on the azimuth (ϕ), the equation of transfer in the absence of sources is[6]

$$(\mu\frac{\partial}{\partial\tau} + 1)\ I(\tau,\mu,\phi) = \frac{1}{4\pi}\int_{-1}^{1} d\mu' \int_{0}^{2\pi} d\phi'\ p(\cos\ \delta)\ I(\tau,\mu',\phi'). \tag{1}$$

The photon mean free path serves as the unit of length. The tacit assumption has been made that polarization effects may be neglected, so that the distribution of radiation can be represented by a single function I.

The scattering function (phase function) $p(\cos\ \delta)$, where δ is the scattering angle, shall be bounded and non-negative, vanishing at most for a discrete set of angles. Anisotropic scattering of arbitrary but finite order will be admitted, which shall mean that

$$p(\cos\ \delta) = \sum_{\ell=0}^{L} \varpi_\ell\ P_\ell(\cos\ \delta). \tag{2}$$

We assume that some absorption is present, hence $0 < \varpi_0 < 1$, postponing the conservative case ($\varpi_0 = 1$) for separate discussion (Sec. 5). The remaining coefficients are limited by $|\varpi_\ell| < (2\ell + 1)\varpi_0$.

Application of the spherical harmonics addition theorem helps to rewrite Eq. (2) as[6,9]

$$p(\cos\ \delta) = \sum_{m=0}^{L} (2 - \delta_{m0})\ p^m(\mu,\mu')(1 - \mu^2)^{m/2}\quad (1 - \mu'^2)^{m/2}\cos\ m(\phi - \phi'), \tag{3}$$

where

$$p^m(\mu,\mu') = \sum_{\ell=m}^{L} c_\ell^m\ p_\ell^m(\mu)\ p_\ell^m(\mu')\ , \tag{4}$$

$$p_\ell^m(\mu) = (d^m/d\mu^m)\ P_\ell(\mu)\ , \tag{5}$$

$$c_\ell^m = \varpi_\ell(\ell - m)!/(\ell + m)!\ . \tag{6}$$

We recall that the $p_\ell^m(\mu)$ (the polynomial factors of the associated Legendre functions) are mutually orthogonal in the sense that

$$\int_{-1}^{1} p_\ell^m(\mu)\ p_k^m(\mu)\ dm(\mu) = \frac{2}{2\ell + 1}\frac{(\ell + m)!}{(\ell - m)!}\delta_{\ell k}\ ,$$

where $dm(\mu) = (1 - \mu^2)^m \, d\mu$.

The azimuthal variable may be separated by a Fourier expansion. We define

$$I^m(\tau,\mu)(1 - \mu^2)^{m/2} \cos m(\phi - \phi_m) = \frac{1}{2\pi} \int_0^{2\pi} I(\tau,\mu,\phi') \cos m(\phi - \phi') \, d\phi' \quad , \tag{7}$$

which also determines ϕ_m . A set of uncoupled integrodifferential equations for the coefficients I^m follows,

$$\left(\mu \frac{\partial}{\partial \tau} + 1\right) I^m(\tau,\mu) = \frac{1}{2} \int_{-1}^{1} p^m(\mu,\mu') \, I^m(\tau, \mu') \, dm(\mu') \quad . \tag{8}$$

There is no need to deal with Eq. (8) for $m > L$ because the right-hand side then vanishes. This means that those higher $I^m(\tau,\mu)$ only contribute to the unscattered distribution (consisting of light that arrives directly from the outside without having been scattered). For any given boundary condition the intensity $I(\tau,\mu,\phi)$ can be reconstructed from the first $(L + 1)$ azimuthal coefficients by separating out the part of the unscattered distribution that is not included in those terms. If light is incident only at the boundary $\tau = 0$, this is written as follows,

$$I(\tau,\mu,\phi) = \sum_{m=0}^{L} (2 - \delta_{m0}) \, I^m(\tau,\mu)(1 - \mu^2)^{m/2} \cos m(\phi - \phi_m)$$

$$+ \left[1 - \theta(\mu)\right] e^{-\tau/\mu} \left[I(0,\mu,\phi) - \sum_{m=0}^{L} (2 - \delta_{m0}) \, I^m(0,\mu)(1 - \mu^2)^{m/2} \cos m(\phi - \phi_m) \right] , \tag{9}$$

where $\theta(\mu) = 0$ for $0 < \mu \leq 1$ and $\theta(\mu) = 1$ otherwise.

Since each equation (8) is to be treated independently, it suffices to discuss one of them. Except when needed, the superscript m with $I^m(\tau,\mu)$ and $p^m(\mu,\mu')$, and with any further functions to be derived therefrom will be suppressed henceforth.

2. EIGENFUNCTIONS AND EIGENVALUES

It is relatively easy to find the eigenmodes, i.e., special solutions of Eq. (8) where the variables τ and μ are separated, but the boundary conditions in general are not obeyed. The unknown $I(\tau,\mu)$ is then expanded in the eigenmodes and the expansion coefficients determined from the boundary conditions. The procedure is much the same as in the well-known method of Fourier, except for one essential difference: a continuous set of singular eigenmodes will be involved, owing to the presence of a continuous part of the eigenvalue spectrum.

The ansatz $I(\tau,\mu) = \emptyset(\nu,\mu) \, e^{-\tau/\nu}$ leads to the following equation for the eigenfunction $\emptyset(\nu,\mu)$,

$$(\nu - \mu) \, \emptyset(\nu,\mu) = \frac{\nu}{2} \int_{-1}^{1} p(\mu,\mu') \, \emptyset(\nu,\mu') \, dm(\mu') \quad . \tag{10}$$

We first discuss the regular (square integrable) eigenfunctions that correspond to some discrete eigenvalues. Obviously these occur in pairs $(\pm\nu_j)$, and they are all bounded, real, and outside the interval $[-1,1]$.[11] We make the additional assumption that all eigenvalues are simple, i.e., that to each of them there corresponds only one eigenfunction. The positive eigenvalues--the so called relaxation lengths--shall be ordered for each m as $1 < \nu_J < \ldots < \nu_2 < \nu_1 < \infty$. The largest among all relaxation lengths (ν_1^0) occurs with the azimuth independent component I^0. It is called the diffusion length and is of particular importance since it determines the asymptotic approximation describing the behavior of the radiation field deep in the interior of the medium. The corresponding eigenfunctions $\phi^0(\pm\nu_1^0,\mu)$ are the only non-negative ones.[11] The second largest relaxation length determines how fast some general solution approaches the asymptotic one. In view of these observations, the eigenvalues and the problem of their existence will be studied at some length.

The integral in Eq. (10) has the form

$$g(\nu,\mu) = \sum_{\ell=m}^{L} c_\ell \, g_\ell(\nu) \, p_\ell(\mu) \quad , \tag{11}$$

where

$$g_\ell(\nu) = \int_{-1}^{1} \phi(\nu,\mu) \, p_\ell(\mu) \, dm(\mu) \quad . \tag{12}$$

The regular eigenfunctions can then be written as

$$\phi(\pm\nu_j,\mu) = \frac{\nu_j}{2} \, \frac{g(\pm\nu_j,\mu)}{\nu_j \mp \mu} \quad . \tag{13}$$

The coefficients $g_\ell(\nu)$ are seen to obey a recurrence relation,

$$(\ell - m) \, g_\ell(\nu) = h_{\ell-1} \, \nu \, g_{\ell-1}(\nu) - (\ell + m - 1) \, g_{\ell-2}(\nu) \tag{14}$$

for $\ell \geq m$, where $h_\ell = 2\ell + 1 - \varpi_\ell$, and $g_{m-1} = 0$. Obviously the lowest coefficient $g_m(\nu)$ cannot be allowed to vanish; it is convenient to choose the following constant,[9]

$$g_m^m = p_m = \prod_{n=0}^{m-1} (2n + 1), \quad m \geq 1 \quad , \tag{15}$$

and $g_0^0 = 1$. By Eq. (12) this implies that

$$\int_{-1}^{1} \phi(\nu,\mu) \, dm(\mu) = 1 \quad . \tag{16}$$

After multiplication by $dm(\mu)$ and integration, Eq. (10) leads to a similar result,

$$\int_{-1}^{1} \mu\, \emptyset(\nu,\mu)\, dm(\mu) = \nu[1 - \varpi_m/(2m+1)] \quad . \tag{17}$$

With the above normalization all $g_\ell(\nu)$ become polynomials, alternatively even and odd, of degree $(\ell - m)$. Linear independence is assured in view of the different degrees. These polynomials have first been introduced by Chandrasekhar,[6] and reinvestigated by a number of authors.[8, 9, 12-17] An explicit expression (a generalization of the one given by Kaper[15] and Inönü[17]) is

$$g_\ell(\nu) = \frac{g_m}{(\ell - m)!} \begin{vmatrix} h_m\nu & 1 & 0 & . & . & 0 \\ (2m+1) & h_{m+1}\nu & 2 & . & . & . \\ 0 & (2m+2) & h_{m+2}\nu & . & . & . \\ 0 & . & . & . & . & 0 \\ . & . & . & . & h_{\ell-2}\nu & (\ell-m-1) \\ 0 & . & . & 0 & (\ell+m-1) & h_{\ell-1}\nu \end{vmatrix} , \quad \ell > m \quad . \tag{18}$$

Condition (16) represents a transcendental equation for the eigenvalues. It may be rewritten as

$$\Lambda(\pm\nu_j) = 0 \quad , \tag{19}$$

where Λ is the so-called dispersion function,

$$\Lambda(z) = 1 - \frac{z}{2}\int_{-1}^{1} \frac{g(z,\mu)}{z-\mu}\, dm(\mu)$$

$$= 1 - \frac{z}{2}\int_{-1}^{1} \frac{g(\mu,\mu)}{z-\mu}\, dm(\mu) \quad . \tag{20}$$

Equality of the two expressions follows from orthogonality of $p_\ell(\mu)$ to any polynomial of lower degree. Incidentally, $g(\mu,\mu)$, which will play an important role in the analysis, equals twice Chandrasekhar's characteristic function $\Psi(\mu)$.[6]

We notice that $\Lambda(z)$ is analytic in the complex plane cut along $(-1,1)$, real for real z outside the cut, and with at most logarithmic singularities at the endpoints of the cut. The boundary values of Λ on both sides of the cut are

$$\Lambda^{\pm}(\nu) \equiv \lim_{\varepsilon \to 0+} \Lambda(\nu \pm i\varepsilon)$$

$$= \lambda(\nu) \pm \frac{1}{2}\pi\, i\nu\, g(\nu,\nu)\, (1 - \nu^2)^m \quad , \tag{21}$$

where

$$\lambda(\nu) = 1 - \frac{\nu}{2} \int_{-1}^{1} \frac{g(\mu,\mu)}{\nu-\mu}\, dm(\mu) \quad , \quad \nu \in (-1,1) \quad . \tag{22}$$

The integral here, as well as subsequent integrals of a similar nature, is to be understood in the Cauchy principal-value sense.

The number of pairs of eigenvalues can be assessed from the argument principle, according to which[14]

$$J = \frac{1}{\pi} \left[\text{Im } \ln \Lambda^{+}(\nu) \right] \Big|_{\nu = 0}^{\nu \to 1} \quad .$$

Plots of the values of $\Lambda^{+}(\nu)$ will be helpful (Fig. 1); those for $m = 0$ and for $m > 0$ have to be investigated separately. In the first case, and if $g(\mu,\mu)$ is positive, $\lambda(\nu)$ goes to $-\infty$ at $\nu \to 1$, while the imaginary part in Eq. (21) reaches a positive limit. Hence $J = 1$, i.e., exactly one pair of eigenvalues exists.[6] If, on the other hand, the sign of $g(\mu,\mu)$ changes once in $0 < \mu < 1$, so that $g(1,1) < 0$, the plot may have the form b on Fig. 1, and we expect $J = 2$. More complicated cases can be conceived.

Since the polynomial $g(\mu,\mu)$, being even and of degree $2L$, can have at most L zeros in the interval $(0,1)$, it follows[14] that the number of pairs of eigenvalues is bounded by $J \leqq L + 1$. For the higher azimuthal components ($m > 0$) the situation is different because $dm(\mu)$ in Eqs. (20) and (22) contains the factor $(1 - \mu^2)^m$. Thereby λ stays bounded while the imaginary part in Eq. (21) vanishes at $\nu = 1$. Hence for a non-negative $g(\mu,\mu)$ we obtain a plot of the type c on Fig. 1, showing that one pair of eigenvalues exists, or none, depending upon whether $\lambda(1) < 0$, or $\geqq 0$.

For not too strongly anisotropic scattering, and certainly for $L \leqq 2$, the functions $g(\mu,\mu)$ are found to be positive, so that for $m = 0$ only one pair of eigenvalues exists. However, this is not generally the case for the strongly peaked scattering functions observed in natural fog. There additional eigenvalues were indeed found, even for $m > 0$.[18,19]

It is instructive to see how the eigenvalues change if ϖ_0 is varied, yet with the shape of the scattering function being kept constant. That is, we study the functions $\nu_j(\varpi_0)$ when $\varpi_\ell = \varpi_0 b_\ell$, b_ℓ = constant. A simple case of linearly anisotropic scattering ($L = 1$, $b_1 = 1$) is illustrated in Fig. 2. For higher values of L, additional curves could appear, some of them possibly connected as in the example shown.

Some of the features of Fig. 2 turn out to hold generally. The curves can be shown to intersect the horizontal axis at the values $(2\ell + 1)/b_\ell$, $\ell = m,\ m+1,\ \ldots\ ,\ L$. It also can be shown by a perturbation calculation that for $0 < \varpi_0 < 1$ all $\nu_j(\varpi_0)$ are monotonically increasing functions. The number of eigenvalues therefore can be determined by counting the number of limiting points s_j (see figure) to the left of the given ϖ_0 . These points are defined by

$$s_j = \lim_{\nu_j \to 1} \varpi_0(\nu_j) \quad .$$

For $m = 0$ they are evaluated by observing that the integral in (20) diverges for $z \to 0+$, unless $g(1,1)$ vanishes. The latter quantity is a polynomial in ϖ_0 , of degree L, and divisible by ϖ_0 . Thus the values s_j, $j = 1,\ \ldots\ ,\ L$, are found as zeros of this polynomial, and one of them is $s_1 = 0$.

For $m > 0$ the evaluation is less simple. Since the integral never diverges none of the s_j can vanish.

We see now that for sufficiently strong absorption (sufficiently small ϖ_0) only one pair of eigenvalues $(\pm\nu_1)$ exists for $m = 0$, and none for $m > 0$. With this observation, we conclude the discussion of the eigenvalues, and turn to the examination of the rest of the ν-spectrum.

Arbitrary functions of μ , say from the Hilbert space $L_2(-1,1)$, obviously cannot be expanded in terms of the finite number of regular eigenfunctions. These must therefore be supplemented by a set of singular eigenfunctions that belong to the continuous spectrum, i.e., to $\nu \in (-1,1)$. (The endpoints, though belonging to the spectrum, are deleted here, because no corresponding eigenfunctions exist; this creates no difficulties, however.)

The singular eigenfunctions are distributions (generalized functions) and include the Dirac delta function. The exact form is inferred from Eq. (10),

$$\phi(\nu,\mu) = \frac{\nu}{2}\,\frac{g(\nu,\mu)}{\nu-\mu} + \frac{\lambda(\nu)}{(1-\nu^2)^m}\,\delta(\nu-\mu), \quad \nu \in (-1,1) \quad . \tag{23}$$

As agreed before, integrals of the first term shall be understood in the Cauchy principal-value sense.

3. HALF-RANGE EXPANSIONS

The full set of eigenfunctions (regular + singular) is complete in the sense that the eigenfunctions can be used to expand arbitrary functions $f(\mu)$ given on the full range $-1 \le \mu \le 1$. The proof of this statement is usually achieved in a constructive way,[14] although it is expected also to follow from some general theorems on selfadjoint operators.[20,21] The evaluation of the expansion coefficients is greatly facilitated by the full-range orthogonality relation

$$\int_{-1}^{1} \phi(\nu,\mu)\ \phi(\nu',\mu)\ \mu\ dm(\mu) = 0 \quad , \tag{24}$$

valid for $\nu \neq \nu'$ and $\nu, \nu' \in (-1,1)$ or $= \pm\nu_1, \ldots, \pm\nu_J$, and by the associated normalization relations.[14,5] Both follow from Eq. (10).

An explanation is needed for the case that $\nu' \to \nu \in (-1,1)$. The ensuing conceptual difficulty, arising from the merging of the two singularities in the integrand, is best avoided if such integrals are understood as convolutions of distributions.[20] The switching of orders of integration, needed in applications to eigenfunction expansions, is then allowed by definition. In carrying out the details, one needs the Poincaré-Bertrand formula.[22,5]

Full-range orthogonality and full-range completeness have only indirect relevance in problems for a semi-infinite atmosphere. Normally, solutions bounded at $\tau \to \infty$ are sought, as in the albedo problem where the incident intensity is given. In such case exponentially increasing eigenmodes ($\nu < 0$) must be excluded. The expansion of $I(\tau,\mu)$ then takes the form

$$I(\tau,\mu) = \sum_{j=1}^{J} A(\nu_j)\, \phi(\nu_j,\mu)\, e^{-\tau/\nu_j} + \int_0^1 A(\nu)\, \phi(\nu,\mu)\, e^{-\tau/\nu} d\nu \quad .$$

This will be abbreviated as

$$I(\tau,\mu) = \int_{\sigma+} A(\nu)\, \phi(\nu,\mu)\, e^{-\tau/\nu} d\nu \quad , \tag{25}$$

where $\sigma+$ denotes the positive half of the spectrum, i. e., the union of the interval $(-1,1)$ and of the set $\nu_1, \nu_2, \ldots, \nu_J$. The reader is reminded that the superscript m denoting the m'th azimuthal Fourier component is suppressed for such quantities as $I^m(\tau,\mu)$, $A^m(\nu)$, c_ℓ^m, ν_j^m, $\phi^m(\nu,\mu)$, $g_\ell^m(\nu)$, $p_\ell^m(\mu)$, $g^m(\nu,\mu)$, $\Lambda^m(z)$, and $\lambda^m(\nu)$.

The unknown coefficients $A(\nu_j)$ and $A(\nu)$ should be determined from the boundary condition at $\tau = 0$. If $I(0,\mu)$ is given for $0 < \mu \leq 1$, then

$$I(0,\mu) = \int_{\sigma+} A(\nu)\, \phi(\nu,\mu)\, d\nu \quad . \tag{26}$$

Thus a function known only upon the half-interval $(0,1]$ is to be expanded in terms of half the set of eigenfunctions. To justify such an expansion, we need a half-range completeness theorem. This was first proved by Mika[14] by way of construction. An easier, indirect way that was worked out by Pahor and Suhadolc in a different context[23] can undoubtedly be adapted to the present problem. The proof combines existence of the solution of the albedo problem (established through a Neumann expansion) and full-range completeness. Formally a full-range expansion is applied to the solution $I(\tau,\mu)$. The coefficients for $\nu < 0$ are found to vanish; hence for $\tau = 0$, the half-range expansion (26) ensues, which completes the proof.

Once completeness is assured, we are left with the task of determining the expansion coefficients in Eq. (26). Noticing that the set of singularities of the reciprocal dispersion function $[\Lambda(z)]^{-1}$ coincides with the whole spectrum of ν, we are led to expect that a corresponding function is needed with singularities in half of the spectrum. The need is met by Chandrasekhar's H-function, defined through the Wiener-Hopf factorization,

$$[\Lambda(z)]^{-1} = H(z)\, H(-z) \quad , \tag{27}$$

where it is required that $H(z)$ be analytic for $\mathrm{Re}(z) > 0$.

An explicit expression for $\ln H(z)$ follows from Eq. (27) through Cauchy's integral theorem:[6]

$$\ln H(z) = \frac{z}{2\pi i} \int_{-i\infty}^{i\infty} \frac{\ln \Lambda(\zeta)}{\zeta^2 - z^2}\, d\zeta \quad , \qquad \mathrm{Re}(z) > 0.$$

By bending the contour and carrying out some manipulation, other expressions are derived, e.g.[24]

$$\frac{1}{H(z)} = (1+z)^{-J} \left[\prod_{j=1}^{J} (1 + z/\nu_j)\right] \exp\left[-\frac{z}{2\pi i} \int_0^1 \ln \frac{\Lambda^+(\nu)}{\Lambda^-(\nu)}\, \frac{d\nu}{\nu(z+\nu)}\right] \tag{28}$$

for $z \notin [-1,0)$. It must be mentioned that for each $\Lambda(z)$ the factorization (27) is unique if the quoted requirement is observed. To prove this, we only have to consider the ratio of two hypothetical H-functions factorizing the same Λ and to call upon Liouville's theorem.[25]

The H-function is regular in the complex plane cut along $(-1,0)$, except for the poles at $-\nu_j$, $j = 1, 2, \ldots, J$. On the real axis outside the cut, $H(z)$ is seen to be real and positive for $z \geq 0$. For $|z| > 1$, we find

$$\Lambda(z) = 1 - \eta_0 - \frac{\eta_2}{z^2} - \frac{\eta_4}{z^4} - \ldots , \tag{29}$$

$$\Lambda(z)\, H(z) = \frac{1}{H(-z)} = 1 - \beta_0 - \frac{\beta_1}{z} - \frac{\beta_2}{z^2} - \ldots , \tag{30}$$

where

$$\eta_{2n} = \frac{1}{2} \int_{-1}^{1} \mu^{2n}\, g(\mu,\mu)\, dm(\mu) \quad ,$$

$$\eta_0 = 1 - \prod_{\ell=m}^{L} \frac{h_\ell}{2\ell+1} \quad ,$$

$$\beta_n = \frac{1}{2} \int_0^1 \mu^n\, g(\mu,\mu)\, H(\mu)\, dm(\mu) \quad ,$$

$$\eta_0 - 2\beta_0 + \beta_0^2 = 0 \quad , \tag{31}$$

$$\eta_2 - 2\beta_2 + 2\beta_0\beta_2 - \beta_1^2 = 0 \quad , \tag{32}$$

etc.[6,14] The β_n are to be expressed in terms of the moments of the H-function,

$$\alpha_n = \int_0^1 \mu^n \, H(\mu) \, dm(\mu) \quad .$$

In view of Eq. (19), the product $\Lambda(z)\, H(z)$ has no singularities at all in the plane cut along (0,1). We apply Cauchy's integral theorem to this function, drawing a contour around the cut. After shrinking the contour onto the cut, we find

$$\Lambda(z)\, H(z) = \frac{1}{2\pi i} \int_0^1 \frac{\Lambda^+(\mu) - \Lambda^-(\mu)}{\mu - z} H(\mu)\, d\mu + \Lambda(\infty)\, H(\infty), \quad z \notin [0,1] \quad . \tag{33}$$

From Eq. (21) we substitute $\Lambda^+(\mu) - \Lambda^-(\mu) = \pi i \mu \, g(\mu,\mu) \, (1 - \mu^2)^m$. Taking $z \to 0$, and combining the result with Eq. (33), we simplify the equation to

$$\frac{z}{2} \int_0^1 \frac{g(\mu,\mu)}{z - \mu} H(\mu) \, dm(\mu) + \Lambda(z)\, H(z) = 1, \quad z \notin [0,1] \quad . \tag{34}$$

The well-known non-linear integral equation[6] is derived by substituting $\Lambda(z)\, H(z) = 1/H(-z)$ from Eq. (27). Such an equation has often been used for computations in preference to Eq. (28).

For $z \to \nu \in (0,1)$ in Eq. (34), we apply Plemelj's formula[22] to obtain

$$\frac{\nu}{2} \int_0^1 \frac{g(\mu,\mu)}{\nu - \mu} H(\mu) \, dm(\mu) + \lambda(\nu)\, H(\nu) = 1 \quad , \tag{35}$$

which represents an inhomogeneous Cauchy singular integral equation for $H(\mu)$. For $z \to \nu_j$, $j = 1 \ldots, J$ a set of subsidiary conditions follows, with $\Lambda(\nu_j)\, H(\nu_j) = 1/H(-\nu_j) = 0$. Because J is the index[22] of Eq. (35), a J-parametric family of solutions exists which is just right to fit the subsidiary conditions in a unique way.

The factor multiplying $H(\mu)$ in the integrand of Eq. (35) looks suspiciously like $\phi(\nu,\mu)$, except that $g(\nu,\mu)$ is replaced by $g(\mu,\mu)$. To gain more insight, we turn from Eq. (34) to a modified relation,

$$\frac{z}{2}\int_0^1 \frac{g(z,\mu)}{z-\mu}\, Q(\mu)\, H(\mu)\, dm(\mu) + Q(z)\, \Lambda(z)\, H(z) = G(z), \quad z \notin [0,1] \quad , \tag{36}$$

where the functions $Q(z)$ and $G(z)$ are yet to be specified. It turns out that if $G(z)$ is a polynomial of maximum degree $L - m$, the same is true of $Q(z)$. This can be seen by observing that the discontinuity across the cut of the first term on the left-hand side is exactly cancelled by that of the second term (by the Plemelj formula). Hence $Q(z)$ is an entire function. The maximum degree of $Q(z)$ easily follows from $g(z,\mu)$ and $G(z)$.

Let us take $G(z) = g_\ell(z)$, $\ell = m, m+1, \ldots, L$, for which choice the corresponding $Q(z)$ define the Busbridge polynomials[8] $q_\ell(z)$.* When z reaches the positive half of the spectrum, a singular integral equation (with subsidiary conditions) follows,

$$\int_0^1 \phi(\nu,\mu)\, q_\ell(\mu)\, H(\mu)\, dm(\mu) = g_\ell(\nu) \quad , \quad \nu \in \sigma+ \quad . \tag{37}$$

It was derived by Pahor[24] from the original definition of Busbridge. A comprehensive discussion by van de Hulst[26] should also be consulted.

Another useful relation ensues when z approaches the negative half of the spectrum,

$$\int_0^1 \phi(-\nu,\mu)\, q_\ell(\mu)\, H(\mu)\, dm(\mu) = g_\ell(-\nu) - \frac{q_\ell(-\nu)}{H(\nu)} \quad , \quad \nu \in \sigma+ \quad . \tag{38}$$

Doubts about existence and uniqueness of the Busbridge polynomials, arising because some determinant involved in the calculation might vanish, can be resolved by resorting to the original definition, i.e. by expressing $q_\ell(\mu)$, $\mu \in (0,1)$, in terms of the solution of the albedo problem and relying upon the existence and uniqueness of this solution. A more direct proof might be obtainable from theorems[22,27] relating the multiplicity of solutions $q_\ell(\mu)\, H(\mu)$ of Eq. (37) to that of the corresponding adjoint dominant equation (36).

For computational purposes both sides of Eq. (34) are multiplied by $q_\ell(z)$ and combined with Eq. (36) (with $Q = q_\ell$ and $G = g_\ell$) to derive the Fredholm-like equation,[24]

$$q_\ell(z) = g_\ell(z) - \frac{z}{2}\int_0^1 \frac{g(z,\mu)\, q_\ell(\mu) - g(\mu,\mu)\, q_\ell(z)}{z-\mu}\, H(\mu)\, dm(\mu) \quad . \tag{39}$$

Multiplying both sides of Eq. (37) by $\frac{1}{2}\nu c_\ell p_\ell(\mu)$ and summing over ℓ we obtain

---

*The sign convention[24,26] differs from that of Busbridge by a factor $(-1)^\ell$.

$$\frac{\nu}{2}\int_0^1 K(\mu,\mu')\,\phi(\nu,\mu')\,H(\mu')\,dm(\mu') = \frac{\nu}{2}\,g(\nu,\mu)$$

$$= (\nu - \mu)\,\phi(\nu,\mu), \quad \nu \in \sigma+ \quad , \tag{40}$$

where

$$K(\mu,\mu') = \sum_{\ell=m}^{L} c_\ell\, p_\ell(\mu)\, q_\ell(\mu') \quad . \tag{41}$$

Thus the Busbridge polynomials have made it possible to construct a half-range integral equation for the eigenfunctions $\phi(\nu,\mu)$, where $K(\mu,\mu')$ has taken the role of $p(\mu,\mu')$ in Eq. (10), and the integrand is weighted with the H-function. This equation will be the key to further analysis.

Since K is not a symmetric kernel (except if scattering is isotropic when $K = \text{const}$), it becomes necessary to study also the adjoint equation,

$$\frac{\nu}{2}\int_0^1 K(\mu',\mu)\,\phi^\dagger(\nu,\mu')\,H(\mu')\,dm(\mu') = (\nu - \mu)\,\phi^\dagger(\nu,\mu) \equiv \frac{\nu}{2}\,g^\dagger(\nu,\mu), \nu \in \sigma^+ \tag{42}$$

(In a different form this equation (for $\nu = \nu_1^0$) has already been formulated by Ambarzumian.[28,7]) A somewhat indirect and lengthy procedure leads to the conclusion[4] that, with appropriate normalization, $\nu^{-1}\,\phi^\dagger(\nu,\mu)$ differs from $\nu^{-1}\,\phi(\nu,\mu)$ only by a polynomial of maximum degree $L - m - 1$ in each variable. This means that $\phi^\dagger$ has the form

$$\phi^\dagger(\nu,\mu) = \frac{\nu}{2}\,\frac{g^\dagger(\nu,\mu)}{\nu - \mu} + \frac{\lambda(\nu)}{(1 - \nu^2)^m}\,\delta(\nu - \mu) \quad , \tag{43}$$

with the same $\lambda(\nu)$ as before; another consequence is that

$$g^\dagger(\mu,\mu) = g(\mu,\mu) \quad . \tag{44}$$

From Eq. (37) we infer that the q_ℓ are linearly independent so we may expand $g^\dagger$ as

$$g^\dagger(\nu,\mu) = \sum_{\ell=m}^{L} c_\ell\, g_\ell^\dagger(\nu)\, q_\ell(\mu) \quad , \tag{45}$$

implying that

$$\int_0^1 \phi^\dagger(\nu,\mu)\, p_\ell(\mu)\, H(\mu)\, dm(\mu) = g_\ell^\dagger(\nu) \quad , \quad \nu \in \sigma+ \quad . \tag{46}$$

In a manner similar to that used to obtain Eq. (38), it follows that

$$\int_0^1 \phi^\dagger(-\nu,\mu)\, p_\ell(\mu)\, H(\mu)\, dm(\mu) = g_\ell^\dagger(-\nu) - \frac{p_\ell(-\nu)}{H(\nu)} \quad , \quad \nu \in \sigma+ \quad . \tag{47}$$

By a standard procedure equations (40) and (42) are combined to derive a biorthogonality relation between the $\phi(\nu,\mu)$ and $\phi^\dagger(\nu,\mu)$. The normalization constants can be evaluated by first generalizing those two equations to complex ν and ν', combining both as before and then taking the appropriate limits. All results can be condensed into one formula,[4]

$$\int_0^1 \phi(\nu,\mu)\, \phi^\dagger(\nu',\mu)\mu\, H(\mu)\, dm(\mu) = [1 - \theta(\nu)]\, N(\nu)\, H(\nu)\, \delta(\nu-\nu')$$

$$- \theta(\nu)\, \frac{\nu\phi^\dagger(\nu',\nu)}{H(-\nu)} - \theta(\nu')\, \frac{\nu'\phi(\nu,\nu')}{H(-\nu')} \quad , \tag{48}$$

with the same $\theta(\nu)$ as in Eq. (9) and

$$N(\nu) = \nu\Lambda^+(\nu)\, \Lambda^-(\nu) = \nu \left| \lambda^2(\nu) + \left[\tfrac{1}{2}\pi\nu\, g(\nu,\nu)(1 - \nu^2)^m\right]^2 \right| , \quad \nu \in (0,1).$$

When $\nu = \nu' = \nu_j$, the last terms must be understood in the sense of the limit as $\nu \to \nu_j$ and $\nu' \to \nu_j$. Thus

$$\int_0^1 \phi(\nu_j,\mu)\, \phi^\dagger(\nu_j,\mu)\, \mu\, H(\mu)\, dm(\mu) = N(\nu_j)\, H(\nu_j) \quad , \tag{49}$$

where $N(\nu_j)$ is expressed with the derivative of Λ,

$$N(\nu_j) = \tfrac{1}{2}\, \nu_j^2\, g(\nu_j,\nu_j)\Lambda'(\nu_j) \quad . \tag{50}$$

A particularly useful example of Eq. (48) is the following transformation, where some of the variables have been renamed,

$$\int_0^1 \phi(\nu,\mu')(\mu'/\mu)\, \phi^\dagger(-\mu,\mu')\, H(\mu)\, H(\mu')\, dm(\mu') = \phi(\nu,-\mu) \quad ,$$

$$\nu \in \sigma+ \quad , \mu \in (0,1) \quad . \tag{51}$$

For $\nu = \nu_1^0$ this equation, as well as Eq. (48) for $\nu' = \nu_1^0$, were already considered by Sobolev.[7]

The $\phi(\nu,\mu)$ and $\phi(\nu,-\mu)$ may be regarded as intensities exchanged at the plane $\tau = 0$ between two halves of an infinite medium.[24] Obviously the single ϕ may be substituted by any linear combination of eigenfunctions. In view of half-range completeness, the transformation (51) represents the reflection law for a semi-infinite medium. It is traditionally stated in terms of Chandrasekhar's S-function,[6]

$$S(\mu,\mu') = (2 - \delta_{m0}) \frac{\mu\,\mu'}{\mu+\mu'} g^{\dagger}(-\mu,\mu')\, H(\mu)\, H(\mu')(1 - \mu^2)^{m/2}\,(1 - \mu'^2)^{m/2} \quad . \tag{52}$$

The reciprocity relation[6] $S(\mu,\mu') = S(\mu',\mu)$ translates into the present notation as

$$g^{\dagger}(-\mu',\mu) = g^{\dagger}(-\mu,\mu') \quad \text{or} \quad \mu\, \phi^{\dagger}(-\mu',\mu) = \mu'\, \phi^{\dagger}(-\mu,\mu') \quad . \tag{53}$$

We are now able to determine the $g_{\ell}^{\dagger}(\nu)$. Combining Eqs. (12), (37), (51), (53), and splitting the range of integration in (12), we obtain

$$\int_0^1 \phi(\nu,\mu)\, q_{\ell}(\mu)\, H(\mu)\, dm(\mu) = \int_0^1 \phi(\nu,\mu) \left[p_{\ell}(\mu) + \right.$$

$$\left. + (-1)^{\ell+m} \int_0^1 \phi^{\dagger}(-\mu,\mu')\, p_{\ell}(\mu')\, H(\mu)\, H(\mu')\, dm(\mu') \right] dm(\mu) \quad .$$

Because of half-range completeness, the bracketed factor on the right must equal the corresponding factor of the left-hand integrand. The equation thus obtained is further modified by substituting a complex μ, invoking the factorization (27), and taking the limit $\mu \to -\nu$, where $\nu \in \sigma+$. The result is

$$\int_0^1 \phi^{\dagger}(\nu,\mu')\, p_{\ell}(\mu')\, H(\mu')\, dm(\mu') = (-1)^{\ell+m}\, q_{\ell}(-\nu) \quad , \quad \nu \in \sigma+ \quad , \tag{54}$$

and hence

$$g_{\ell}^{\dagger}(\nu) = (-1)^{\ell+m}\, q_{\ell}(-\nu) \tag{55}$$

by comparison with Eq. (46). Thus finally[8,24]

$$g^{\dagger}(\nu,\mu) = \sum_{\ell=m}^{L} (-1)^{\ell+m}\, c_{\ell}\, q_{\ell}(-\nu)\, q_{\ell}(\mu) \quad . \tag{56}$$

With expression (56) inserted in Eq. (54), we recover Busbridge's definition of the q_ℓ-polynomials, i.e., her Eq. (48.4).[8] On the other hand, with (55) and (56) substituted, Eq. (46) becomes equivalent to an equation given by van de Hulst.[26]

4. ALBEDO AND MILNE PROBLEMS

After the preceding lengthy preparation, problems can be solved in a very expedient way by only carrying out quadratures. For the albedo problem the coefficients in Eq. (26) are determined by multiplying both sides by $\phi^\dagger(\nu,\mu)\ \mu\ H(\mu)\ dm(\mu)$, and integrating. The result from Eq. (48) is

$$I(0,\mu) = \int_{\sigma+} d\nu\ \frac{\phi(\nu,\mu)}{N(\nu)\ H(\nu)} \int_0^1 dm(\mu')\ I(0,\mu)\ \phi^\dagger(\nu,\mu')\ \mu'\ H(\mu')\ ,\quad \mu\ \varepsilon\ (0,1)\ . \tag{57}$$

As it stands, expansion (57) is of no direct use because it only reproduces the given incident distribution on the surface. This is made clear by stating the closure relation

$$\delta(\mu - \mu') = (1 - \mu'^2)^m\ \mu'\ H(\mu') \int_{\sigma+} \frac{\phi(\nu,\mu)\,\phi^\dagger(\nu,\mu')}{N(\nu)\ H(\nu)}\ d\nu\ , \tag{58}$$

which is a concise expression of the half-range completeness property of the eigenfunctions.

Meaningful results quickly follow from expansion (57). If the factor $e^{-\tau/\nu}$ is included in the integrand, we obtain the m-th azimuthal component of the distribution inside the medium. The angle integrated intensity $\rho(\tau)$ and the net flux $j(\tau)$ then follow (for $m = 0$) by integration and by aid of Eqs. (16) and (17). If we are interested in the distribution emerging from the surface, we need only replace μ in Eq. (57) by $-\mu$, where $\mu > 0$. With $\phi(\nu, -\mu)$ from Eq. (51) substituted and with reciprocity taken into account, we have

$$I(0, \mu) = \int_0^1 I(0,\mu')\ \tilde{\phi}^\dagger(-\mu',\mu)\ H(\mu)\ H(\mu')\ dm(\mu')\ ,\quad \mu\ \varepsilon\ (0,1)\ . \tag{59}$$

Equation (59) for $m = 0$ may be used to calculate the angle-integrated intensity and net flux at the surface of the semi-infinite medium. After switching the orders of integration, we conclude from Eq. (47) that[29]

$$\rho(0) = \int_{-1}^1 d\mu \int_0^{2\pi} d\phi\ I(0,\mu,\phi) = 2\pi \int_0^1 I^0(0,\mu)\ q_0^0(\mu)\ H^0(\mu)\ d\mu\ , \tag{60}$$

$$j(0) = \int_{-1}^1 \mu\ d\mu \int_0^{2\pi} d\phi\ I(0,\mu,\phi) = 2\pi \int_0^1 I^0(0,\mu)\ q_1^0(\mu)\ H^0(\mu)\ d\mu\ . \tag{61}$$

Let us consider the specific albedo problem where a parallel incident beam is given by

$$I(0,\mu,\phi) = \delta(\mu - \mu_0)\ \delta(\phi - \phi_0)/\mu_0 \quad , \quad 0 < \mu \leq 1 \quad . \tag{62}$$

According to Eq. (7), we have $\phi_m = \phi_0$ and

$$I(0,\mu) = \frac{\delta(\mu - \mu_0)}{2\pi\mu_0(1 - \mu_0^2)^{m/2}} \quad , \quad 0 < \mu \leq 1 \quad . \tag{63}$$

From Eq. (59), we obtain the value of $I(0,-\mu)$ to be used in Eq. (9) for calculating $I(0,-\mu,\phi)$,

$$I(0,-\mu) = \frac{(1 - \mu_0^2)^{m/2}}{2\pi\mu_0}\ \phi^{\dagger}(-\mu_0,\mu)\ H(\mu_0)\ H(\mu) \quad , \quad 0 < \mu \leq 1 \quad . \tag{64}$$

Equations (60) and (61) reduce to

$$\rho(0) = \mu_0^{-1}\ q_0^0(\mu_0)\ H^0(\mu_0) \quad , \quad j(0) = \mu_0^{-1}\ q_1^0(\mu_0)\ H^0(\mu_0) \quad . \tag{65}$$

In general, we see that any spherical-harmonics moment of the surface intensity can be expressed in terms of the corresponding $q_\ell^m(\mu_0)\ H^m(\mu_0)$ in the manner of Eqs. (60) and (61).

It is also interesting to know the distribution in the deep interior of the atmosphere. Let it suffice to quote the asymptotic approximation, consisting of the dominant term in the expansion, i.e., the one depending upon the longest relaxation length ν_1^0 (hence $m = 0$),

$$I_{as}(\tau,\mu,\phi) = A(\nu_1)\ \phi(\nu_1,\mu)\ \exp(-\tau/\nu_1) \quad , \tag{66}$$

$$\rho_{as}(\tau) = 2\pi\ A(\nu_1)\ \exp(-\tau/\nu_1) \quad , \tag{67}$$

$$j_{as}(\tau) = 2\pi h_0 \nu_1\ A(\nu_1)\ \exp(-\tau/\nu_1) \quad . \tag{68}$$

Here

$$A(\nu_1) = \frac{1}{2\pi}\ \frac{\phi^{\dagger}(\nu_1,\mu_0)\ H(\mu_0)}{N(\nu_1)\ H(\nu_1)} \tag{69}$$

according to Eq. (58), with $N(\nu_1)$ to be taken from Eq. (50). Significant deviations from this approximation can be expected only in a boundary layer near the surface. The thickness of this layer is a few times the next largest relaxation length if it exists, or a few mean free paths if it does not.

Another albedo problem of some interest is that with a uniformly diffuse illumination. For a unit incident flux, the boundary condition is

$$I(0,\mu,\phi) = \pi^{-1} \quad , \quad 0 < \mu \leqq 1 \quad .$$

Multiplying expression (64) for $m = 0$ by $2\,\mu_0 d\mu_0$ and integrating, we obtain

$$I(0,-\mu) = \pi^{-1}\left[1 - \mu^{-1}\, q_1(\mu)\, H(\mu)\right] \quad , \quad 0 < \mu \leqq 1 \quad , \tag{70}$$

and then

$$\rho(0) = 4 - 2\int_0^1 \mu^{-1}\, q_1(\mu)\, H(\mu)\, d\mu \quad , \tag{71}$$

$$j(0) = 2\int_0^1 q_1(\mu)\, H(\mu)\, d\mu \quad . \tag{72}$$

Another expression for $\rho(0)$ follows from the first of Eqs. (65) through integration with $2\,\mu_0 d\mu_0$, or from (71) by aid of the identity

$$2 - \int_0^1 \mu^{-1}\, q_1(\mu)\, H(\mu)\, d\mu = \int_0^1 q_0(\mu)\, H(\mu)\, d\mu \quad ,$$

which is derived from Eq. (47).

In expressions of the form (66) - (68), we now have

$$A(\nu_1) = -\pi^{-1}\, q_1(-\nu_1)/N(\nu_1)\, H(\nu_1) \quad . \tag{73}$$

In a similar way the Milne problem is solved, where an azimuth-independent distribution is postulated satisfying the boundary conditions

$$I(0,\mu) = 0 \quad , \quad 0 < \mu \leqq 1 \quad , \tag{74}$$

$$I(\tau,\mu) = \phi^0(-\nu_1^0,\mu)\, \exp(\tau/\nu_1^0), \quad \tau \to \infty \quad . \tag{75}$$

We drop the superscript $m = 0$ henceforth.

The increasing term from Eq. (75) must now be added to the expansion (25). However, when fitting the boundary condition, we transfer this term to the left-hand side, so that the function to be expanded according to the half-range procedure, Eq. (57), now is $-\emptyset(-\nu_1,\mu)$. In switching to the emerging intensity via Eq. (59), however, some care is needed since we must add the term $\emptyset(-\nu_1,-\mu)$, to obtain $I(0,-\mu)$. Use of Eq. (48) then gives

$$I(0,-\mu) = \emptyset^{\dagger}(\nu_1,\mu)\, H(\mu)/H(\nu_1) \quad , \quad 0 < \mu \leqq 1 \quad . \tag{76}$$

In passing, the generalized Milne problem may be mentioned,[2] where instead of Eq. (75) we prescribe that at $\tau \to \infty$ the intensity be proportional to some other increasing eigenmode. The problem is only of mathematical interest because the solution is partly negative or even singular. It is worth noticing, however, that a picture of all the adjoint eigenfunctions for $\nu \in \sigma+$ is obtained, since

$$I(0,-\mu) \propto \emptyset^{\dagger}(\nu,\mu)\, H(\mu) \quad . \tag{77}$$

Integrating Eq. (76) with $2\pi d\mu$ or $-2\pi\mu\, d\mu$, respectively, we derive by aid of Eq. (54) the angle-integrated intensity and net flux at the surface,

$$\rho(0) = 2\pi q_0(-\nu_1)/H(\nu_1) \quad , \quad j(0) = 2\pi q_1(-\nu_1)/H(\nu_1) \quad . \tag{78}$$

It is sometimes convenient, especially when $\varpi_0 \to 1$, to renormalize the Milne solution to unit emerging net flux by multiplying everything by $[-H(\nu_1)/2\pi q_1(-\nu_1)]$.

The asymptotic approximation is now defined with the two terms

$$I_{as}(\tau,\mu) = \emptyset(-\nu_1,\mu)\, \exp(\tau/\nu_1) + A(\nu_1)\, \emptyset(\nu_1,\mu)\, \exp(-\tau/\nu_1) \quad , \tag{79}$$

where the expansion coefficient is found as before,

$$A(\nu_1) = -\, \frac{\nu_1 g^{\dagger}(\nu_1,-\nu_1)}{4\, N(\nu_1)\, H^2(\nu_1)} \quad . \tag{80}$$

In writing the angle-integrated intensity and net flux it is convenient to lump both terms together in the form

$$\rho_{as}(\tau) = 4\pi\, \exp(-\tau^*/\nu_1)\, \sinh[(\tau + \tau^*)/\nu_1] \quad , \tag{81}$$

$$j_{as}(\tau) = -4\pi h_0 \nu_1\, \exp(-\tau^*/\nu_1)\, \cosh[(\tau + \tau^*)/\nu_1] \quad . \tag{82}$$

The so-called extrapolation length τ^* is defined by the condition $\rho_{as}(-\tau^*) = 0$, so that from Eq. (79)

$$\exp[-2\tau^*/\nu_1] = -A(\nu_1) \quad . \tag{83}$$

With expression (80) substituted, this formula has been used in a few numerical calculations.[30]

Next we consider a weakly absorbing atmosphere of finite but large thickness $(0 \leq \tau \leq \tau_0 \, , \, \tau_0 >> 1)$, resting upon a ground of albedo $\underline{a}$ and reflecting light according to Lambert's law. This corresponds to the boundary condition

$$I(\tau_0,-\mu,\phi) = \frac{a}{\pi}\int_0^1 \mu' \, d\mu' \int_0^{2\pi} d\phi' \; I(\tau_0,\mu',\phi') \quad , \quad 0 < \mu \leq 1 \quad . \tag{84}$$

As before we take a parallel incident beam, Eq. (62).

A matched asymptotic approximation[31] will be constructed from the solutions for the semi-infinite atmosphere. These will be distinguished by subscripts p (parallel incident beam), d (diffuse source) and M (Milne). In the case of $a = 0$, we argue that at the bottom of the atmosphere, where the unscattered contribution shown in Eq. (9) becomes negligible, the solution must approximately equal that of the homogeneous problem--the Milne problem. More generally, if reflection from the ground is present, a multiple of the albedo solution for a diffuse source must be added. Thus with an obvious change of variables,

$$I(\tau,\mu,\phi) \approx C_1 \, I_M(\tau_0 - \tau,-\mu) + C_2 \, I_d(\tau_0 - \tau,-\mu) \quad , \quad \tau >> 1 \quad . \tag{85}$$

Actually this approximate equality is expected to hold within most of the atmosphere, with only a top boundary layer (b_1 on Fig. 3) excepted, according to what was said before.

By similar reasoning the solution in the upper part of the atmosphere can, with neglect of a bottom boundary layer (b_2 on Fig. 3), be represented as a superposition of the solutions I_p and I_M,

$$I(\tau,\mu,\phi) \approx I_p(\tau,\mu,\phi) - C_3 \, I_M(\tau,\mu) \quad , \quad \tau_0 - \tau >> 1 \quad . \tag{86}$$

In the asymptotic region (as on Fig. 3), where both boundary layers are excluded, we keep only the terms proportional to $\exp(\pm\tau/\nu_1)$ in the eigenmode expansions of I_p, I_d, and I_M. Equations (85) and (86) thereby yield two relations for the coefficients C_1, C_2, C_3. It suffices to equate angle-integrated intensities, and to then take $\tau = -\tau^*$ and $\tau = \tau_0 + \tau^*$ to obtain

$$2 \, C_1 \sinh \frac{\tau_0 + 2\tau^*}{\nu_1} + C_2 \, A_d(\nu_1) \exp(-\tau_0/\nu_1) = A_p(\nu_1) \exp(2\tau^*/\nu_1) \quad , \tag{87}$$

$$C_2\, A_d(\nu_1)\, \exp(2\tau^*/\nu_1) = A_p(\nu_1)\, \exp(-\tau_0/\nu_1) - 2\, C_3\, \sinh \frac{\tau_0 + 2\tau^*}{\nu_1} \quad . \tag{88}$$

The third equation follows from relating the net fluxes emerging and reflected at $\tau = \tau_0$ according to the boundary condition (84),

$$C_2 = a \left[C_1\, |j_M(0)| + C_2\, |1 - j_d(0)| \right] . \tag{89}$$

The system (87) - (89) is easily solved. We then only have to substitute the previous results in Eqs. (85) and (86) to obtain the quantities relevant to the thick atmosphere. For instance, if there is no ground reflection ($a = 0$, $C_2 = 0$), we find

$$C_1 = A_p(\nu_1)\, \frac{\exp(2\tau^*/\nu_1)}{2\, \sinh[(\tau_0 + 2\tau^*)/\nu_1]} \quad , \quad C_3 = C_1\, \exp[-(\tau_0 + 2\tau^*)/\nu_1] \quad ,$$

and then (for $0 < \mu \leq 1$)

$$I(\tau_0,\mu,\phi) \simeq \frac{\phi^\dagger(\nu_1,\mu_0)\, \phi^\dagger(\nu_1,\mu)\, H(\mu_0)\, H(\mu)}{\pi\, \nu_1\, \sinh[(\tau_0 + 2\tau^*)/\nu_1]\, g^\dagger(\nu_1,-\nu_1)} \quad , \tag{90}$$

$$I(0,-\mu,\phi) \simeq I_p(0,-\mu,\phi) - \exp[-(\tau_0 + 2\tau^*)/\nu_1]\, I(\tau_0,\mu,\phi) \quad . \tag{91}$$

The appearance of the argument $(\tau_0 + 2\tau^*)/\nu_1)$ can be understood from Fig. 3.

A rigorous justification of the above approximations must start with full-range expansions for the exact solution.[5,32,33] Equations (85) and (86) coincide with the initial approximations in an iterative procedure, obtained by neglecting the terms decreasing or increasing with τ, respectively, except for the dominant terms that involve $\exp(\pm\tau/\nu_1)$.

Alternatively, for atmospheres of any thickness (if no ground reflection is present), the reflected and transmitted intensities can be expressed exactly in terms of Chandrasekhar's X- and Y-functions and by a generalization of the Busbridge polynomials.[7] Gibbs has succeeded in linking this formalism (so far for isotropic scattering) to the method of singular eigenfunctions.[34] However, no closed-form expressions have been found for the functions $X(\mu)$ and $Y(\mu)$.

5. THE CONSERVATIVE CASE

In the conservative case, i.e., when there is no true absorption, a few modifications become necessary. These only affect the azimuth-independent component, and the reason is that the eigenvalues ν_1^0 and $-\nu_1^0$ merge at infinity. Rather than make a fresh start, we are going to derive the results

by taking limits with $\varpi_0 \to 1$ (or $h_0 \to 0$). As before, the superscript $m = 0$ will be omitted.

The diffusion length can be seen to approach infinity like $\nu_1 \simeq (h_0\, h_1)^{-1/2}$. Equation (30) shows that $H(\nu_1) \simeq \nu_1/2\beta_1$. Next, we notice that in the unit $\beta_0 = \eta_0 = 1$ and $\beta_1^2 = \eta_2$. The latter quantity now allows a concise expression,

$$\eta_2 = \frac{1}{3} \prod_{\ell=2}^{L} \frac{h_\ell}{2\ell + 1} \quad .$$

While two of the eigenmodes become identical,

$$\lim_{\varpi_0 \to 1} \phi(\mp\nu_1, \mu) \exp(\mp\tau/\nu_1) = \frac{1}{2} \quad , \tag{92}$$

a new linearly independent eigenmode arises in the following way:

$$\lim_{\varpi_0 \to 1} \frac{1}{2} h_1 \nu_1 \left[\phi(-\nu_1, \mu) \exp(\tau/\nu_1) - \phi(\nu_1, \mu) \exp(-\tau/\nu_1)\right] = \frac{1}{2}(h_1 \tau - 3\mu) \quad . \tag{93}$$

Half-range completeness remains intact if the eigenfunction from Eq. (92) is included. That is, we agree that the set $\sigma+$ shall include the point $\nu_1 = \infty$.

The polynomials $g_\ell(\nu)$ now become $g_0 = 1$, $g_1 = 0$, $g_2 = -\frac{1}{2}$, $g_3 = -h_2\nu/3!$, etc. To obtain the higher g_ℓ's, the first two rows and columns of the determinant (18) may be deleted and the sign changed.[15] Except for g_0, the degree is $\ell - 2$, and linear independence is preserved only for $g_2, \ldots, g_L$.

Equation (92) implies that

$$\lim_{\varpi_0 \to 1} g_\ell(\nu_1) = \delta_{\ell 0} \quad . \tag{94}$$

(In fact, $g_\ell(\nu_1) = O(\nu_1^{-\ell})$,[4] so that for weakly absorbing atmospheres ν_1 can be calculated efficiently from the higher g_ℓ's.[13]) Notice that first the substitution $\nu = \nu_1$ is made and only then the limit taken. It can be shown, moreover, that[4]

$$\lim_{\varpi_0 \to 1} g(\nu_1, \nu_1) = 1/h_1\eta_2 \quad . \tag{95}$$

The Busbridge polynomials are still uniquely defined by the set of equations (37) provided we include the equation for $\nu = \nu_1 \to \infty$, i.e.

$$\frac{1}{2}\int_0^1 q_\ell(\mu)\, H(\mu)\, d\mu = \delta_{\ell 0} \quad , \tag{96}$$

which must also be used with Eq. (39). We notice that $q_1(z)$ vanishes because $g_1 = 0$. Taking into account that $H(z)$ now has a simple pole at infinity, we find that the maximum degree of the $q_\ell(z)$ is lowered to $L - 1$ for $L \geq 2$.

If condition (96) is disregarded, the homogeneous versions of Eqs. (37) and (39) become solvable. The solution is $q_0(z) + 2q_2(z)$, in view of $g_0 + 2g_2 = 0$.

Examination of Eq. (39) indicates that the following limits are bounded too,

$$\phi_1^\dagger(\mu) = \lim_{\varpi_0 \to 1} \phi^\dagger(\nu_1,\mu) = \frac{1}{2} \sum_{\ell=0}^{L} \varpi_\ell \gamma_\ell q_\ell(\mu) \quad , \tag{97}$$

$$\gamma_\ell = (-1)^\ell \lim_{\varpi_0 \to 1} q_\ell(-\nu_1) = \int_0^1 \phi_1^\dagger(\mu) P_\ell(\mu) H(\mu) \, d\mu \quad . \tag{98}$$

Of course, $\phi_1^\dagger(\mu)$ is orthogonal to $\phi(\nu,\mu)$, $\nu \in \sigma+$, except for $\nu = \infty$. There we find

$$\int_0^1 \phi_1^\dagger(\mu) \, \mu \, H(\mu) \, d\mu = \gamma_1 = 1/h_1\beta_1 \tag{99}$$

by taking the limit of expressions (49), (50), and using Eqs. (29) and (95). We shall also need the quantity

$$\lim_{\varpi_0 \to 1} g^\dagger(\nu_1,-\nu_1) = \sum_{\ell=0}^{L} (-1)^\ell \varpi_\ell \gamma_\ell^2 = \frac{1}{h_1 n_2} \quad , \tag{100}$$

where the last expression is derived from Eqs. (48) and (99).

The orthogonality relation between $\phi(\nu,\mu)$ and $\phi_1^\dagger(\mu)$ may be regarded as a homogeneous integral equation for the function $\mu\phi_1^\dagger(\mu)$. Since the operator is the same as in Eq. (37), we conclude that $\mu \phi_1^\dagger(\mu)$ equals a solution of the homogeneous version of that equation, and hence is a multiple of $q_0(\mu) + 2q_2(\mu)$. Comparing the normalization condition (99) with (96) we have finally

$$\phi_1^\dagger(\mu) = \frac{q_0(\mu) + 2q_2(\mu)}{2 \, \mu \, h_1\beta_1} \quad . \tag{101}$$

With this expression substituted, we may find the remaining γ_ℓ from Eq. (98).

After such explanations, it is clear how Eq. (48) is to be applied in the limiting case. A useful supplementary equation,[4] with (101) substituted, is

$$\int_0^1 \phi^\dagger(\nu,\mu)\, \mu^2\, H(\mu)\, d\mu = -\frac{\theta(\nu)\nu^2}{H(-\nu)} + \frac{1}{3}\left[q_0(-\nu) + 2q_2(-\nu)\right] \quad . \tag{102}$$

The results (64) and (65) for the albedo problem for a semi-infinite atmosphere remain valid without modification. Taking the limit of expression (69) we find that

$$\rho(\infty) = 2h_1\, \beta_1\, \phi_1^\dagger(\mu_0)\, H(\mu_0) \quad , \tag{103}$$

while of course $j(\tau) = 0$. For a uniformly diffuse illumination, we can verify that $I(\tau,\mu,\phi) = \text{const.}$

It remains to deal with the Milne problem.[24] Setting $j = -1$, we find

$$I(0,-\mu) = \frac{\phi_1^\dagger(\mu)\, H(\mu)}{2\pi\gamma_1} = \frac{[q_0(\mu) + 2q_2(\mu)]H(\mu)}{4\pi\mu} \quad , \quad 0 < \mu \leqq 1 \quad . \tag{104}$$

The Hopf-Bronstein relation, well known for isotropic scattering,[6] generalizes in the following way,[36]

$$(2\pi)^2 \int_0^1 d\mu \int_0^1 d\mu'\; I(0,-\mu)\, p(\mu,-\mu')\, I(0,-\mu') = h_1 \quad , \tag{105}$$

which checks with Eq. (101). Next we find

$$\rho(0) = \gamma_0/\gamma_1 \quad , \tag{106}$$

$$\rho_{as}(\tau) = h_1(\tau + \tau^*) \quad , \tag{107}$$

$$\tau^* = \left\{\frac{1}{2}\int_0^1 \left[q_0(\mu) + 2q_2(\mu)\right] \mu\, H(\mu)\, d\mu\right\}\frac{3}{h_1} \quad . \tag{108}$$

The factor multiplying $(3/h_1)$ is always found to be very close to 0.71.[3,18]

Expression (90) for the intensity transmitted through a thick plane layer simplifies by aid of Eqs. (100) and (101) to

$$I(\tau_0,\mu,\phi) \approx \frac{[q_0(\mu_0) + 2q_2(\mu_0)][q_0(\mu) + 2q_2(\mu)]\, H(\mu_0)\, H(\mu)}{4\pi h_1\, \mu_0\, \mu(\tau_0 + 2\tau^*)} \quad . \tag{109}$$

Integration leads to values of the angle-integrated intensity and net flux.[24,36]

Results for different nonabsorbing plane atmospheres can approximately be compared in a way that has been known in neutron transport theory,[3,37] and that is concisely formulated by the similarity rules of van de Hulst.[38,39] Two atmospheres permit a comparison if the values of $h_1\tau_0$ are the same. That is, the thickness measured in transport mean free paths must be the same, the latter parameter being equal to $3/h_1 = 3/(3 - \varpi_1)$ in our notation. Under such condition the transmitted and the azimuth-averaged reflected intensities are found to be very insensitive to details of the scattering law.

To see what is happening, we consider the case with $m = 0$ and $\varpi_0 = 1$, keeping all the higher ϖ_ℓ, $\ell = 2, 3, \ldots, L$, constant, but varying ϖ_1. We notice that $g(\nu,\mu)$ is independent of ϖ_1, and consequently the functions $\Lambda(z)$, $\lambda(\nu)$, $H(z)$ do not depend upon this parameter either. The same is true for all the eigenfunctions $\phi(\nu,\mu)$ and, according to Eq. (37), also for the Busbridge polynomials and the adjoint eigenfunctions $\phi^\dagger(\nu,\mu)$, with $\phi_1^\dagger(\mu)$ excepted, however. Along with the latter function, the coefficient γ_1 is proportional to h_1^{-1}.

The most important occurrence of ϖ_1 is in the new eigenmode (93), which shows that

$$j_{as}(\tau) = -\frac{1}{h_1}\,\frac{d\rho_{as}(\tau)}{d\tau} \quad ,$$

implying a diffusion coefficient $1/h_1$. This is where the idea of the transport mean free path comes from.

Clearly the solution of the albedo problem is independent of ϖ_1, as witnessed by Eq. (64). However, the same cannot be said for the Milne problem where the mode (93) comes into play because of the non-vanishing net flux. If the solution is normalized to $j = -1$, the intensity can be shown[3] to depend upon ϖ_1 according to

$$I(\tau,\mu) = (4\pi)^{-1}\, h_1\tau + I'(\tau,\mu) \quad , \tag{110}$$

where I' is independent of ϖ_1. Consequently the same independence holds for $I(0,-\mu)$, as is also clear from Eq. (104). We should note that with such normalization the gradient of $\rho_{as}(\tau)$ is proportional to h_1.

Turning to finite thick atmospheres, we conclude from the last observation that for two different ϖ_1's the net flux, and thereby the emerging intensities, will be approximately the same only if the values of $h_1\tau_0$ agree. An example of this is in Eq. (109).

Similarity can approximately be extended to cases with weak absorption, provided we impose as a second condition that τ_0/ν_1^0 (the thickness measured in diffusion lengths) be the same. Since $\nu_1^0 \simeq (h_0h_1)^{-1/2}$, an equivalent condition is that the values of h_0/h_1 must be equal.

It remains to explain why the azimuth-averaged intensities only very weakly depend upon the higher ϖ_ℓ, $\ell = 2, 3, \ldots, L$. The reason is that for $\varpi_0 = 1$ the leading eigenmodes (92) and (93) that compose the asymptotic approximation are independent of those coefficients. Relatively small deviations from this approximation (the curly tails on Fig. 3) only arise in the boundary layers. Inevitably, variations due to changes in the higher ϖ_ℓ should be smaller still.

None of the above arguments hold for the azimuth-dependent components ($m \geq 1$), which behave as if strong absorption were present. Therefore, anisotropy in single scattering always shows up strongly in the azimuthal dependence of the intensity reflected by a plane layer.

6. COMMENTS

So far we have adhered to the assumption of a finite expansion of the scattering kernel $p(\cos\delta)$. This, of course, in itself is an approximation, justified less by the nature of the problem than by the desire to avoid annoying problems of convergence. We should honestly ask what happens when $L \to \infty$. Then $g(\nu,\mu)$ ceases to be a polynomial, and Busbridge's $q_\ell(\mu)$ also become transcendental functions, no longer expressible in closed form. This makes the various factorizations apparently meaningless, in particular the extraction of $H(\mu)\,H(\mu_0)$ from $S(\mu,\mu_0)$, since the remaining factor still is an infinite bilinear sum of transcendental q_ℓ's.

Two arguments may be raised against such opinion. Several of the formulas quoted in Sections 4 and 5 contain only one or a few of the q_ℓ's, which can still be evaluated from the (now non-degenerate) Fredholm-like equation (39). The other argument is purely mathematical and refers to the analytical properties of the functions involved. A natural assumption that must be made in this context is that $p(\cos\delta)$ can be expanded in a series that converges absolutely for $|\cos\delta| \leq 1$. This suffices to make all the $p^m(\mu,\mu')$ analytic functions for complex values of μ and μ' in the ranges $|\mu| \leq 1$, $|\mu'| \leq 1$. A study of the g-polynomials shows[17] that the functions $g(\nu,\mu)$ too are analytic for $|\nu| \leq 1$ and $|\mu| \leq 1$. Analyticity also appears to hold in some vicinity of the eigenvalues $\pm\nu_j$. Presumably it should then be possible to prove that the $q_\ell(\mu)$ are analytic for $|\mu| \leq 1$, as well as for $\mu \to -\nu_j$, and that a corresponding statement applies to $g^\dagger(\nu,\mu)$.

If these conjectures can be confirmed, the factorization in Eq. (52), for example, at least retains an aesthetic justification. The factors $H(\mu)$, $H(\mu_0)$, and $(\mu + \mu_0)^{-1}$ carry all the singularities within the unit circles, i.e., the cuts $-1 < \mu < 0$ and $-1 < \mu_0 < 0$ and the pole at $\mu = -\mu_0$, respectively, whereas the remaining factor $g^\dagger(-\mu,\mu_0)$ is analytic within $|\mu| \leq 1$, $|\mu_0| \leq 1$.

A second comment refers to polarization. Until polarization effects are properly taken into account, we cannot be fully satisfied with having solved radiative-transfer problems for more than artificial models.

Instead of one function describing the radiation field, one now has to use a 2×2 density matrix $\underline{I}(\tau,\mu,\phi)$, or equivalently a "vector" consisting of the four Stokes parameters I, Q, U, V.[6,40] The scattering function then becomes a fourth-order $2 \times 2 \times 2 \times 2$ matrix, or a second-order 4×4 matrix in the Stokes representation.

By nature, the scattering matrix $\underset{\sim}{p}(\cos\delta)$ is given in a coordinate system attached to the incident and scattered beams. Before azimuthal integration can be carried out to derive the $\underset{\sim}{p}^m(\mu,\mu')$, the matrix must be transformed to a fixed coordinate system. For Rayleigh scattering the result is well-known.[6] Also in more general cases this step can be carried out smoothly[40] if the components of $\underset{\sim}{p}(\cos\delta)$ are expanded in terms of generalized spherical functions.[41] A modified representation referring to circular polarization must be used for this purpose.

While a great deal of analysis, including work with singular eigenfunctions, has been accomplished for Rayleigh scattering, relatively little use has been made of the more general formalism.[40,42] Yet no insurmountable obstacles appear to impede a more extensive application of singular eigenfunctions in a manner analogous to that shown in the preceding sections. However, since matrices are involved, the calculations inevitably become more tedious. In particular, a matrix Wiener-Hopf factorization has to be carried out,

$$[\underline{\Lambda}(z)]^{-1} = \underline{H}(z) \cdot \underline{H}^{T}(-z) \quad .$$

In general this cannot be done in closed form, as seen from the work of Siewert and co-workers[43-45] for the example of a mixture of Rayleigh and isotropic scattering. Pure Rayleigh scattering represents an exception in this respect.[6]

We finally have to face the unpleasant question about the practical usefulness of this kind of analysis in problems of radiative transfer. The method of singular eigenfunctions turns out to be quite elegant for simple scattering kernels, in particular for $L = 0$ or 1. Occasionally it has been applied to considerably more complicated cases, with L up to 15.[18,19] However, as these cases clearly indicate, with increasing L the calculations become more time consuming and they cannot compete in efficiency with some of the direct techniques, such as the doubling method of van de Hulst and Grossman.[38,39] This method also was successfully applied by Hansen[46] and Hovenier[47] to problems involving polarization. While acknowledging the practical advantage of such an approach, one can still argue that mathematical enthusiasm need not be the only excuse for advancing analytical methods beyond their direct applicability. Understanding of the mathematical structure of the solutions can be and has been of help in preparing computational programs, even if they do not follow the same analytical approach. Let us recall, for instance, that the often used asymptotic approximations are clearly defined and understood only in terms of eigenmode expansions.

Sometimes the solution of a problem is not required in full detail, but only the value of some characteristic quantity. It may happen, as in the case of the intensity transmitted by a thick nonabsorbing atmosphere, Eq. (109), that a particularly simple and computationally efficient expression exists for that quantity. Then the analytic approach, perhaps with some approximation for the H-functions,[48] should facilitate an almost direct study of the influence of the various parameters.

We ought to think also of the inverse transfer problem, which requires the determination of $p(\cos\delta)$ from observed intensities reflected and/or transmitted by a plane layer. Evidently this is a problem of central relevance to the present conference, and we should recall that Professor Sekera was among the first to initiate its study.[49] It appears that methods of solution are still not fully satisfactory and that advances are being tried in several ways. However, regardless of whether parameterized models[50] or model-independent approaches[51,52] will be used, it appears likely that mathematical understanding of the direct problems will be helpful, if not essential, to further progress in this field.

ACKNOWLEDGMENTS

Helpful suggestions from Professors R. Aronson, H. C. van de Hulst, and S. Pahor were appreciated. One of the authors (NJM) expresses his gratitude for the hospitality of the Slovene Academy of Sciences and Arts and the University of Ljubljana under the exchange program of the U. S. National Academy of Sciences and the Council of the Academies of Yugoslavia.

REFERENCES

1. M. M. R. Williams, "Advances in Nuclear Science and Technology" (E. J. Henley and J. Lewins, eds.), Vol. 7, Academic Press, New York, 283, (1973).

2. K. M. Case, Ann. Phys., 9, 1, (1960).

3. K. M. Case and P. F. Zweifel, "Linear Transport Theory," Addison-Wesley, Reading, MA, (1967).

4. N. J. McCormick and I. Kuščer, J. Math. Phys., 7, 2036, (1966).

5. N. J. McCormick and I. Kuščer, "Advances in Nuclear Science and Technology" (E. J. Henley and J. Lewins, eds.), Vol. 7, Academic Press, New York, 181, (1973).

6. S. Chandrasekhar, "Radiative Transfer," Oxford Univ. Press, London and New York, (1950); Dover Publications, New York, (1960).

7. V. V. Sobolev, "Perenos luchistoĭ energii v atmosferakh zvezd i planet," Gostekhizdat, Moscow, (1956). [English transl.: "A Treatise on Radiative Transfer," Van Nostrand, Princeton, (1963)]. Also "Rasseyanie sveta v atmosferakh planet," Nauka, Moscow, (1972).

8. I. W. Busbridge, "The Mathematics of Radiative Transfer," Cambridge Univ. Press, London and New York, (1960).

9. T. W. Mullikin, Astrophys. J., 139, 379 and 1267, (1964).

10. M. V. Maslennikov, Atomic Energy Rev., 5, 59, (1967).

11. I. Kuščer and I. Vidav, J. Math. Anal. Appl., 25, 80, (1969).

12. B. Davison, "Neutron Transport Theory," Oxford Univ. Press, London and New York, (1957).

13. I. Kuščer, J. Math. & Phys., 34, 256, (1956); 37, 52, (1958).

14. J. R. Mika, Nucl. Sci. Eng., 11, 415, (1961).

15. H. G. Kaper, "One Speed Transport Theory with Anisotropic Scattering. Application to the Slab Albedo Problem. Part I, Theory," Rep. TW-37, Math. Inst. Univ. Groningen, Groningen, (1966).

16. G. W. Eccleston, Jr., and N. J. McCormick, J. Nucl. Energy, 24, 23, (1970).

17. E. Inönü, J. Math. Phys., 11, 568, (1970).

18. S. Pahor and M. Gros, Tellus, 22, 321, (1970).

19. D. L. Feinstein, F. E. Butler, K. R. Piech, and A. Leonard, Phys. Fluids, 15, 1641, (1972).

20. I. M. Gel'fand and G. E. Shilov, "Generalized Functions," (Transl. of Russian 1958 ed.), Academic Press, New York, (1967).

21. Yu. M. Berezanskiĭ, "Expansions in Eigenfunctions of Selfadjoint Operators," (Transl. of Russian 1965 ed.), Transl. of Math. Monographs, Vol. 17, Amer. Math. Soc., Providence, RI, (1968).

22. N. I. Muskhelishvili, "Singulyarnie integral'nie uravneniya," Third ed., Nauka, Moscow, (1968). (English transl. of First ed.: "Singular Integral Equations," Noordhoff, Groningen, 1953).

23. S. Pahor and A. Suhadolc, Transport Theory Statist. Phys., 2, 335, (1972).

24. S. Pahor, Nucl. Sci. Eng., 26, 192, (1966); 29, 248, (1967).

25. S. Pahor, Nucl. Sci. Eng., 31, 110, (1968).

26. H. C. van de Hulst, Astron. & Astrophys., 9, 359, (1970).

27. F. D. Gakhov, "Kraevye zadachi," Fitmatgiz, Moscow, (1963). (English transl.: "Boundary Value Problems," Pergamon Press, Oxford, 1966).

28. V. A. Ambarzumian, Doklady, 43, 106, (1944); also in "Nauchnye trudy," Izd. Arm. Akad., Erevan, Vol. I, 256, (1960).

29. N. J. McCormick and I. Kuščer, Transport Theory Statist. Phys., 1, 1, (1971).

30. S. F. Su and N. J. McCormick, J. Nucl. Energy, 25, 657, (1971).

31. I. Kuščer, Canad. J. Phys., 31, 1187, (1953).

32. H. G. Kaper, J. K. Shultis, and J. G. Veninga, J. Computational Phys., 6, 288, (1970); One-Speed Transport Theory with Anisotropic Scattering. Part 2: Numerical Evaluation of the Exact Slab Albedo Problem Solution. Rep. TW-65, Math. Inst. Univ. Groningen, Groningen, (1969).

33. J. K. Shultis and H. G. Kaper, Astron. & Astrophys., 3, 110, (1969).

34. A. G. Gibbs, in "Second Conference on Transport Theory," Rep. CONF-710107, U. S. Atomic Energy Commission, 464, (1971).

35. I. Kuščer, J. Nucl. Energy (A/B), 16, 379, (1962).

36. I. W. Busbridge and S. E. Orchard, Astrophys. J., 154, 729, (1968).

37. A. M. Weinberg and E. P. Wigner, "The Physical Theory of Neutron Chain Reactors," Chicago Univ. Press, (1958).

38. H. C. van de Hulst and K. Grossman, "The Atmospheres of Venus and Mars," (J. C. Brandt and M. B. McElroy, eds.), Gordon & Breach, New York, 35, (1968).

39. H. C. van de Hulst, "Planetary Atmospheres," (C. Sagan, et al., ed.), Reidel, Dordrecht, 177, (1971); J. Quant. Spectrosc. Radiative Transfer, 11, 785, (1971).

40. I. Kuščer and M. Ribarič, Optica Acta, 6, 42, (1959).

41. I. M. Gel'fand and Z. Ya. Shapiro, Uspekhi matem. nauk., 7, 3, (1952); English transl.: Amer. Math. Soc. Translations, 2, 207, (1956). See especially §§ 7.4, 8.3.

42. J. Lenoble, Comptes Rendus, 260, 468, (1965).

43. E. E. Burniston and C. E. Siewert, J. Math. Phys., 11, 3416, (1970); 12, 1057, (1971).

44. G. R. Bond and C. E. Siewert, Astrophys. J., 164, 97, (1971).

45. C. E. Siewert, J. Quant. Spectrosc. Radiative Transfer, 12, 683, (1972).

46. J. E. Hansen, J. Atmos. Sci., 28, 120 and 1400, (1971).

47. J. W. Hovenier, Astron. & Astrophys., 13, 7, (1971).

48. I. K. Abu-Shumays, Nucl. Sci. Eng., 26, 430, (1966); 27, 607, (1967).

49. Z. Sekera, Icarus, 6, 348, (1967).

50. J. G. Kuriyan, this Conference.

51. S. Pahor, Phys. Rev., 175, 218, (1968).

52. K. M. Case, 1973: Phys. Fluids, 16, 1607.

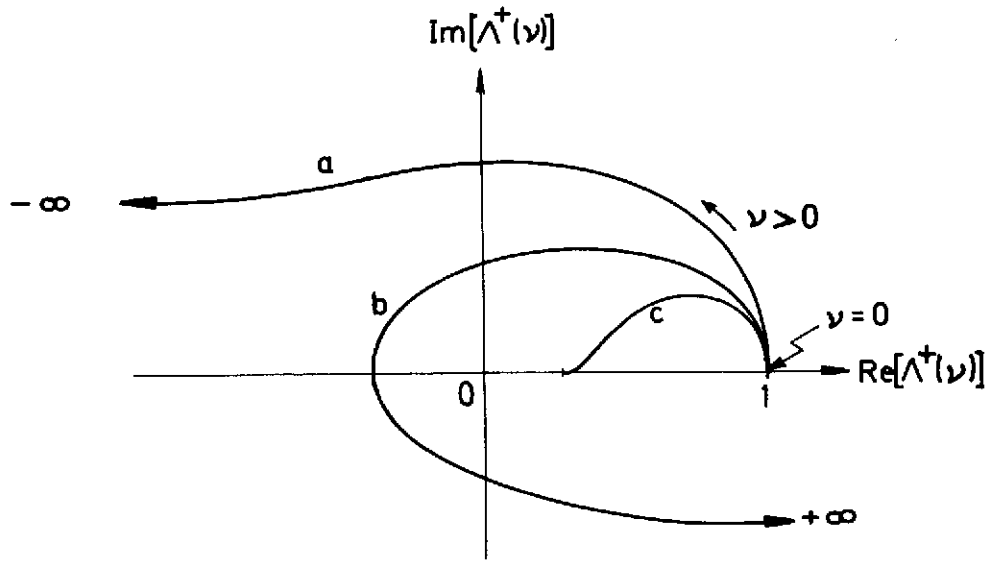

Fig. 1. Schematic plots of $\Lambda^+(\nu)$ for $0 \leq \nu < 1$ for three typical cases. The curves a and b are for $m = 0$, with $g(\mu,\mu)$ positive and with $g(\mu,\mu)$ changing its sign once in $0 < \mu < 1$, respectively. The plot c is for $m > 0$, $g(\mu,\mu) > 0$, $\lambda(1) > 0$, when no eigenvalue exists.

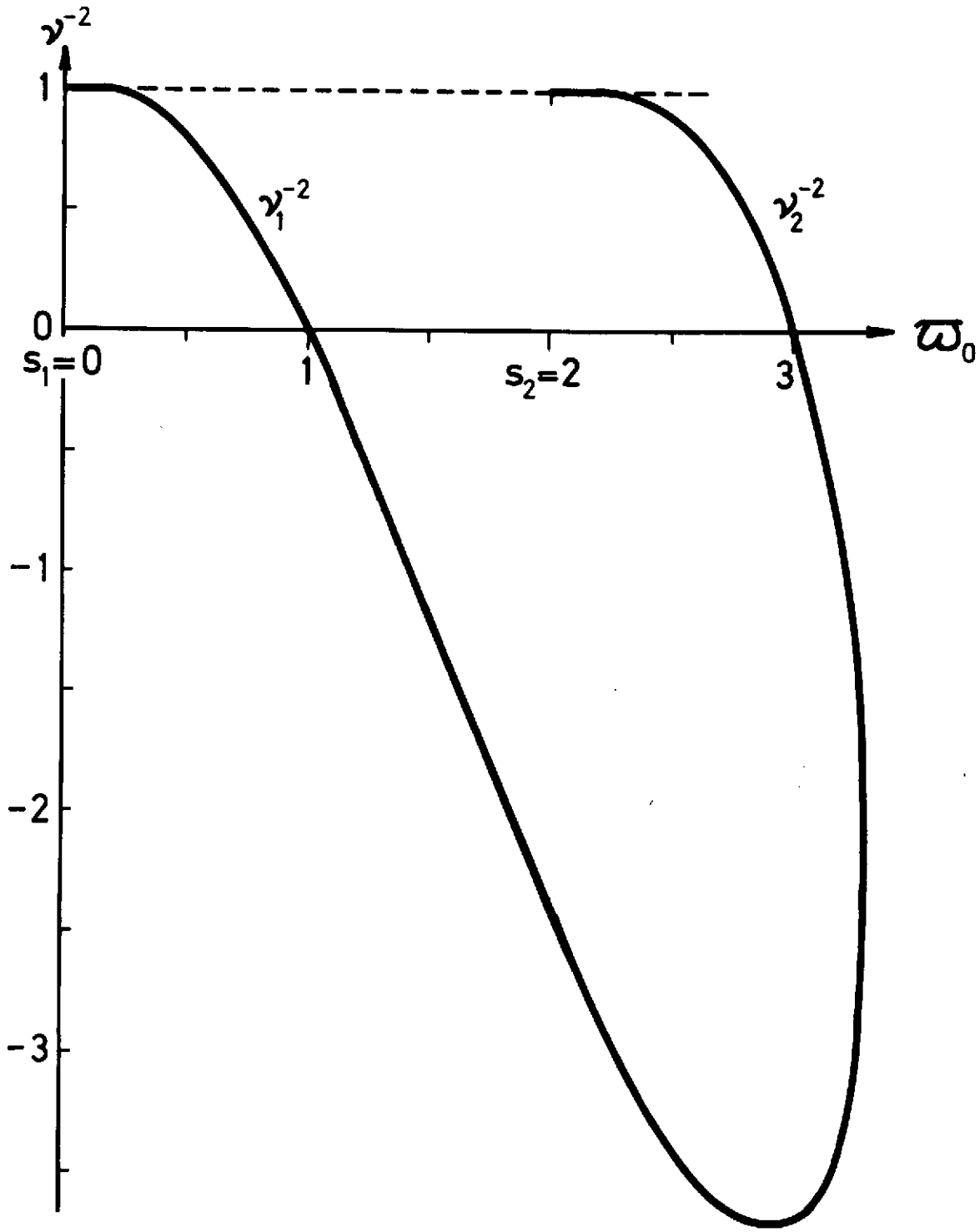

Fig. 2. Squared reciprocal eigenvalues versus ϖ_0 for $m = 0$ and for the scattering function $p(\cos\delta) = \varpi_0(1 + \cos\delta)$.

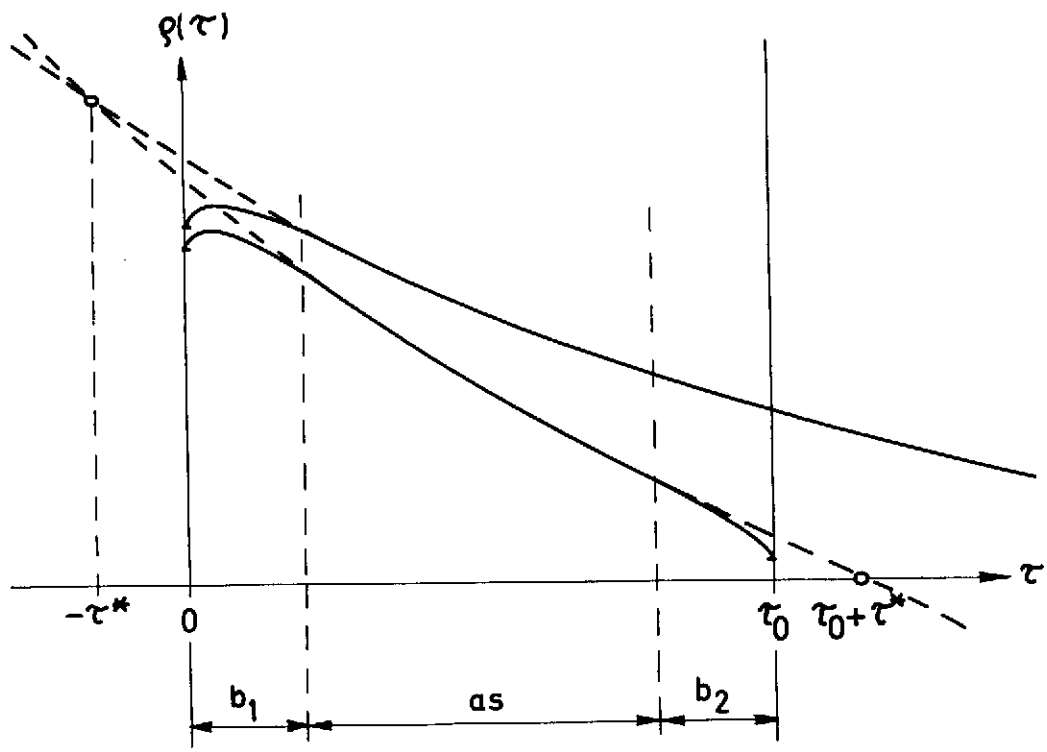

Fig. 3. Angle-integrated intensity in a thick atmosphere illuminated at $\tau = 0$, with no reflection at the ground. The boundary layers (b_1, b_2) and the asymptotic region (as) are indicated. Equations (85) and (86) approximately hold in the regions as + b_2 and b_1 + as, respectively. The upper curve refers to a semi-infinite atmosphere.

LECTURES ON THE

SCATTERING OF LIGHT

David S. Saxon
Department of Physics
University of California
Los Angeles, California 90024 *

ABSTRACT

The exact (Mie) theory for the scattering of a plane wave by a dielectric sphere is presented in more detail and using somewhat more modern methods than is customary in the literature. Since this infinite series solution is computationally impractical for large spheres, another formulation is given in terms of an integral equation valid for a bounded but otherwise general array of scatterers. This equation is applied to the scattering by a single sphere, and several methods are suggested for approximating the scattering cross-section in closed form. Finally, a tensor scattering matrix is introduced, in terms of which some general scattering theorems are derived. The application of the formalism to multiple scattering is briefly considered.

INTRODUCTION

When considering transfer of solar radiation through the earth's atmosphere, the scattering of the radiation by particles whose size is of the order of or larger than the wavelength is of fundamental importance. An exact theory for the scattering of an incident plane wave by a sphere was first presented by Mie (1908). Although the Mie theory is given in many places, it is presented here in more detail and using somewhat more modern methods than is customary. The infinite series solution of Mie can be applied to many problems in atmospheric optics but becomes computationally impractical when the sphere is larger than the wavelength of the incident light. Hence, it is desirable to see if other methods can be made available for computing the scattering by large spheres.

To investigate possible approximate solutions, the radiation field is examined using an integral equation formulation in terms first of the electric field and then of the magnetic field. These equations are deduced from Maxwell's equations with the aid of a tensor Green's function. In the electric field case, several approximations for the field interior to the sphere, in terms of which the scattering is completely defined, are considered as follows: a Kirchhoff-Born approximation, a modified Born approximation, a W.K.B. interior wave, a W.K.B. interior wave with refraction, and an asymptotic approximation to the exact interior solution. Estimates are also discussed using the more complicated magnetic field integral equation. Apparently, the W.K.B. interior wave gives the most realistic approximation in both cases although no actual computations have yet been performed.

* Notes prepared by Robert S. Fraser, May 1955. Lectures delivered at the Department of Meteorology, University of California, Los Angeles.

To arrive at the underlying character of the scattering process, some general relations are derived. Using a tensor scattering matrix, the field at large distances from the scattering object, the reciprocity principle, the total scattering cross-section theorem, and the relation between the scattering matrix and the plane wave scattering amplitudes are studied. The application of the formalism to multiple scattering is briefly discussed.

Although these problems are developed somewhat within the context of atmospheric optics, the principles are quite general. For instance, only dielectric spheres are discussed, but many of the results become applicable to conducting spheres if the real propagation constant is made complex; or the scattering particles can be imbedded in a medium other than free space; etc.

I. MIE THEORY

A. Solutions of the Vector Wave Equation in Spherical Coordinates

As a mathematical preliminary, we discuss the properties of the solutions in spherical coordinates of the vector Helmholtz equation

$$\nabla \times \nabla \times \underset{\sim}{A} - \nabla\nabla \cdot \underset{\sim}{A} - k^2 \underset{\sim}{A} = 0 \quad .$$

For our applications, we require only divergenceless solutions, that is, $\nabla \cdot \underset{\sim}{A} = 0$; and accordingly we restrict ourselves to the simplified Helmholtz equation

$$\nabla \times \nabla \times \underset{\sim}{A} - k^2 \underset{\sim}{A} = 0 \quad . \tag{1}$$

We now show that if $\psi(\underset{\sim}{r})$ satisfies the scalar Helmholtz equation

$$(\nabla^2 + k^2)\, \psi(\underset{\sim}{r}) = 0 \quad , \tag{2}$$

then the vector functions $\underset{\sim}{M}$ and $\underset{\sim}{N}$ defined by

$$\underset{\sim}{M}(r,\theta,\phi) \equiv \nabla \times \underset{\sim}{r}\psi(r,\theta,\phi) = \nabla\psi \times \underset{\sim}{r} \tag{3}$$

and

$$\underset{\sim}{N}(r,\theta,\phi) \equiv \frac{1}{k} \nabla \times \nabla \times (\underset{\sim}{r}\psi) \tag{4}$$

satisfy the vector Helmholtz equation (1). As indicated in Fig. 1, r,θ,ϕ are the usual spherical coordinates (unit vectors are also shown).

To show that $\underset{\sim}{M}$ satisfies (1), we have first

$$\nabla \times \underset{\sim}{M} = \nabla \times \nabla \times \underset{\sim}{r}\psi$$

$$= -\nabla^2(\underset{\sim}{r}\psi) + \nabla[\nabla \cdot (\underset{\sim}{r}\psi)] \quad .$$

Using the relation

$$\nabla^2(\underset{\sim}{r}\psi) = \underset{\sim}{r}\nabla^2\psi + 2\nabla\psi \quad ,$$

we find

$$\nabla \times \underset{\sim}{M} = -\underset{\sim}{r}\nabla^2\psi - 2\nabla\psi + \nabla[\nabla \cdot (\underset{\sim}{r}\psi)] \quad .$$

Since ψ satisfies the scalar Helmholtz equation, we then have

$$\nabla \times \underset{\sim}{M} = k^2\underset{\sim}{r}\psi + \nabla[\nabla \cdot (\underset{\sim}{r}\psi) - 2\psi] \quad ;$$

and hence

$$\nabla \times \nabla \times \underset{\sim}{M} = k^2(\nabla \times \underset{\sim}{r}\psi) = k^2\underset{\sim}{M} \quad ,$$

which is Helmholtz's equation as asserted. Further, since $\underset{\sim}{N} \sim \nabla \times \underset{\sim}{M}$, it obviously satisfies the vector Helmholtz equation if $\underset{\sim}{M}$ does. Note that when both $\underset{\sim}{M}$ and $\underset{\sim}{N}$ are derived from the same ψ

$$\underset{\sim}{N} = \frac{1}{k}\nabla \times \underset{\sim}{M} \; ; \quad M = \frac{1}{k}\nabla \times \underset{\sim}{N} \quad . \tag{5}$$

The general solutions of the scalar Helmholtz equation in spherical coordinates have the form

$$\psi_{\ell m}(r,\Theta,\phi) = C_\ell(kr)\, Y_\ell^m(\theta,\phi) \tag{6}$$

where $C_\ell(kr)$ is a general spherical Bessel function

$$C_\ell(kr) = \left(\frac{\pi}{2kr}\right)^{1/2} + Z_{\ell+1/2}\,(kr)$$

and satisfies

$$\frac{1}{r^2}\,\frac{\partial}{\partial r}\left(r^2\,\frac{\partial C_\ell}{\partial r}\right) + \left[k^2 - \frac{\ell(\ell+1)}{r^2}\right] C_\ell = 0 \quad .$$

The $Y_\ell^m(\Theta,\phi)$ are normalized spherical harmonics, which we can write in the form

$$Y_\ell^m(\Theta,\phi) = \left[\frac{(2\ell + 1)}{4\pi} \frac{(\ell - |m|)!}{(\ell + |m|)!}\right]^{\frac{1}{2}} P_\ell^{|m|} (\cos \Theta) e^{im\phi} ; \tag{7}$$

$$\ell = 0, 1, 2, \ldots, \quad m = 0, \pm 1, \pm 2, \ldots, \quad \ell \geq |m| .$$

The $Y_\ell^m(\Theta,\phi)$ satisfy the orthonormality condition

$$\int_0^{2\pi} \int_0^{\pi} Y_\ell^m \; Y_{\ell'}^{m'*} \; d\Omega = \delta_{\ell\ell'} \; \delta_{mm'} , \tag{8}$$

where

$$\delta_{nn'} = \begin{cases} 0, & n \neq n' \\ 1, & n = n' \end{cases} \qquad d\Omega = \sin \Theta \; d\Theta d\phi ,$$

and Y_ℓ^{m*} denote the complex conjugate of Y_ℓ^m . The spherical harmonics are solutions of the differential equation

$$(\underset{\sim}{r} \times \nabla)^2 \; Y_\ell^m(\Theta, \phi) + \ell(\ell + 1) \; Y_\ell^m(\Theta, \phi) = 0 ;$$

that is

$$\frac{1}{\sin \Theta} \frac{\partial}{\partial \Theta} \left(\sin \Theta \frac{\partial Y_\ell^m}{\partial \Theta}\right) + \frac{1}{\sin^2 \Theta} \frac{\partial^2 Y_\ell^m}{\partial \phi^2} + \ell(\ell + 1) \; Y_\ell^m = 0 .$$

We shall frequently use the abbreviation

$$\underset{\sim}{L} = \underset{\sim}{r} \times \nabla \tag{9}$$

so that equivalently

$$\underset{\sim}{L}^2 Y_\ell^m + \ell(\ell + 1) \; Y_\ell^m = 0 . \tag{10}$$

The normalization constant for these functions is most easily derived using the relation

$$P_n^m(\cos\Theta) = P_n^m(x) = \frac{(1 - x^2)^{n/2}}{2^n n!} \frac{d^{n+m}(x^2 - 1)^n}{dx^{n+m}}$$

and successive integration by parts. The orthogonality properties are most easily derived from the differential equations.

From their definitions (3) and (4), the vector wave functions we shall deal with, are thus seen to have the form

$$\underset{\sim}{M}_{\ell m} = \nabla \times \underset{\sim}{r}\psi_{\ell m}$$

$$= \frac{im}{\sin\Theta} C_\ell(kr)\, Y_\ell^m(\Theta, \phi)\underset{\sim}{e}_\Theta - C_\ell(kr) \frac{\partial}{\partial\Theta} Y_\ell^m(\Theta, \phi)\underset{\sim}{e}_\phi , \qquad (11)$$

and

$$\underset{\sim}{N}_{\ell m} = \frac{1}{k} \nabla \times \nabla \times \underset{\sim}{r}\, \psi_{\ell m}$$

$$= \frac{\ell(\ell + 1)}{kr} C_\ell(kr)\, Y_\ell^m(\Theta, \phi)\underset{\sim}{e}_r$$
$$+ \frac{1}{kr} \frac{\partial}{\partial r} \left[rC_\ell(kr)\right] \frac{\partial Y^m_\ell}{\partial\Theta} \underset{\sim}{e}\Theta$$
$$+ \frac{im}{kr \sin\Theta} \frac{\partial}{\partial r} \left[rC_\ell(kr)\right] Y^m_\ell \underset{\sim}{e}_\phi \qquad (12)$$

We shall use superscripts (1), (2), (3) to denote spherical Bessel functions j_ℓ, y_ℓ, and $h_\ell^{(1)}$ respectively; that is, $M_{\ell m}^{(1)} \sim j_\ell(kr)$, etc.

Note from (5) that if the electric vector $\underset{\sim}{E} \sim \underset{\sim}{M}$, then the magnetic vector $\underset{\sim}{H} \sim \underset{\sim}{N}$, and vice versa. Hence, these are essentially transverse electric and transverse magnetic waves with respect to the radial direction.

Stratton (Stratton, 1941a) gives the following orthogonality relations for the N's and M's:

$$\int_0^{2\pi}\int_0^{\pi} \underset{\sim}{M}_{\ell m}\cdot\underset{\sim}{M}^{*}_{\ell' m'}\,d\Omega = \ell(\ell+1)\left[C_\ell(kr)\right]^2\delta_{\ell\ell'}\,\delta_{mm'}\ ,$$

$$\int_0^{2\pi}\int_0^{\pi} \underset{\sim}{M}_{\ell m}\cdot\underset{\sim}{N}^{*}_{\ell' m'}\,d\Omega = 0\ ,$$

$$\int_0^{2\pi}\int_0^{\pi} \underset{\sim}{N}_{\ell m}\cdot\underset{\sim}{N}^{*}_{\ell' m'}\,d\Omega = \frac{\ell(\ell+1)}{2\ell+1}\Big\{(\ell+1)\left[C_{\ell-1}(kr)\right]^2 + \ell\left[C_{\ell+1}(kr)\right]^2\Big\}\delta_{\ell\ell'}\,\delta_{mm'}\ . \tag{13}$$

(Note that Stratton uses unnormalized real spherical harmonics in his definition of the $\underset{\sim}{M}$'s and $\underset{\sim}{N}$'s.) These relations are a little special for our purposes, because they are tied to the radial factor which arises from the wave equation. Since only angular integrations are involved, however, the basic character of the results cannot depend on the radial functions in any essential way. To remove the apparent dependence, we now introduce general "vector spherical harmonics." These are suggested by the form of the defining equations for $\underset{\sim}{M}$ and $\underset{\sim}{N}$. We write as follows:

$$\underset{\sim}{\mu}_{\ell m}(\Theta,\phi) \equiv \nabla\times\underset{\sim}{r}Y^m_\ell(\Theta,\phi) = -\underset{\sim}{L}Y^m_\ell\ ,$$

$$\underset{\sim}{\tau}_{\ell m}(\Theta,\phi) \equiv \left[\underset{\sim}{e}_r\cdot(\nabla\times\nabla\times\underset{\sim}{r}rY^m_\ell)\right]\underset{\sim}{e}_r$$

$$= -\underset{\sim}{L}^2Y^m_\ell\underset{\sim}{e}_r = \ell(\ell+1)\,Y^m_\ell\underset{\sim}{e}_r\ ,$$

$$\underset{\sim}{\nu}_{\ell m}(\Theta,\phi) \equiv \nabla\times\nabla\times\underset{\sim}{r}rY^m_\ell - \underset{\sim}{\tau}_{\ell m}$$

$$= -2(\underset{\sim}{e}_r\times\underset{\sim}{L}Y^m_\ell) = 2r\nabla Y^m_\ell\ . \tag{14}$$

The alternative expressions for $\underset{\sim}{\tau}_{\ell m}$ and $\underset{\sim}{\nu}_{\ell m}$ follow after some vector algebra. Upon inspection of (11) and (12), it is easily seen that, in terms of these functions,

$$\underset{\sim}{M}_{\ell m} = C_\ell(kr)\underset{\sim}{\mu}_{\ell m} \tag{15}$$

and

$$\underset{\sim}{N}_{\ell m} = \frac{C_\ell(kr)}{kr}\ \underset{\sim}{\tau}_{\ell m} + \frac{1}{2kr}\frac{\partial}{\partial r}\left[rC_\ell(kr)\right]\ \underset{\sim}{\nu}_{\ell m} \quad . \tag{16}$$

These relations can also be established directly from the definitions (3), (4), and (14) after a certain amount of vector algebra.

We now show that the vector spherical harmonics satisfy the following orthogonality relations:

$$\text{(A)} \qquad \int \underset{\sim}{\mu}_{\ell m} \cdot \underset{\sim}{\mu}^*_{\ell' m'}\, d\Omega = \ell(\ell+1)\,\delta_{\ell\ell'}\,\delta_{mm'} \quad ,$$

$$\text{(B)} \qquad \int \underset{\sim}{\tau}_{\ell m} \cdot \underset{\sim}{\tau}^*_{\ell' m'}\, d\Omega = \ell^2(\ell+1)^2\,\delta_{\ell\ell'}\,\delta_{mm'} \quad ,$$

$$\text{(C)} \qquad \int \underset{\sim}{\nu}_{\ell m} \cdot \underset{\sim}{\nu}^*_{\ell' m'}\, d\Omega = 4\ell(\ell+1)\,\delta_{\ell\ell'}\,\delta_{mm'} \quad ,$$

$$\text{(D)} \qquad \int \underset{\sim}{\mu}_{\ell m} \cdot \underset{\sim}{\nu}^*_{\ell' m'}\, d\Omega = \int \underset{\sim}{\mu}_{\ell m} \cdot \underset{\sim}{\tau}^*_{\ell' m'}\, d\Omega$$

$$= \int \underset{\sim}{\nu}_{\ell m} \cdot \underset{\sim}{\tau}^*_{\ell' m'}\, d\Omega = 0 \quad . \tag{17}$$

Note that (B) follows at once from the orthonormality relation (8) for the Y_ℓ^m, that (C) follows immediately once (A) is established (since $\underset{\sim}{\nu}_{\ell m} = 2\underset{\sim}{e}_r \times \underset{\sim}{\mu}_{\ell m}$), and that since the μ's and ν's are orthogonal to the τ's, only the first equation of (D) and (A) require proof. We first prove (A) as follows: convert the angular integral to an integral over all space by writing

$$\int \underset{\sim}{\mu}_{\ell m} \cdot \underset{\sim}{\mu}^*_{\ell' m'}\, d\Omega = \int_{\text{all space}} \frac{\delta(r-r_0)}{r^2}\ \underset{\sim}{\mu}_{\ell m} \cdot \underset{\sim}{\mu}^*_{\ell' m'}\, r^2\, dr d\Omega \quad ,$$

where the Dirac δ function is defined by

$$\delta(r - r_0) = \delta(r_0 - r) = 0, \; r \neq r_0 \; ; \tag{18}$$

$$\int \delta(r - r_0)\, dr = 1 \; ,$$

provided the interval of integration includes r_0. Now from the definition of $\underset{\sim}{\mu}_{\ell m}$ (and since $\underset{\sim}{L}$ involves no radial derivatives),

$$\int \underset{\sim}{\mu}_{\ell m} \cdot \underset{\sim}{\mu}^{*}_{\ell' m'} \, d\Omega = \int_{\substack{\text{all} \\ \text{space}}} \underset{\sim}{L} Y^{m}_{\ell} \cdot \underset{\sim}{L} \left[Y^{m'*}_{\ell'} \frac{\delta(r - r_0)}{r^2} \right] r^2 \, dr d\Omega$$

$$= \int_{\substack{\text{all} \\ \text{space}}} \underset{\sim}{L} \cdot \left[\frac{\delta(r - r_0)}{r^2} \, Y^{m'*}_{\ell'} \, \underset{\sim}{L} Y^{m}_{\ell} \right] r^2 \, dr d\Omega \; -$$

$$- \int_{\substack{\text{all} \\ \text{space}}} \frac{\delta(r - r_0)}{r^2} \, Y^{m'*}_{\ell'} \, \underset{\sim}{L}^2 Y^{m}_{\ell} \, r^2 \, dr d\Omega \; .$$

The first integral is easily seen to integrate to zero, since the integrated part vanishes at infinity; hence, performing the radial integration in the second integral,

$$\int \underset{\sim}{\mu}_{\ell m} \cdot \underset{\sim}{\mu}^{*}_{\ell' m'} \, d\Omega = - \int Y^{m'*}_{\ell'} \, \underset{\sim}{L}^2 Y^{m}_{\ell} \, d\Omega \; .$$

In conjunction with the differential equation (10) satisfied by the orthonormal Y^{m}_{ℓ}, this completes the proof of (17A). (The artifice of converting to a volume integral is rather annoying, but it seems difficult to avoid without destroying the essential simplicity of the proof.)

To prove the first equation of (D), which is all that remains for the verification of (17), we have

$$\int \underset{\sim}{\mu}_{\ell m} \cdot \underset{\sim}{\nu}^{*}_{\ell' m'} \, d\Omega = \int (-\underset{\sim}{L} Y^{m}_{\ell}) \cdot (2r\nabla Y^{m'*}_{\ell'}) \, d\Omega$$

$$= \int (-\underset{\sim}{L} Y^{m}_{\ell}) \cdot \nabla (2r Y^{m'*}_{\ell'}) \, d\Omega$$

since $\underset{\sim}{L} Y^{m}_{\ell}$ has no radial component. Further, since $\nabla \cdot \underset{\sim}{L} Y^{m}_{\ell} = 0$,

$$\int \underset{\sim}{\mu}_{\ell m} \cdot \underset{\sim}{\nu}^{*}_{\ell' m'} \, d\Omega = - \int \nabla \cdot (2r Y^{m'*}_{\ell'} \underset{\sim}{L} Y^{m}_{\ell}) \, d\Omega$$

$$= - \int \frac{1}{\sin\theta} \frac{\partial}{\partial\theta} (2 \sin\theta \, Y^{m'*}_{\ell'} \underset{\sim}{e}_{\theta} \cdot \underset{\sim}{L} Y^{m}_{\ell}) \, d\Omega +$$

$$+ \int \frac{1}{\sin\theta} \frac{\partial}{\partial\phi} (2 Y^{m'*}_{\ell'} \underset{\sim}{e}_{\phi} \cdot \underset{\sim}{L} Y^{m}_{\ell}) \, d\Omega \, .$$

The first term gives zero when the θ integration is performed because the $\sin\theta$ factor vanishes at the limits. The second term likewise is seen to vanish when the ϕ integration is performed because the Y^{m}_{ℓ} are single-valued functions, thus completing the proof.

Equations (17) are the general orthogonality conditions we require -- freed from all dependence on radial factors. We note that the previously mentioned special relations (13) (from Stratton) are easily recovered using (15), (16), (17), and standard recursion formulae for the spherical Bessel functions.

As final mathematical preliminary, we now derive some expansion theorems for vector plane waves which we shall require later. Specifically, we seek expansions in spherical coordinates of $\underset{\sim}{e}_x e^{ikz}$ and $\underset{\sim}{e}_y e^{ikz}$. Since these functions are divergenceless solutions of the vector wave equation, they must be expressible in terms of the fundamental vector solutions $\underset{\sim}{M}_{\ell m}$ and $\underset{\sim}{N}_{\ell m}$; that is

$$\underset{\sim}{e}_x e^{ikz} = \sum_{m} \sum_{\ell} (\alpha_{\ell m} \underset{\sim}{M}^{(1)}_{\ell m} + \beta_{\ell m} \underset{\sim}{N}^{(1)}_{\ell m}) \, , \tag{19}$$

and since

$$\underset{\sim}{e}_y e^{ikz} = \frac{1}{ik} \nabla \times \underset{\sim}{e}_x e^{ikz} \, ,$$

therefore, also

$$\underset{\sim}{e}_y e^{ikz} = \frac{1}{i} \sum_m \sum_\ell \left(\beta_{\ell m} \underset{\sim}{M}^{(1)}_{\ell m} + \alpha_{\ell m} \underset{\sim}{N}^{(1)}_{\ell m}\right) \quad . \tag{20}$$

As indicated by the superscript (1), only Bessel functions of the first kind $j_\ell(kr)$ enter -- the reason being that the other Bessel functions are irregular at the origin. Observe that since

$$\underset{\sim}{e}_x e^{ikz} = (\underset{\sim}{e}_r \sin\Theta\cos\phi + \underset{\sim}{e}_\Theta \cos\Theta\cos\phi - \underset{\sim}{e}_\phi \sin\phi)\, e^{ikr\cos\Theta} \ ,$$

the angle ϕ enters only through the factors $e^{i\phi}$ and $e^{-i\phi}$. Hence, only terms for which $m = \pm 1$ can occur in the final result.

The coefficients $\alpha_{\ell m}$ and $\beta_{\ell m}$ can be determined directly using the orthogonality properties of $\underset{\sim}{M}_{\ell m}$ and $\underset{\sim}{N}_{\ell m}$, but this involves integrals of $\underset{\sim}{M}^*_{\ell m} \cdot \underset{\sim}{e}_x e^{ikz}$ and $\underset{\sim}{N}^*_{\ell m} \cdot \underset{\sim}{e}_x e^{ikz}$, the evaluation of which is somewhat involved. We derive the result from the much simpler expansion of a scalar plane wave, namely

$$e^{ikz} = e^{ikr\cos\Theta} = \sum_{\ell=0}^{\infty} i^\ell (2\ell+1)\, j_\ell(kr)\, P_\ell(\cos\Theta)$$

$$= \sqrt{4\pi} \sum_{\ell=0}^{\infty} i^\ell \sqrt{2\ell+1}\ \psi^{(1)}_{\ell,0} \quad . \tag{21}$$

(See Stratton (1941b) for details.) As a first step, we construct expansions of xe^{ikz} and ye^{ikz} as follows:

$$xe^{ikz} = r\sin\Theta\cos\phi\, e^{ikr\cos\Theta}$$

$$= -\frac{1}{2ik}\left(e^{i\phi} + e^{-i\phi}\right)\frac{\partial}{\partial\Theta} e^{ikr\cos\Theta}$$

which, together with (21), yields

$$xe^{ikz} = -\frac{1}{2ik}\sum_{\ell=1} i^{\ell}(2\ell+1)\, j_{\ell}(kr)\,(e^{i\phi}+e^{-i\phi})\,\frac{d[P_{\ell}(\cos\Theta)]}{d\Theta} \quad .$$

Using

$$\frac{dP_{\ell}(\cos\Theta)}{d\Theta} = -P_{\ell}^{1}(\cos\Theta) \quad ,$$

and also (6) and (7), we obtain

$$xe^{ikz} = \frac{\sqrt{\pi}}{ik}\sum_{\ell=1}^{\infty} i^{\ell}\sqrt{2\ell+1}\sqrt{\ell(\ell+1)}\left[\Psi_{\ell,1}^{(1)} + \Psi_{\ell,-1}^{(1)}\right] \quad ; \qquad (22)$$

and similarly,

$$ye^{ikz} = -\frac{\sqrt{\pi}}{k}\sum_{\ell=1}^{\infty} i^{\ell}\sqrt{2\ell+1}\sqrt{\ell(\ell+1)}\left[\Psi_{\ell,1}^{(1)} - \Psi_{\ell,-1}^{(1)}\right] \quad .$$

To find the expansion coefficients $\alpha_{\ell m}$ and $\beta_{\ell m}$, take the scalar product of (19) with $\underset{\sim}{r}$. Since $\underset{\sim}{M}_{\ell m}^{(1)}$ has no radial component,

$$\underset{\sim}{r}\cdot\underset{\sim}{e}_x e^{ikz} = xe^{ikz} = \sum_{m}\sum_{\ell}\beta_{\ell m}\,\underset{\sim}{r}\cdot\underset{\sim}{N}_{\ell m}^{(1)} \quad .$$

Thus, from the expression (12) for $\underset{\sim}{N}_{\ell m}$, we obtain

$$xe^{ikz} = \sum_{m}\sum_{\ell}\beta_{\ell m}\frac{\ell(\ell+1)}{k}\,\Psi_{\ell m}^{(1)} \quad ;$$

and hence, upon comparison with (22) we have

$$\beta_{\ell,1} = \beta_{\ell,-1} = \sqrt{\pi}\, i^{\ell-1} \sqrt{\frac{2\ell+1}{\ell(\ell+1)}} .$$

Considering $\underset{\sim}{r} \cdot \underset{\sim}{e}_y e^{ikz}$, we find in the same way

$$\alpha_{\ell,1} = -\alpha_{\ell,-1} = \sqrt{\pi}\, i^{\ell-1} \sqrt{\frac{2\ell+1}{\ell(\ell+1)}} .$$

Finally, the vector plane waves are expressible as

$$\begin{aligned}
\underset{\sim}{e}_x e^{ikz} &= \sqrt{\pi} \sum_{\ell=1}^{\infty} i^{\ell-1} \sqrt{\frac{2\ell+1}{\ell(\ell+1)}} \left[\underset{\sim}{M}^{(1)}_{\ell,1} - \underset{\sim}{M}^{(1)}_{\ell,-1} + \underset{\sim}{N}^{(1)}_{\ell,1} + \underset{\sim}{N}^{(1)}_{\ell,-1} \right] , \\
\underset{\sim}{e}_y e^{ikz} &= -i\sqrt{\pi} \sum_{\ell=1}^{\infty} i^{\ell-1} \sqrt{\frac{2\ell+1}{\ell(\ell+1)}} \left[\underset{\sim}{M}^{(1)}_{\ell,1} + \underset{\sim}{M}^{(1)}_{\ell,-1} + \underset{\sim}{N}^{(1)}_{\ell,1} - \underset{\sim}{N}^{(1)}_{\ell,-1} \right] .
\end{aligned} \tag{23}$$

These expansions in spherical coordinates complete the preliminary discussion.

B. Scattering from a Dielectric Sphere

In an isotropic medium with dielectric constant ε and with permeability $\mu = 1$, Maxwell's equations (in Gaussian units) in the absence of sources are

$$\nabla \times \underset{\sim}{E} = -\frac{1}{c}\frac{\partial \underset{\sim}{H}}{\partial t} ,$$

$$\nabla \times \underset{\sim}{H} = \frac{\varepsilon}{c}\frac{\partial \underset{\sim}{E}}{\partial t} ,$$

where c is the velocity of light in free space. When the fields have harmonic time dependence $e^{-i\omega t}$, these reduce to

$$\nabla \times \underset{\sim}{E} = ik\underset{\sim}{H} ,$$

$$\nabla \times \underset{\sim}{H} = -i\varepsilon k\underset{\sim}{E}, \tag{24}$$

where $k = \frac{\omega}{c} = \frac{2\pi}{\lambda_0}$ is the free space propagation constant and λ_0 is the free space wavelength. From (24) we see at once that $\underset{\sim}{E}$ and $\underset{\sim}{H}$ satisfy the vector Helmholtz equation

$$\nabla \times \nabla \times \underset{\sim}{E} = \varepsilon k^2 \underset{\sim}{E} \equiv \kappa^2 \underset{\sim}{E} \equiv n^2 k^2 \underset{\sim}{E} ,$$

$$\nabla \times \nabla \times \underset{\sim}{H} = \varepsilon k^2 \underset{\sim}{H}. \tag{25}$$

Therefore, $\underset{\sim}{E}$ and $\underset{\sim}{H}$ are expressible in terms of the solutions previously described. In (25) κ is the propagation constant in a medium of dielectric constant ε or the index of refraction n.

Specifically, the problem that we wish to solve is this: A plane, polarized wave is incident on a non-conducting sphere of dielectric constant ε and radius a. The sphere is imbedded in free space with $\varepsilon = 1$. Find the electric and magnetic fields interior and exterior to the sphere.

Choose the coordinate system such that the z-direction is the direction of propagation of the incident wave, the x-axis is in the direction of the incident electric field, and the origin of coordinates is the center of the sphere.

The differential equations are, from (25),

Interior of sphere, $r < a$:

$$\nabla \times \nabla \times \underset{\sim}{E} = \kappa^2 \underset{\sim}{E},$$

$$\nabla \times \nabla \times \underset{\sim}{H} = \kappa^2 \underset{\sim}{H};$$

Exterior of the sphere, $r > a$:

$$\nabla \times \nabla \times \underset{\sim}{E} = k^2 \underset{\sim}{E},$$

$$\nabla \times \nabla \times \underset{\sim}{H} = k^2 \underset{\sim}{H}. \tag{26}$$

The boundary consitions are:

(a) The tangential conponents of $\underset{\sim}{E}$ and $\underset{\sim}{H}$ are continuous at $r = a$;

(b) The wave at large distances from the sphere is composed only of the incident plane wave and the scattered, outgoing wave; that is

$$r \to \infty: \quad \underset{\sim}{E} \cong \underset{\sim}{E}_{inc} + \underset{\sim}{E}_{sctd},$$

$$\underset{\sim}{H} \cong \underset{\sim}{H}_{inc} + \underset{\sim}{H}_{sctd}; \tag{27}$$

where

$$\underset{\sim}{E}_{inc} = \underset{\sim}{e}_x e^{ikz},$$

$$\underset{\sim}{H}_{inc} = \underset{\sim}{e}_y e^{ikz}. \tag{28}$$

As $r \to \infty$, $\underset{\sim}{E}_{sctd}$ has the following form:

$$\underset{\sim}{E}_{sctd} \cong \underset{\sim}{A}(\theta, \phi) \frac{e^{ikr}}{r} \tag{29}$$

with $\underset{\sim}{A} \cdot \underset{\sim}{r} = 0$, of course. Similarly,

$$\underset{\sim}{H}_{sctd} \cong \underset{\sim}{e}_r \times \underset{\sim}{A} \frac{e^{ikr}}{r}. \tag{30}$$

$\underset{\sim}{A}(\theta, \phi)$ is called the scattering amplitude.

The mean energy flux in the incident wave is given by the Poynting vector; that is,

$$\underset{\sim}{\overline{S}}_{inc} = \frac{1}{8\pi} \text{ Re } \left\{ \underset{\sim}{E}_{inc} \times \underset{\sim}{H}^{*}_{inc} \right\} \quad \frac{\text{ergs}}{\text{cm}^2 \times \text{sec}}$$

$$= \frac{1}{8\pi} \underset{\sim}{e}_z \ .$$

Similarly,

$$\underset{\sim}{\overline{S}}_{sctd} = \frac{1}{8\pi} \text{ Re } \left\{ \underset{\sim}{E}_{sctd} \times \underset{\sim}{H}^{*}_{sctd} \right\}$$

$$= \frac{1}{8\pi r^2} \text{ Re } \left\{ \underset{\sim}{A} \times (\underset{\sim}{e}_r \times \underset{\sim}{A}^{*}) \right\} \ .$$

Using the identity

$$\underset{\sim}{A} \times (\underset{\sim}{B} \times \underset{\sim}{C}) \equiv (\underset{\sim}{A} \cdot \underset{\sim}{C}) \underset{\sim}{B} - (\underset{\sim}{A} \cdot \underset{\sim}{B}) \underset{\sim}{C}$$

and the fact that $\underset{\sim}{A} \cdot \underset{\sim}{r} = 0$, we then have

$$\underset{\sim}{\overline{S}}_{sctd} = \frac{1}{8\pi r^2} \underset{\sim}{A} \cdot \underset{\sim}{A}^{*} \underset{\sim}{e}_r \ .$$

Hence, the differential cross-section, defined as the energy scattered into $d\Omega$ per unit incident flux, is

$$d\sigma(\theta, \phi) = \frac{\left| \underset{\sim}{\overline{S}}_{sctd} \right| r^2 \, d\Omega}{\left| \underset{\sim}{\overline{S}}_{inc} \right|} = \underset{\sim}{A} \cdot \underset{\sim}{A}^{*} \, d\Omega = |A|^2 \, d\Omega \ ; \tag{31}$$

and the total scattering cross-section is

$$\sigma_{tot} = \int_0^{2\pi} \int_0^{\pi} |A|^2 \, d\Omega \, . \tag{32}$$

The actual solutions of the scattering problem are obtained as follows: First, exterior to the sphere, $r > a$, we write

$$\underset{\sim}{E} = \underset{\sim}{e}_x e^{ikz} + \sum_{\ell=1;m=1,-1}^{\infty} \left[a_{\ell m} \underset{\sim}{M}^{(3)}_{\ell m}(kr) + b_{\ell m} \underset{\sim}{N}^{(3)}_{\ell m}(kr) \right] \times$$

$$\times \sqrt{\pi} \, i^{\ell-1} \sqrt{\frac{2\ell+1}{\ell(\ell+1)}} \, ; \tag{33}$$

and using (24),

$$\underset{\sim}{H} = \underset{\sim}{e}_y e^{ikz} + \frac{1}{i} \sum_{\ell=1;m=1,-1}^{\infty} \left[a_{\ell m} \underset{\sim}{N}^{(3)}_{\ell m}(kr) + b_{\ell m} \underset{\sim}{M}^{(3)}_{\ell,m}(kr) \right] \times$$

$$\times \sqrt{\pi} \, i^{\ell-1} \sqrt{\frac{2\ell+1}{\ell(\ell+1)}} \, .$$

The superscript (3), meaning $h^{(1)}_{\ell}(kr)$, is required to satisfy the boundary condition at infinity. Substitution of the plane wave expansions (23) then yields

$$\underset{\sim}{E} = \sqrt{\pi} \sum_{\ell=1}^{\infty} i^{\ell-1} \sqrt{\frac{2\ell+1}{\ell(\ell+1)}} \left[\underset{\sim}{M}^{(1)}_{\ell,1} + a_{\ell,1} \underset{\sim}{M}^{(3)}_{\ell,1} - \underset{\sim}{M}^{(1)}_{\ell,-1} + \right.$$

$$+ a_{\ell,-1} \underset{\sim}{M}^{(3)}_{\ell,-1} + \underset{\sim}{N}^{(1)}_{\ell,1} + b_{\ell,1} \underset{\sim}{N}^{(3)}_{\ell,1} +$$

$$\left. + \underset{\sim}{N}^{(1)}_{\ell,-1} + b_{\ell,-1} \underset{\sim}{N}^{(3)}_{\ell-1} \right] \, ;$$

and

$$\underset{\sim}{H} = \frac{\sqrt{\pi}}{i} \sum_{\ell=1}^{\infty} i^{\ell-1} \sqrt{\frac{2\ell+1}{\ell(\ell+1)}} \left[\underset{\sim}{M}^{(1)}_{\ell,1} + b_{\ell,1} \underset{\sim}{M}^{(3)}_{\ell,1} + \underset{\sim}{M}^{(1)}_{\ell,-1} + \right.$$

$$+ b_{\ell,-1} \underset{\sim}{M}^{(3)}_{\ell,-1} + \underset{\sim}{N}^{(1)}_{\ell,1} + a_{\ell,1} \underset{\sim}{N}^{(3)}_{\ell,1} - \underset{\sim}{N}^{(1)}_{\ell,-1} +$$

$$\left. + a_{\ell,-1} \underset{\sim}{N}^{(3)}_{\ell,-1} \right] .$$

In the above, kr is the argument of all the spherical Bessel functions.

Now consider the region interior to the sphere, $r < a$. We write

$$\underset{\sim}{E} = \sqrt{\pi} \sum_{\ell=1}^{\infty} i^{\ell-1} \sqrt{\frac{2\ell+1}{\ell(\ell+1)}} \left[c_{\ell,1} \underset{\sim}{M}^{(1)}_{\ell,1} + c_{\ell,-1} \underset{\sim}{M}^{(1)}_{\ell,-1} + \right.$$

$$\left. + d_{\ell,1} \underset{\sim}{N}^{(1)}_{\ell,1} + d_{\ell,1} \underset{\sim}{N}^{(1)}_{\ell,-1} \right] , \tag{34a}$$

$$\underset{\sim}{H} = \frac{\sqrt{\pi}}{i} \frac{\kappa}{k} \sum_{\ell=1}^{\infty} i^{\ell-1} \sqrt{\frac{2\ell+1}{\ell(\ell+1)}} \left[d_{\ell,1} \underset{\sim}{M}^{(1)}_{\ell,1} + \right.$$

$$\left. + d_{\ell,-1} \underset{\sim}{M}^{(1)}_{\ell-1} + c_{\ell,1} \underset{\sim}{N}^{(1)}_{\ell,1} + c_{\ell,-1} \underset{\sim}{N}^{(1)}_{\ell,-1} \right] , \tag{34b}$$

where now the argument of all the spherical Bessel functions is κr. Only functions of the first kind enter since the interior solutions must be regular at the origin. The factor κ/k arises because $\underset{\sim}{M}(\kappa r) = \frac{1}{\kappa} \nabla \times \underset{\sim}{N}$ and $\underset{\sim}{N}(\kappa r) = \frac{1}{\kappa} \nabla \times \underset{\sim}{M}$ but $\underset{\sim}{H} = \frac{1}{ik} \nabla \times \underset{\sim}{E} = \frac{\kappa}{ik} \frac{1}{\kappa} \nabla \times \underset{\sim}{E}$.

It remains only to satisfy the requirement that tangential $\underset{\sim}{E}$ and $\underset{\sim}{H}$ be continuous at $r = a$; that is, that

$$\underset{\sim}{E}_{tan}(r < a) = \underset{\sim}{E}_{tan}(r > a),$$

$$\underset{\sim}{H}_{tan}(r < a) = \underset{\sim}{H}_{tan}(r > a). \tag{35}$$

Taking the scalar product of the first equation with $\underset{\sim}{\mu}^{*}_{\ell',1}$ and integrating over all solid angles, we find at once, using the orthogonality relations (17),

$$\ell(\ell+1)\sqrt{\pi}\; i^{\ell-1}\sqrt{\frac{2\ell+1}{\ell(\ell+1)}}\; c_{\ell,1}\; j_\ell(\kappa a)$$

$$= \ell(\ell+1)\sqrt{\pi}\; i^{\ell-1}\sqrt{\frac{2\ell+1}{\ell(\ell+1)}}\left[j_\ell(ka) + a_{\ell,1}\, h_\ell^{(1)}(ka)\right] \quad .$$

Similarly, taking the scalar product of the second equation of (35) with $\underset{\sim}{\nu}^{*}_{\ell',1'}$ we find, after integrating over all solid angles,

$$\frac{\ell(\ell+1)}{a^2}\frac{\sqrt{\pi}}{i}\frac{\kappa}{k}\; i^{\ell-1}\sqrt{\frac{2\ell+1}{\ell(\ell+1)}}\; c_{\ell,1}\; \frac{d}{dr}\left[r\,\frac{j_\ell(\kappa r)}{\kappa}\right]_{r=a}$$

$$= \frac{\ell(\ell+1)}{a^2}\frac{\sqrt{\pi}}{i}\; i^{\ell-1}\sqrt{\frac{2\ell+1}{\ell(\ell+1)}}\left\{\frac{d}{dr}\left[r\,\frac{j_\ell(kr)}{k}\right]\right.$$

$$\left. + a_{\ell,1}\,\frac{d}{dr}\left[r\,\frac{h_\ell^{(1)}(kr)}{k}\right]\right\}_{r=a} \quad .$$

Introducing

$$\alpha = ka \quad \text{and} \quad \beta = \kappa a$$

and letting a prime denote differentiation with respect to the arguments, these equations become, upon cancelling common factors,

$$c_{\ell,1} j_\ell(\beta) = j_\ell(\alpha) + a_{\ell,1} h_\ell^{(1)}(\alpha) \quad ,$$

$$c_{\ell,1}\,[\beta j_\ell(\beta)]' = [\alpha j_\ell(\alpha)]' + a_{\ell,1}\,[\alpha h_\ell^{(1)}(\alpha)]' \quad ,$$

which determines $a_{\ell,1}$ and $c_{\ell,1}$. The pair of equations for $(-c_{\ell,-1})$ and $(-a_{\ell,-1})$ are identical. Hence, we have

$$a_{\ell,1} = -a_{\ell,-1} = -\frac{j_\ell(\beta)\left[\alpha j_\ell(\alpha)\right]' - j_\ell(\alpha)\left[\beta j_\ell(\beta)\right]'}{j_\ell(\beta)\left[\alpha h_\ell^{(1)}(\alpha)\right]' - h_\ell^{(1)}(\alpha)\left[\beta j_\ell(\beta)\right]'} ,$$

$$c_{\ell,1} = -c_{\ell,-1} = \frac{j_\ell(\alpha)\left[\alpha h_\ell^{(1)}(\alpha)\right]' - h_\ell^{(1)}(\alpha)\left[\alpha j_\ell(\alpha)\right]'}{j_\ell(\beta)\left[\alpha h_\ell^{(1)}(\alpha)\right]' - h_\ell^{(1)}(\alpha)\left[\beta j_\ell(\beta)\right]'} .$$

If in the numerators we let $h_\ell^{(1)} = j_\ell + iy_\ell$, perform the differentiations, and use the Wronskian relation

$$j_\ell(z)y'_\ell(z) - y_\ell(z)j'_\ell(z) = \frac{1}{z^2} ,$$

we obtain

$$c_{\ell,1} = -c_{\ell,-1} = \frac{i/\alpha}{j_\ell(\beta)\left[\alpha h_\ell^{(1)}(\alpha)\right]' - h_\ell^{(1)}(\alpha)\left[\beta j_\ell(\beta)\right]'} . \tag{36}$$

Note that the expression for $a_{\ell,1}$ has the form $-\frac{x}{x+iy}$, so that introducing

$$x = R \sin \delta_\ell , \quad y = R \cos \delta_\ell ,$$

we obtain

$$a_{\ell,1} = -a_{\ell,-1} = i \sin \delta_\ell \, e^{i\delta\ell} , \tag{37}$$

where

$$\tan \delta_\ell = \frac{j_\ell(\beta)\left[\alpha j_\ell(\alpha)\right]' - j_\ell(\alpha)\left[\beta j_\ell(\beta)\right]'}{j_\ell(\beta)\left[\alpha y_\ell(\alpha)\right]' - y_\ell(\alpha)\left[\beta j_\ell(\beta)\right]'} . \tag{38}$$

Next, consider the b's and d's. Multiplying the equation for $\underset{\sim}{E}_{tan}$ by $\underset{\sim}{\nu}^{*}_{\ell',1}$ and for $\underset{\sim}{H}_{tan}$ by $\underset{\sim}{\mu}^{*}_{\ell,1}$, integrating over all solid angles, and proceeding just as before, we find, after cancelling common factors,

$$\frac{1}{n} d_{\ell,1} \left[\beta j_\ell(\beta)\right]' = \left[\alpha j_\ell(\alpha)\right]' + b_{\ell,1} \left[\alpha h_\ell^{(1)}(\alpha)\right]' ,$$

$$n d_{\ell,1} j_\ell(\beta) = j_\ell(\alpha) + b_{\ell,1} h_\ell^{(1)}(\alpha) .$$

An identical pair of equations holds for $b_{\ell,-1}$ and $d_{\ell,-1}$. These equations are the same as the previous set execpt that $j_\ell(\beta)$ is replaced by $n j_\ell(\beta)$ and $[\beta j_\ell(\beta)]'$ is replaced by $\frac{1}{n}[\beta j_\ell(\beta)]'$. Hence,

$$b_{\ell,1} = b_{\ell,-1} = - \frac{n^2 j_\ell(\beta)\left[\alpha j_\ell(\alpha)\right]' - j_\ell\, \alpha \left[\beta j_\ell(\beta)\right]}{n^2 j_\ell(\beta)\left[\alpha h_\ell^{(1)}(\alpha)\right]' - h_\ell^{(1)}(\alpha)\left[\beta j_\ell(\beta)\right]'} .$$

or

$$b_{\ell,1} = b_{\ell,-1} = i\, e^{i\eta_\ell} \sin \eta_\ell \tag{39}$$

where

$$\tan \eta_\ell = \frac{n^2 j_\ell(\beta)\left[\alpha j_\ell(\alpha)\right]' - j_\ell(\alpha)\left[\beta j_\ell(\beta)\right]'}{n^2 j_\ell(\beta)\left[\alpha y_\ell(\alpha)\right]' - y_\ell(\alpha)\left[\beta j_\ell(\beta)\right]'} . \tag{40}$$

Also,

$$d_{\ell,1} = d_{\ell,-1} = \frac{i\, n/\alpha}{n^2 j_\ell(\beta)\left[\alpha h_\ell^{(1)}(\alpha)\right]' - h_\ell^{(1)}(\alpha)\left[\beta j_\ell(\beta)\right]'} . \tag{41}$$

We return to the interior fields much later -- for now we require only the a's and b's. The scattered fields are given from (33) by

$$\underset{\sim}{E}_{sctd} = \sqrt{\pi} \sum_{\ell=1}^{\infty} i^{\ell-1} \sqrt{\frac{2\ell+1}{\ell(\ell+1)}} \chi \left\{ a_{\ell,1} \left[\underset{\sim}{M}^{(3)}_{\ell,1} - \underset{\sim}{M}^{(3)}_{\ell,-1} \right] + b_{\ell,1} \left[\underset{\sim}{N}^{(3)}_{\ell,1} + \underset{\sim}{N}^{(3)}_{\ell,-1} \right] \right\}$$

$\underset{\sim}{H}_{sctd}$ is similar. Asymptotically, using

$$h^{(1)}_{\ell}(kr) \simeq (-i)^{\ell+1} \frac{e^{ikr}}{kr} , \quad r \to \infty ,$$

we obtain from (15) and (16)

$$\underset{\sim}{M}^{(3)}_{\ell m}(kr) \simeq (-i)^{\ell+1} \frac{e^{ikr}}{kr} \underset{\sim}{\mu}_{\ell,m} = - (-i)^{\ell+1} \frac{e^{ikr}}{kr} \underset{\sim}{L} Y^{m}_{\ell} ,$$

$$\underset{\sim}{N}^{(3)}_{\ell,m}(kr) \simeq - (-i)^{\ell+2} \frac{e^{ikr}}{2kr} \underset{\sim}{\nu}_{\ell,m} = i \underset{\sim}{e}_{r} \chi \underset{\sim}{M}^{(3)}_{\ell,m} ,$$

where terms of order $\frac{1}{r^2}$ and higher have been neglected. Consequently, we have for $r \to \infty$,

$$\underset{\sim}{E}_{sctd} = \frac{e^{ikr}}{r} \frac{\sqrt{\pi}}{k} \sum_{\ell=1}^{\infty} i^{\ell-1} \sqrt{\frac{2\ell+1}{\ell(\ell+1)}} \left\{ (-i)^{\ell+1} \chi \right.$$

$$\chi \left[\underset{\sim}{\mu}_{\ell,1} - \underset{\sim}{\mu}_{\ell,-1} \right] a_{\ell,1} - \frac{1}{2} (-i)^{\ell+2}$$

$$\left. \chi \left[\underset{\sim}{\nu}_{\ell,1} + \underset{\sim}{\nu}_{\ell,-1} \right] b_{\ell,1} \right\} .$$

Comparing this with (29), the scattering amplitude $\underset{\sim}{A}(\Theta, \phi)$ is then

$$\underset{\sim}{A}(\Theta, \phi) = -\frac{\sqrt{\pi}}{k} \sum_{\ell=1}^{\infty} \sqrt{\frac{2\ell + 1}{\ell(\ell + 1)}} \left\{ \left[\underset{\sim}{\mu}_{\ell,1} - \underset{\sim}{\mu}_{\ell,-1}\right] a_{\ell,1} + \frac{i}{2} \left[\underset{\sim}{\nu}_{\ell,1} + \underset{\sim}{\nu}_{\ell,-1}\right] b_{\ell,1} \right\} ,$$

or alternatively,

$$\underset{\sim}{A}(\Theta, \phi) = \frac{\sqrt{\pi}}{k} \sum_{\ell=1}^{\infty} \sqrt{\frac{2\ell + 1}{\ell(\ell + 1)}} \left\{ a_{\ell,1} \left[\underset{\sim}{L}Y_{\ell}^{1} - \underset{\sim}{L}Y_{\ell}^{-1}\right] + i b_{\ell,1} \underset{\sim}{e}_r \times \left[\underset{\sim}{L}Y_{\ell}^{1} + \underset{\sim}{L}Y_{\ell}^{-1}\right] \right\} .$$

$\underset{\sim}{H}_{sctd}$ is given by (30).

The differential cross-section is simply $|A|^2 \, d\Omega = \underset{\sim}{A} \cdot \underset{\sim}{A}^{*} \, d\Omega$ while the total cross-section is given by

$$\sigma_{tot} = \int_0^{\pi} \int_0^{2\pi} |A|^2 \, d\Omega = \frac{2\pi}{k^2} \sum_{\ell=1}^{\infty} (2\ell + 1) \left\{ |a_{\ell,1}|^2 + |b_{\ell,1}|^2 \right\} \tag{42}$$

$$= \frac{2\pi}{k^2} \sum_{\ell=1}^{\infty} (2\ell + 1) (\sin^2 \delta_{\ell} + \sin^2 \eta_{\ell}) .$$

The orthogonality relation (17) and the expression (37) and (39) for $a_{\ell,1}$ and $b_{\ell,1}$ have been used.

The physical significance of the quantities δ_{ℓ} and η_{ℓ} is easily established. For the ℓ^{th} vector spherical harmonic, $\underset{\sim}{M}_{\ell,1}$ say, the incident wave can be shown to behave asymptotically like

$$\underset{\sim}{E}^{(\ell)}_{inc} \simeq \frac{\sqrt{\pi}}{2k}\sqrt{\frac{2\ell+1}{\ell(\ell+1)}}\left[(-1)^{\ell}\frac{e^{-ikr}}{r} - \frac{e^{ikr}}{r}\right]\underset{\sim}{\mu}_{\ell,1} \ ,$$

that is, as a combination of incoming and outgoing waves. From the last expression for $\underset{\sim}{E}_{sctd}$, the corresponding harmonic for the scattered wave, which is of course purely outgoing, behaves like

$$\underset{\sim}{E}^{(\ell)}_{sctd} \simeq -\frac{\sqrt{\pi}}{k}\sqrt{\frac{2\ell+1}{\ell(\ell+1)}}\frac{e^{ikr}}{r}\ a_{\ell,1}\underset{\sim}{\mu}_{\ell,1} \ .$$

Hence, substituting the expression (37) for $a_{\ell,1}$,

$$\underset{\sim}{E}^{(\ell)}_{inc} + \underset{\sim}{E}^{(\ell)}_{sctd} \simeq \frac{\sqrt{\pi}}{2k}\sqrt{\frac{2\ell+1}{\ell(\ell+1)}}\left[(-1)^{\ell}\frac{e^{-ikr}}{r}\right.$$

$$\left. - \frac{e^{ikr}}{r}(1 + 2i\sin\delta_{\ell}\ e^{i\delta_{\ell}})\right]\underset{\sim}{\mu}_{\ell,1}$$

$$\simeq \frac{\sqrt{\pi}}{2k}\sqrt{\frac{2\ell+1}{\ell(\ell+1)}}\left[(-1)^{\ell}\frac{e^{-ikr}}{r} - e^{\frac{ikr+2i\delta_{\ell}}{r}}\right]\underset{\sim}{\mu}_{\ell,1} \ .$$

Similarly for the vector harmonic $\underset{\sim}{N}_{\ell,m}$ with η_{ℓ} replacing δ_{ℓ} and $\underset{\sim}{\nu}_{\ell}$ replacing $\underset{\sim}{\mu}_{\ell}$. Therefore, the entire effect of the scattering center on the far field is simply to shift the phases of the outgoing waves by $2\delta_{\ell}$ and $2\eta_{\ell}$ respectively relative to their values in the absence of scattering. One may think of a given spherical vector wave as impinging on the obstacle, being reflected at the origin, and then returning to infinity with amplitude unchanged (as required by energy conservation, since different vector harmonics are not coupled by the spherical scatterer) but with phase shifted by $2\delta_{\ell}$ or $2\eta_{\ell}$. In virtue of this interpretation, δ_{ℓ} and η_{ℓ} are customarily called "phase shifts."

It is perhaps of interest to make a few brief comments about the character of the solutions. As a check we note first that as the index of refraction n approaches unity, the phase shifts and hence also the scattered wave, properly vanish.

Note also that, as expected, the scattered light is generally elliptically polarized. (The light is linearly polarized for $\phi = 0, \ \pi/2, \ \pi, \ (3\pi)/2.$) If two scattered components, say E_{Θ} and E_{ϕ}, are compared, the ratio is seen to be complex; that is, a phase difference exists

between the two components.

As a second check, consider the limit in which the radius of the scattering sphere is very small; that is, in which $\alpha = (2\pi a)/\lambda << 1$. The coefficient $b_{1,1}$ is seen to be dominant in this limit, and the scattered field thus corresponds to that of an induced dipole oriented in the direction of the incident electric vector. The total cross-section is easily found to be

$$\sigma_{tot} = \frac{128}{3}\pi^5 \frac{a^6}{\lambda^4}\left(\frac{n^2 - 1}{n^2 + 2}\right)^2 \quad . \tag{43}$$

This is Rayleigh's well known law of scattering in which the energy radiated is proportional to λ^{-4}.

Next, consider briefly the geometrical optical limit $\alpha >> 1$. In this case, the series for the scattered field converges very slowly, the phase shifts becoming small only when $\ell \gtrsim \alpha$. Further, for the important terms in the series $\ell \lesssim \alpha$, the Bessel functions in the determining expressions for the phase shifts are rapidly fluctuating functions of α, while the differential cross-section is a rapidly varying function of the scattering angle (because of the complicated interference between the very many vector harmonics). Hence, calculation of the scattering from the exact Mie solution becomes impractical -- even using high speed computers. For this reason, in Section II we shall consider methods for obtaining closed form approximations to the scattering cross-section.

Next, we say a few words about the total cross-section in the geometrical limit. This is not too difficult to estimate, at least in the case $n >> 1$ (nearly opaque spheres). In this case $\sin^2 \delta_\ell$ and $\sin^2 \eta_\ell$ are easily seen to fluctuate rapidly between zero and unity as functions of ℓ for $\ell < \alpha$ and to become small rather rapidly when ℓ exceeds α. Thus, we write (42) approximately as

$$\sigma_{tot} \simeq \frac{2\pi}{k^2} \sum_{\ell=1}^{\alpha} (2\ell + 1)(\sin^2 \delta_\ell + \sin^2 \eta_\ell) \quad .$$

Replacing $\sin^2 \delta_\ell$ and $\sin^2 \eta_\ell$ by their average value 1/2, we find at once

$$\sigma_{tot} \simeq 2\pi a^2 \quad .$$

The exact total cross-section fluctuates rapidly, but with ever smaller amplitude, about this value as α increases. The situation is similar for the more general case in which the sphere is not opaque. Hence, the total cross-section is very much more stable than the differential cross-section.

It is of interest to remark on the fact that the total cross-section above is twice the geometrical cross-section of the sphere. This is a consequence of our definition (27) of the scattered field as the correction to the incident field. The fact that a shadow is formed in the geometrical optical limit means that the incident wave is annihilated behind the sphere by a wave which exists only over the shadow and is exactly out of phase with the incident wave. By our definition, however, this annihilating wave must be counted as part of the scattered field, and it evidently contributes πa^2 to the total cross-section. Together with the contribution πa^2 arising from the geometrical optical specular reflection, this yields the result found above.

Finally, we comment on the requirements of energy conservation and its relation to interference between the incident and scattered field. Evidently, the normal component of Poynting's vector for the total field (incident plus scattered) must give zero when integrated over the sphere at infinity, as over any closed surface. Now the incident field alone integrates to zero, but the scattered field alone does not, since it contains only outgoing waves. Indeed, it gives just the total cross-section times the incident flux. Hence, the interference term between the scattered and incident field must compensate this if energy is to be conserved. Since this interference term is linear in the scattering amplitude $\underset{\sim}{A}$, this implies that the total cross-section is linearly related to $\underset{\sim}{A}$. This relation is the famous cross-section theorem which states that for scattering from a sphere, σ_{tot} is $4\pi/k$ times the imaginary part of the scalar amplitude of the scattering in the forward direction. A proof of this result is deferred until Section III, but some use will be made of it in the following.

II. INTEGRAL EQUATION FORMULATION

A. Derivation of the Integral Equation

In the following we shall present an integral equation formulation of the scattering problem which automatically incorporates all of the boundary conditions. We shall then use this formulation to find approximate closed form expressions for the scattering amplitude. We start, naturally, with Maxwell's equations, which for harmonic time dependence become (in Gaussian units and with $\mu = 1$)

$$\nabla \times \underset{\sim}{E} = \frac{i\omega}{c} \underset{\sim}{H} ,$$

$$\nabla \times \underset{\sim}{H} = - \frac{i\omega}{c} \underset{\sim}{D} = - \frac{i\omega \varepsilon(\underset{\sim}{r})}{c} \underset{\sim}{E} . \tag{44}$$

As indicated, we consider a medium in which $\varepsilon = \varepsilon(\underset{\sim}{r})$. We shall assume that ε is continuous except, perhaps, for surface discontinuities. Also, we assume the condition $\varepsilon \to 1$ as $r \to \infty$; that is, all of the scattering centers can be enclosed within a sphere of finite radius. The wave equations satisfied by $\underset{\sim}{E}$ and $\underset{\sim}{H}$ then become

$$\nabla \times \nabla \times \underset{\sim}{E} - \varepsilon (\underset{\sim}{r}) \, k^2 \underset{\sim}{E} = 0, \quad k^2 = \frac{\omega^2}{c^2} ,$$

$$\nabla \times \nabla \times \underset{\sim}{E} - \kappa^2 (\underset{\sim}{r}) \, \underset{\sim}{E} = 0, \quad \kappa^2 = \varepsilon k^2 ; \tag{45}$$

and

$$\nabla \times \left[\frac{1}{\varepsilon(\underset{\sim}{r})} \nabla \times \underset{\sim}{H} \right] - k^2 \underset{\sim}{H} = 0 . \tag{46}$$

Evidently, it is easiest to work with the equation for $\underset{\sim}{E}$ and to regard $\underset{\sim}{H}$ as determined in terms of $\underset{\sim}{E}$ by (44). At least we shall start that way. Note that $\underset{\sim}{E}$ is not divergenceless, but rather that

$$\nabla \cdot (\varepsilon E) = 0 \ ,$$

so that in fact

$$\nabla \cdot \underset{\sim}{E} = - \frac{1}{\varepsilon} \ \underset{\sim}{E} \cdot \nabla \varepsilon \ .$$

Substitution of this result into (45) yields the alternative form of the wave equation

$$\nabla^2 \underset{\sim}{E} + \nabla \left| \frac{1}{\varepsilon(\underset{\sim}{r})} \ \underset{\sim}{E} \cdot \nabla \varepsilon(\underset{\sim}{r}) \right| + \varepsilon(\underset{\sim}{r}) \ k^2 \ \underset{\sim}{E} = 0 \ . \tag{47}$$

It is understood that the Laplacian operates on the rectangular components of $\underset{\sim}{E}$. We now derive the integral equation for $\underset{\sim}{E}$ using the methods of Levine and Schwinger.

1. Schwinger-Levine Method (Levine and Schwinger, 1950)

We start with Green's identity for vectors, namely

$$\int_S d\underset{\sim}{s}\underset{\sim}{n} \cdot [\underset{\sim}{B} \times (\nabla \times \underset{\sim}{A}) - \underset{\sim}{A} \times (\nabla \times \underset{\sim}{B})] =$$

$$\int_V dv[\underset{\sim}{A} \cdot (\nabla \times \nabla \times \underset{\sim}{B}) - \underset{\sim}{B} \cdot (\nabla \times \nabla \times \underset{\sim}{A})] \ . \tag{48}$$

This identity can be established, using

$$\nabla \cdot (\underset{\sim}{C} \times \underset{\sim}{D}) = \underset{\sim}{D} \cdot (\nabla \times \underset{\sim}{C}) - \underset{\sim}{C} \cdot (\nabla \times \underset{\sim}{D}) \ ,$$

as follows: first, identify $\underset{\sim}{D}$ with $\underset{\sim}{A}$ and $\underset{\sim}{C}$ with $\nabla \times \underset{\sim}{B}$; then identify $\underset{\sim}{D}$ with $\underset{\sim}{B}$ and $\underset{\sim}{C}$ with $\nabla \times \underset{\sim}{A}$; subtract; integrate over the volume; and finally, use Gauss' theorem to obtain the surface integral.

Now introduce the tensor Green's function $\underset{\sim}{\Gamma}$ satisfying the equation

$$\nabla \times \nabla \times \underset{\sim}{\Gamma} (\underset{\sim}{r}, \underset{\sim}{r}') - k^2 \underset{\sim}{\Gamma} (\underset{\sim}{r}, \underset{\sim}{r}') = \underset{\sim}{\varepsilon} \delta(|\underset{\sim}{r} - \underset{\sim}{r}'|) \ , \tag{49}$$

where $\underset{\sim}{\varepsilon}$ is the identity tensor,

$$\underset{\sim}{\varepsilon} = \underset{\sim\sim}{ii} + \underset{\sim\sim}{jj} + \underset{\sim\sim}{kk} \ .$$

The Dirac delta function $\delta(|\underset{\sim}{r} - \underset{\sim}{r}'|)$, which is the generalization to three dimensions of that introduced earlier (18), has the properties that

$$\delta(|\underset{\sim}{r} - \underset{\sim}{r}'|) = \delta(|\underset{\sim}{r}' - \underset{\sim}{r}|) = 0, \ \underset{\sim}{r} \neq \underset{\sim}{r}' \ ,$$

$$\int_V \delta(|\underset{\sim}{r} - \underset{\sim}{r}'|) \, dv' \equiv 1 \ ,$$

$$\int_V f(\underset{\sim}{r}') \, \delta(|\underset{\sim}{r} - \underset{\sim}{r}'|) \, dv' = f(\underset{\sim}{r}) \ .$$

The physical significance of $\underset{\sim}{\Gamma}$ can be seen as follows: Take the scalar product of (49) with the arbitrary vector $\underset{\sim}{j}(\underset{\sim}{r}')$. Then $\underset{\sim}{\Gamma}(\underset{\sim}{r}, \underset{\sim}{r}') \cdot \underset{\sim}{j}(\underset{\sim}{r}')$ is the vector field at the position $\underset{\sim}{r}$ generated by a vector point source of strength $\underset{\sim}{j}$ located at the position $\underset{\sim}{r}'$.

Following Schwinger and Levine, upon taking the divergence of (49), it follows that

$$k^2 \nabla \cdot \underset{\sim}{\Gamma} = - \nabla \delta(|\underset{\sim}{r} - \underset{\sim}{r}'|) = \nabla' \delta(|\underset{\sim}{r} - \underset{\sim}{r}'|) \ , \tag{50}$$

where ∇' denotes the operator ∇ acting on $\underset{\sim}{r}'$. Using the relation

$$\nabla \chi \nabla \chi = - \nabla^2 + \nabla (\nabla \cdot \quad ,$$

equation (49) becomes

$$(\nabla^2 + k^2) \underset{\sim}{\Gamma} = - (\underset{\sim}{\varepsilon} - \frac{1}{k^2} \nabla \nabla') \, \delta(|\underset{\sim}{r} - \underset{\sim}{r}'|) \ .$$

If we introduce the scalar Green's function

$$G(\underset{\sim}{r}, \underset{\sim}{r}') = \frac{e^{ik|\underset{\sim}{r} - \underset{\sim}{r}'|}}{4\pi \, |\underset{\sim}{r} - \underset{\sim}{r}'|} \ , \tag{51}$$

which satisfies the scalar equation

$$(\nabla^2 + k^2)\, G(\underset{\sim}{r}, \underset{\sim}{r}') = -\delta(|\underset{\sim}{r} - \underset{\sim}{r}'|) \quad , \tag{52}$$

then a solution for $\underset{\sim}{\Gamma}$ is

$$\underset{\sim}{\Gamma}(\underset{\sim}{r}, \underset{\sim}{r}') = (\underset{\sim}{\varepsilon} - \frac{1}{k^2}\, \nabla\nabla')\, G(\underset{\sim}{r}, \underset{\sim}{r}') = \underset{\sim}{\Gamma}(\underset{\sim}{r}', \underset{\sim}{r}) \quad , \tag{53}$$

since the scalar operator $\nabla^2 + k^2$ commutes with $\underset{\sim}{\varepsilon} - \frac{1}{k^2}\nabla\nabla'$. Note that

$$\underset{\sim}{\Gamma}(r, r') = \tilde{\underset{\sim}{\Gamma}}(\underset{\sim}{r}', \underset{\sim}{r}) \quad ,$$

where $\tilde{\underset{\sim}{\Gamma}}$ is the transpose of $\underset{\sim}{\Gamma}$; that is,

$$(\tilde{\underset{\sim}{\Gamma}})_{ij} = \underset{\sim}{\Gamma}_{ji} \, .$$

Now apply Green's theorem (48) to $\underset{\sim}{E}(\underset{\sim}{r}')$ and $\underset{\sim}{\Gamma}(\underset{\sim}{r}', \underset{\sim}{r}) \cdot \underset{\sim}{e}$, where $\underset{\sim}{e}$ is an arbitrary constant vector, and let the integral extend over all space. We then find at once

$$\underset{\sim}{E}(\underset{\sim}{r}) \cdot \underset{\sim}{e} = \underset{\sim}{E}_{inc} \cdot \underset{\sim}{e} + \int_V dv' \left\{ k^2[\varepsilon(\underset{\sim}{r}')-1]\, \underset{\sim}{E}(\underset{\sim}{r}') \cdot \underset{\sim}{\Gamma}(\underset{\sim}{r}', \underset{\sim}{r}) \cdot \underset{\sim}{e} \right\}$$

where the integral over the surface at infinity supplies the incident wave. Since $\underset{\sim}{e}$ is an arbitrary, constant vector, this last equation is equivalent to

$$\underset{\sim}{E}(\underset{\sim}{r}) = \underset{\sim}{E}_{inc}(\underset{\sim}{r}) + \int_V dv' \left\{ k^2[\varepsilon(\underset{\sim}{r}')-1]\, \underset{\sim}{E}(\underset{\sim}{r}') \cdot \underset{\sim}{\Gamma}(\underset{\sim}{r}', \underset{\sim}{r}) \right\} .$$

Using

$$\underset{\sim}{E} \cdot \underset{\sim}{\Gamma}(\underset{\sim}{r}', \underset{\sim}{r}) = \tilde{\underset{\sim}{\Gamma}}(\underset{\sim}{r}', \underset{\sim}{r}) \cdot \underset{\sim}{E} = \underset{\sim}{\Gamma}(\underset{\sim}{r}, \underset{\sim}{r}') \cdot \underset{\sim}{E} \quad ,$$

we obtain the somewhat more convenient form

$$\underset{\sim}{E}(\underset{\sim}{r}) = \underset{\sim}{E}_{inc}(\underset{\sim}{r}) + \int_V dv' \left\{ k^2[\varepsilon(\underset{\sim}{r}')-1]\, \underset{\sim}{\Gamma}(\underset{\sim}{r}, \underset{\sim}{r}') \cdot \underset{\sim}{E}(\underset{\sim}{r}') \right\} \quad . \tag{54}$$

In view of our previous interpretation of $\underset{\sim}{\Gamma}$, this equation simply states that $\underset{\sim}{E}$ is the incident field plus a superposition of the fields created at each point $\underset{\sim}{r}'$ by sources of strength $k^2[\varepsilon(\underset{\sim}{r}')-1]\,\underset{\sim}{E}(\underset{\sim}{r}')$.

It is easily verified that $\underset{\sim}{E}$ satisfies its wave equation. It is interesting to show, however, that $\underset{\sim}{E}$ satisfies the proper divergence condition. Using $\nabla \cdot \underset{\sim}{E}_{inc} = 0$, we have

$$\nabla \cdot \underset{\sim}{E} = \int_V dv' \left\{ k^2[\varepsilon(\underset{\sim}{r}')-1]\, \nabla \cdot \underset{\sim}{\Gamma}(\underset{\sim}{r}, \underset{\sim}{r}') \cdot \underset{\sim}{E}(\underset{\sim}{r}') \right\} .$$

With the help of (50), we find

$$\nabla \cdot \underset{\sim}{E} = \int_V dv' \left\{ [\varepsilon(\underset{\sim}{r}')-1]\, \nabla' \, \delta(|\underset{\sim}{r} - \underset{\sim}{r}'|) \cdot \underset{\sim}{E}(\underset{\sim}{r}') \right\}$$

$$= - \int_V dv' \left\{ \delta(|\underset{\sim}{r} - \underset{\sim}{r}'|)\, \nabla' \cdot [(\varepsilon(\underset{\sim}{r}')-1)\, \underset{\sim}{E}(\underset{\sim}{r}')] \right\}$$

$$= - \nabla \cdot [(\varepsilon(\underset{\sim}{r})-1)\, \underset{\sim}{E}(\underset{\sim}{r})] ,$$

and hence, properly

$$\nabla \cdot \varepsilon \underset{\sim}{E} = 0 .$$

Note that since $\underset{\sim}{\Gamma}$ is outgoing at infinity, the correct boundary conditions at infinity are incorporated into the integral equation. Further, since no derivatives of ε or $\underset{\sim}{E}$ are involved, this formulation is valid even if $\varepsilon(\underset{\sim}{r})$ has surfaces of discontinuity.

If we introduce the actual form of $\underset{\sim}{\Gamma}$ (53) into (54), we have more explicitly

$$\underset{\sim}{E}(\underset{\sim}{r}) = \underset{\sim}{E}_{inc}(\underset{\sim}{r}) + k^2 \int_V dv'[\varepsilon(\underset{\sim}{r}')-1]\, \underset{\sim}{E}(\underset{\sim}{r}')\, G(\underset{\sim}{r}, \underset{\sim}{r}')$$

$$- \nabla \int_V dv'\, \nabla' \, G(\underset{\sim}{r}, \underset{\sim}{r}') \cdot \underset{\sim}{E}(\underset{\sim}{r}')[\varepsilon(\underset{\sim}{r}')-1] . \qquad (55)$$

This is the formula with which we shall work.

2. Alternative Derivations of the Integral Equation

Before proceeding further, it might be helpful to give a less abstract derivation of our results. To this end we now construct the integral equation without the use of tensors. We start with the vector wave equation (45), and write it in the form

$$(\nabla^2 + k^2)\, \underset{\sim}{E}(\underset{\sim}{r}) = -\,[\varepsilon(\underset{\sim}{r})-1]\, k^2\, \underset{\sim}{E}(\underset{\sim}{r}) + \nabla\,\nabla\cdot\,\underset{\sim}{E}(\underset{\sim}{r}) \quad .$$

In rectangular coordinates this represents three scalar equations, each of which can be written

$$(\nabla^2 + k^2)\, E_i(\underset{\sim}{r}) = f_i(\underset{\sim}{r}), \quad i = 1, 2, 3,$$

where

$$f_i(\underset{\sim}{r}) = -\,[\varepsilon(\underset{\sim}{r})-1]\, k^2 E_i\,(\underset{\sim}{r}) + \frac{\partial}{\partial x_i}\,\nabla\cdot\,\underset{\sim}{E}(\underset{\sim}{r}) \quad .$$

Now we know the solution of this equation to be

$$E_i(\underset{\sim}{r}) = E_{i,inc}(\underset{\sim}{r}) - \int_V f_i(\underset{\sim}{r}')\, G(\underset{\sim}{r},\underset{\sim}{r}')\, dv' \quad .$$

If we multiply by the corresponding unit vectors and add, we have

$$\underset{\sim}{E}(\underset{\sim}{r}) = \underset{\sim}{E}_{inc}(\underset{\sim}{r}) + k^2 \int_V [\varepsilon(\underset{\sim}{r}')-1]\, \underset{\sim}{E}(\underset{\sim}{r}')\, G(\underset{\sim}{r}, \underset{\sim}{r}')\, dv'$$

$$- \int_V G(\underset{\sim}{r}, \underset{\sim}{r}')\, \nabla'\,\nabla'\cdot\,\underset{\sim}{E}(\underset{\sim}{r}')\, dv' \quad . \tag{56}$$

Using

$$G(\underset{\sim}{r}, \underset{\sim}{r}')\, \nabla'\,\nabla'\cdot\,\underset{\sim}{E}(\underset{\sim}{r}') = \nabla'\,[G(\underset{\sim}{r}, \underset{\sim}{r}')\, \nabla'\cdot\,\underset{\sim}{E}(\underset{\sim}{r}')]$$

$$- \nabla' G(\underset{\sim}{r}, \underset{\sim}{r}')\, \nabla'\cdot\,\underset{\sim}{E}(\underset{\sim}{r}')$$

$$= \nabla'\,[G(\underset{\sim}{r}, \underset{\sim}{r}')\, \nabla'\cdot\,\underset{\sim}{E}(\underset{\sim}{r}')]$$

$$+ \nabla\, G(\underset{\sim}{r}, \underset{\sim}{r}')\, \nabla'\cdot\,\underset{\sim}{E}(\underset{\sim}{r}') \quad ,$$

we obtain

$$\underset{\sim}{E}(\underset{\sim}{r}) = \underset{\sim}{E}_{inc}(\underset{\sim}{r}) + k^2 \int_V [\varepsilon(\underset{\sim}{r}')-1]\, \underset{\sim}{E}(\underset{\sim}{r}')\, G(\underset{\sim}{r}, \underset{\sim}{r}')\, dv'$$

$$- \nabla \int_V G(r, r')\, \nabla' \cdot \underset{\sim}{E}(\underset{\sim}{r}')\, dv',$$

the integral of $\nabla'[G\, \nabla' \cdot E]$ vanishing because $\underset{\sim}{E}$ is divergenceless at infinity. Next, consider

$$G(r, r')\, \nabla' \cdot \underset{\sim}{E} = - G(\underset{\sim}{r}, \underset{\sim}{r}')\, \nabla' \cdot [\underset{\sim}{E}(\varepsilon - 1)] \quad ,$$

since $\varepsilon\underset{\sim}{E}$ is divergenceless everywhere. Thus,

$$G(\underset{\sim}{r}, \underset{\sim}{r}')\, \nabla' \cdot \underset{\sim}{E} = - \nabla' \cdot [G\underset{\sim}{E}(\varepsilon - 1)] + \nabla' G \cdot \underset{\sim}{E}(\varepsilon - 1) \quad ;$$

and hence, upon substitution, we recover our original result (55), the surface integral vanishing because $\varepsilon - 1 = 0$ at infinity.

Still another derivation of this result is discussed in Morse and Feshbach (1953b). The tensor Green's function used there is simpler than that of Schwinger and Levine. However, this derivation immediately leads to the expression (56), and we shall not bother to give details.

3. The Scattering Amplitude

We now obtain an expression for the scattering amplitude by considering the far field as given by the integral equation (55). We start with the easily derived asymptotic form

$$G(\underset{\sim}{r}, \underset{\sim}{r}') \simeq \frac{e^{ikr}}{4\pi r}\, e^{-ik\underset{\sim}{n}' \cdot \underset{\sim}{r}'}, \quad r \to \infty$$

where $\underset{\sim}{n}'$ is a unit vector along $\underset{\sim}{r}$, that is in the direction of observation (we reserve $\underset{\sim}{n}$ to denote the direction of incidence). The first integral in (55) then becomes for $r \to \infty$,

$$\int_V G(\underset{\sim}{r}, \underset{\sim}{r}')\, k^2[\varepsilon(\underset{\sim}{r}')-1]\, \underset{\sim}{E}(\underset{\sim}{r}')\, dv'$$
$$\simeq \frac{e^{ikr}}{r}\, \frac{k^2}{4\pi} \int_V e^{-ik\underset{\sim}{n}' \cdot \underset{\sim}{r}'}\, (\varepsilon - 1)\underset{\sim}{E}\, dv' \equiv \frac{e^{ikr}}{r}\, \underset{\sim}{D}(\underset{\sim}{n}') \quad ,$$

where

$$\underset{\sim}{D}(\underset{\sim}{n}') = \frac{k^2}{4\pi} \int_V e^{-ik\underset{\sim}{n}' \cdot \underset{\sim}{r}} [\varepsilon(r)-1] \, \underset{\sim}{E}(\underset{\sim}{r}) \, dv \quad . \tag{57}$$

The second integral of (55) becomes

$$\nabla \int_V \nabla' \, G(\underset{\sim}{r}, \underset{\sim}{r}') \cdot \underset{\sim}{E}(\underset{\sim}{r}') \, [\varepsilon(\underset{\sim}{r}')-1] \, dv'$$

$$\simeq \nabla \left(\frac{e^{ikr}}{4\pi r}\right) \int \nabla' \, e^{-ik\underset{\sim}{n}' \cdot \underset{\sim}{r}'} \cdot \underset{\sim}{E}(\varepsilon - 1) \, dv'$$

$$\simeq \frac{e^{ikr}}{r} \, \frac{k^2}{4\pi} \, \underset{\sim}{n}' \, [\underset{\sim}{n}' \cdot \int e^{-ik\underset{\sim}{n}' \cdot \underset{\sim}{r}'} \, \underset{\sim}{E}(\varepsilon - 1) \, dv']$$

$$= \frac{e^{ikr}}{r} \, (\underset{\sim}{n}' \cdot \underset{\sim}{D})\underset{\sim}{n}' \quad .$$

Accordingly,

$$\underset{\sim}{E}_{sctd} \simeq [\underset{\sim}{D} - (\underset{\sim}{n}' \cdot \underset{\sim}{D})\underset{\sim}{n}'] \, \frac{e^{ikr}}{r} \quad .$$

From its definition, consequently, the amplitude of the wave scattered in the direction $\underset{\sim}{n}'$ when the incident wave is in the direction $\underset{\sim}{n}$ is given by

$$\underset{\sim}{A}_1 (\underset{\sim}{n}, \underset{\sim}{n}') = \underset{\sim}{D} - (\underset{\sim}{n}' \cdot \underset{\sim}{D})\underset{\sim}{n}' = - \underset{\sim}{n}' \times (\underset{\sim}{n}' \times \underset{\sim}{D}) \quad . \tag{58}$$

If the polar axis is chosen to lie along $\underset{\sim}{n}$, and if Θ, ϕ specify the orientation of $\underset{\sim}{n}'$ with respect to the polar axis, then we write $\underset{\sim}{A}(\underset{\sim}{n}, \underset{\sim}{n}')$ as $\underset{\sim}{A}(\Theta, \phi)$ as in the past. The present more general notation is only intended to describe the scattering in a more explicit way. It perhaps ought to be mentioned in this connection that the direction of incidence (and the polarization direction) appear in the expressions for $\underset{\sim}{D}$ and hence for $\underset{\sim}{A}$, only implicitly through the dependence of the field $\underset{\sim}{E}$ upon these directions.

The essential feature of these results is that the scattering amplitude is expressed in terms of a relatively simple (looking) integral of the electric field over the scattering objects. Choosing "reasonable" approximations for the field internal to a single scattering object, one hopes to obtain correspondingly reasonable approximations to the scattering amplitude for that object. This is the main point of the formulation. Before proceeding with such considerations, however, we briefly present a second formulation in terms of the magnetic rather than the electric field.

4. Magnetic Field Integral Equation

Here, of course, we start with equation (46) for $\underset{\sim}{H}$, namely

$$\nabla \chi \left[\frac{1}{\varepsilon(\underset{\sim}{r})} \nabla \chi \underset{\sim}{H}(\underset{\sim}{r}) \right] - k^2 \underset{\sim}{H}(\underset{\sim}{r}) = 0 \ .$$

Now

$$\nabla \chi \left[\frac{1}{\varepsilon(\underset{\sim}{r})} \nabla \chi \underset{\sim}{H}(\underset{\sim}{r}) \right] = \frac{1}{\varepsilon} \nabla \chi \nabla \chi \underset{\sim}{H} + \nabla \frac{1}{\varepsilon} \chi \nabla \chi \underset{\sim}{H}$$

$$= \frac{1}{\varepsilon} \nabla \chi \nabla \chi \underset{\sim}{H} + \frac{ik}{\varepsilon} \nabla \varepsilon \chi \underset{\sim}{E} \ ,$$

using the second Maxwell equation. Hence we have

$$\nabla \chi \nabla \chi \underset{\sim}{H} + ik \nabla \varepsilon \chi \underset{\sim}{E} - \kappa^2 \underset{\sim}{H} = 0 \ .$$

Applying Green's theorem (48), we obtain in the same way as before

$$\underset{\sim}{H}(\underset{\sim}{r}) = \underset{\sim}{H}_{inc}(\underset{\sim}{r}) + \int_V k^2[\varepsilon(\underset{\sim}{r}')-1] \underset{\sim}{\Gamma}(\underset{\sim}{r}, \underset{\sim}{r}') \cdot \underset{\sim}{H}(\underset{\sim}{r}') \, dv'$$

$$- ik \int_V \underset{\sim}{\Gamma}(\underset{\sim}{r}, \underset{\sim}{r}') \cdot [\nabla \varepsilon(\underset{\sim}{r}') \chi \underset{\sim}{E}(\underset{\sim}{r}')] \, dv' \ .$$

Asymptotically, we then find

$$\underset{\sim}{H}_{sctd}(\underset{\sim}{r}) \equiv \frac{e^{ikr}}{r} \underset{\sim}{A}_2(\underset{\sim}{n}') \tag{59}$$

where

$$\underset{\sim}{A}_2 = \underset{\sim}{D}'(\underset{\sim}{n}') - \underset{\sim}{n}' \ (\underset{\sim}{n}' \cdot \underset{\sim}{D}') + \underset{\sim}{D}'' \ (\underset{\sim}{n}') - \underset{\sim}{n}'(\underset{\sim}{n}' \cdot \underset{\sim}{D}'')$$

$$= - \underset{\sim}{n}' \times [\underset{\sim}{n}' \times \ (\underset{\sim}{D}' + \underset{\sim}{D}'')] \ , \tag{60}$$

with

$$\underset{\sim}{D}' \ (\underset{\sim}{n}') = \frac{1}{4\pi} \int_V e^{-ik\underset{\sim}{n}' \cdot \underset{\sim}{r}} \ k^2[\varepsilon(\underset{\sim}{r})-1] \ \underset{\sim}{H}(\underset{\sim}{r}) \ dv \ , \tag{61}$$

and

$$\underset{\sim}{D}''(\underset{\sim}{n}') = - \frac{ik}{4\pi} \int_V e^{-ik\underset{\sim}{n}' \cdot \underset{\sim}{r}} \ \nabla \varepsilon \ (\underset{\sim}{r}) \times \underset{\sim}{E}(\underset{\sim}{r}) \ dv \ .$$

One interesting feature is already apparent. In the electric field case, any approximations in which the interior $\underset{\sim}{E}$ has the fixed polarization $\underset{\sim}{e}$ of the incident wave gives rise to a dipole-like polarization of the scattered wave (that is, $\underset{\sim}{A} \sim \underset{\sim}{n}' \times (\underset{\sim}{n}' \times \underset{\sim}{e})$). In the magnetic field case this is not so -- the contribution from $\underset{\sim}{D}''$ automatically contains polarization corrections.

A second interesting feature appears if there are surfaces of discontinuity present, since then surface integrals occur. Now in the geometrical limit, specular reflection at the surface must play an important role. This seems to be a rather promising aspect. To make the character of these terms more apparent, let us specialize to the case of a sphere of dielectric constant ε and radius a by writing

$$\varepsilon(\underset{\sim}{r}) = \varepsilon - (\varepsilon - 1) \ u(r - a) \ ,$$

where

$$u(r - a) = \begin{cases} 0, & r < a \\ 1, & r > a \ . \end{cases}$$

Then

$$\nabla \varepsilon(r) \equiv \frac{d\varepsilon}{dr} \underset{\sim}{e}_r = - (\varepsilon - 1)\, \delta(r - a)\, \underset{\sim}{e}_r \quad ,$$

as is easily verified by integrating this expression for $\frac{d\varepsilon}{dr}$. Hence,

$$\underset{\sim}{D}''(\underset{\sim}{n}') = \frac{ik(\varepsilon - 1)}{4\pi} \int_S e^{-ik\underset{\sim}{n}' \cdot \underset{\sim}{r}} \underset{\sim}{e}_r \times \underset{\sim}{E}(\underset{\sim}{r})\, ds \quad . \tag{62}$$

This explicitly exhibits the surface integral contribution to $\underset{\sim}{H}$.

B. Calculation of the Scattered Field by Various Approximations to $\underset{\sim}{E}$

We now specialize to the scattering from a sphere and consider several approximations to the interior electric field $\underset{\sim}{E}$. Although $\underset{\sim}{E}$ is known exactly in principle from the theory developed in I(B), the infinite series obtained is impractical in the general case. On the other hand, the approximations give answers in closed form.*

1. Kirchhoff (or Born) Approximation

Recall the integral equation (54) satisfied by $\underset{\sim}{E}(\underset{\sim}{r})$,

$$\underset{\sim}{E}(\underset{\sim}{r}) = \underset{\sim}{E}_{inc}(\underset{\sim}{r}) + \int_V dv' \left\{ k^2[\varepsilon(\underset{\sim}{r}')-1]\, \underset{\sim}{\Gamma}(\underset{\sim}{r}, \underset{\sim}{r}') \cdot \underset{\sim}{E}(\underset{\sim}{r}') \right\} \quad .$$

If $\varepsilon(\underset{\sim}{r}')-1$ is small, and if the volume of integration is not too large, then the integral amounts to a correction term. The electric field will then be given to good approximation by

$$\underset{\sim}{E}(\underset{\sim}{r}) \sim \underset{\sim}{E}_{inc}(\underset{\sim}{r}) \quad .$$

Applying this assumption to a small, dielectric sphere of radius a, we write for the internal field

---

* The total scattering cross-section is not so hard to evaluate; its fluctuations are relatively small. Hence, the exact total cross-section can be used to normalize the estimates.

$$\underset{\sim}{E} \approx \underset{\sim}{e}_0 e^{ik\underset{\sim}{n} \cdot \underset{\sim}{r}} ,$$

where $\underset{\sim}{n}$ is the direction of propagation of the incident wave, and $\underset{\sim}{e}_0$ is a unit vector along the direction of polarization such that $\underset{\sim}{e}_0 \cdot \underset{\sim}{n} = 0$ but otherwise arbitrary. From (57)

$$\underset{\sim}{D}(\underset{\sim}{n}, \underset{\sim}{n}') = \frac{1}{4\pi} (\varepsilon - 1) k^2 \underset{\sim}{e}_0 \int_{\text{sphere}} e^{-ik\underset{\sim}{n}' \cdot \underset{\sim}{r}} e^{ik\underset{\sim}{n} \cdot \underset{\sim}{r}} dv .$$

To evaluate the integral, choose the polar axis in the direction of $n' - n$ leading at once to

$$D(n, n') = \frac{(\varepsilon - 1)k^2}{k^3 |\underset{\sim}{n}' - \underset{\sim}{n}|^3} \underset{\sim}{e}_0 \left[\sin (k|\underset{\sim}{n}' - \underset{\sim}{n}|a) \right.$$

$$\left. - (k|\underset{\sim}{n}' - \underset{\sim}{n}|a) \cos (k|\underset{\sim}{n}' - \underset{\sim}{n}|a) \right] .$$

Introducing the spherical Bessel function

$$j_1(z) = \frac{\sin z}{z^2} - \frac{\cos z}{z} ,$$

and noting that

$$|\underset{\sim}{n}' - \underset{\sim}{n}| = 2 \sin \frac{\Theta}{2} ,$$

where Θ is the scattering angle, we thus have

$$\underset{\sim}{D}(\underset{\sim}{n}, \underset{\sim}{n}') = (\varepsilon - 1) a(ka)^2 \frac{j_1(2ka \sin \frac{\Theta}{2})}{2ka \sin \frac{\Theta}{2}} \underset{\sim}{e}_0 .$$

From (58), it is apparent that the scattered electric field is polarized in the plane of $\underset{\sim}{e}_0$,

the plane of the inducing dipole. From (31) and (58), the differential cross-section is easily seen to be

$$\frac{d\sigma}{d\Omega} = (\varepsilon - 1)^2 a^2 (ka)^4 \left[\frac{j_1(2ka \sin\frac{\Theta}{2})}{2ka \sin\frac{\Theta}{2}}\right]^2 [1 - (\underset{\sim}{n}' \cdot \underset{\sim}{e}_0)^2] \quad .$$

In the Rayleigh limit, $ka << 1$, this becomes (using $j_1(z) \simeq z/3$ for $z << 1$),

$$\frac{d\sigma}{d\Omega} = \frac{(\varepsilon - 1)^2}{9} a^2 (ka)^4 [1 - (\underset{\sim}{n}' \cdot \underset{\sim}{e}_0)^2] \quad .$$

The total scattering cross-section for the Rayleigh limit is

$$\sigma_{tot} = \frac{128}{3} \pi^5 \frac{a^6}{\lambda^4} \left(\frac{n^2 - 1}{3}\right)^2 \quad ,$$

which agrees very well with the exact result (43), provided our original condition that $\varepsilon - 1$ be small holds.

The angular dependence of the differential scattering cross-section $d\sigma/d\Omega$ is shown schematically in Fig. 2 and is a typical Fraunhofer diffraction pattern. Of course, the Kirchhoff-Born approximation is more realistic the smaller the quantity $(\sqrt{\varepsilon} - 1)\, ka$; in other words, if the dielectric constant of the sphere differs little from that of free space, the incident plane wave will suffer little distortion upon entering the sphere.

The total scattering cross-section for the Kirchhoff-Born approximation is good beyond the Rayleigh limit, $\alpha << 1$, as indicated in Fig. 3, but it becomes very bad if α becomes too large. Indeed for large α, this approximation yields a cross-section which increases without limit (as α^2).

2. Modified Born Approximation

For this case let the field interior to the sphere be given by

$$\underset{\sim}{E} = \underset{\sim}{e}_0 e^{i\kappa z} = \underset{\sim}{e}_0 e^{i\kappa \underset{\sim}{n} \cdot \underset{\sim}{r}}, \text{ where}$$

$$\underset{\sim}{n} \cdot \underset{\sim}{e}_0 = 0 \quad \text{and} \quad \kappa = \sqrt{\varepsilon}\, k \quad .$$

The phase is thus modified in the interior of the sphere, but the rays are assumed to propagate rectilinearly. Also, the amplitude of the interior wave is unity, but as noted before, the total scattering cross-section can be normalized to that computed from the Mie theory.

A straightforward calculation yields

$$\underset{\sim}{D}(\underset{\sim}{n}') = \frac{1}{4\pi} k^2(\epsilon - 1)\, \underset{\sim}{e}_0 \int_v e^{-i(k\underset{\sim}{n}' - \kappa\underset{\sim}{n}) \cdot \underset{\sim}{r}}\, dv'$$

$$= (\epsilon - 1)\, a\, (ka)^2\, \underset{\sim}{e}_0\, \frac{j_1(|\kappa\underset{\sim}{n} - k\underset{\sim}{n}'|a)}{|\kappa\underset{\sim}{n} - k\underset{\sim}{n}'|a}\,, \tag{63}$$

where

$$|\kappa\underset{\sim}{n} - k\underset{\sim}{n}'| = (\kappa^2 + k^2 - 2k\kappa\cos\Theta)^{\frac{1}{2}}$$

$$= k\left[(\sqrt{\epsilon} - 1)^2 + 4\sqrt{\epsilon}\,\sin^2\frac{\Theta}{2}\right]^{\frac{1}{2}}$$

This approximation has the same general limitations as the previous one. However, this result has the additional disadvantage that in the forward direction ($\Theta = 0$) $\underset{\sim}{D}$ oscillates about zero as a function of $(n-1)ka$ although we know that the main diffraction peak is in the forward direction. Hence, this approximation is restricted to $(n-1)ka \lesssim 1$.

3. W. K. B. Interior Wave Number

For this case we assume that the wave is propagated rectilinearly inside the sphere with no change in the polarization. The phase, however, is not assumed to be constant over the wave front (the previous case), but is determined by the distance the plane wave has moved in the drop. Using the notation in Fig. 4, the phase at an arbitrary point P equals the phase at C, plus the difference phase from C to D, plus the difference in phase from D to P: or

$$\text{phase at } P = -ka + k\left(a - \sqrt{a^2 - \rho^2}\right) + \kappa\left(\sqrt{a^2 - \rho^2} + z\right)$$

$$= (\kappa - k)\left(\sqrt{a^2 - \rho^2} + z\right) + kz\,.$$

Actually, the phase at P is slightly different because the ray arriving ar P is refracted at the surface of the sphere.

In any case, using this phase, we take the interior field to be

$$\underset{\sim}{E} = \underset{\sim}{e}_0 e^{ikz + i(\kappa - k)[z+(a^2 - \rho^2)^{\frac{1}{2}}]}$$

Note that the transmission coefficient for a plane wave incident normally on a plane surface of dielectric constant ε is $2/(\sqrt{\varepsilon} + 1)$, so that this might be inserted as a reasonable amplitude factor.

Upon substituting the interior field into (57), we then have

$$\underset{\sim}{D} \simeq \frac{(\varepsilon - 1)}{4\pi} k^2 \underset{\sim}{e}_0 \int_{\text{sphere}} e^{-k\underset{\sim}{n}' \cdot \underset{\sim}{r}} e^{-ik(a^2 - \rho^2)^{\frac{1}{2}}} \chi\, e^{i\kappa [z + (a^2 - \rho^2)^{\frac{1}{2}}]}\, dv \quad . \tag{64}$$

In cylindrical coordinates

$$\underset{\sim}{n}' \cdot \underset{\sim}{r} = (\cos\Theta \underset{\sim}{e}_z + \sin\Theta \underset{\sim}{e}_{\rho'}) \cdot (z\underset{\sim}{e}_z + \rho \underset{\sim}{e}_\rho)$$

$$= z\cos\Theta + \rho \sin\Theta \cos\phi \ ,$$

where Θ is the scattering angle and φ is the angle between $\underset{\sim}{e}_\rho$ and $\underset{\sim}{e}_{\rho'}$. Thus we have

$$\underset{\sim}{D} \simeq \frac{(\varepsilon - 1)}{4\pi} k^2 \underset{\sim}{e}_0 \int_{\text{sphere}} e^{iz(\kappa - k\cos\Theta)} e^{-ik\rho \sin\Theta \cos\phi} \chi\, e^{i(\kappa - k)(a^2 - \rho^2)^{\frac{1}{2}}} \rho \, d\rho d\phi dz \quad .$$

After evaluation of the z and ϕ integrals,

$$\underset{\sim}{D} \simeq \frac{(\varepsilon - 1)k}{\sqrt{\varepsilon} - \cos\Theta} \underset{\sim}{e}_0 \int_0^a \rho \, d\rho \sin[(\kappa - k\cos\Theta)(a^2 - \rho^2)^{\frac{1}{2}}] \chi\, e^{i(\kappa - k)(a^2 - \rho^2)^{\frac{1}{2}}} J_0(k\rho \sin\Theta) \quad .$$

In general, the integral can be evaluated only approximately. However, it can be evaluated exactly for the two special cases of forward and backward scattering. These will serve as a check on our approximate methods. Also, as mentioned earlier, the total cross-section can be estimated from the forward scattering.

Consider the case of forward scattering, that is $\Theta = 0$, first. Let us change variables by writing

$$\rho = a \sin \psi \quad .$$

Then

$$\underset{\sim}{D} \simeq \frac{(\varepsilon - 1)\, a^2 k}{\sqrt{\varepsilon} - \cos\Theta}\, \underset{\sim}{e}_0 \int_0^{\pi/2} \sin\psi \cos\psi \, d\psi \chi \sin[(\kappa - k\cos\Theta)\, a \cos\psi] \chi e^{i(\kappa - k)a\cos\psi} \chi J_0(ka \sin\Theta \sin\psi) \quad . \tag{65}$$

Now let $\Theta = 0$. Then we obtain

$$\underset{\sim}{D} \simeq (\sqrt{\varepsilon} + 1)\, ka^2\, \underset{\sim}{e}_0 \int_0^{\pi/2} \sin\psi \cos\psi \, d\psi \chi \sin[(\kappa - k)\, a \cos\psi] \, e^{i(\kappa - k)\, a \cos\psi} ,$$

$$\simeq \frac{i(\sqrt{\varepsilon} + 1)\, ka^2}{2}\, \underset{\sim}{e}_0 \left[\frac{1}{2} - \frac{e^{2i(\kappa - k)\, a}}{2i(\kappa - k)\, a} - \frac{1 - e^{2i(\kappa - k)\, a}}{[2i(\kappa - k)\, a]^2}\right] . \tag{66}$$

In the geometrical optical limit, $ka \to \infty$, the second and third terms appear merely as correction terms.

From the cross-section theorem, the total scattering cross-section is given by

$$\sigma_t = \frac{4\pi}{k} \operatorname{Im} \left\{ |\underset{\sim}{D}| \right\} \quad ,$$

where $\underset{\sim}{D}$ is computed for $\Theta = 0$ (since $\underset{\sim}{A} = \underset{\sim}{D}$ for forward scattering). Hence we observe that

$$\sigma_t = f\,[(n - 1)\alpha] \quad ;$$

more specifically, it contains terms in $\begin{matrix}\cos \\ \sin\end{matrix}\,[2(n - 1)\alpha]$. Hence, σ_t has a periodicity of approximately $(n - 1)\alpha = \pi$. Penndorf (private communication) computed the position of the maxima from the series solution (Mie theory) to be

$$(n - 1)\alpha \simeq 2.15 + 3.18(p - 1) \quad ,$$

where p is the order of the maxima. He also found the position of the minima to be

$$(n - 1)\alpha \simeq 3.90 + 3.18(q - 1) \quad ,$$

where q is the order of the minima. These computed periods are thus quite comparable to π.

For the case of backward scattering $\Theta = \pi$, (65) becomes

$$\underset{\sim}{D} \simeq \frac{(\sqrt{\epsilon} - 1)\, ka^2}{2i}\, \underset{\sim}{e}_0 \left[\frac{e^{2i\kappa a}}{2i\kappa a} + \frac{1 - e^{2i\kappa a}}{(2i\kappa a)^2} + \frac{e^{-2ika}}{2ika} - \frac{1 - e^{-2ika}}{(2ika)^2} \right] .$$

Here the amplitude is much smaller than in the forward direction, and it oscillates rapidly with changing α; the polarization is the same as the incident field.

Next we give an exact evaluation (but not in closed form) of the expression for $\underset{\sim}{D}$. Consider

$$f(z, \rho) = \int_0^{\pi/2} \sin\psi \cos\psi \, d\psi \, e^{iz \cos\psi} J_0(\rho \sin\psi) \quad ,$$

so that (65) becomes

$$\underset{\sim}{D} \simeq \frac{(\varepsilon - 1)\, ka^2}{(\sqrt{\varepsilon} - \cos \Theta)\, 2i}\ \underset{\sim}{e}_0 \Big\{ f[(\kappa - k)\, a + (\kappa - k \cos \Theta)\, a,\ ka \sin \Theta] - f\left[-2ka \sin^2 \frac{\Theta}{2},\ ka \sin \Theta\right] \Big\} .$$

Now, $f(z, \rho)$ satisfies $(\nabla^2 + 1)\, f(z, \rho) = 0$. Hence introducing spherical coordinates r, γ, ϕ, defined by

$$\rho = r \sin \gamma$$

$$z = r \cos \gamma ,$$

we note that f must be expressible in the form

$$f = \sum a_\ell j_\ell (r)\, P_\ell(\cos \gamma) .$$

Indeed, in Watson (1944)

$$J_0(r \sin \psi \sin \gamma)\, e^{ir \cos \psi \cos \gamma}$$

$$= \sum i^\ell (2\ell + 1)\, j_\ell (r) P_\ell (\cos \psi) P_\ell (\cos \gamma) .$$

Hence, with

$$r = \sqrt{z^2 + \rho^2} , \quad \cos \gamma = \frac{z}{\sqrt{z^2 + \rho^2}} ,$$

we obtain

$$f(z, \rho) = \int_0^{\pi/2} \sin\psi \cos\psi \, d\psi \sum i^{\ell}(2\ell + 1)\, j_{\ell}(r)$$

$$\times P_{\ell}(\cos\psi)\, P_{\ell}(\cos\gamma)$$

$$= \sum i^{\ell}(2\ell + 1)\, a_{\ell}\, j_{\ell}(r)\, P_{\ell}(\cos\gamma) \quad .$$

For ℓ even $= 2m$,

$$a_{2m} = \sum_{s=0} (-1)^{s+m} \frac{1 \cdot 3 \cdot 5 \cdots (2m + 2s - 1)}{(m - s)!\,(2s)!} \frac{1}{(2s + 2)2^{m-s}} \quad ;$$

$$a_0 = \frac{1}{2}, \quad a_2 = \frac{1}{8}, \quad a_4 = -\frac{1}{48} \quad .$$

For ℓ odd $= 2m + 1$, $a_{2m+1} = \frac{1}{3}$ for $m = 0$ and is zero otherwise. Thus we have obtained explicit expressions for $f(z, \rho)$ and therefore have evaluated $\underset{\sim}{D}$ exactly. Unfortunately, the result converges slowly and is consequently not very useful.

Finally, we evaluate the expression (65) for $\underset{\sim}{D}$ approximately by using saddle point methods. Breaking $\sin[(\kappa - k\cos\Theta)\, a\cos\psi]$ into exponentials, we write (65) as

$$\underset{\sim}{D} \simeq \frac{(\varepsilon - 1)\, ka^2}{2i(\sqrt{\varepsilon} - \cos\Theta)}\, \underset{\sim}{e}_0 \, (I_1 - I_2) \quad ;$$

$$I_1 = \int_0^{\pi/2} \sin\psi \cos\psi \, d\psi \; e^{2ika[\sqrt{\varepsilon} - \cos^2(\Theta/2)]\cos\psi}$$

$$\times J_0(ka \sin\Theta \sin\psi) \, ,$$

$$I_2 = \int_0^{\pi/2} \sin\psi \cos\psi \, d\psi \; e^{-2ika \sin^2(\Theta/2)\cos\psi} \qquad (67)$$

$$\times J_0(ka \sin\Theta \sin\psi) \quad .$$

Since we shall be interested in the geometrical limit, we assume not only $ka >> 1$, but also $(\sqrt{\varepsilon} - 1)\, ka >> 1$. We now consider two domains for the scatteirng.

a. Main diffraction peak

This will include small angles around the forward direction. The assumption is that

$$ka\,\theta^2 << 1$$

(but not necessarily $ka\,\theta << 1$). I_1 contributes little to the integration because of the extremely rapid oscillations of the exponential. The major contribution comes from I_2 and we have

$$I_2 \simeq \int_0^{\pi/2} \sin\psi \cos\psi \, d\psi \, J_0(ka\,\theta \sin\psi) \ .$$

Letting $ka\,\theta \sin\psi = x$, we thus have

$$I_2 = \frac{1}{(ka\,\theta)^2} \int_0^{ka\theta} x\, J_0(x)\, dx = \frac{J_1(ka\,\theta)}{ka\,\theta} \ .$$

This is the typical Fraunhofer diffraction pattern for a circular aperture. For $\theta = 0$, it properly gives the leading term of (66).

b. Outside main diffraction peak

This region is treated on the assumption that

$$ka \sin\theta >> 1. \tag{68}$$

It should be pointed out that for ka large enough, this domain can overlap with the previous one. For example, suppose $ka = 1000$. The previous domain extends from $\theta = 0$ to say 1/100 radian; but for $\theta = 1/100$ radian, $ka \sin\theta \simeq 10$, which satisfies (68). For this region use the asymptotic expansion*

* This expansion breaks down for $\psi = 0$ and, strictly speaking, the region from $\psi = 0$ to say $1/(ka \sin\theta)$ should be treated separately. However, it is easily verified that this region contributes only higher order terms.

$$J_0(ka \sin \alpha \sin \psi) \simeq \sqrt{\frac{2}{\pi ka \sin \alpha}} \frac{1}{\sqrt{\sin \psi}}$$

$$\times \left[\frac{e^{ika \sin \alpha \sin \psi - i(\pi/4)}}{2} + \frac{e^{-(ika \sin \alpha \sin \psi - i(\pi/4))}}{2} \right].$$

From (67) consider I_2 first, writing

$$I_2 = I_{2+} + I_{2-} ,$$

$$I_{2\pm} = \sqrt{\frac{2}{\pi ka \sin \alpha}} \frac{e^{\mp i(\pi/4)}}{2} \int_0^{\pi/2} \sqrt{\sin \psi} \cos \psi \, d\psi$$

$$\times e^{-ika [2 \sin^2(\alpha/2) \cos \psi \mp \sin \alpha \sin \psi]}$$

$$= \frac{e^{\mp i(\pi/4)}}{\sqrt{2\pi ka \sin}} \int_0^{\pi/2} \sqrt{\sin \psi} \cos \psi \, d\psi$$

$$\times e^{-2ika \sin(\alpha/2) \sin [(\alpha/2) \mp \psi]} .$$

The saddle points occur for $\frac{\alpha}{2} \mp \psi = (2n + 1) \frac{\pi}{2}$, $n = 0, \pm 1, \pm 2, \ldots$, or $\psi = \pm \frac{\alpha}{2} + (2n + 1) \frac{\pi}{2}$. The only saddle point in the range of integration occurs for I_{2-} with $\psi = \frac{\pi}{2} - \frac{\alpha}{2}$. Hence, letting

$$\psi = \frac{\pi}{2} - \frac{\alpha}{2} + \delta,$$

$$I_{2-} \simeq \frac{1}{\sqrt{2\pi ka \sin}} e^{i(\pi/4)} \int_{-(\frac{\pi}{2} - \frac{\alpha}{2})}^{\frac{\alpha}{2}} \sqrt{\cos \frac{\alpha}{2}} \sin \frac{\alpha}{2}$$

$$\times e^{-2ika \sin (\alpha/2) [1 - (\delta^2/2)]} d\delta$$

$$\simeq \frac{e^{i(\beta/4)}\, e^{-2ika \sin(\Theta/2)}}{2ka\sqrt{\pi}\sqrt{-i}} \int_{-\sqrt{-ika\sin(\Theta/2)}\ (\pi/2 - \Theta/2)}^{\sqrt{-ika\sin(\Theta/2)}\ \Theta/2} e^{-x^2}\, dx$$

$$\simeq -i \frac{e^{-2ika\sin(\Theta/2)}}{2ka} \left\{ 1 + O\left[\frac{1}{\sqrt{ka\sin(\Theta/2)}} \times \left(\frac{1}{\frac{\Theta}{2}} \text{ and / or } \frac{1}{\frac{\pi}{2} - \frac{\Theta}{2}} \right) \right] \right\} .$$

The contribution to the differential scattering cross-section of I_{2-} alone can be seen to lead to isotropic scattering outside the main diffraction peak. This is the approximation made by Wiener.

Similarly, we find

$$I_{2+} \simeq I_{2-} \times O\left(\frac{1}{\sqrt{ka \sin\frac{\Theta}{2}}} \times \frac{1}{\frac{\pi}{2} - \frac{\Theta}{2}} \right) ,$$

and hence, retaining only the dominant term,

$$I_2 \simeq I_{2-} .$$

This evaluation of I_2 is valid provided Θ is not too close to zero or π -- we must essentially have $\frac{1}{\sqrt{ka}\ \sin(\Theta/2)^{3/2}} << 1$. This is a stronger condition than (68). When (68) is satisfied, but the preceeding one is not, saddle point methods can still be used, but the saddle point is then close to one or the other limits of integration; the integral can no longer be regarded as extending from $-\infty$ to $+\infty$. Hence, these are two intermediate regions to consider -- one near $\Theta = 0$, the other near $\Theta = \pi$. All of this is essentially a refinement which we shall not pursue further.

In a similar way, the contributions of I_1 must be included, but we shall not work out the details of this either. We only mention that outside of the main diffraction peak its value is something like

$$I_1 \simeq \pm \frac{1}{2ka} \frac{\sqrt{\epsilon} - \cos^2 \frac{\Theta}{2}}{A^2} e^{\pm 2ikA} ,$$

where

$$A = \sqrt{\epsilon - (2\sqrt{\epsilon} - 1) \cos^2 \frac{\Theta}{2}} ,$$

and hence is of the same order as I_2.

4. W. K. B. Interior Wave Number with Refraction

Here we take the sphere as behaving something like a converging lens and write for the internal field,

$$\underset{\sim}{E}(\underset{\sim}{r}') = \underset{\sim}{Ce}(\Theta', \phi') \frac{e^{-ik |\underset{\sim}{r}' - f\underset{\sim}{e}_z|}}{|\underset{\sim}{r}' - f\underset{\sim}{e}_z|} ,$$

where f is a kind of focal length, determined say for paraxial rays, in which case

$$f = \frac{a}{\sqrt{\epsilon} - 1} .$$

We thus have from (57),

$$\underset{\sim}{D}(\underset{\sim}{n}') = \frac{C(\epsilon - 1) k^2}{4\pi} \int_{\text{sphere}} \underset{\sim}{e}(\Theta', \phi') \frac{e^{-ik|\underset{\sim}{r}' - f\underset{\sim}{e}_z|}}{|\underset{\sim}{r}' - f\underset{\sim}{e}_z|}$$

$$\times e^{-ik\underset{\sim}{n}' \cdot \underset{\sim}{r}'} dv' .$$

Now introduce a new variable

$$\underset{\sim}{\rho} = \underset{\sim}{r}' - f\underset{\sim}{e}_z ,$$

so that

$$\underset{\sim}{D} = \frac{C(\varepsilon - 1)\, k^2}{4\pi} \int_{\text{sphere}} \underset{\sim}{e}(\Theta_\rho, \phi_\rho)\ \frac{e^{-ik\rho}}{\rho}\ e^{-ik\underset{\sim}{n}' \cdot (f\underset{\sim}{e}_z + \rho)}$$

$$\rho^2\, d\rho \sin\Theta_\rho\, d\Theta_\rho\ d\phi_\rho\ ,$$

where the integration still is to be carried out over the original sphere; that is, ϕ_ρ varies from zero to 2π, and, since we must have

$$r'^2 = \rho^2 + f^2 + 2\rho f \cos\Theta_\rho \leq a^2\ ,$$

ϕ_ρ varies from $\cos^{-1}\frac{a^2 - \rho^2 - f^2}{2\rho f}$ to π; while ρ varies from $f - a$ to $f + a$. With this understanding and the fact that

$$\underset{\sim}{n}' \cdot \underset{\sim}{\rho} = \cos\Theta\cos\Theta_\rho + \sin\Theta\sin\Theta_\rho\cos(\phi - \phi_\rho),$$

we obtain

$$\underset{\sim}{D} = \frac{C(\varepsilon - 1)\, k^2}{4\pi}\ e^{-ikf\cos\Theta} \int_{\text{sphere}} \underset{\sim}{e}(\Theta_\rho, \phi_\rho)\ \frac{e^{-ik\rho}}{\rho}$$

$$\chi\ e^{-ik\rho\cos\Theta\cos\Theta_\rho}$$

$$\chi\ e^{-ik\rho\sin\Theta\sin\Theta_\rho\cos(\phi - \phi_\rho)}$$

$$\chi\ \rho^2\, d\rho d\phi_\rho \sin\Theta\rho\, d\Theta_\rho\ .$$

Now, we attempt to take into account the change of direction of the electric field on refraction. We do this only approximately -- neglecting from the beginning the change in the plane of polarization on transmission for rays incident outside of the xz or yz planes. However, we shall demand that the electric field be perpendicular to the direction of propagation of the ray. We write

$$\underset{\sim}{e} = \alpha\underset{\sim}{e}_x + \beta\underset{\sim}{e}_z\ ;$$

(plane of polarization of ray is not rotated, as it really should be). Also, we require that

$$\underset{\sim}{e} \cdot \underset{\sim}{e}_\rho = 0 \ ,$$

so that the field is transverse. Now,

$$\underset{\sim}{e}_\rho = \underset{\sim}{e}_x \sin \Theta_\rho \cos \phi_\rho + \underset{\sim}{e}_y \sin \Theta_\rho \sin \phi_\rho + \underset{\sim}{e}_z \cos \Theta_\rho \ .$$

Hence,

$$\underset{\sim}{e} \cdot \underset{\sim}{e}_\rho = 0 = \alpha \sin \Theta_\rho \cos \phi_\rho + \beta \cos \Theta_\rho \ ,$$

and along with

$$\alpha^2 + \beta^2 = 1 \ ,$$

this yields at once

$$\alpha = \frac{1}{\sqrt{1 + \tan^2 \Theta_\rho \cos^2 \phi_\rho}}$$

$$\beta = - \frac{\tan \Theta_\rho \cos \phi_\rho}{\sqrt{1 + \tan^2 \Theta_\rho \cos^2 \phi_\rho}} \ .$$

If f is appreciably larger than a, then Θ_ρ is always close to π, and

$$\tan^2 \Theta_\rho << 1 \ .$$

Thus we shall make the further approximation

$$\alpha \simeq 1, \ \beta \simeq -\tan \Theta_\rho \cos \phi_\rho \simeq \sin \Theta_\rho \cos \phi_\rho \ ;$$

that is, $\underset{\sim}{e}$ is very nearly in the x direction but has a first order component in the z-direction. The errors involved in these last approximations are <u>probably</u> of the same order as those involved in neglecting rotations of the plane of polarization (and probably smaller than those incurred in neglecting amplitude variations of the refracted ray with angle of incidence). In any case, we obtain

C-4

$$D_x = \frac{C(\varepsilon - 1)\, k^2}{4\pi}\; e^{-ikf\cos\Theta} \int_{\text{sphere}} \frac{e^{-ik\rho}}{\rho}\; e^{-ik\rho\cos\Theta\cos\Theta_\rho}$$

$$\chi\; e^{-ik\rho\sin\Theta\sin\Theta_\rho\cos(\phi - \phi_\rho)}$$

$$\chi\; \rho^2\, d\rho d\phi_\rho \sin\Theta_\rho\, d\Theta_\rho$$

$$= \frac{C(\varepsilon - 1)\, k^2}{2}\; e^{-ikf\cos\Theta} \int_{f-a}^{f+a} \rho\, d\rho\, e^{-ik\rho} \int_{\cos^{-1}\frac{a^2 - \rho^2 - f^2}{2\rho f}}^{\pi}$$

$$\chi \sin\Theta_\rho\; d\Theta_\rho\, e^{-ik\rho\cos\Theta\cos\Theta_\rho}$$

$$\chi\; J_0(k\rho\sin\Theta\;\sin\Theta_\rho).$$

$$D_z = \frac{C(\varepsilon - 1)\, k^2}{4\pi}\; e^{-ikf\cos\Theta} \int_{\text{sphere}} \frac{e^{-ik\rho}}{\rho}\, e^{-ik\rho\cos\Theta\cos\Theta_\rho}$$

$$\chi\; e^{-ik\rho\sin\Theta\sin\Theta_\rho\;\cos(\phi - \phi_\rho)}$$

$$\chi \sin\Theta_\rho\cos\phi_\rho\; \rho^2\, d\rho$$

$$\chi\; d\phi_\rho \sin\Theta_\rho\, d\Theta_\rho$$

$$D_z = -\frac{iC(\varepsilon - 1)\, k^2}{2}\; \cos\phi\;\; e^{-ikf\cos\Theta} \int_{f-a}^{f+a} \rho\, d\rho\, e^{-ik\rho}$$

$$\chi \int_{\cos^{-1}\frac{a^2 - \rho^2 - f^2}{2\rho f}}^{\Pi} \Big[\sin^2\Theta_\rho\, d\Theta_\rho\; e^{-ik\rho\cos\Theta\cos\Theta_\rho}$$

$$\chi\; J_1\,(k\rho\sin\Theta\;\sin\Theta_\rho)\Big]\quad ,$$

where the relation

$$\int_0^{2\pi} \cos \phi_\rho \; e^{-i\gamma \cos (\phi - \phi_\rho)} \; d\phi_\rho = 2\pi i \cos \phi \; J_1(\gamma)$$

has been used. In spite of the approximations, the integrals for D_x and D_z are still difficult to integrate. At least for now, we examine only the forward scattering. For this case,

$$D_z = 0 \; ;$$

and

$$D_x = \frac{C(\varepsilon - 1)\, k^2 e^{-ikf}}{2} \int_{f-a}^{f+a} \rho \, d\rho \, e^{-i\kappa\rho}$$

$$\times \int_{\cos^{-1} \frac{a^2 - \rho^2 - f^2}{2\rho f}}^{\pi} \sin \Theta_\rho \; \Theta_\rho \; e^{-ik\rho \cos \Theta_\rho}$$

$$= \frac{C(\varepsilon - 1)\, k e^{-ikf}}{2i} \int_{f-a}^{f+a} d\rho \, e^{-i(\kappa - k)\rho}$$

$$\times \left\{ e^{ik\rho} - e^{ik\rho \frac{f^2 + \rho^2 - a^2}{2\rho f}} \right\}$$

$$D_x = \frac{C(\varepsilon - 1)\, k e^{-ikf}}{2i} \int_{f-a}^{f+a} d\rho \left\{ e^{-i(\kappa - k)\rho} \right.$$

$$\left. - e^{ik \frac{f^2 - a^2}{2f}} \; e^{i \left(\frac{k\rho^2}{2f} - \kappa\rho \right)} \right\}$$

$$= \frac{C(\varepsilon - 1)\, k}{2i} \left\{ \frac{2 \sin (\kappa - k)\, a}{\kappa - k}\, e^{-i\kappa f} \right.$$

$$\left. - e^{ik \frac{f^2 - a^2}{2f}} - ikf - i\, \frac{f\kappa^2}{2k} \int_{f-a}^{f+a} e^{i \frac{k}{2f} \left(\rho - \frac{f\kappa}{k}\right)^2} d\rho \right\} .$$

Consider just the integral:

$$\int_{f-a}^{f+a} e^{\frac{ik}{2f} \left(\rho - \frac{f\kappa}{k}\right)^2} d\rho = \sqrt{\frac{2f}{k}} \int_{[f(1 - \frac{\kappa}{k}) - a] \sqrt{\frac{k}{2f}}}^{[f(1 - \frac{\kappa}{k}) + a] \sqrt{\frac{k}{2f}}} e^{iu^2}\, du .$$

Using $f = \frac{a}{\sqrt{\varepsilon} - 1}$, $\frac{\kappa}{k} = \sqrt{\varepsilon}$, the upper limit is seen to be zero, the lower to be $-\sqrt{\frac{k(\sqrt{\varepsilon} - 1)}{2a}}\, 2a = -\sqrt{2ka\,(\sqrt{\varepsilon} - 1)}$; that is, large and negative. Then replacing u by - u, the integral becomes

$$\sqrt{\frac{2f}{k}} \left\{ \int_0^\infty e^{iu^2}\, du - \int_{\sqrt{2ka\,(\sqrt{\varepsilon} - 1)}}^\infty e^{iu^2}\, du \right\}$$

$$= \sqrt{\frac{2f}{k}} \left\{ \sqrt{\frac{\pi i}{4}} + \frac{e^{2ika\,(\sqrt{\varepsilon} - 1)}}{2i \sqrt{2ka\,(\sqrt{\varepsilon} - 1)}} + \ldots \right\}$$

$$= \sqrt{\frac{\pi i a}{2(\sqrt{\varepsilon} - 1)\, k}} + \frac{e^{2ika\,(\sqrt{\varepsilon} - 1)}}{2ik\,(\sqrt{\varepsilon} - 1)} + \ldots$$

Using

$$e^{-ik\kappa f} = e^{-i\sqrt{\varepsilon}\, ka/(\sqrt{\varepsilon} - 1)} ;$$

$$e^{ik \frac{f^2 - a^2}{2f} - ikf - \frac{if\kappa^2}{2k}} = e^{-\frac{ika}{\sqrt{\varepsilon} - 1} (1 - \sqrt{\varepsilon} + \varepsilon)}$$

we obtain finally

$$D_x = \frac{C(\varepsilon - 1)}{2i} k \left\{ \frac{2 \sin (\sqrt{\varepsilon} - 1) ka}{(\sqrt{\varepsilon} - 1) k} e^{-i\sqrt{\varepsilon}\, ka/(\sqrt{\varepsilon} - 1)} \right.$$

$$\left. + e^{-\frac{ika}{\sqrt{\varepsilon} - 1} (1 - \sqrt{\varepsilon} + \varepsilon)} \left[\sqrt{\frac{\pi i a}{2(\sqrt{\varepsilon} - 1) k}} + \cdots \right] \right\} .$$

Unfortunately, this does not seem to behave properly, which is rather surprising since the approximation used for the internal field seems so reasonable. Presumably, the situation could be improved by adjusting the phase of the diffracted ray more accurately -- that is, by introducing a factor $e^{i\gamma(\theta_\rho)}$ in the expression for $\underset{\sim}{E}$ with which we started. However, this possibility has not been examined.

5. Interior Solution Estimated from the Exact

The exact solution (34a) in the interior was found earlier to be

$$\underset{\sim}{E} = \sqrt{\pi} \sum_{\ell=1}^{\infty} i^{\ell-1} \sqrt{\frac{2\ell + 1}{\ell(\ell + 1)}} \left[c_{\ell, 1} \underset{\sim}{M}^{(1)}_{\ell, 1} + c_{\ell, -1} \underset{\sim}{M}^{(1)}_{\ell, -1} \right.$$

$$\left. + d_{\ell, 1} \underset{\sim}{N}^{(1)}_{\ell, 1} + d_{\ell, -1} \underset{\sim}{N}^{(1)}_{\ell, -1} \right] ,$$

where $C_{\ell,1}$ is given by (36) and $d_{\ell,1}$ by (41). Since we are interested in $\alpha, \beta >> 1$, we approximate the interior solution by using asymptotic forms for $C_{\ell,1}$ and $d_{\ell,1}$. (This has been done for scalar fields by Hart (1951) and Latter (1951).) The asymptotic forms of the spherical Bessel functions (Stratton, 1941c) are

$$j_\ell(z) \simeq \frac{1}{z} \cos\left(z - \frac{\ell + 1}{2}\pi\right) ,$$

$$h_\ell(z) \simeq \frac{e^{i\left(z - \frac{\ell + 1}{2}\pi\right)}}{z} ;$$

and hence

$$[z j_\ell(z)]' \simeq - \sin\left(z - \frac{\ell + 1}{2}\pi\right) ,$$

$$[z h_\ell^{(1)}(z)]' \simeq i e^{i\left(z - \frac{\ell + 1}{2}\pi\right)} .$$

Using the asymptotic expressions indiscriminately, we have at once

$$c_{2p,\,1} \simeq d_{2p+1,\,1} \simeq d_{1,\,1} = \frac{e^{-i\alpha}}{\cos\beta - \frac{i}{\sqrt{\epsilon}} \sin\beta} \equiv d ,$$

$$d_{2p,\,1} \simeq c_{2p+1,\,1} \simeq c_{1,\,1} = \frac{e^{-i\alpha}}{\frac{1}{\sqrt{\epsilon}} \cos\beta - i \sin\beta} \equiv c .$$

Hence, to this approximation, the interior field becomes (for $r < a$)

$$\underset{\sim}{E} \simeq \frac{\sqrt{\pi}}{2} c \sum_{\ell=1}^{\infty} i^{\ell-1} \sqrt{\frac{2\ell + 1}{\ell(\ell + 1)}} \left\{ [1 - (-1)^\ell] \right.$$

$$\left. \times \left[\underset{\sim}{M}_{\ell,\,1}^{(1)} - \underset{\sim}{M}_{\ell,\,-1}^{(1)}\right] + [1 + (-1)^\ell] \left[\underset{\sim}{N}_{\ell,\,1}^{(1)} + \underset{\sim}{N}_{\ell,\,-1}^{(1)}\right] \right\}$$

$$+ \frac{\sqrt{\pi}}{2} d \sum_{\ell=1}^{\infty} i^{\ell-1} \sqrt{\frac{2\ell + 1}{\ell(\ell + 1)}} \left\{ [1 + (-1)^\ell] \right.$$

$$\left. \times \left[\underset{\sim}{M}_{\ell,\,1}^{(1)} - \underset{\sim}{M}_{\ell,\,-1}^{(1)}\right] + [1 - (-1)^\ell] \left[\underset{\sim}{N}_{\ell,\,1}^{(1)} + \underset{\sim}{N}_{\ell,\,-1}^{(1)}\right] \right\} ;$$

or

$$\underset{\sim}{E} \simeq \frac{\sqrt{\pi}}{2}(c+d) \sum_{\ell=1}^{\infty} i^{\ell-1} \sqrt{\frac{2\ell+1}{\ell(\ell+1)}} \left\{ \underset{\sim}{M}^{(1)}_{\ell,1} - \underset{\sim}{M}^{(1)}_{\ell,-1} + \underset{\sim}{N}^{(1)}_{\ell,1} + \underset{\sim}{N}^{(1)}_{\ell,-1} \right\} +$$

$$+ \frac{\sqrt{\pi}}{2}(c-d) \sum_{\ell=1}^{\infty} i^{\ell-1} \sqrt{\frac{2\ell+1}{\ell(\ell+1)}} (-1)^{\ell} \left\{ -\underset{\sim}{M}^{(1)}_{\ell,1} + \underset{\sim}{M}^{(1)}_{\ell,-1} + \underset{\sim}{N}^{(1)}_{\ell,1} + \underset{\sim}{N}^{(1)}_{\ell,-1} \right\} .$$

Recall the identity (23),

$$\underset{\sim}{e}_x e^{i\kappa z} = \sqrt{\pi} \sum_{\ell=1}^{\infty} i^{\ell-1} \sqrt{\frac{2\ell+1}{\ell(\ell+1)}} \left\{ \underset{\sim}{M}^{(1)}_{\ell,1} - \underset{\sim}{M}^{(1)}_{\ell,-1} + \underset{\sim}{N}^{(1)}_{\ell,1} + \underset{\sim}{N}^{(1)}_{\ell,-1} \right\} ,$$

Taking the complex conjugate, we also have

$$\underset{\sim}{e}_x e^{-i\kappa z} = \sqrt{\pi} \sum_{\ell=1}^{\infty} (-i)^{\ell-1} \sqrt{\frac{2\ell+1}{\ell(\ell+1)}} \left\{ \underset{\sim}{M}^{(1)}_{\ell,-1} - \underset{\sim}{M}^{(1)}_{\ell,1} + \underset{\sim}{N}^{(1)}_{\ell,1} + \underset{\sim}{N}^{(1)}_{\ell,-1} \right\} ,$$

where we have used

$$\underset{\sim}{M}^{(1)*}_{\ell,1} = \underset{\sim}{M}^{(1)}_{\ell,-1} \quad ; \quad \underset{\sim}{N}^{(1)*}_{\ell,1} = \underset{\sim}{N}^{(1)}_{\ell,-1} .$$

Consequently, this approximation for the internal field takes the simple form

$$\underset{\sim}{E} \simeq \frac{c+d}{2} \underset{\sim}{e}_x e^{i\kappa z} - \frac{c-d}{2} \underset{\sim}{e}_x e^{-i\kappa z} ,$$

the new feature being the appearance of the wave travelling in the backward direction.

The results are very similar to those of the modified Born approximation, given in (63), except that an additional term in $|\kappa \underset{\sim}{n}' + k\underset{\sim}{n}|$ appears. This results in a small backward peak, which is common and improves the large angle scattering. The approximation is presumably valid only when ε is small; or better when $(\sqrt{\varepsilon} - 1)\, ka \lesssim 1$.

The form of the internal field obtained by the arguments presented above suggests that the earlier approximations might be improved by adding a backward travelling wave. However, we have not pursued this point.

6. Estimate Using the Magnetic Field Integral Equation Including Surface Terms

This approximation will lead to polarization effects. To carry it out we use the W.K.B. interior wave number approximation, the third approximation discussed, since this seems to work best of those tried. From (59), (60), (61) and (62), we want to evaluate

$$\underset{\sim}{A}_2 = -\underset{\sim}{n}' \times \underset{\sim}{n}' \times [\underset{\sim}{D}' + \underset{\sim}{D}''] = - \underset{\sim}{n}' \times \underset{\sim}{n}' \times \underset{\sim}{D}_2 \ ;$$

where

$$\underset{\sim}{D}' = \frac{\varepsilon - 1}{4\pi} \ k^2 \int_{\text{sphere}} e^{-ik\underset{\sim}{n}' \cdot \underset{\sim}{r}'} \ \underset{\sim}{H}(\underset{\sim}{r}') \ dv' \ ,$$

and

$$D'' = \frac{ik(\varepsilon - 1)}{4\pi} \int_{\text{sphere}} e^{-ik\underset{\sim}{n}' \cdot \underset{\sim}{r}} \ \underset{\sim}{e}_r \times \underset{\sim}{E}(\underset{\sim}{r}) \ ds \ .$$

As before, for $r < a$, take

$$\underset{\sim}{E} = \frac{2}{\sqrt{\varepsilon} + 1} \ \underset{\sim}{e}_0 \ e^{ikz + i(\kappa - k)[z + \sqrt{a^2 - \rho^2}]},$$

except that the transmission coefficient at normal incidence, $2/(\sqrt{\varepsilon} + 1)$, has been introduced as a factor. On the surface S of the sphere

$$\underset{\sim}{E} = \frac{2}{\sqrt{\varepsilon} + 1} \ \underset{\sim}{e}_0 \ e^{ikz}, \quad \pi/2 \leq \Theta \leq \pi \ ;$$

$$\underset{\sim}{E} = \frac{2}{\sqrt{\varepsilon} + 1} \ \underset{\sim}{e}_0 \ e^{ikz + 2k(\kappa - k)z}, \quad 0 \leq \Theta \leq \pi/2 \ .$$

Corresponding to $\underset{\sim}{E}$, $\underset{\sim}{H}$ can be obtained by (24) and yields $(r < a)$

$$\underset{\sim}{H} = \frac{2\sqrt{\varepsilon}}{\sqrt{\varepsilon}+1}\,(\underset{\sim}{e}_z \times \underset{\sim}{e}_0)e^{ikz + i(\kappa - k)\left[z + \sqrt{a^2 - \rho^2}\right]} \quad .$$

Upon substitution, it then follows from (64) and (67) that

$$\underset{\sim}{D}' = \frac{2\sqrt{\varepsilon}}{\sqrt{\varepsilon}+1}\,(\underset{\sim}{e}_z \times \underset{\sim}{e}_0)\,\frac{(\varepsilon - 1)\,ka^2}{2i(\sqrt{\varepsilon} - \cos\Theta)}\,(I_1 - I_2) \quad ,$$

where I_1 and I_2 are given in (67). Now look at $\underset{\sim}{D}''$ noting that

$$\underset{\sim}{e}_r \times \underset{\sim}{e}_0 = (\underset{\sim}{e}_z \times \underset{\sim}{e}_0)\,\underset{\sim}{e}_r \cdot \underset{\sim}{e}_z - \underset{\sim}{e}_z\,\underset{\sim}{e}_r \cdot (\underset{\sim}{e}_z \times \underset{\sim}{e}_0)$$

$$= (\underset{\sim}{e}_z \times \underset{\sim}{e}_0)\cos\Theta - \underset{\sim}{e}_z \sin\Theta \sin\phi \ ,$$

where $\underset{\sim}{e}_0$ is taken as the reference axis for ϕ. Then we find

$$\underset{\sim}{D}'' = \frac{2}{\sqrt{\varepsilon}+1}\,\frac{ik(\varepsilon - 1)}{4\pi}\,a^2 \Bigg\{ \Bigg[\int_{\pi/2}^{\pi} e^{2ika \sin^2\Theta/2 \cos\Theta} + \int_0^{\pi/2} e^{2ia(\kappa - k\cos^2\Theta/2)\cos\Theta} \Bigg]$$

$$\times \int_0^{\pi/2} e^{-ika \sin\Theta \sin\Theta \cos(\phi - \phi')}$$

$$\times \left[(\underset{\sim}{e}_z \times \underset{\sim}{e}_0)\cos\Theta - \underset{\sim}{e}_z \sin\Theta \sin\phi \right]$$

$$\times \sin\Theta \, d\Theta d\phi \Bigg\}$$

$$= \frac{2}{\sqrt{\varepsilon}+1}\,\frac{ik(\varepsilon - 1)}{2}\,a^2 \left\{ (\underset{\sim}{e}_z \times \underset{\sim}{e}_0)\,[I_1 - I_2] + \underset{\sim}{e}_z\,[I_3 + I_4] \sin\phi' \right\} \quad ,$$

where ϕ' is the aximuth from $\underset{\sim}{e}_0$ of $\underset{\sim}{n}'$. The following relation

$$\int_0^{2\pi} \sin\phi\, e^{-i\gamma \cos(\phi - \phi')}\, d\phi = -2\pi i \sin\phi'\, J_1(\gamma)$$

is used to obtain

$$I_3 = i \int_0^{\pi/2} e^{2ika[(\varepsilon)^{\frac{1}{2}} - \cos^2\Theta/2]} \cos\theta \; \chi\, J_1(ka \sin\Theta \sin\theta) \sin^2\theta\, d\theta$$

and

$$I_4 = i \int_0^{\pi/2} e^{-2ika \sin^2\Theta/2 \cos\theta} \; \chi\, J_1(ka \sin\Theta \sin\theta) \sin^2\theta\, d\theta \; .$$

As before, I_1 and I_2 are given by (67). Finally, collecting results,

$$D_2 = i(\sqrt{\varepsilon} - 1)\, ka^2 \frac{\cos\Theta}{\sqrt{\varepsilon} - \cos\Theta} (I_2 - I_1)(\underset{\sim}{e}_z \times \underset{\sim}{e}_0) + i(\sqrt{\varepsilon} - 1)\, ka^2 \sin\phi' (I_3 + I_4)\, \underset{\sim}{e}_z \; .$$

Comparing with expression (67) for $\underset{\sim}{D}$, we see that the first term above is just $\underset{\sim}{D}$, multiplied by the factor $\cos\Theta$; the second term, which is the new feature, changes the plane of polarization. I_3 and I_4 can be evaluated by precisely the same saddle point methods as are used for I_1 and I_2. In the main diffraction peak, $ka\,\Theta^2 << 1$ (but not necessarily $ka\,\Theta << 1$), the main contribution comes from I_4;

$$I_4 \simeq i \int_0^{\pi/2} J_1(ka\,\mu\sin\theta)\sin^2\theta \; d\theta \simeq i j_1(ka\,\Theta) \quad .$$

This at least indicates how the polarization shifts in the main diffraction peaks. Outside the main diffraction peak, we merely remark that I_1, I_2, I_3, I_4 are all of the same order of magnitude, and hence the polarization at large angles is not simply related to the polarization of the incident wave. One final remark: for $\Theta = 0, \pi$, I_3 and I_4 vanish (as expected) and the integrals can be evaluated exactly. The result for forward scattering is exactly that of (66); for backward scattering it is the negative of the previous result. In both cases, the earlier results must be multiplied by the normalization factor $2/(\sqrt{\varepsilon} + 1)$.

III. SCATTERING MATRIX*

A. Definition

In the following we attempt to isolate the essential character of the scattering process. That is, we seek those properties which are independent of the detailed character of the scattering object (except that it be lossless) and depend only on the linearity of Maxwell's equations and on their asymptotic form. This asymptotic form is, of course,

$$r \to \infty : \quad \nabla \times \underset{\sim}{E} = ik\underset{\sim}{H}, \quad \nabla \times \underset{\sim}{H} = - ik\underset{\sim}{E} \quad , \tag{69}$$

since we assume $\varepsilon(\underset{\sim}{r}) \to 1, \quad r \to \infty$.

We now decompose the asymptotic solution for $\underset{\sim}{r} = \underset{\sim}{n}r, \; r \to \infty,$ into incoming and outgoing waves along $\underset{\sim}{n}$; that is, we write

$$\underset{\sim}{E}(\underset{\sim}{n}r) = \underset{\sim}{F}_1(\underset{\sim}{n}) \frac{e^{-ikr}}{r} + \underset{\sim}{F}_2(\underset{\sim}{n}) \frac{e^{ikr}}{r} \quad . \tag{70}$$

Since $\nabla \cdot \underset{\sim}{E} = 0,$ if we neglect higher order terms,

$$\underset{\sim}{F}_1 \cdot \underset{\sim}{n} = \underset{\sim}{F}_2 \cdot \underset{\sim}{n} = 0 \quad ; \tag{71}$$

the fields are thus transverse. Also,

$$\underset{\sim}{H}(\underset{\sim}{n}r) = \frac{1}{ik} \nabla \times \underset{\sim}{E} = - (\underset{\sim}{n} \times \underset{\sim}{F}_1) \frac{e^{-ikr}}{r} + (\underset{\sim}{n} \times \underset{\sim}{F}_2) \frac{e^{ikr}}{r} \tag{72}$$

Next, we examine the requirements imposed by energy conservation. The mean power flow is

$$\overline{\underset{\sim}{S}} = \frac{c}{8\pi} \mathrm{Re} \left\{ \underset{\sim}{E} \times \underset{\sim}{H}^* \right\} = \frac{c}{8\pi r^2} \mathrm{Re} \Big\{ - \underset{\sim}{F}_1 \times (\underset{\sim}{n} \times \underset{\sim}{F}_1^*) + \underset{\sim}{F}_2 \times (\underset{\sim}{n} \times \underset{\sim}{F}_2^*)$$

$$+ \underset{\sim}{F}_1 \times (\underset{\sim}{n} \times \underset{\sim}{F}_2^*) e^{-2ikr} - \underset{\sim}{F}_2 \times (\underset{\sim}{n} \times \underset{\sim}{F}_1^*) e^{2ikr} \Big\} \quad .$$

---

* For a parallel discussion in the acoustic case, see Gerjuoy and Saxon (1954).

Using (71), we then find

$$\bar{\underset{\sim}{S}} = \frac{c}{8\pi r^2} \mathrm{Re} \left\{ \underset{\sim}{n}(\underset{\sim}{F}_2 \cdot \underset{\sim}{F}_2^* - \underset{\sim}{F}_1 \cdot \underset{\sim}{F}_1^*) + \underset{\sim}{n}(\underset{\sim}{F}_1 \cdot \underset{\sim}{F}_2^* \; e^{-2ikr} - \underset{\sim}{F}_2 \cdot \underset{\sim}{F}_1^* \; e^{2ikr}) \right\}$$

$$= \frac{c}{8\pi r^2} \underset{\sim}{n}(\underset{\sim}{F}_2 \cdot \underset{\sim}{F}_2^* - \underset{\sim}{F}_1 \cdot \underset{\sim}{F}_1^*) \; ;$$

since we assume no sources except at infinity, conservation of energy requires

$$\int \bar{\underset{\sim}{S}} \cdot \underset{\sim}{n} r^2 \, d\Omega_n = 0 \; .$$

Therefore, we have derived the important relation

$$d\Omega_n \, [\underset{\sim}{F}_2(\underset{\sim}{n}) \cdot \underset{\sim}{F}_2^*(\underset{\sim}{n}) - \underset{\sim}{F}_1(\underset{\sim}{n}) \cdot \underset{\sim}{F}_1^*(\underset{\sim}{n})] = 0 \; , \tag{73}$$

which simply states that as much energy flows out of the closed region as flows in.

We now assert that the $\underset{\sim}{F}_1$ and $\underset{\sim}{F}_2$ must be linearly related as a consequence of the linearity of Maxwell's equations. Because $\underset{\sim}{F}_1$ and $\underset{\sim}{F}_2$ are vectors, the linear connective must be a tensor $\underset{\sim}{S}(\underset{\sim}{n}, \underset{\sim}{n}')$ which is called the scattering matrix, and which we define as follows:

$$\underset{\sim}{F}_2(\underset{\sim}{n}) = - \int d\Omega_{n'} \, \underset{\sim}{S}(\underset{\sim}{n}, \underset{\sim}{n}') \cdot \underset{\sim}{F}_1(-\underset{\sim}{n}') \; . \tag{74}$$

$\underset{\sim}{F}_2(\underset{\sim}{n})$ is the amplitude of an outgoing wave proceeding along $\underset{\sim}{n}$ and is thus given in terms of the amplitudes $\underset{\sim}{F}_1(-\underset{\sim}{n}')$ of the incoming waves proceeding along $(-\underset{\sim}{n}')$. In the definition, the choice of signs is not essential, but has the virtue that $\underset{\sim}{S}$ reduces to the unit matrix when there is no scattering. Note that dotting (74) with $\underset{\sim}{n}$,

$$\underset{\sim}{n} \cdot \underset{\sim}{F}_2(\underset{\sim}{n}) = - \int d\Omega_{n'} \underset{\sim}{n} \cdot \underset{\sim}{S}(\underset{\sim}{n}, \underset{\sim}{n}') \cdot \underset{\sim}{F}_1(-\underset{\sim}{n}') = 0 \; ,$$

because of (71). Since $\underset{\sim}{F}_1(-\underset{\sim}{n}')$ is arbitrary, this implies that $\underset{\sim}{n} \cdot \underset{\sim}{S}(\underset{\sim}{n}, \underset{\sim}{n}') = 0$.

B. General Properties of the Scattering Matrix

The detailed structure of the scattering matrix depends, of course, on the precise details of the scattering process, that is, on the particular behavior of $\underset{\sim}{S}(\underset{\sim}{r})$. However, there exists certain general characteristics of $\underset{\sim}{S}$ which are quite independent of such details. These follow from correspondingly general properties of Maxwell's equations -- namely, their symmetry properties and the property that energy must be conserved. We first establish the consequences of energy conservation as expressed by (73). Substitution of the definition (74) of $\underset{\sim}{S}$ then yields

$$\int d\Omega_n \left\{ \int\int \left[\underset{\sim}{S}(\underset{\sim}{n}, \underset{\sim}{n}') \cdot \underset{\sim}{F}_1(-\underset{\sim}{n}') \right] \cdot \left[\underset{\sim}{S}^*(\underset{\sim}{n}, \underset{\sim}{n}'') \cdot \underset{\sim}{F}_1^*(-\underset{\sim}{n}'') \right] \times d\Omega_{n''}\, d\Omega_{n'} - \underset{\sim}{F}_1(\underset{\sim}{n}) \cdot \underset{\sim}{F}_1^*(\underset{\sim}{n}) \right\} = 0 \quad . \tag{75}$$

Now,

$$\left[\underset{\sim}{S}(\underset{\sim}{n}, \underset{\sim}{n}') \cdot \underset{\sim}{F}_1(-\underset{\sim}{n}') \right] \cdot \left[\underset{\sim}{S}^*(\underset{\sim}{n}, \underset{\sim}{n}'') \cdot \underset{\sim}{F}_1^*(-\underset{\sim}{n}'') \right]$$

$$= \underset{\sim}{F}_1(-\underset{\sim}{n}') \cdot \tilde{\underset{\sim}{S}}(\underset{\sim}{n}, \underset{\sim}{n}') \cdot \underset{\sim}{S}^*(\underset{\sim}{n}, \underset{\sim}{n}'') \cdot \underset{\sim}{F}_1^*(-\underset{\sim}{n}'') \quad ,$$

where

$$\left[\tilde{\underset{\sim}{S}}(\underset{\sim}{n}, \underset{\sim}{n}') \right]_{ij} = \underset{\sim}{S}(\underset{\sim}{n}, \underset{\sim}{n}')_{ji} \quad .$$

Let

$$\int d\Omega_n \, \tilde{\underset{\sim}{S}}(\underset{\sim}{n}, \underset{\sim}{n}') \cdot \underset{\sim}{S}^*(\underset{\sim}{n}, \underset{\sim}{n}'') = \underset{\sim}{Q}(\underset{\sim}{n}', \underset{\sim}{n}'') \quad .$$

Define $\underset{\sim}{Q}_\perp(\underset{\sim}{n}', \underset{\sim}{n}'')$, the transverse part of $\underset{\sim}{Q}(\underset{\sim}{n}', \underset{\sim}{n}'')$ by $\underset{\sim}{Q} = \underset{\sim}{Q}_\perp + (\underset{\sim}{n}'\,\underset{\sim}{n}') \cdot \underset{\sim}{Q} + \underset{\sim}{Q} \cdot (\underset{\sim}{n}''\,\underset{\sim}{n}'') - (\underset{\sim}{n}'\,\underset{\sim}{n}') \cdot \underset{\sim}{Q} \cdot (\underset{\sim}{n}''\,\underset{\sim}{n}'')$; hence, $\underset{\sim}{n}' \cdot \underset{\sim}{Q}_\perp = \underset{\sim}{Q}_\perp \cdot \underset{\sim}{n}'' = 0$. Then if $\underset{\sim}{a}$ and $\underset{\sim}{b}$ are vectors perpendicular to $\underset{\sim}{n}'$ and $\underset{\sim}{n}''$ respectively, we see that

$$\underset{\sim}{a} \cdot \underset{\sim}{Q} \cdot \underset{\sim}{b} = \underset{\sim}{a} \cdot \underset{\sim}{Q}_\perp \cdot \underset{\sim}{b} \quad .$$

Replacing the dummy variable n in the last term of (75) by $\underset{\sim}{n}'$, we then have

$$\int d\Omega_{n'} \left\{ \underset{\sim}{F}_1(-\underset{\sim}{n}') \cdot \int d\Omega_{n''} \underset{\sim}{Q}_{\perp}(\underset{\sim}{n}', \underset{\sim}{n}'') \cdot \underset{\sim}{F}_1^*(-\underset{\sim}{n}'') - \underset{\sim}{F}_1(\underset{\sim}{n}') \cdot \underset{\sim}{F}_1^*(\underset{\sim}{n}') \right\} = 0 \quad .$$

Since $\underset{\sim}{F}_1(-\underset{\sim}{n})$ is arbitrary (except that it must remain transverse -- which is the reason only the transverse part of $\underset{\sim}{Q}$ appears); this implies

$$\underset{\sim}{Q}_{\perp}(\underset{\sim}{n}', \underset{\sim}{n}'') = \underset{\sim}{\varepsilon}_{\perp}(\underset{\sim}{n}')\, \delta(|\underset{\sim}{n}' - \underset{\sim}{n}''|) = \underset{\sim}{\varepsilon}_{\perp}(\underset{\sim}{n}'')\, \delta(|\underset{\sim}{n}' - \underset{\sim}{n}''|), \tag{76}$$

where $\underset{\sim}{\varepsilon}_{\perp}(\underset{\sim}{n})$ is the part of the unit dyad transverse to $\underset{\sim}{n}$; that is,

$$\underset{\sim}{\varepsilon}_{\perp}(n) = \underset{\sim}{\varepsilon} - \underset{\sim}{n}\,\underset{\sim}{n} \tag{77}$$

so that

$$\underset{\sim}{n} \cdot \underset{\sim}{\varepsilon}_{\perp}(\underset{\sim}{n}) = \underset{\sim}{\varepsilon}_{\perp}(\underset{\sim}{n}) \cdot \underset{\sim}{n} = 0 \quad . \tag{78}$$

Therefore, if $\underset{\sim}{A}$ is any vector perpendicular to $\underset{\sim}{n}$,

$$\underset{\sim}{\varepsilon}_{\perp} \cdot \underset{\sim}{A} = \underset{\sim}{A} \cdot \underset{\sim}{\varepsilon}_{\perp} = \underset{\sim}{A} \quad . \tag{79}$$

Now recall that $\underset{\sim}{n} \cdot \underset{\sim}{S}(\underset{\sim}{n}, \underset{\sim}{n}') = 0$ and note therefore that the definition (74) of $\underset{\sim}{S}$ is such that only $\underset{\sim}{S}_{\perp}$ is actually defined. Consequently, we can assume without loss of generality that also $\underset{\sim}{S} \cdot \underset{\sim}{n}' = 0$. Using

$$\underset{\sim}{n}' \cdot \underset{\sim}{\tilde{S}}(\underset{\sim}{n}, \underset{\sim}{n}') = \underset{\sim}{S}(\underset{\sim}{n}, \underset{\sim}{n}') \cdot \underset{\sim}{n}' = 0 \quad ,$$

it then follows that

$$\underset{\sim}{n}' \cdot \underset{\sim}{Q}(\underset{\sim}{n}', \underset{\sim}{n}'') = \underset{\sim}{Q}(\underset{\sim}{n}', \underset{\sim}{n}'') \cdot \underset{\sim}{n}'' = 0$$

and hence that $\underset{\sim}{Q} = \underset{\sim}{Q}_{\perp}$. Therefore, (76) yields the important relation

$$\int d\Omega_n \, \underset{\sim}{\tilde{S}}(\underset{\sim}{n}, \underset{\sim}{n}') \cdot \underset{\sim}{S}^*(\underset{\sim}{n}, \underset{\sim}{n}'') = \underset{\sim}{\varepsilon}_{\perp}(\underset{\sim}{n}') \, \delta(|\underset{\sim}{n}' - \underset{\sim}{n}''|) \quad . \tag{80}$$

Next, we derive a general reciprocity relation upon noting the following symmetry property of Maxwell's equations: If we take the complex conjugate of Maxwell's equations in the form (24), we see that

$$\nabla \times \underset{\sim}{E}^* = - ik\underset{\sim}{H}^*; \quad \nabla \times \underset{\sim}{H}^* = ik\underset{\sim}{\varepsilon}\underset{\sim}{E}^* \quad .$$

Accordingly, if $\underset{\sim}{E}$ and $\underset{\sim}{H}$ are solutions to Maxwell's equations, so are $\underset{\sim}{E}^*$ and $-\underset{\sim}{H}^*$; stated otherwise, if $\underset{\sim}{E}$, $\underset{\sim}{H}$ is a solution, a second solution can be constructed by the transformation $\underset{\sim}{E}^* \to \underset{\sim}{E}$ and $\underset{\sim}{H}^* \to -\underset{\sim}{H}$. Corresponding to the asymptotic solution (70), we thus construct a new asymptotic solution, namely

$$\underset{\sim}{E}(\underset{\sim}{n}r) = \underset{\sim}{F}_2^*(\underset{\sim}{n}) \, \frac{e^{-ikr}}{r} + \underset{\sim}{F}_1^*(\underset{\sim}{n}) \, \frac{e^{ikr}}{r} \, .$$

By the definition (74) of $\underset{\sim}{S}$, we thus have

$$\underset{\sim}{F}_1^*(\underset{\sim}{n}) = - \int d\Omega_{n'} \, \underset{\sim}{S}(\underset{\sim}{n}, \underset{\sim}{n}') \cdot \underset{\sim}{F}_2^*(-\underset{\sim}{n}') \quad .$$

Taking the complex conjugate and substituting (74) obtain

$$\underset{\sim}{F}_1(\underset{\sim}{n}) = \int d\Omega_{n'} \int d\Omega_{n''} \, \underset{\sim}{S}^*(\underset{\sim}{n}, \underset{\sim}{n}') \cdot \underset{\sim}{S}(-\underset{\sim}{n}', \underset{\sim}{n}'') \cdot \underset{\sim}{F}_1(-\underset{\sim}{n}'') \quad ,$$

which implies

$$\int d\Omega_{n'} \, \underset{\sim}{S}^*(\underset{\sim}{n}, \underset{\sim}{n}') \cdot \underset{\sim}{S}(-\underset{\sim}{n}', -\underset{\sim}{n}'') = \underset{\sim}{\varepsilon}_{\perp} \, \delta(|\underset{\sim}{n} - \underset{\sim}{n}''|) \quad . \tag{81}$$

Multiplying by $\underset{\sim}{\tilde{S}}(\underset{\sim}{n}, \underset{\sim}{n}''')$ and integrating with respect to $d\Omega_n$, we obtain $\underset{\sim}{\tilde{S}}(\underset{\sim}{n}'', \underset{\sim}{n}''')$ for the right side; using also (80), we obtain on the left $\underset{\sim}{S}(-\underset{\sim}{n}''', -\underset{\sim}{n}'')$. Thus, after the indices are relabeled, we arrive at the <u>reciprocity theorem</u> in its most general form:

$$\underset{\sim}{S}(\underset{\sim}{n}, \underset{\sim}{n}') = \underset{\sim}{\tilde{S}}(-\underset{\sim}{n}', -\underset{\sim}{n}) \quad . \tag{82}$$

It states that we obtain essentially the same results when we have an incident wave along $\underset{\sim}{n}'$, and observe along n, as when we have an incident wave along $-\underset{\sim}{n}$ and observe along $-\underset{\sim}{n}'$ (that is, interchange the source and the observer.)

The physical content of the proof is best understood upon remarking that the operation of taking the complex conjugate for harmonic time dependence is equivalent to changing the sign of the time t. Thus, the symmetry property invoked above is that Maxwell's equations are invariant under time reversal provided $\underset{\sim}{H}$ is replaced by $-\underset{\sim}{H}$. Since reversing the sign of t reverses the direction of travel of the waves, this sign change in $\underset{\sim}{H}$ is required to preserve the correct sense of energy flow. The reciprocity relation is thus easily seen to be a direct consequence of this invariance,for the incoming and outgoing waves are simply interchanged under time reversal.

Next we show that $\underset{\sim}{S}$ is unitary. This follows from (81) which, upon use of the reciprocity relation, becomes

$$\int d\Omega_n, \underset{\sim}{S}^*(\underset{\sim}{n}, \underset{\sim}{n}') \cdot \underset{\sim}{S}(\underset{\sim}{n}'', \underset{\sim}{n}') = \underset{\sim}{\varepsilon}_{\perp} \delta(\underset{\sim}{n} - \underset{\sim}{n}'') \quad . \tag{83}$$

This completes the proof, since regarding $\underset{\sim}{\tilde{S}}$ as a continuous super matrix, the conjugates of (80) and (83) can be written symbolically as

$$\underset{\sim}{S}^+ \underset{\sim}{S} = 1 \ ,$$

$$\underset{\sim}{S} \underset{\sim}{S}^+ = 1 \ ,$$

where the adjoint sign means to take the conjugate and to transpose all indices continuous and discreet.

B. Relation Between the Scattering Matrix and the Scattering Amplitude

We now relate the scattering amplitude $\underset{\sim}{A}(\underset{\sim}{n}, \underset{\sim}{n}_0)$, defined only for plane wave excitation, to the general scattering matrix $\underset{\sim}{S}$. For a plane wave incident along $\underset{\sim}{n}_0$, the field at infinity in the direction $\underset{\sim}{n}$ has the form

$$\underset{\sim}{E}(\underset{\sim}{n}r) = \underset{\sim}{e}\, e^{ikr\underset{\sim}{n}_0 \cdot \underset{\sim}{n}} + \underset{\sim}{A}(\underset{\sim}{n}, \underset{\sim}{n}_0) \frac{e^{ikr}}{r} \ ; \tag{84}$$

$\underset{\sim}{e}$ is a unit vector in the direction of polarization and is such that $\underset{\sim}{e} \cdot \underset{\sim}{n}_0 = 0$; the first term on the right is the plane incident, exciting wave; the second term is the scattered wave.

From (21)

$$e^{ikr\underset{\sim}{n}_0 \cdot \underset{\sim}{n}} = 4\pi \sum_{\ell=0}^{\infty} \sum_{m=0}^{m=\ell} i^{\ell} j_{\ell}(kr)\, Y_{\ell}^{m}(\underset{\sim}{n}_0)\, Y_{\ell}^{m*}(\underset{\sim}{n}) ,$$

where we have used the addition theorem for Legendre functions (Morse and Feshbach, 1953a)

$$Y_{\ell}(\underset{\sim}{n}_0, \underset{\sim}{n}) = \sum_{m=0}^{\ell} \sqrt{\frac{4\pi}{2\ell + 1}}\, Y_{\ell}^{m}(\underset{\sim}{n}_0)\, Y_{\ell}^{m*}(\underset{\sim}{n}) .$$

If we substitute the asymptotic form for $j_{\ell}(kr)$, we thus have

$$e^{ikr\underset{\sim}{n}_0 \cdot \underset{\sim}{n}} = \frac{4\pi}{kr} \sum_{\ell=0}^{\infty} \sum_{m=0}^{\ell} i^{\ell} \cos\left(kr - \frac{\ell + 1}{2}\pi\right) Y_{\ell}^{m}(\underset{\sim}{n}_0)\, Y_{\ell}^{m*}(\underset{\sim}{n})$$

$$= \frac{2\pi}{kr} \sum_{\ell=0}^{\infty} \sum_{m=0}^{\ell} i^{\ell} \left\{ e^{ikr}(-i)^{\ell+1} + e^{-ikr}(i)^{\ell+1} \right\}$$

$$\times\, Y_{\ell}^{m}(\underset{\sim}{n}_0)\, Y_{\ell}^{m*}(\underset{\sim}{n})$$

$$= \frac{2\pi i}{k} \left\{ -\frac{e^{ikr}}{r} \sum_{\ell=0}^{\infty} \sum_{m=0}^{\ell} Y_{\ell}^{m}(\underset{\sim}{n}_0)\, Y_{\ell}^{m*}(\underset{\sim}{n}) \right.$$

$$\left. + \frac{e^{-ikr}}{r} \sum_{\ell=0}^{\infty} \sum_{m=0}^{\ell} (-i)^{\ell} Y_{\ell}^{m}(\underset{\sim}{n}_0)\, Y_{\ell}^{m*}(\underset{\sim}{n}) \right\} .$$

Because the Y_{ℓ}^{m} form a complete, orthonormal set, this becomes

$$r \to \infty : \quad e^{ikr\underset{\sim}{n}_0 \cdot \underset{\sim}{n}} = \frac{2\pi i}{k} \left\{ -\frac{e^{ikr}}{r}\, \delta(|\underset{\sim}{n}_0 - \underset{\sim}{n}|) \right.$$

$$\left. + \frac{e^{-ikr}}{r}\, \delta\,|\underset{\sim}{n}_0 + \underset{\sim}{n}|) \right\} .$$

Substitution into (84) then yields

$$\underset{r \to \infty}{\underset{\sim}{E}(\underset{\sim}{n}r)} \simeq \frac{2\pi i}{k} \underset{\sim}{e}\, \delta(|\underset{\sim}{n}_0 + \underset{\sim}{n}|) \frac{e^{-ikr}}{r}$$

$$+ \left[\underset{\sim}{A}(\underset{\sim}{n}, \underset{\sim}{n}_0) - \frac{2\pi i}{k} \underset{\sim}{e}\, \delta(|\underset{\sim}{n}_0 - \underset{\sim}{n}|)\right] \frac{e^{ikr}}{r} \quad . \tag{85}$$

This is a special case of the general formulation in terms of incoming and outgoing waves with

$$\underset{\sim}{F}_1(\underset{\sim}{n}) = \frac{2\pi i}{k}\, \delta(|\underset{\sim}{n}_0 + \underset{\sim}{n}|)\, \underset{\sim}{e} \ ,$$

and

$$\underset{\sim}{F}_2(\underset{\sim}{n}) = \underset{\sim}{A}(\underset{\sim}{n}, \underset{\sim}{n}_0) - \frac{2\pi i}{k}\, \delta(|\underset{\sim}{n}_0 - \underset{\sim}{n}|)\, \underset{\sim}{e} \quad .$$

From the definition (74) of the scattering matrix, we thus have

$$\underset{\sim}{A}(\underset{\sim}{n}, \underset{\sim}{n}_0) = \frac{2\pi i}{k}\, \delta(|\underset{\sim}{n}_0 - \underset{\sim}{n}|)\, \underset{\sim}{e} - \frac{2\pi i}{k}\, \underset{\sim}{S}(\underset{\sim}{n}, \underset{\sim}{n}_0) \cdot \underset{\sim}{e} \quad . \tag{86}$$

Several interesting scattering properties follow from this result. The first is obtained by using the reciprocity relation. Let a plane, parallel wave be incident along $-\underset{\sim}{n}$, and consider the scattering along $-\underset{\sim}{n}_0$; let the polarization of the incident wave be along $\underset{\sim}{e}'$ ($\underset{\sim}{e}' \cdot \underset{\sim}{n} = 0$). Then, from (86)

$$\underset{\sim}{A}(-\underset{\sim}{n}_0, -\underset{\sim}{n}) = \frac{2\pi i}{k}\, \delta(|\underset{\sim}{n} - \underset{\sim}{n}_0|)\, \underset{\sim}{e}' - \frac{2\pi i}{k}\, \underset{\sim}{S}(-\underset{\sim}{n}_0, -\underset{\sim}{n}) \cdot \underset{\sim}{e}'$$

$$= \frac{2\pi i}{k}\, \delta(|\underset{\sim}{n} - \underset{\sim}{n}_0|)\, \underset{\sim}{e}' - \frac{2\pi i}{k}\, \underset{\sim}{e}' \cdot \tilde{\underset{\sim}{S}}(-\underset{\sim}{n}_0, -\underset{\sim}{n})$$

$$= \frac{2\pi i}{k}\, \delta(|\underset{\sim}{n} - \underset{\sim}{n}_0|)\, \underset{\sim}{e}' - \frac{2\pi i}{k}\, \underset{\sim}{e}' \cdot \underset{\sim}{S}(\underset{\sim}{n}, \underset{\sim}{n}_0) \ ,$$

with the aid of the reciprocity relation. If we dot this result with $\underset{\sim}{e}$ and (86) with $\underset{\sim}{e}'$, then subtract, we obtain

$$\underset{\sim}{e} \cdot \underset{\sim}{A}(-\underset{\sim}{n}_0, -\underset{\sim}{n}) = \underset{\sim}{e}' \cdot \underset{\sim}{A}(\underset{\sim}{n}, \underset{\sim}{n}_0) \ ;$$

that is, if the source and observer are interchanged, the scattering amplitude along the incident plane of polarization is the same in both cases. In the special case $\underset{\sim}{n} = \underset{\sim}{n}_0$ (forward scattering), this implies that for fixed plane of polarization

$$\underset{\sim}{A}(-\underset{\sim}{n}_0, -\underset{\sim}{n}_0) = \underset{\sim}{A}(\underset{\sim}{n}_0, \underset{\sim}{n}_0) \quad .$$

In words, regardless of the shape of the scatterer, when the observer is on the axis of transmission, the scattered wave he sees is unchanged if he interchanges position with the source.

A second relation is the previously mentioned cross-section theorem. To get this use equation (80):

$$\int d\Omega_n \, \underset{\sim}{\tilde{S}}(\underset{\sim}{n}, \underset{\sim}{n}_0) \cdot \underset{\sim}{S}^*(\underset{\sim}{n}, \underset{\sim}{n}_0') = \underset{\sim}{\varepsilon}_\perp \, \delta(|\underset{\sim}{n}_0 - \underset{\sim}{n}_0'|) \quad ;$$

or

$$\int d\Omega_n \left[\underset{\sim}{S}(\underset{\sim}{n}, \underset{\sim}{n}_0) \cdot \underset{\sim}{e}\right] \cdot \left[\underset{\sim}{S}^*(\underset{\sim}{n}, \underset{\sim}{n}_0') \cdot \underset{\sim}{e}'\right] = \underset{\sim}{e} \cdot \underset{\sim}{e}' \, \delta(|\underset{\sim}{n}_0 - \underset{\sim}{n}_0'|) .$$

By means of (86) express the $\underset{\sim}{S}$ in terms of the corresponding $\underset{\sim}{A}$'s, giving

$$\begin{aligned} &\int d\Omega_n \left[\frac{ik\underset{\sim}{A}_e(\underset{\sim}{n}, \underset{\sim}{n}_0)}{2\pi} + \delta(|\underset{\sim}{n}_0 - \underset{\sim}{n}|)\, \underset{\sim}{e}\right] \cdot \\ &\cdot \left[-\frac{ik\underset{\sim}{A}^*_{e'}(\underset{\sim}{n}, \underset{\sim}{n}_0')}{2\pi} + \delta(|\underset{\sim}{n}_0' - \underset{\sim}{n}|)\, \underset{\sim}{e}'\right] \\ &= \underset{\sim}{e} \cdot \underset{\sim}{e}' \, \delta(|n_0 - n_0'|) \quad , \end{aligned} \tag{87}$$

or

$$\begin{aligned} &\frac{k^2}{4\pi^2} \int \underset{\sim}{A}_e(\underset{\sim}{n}, \underset{\sim}{n}_0) \cdot \underset{\sim}{A}^*_{e'}(\underset{\sim}{n}, \underset{\sim}{n}_0') \, d\Omega_n \\ &= -\frac{ik}{2\pi} \left[\underset{\sim}{e}' \cdot \underset{\sim}{A}_e(\underset{\sim}{n}_0', \underset{\sim}{n}_0) - \underset{\sim}{e} \cdot \underset{\sim}{A}^*_{e'}(\underset{\sim}{n}_0, \underset{\sim}{n}_0')\right], \end{aligned}$$

where $\underset{\sim}{A}_e$ is the scattering amplitude arising from an incident wave whose plane of polarization is given by $\underset{\sim}{e}$. This in itself is a rather unusual and occasionally useful relation. The special case in which $\underset{\sim}{n}_0' = \underset{\sim}{n}_0$, $\underset{\sim}{e} = \underset{\sim}{e}'$ gives the famous cross-section theorem at once

$$\sigma_{tot} = \frac{4\pi}{k} \operatorname{Im} \left\{ \underset{\sim}{e} \cdot \underset{\sim}{A}(\underset{\sim}{n}_0, \underset{\sim}{n}_0) \right\} \quad . \tag{88}$$

To relate this back to the discussion at the end of Section I in terms of interference between the incident and scattered waves, note that in this treatment the incident wave is represented by the δ functions. Thus, the term on the left of (87), representing the total outgoing energy, contains the scattered energy, the outgoing energy in the incident wave, and the interference or product terms. The right side represents the incoming energy -- arising only from the incident wave, of course. The purely incident wave terms cancel, as they must; and hence, we are left with the scattering term plus the interference term. As asserted earlier, these give rise to the cross-section theorem.

We note in passing that for scattering from a sphere, the forward scattering amplitude $\underset{\sim}{A}$ is in the direction of $\underset{\sim}{e}$. Hence, $\sigma_{tot} = \frac{4\pi}{k}$ times the imaginary part of the scalar amplitude of $\underset{\sim}{A}$ for forward scattering. For example, for the W.K.B. interior wave number approximation, if formulas (58) and (66) are substituted into (88), together with the normalization factor $\frac{2}{(\varepsilon)^{\frac{1}{2}} + 1}$, then

$$\sigma_{tot} = 2\pi a^2 \left[1 - \frac{\sin 2(n-1)\alpha}{(n-1)\alpha} + \frac{1 - \cos 2(n-1)\alpha}{2(n-1)^2 \alpha^2} \right].$$

This has reasonable features such as the approximately correct period, $(n-1)\alpha = \pi$, and in the geometrical optical limit, $(n-1)\alpha \to \infty$, $\sigma_{tot} = 2\pi a^2$.

Finally, we observe that $\underset{\sim}{A}_e(\underset{\sim}{n}, \underset{\sim}{n}_0)$ as given in (86) can be written in the form

$$\underset{\sim}{A}_e(\underset{\sim}{n}, \underset{\sim}{n}_0) = \frac{2\pi i}{k} \left[\delta(|\underset{\sim}{n}_0 - \underset{\sim}{n}|)\, \underset{\sim}{\varepsilon} - \underset{\sim}{S}(\underset{\sim}{n}, \underset{\sim}{n}_0) \right] \cdot \underset{\sim}{e}$$

using (79). Hence, we are led to the idea of a tensor scattering amplitude $\mathcal{A}(n, n_0)$ given by

$$\underset{\sim}{\mathscr{A}}(\underset{\sim}{n}, \underset{\sim}{n}_0) = \frac{2\pi i}{k} \left| \delta(|\underset{\sim}{n} - \underset{\sim}{n}_0|) \underset{\sim}{\varepsilon}_\perp - \underset{\sim}{S}(\underset{\sim}{n}, \underset{\sim}{n}_0) \right| \tag{89}$$

Note that $\underset{\sim}{n} \cdot \underset{\sim}{\mathscr{A}} = \underset{\sim}{\mathscr{A}} \cdot \underset{\sim}{n}_0 = 0$, and that evidently

$$\underset{\sim}{A}_e = \underset{\sim}{\mathscr{A}} \cdot \underset{\sim}{e} \ .$$

Now suppose $\underset{\sim}{e}_1$ and $\underset{\sim}{e}_2$ are two mutually perpendicular polarization directions, and $\underset{\sim}{A}_1$ and $\underset{\sim}{A}_2$ are the corresponding amplitudes. We then assert that

$$\underset{\sim}{\mathscr{A}} = \underset{\sim}{A}_1\underset{\sim}{e}_1 + \underset{\sim}{A}_2\underset{\sim}{e}_2 \ , \tag{90}$$

since this satisfies all of the requirements, namely

$$\underset{\sim}{\mathscr{A}} \cdot \underset{\sim}{e}_1 = \underset{\sim}{A}_1, \quad \underset{\sim}{\mathscr{A}} \cdot \underset{\sim}{e}_2 = \underset{\sim}{A}_2; \quad \underset{\sim}{n} \cdot \underset{\sim}{\mathscr{A}} = \underset{\sim}{\mathscr{A}} \cdot \underset{\sim}{n}_0 = 0 \ .$$

Of course, for a general incident plane of polarization given by $\underset{\sim}{e}$

$$\underset{\sim}{\mathscr{A}} \cdot \underset{\sim}{e} = \underset{\sim}{A}_e = \underset{\sim}{A}_1(\underset{\sim}{e}_1 \cdot \underset{\sim}{e}) + \underset{\sim}{A}_2(\underset{\sim}{e}_2 \cdot \underset{\sim}{e}) \ ,$$

which is certainly correct since it is just the superposition principle. Accordingly, the final explicit expression for $\underset{\sim}{S}$, obtained by substituting (90) into (89), is

$$\underset{\sim}{S}(\underset{\sim}{n}, \underset{\sim}{n}_0) = \underset{\sim}{\varepsilon}_\perp \delta(|\underset{\sim}{n}_0 - \underset{\sim}{n}|) - \frac{k}{2\pi i} (\underset{\sim}{A}_1\underset{\sim}{e}_1 + \underset{\sim}{A}_2\underset{\sim}{e}_2) \ . \tag{91}$$

D. Multiple Scattering

We conclude with a few (unfortunately rather superficial) remarks about multiple scattering using the scattering matrix as a mechanism for the discussion. Consider an arbitrary array of scatterers 1, 2, 3, ... i ... j ... N, but for the simplicity take them to be far enough apart that the scattered field originating at any one of them is a pure radiation field when it reaches any other. With respect to a convenient origin, let $\underset{\sim}{r} = r\underset{\sim}{n}$ be the position vector to the point of observation, $\underset{\sim}{R}_i$ be the position vector of the i^{th} scatterer, and $\underset{\sim}{r}_i = \underset{\sim}{n}_i r_i = \underset{\sim}{n}_i|\underset{\sim}{r}-\underset{\sim}{R}_i|$ be the position of the observer with respect to the i^{th} scatterer.

Consider a plane wave

$$\underset{\sim}{E}_{inc} = \underset{\sim}{e}\, e^{ikr\underset{\sim}{n} \cdot \underset{\sim}{n}_0}, \quad \underset{\sim}{e} \cdot \underset{\sim}{n}_0 = 0 ,$$

incident along the direction $\underset{\sim}{n}_0$ on the array of scatterers. The total field at any point exterior to the scatterers is rigorously expressible as

$$\underset{\sim}{E}(\underset{\sim}{n}r) = \underset{\sim}{E}_{inc} \sum_{i=1}^{N} \underset{\sim}{E}_i(\underset{\sim}{n}_i r_i) , \tag{92}$$

where $\underset{\sim}{E}_i$ is the outgoing (scattered) field from the i^{th} scatterer. For large enough $r_i = | \underset{\sim}{r} - \underset{\sim}{R}_i |$,

$$\underset{\sim}{E}_i(\underset{\sim}{n}_i r_i) \simeq \underset{\sim}{f}_i(\underset{\sim}{n}_i) \frac{e^{ik | \underset{\sim}{r} - \underset{\sim}{R}_i |}}{| \underset{\sim}{r} - \underset{\sim}{R}_i |} .$$

Further, for $r \to \infty$, $| \underset{\sim}{r} - \underset{\sim}{R}_i | \simeq r - \underset{\sim}{R}_i \cdot \underset{\sim}{n}$, and $\underset{\sim}{n}_i \to \underset{\sim}{n}$, so that

$$\underset{\sim}{E}_i(\underset{\sim}{n}_i r_i) \simeq \underset{\sim}{f}_i(\underset{\sim}{n})\, e^{-ik\underset{\sim}{n} \cdot \underset{\sim}{R}_i} \frac{e^{ikr}}{r}$$

The total scattered field at infinity is thus expressible as

$$\underset{\sim}{E}_{sctd}(\underset{\sim}{n}r) \simeq \frac{e^{ikr}}{r} \sum_{i=1}^{N} \underset{\sim}{f}_i(\underset{\sim}{n})\, e^{-ik\underset{\sim}{n} \cdot \underset{\sim}{R}_i} .$$

The total scattering amplitude is seen to be the sum of the individual scattering amplitudes modified by a phase factor appropriate to the choice of origin. The individual scattering amplitudes are not to be confused with the plane wave, single scattering amplitudes treated earlier. The individual scattering amplitudes discussed in this section involve the total interaction of the scatterers with each other and with the incident field.

To determine the $\underset{\sim}{f}$'s we now decompose the total field in the neighborhood of the j^{th} scatterer into its incoming and outgoing parts with respect to that scatterer, since the fields are related by the (assumed known) scattering matrix. Consider first the incident field. We have

$$\underset{\sim}{E}_{inc}(\underset{\sim}{n}\underset{\sim}{r}) = \underset{\sim}{e}e^{ik\underset{\sim}{n}_0 \cdot \underset{\sim}{r}} = \underset{\sim}{e}e^{i\underset{\sim}{n}_0 \cdot \underset{\sim}{R}_j}e^{ik\underset{\sim}{n}_0 \cdot (\underset{\sim}{r} - \underset{\sim}{R}_j)}$$

$$= \underset{\sim}{e}e^{ik\underset{\sim}{n}_0 \cdot \underset{\sim}{R}_j}e^{ikr_j\underset{\sim}{n}_0 \cdot \underset{\sim}{n}_j} ;$$

or, using the plane wave expression (85),

$$\underset{\sim}{E}_{inc} \simeq \underset{\sim}{e}e^{ik\underset{\sim}{n}_0 \cdot \underset{\sim}{R}_j} \frac{2\pi i}{k} \left[\delta_0(|\underset{\sim}{n}_0 + \underset{\sim}{n}_j|) \frac{e^{-ikr_j}}{r_j} - \delta_0(|\underset{\sim}{n}_0 - \underset{\sim}{n}_j|) \frac{e^{ikr_j}}{r_j}\right] . \tag{93}$$

Next, consider the scattered wave $\underset{\sim}{E}_i(\underset{\sim}{n}_i\underset{\sim}{r}_i)$, $i \neq j$. Because of our assumption that the scatterers are far apart,

$$\underset{\sim}{E}_i(\underset{\sim}{n}_i\underset{\sim}{r}_i) \simeq \underset{\sim}{f}_i(\underset{\sim}{n}_i) \frac{e^{ik|\underset{\sim}{r} - \underset{\sim}{R}_i|}}{|\underset{\sim}{r} - \underset{\sim}{R}_i|} = \underset{\sim}{f}_i(\underset{\sim}{n}_i) \frac{e^{ik|\underset{\sim}{r}_j + \underset{\sim}{R}_{ij}|}}{|\underset{\sim}{r}_j + \underset{\sim}{R}_{ij}|} ,$$

where

$$\underset{\sim}{r}_j = \underset{\sim}{r} - \underset{\sim}{R}_j = \underset{\sim}{n}_j r_j, \quad \underset{\sim}{R}_{ij} = \underset{\sim}{R}_j - \underset{\sim}{R}_i = \underset{\sim}{n}_{ij}R_{ij} .$$

Assuming now that $R_{ij} >> r_j$, that is, that we are in the neighborhood of the j^{th} scatterer (but still in its radiation field), we have

$$|\underset{\sim}{r}_j + \underset{\sim}{R}_{ij}| \simeq R_{ij} + \underset{\sim}{n}_{ij} \cdot \underset{\sim}{n}_j r_j .$$

Therefore, for $i \neq j$,

$$\underset{\sim}{E}_i \simeq \underset{\sim}{f}_i(\underset{\sim}{n}_i) \frac{e^{ikR_{ij}}}{R_{ij}} e^{ikr_j \underset{\sim}{n}_{ij} \cdot \underset{\sim}{n}_j}$$

so that from the familiar expansion for a plane wave we have,

$$i \neq j, \quad \underset{\sim}{E}_i \simeq \underset{\sim}{f}_i(\underset{\sim}{n}_i) \frac{e^{ikR_{ij}}}{R_{ij}} \frac{2\pi i}{k} \left[\delta(|\underset{\sim}{n}_j + \underset{\sim}{n}_{ij}|) \right.$$

$$\left. \frac{e^{-ikr_j}}{r_j} - \delta(|\underset{\sim}{n}_j - \underset{\sim}{n}_{ij}|) \frac{e^{ikr_j}}{r_j} \right] .$$

Substitution of this result, along with (93), into the expression (92) for the total field then yields for the field in the neighborhood of the j^{th} scatterer,

$$\underset{\sim}{E} \simeq \frac{2\pi i}{k} \left\{ e^{ik\underset{\sim}{n}_0 \cdot \underset{\sim}{R}_{j\underset{\sim}{e}}} \delta(|\underset{\sim}{n}_0 + \underset{\sim}{n}_j|) \right.$$

$$\left. + \sum_{\substack{i=1 \\ i \neq j}}^{N} \frac{e^{ikR_{ij}}}{R_{ij}} \underset{\sim}{f}_i(\underset{\sim}{n}_i) \delta(|\underset{\sim}{n}_{ij} + \underset{\sim}{n}_j|) \right\} \frac{e^{-ikr_j}}{r_j}$$

$$+ \left\{ \underset{\sim}{f}_j(\underset{\sim}{n}_j) - \frac{2\pi i}{k} \left[e^{ik\underset{\sim}{n}_0 \cdot \underset{\sim}{R}_{j\underset{\sim}{e}}} \delta(|\underset{\sim}{n}_0 - \underset{\sim}{n}_j|) \right.\right.$$

$$\left.\left. + \sum_{\substack{i=1 \\ i \neq j}}^{N} \frac{e^{ikR_{ij}}}{R_{ij}} \underset{\sim}{f}_i(\underset{\sim}{n}_i) \delta(|\underset{\sim}{n}_{ij} - \underset{\sim}{n}_j|) \right] \right\} \frac{e^{ikr_j}}{r_j} .$$

This completes the decomposition into incoming and outgoing waves with respect to the j^{th} scatterer. From the definition (74) of the scattering matrix $\underset{\sim}{S}_j$ for the j^{th} scatterer, we must then have

$$\underset{\sim}{f}_j(\underset{\sim}{n}_j) - \frac{2\pi i}{k} e^{ik\underset{\sim}{n}_0 \cdot \underset{\sim}{R}_{je}} \delta(|\underset{\sim}{n}_0 - \underset{\sim}{n}_j|)$$

$$+ \sum_{\substack{i=1 \\ i\neq j}}^{N} \frac{e^{ikR_{ij}}}{R_{ij}} \underset{\sim}{f}_i(\underset{\sim}{n}_{ij}) \delta(|\underset{\sim}{n}_{ij} - \underset{\sim}{n}_j|)$$

$$= -\frac{2\pi i}{k} \left[e^{ik\underset{\sim}{n}_j \cdot \underset{\sim}{R}_j} \underset{\sim}{S}_j(\underset{\sim}{n}_j, \underset{\sim}{n}_0) \cdot \underset{\sim}{e} \right.$$

$$\left. + \sum_{\substack{i=1 \\ i\neq j}}^{N} \frac{e^{ikR_{ij}}}{R_{ij}} \underset{\sim}{S}_j(\underset{\sim}{n}_j, \underset{\sim}{n}_{ij}) \cdot \underset{\sim}{f}_i(\underset{\sim}{n}_{ij}) \right] ;$$

or using (89),

$$\underset{\sim}{f}_j(\underset{\sim}{n}_j) = \underset{\sim}{A}_j(\underset{\sim}{n}_j, \underset{\sim}{n}_0) \cdot \underset{\sim}{e}$$

$$+ \sum_{\substack{i=1 \\ i\neq j}}^{N} \frac{e^{ikR_{ij}}}{R_{ij}} \underset{\sim}{A}_j(\underset{\sim}{n}_j, \underset{\sim}{n}_{ij}) \cdot \underset{\sim}{f}_i(\underset{\sim}{n}_{ij}) \quad . \tag{94}$$

This is a set of N simultaneous equations (one for each value of j) for the N unknown scattering amplitudes $\underset{\sim}{f}_j$. The structure of these equations, physically, is quite clear: the scattering amplitude of each scattering center is just the sum of the amplitude for scattering the incident plane wave, and the amplitudes for scattering the waves originating at all the other scatterers (these waves being treated as plane waves of amplitude $\frac{e^{ikR_{ij}}}{R_{ij}} \underset{\sim}{f}_i(\underset{\sim}{n}_{ij})$, because of the assumption that the scatterers are far apart).

The solution of the multiple scattering equations is another matter, of course. We only remark on the obvious limit in which the scattering is small. In this case, the sum in (94) can be regarded as a correction, and the zero order approximation to $\underset{\sim}{f}$ is then the single scattering result

$$\underset{\sim}{f}_j^{(0)}(\underset{\sim}{n}_j) = \underset{\sim}{A}_j(\underset{\sim}{n}_j, \underset{\sim}{n}_0) \cdot \underset{\sim}{e} \quad .$$

Substituting this zero order approximation into the summation, we obtain the first order result

$$\underset{\sim}{f}_j^{(1)}(\underset{\sim}{n}_j) = \underset{\sim}{\mathcal{A}}_j(\underset{\sim}{n}_j, \underset{\sim}{n}_0) \cdot \underset{\sim}{e} + \sum_{\substack{i=1 \\ i\neq j}}^{N} \frac{e^{ikR_{ij}}}{R_{ij}} \times \underset{\sim}{\mathcal{A}}_j(\underset{\sim}{n}_j, \underset{\sim}{n}_{ij}) \cdot \underset{\sim}{f}_i^{(0)}(\underset{\sim}{n}_{ij})$$

$$= \underset{\sim}{\mathcal{A}}_j(\underset{\sim}{n}_j, \underset{\sim}{n}_0) \cdot \underset{\sim}{e} + \sum_{\substack{i=1 \\ k\neq j}}^{N} \frac{e^{ikR_{ij}}}{R_{ij}} \underset{\sim}{\mathcal{A}}_j(\underset{\sim}{n}_j, \underset{\sim}{n}_{ij}) \cdot \underset{\sim}{\mathcal{A}}_j(\underset{\sim}{n}_{ij}, \underset{\sim}{n}_0) \cdot \underset{\sim}{e} \quad .$$

This is just the sum of single and double scattering. Repeating the process, we then obtain the iterative "solution"

$$\underset{\sim}{f}_j^{(\rho)}(\underset{\sim}{n}_j) = \underset{\sim}{\mathcal{A}}_j(\underset{\sim}{n}_j, \underset{\sim}{n}_0) \cdot \underset{\sim}{e} + \sum_{\substack{i=1 \\ i\neq j}}^{N} \frac{e^{ikR_{ij}}}{R_{ij}} \times \underset{\sim}{\mathcal{A}}_j(\underset{\sim}{n}_j, \underset{\sim}{n}_{ij}) \cdot \underset{\sim}{f}_i^{(\rho-1)}(\underset{\sim}{n}_{ij}) \quad .$$

It need hardly be added that this is not very useful in practice.

REFERENCES*

E. Gerjuoy and D. S. Saxon, 1954: "Variational principles for the acoustic field." Phys. Rev. 94, 1445-1458.

R. W. Hart, 1951" "Sound scattering of a plane wave from a nonabsorbing sphere." J. Acoust. Soc. America. 23, 323-329.

R. Latter, 1951: "A scattering approximation." Phys. Rev. 83, 1056-1057.

H. Levine and J. Schwinger, 1950: "On the theory of electromagnetic wave diffraction by an aperture in an infinite plane conducting screen." Commun. on Applied Math. [1], 3, 355-391.

G. Mie, 1908: "Beitrage zur optik truber medien, speziell kolloidaler Metallosungen." Ann. der Physik. [4], 25, 377-445.

P. M. Morse and H. Feshbach, 1953a: Methods of theoretical physics, p. 1274, eqn. 10.3.38. New York: McGraw-Hill Book Co., Inc.

P. M. Morse and H. Feshbach, 1953b: Methods of theoretical physics, p. 1763-1791, New York: McGraw-Hill Book Co., Inc.

J. A. Stratton, 1941a: Electromagnetic theory, p. 418. New York: McGraw-Hill Book Co.,Inc.

J. A. Stratton, 1941b: Electromagnetic theory, p. 408-409. New York: McGraw-Hill Book Co., Inc.

J. A. Stratton, 1941c: Electromagnetic theory, p. 406. New York: McGraw-Hill Book Co., Inc.

G. N. Watson, 1944: A treatise on the theory of Bessel functions, 2nd ed., p. 370, eqn. 9. New York: The Macmillan Co.

* No attempt has been made to give a complete list of references. Additional references can be found in some of the standard texts -- e.g., Morse and Feshbach.

FIGURES

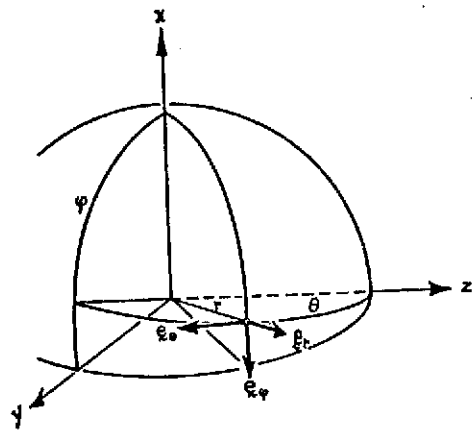

FIGURE 1

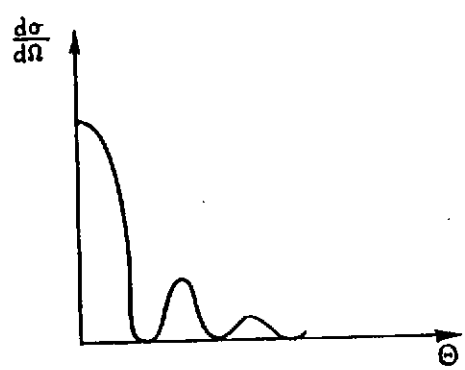

FIGURE 2

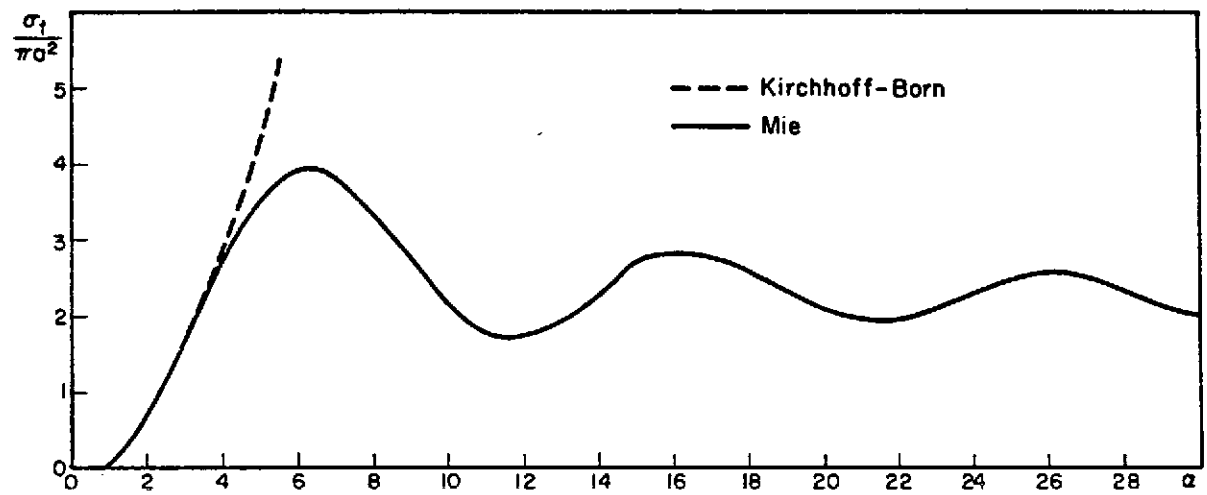

FIGURE 3

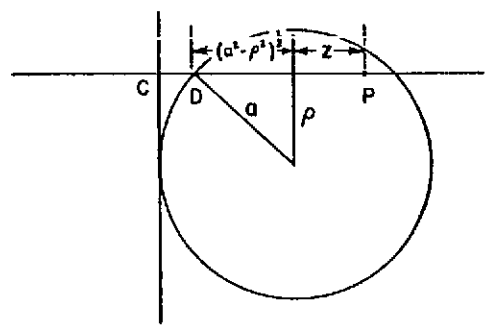

FIGURE 4

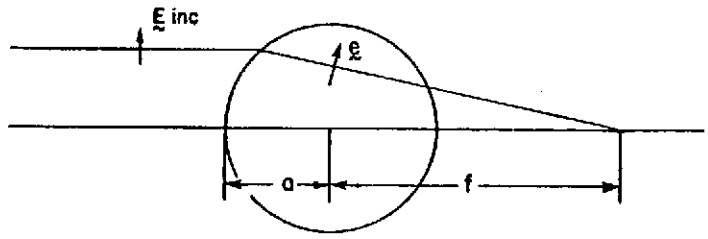

FIGURE 5

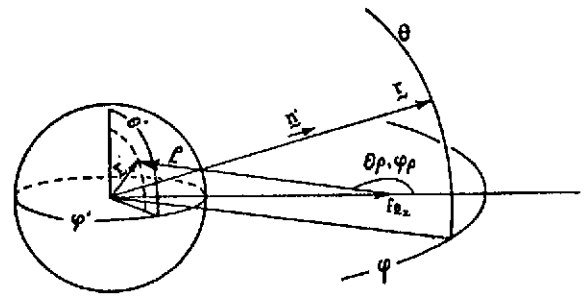

FIGURE 6

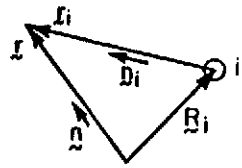

FIGURE 7

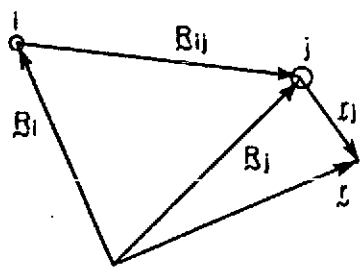

FIGURE 8

INFLUENCE OF THE ATMOSPHERE ON SPECTRAL RADIANCE AND CONTRASTS OF NATURAL FORMATIONS MEASURED FROM SPACE

K. Ya. Kondratyev, A. A. Buznikov, O. B. Vasilyev, and O. I. Smokty
Leningrad University
Leningrad, U.S.S.R.

Professor Z. Sekera's outstanding contribution to the theory of multiple scattering in the atmosphere created a basis for the consideration of various applications of this theory. One significant application is connected with the incorporation of atmospheric effects in solving various problems of remote sensing from space.

While studying the surfaces of such planets as the Earth or Mars by means of spectrophotometric instruments installed on board the space vehicle, it is necessary to take into account the transforming influence of the whole atmospheric thickness. Therefore, the problem on the correct reduction of the corresponding data of spectral measurements to the level of the underlying surface of the planet is urgent (1,2). A similar problem occurs in the interpretation of aerial photography data or in the recording of natural formations spectra from high-altitude aircrafts. In such cases, it is convenient to introduce the atmospheric transfer function of the surface-atmosphere system. The knowledge of this function permits, from spectral radiance of natural formations and contrasts of spectral radiance measured from a space vehicle or aircraft, the derivation of the corresponding characteristics at the lower boundary of the atmosphere.

In the reduction of space spectrophotometric data to the level of the underlying surface, two types of problems have to be solved. On the one hand, one must determine the transfer function and the possible limits of its variability depending on a) the optical characteristics of the atmosphere and the surface; b) the direction of viewing; and c) the geometry of the illumination of the upper atmospheric boundary by solar radiation. On the other hand, in the interest of the solution of inverse problems of atmospheric space optics, it is important to determine such characteristics as radiance of the atmospheric haze, $I_{h,\lambda}$, and the atmospheric transparency, T_λ, over the geographical regions investigated.

The possibility of determining the atmospheric transfer functions of the surface-atmosphere system based upon the experiment was first realized in papers (2-5), a theoretical solution of the corresponding problems was made in (6-10). However, a complete study of the problem, i.e., a detailed comparison between the experimental and theoretical values of the transfer functions has not been made. The objective of the present paper is to discuss the technique for determining the transfer functions and their components from the results of a combined sub-satellite experiment and to compare in detail the corresponding theoretical and experimental data.

1. FORMULATION OF THE PROBLEM

We shall regard the planetary atmosphere as restricted from below by the surface that reflects the solar radiation incident on it. The processes of scattering and absorption of radiation in the atmosphere will be allowed for. Refraction and polarization of radiation scattered by the atmosphere and reflected from the surface will be neglected.

Let the radiance of the surface objects $I_{ob,\lambda}$ and of the background $I_{b,\lambda}$ be measured from space in various spectral regions $\Delta\lambda$ where λ is the wavelength. We must estimate the influence of the whole atmospheric thickness on radiance $I^{o}_{ob,\lambda}$ and $I^{o}_{b,\lambda}$ where the superscript o refers to the surface level. Let us define the spectral transfer functions of the surface-atmosphere system for radiance of the background $\Pi_{b,\lambda}$ and the object $\Pi_{ob,\lambda}$ by the following relations (for simplicity, the subscript λ will be omitted):

$$I^{0}_{b} = \Pi_{b} \cdot I_{b} \tag{1}$$

$$I^{0}_{ob} = \Pi_{ob} \cdot I_{ob} \tag{2}$$

One can represent spectral radiance of the background I_b and of the object I_{ob} in the form:

$$I_{b} = I^{0}_{b} \cdot T + I_{h,b} \tag{3}$$

$$I_{ob} = I^{0}_{ob} \cdot T + I_{h,ob} \tag{4}$$

where $I_{h,ob}$ and $I_{h,b}$ are spectral radiances of the atmospheric haze over the object and the background, T is the spectral transmission factor (atmospheric transparency) in the fixed direction whose values are assumed equal over the object and the background.

Using (3) - (4), we shall represent relations (1) - (2) in the form:

$$\Pi_{b} = \frac{1}{P_{b} \cdot T} \quad ; \quad \Pi_{ob} = \frac{1}{P_{ob} \cdot T} \tag{5}$$

where

$$P_{b} = 1 + \frac{I^{b}_{h}}{I^{0}_{b} \cdot T} \quad ; \quad P_{ob} = 1 + \frac{I^{ob}_{h}}{I^{0}_{ob} \cdot T} \tag{6}$$

The transfer functions Π_b and Π_{ob} permit not only the reduction of satellite radiation data to the level of the surface but also the determination of the haze effect, which is important for the solution of some inverse problems of atmospheric optics. Substituting (1) - (2) into (3) - (4) and allowing for (5) - (6), we find:

$$I^{b}_{h} = I_{b}(1 - P^{-1}_{b}) = I_{b}(1 - \Pi_{b} \cdot T) \tag{7}$$

$$I_h^{ob} = I_{ob}(1 - P_{ob}^{-1}) = I_{ob}(1 - \Pi_{ob} \cdot T) \qquad (8)$$

Relations similar to (1) - (8) may be written for the spectral radiance coefficients Γ_{ob} and Γ_b defined as the ratio of the radiation reflected from the object and the background to the radiation incident on them.

According to the determination of the spectral contrast $(\kappa \geq 0)$ between radiance of the background and that of the object, we have

$$\kappa = \frac{I_{ob} - I_b}{I_{ob}} \qquad (9)$$

if $I_{ob} \geq I_b$. If $I_b > I_{ob}$, the modification of (9) is evident.

Substituting (3) and (4) into (9), we find

$$\kappa_0 = \mathcal{G} \cdot \kappa \qquad (10),$$

where κ_0 is the spectral contrast between radiance of the object and that of the background at the level of the surface,

$$\kappa_0 = \frac{I^0_{ob} - I^0_b}{I^0_{ob}} \qquad (11).$$

The following expression is valid for the function $\mathcal{G}$, (6)

$$\mathcal{G} = \frac{\kappa_h}{\kappa} + \mathcal{G}_{ob}\left(1 - \frac{\kappa_h}{\kappa}\right) \qquad (12),$$

where κ_h is the spectral contrast of the haze radiance over the object and the background

$$\kappa_h = \frac{I_h^{ob} - I_h^b}{I_h^{ob}} \qquad (13).$$

In the case of $\kappa_h \approx 0$, from (12) it follows that $\mathcal{G} \approx P_{ob}$.

We shall call the function $\mathcal{G}$ the spectral transfer function for the contrasts of radiance of the object and the background when $I_{ob} \geq I_b$. A similar determination may be obtained for the case $I_b \geq I_{ob}$.

It is to be emphasized that the reduction of satellite spectrophotometric data to the level of the underlying surface cannot be strictly performed in the framework of a satellite experiment (without using the data of aircraft and surface measurements). This may be explained by the fact that for a correct determination of the transfer functions Π and $\mathcal{G}$ from a satellite experiment it is necessary to solve a number of inverse problems of atmospheric optics: from the radiance of the

medium measured from space it is necessary, in the first place, to retrieve the optical characteristics of the medium at different levels of the atmosphere up to the surface of the planet and only then can one perform the reduction of spectrophotometric data for a specific type of surface. As is known, a strict formulation and the methods for the solution of inverse problems of atmospheric space optics (in the presence of multiple scattering in the surface-atmosphere system) has not yet been developed. Therefore, it is timely to develop different semi-empirical techniques which would permit a sufficiently accurate consideration of the influence of atmospheric effects on spectral radiance of natural formations during space survey. One such technique based upon the parameterization of the expressions for I_b and I_{ob} and the usage of the data on radiance of natural formations measured from several points of the spacecraft orbit is proposed in (9) . The determination of transfer functions and of their components is much easier in the case of combined subsatellite experiments, where the transfer functions Π and $\mathcal{J}$ may be found from a simple comparison of radiance measured from the spacecraft and the aircraft.

The second possibility of determining transfer functions consists in the preliminary determination of their components, viz., of the haze radiance and the atmospheric transparency from relations (3)-(4) considered as a system of linear algebraic equations. Thereupon, it is necessary that the radiance of the object and the background at the level of the underlying surface should be known from the aircraft (surface) measurements synchronized with satellite measurements in time and space. In a general case, the system of algebraic equations (3)-(4) is indefinite since $I_h^b \neq I_h^{ob}$. Consequently, the solution of the given system is possible only if the values for I_h^b and I_h^{ob} are coincident or close to each other. The technique of "smoothing" the values for haze radiance over the background I_h^b and the object I_h^{ob} is given in (3,6,9).

2. THEORETICAL DETERMINATION OF TRANSFER FUNCTIONS.

A theoretical determination of the transfer function for spectral radiance Π and the contrasts $\mathcal{J}$ involves the main problems of the transfer theory of nonpolarized solar radiation: the consideration of multiple scattering at a strong elongation of the aerosol scattering function and the reflection from the nonuniform underlying surface. A detailed investigation of these problems is made in (11-12).

The application of a theory of anisotropic light scattering to the determination of the transfer functions Π and $\mathcal{J}$ is given in (6, 9, 13) .

Considering the formulation of the problem on the theoretical determination of the transfer function for the surface-atmosphere system radiance is known, we shall present the main formulas and relations which may be interesting for a subsequent analysis and comparison with the experimental data.

2.1 The case of the uniform infinitely extensive underlying surface.

In this case we have: $I_b = I_{ob} = I(\eta, \xi, \phi, \tau_0)$; $I_h^b = I_h^{ob} = I_h(\eta, \xi, \phi, \tau_0)$; $\Pi_b = \Pi_{ob} = \Pi(\eta, \xi, \phi, \tau_0)$. The angular coordinates η, ξ, ϕ and the optical thickness τ_0 are determined according to (6, 7). The expression for the transfer function has a form:

$$\Pi(\eta, \xi, \phi, \tau_0) = \frac{A\mu(\xi, \tau_0)}{[1 - Ac(\tau_0)]\,\rho(\eta, \xi, \phi, \tau_0) + A\mu(\eta, \tau_0)\,\mu(\xi, \tau_0)} \qquad (14),$$

where A is the albedo of the underlying surface, the functions $\mu(\xi, \tau_0)$, $\rho(\eta, \xi, \phi, \tau_0)$ and $C(\tau_0)$ are determined in (11).

As shown in (9), the tabulation of the functions $\mu(\xi, \tau_0)$ and $\nu(\eta, \tau_0)$ associated with the reflection and transmission coefficients for the plane layer at $\tau = \tau_0$ is very important for the calculation of the transfer function. According to (12) for an arbitrary scattering function, the functions μ and ν are simply expressed through ϕ_i^m and $\bar{\psi}_i^m$, i.e., Ambartsumyan's functions

$$\mu(\eta, \tau_0) = \psi_i^0(\eta, \tau_0) \cdot \frac{1}{\eta} \quad ; \quad \nu(\eta, \tau_0) = 1 - \frac{\phi_1^0(\eta, \tau_0)}{\eta} \qquad (15).$$

The tabulation of these functions which depend only on the optical atmospheric model permits the determination of the transfer functions of the surface-atmosphere system for any fixed albedo of the reflecting bottom.

2.2 The case of the infinitely extensive underlying surface formed of two uniform semiplanes with the albedo A_i $(i = 1, 2)$.

First, let us consider spectrophotometric radiance measurements of the nonuniform underlying surface formed of two semiplanes with different albedo A_i $(i = 1, 2)$ far from the boundary of two types of the underlying surface. The subscripts $i=1$ and $i=2$ indicate the position of the uniform semiplane relative to the boundary (on its right or left). It is natural to suppose the optical properties of the atmosphere to be unchangeable in the horizontal direction.

In this case the expressions for radiance of the atmospheric haze $I_{h,i}$, radiance of the underlying surface $I_{o,i}$ and the transfer functions are $\Pi_i = \frac{I_{o,i}}{I_i}$ obtained by substituting the albedo A_i for the albedo of the underlying surface A.

For the transfer function of the contrasts of radiance $P_i = \frac{\kappa_i}{\kappa_{oi}}$ where

$$\kappa_i = \frac{|I_1 - I_2|}{I_i} \geq 0 \qquad \kappa_{o,i} = \frac{|I_{o,1} - I_{o,2}|}{I_{o,i}} \qquad (16)$$

we have the expression

$$P_i = 1 + \frac{S\xi\rho(\eta, \xi, \phi)}{I_{o,1}\,\mu(\xi)} \qquad (17).$$

The value of the subscript $i = 1,2$ varies in (16)-(17) depending on the relations $I_1 > I_2$ or $I_2 > I_1$. The transfer function Π_i and P_i are related in a simple way

$$\Pi_i = \frac{1}{P_i \mu} \tag{18}.$$

In the case of spectrophotometric measurements near the boundary between two types of the underlying surface the radiance field is formed under the influence of the albedo of both semiplanes, whereas, far from the boundary the radiance field depends either on A_1 or on A_2 (see, e.g., (14, 15)).

Let us consider that in the vicinity of the boundary (on both sides) radiance of the atmospheric haze is approximately equal and determined by the reflection from the underlying surface with the mean albedo $\overline{A} = \frac{1}{2}(A_1 + A_2)$:

$$\overline{I}_h = I_{h,i} = S\xi\left[\rho(n, \xi, \phi, \tau_0) + \frac{\overline{A}\mu(\xi, \tau_0)\, T_{\tau}(n, \tau_0)}{1 - \overline{AC}(\tau_0)}\right] \tag{19}$$

Radiance of the underlying surfaces $I_{0,i}$ may be presented as a sum of the mean radiance determined by the albedo $\overline{A}$ and the addition due to the deviation of the albedo from the mean value $\overline{A}$.

$$\overline{I}_{0,i} = \frac{\overline{A}\mu(\xi, \tau_0)\, S\xi}{1 - \overline{AC}(\tau_0)} + \frac{(A_i - \overline{A})}{1 - AC}\, \mu(\xi, \tau_0)\, S\xi = \frac{A_i \mu(\xi, \tau_0) S\xi}{1 - \overline{AC}} \tag{20}$$

As shown in (9), the transfer functions $\overline{\Pi}$ and P have the form:

$$\Pi_i = \frac{A_i\, \mu(\xi, \tau_0)}{[1 - \overline{AC}(\tau_0)]\, \rho(n, \xi, \phi, \tau_0) + \mu(\xi, \tau_0)[\overline{A} \cdot T_{\tau}(n, \tau_0) + A_i \cdot T(n, \tau_0)}} \tag{21},$$

$$\overline{P}_i = \frac{1}{\overline{\Pi}_i \cdot T} \tag{22}.$$

3. EXPERIMENTAL DETERMINATION OF TRANSFER FUNCTIONS.

During the flights of the spacecraft "Soyuz-7", "Soyuz-9" and the first orbital station "Salyut" the synchronous subsatellite geophysical experiments have been performed. The technique of these experiments was based on spatial and temporal synchronization of the measurements of spectral radiance of the individual parts of the earth's surface from the spacecraft and aircraft. Let us consider, briefly, the methodical peculiarities of the processing of the results of spectrophotometric measurements necessary for the determination of the surface-atmosphere system transfer functions from experiment. When the Earth is viewed from space ($h \sim 250$ km) in nadir the image of the earth's surface of the total area of 8×0.45 km^2 is projected onto the entrance slit of the spectrograph RSS-2 (2). Spectral radiance of the individual parts of the earth's surface is independently fixed on the film of the spectrograph. Thereupon, the spectra of two or more types of the underlying surface can be obtained simultaneously if the spectrophotometric measurements are conducted over their boundary.

The processing of the negatives on the standard microphotometer permitted us to obtain, from one frame, 18-19 reflection spectra of the individual parts of the underlying surface situated in the immediate proximity to each other. Their minimum area (0.40 x 0.45 km^2) is determined by the product of the limiting resolution of the spectrograph RSS-2 over the height of the slit (~ 2') by the slitwidth (~ 3'). Thus the spectrograph used allowed a simultaneous determination of spectral radiance of two and more parts of the underlying surface with the different values of albedo even from one frame. A series of frames gave the possibility of obtaining the radiance values for the underlying surfaces situated at any distance from the boundary.

As has been mentioned, a direct comparison between the results of synchronous spectrophotometric measurements of the same parts of the underlying surface from space and the low-altitude aircraft permitted the determination of the surface-atmosphere system transfer function immediately from formulas (1)-(2). Yet, it is rather difficult to ensure synchronous satellite and aircraft measurements of the same part of the underlying surface. A complete synchronization of measurements was achieved only once during the "Soyuz-7" flight over the Caspian coast (cape Begdash, October 13, 1969,13 hr, 27 min., Moscow time). However, a large number of spectra obtained permitted the performance of "quasisynchronized" experiments. In this case the transfer function Π was determined by comparing satellite data with the corresponding spectrophotometric characteristics of similar parts of the underlying surface measured from the aircraft or at the earth's surface at different times.

It is natural that the data corresponding to the meteorological conditions and sun elevations of a satellite experiment have been selected. Fig. 1a presents the results of synchronous spectrophotometric measurements of the same part of the desert on the cape Begdash from the spacecraft "Soyuz-7" (the height of the orbit is 220 km) and the aircraft LI-2 (the height of the aircraft is 2.7 km). The curves of spectral radiance show the influence of the atmospheric haze. As has been expected, the strongest effect of the atmospheric haze was observed in the shortwave region (λ = 450-570nm): curve 1 obtained from space is above curve 2 derived from the airborne measurements. In the wavelength range of λ = 570-610 nm the values of spectral radiance measured from space and at the earth's surface become equal. At λ = 620-680 nm the values of spectral radiance measured from the satellite are somewhat smaller compared to the aircraft measurements, which may be explained by absorption of reflected radiation by the atmospheric thickness. The values of the spectral transfer function calculated from these data are given in Fig. 1b.

Spectrophotometric measurements of natural formations from the "Soyuz-9" spacecraft were made on June 15 and 17, 1970 over the path - the North Caucasus-Caspian sea - UstUrt plateau. Since a complete temporal synchronization of the "Soyuz-9" and aircraft measurements was not achieved, in order to determine the transfer function Π_λ the quasisynchronization technique was used. "Space" spectra were compared with the spectra of the identified surfaces obtained from the aircraft and at the earth's surface.

Fig. 2 presents the experimental values of the transfer functions Π_λ for sand and water surfaces and continuous cloudiness obtained from the direct comparison of the results of spectral measurements. The measurements were taken at zenith distance of the sun Θ_0 = 33-45°. The difference between the transfer functions for a sand surface from the "Soyuz-7" (curve 1) and "Soyuz-9" (curve 3) data is due to the fact that curve 1 takes into account the influence of the atmospheric layer from 700 mb and higher, whereas, curve 3 corresponds to the transfer functions for the entire

atmospheric thickness.

To find the components of the transfer function, use was made of the results of spectrophotometric satellite and airborne measurements of the underlying surface radiance near the boundary of two areas with different albedo $A_i (i = 1, 2)$. In the subsequent solution of the equation system (3)-(4) radiance of the haze was considered equal near the boundary of two types of the underlying surface $(I_{h,i} = \overline{I}_h)$.

Of the "Soyuz-7" and aircraft spectra (UstUrt plateau, October 13, 1969) the spectra of two types of natural formations similar by their outer features on the RSS-2 photo have been selected: thick white cloudiness and the shaded dark areas of the desert (about 30 spectra). From these spectra the absolute values of spectral radiance in the wavelength range of 430-690 nm have been determined and then averaged for each type of the underlying surface. The values for I'_{ob}, I'_{b}, I''_{ob} and I''_{b} obtained correspond to the values of spectral radiance of the shaded parts of the desert and cloudiness measured from the spacecraft and aircraft (a height of the aircraft is 2700 m). The results of the solution of the (3)-(4) system are given in Fig. 3 a. Fig. 3 b presents the values of spectral transparency of the atmosphere and the mean coefficient of spectral radiance of haze obtained in a similar way using the spectral radiance coefficients measured from "Soyuz-9" and at the earth's surface near the boundary between the sand and the sea. From the results of space and aircraft measurements of spectral radiance, spectral contrasts of radiance of some natural formations have been calculated (1, 3). Fig. 4 presents spectral variation of transfer functions for the contrasts of radiance of the underlying surfaces: "desert-water surface" and desert-cloudiness". These transfer functions were constructed from the measurements taken on "Soyuz-9", the low-altitude aircraft and at the earth's surface.

4. COMPARISON OF THE MEASURED AND THEORETICALLY CALCULATED VALUES OF THE SPECTRAL TRANSFER FUNCTION.

For a detailed comparison between the measured and theoretically calculated values for the transfer functions Π_λ and $\mathcal{G}_\lambda$ it is necessary, first of all, to classify the experimental data according to the type of the nonuniformity of the underlying surface whose areas were projected on the entrance slit of the spectrograph during the measurements from space. Fig. 5 presents a schematic of the spectrograph RSS-2 frame and the calssification of the photos of the spectra of natural formations according to the type of the nonuniformity of the underlying surface measured. Let us compare theoretical and experimental data of the cases shown in Fig. 5.

Fig. 2 presents the experimental and theoretical curves of the transfer function Π_λ for three types of the uniform underlying surfaces: cloudiness, the desert and a water surface. The experimental values have been obtained from the results of the combined satellite and aircraft (surface) experiments. The corresponding theoretical values have been calculated by formula (14) according to the technique given in (13).

For the case of a large albedo of the underlying surface (cloudiness, $A = 0.78$, curves 2 and 6) a rather good coincidence between the theoretical and experimental curves is observed.

The experimental values of Π_λ for the desert surface according to the "Soyuz-7" data (curve 1) are slightly above the theoretical values (curve 5, A = 0.24). Similar curves obtained during the "Soyuz-9" flight coincide with the Π_λ -values calculated for a sand surface (curve 3). This behaviour of the experimental curves may be explained by the conditions under which the combined aircraft and satellite experiments were performed. As has been mentioned above, during the "Soyuz-7" flight the measurements of radiance of the underlying surfaces in the subsatellite region were conducted from the aircraft LI-2 at a height of 2700 m. Therefore the experimental Π_λ-values (curve 1) are somewhat overestimated as compared to the case when instead of the aircraft data the surface measurements were used (curve 3). A good coincidence between the experimental and theoretical curves for the overcast case may be explained by a large value for the cloud albedo, i.e., by a large contribution of the radiation reflected from the underlying surface and by the fact that during the combined experiment the cloud-top height (2200 m) was close to the height of the aircraft. The calculated values (curve 6) for a water surface are situated above the experimental values (curve 4). A comparison between the transfer functions in this case is difficult because of a small albedo value of the water surface and the prevailing influence of radiation scattered by the atmosphere.

Now, let us compare the experimental and theoretical values of transfer functions for the most interesting case of the nonuniform underlying surface formed by two uniform semiplanes with different albedos A_1 and A_2 (Fig. 5 b). As has been mentioned in section 2, this case may be reduced to the above example (Fig. 5 a) if the values of spectral radiance are determined far from the boundary of two underlying surfaces (at a distance exceeding the scale height). However, a comparison between the reflection spectra of natural formations obtained over the boundary of two underlying surfaces and the corresponding theoretical calculation is more difficult. This may be due to the complexity of the combined experiment over the boundary and an approximate character of expressions (19)-(22).

The transfer function near the boundary of two underlying surfaces, as in the case of the uniform underlying surface, may be determined from a direct comparison between the aircraft and satellite measurements. Yet, here arises an additional difficulty which is very important. It lies in the fact that in the spectrophotometric measurements of natural formations from the aircraft and space, the linear dimensions of the areas projected on the entrance slit of the spectrograph differ from each other by several orders. Due to the essential nonuniformity of the real underlying surfaces, a larger area of the underlying surface on the "space" frame causes a certain inadequacy with the corresponding "aircraft" frame.

Fig. 6 presents a comparison between the theoretical and the experimental values of the transfer functions Π_λ near the boundary of two underlying surfaces: cloudiness-sand. The experimental curves were obtained during the "Soyuz-9" and LI-2 flights, the theoretical Π_λ-values were calculated by formula (21). In the case of the sand-sea boundary a good coincidence between the experimental (curve 1) and theoretical (curve 2) data is observed. This shows the validity of the assumption stating that the values for haze radiance near the boundary of two underlying surfaces are equal. The approximate formula (21) is based on this assumption. A comparison between the theoretical and experimental Π_λ-values for other cases of the nonuniform underlying surfaces is difficult since reliable experimental data is lacking.

Comparing the calculated curves for the cases of the uniform and nonuniform underlying surfaces it is possible to draw an interesting conclusion on the degree of the influence of the boundary between two underlying surfaces on the value for the transfer functions. For example, for the sand desert (A = 0.24) situated near the water surface (A = 0.06) the Π_λ-values increase as compared to the case of the uniform sand surface (A = 0.24), whereas, for the sand surface situated near the edge of cloudiness they remain nearly the same as in the case of the uniform sand surface. This shows a different influence of the "backlighting" from the underlying surfaces with different albedo on the transformation of radiance of natural formations by the atmospheric thickness.

Along with the above comparison of the theoretical and experimental values of the transfer function Π_λ, it is of interest to investigate the influence of the nonuniformity of the underlying surface (i.e. as the boundary of two underlying surfaces is approached). Fig. 7 presents a number of sequential photometric profiles of spectral radiance of the water surface and the shore of the lake in south-western Afganistan according to the "Soyuz-9" data. In the right-hand side of the figure one can see the position of the slit of the spectrograph relative to the underlying surfaces measured. The horizontal lines show the position of the photometric profiles relative to the boundary of two underlying surfaces. From the data of Fig. 7 one can see the transformation of spectral radiance of the nonuniform underlying surface in the transitional region-"the water surface-the shore": as the shoreline is approached, spectral radiance of the water surface increases, whereas, radiance of the land decreases tending to the mean value at the boundary (curve 10). The top (2) and the bottom (18) curves are the spectra of the uniform underlying surfaces. The corresponding calculated data are shown in the form of curves 19, 20, 21, 22.

To illustrate the influence of the boundary between two underlying surfaces on radiance of the uniform underlying surfaces with the different albedo near and far from the boundary Fig. 8 a, b gives the theoretically calculated values of spectral radiance of the haze, sand and cloudiness when observed from space. The calculation of spectral radiance near and far from the boundary was made using the formulas of paper (9). The intermediate cases were calculated by the following approximate formulas

$$I_{h,i} = S\xi\left[\frac{A_i\mu(\xi, \tau_0) \cdot T_\varphi(\eta, \tau_0)}{1 - \overline{AC}} + \rho(\eta, \xi, \phi, \tau_0)\right] \quad (23),$$

$$I_i = S\xi\left[\frac{A_i\mu(\xi, \tau_0)\,\mu(\eta, \tau_0)}{1 - \overline{AC}} + \rho(\eta, \xi, \phi, \tau_0)\right] \quad (24).$$

A comparison between the theoretical and experimental data for the case shown in Fig. 5 has not been made because the object measured was an extensive bank of small cumulus clouds and the corresponding theoretical expressions for the transfer functions were obtained only for the case of a single small object on the earth's surface (9).

The influence of the atmosphere on the natural formation spectra obtained from space may be estimated accurately if radiance of the atmospheric haze is calculated by formulas (7)-(8) in which the values for transfer functions are taken from a direct comparison between satellite and aircraft (surface) experiments (Fig. 1, 2). But in this case according to (7)-(8), the independent determination of the atmospheric transparency over the areas of the underlying surface measured is needed.

Since the direct measurement of the atmospheric transparency during the combined subsatellite 1969-1971 experiments has not been made, the only possibility of the experimental estimation of the haze radiance and of the atmospheric transparency is in the solution of the equation system (3)-(4).

Fig. 9 presents a comparison between the theoretical and experimental values of $I_{h,\lambda}$ and T_λ over the boundary of two surfaces: sand-sea. The data of synchronous aircraft and satellite measurements conducted during the "Soyuz-9" flight (2) were used as the experimental values. Theoretical values were calculated by formula (19) under the assumption of the equality of haze radiance near the boundary of two uniform underlying surfaces. A comparison between the experimental and calculated data shows a good coincidence in the wavelength range considered.

The efficiency of using the equation system (3)-(4) for the determination of the components of the transfer function may be further checked by comparing the solution of this system with the results of the experimental determination of the atmospheric transparency T_λ and haze radiance $I_{h,\lambda}$ by the formulas (7)-(8).

Now let us compare the experimental and theoretical curves of the transfer functions for the contrasts of spectral radiance of two uniform semiplanes with different albedo.

Besides the experimental curves, Fig. 4 shows the theoretical values $\mathcal{J}_i$ calculated by formulas (21)-(22) under the assumption of $\varkappa_h = 0$. According to the experimental and theoretical data, at the small albedo values for contrasting surfaces (e.g. sand-sea) a considerable worsening of the transfer of contrasts to the top of the atmosphere is observed as compared to the case of large albedo (cloudiness-sand). However, with increasing wavelength this difference is considerably smoothed due to the decrease in the capability of the atmosphere to scatter.

For the cloudiness-sand system the theoretical experimental $\mathcal{J}_\lambda$-values coincide throughout the entire spectral range considered, which may be explained by rather large values of the albedo of sand and cloudiness. A large discrepancy is observed for the sand-water system in the interval of λ = 450-550 nm where the attenuation influence of the atmospheric haze smoothing the contrasts with small albedo is the strongest. With increasing wavelength (550 nm) the consistency between the experimental and theoretical curves improves considerably.

5. CONCLUSION

Spectrophotometric measurements of natural formations first performed from the spacecraft "Soyuz-7" and "Soyuz-9" and a subsequent analysis of the data from combined aircraft-satellite experiments permitted the construction of the technique for the reduction of "space" spectra to the earth's surface with the help of the transfer functions Π_λ and $\mathcal{J}_\lambda$. The results obtained gave the possibility to estimate the variations in the transfer functions in the visible spectral region depending on the albedo of the underlying surface both for the uniform surfaces and near the boundary between two uniform underlying surfaces.

Experimental values of the transfer functions and of their components correspond to a certain optical state of the atmosphere and the underlying surface. However, they give a good notion on the degree of the atmospheric effect on spectral radiance of natural formations and their contrasts during spectrophotometric measurements from space.

A comparison with the theoretical data obtained for the mean optical models of the atmosphere and with the Lambert underlying surface shows a good qualitative and, in some cases, quantitative agreement between theory and experiment.

A general task of theory and experiment is the development of the generalized mean transfer functions which would permit a reliable reduction of satellite spectral data to the level of the underlying surface.

For the practical solution of this perspective problem it is necessary to take into account an important influence of the following main factors:

1. Inaccuracy of the photographic method of recording spectral radiance of natural formations.

2. The inadequacy of experimental data depending on the degree of the nonsynchronization of the aircraft and satellite measurements as well as various scales of smoothing.

3. Inadequacy between the optical models of the atmosphere and the underlying surface (scattering function, the probability of the quantum survival, the optical thickness, the reflection coefficient or the albedo) used in theoretical calculations of Π_λ, $\mathfrak{S}_\lambda$ and the real optical state of the atmosphere and underlying surface in the subsatellite region during the combined subsatellite experiment.

4. The error of theoretical modeling of the field of the multiple scattered radiation in the presence of the atmosphere of aerosol particles and anisotropic reflection from the nonuniform underlying surface.

Each of the problems mentioned is interesting in itself and requires special investigation.

Though these problems have not been considered in detail in the present paper, the experimental technique and the processing of the results of measurements (17) called for the reduction of the influence of the first two factors to minimum. As to the analysis of the errors of theoretical interpretation of the experimental data, it can be performed for the real models of the atmosphere and the underlying surface, most efficiently, using the Monte Carlo method or the numerical solution of the initial transfer equation.

ACKNOWLEDGEMENTS

The authors acknowledge their gratitude to V. M. Orlov and V. P. Bulychev for their help in the calculation and processing the experimental data.

REFERENCES

1. K Ya. Kondratyev, A. A. Buznikov, B. V. Vinogradov, V. N. Volkov, V. V. Gorbatko, O. I. Smokty and V. M. Orlov, 1970: "Some Results of Spectrophotometric Measurements of the Earth from the Spacecraft "Soyuz-7" ". Doklady Akad. Nauk USSR, v. 195, No. 5.

2. K. Ya. Kondratyev, A. A. Buznikov, O. B. Vasilyev, B. V. Vinogradov, V. M. Orlov and O. I. Smokty, 1972: "Some Results of Spectrophotometric Measurements of Natural Formations from the Manned Spacecraft "Soyuz-9" ". Kosmicheskie Issled, No. 2.

3. K. Ya. Kondratyev, A. A. Buznikov, O. B. Vasilyev, B. V. Vinogradov, V. M. Orlov and O. I. Smokty, 1972: "Study of Earth Resources with the Help of the Combined Complex Optical Experiments from the "Spacecraft "Soyuz-7" and the Instrumented Aircraft". Problems of Atmopheric Physics, issue 10, No. 3, Leningrad Univ. Press.

4. K. Ya. Kondratyev, A. A. Buznikov, O. B. Vasilyev, V. S. Grishechkin and O. I. Smokty, 1971: "The Aircraft Subsatellite Optical Experiment, the Atmospheric Transfer Function and its Influence on the Spectral Albedo of the Surface Object during Space Observations." Proc. of the All-union Conference on the Problems of the Meteorological Security of the Supersonic Aviation, Leningrad Univ. Press.

5. K. Ya. Kondratyev, A. A. Buznikov, O. B. Vasilyev, B. V. Vinogradov, A. A. Grigoryev, Yu. I. Rabinovich and L. I. Chapursky, 1971: "Some Results of the Combined Sunsatellite Optical Experiment." Doklady Akad. Nauk, USSR, v. 197, No. 5.

6. K. Ya. Kondratyev and O. I. Smokty, 1972: "On the Determination of the Transfer Function in the Spectrophotometric Measurements of the Surface of a Planet from Space." Doklady Akad. Nauk, USSR, v. 206, No. 5.

7. K. Ya. Kondratyev and O. I. Smokty, 1972: "Determination of the Transfer Function for the Spectral Albedo of the Surface-Atmosphere System." Doklady Akad. Nauk, USSR, v. 206, No. 6.

8. K. Ya. Kondratyev and O. I. Smokty, 1972: "On the Influence of the Atmospheric Haze on the Color of Natural Formation Measured from Space." Doklady Akad. Nauk, USSR, v. 207, No. 1.

9. K. Ya. Kondratyev and O. I. Smokty, 1973: "On the Determination of Spectral Transfer Functions for Radiance of Natural Formation and their Contrasts in the Spectrophotometric Measurements of the Surface-Atmosphere System." Trudy GGO, issue 296, p. 135.

10. K. Ya. Kondratyev and O. I. Smokty, 1973: "On the Determination of the Transfer Function for Polarization in the Spectrophotometric Measurements of the Surface of a Planet from Space." Doklady Akad. Nauk, USSR, v. 208, No. 1.

11. V. V. Sobolev, 1956: "Transfer of the Radiative Energy in the Atmospheres of Stars and Planets." Gostekhteorizdat, Leningrad.

12. V. V. Sobolev, 1972: "Light Scattering in the Planetary Atmospheres." "Nauka", Moscow.

13. K. Ya. Kondratyev (Ed.), 1972: "Studies in the Environment from Manned Orbital Stations." Hydrometeoizdat. Leningrad.

14. M. S. Malkevich, 1957: "On the Consideration of the Nonuniformities of the Underlying Surface in the Problems of Light Scattering in the Atmosphere." Izv. Akad. Nauk, USSR, ser Geography and Geophysics, No. 5.

15. M. S. Malkevich, 1958: "On the Influence of the Horizontal Changes in the Albedo of the Underlying Surface on Light Scattering in the Uniform Atmosphere." Izv. Akad. Nauk, USSR, ser. Geography and Geophysics, No. 8.

16. L. Elterman, 1968: "UV, Visible and IR Attenuation for Altitudes to 50 km", AFCRL-68-0153, Environ. Res. Papers, No. 285, April.

FIGURE CAPTIONS

Fig. 1. a) Spectral radiance of the underlying surface (cape Begdash, the Caspian coast):
1. From the spacecraft "Soyuz-7" (220 km).
2. From the aircraft (2.7 km).
b) The transfer function of the surface-atmosphere system (cape Begdash).

Fig. 2. A comparison between the experimental and theoretical spectral transfer functions for the case of the uniform underlying surfaces (solar zenith distance Θ_o = 33 - 45°).
I. "Soyuz-7", the aircraft (2.7 km):
1. The sand desert.
2. Continuous cloudiness.
II. "Soyuz-9", surface measurements:
3. The sand desert.
4. A water surface.
III. The calculated data (Elterman's model (16), the atmospheric scattering function $\chi(j)$ is taken from (11), Θ_o = 40°).
5. Sand, A = 0.24.
6. Cloudiness, A = 0.78.
7. The sea, A = 0. 06.

Fig. 3. a) Dependence of the haze radiance and of the atmospheric transparency on the wavelength: 1 - T_λ , 2 - $I_{h,\lambda}$.
b) Dependence of the atmospheric transparency and of the mean value of the spectral radiance coefficients for the atmospheric haze near the sand-sea boundary: 1 - T_λ , 2 - $I_{h,\lambda}$.

Fig. 4. Transfer functions for the contrasts of radiance of the underlying surfaces.
1. The desert-water surface, according to the "Soyuz-9" data.
2. Cloudiness-desert, according to the "Soyuz-7" data.
3. Cloudiness-desert, according to the "Soyuz-9" data
4. Sand-sea, calculated data, A_1 = 0.24; A_2 = 0.06; Θ_o = 40°.
5. Sand-cloudiness, calculated data, A_1 = 0.78, A_2 = 0.24, Θ_o = 40°.

Fig. 5. Schematic of the frame of the RSS-2 spectrograph, and the classification of the photos of spectra of natural formations according to the degree of the nonuniformity of the underlying surfaces projected on the slit of the spectrograph during the measurement from space:
1. photo,
2. The position of the spectrographic slit,
3. The clock,
4. The spectrum:
a) the uniform underlying surface with the albedo A_1:
b) two uniform surfaces with the albedo A_1 and A_2 near the boundary;
c) the areas of uniform surfaces with the albedo A_1 against the background of the extensive uniform surface with the albedo A_2.

Fig. 6 A comparison between the experimental and theoretical values of the atmospheric transfer functions near the boundary of two underlying surfaces. Sand near the water surface:

1. The experiment: "Soyuz-9", the aircraft (2.7 km).
2. The calculated data: $A_1 = 0.24$, $A_2 = 0.06$. Sand near the edge of continuous cloudiness:
3. The calculated data: $A_1 = 0.24$, $A_2 = 0.78$. The uniform sand surface:
4. The calculated data, $A = 0.24$.
   Sea near the sand surface:
5. The calculated data, $A_1 = 0.06$, $A_2 = 0.24$.
   The uniform water surface:
6. The calculated data, $A = 0.06$.
   The data were calculated according to Elterman's model (16). $\chi(j)$ according to (11). $\Theta_o = 30^o$.

Fig. 7. Spectral radiance of the underlying surface near the boundary of two underlying surfaces ("Soyuz-9", the shore of the lake in south-western Afganistan, $\Theta_o = 33.8^o$):

a) the position of the split projection and of the photometric profiles on the underlying surface measured;

b) spectral radiance: 2 is the sand surfaces; 18 is a water surface; 20 is a water surface, the calculation was made at $\Theta_o = 30^o$; 21 is the sand near the water surface, the calculation was made at $\Theta_o = 30^o$; 22 is the sand far from the water surface, the calculation was made at $\Theta_o = 30^o$.

Fig. 8. a) Spectral radiance (relative to the solar radiation flux) of cloudiness and of the sand surface near the boundary (calculation was made at $\Theta_o = 40^o$, $\chi(j)$ according to (11) Elterman's model (16):

1. Cloudiness far from the boundary.
2. Cloudiness not far from the boundary (the intermediate case).
3. Cloudiness near the boundary.
4. Sand near the boundary.
5. Sand not far from the boundary (the intermediate case).
6. Sand far from the boundary.

b) Spectral radiance of the atmopsheric haze over the boundary and far from it (the calculation was made at $\Theta_o = 40^o$, $\chi(j)$ according to (11), Elterman's model (16):

1. over the boundary, sand-cloudiness;
2. over the sand not far from the boundary (the intermediate case);
3. over cloudiness not far from the boundary (the intermediate case);
4. over the sand far from the boundary;
5. over cloudiness far from the boundary.

Fig. 9. Comparison between the experimental and theoretical values for the haze radiance $I_{h,\lambda}$ and the atmospheric transparency T_λ.

1. $I_{h,\lambda}$ over the sand-sea boundary according to the "Soyuz-9" data,

2. $I_{h,\lambda}$ over the sand-sea boundary, a theoretical calculation,

3. T_λ according to the "Soyuz-9" data.

4. T_λ calculated theoretically ($\Theta_o = 40^o$, $\chi(j)$ according to (11), Elterman's model (16).

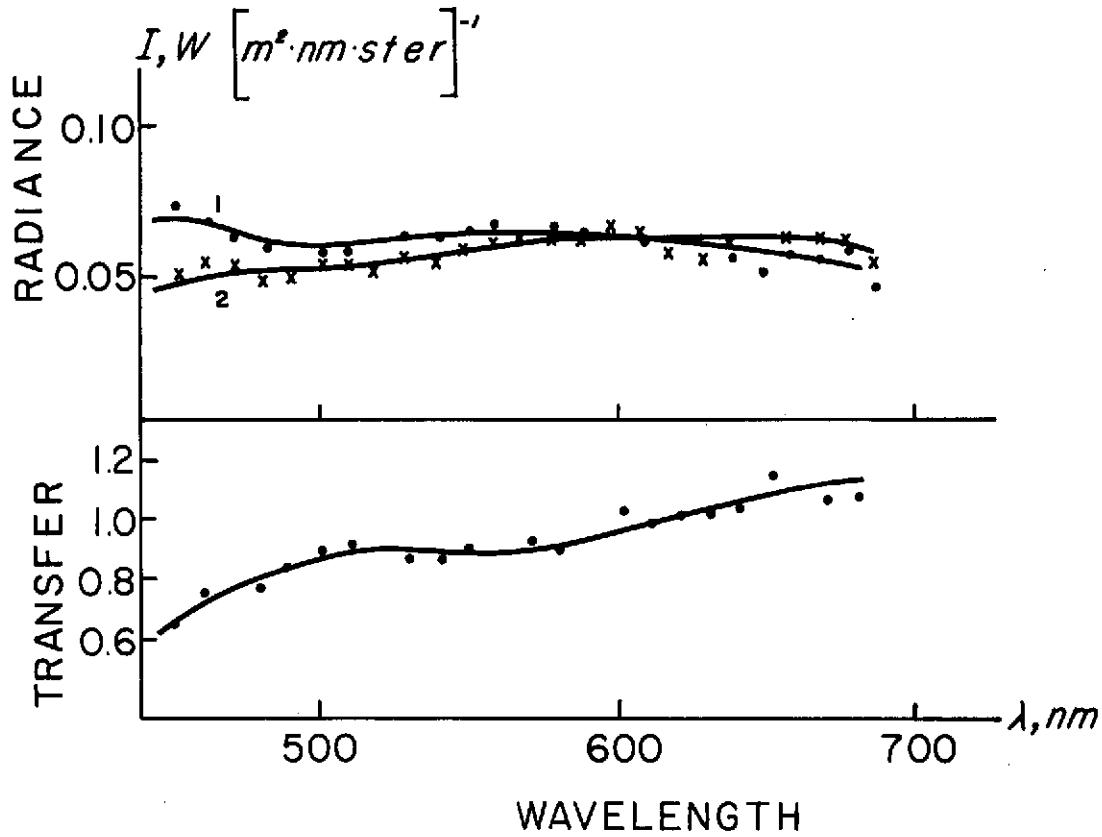
I, W [m² · nm · ster]⁻¹
RADIANCE
0.10
0.05
1
2
TRANSFER
1.2
1.0
0.8
0.6
λ, nm
500
600
700
WAVELENGTH

FIGURE 1 a, b

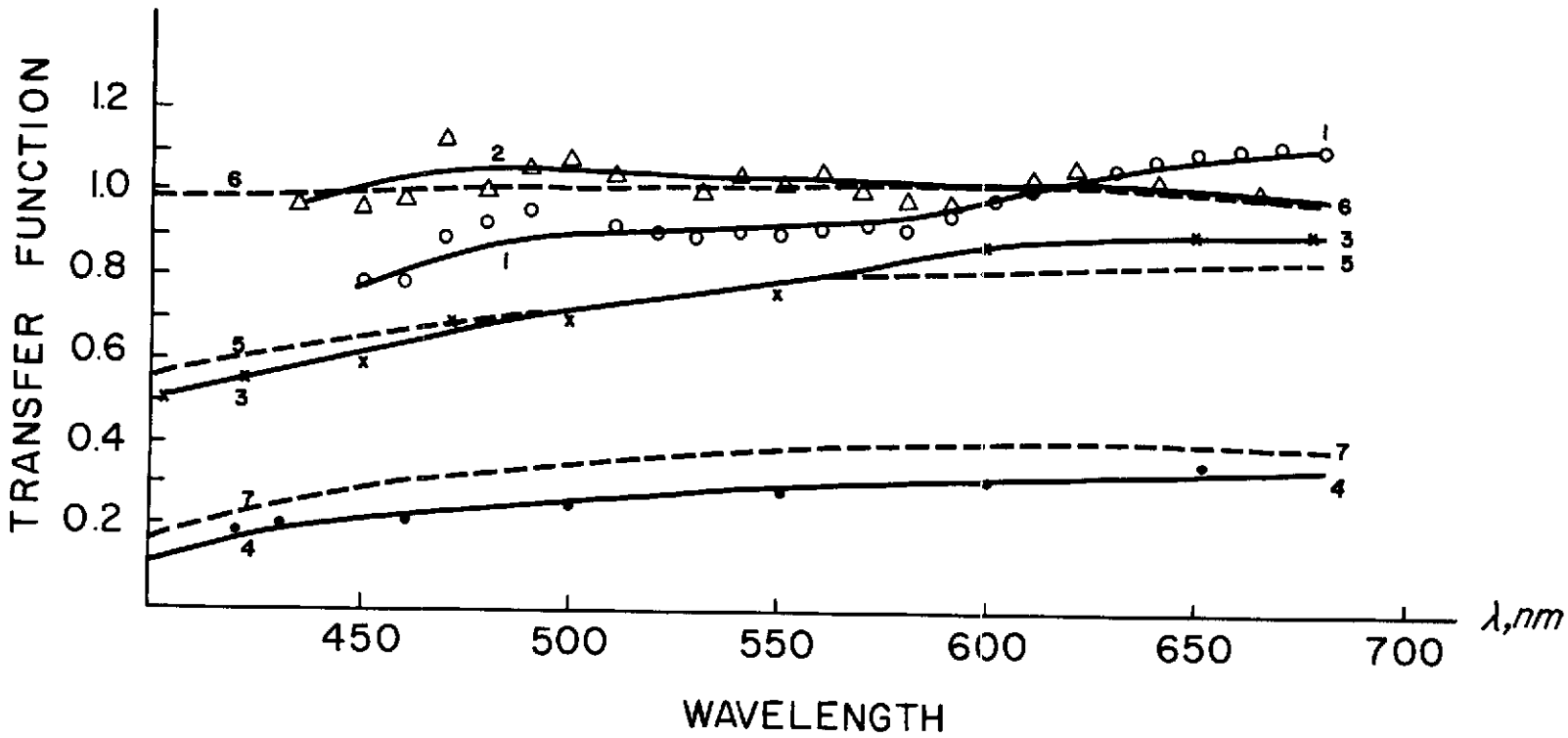
TRANSFER FUNCTION
1.2
1.0
0.8
0.6
0.4
0.2
450
500
550
600
650
700
λ,nm
WAVELENGTH
1
2
3
4
5
6
7

FIGURE 2

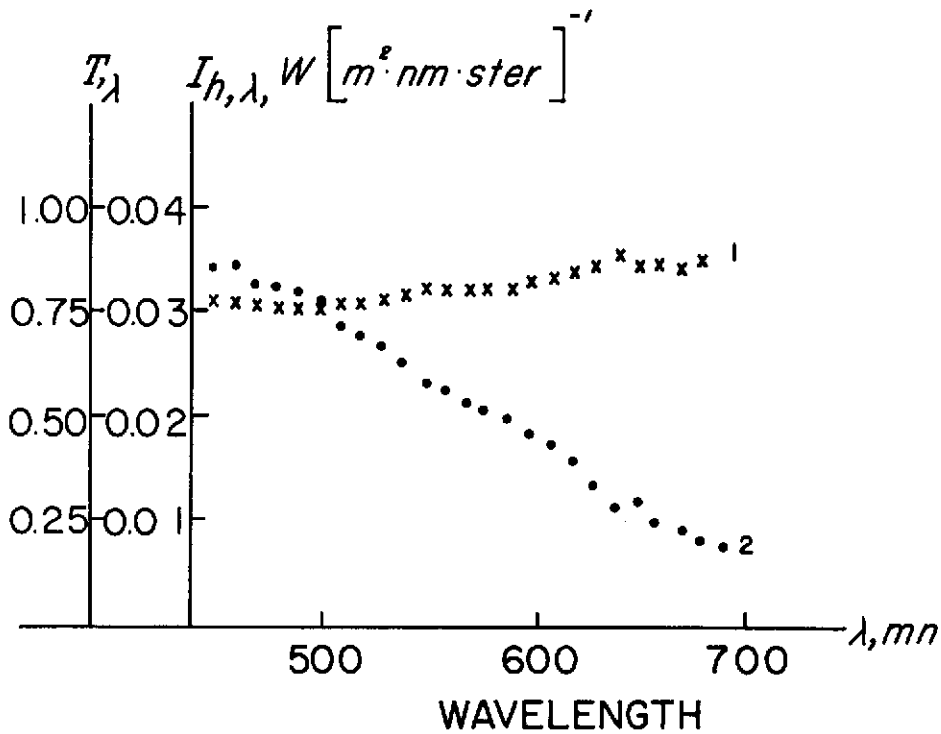
T,λ
$I_{h,\lambda}$, $W\left[m^2 \cdot nm \cdot ster\right]^{-1}$
1.00
0.75
0.50
0.25
0.04
0.03
0.02
0.01
1
2
500
600
700
λ, mn
WAVELENGTH

FIGURE 3 a

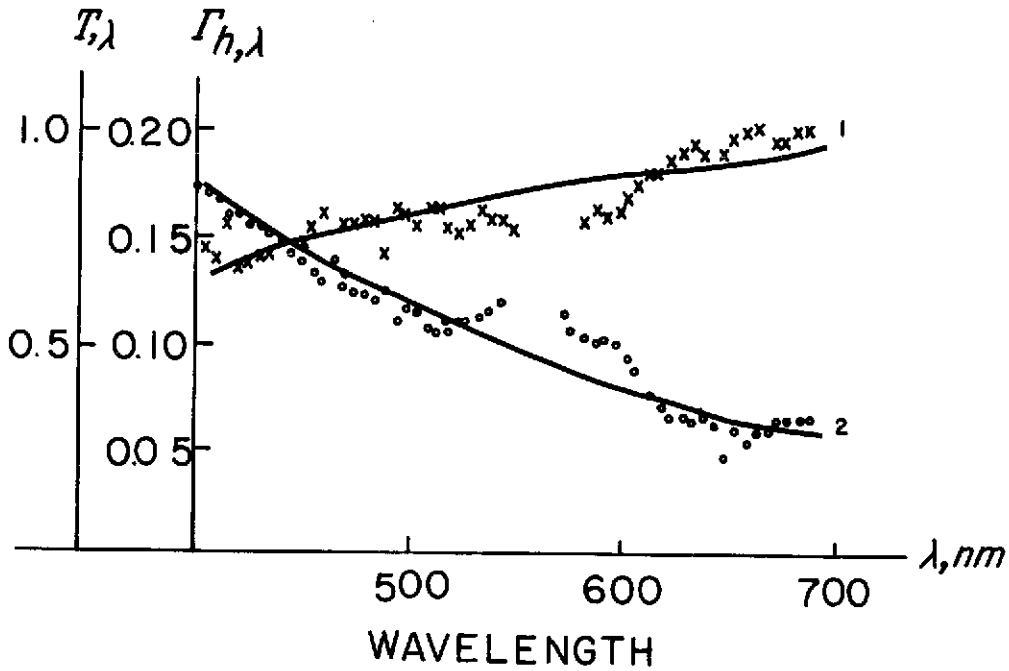

FIGURE 3 b

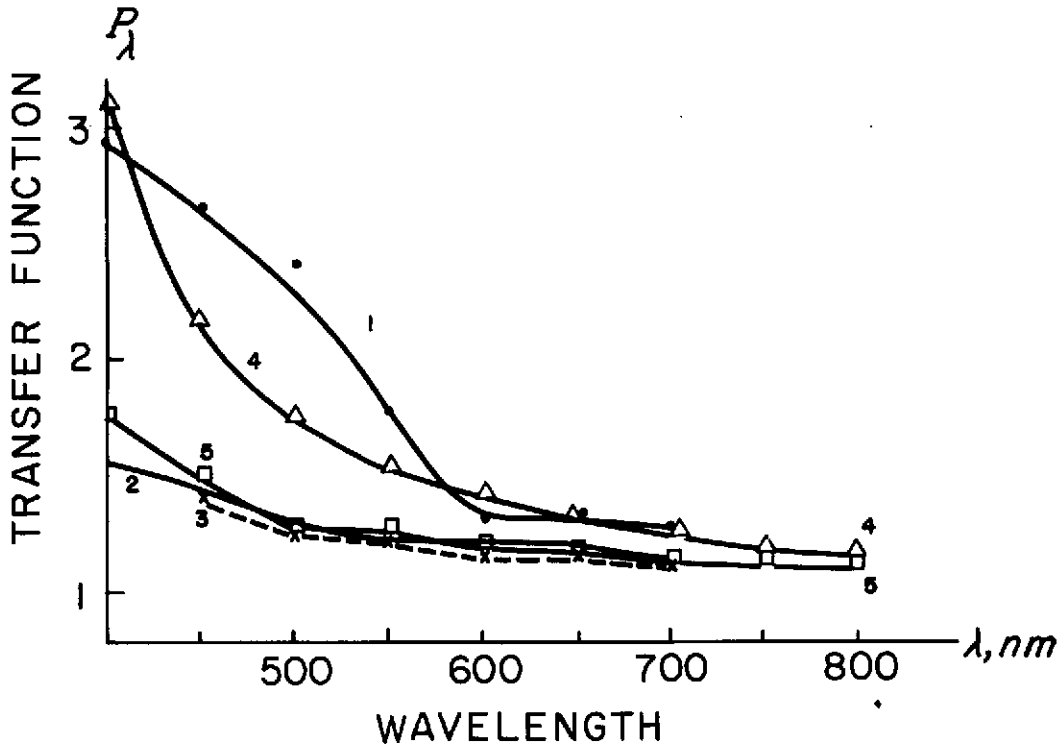
P_λ
TRANSFER FUNCTION
3
2
1
500
600
700
800
λ, nm
WAVELENGTH
1
2
3
4
5

FIGURE 4

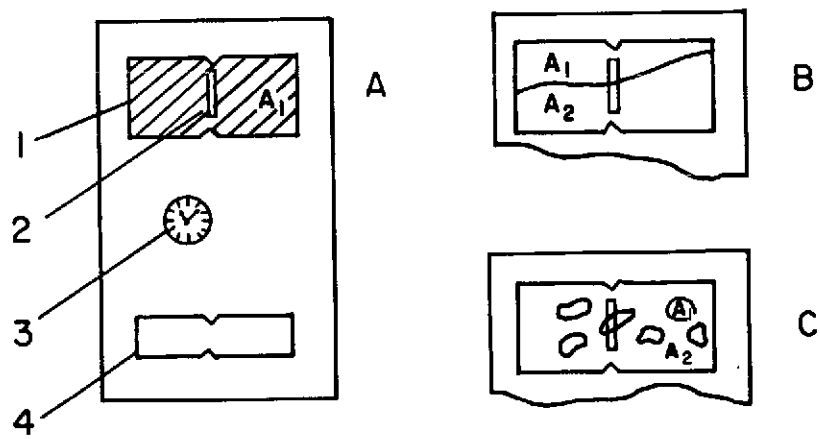

FIGURE 5

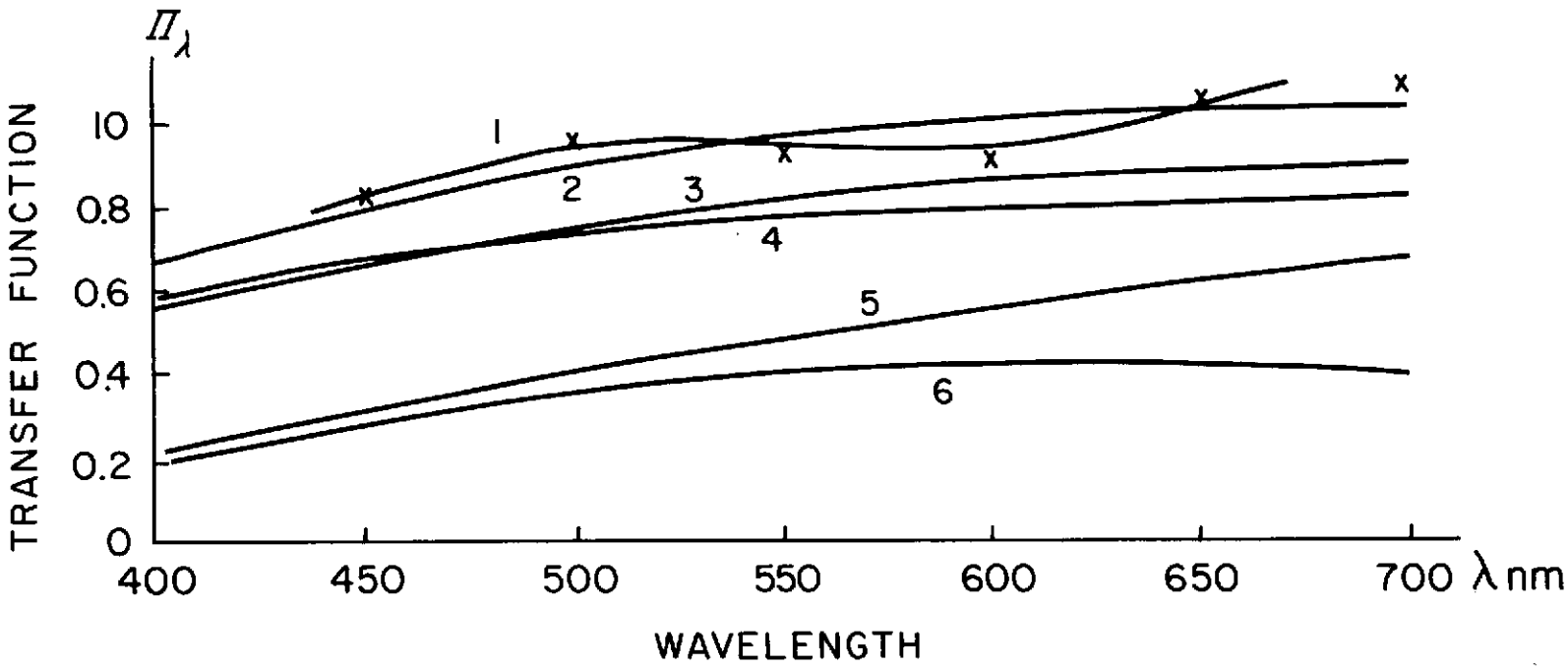
Π_λ
TRANSFER FUNCTION
10
0.8
0.6
0.4
0.2
0
1
2
3
4
5
6
400
450
500
550
600
650
700 λ nm
WAVELENGTH

FIGURE 6

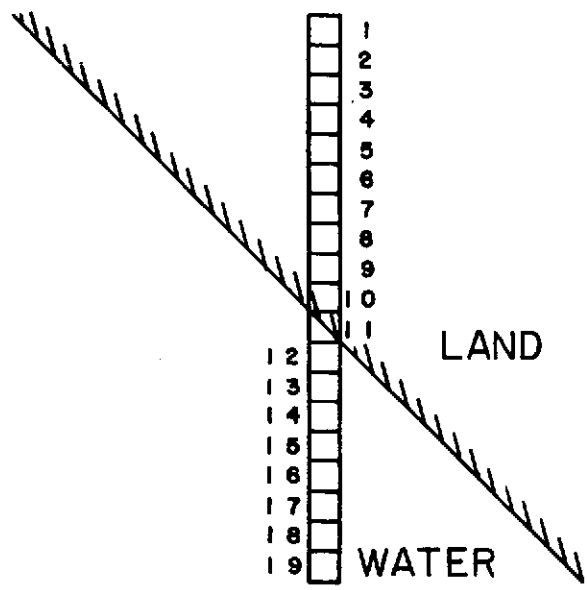

FIGURE 7 a

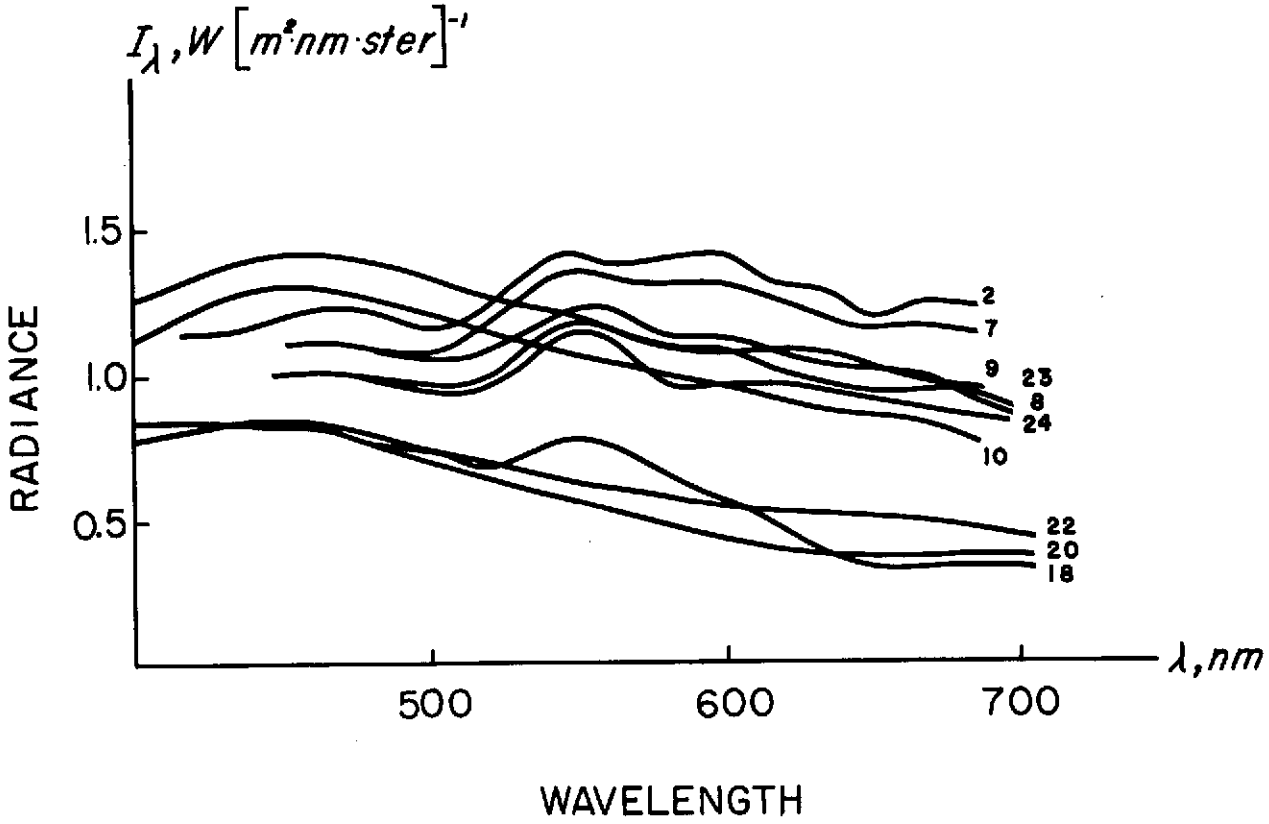
I_λ, W $[m^2 nm \cdot ster]^{-1}$
1.5
1.0
0.5
RADIANCE
2
7
9
23
8
24
10
22
20
18
500
600
700
λ, nm
WAVELENGTH

FIGURE 7 b

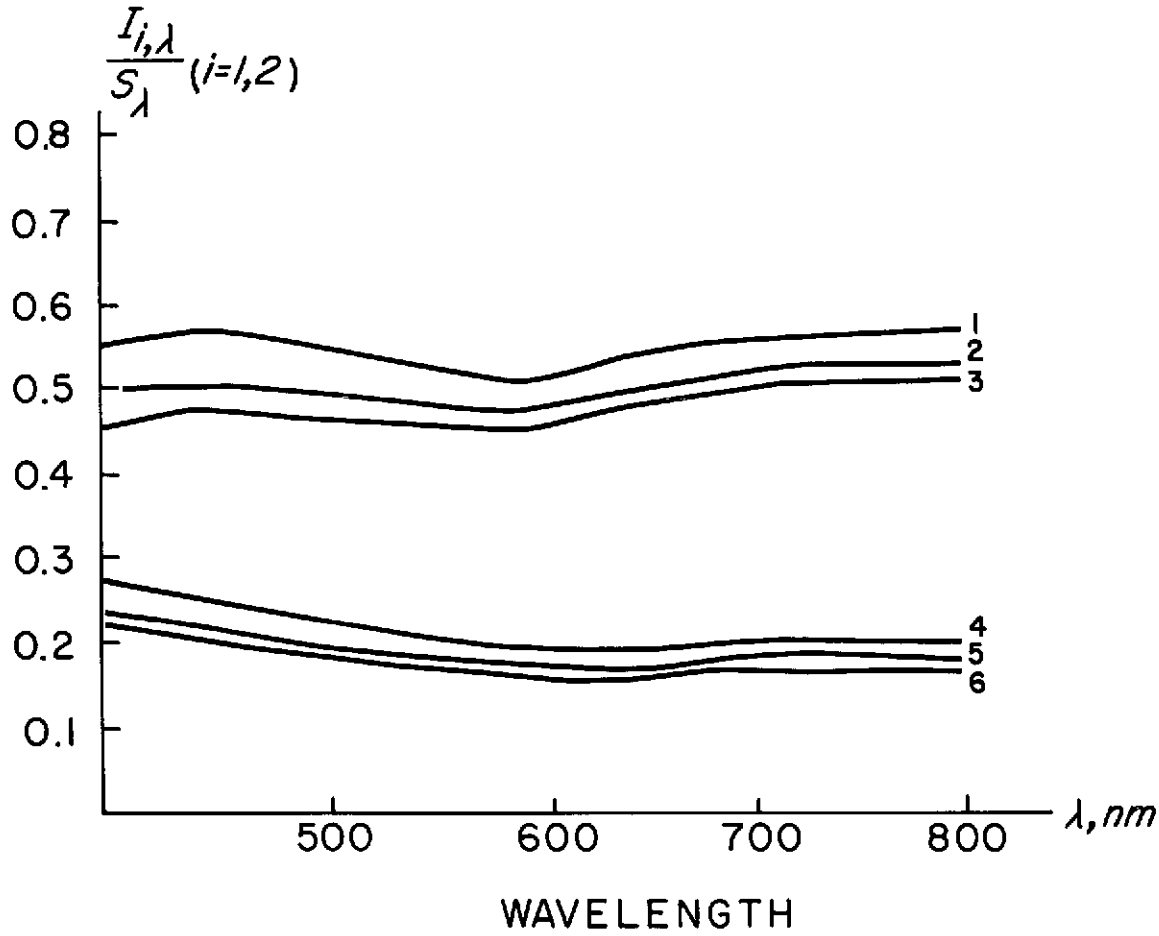
$\frac{I_{i,\lambda}}{S_\lambda}$ (i=1,2)
0.8
0.7
0.6
0.5
0.4
0.3
0.2
0.1
1
2
3
4
5
6
500
600
700
800
λ, nm
WAVELENGTH

FIGURE 8 a

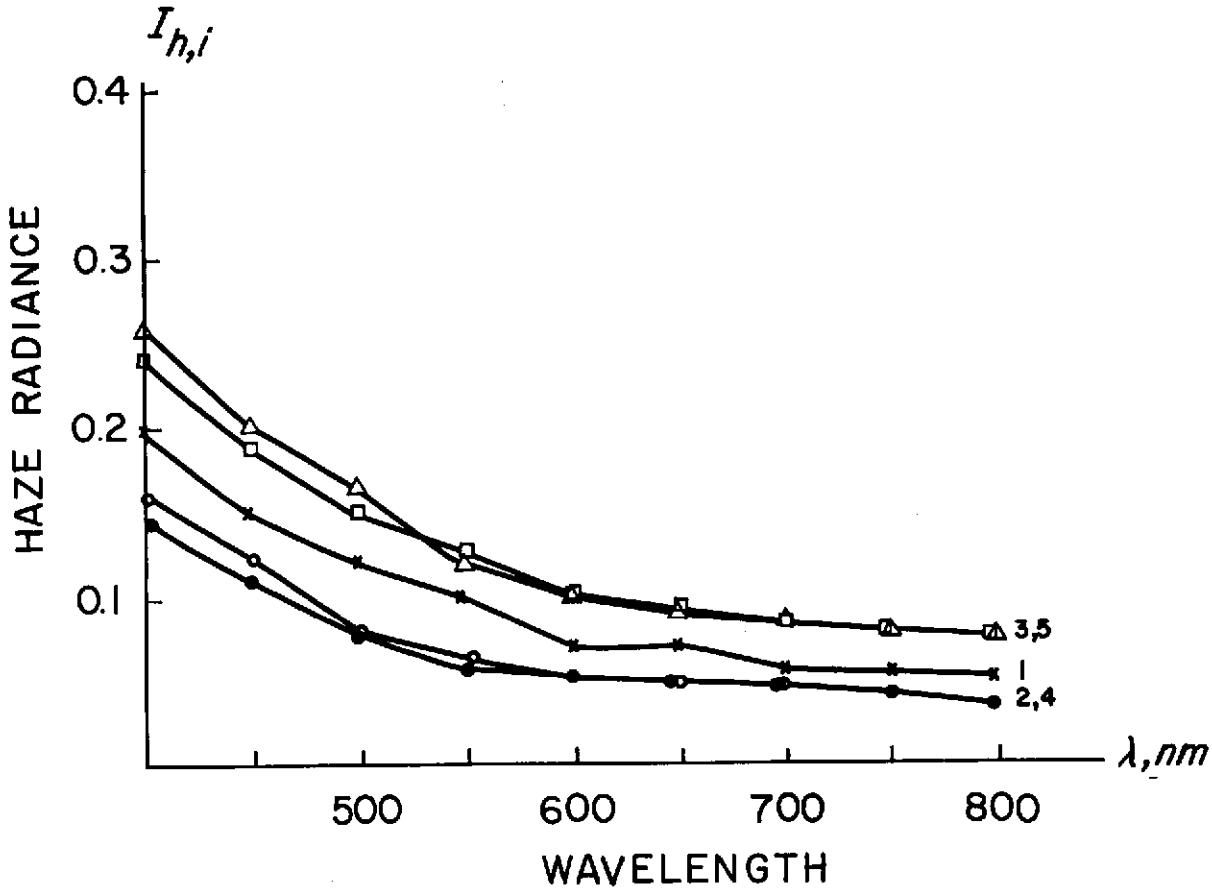
$I_{h,i}$
0.4
0.3
0.2
0.1
HAZE RADIANCE
3,5
1
2,4
λ,nm
500
600
700
800
WAVELENGTH

FIGURE 8 b

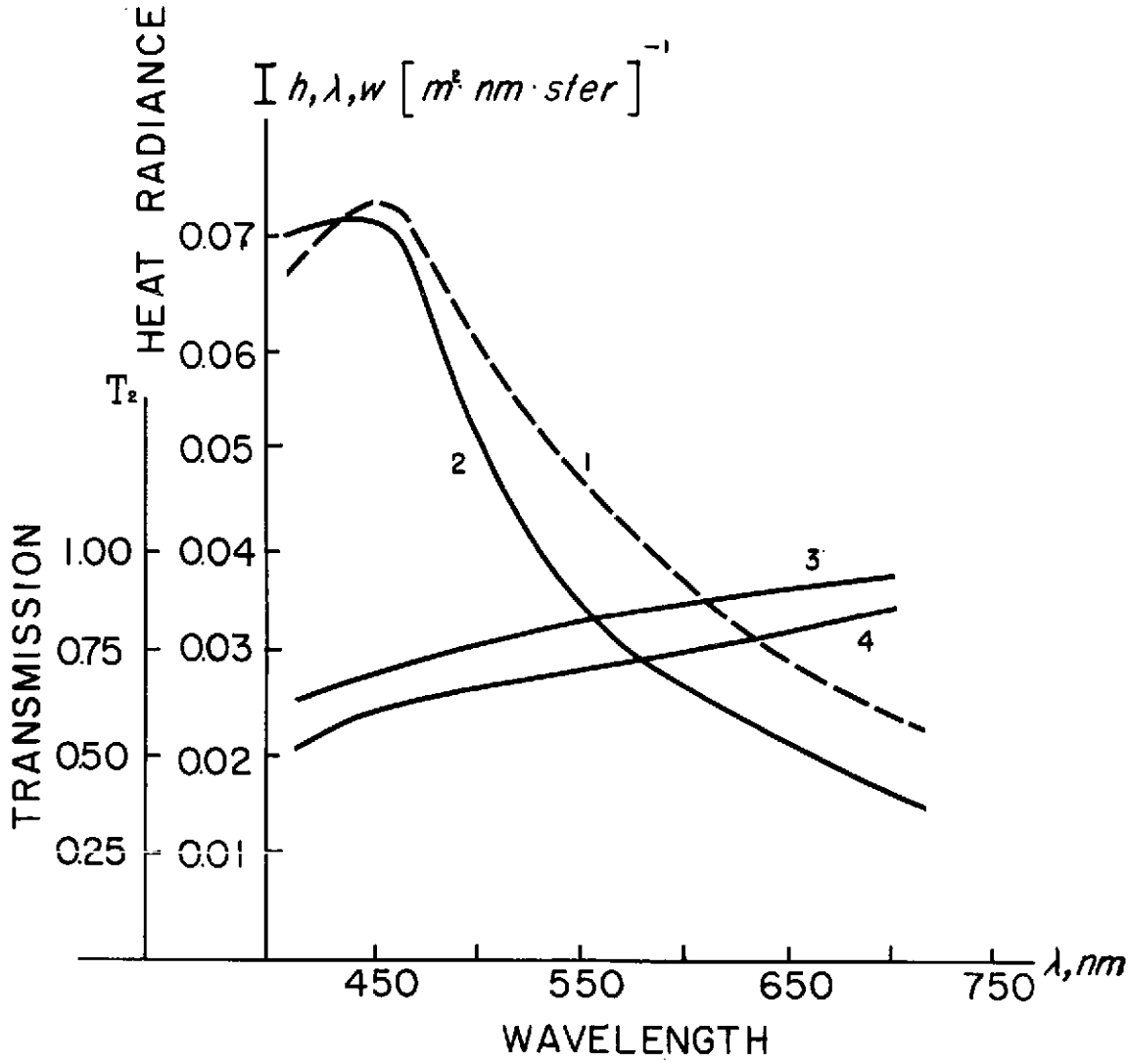
HEAT RADIANCE
I h,λ,w [m² nm·ster]⁻¹
0.07
0.06
0.05
0.04
0.03
0.02
0.01
T₂
TRANSMISSION
1.00
0.75
0.50
0.25
1
2
3
4
450
550
650
750
λ,nm
WAVELENGTH

FIGURE 9

PARTICULATE SIZES FROM POLARIZATION MEASUREMENTS

by Jacob G. Kuriyan
Department of Meteorology
University of California
Los Angeles 90024 CA

The theoretical aspects of the transfer of radiation through an atmosphere have been discussed by Professors Chandrasekhar and Yamamoto. The thrust of my talk will be to describe an experiment that uses the results of these sophisticated studies to obtain information on particles in the atmosphere. To be specific, I shall describe an experiment with a ground based polarimeter (constructed and donated for our research use by TRW Systems, Redondo Beach), and explain the theory that is necessary to infer the optical properties of particles in the atmosphere, from measurements of the radiation field. It is my hope that the successful conclusion of this experiment will encourage the widespread use of the polarimeter as a remote probe of atmospheric particulates.

Professor Sekera's pioneering theoretical and experimental work contributed significantly to the development and use of the polarimeter as an experimental tool. The last project in which he participated was the NASA - AAFE experiment in which a polarimeter was flown in an aircraft to infer the particulate sizes. Unfortunately his illness prevented a serious study of the theory and thus the few measurements that were made could not be interpreted satisfactorily.[1] My interest in this field was aroused by the short association I had with him, during which we tried to obtain analytical approximations to the phase matrix. After his untimely death, serious doubts were cast on the feasibility of this approach. Fortunately, TRW Systems Group, Redondo Beach, offered to construct and donate a polarimeter for my use, if it would help establish the viability of the method. This is, therefore, the result of a frantic and furious effort, since March 1973, to settle this question.

What concerns us is the so-called inverse problem in atmospheric optics. Here, the incident and the emergent beams are prescribed and it is necessary to deduce the properties of the scatterers. The complicated nature of the equations and the inherent lack of uniqueness suggests to me that it is impossible to obtain a solution to this inverse problem. However a 'back-door', yet useful, resolution is possible and this will be the content of my talk.

I will attempt to calculate the emergent radiation for all possible particulate distributions, and catalogue these results. Then any measurement will be matched against these tables so as to infer the relevant optical characteristics. Sekera's[2] compilation of Chandrasekhar's results have served as a similar catalogue for molecular atmospheres, and it is possible, from these tables to infer the reflectivity and optical thickness, if the incident and emergent radiation fields are specified.[3] In order to incorporate the effects of particulates it is necessary to parameterize them and devise a method of searching for a fit.

The mathematical details of my talk are available in a paper[4] that has been submitted for publication in the Quarterly Journal of the Royal Meteorological Society and here I will emphasize the physics of the problem, explaining the assumptions and the underlying philosophy.

The auxiliary equation for the source function J in a turbid atmosphere in the absence of ground reflection when unpolarized radiation $\pi F\,(0, -\mu_0)$ is incident in the top of the atmosphere is given by

$$J(\tau, \Omega) = \frac{1}{4} e^{\frac{-\tau}{\mu_0}} \left\{ \sum_i \beta_i(\tau)\, P_i(\tau, \Omega, -\Omega_0) \right\} F(0, -\Omega_0)$$

$$+ \frac{1}{4}\pi \int_0^{2\pi} d\phi' \int_0^1 \frac{d\mu'}{\mu'} \left\{ \sum_i \beta_i(\tau)\, P_i\,(\tau, \Omega, +\Omega') \right\} \int_\tau^{\tau_{Bottom}} e^{-\frac{|\tau - t|}{\mu'}} J(\tau, +\Omega')\, dt$$

$$+ \frac{1}{4}\pi \int_0^{2\pi} d\phi' \int_{-1}^{0} \frac{d\mu'}{\mu'} \left\{ \sum_i \beta_i(\tau)\, P_i(\tau, \Omega, -\Omega') \right\} \int_0^{\tau} e^{-\frac{|t - \tau|}{\mu'}} J(\tau, -\Omega')\, dt \qquad (1)$$

with the definition

$$\sum_i \beta_i(\tau)\, P_i(\tau, \Omega, \Omega') \equiv \frac{\beta_R(\tau)\, P_R(\tau, \Omega, \Omega') + \beta_A(\tau)\, P_A(\tau, \Omega, \Omega')}{\beta_R(\tau) + \beta_A(\tau)} \qquad (2)$$

where $\beta_R(\tau)$, $\beta_A(\tau)$ are the volume scattering coefficients; while $P_R(\tau, \Omega, \Omega)$, $P_A(\tau, \Omega, \Omega')$ are the phase matrices for the Rayleigh and the aerosol parts, respectively.

The diffuse component of the intensity is then given as

$$I_{DIFF}(\tau, \Omega') = \frac{1}{\mu'} \int_t^{\tau_{Bottom}} J(t, +\Omega')\, e^{-\frac{|t - \tau|}{\mu'}} dt \quad . \qquad (3)$$

$$I_{DIFF}\ (\tau, -\Omega') = \frac{1}{\mu'} \int_0^{\tau} J(t, -\Omega')\, e^{-\frac{|t - \tau|}{\mu'}} dt \qquad (4)$$

The solution, therefore, requires a knowledge of $P_A(\tau, \Omega, \Omega')$ and $\beta_A(\tau, \Omega, \Omega')$ the aerosol phase function and the volume scattering coefficient. The reflection at the ground is assumed to be Lambertian and this adds another term $\underset{\sim}{J}^*(\tau, \Omega)$ to the above source function, where

$$\underset{\sim}{J}^{*}(\tau, \Omega) = \frac{1}{4}\pi \int_0^1 d\mu_1 \int_0^{2\pi} d\phi_1 \, \underset{\sim}{P}(\mu\phi : \mu_1\phi_1) \, \underset{\sim}{I}_g \, e^{-\frac{\tau_1 - \tau}{\mu_1}}$$

$$+ \frac{1}{4}\pi \int_{-1}^{+1} d\mu' \int_0^{2\pi} d\phi' \, \underset{\sim}{P}(\mu\phi : \mu'\phi') \, \underset{\sim}{I}^{*}(\tau, \mu'\phi'). \qquad (5)$$

Here the radiation reflected by the ground is assumed to be unpolarized and isotropic, represented by the matrix

$$\underset{\sim}{I}_g = I_g \begin{pmatrix} 1/2 \\ 1/2 \\ 0 \\ 0 \end{pmatrix}. \qquad (6)$$

$\underset{\sim}{I}^{*}(\tau, \mu', \phi')$ is related to $\underset{\sim}{J}^{*}(\tau, \Omega)$ in the same way as $\underset{\sim}{I}(\tau, \mu', \phi')$ was to $\underset{\sim}{J}(\tau, \Omega)$, as in equations (3) and (4). The reflectivity of the ground, A, will determine the magnitude of I_g and the relevant expressions have been obtained by Dave (1964). In our discussion we will borrow Dave's general treatment and focus our attention on the contribution that aerosols make to the transfer problem.

The source function has the phase matrix P_A and the volume scattering coefficient β_A which depend on the interaction of the EM radiation with the particles in the atmosphere. The model that we assume will enable us to calculate these quantities.

It has been the convention to describe aerosol particles by spheres of varying radii and a uniform refractive index. Deirmendjian attributes to Sekera the suggestion that the size of particles be represented by a continuous function $n(r)$, the size distribution function, for reasons of mathematical elegance and convenience. It has become the practice to take such distributions literally, as an actual representation of the state of affairs. This is unwarranted and I shall, later on, give a consistent and defensible interpretation of the use of such size distribution functions.

With this assumption it is possible to integrate over all radii (with the size distribution as a weight function) the Mie result for scattering for a single sphere, to obtain the polydisperse phase matrix element P_A^5. The parameters of the polydispersions are allowed to take all possible physically realizable values and the corresponding phase matrices calculated. This will then be used to determine and compile our catalogue of the radiation field.

Professor Sekera tried, many years ago, to write the phase function as a Legendre series to solve the equation of transfer. Dr. R. S. Fraser, then a student at UCLA, found[6] that a realistic phase function requires 50 to 60 terms in the Legendre expansion and each of the coefficients depends on wavelength, refractive index etc. This was indeed impractical and, therefore, abandoned. Professor Sekera speculated that an inordinately large number of terms was necessary because the aerosol phase function had a pronounced forward peak and if this could, in some sense, be subtracted, then the remainder could perhaps be fit by a few Legendre polynomials. This is what he called the 'separation of the forward peak' in his paper.[3] In the discipline that I came from, (Elementary Particle Physics), it was conventional, in many problems, to consider only forward scattering and ignore the rest. Thus we sought to obtain analytical approximations to the forward scattering so as to simplify the radiative transfer equation.

In the literature Saxon,[7] van de Hulst[8] and Shifrin[9], have described a variety of such approximations. Then the only problem that remained was to generalize these results to polydispersions and obtain an analytical approximation. The size distribution popularized by my fellow Armenian, Diran Deirmendjian, lent itself well since it was well behaved at small and large values of r. (Junge's[10] distribution $\frac{1}{r^{\nu+1}}$ would have required a cutoff in the integral).

Diran uses the size distribution $n(r) = ar^{\alpha} e^{-br^{\gamma}}$ and classifies naturally occurring aerosol particles into 3 groups

haze H $\alpha = 2$ $\gamma = 1$

" L $\alpha = 2$ $\gamma = \frac{1}{2}$

" M $\alpha = 1$ $\gamma = 1/2$.

We used the haze H model and the Born approximation for scattering due to a single sphere (here it is assumed that particles are smaller than or of the same size as the wavelength of light). The normalized phase matrix element became a simple expression[11]

$$P_1(\Theta) = \frac{P_1(\Theta)}{P_1(\Theta = 0)} = \frac{3Z^3 + 16Z^2 + 35Z + 70}{70(1 + Z)^5}$$

$$\text{with } Z = \frac{16k^2}{b^2} \sin^2 \frac{\Theta}{2}$$

where $k = \frac{2\pi}{\lambda}$ is the wavenumber and Θ the scattering angle.

This was then compared against Deirmendjian's exact result and the agreement (even when the value of the normalized phase function was 20%) was quite reasonable (See Fig. 1). Unfortunately the case of haze L and M did not yield a simple expression and it seemed that we would have to resort to numerical methods. Of course, if we had to use numerical methods then there was no need to concern ourselves with approximations. The source of the problem was due to γ taking the value of $\frac{1}{2}$ for haze L and M giving rise to $e^{-B\sqrt{r}}$ instead of e^{-br} as in haze H. If $\int f(r)e^{-B\sqrt{r}}dr$ was approximately equal to $\int f(r)e^{-br}dr$ then our analytic function would apply for haze L and M as well.

Please observe that, our expression for $\overline{P}_1(\Theta)$ is only a function of one variable $k \sin \Theta/2$. So if we plot $P_1(\Theta)$ against $k \sin \Theta/2$ we must obtain a recognizable curve, if it is only a function of one variable, and a scatter of points, if it is a function of two variables k and Θ. When Deirmendjian's haze M tables 1 - 18 for $0.45\mu < \lambda < 16.6\mu$ were used to plot (See Fig. 2) $\overline{P}_1(\Theta)$ against $k \sin \Theta/2$ the curve that was obtained helped us to conclude that it may be possible to obtain the haze L and M results of the Mie theory from our haze H formula by allowing b to vary. The figures 3,4 compare Deirmendjian's haze M ($\gamma = \frac{1}{2}$ $\alpha = 1$ $b_M^2 = 8 \times 10^5$) against our haze H ($\gamma = 1$ $\alpha = 2$ $b = 7.4 \times 10^8$) and haze L ($\gamma = \frac{1}{2}$ $\alpha = 2$ $b_L^2 = 2.3 \times 10^6$) against the haze H ($\gamma = 1$ $\alpha = 2$ $b = 40 \times 10^8$).

The agreement that we have obtained led us to suspect that there is a redundancy in the description of aerosol distributions if haze H, L and M are used. To clinch the argument we must obtain this equivalence even when the Mie theory is used. In fig. (5), we have compared the exact Mie results for the phase matrix elements for haze L and M against an equivalent haze H distribution. The same values of the haze H parameters reproduce the corresponding haze L and M distribution even when the wave length has become 0.7μ (fig. 6). Thus over the visible range we have explicitly displayed the redundancy in the description.

Events conspired to accelerate my sedentary pace to solve the full radiative transfer problem and infer the size of particulates from polarimeter measurements. I am referring to the donation of a polarimeter by the TRW Systems Group and a contract from Don Lawrence's NASA - Langley to complete the investigation before this conference.

Our analytic study helped us weed out the redundancy in the description of the aerosol particles and arrive at a basic or irreducible set of parameters - the optical thickness, refractive index, ground reflectivity, vertical profile and the parameter b from the size distribution which is proportional to the reciprocal of the modal radius. It is obvious that some simplifying physical assumptions are needed in order to make the problem tractable.

We shall assume that the ground is a Lambert reflector. While this is certainly not the case, our method of interpretation is to calibrate the ground effect by our set of measurements and use subsequent measurements to make relative statements with respect to the calibration. This will minimize the error due to our assumption. We shall also assume that the refractive index is real in the visible region and make use of the Elterman vertical profile.

The program to solve the radiative transfer equation in a vertically inhomogeneous medium with various aerosol size distributions has been developed by many scientists and the one that I use will be that due to Dr. J. V. Dave,[12] made available to us through the kind efforts of Dr. R. S. Fraser and Dr. M. P. Mc Cormick of NASA. Dave uses the iterative solution to the auxiliary equation and the program is large and quite expensive to run. The cost would have been prohibitive and the analysis impossible had we not simplified the parameterization of the aerosol size distribution to include only haze H at all times.

The polarimeter is mounted on an alt-azimuth tracker and the base has angular read out scales in both azimuth and elevation, facilitating the precise determination of the Zenith angle of observation of the polarimeter. A set of measurements consists of fixing the Zenith angle of observation and varying the azimuth defined with respect to the solar vertical plane from 0^{o} to 180^{o}. If 0^{o} azimuth corresponds to the smallest scattering angle then it is expedient to normalize all the measured intensity values with respect to this intensity at $\phi = 0$ azimuth and avoid the measurement of exact intensities. The experimentally normalized intensities (I) and degree of polarization (P) can be plotted as a function of the azimuth ϕ .

The theoretical analysis consists of studying the sensitivity of the (normalized) intensity and polarization to the parameters τ, n, b and A. It was observed that they were smoothly varying functions of those parameters and hence it was possible to extrapolate and interpolate the obtained results with a great degree of confidence. Thus typical variations are given in figs. 7-10. Our analysis enabled us to arrive at the following conclusion.

1) The width of the normalized I curve is determined by b.
2) Increase of τ and A raises the tail of the I curve and lowers the degree of polarization.
3) The depolarization due to an increase of m was considerably more drastic.

Thus in order to fit a set of measurements we arrive at the following set of rules.

1) Change b to fit the width of the normalized intensity curve.
2) Fix a reasonable value of the ground albedo, (For $\lambda = 0.7$ we chose $A = 0.2$) in order to calibrate the ground effect. Here we are considering downward radiation and hence the ground effect is not very serious.
3) Vary τ and m so that I and P curves fit the data.
4) Repeat measurements, but use same value of A to obtain fits.

Using this recipe we have fit 3 sets of data taken on August 12, 1973 on the roof-top at UCLA. The relevant parameters are given in figs 11 - 14. It is important to notice the temporal change in size distribution (parameter b) which implies a change in the "average" size of a particle. This is presumably a meteorological feature peculiar to the LA basin where due to the changing wind patterns the marine aerosols and continental aerosols are moving in different directions. A more detailed study, including the correlation with meteorological conditions, is being undertaken by my student R. Willson, for his Ph.D. dissertation.

INTERPRETATION

For the set of haze H parameters we can arrive at the equivalent haze L and M parameters. Those are given in figs. 15-17 and tables I and II. This suggests that the radiation field measurements alone will not enable the determination of exact size distributions. What it does provide is an equivalent optical description which can be used to calculate radiative effects, such as, cooling, heating, etc. Further, relative statements seem to be valid no matter which description of haze H, L, or M is used. For instance, our measurements indicate the increase of modal radius from data set 1 to data set 2 and the decrease from data set 2 to data set 3, when b takes on the values of 18, 12.6, and 25. We observe that this trend holds for haze L and M descriptions as well. The other parameters m, τ and A are unaffected by this model dependency.

It may be argued that in situ techniques will provide exact measurements and are, therefore, more useful. I think in situ sampling mutilates the object that is being studied and so measurements of this nature must be viewed with caution. It would be most desirable to couple in situ techniques with polarimeter measurements and then check if the in situ results, when introduced in the radiative transfer equation reproduce the radiation field that is measured by the polarimeter. I must emphasize that the radiative calculations of aerosol effects are expressed in terms of an effective optical model (such as haze H) and, therefore, the determination of these effective optical parameters, even if they have nothing to do with the actual shape or size of the particles, is most essential. I hope that I have been able to convince you that it is possible, from remote measurements of polarization and intensity, to continually monitor our turbid atmosphere and infer the values of optical parameters essential for calculations in meteorology.

ACKNOWLEDGEMENTS

I am grateful to Professor S. Venkateswaran for his support of this Project. This was the outgrowth of research sponsored in part by the NASA-Langley Research Center and by the U. S. Department of Transportation. My students, Richard Willson and Daniel Phillips have contributed enormously to the success of this experiment while Mr. Dennis St. John and Mr. Bijoy M. Gerge assisted in the programming.

FOOTNOTES AND REFERENCES

1. Z. Sekera and R. E. Bradbury, 1973: "Development of an experiment for visible radiation polarization measurements from a Satellite". NASA CR-2297.

2. Z. Sekera, K. L. Coulson, J. V. Dave, 1960: "Tables related to radiation emerging from a planetary atmosphere with Rayleigh scattering." University of California Press, Berkeley and Los Angeles.

3. Z. Sekera, 1967: Icarus 6, 348.

4. J. G. Kuriyan, D. H. Phillips and R. Willson, 1973: "Determination of optical parameters from ground based polarimeter measurements". UCLA preprint.

5. D. Deirmendjian, 1969: "Electromagnetic Scatterings from spherical polydispersions". American Elsevier.

6. R. S. Fraser, UCLA Thesis, 1959: "Scattering properties of atmospheric aerosols".

7. D. S. Saxon, 1955: "Lectures on the scattering of light". UCLA Department of Meteorology.

8. H. C. van de Hulst, 1957: "Light scattering by small particles". John Wiley, New York.

9. K. Shifrin, 1968: "Light scattering in a turbid medium". NASA Technical translation TT-F472.

10. C. E. Junge, 1963: "Air chemistry and radioactivity". Academic Press.

11. J. G. Kuriyan and Z. Sekera, 1974: Quarterly Journal of the Royal Meteorological Society, 100.67 .

12. J. V. Dave, "Program for computing characteristics of UV radiation". NASA Contract 5-21680.

FIGURES

Figure 1 Normalized forward scattering for Haze H as a Function of Z. Points are obtained from Deirmendjian's Tables 27-32. The curve is that of the analytic formula $\bar{P}_1(z) = \frac{3z^3 + 16z^2 + 35z + 70}{70(1+z)^5}$

Figure 2 Normalized forward scattering as a function of Θ.

Figure 3 Normalized forward scattering for Haze M as a function of Z. Points are obtained from Deirmendjian's Tables 12-16, $b^2 = 8 \times 10^5$, $\gamma = \frac{1}{2}$, $\alpha = 1$. The curve is that of $\bar{P}_1(z)$ with new $b^2 = 7.4 \times 10^8$, $\gamma = 1$, $\alpha = 2$.

Figure 4 Normalized forward scattering for Haze L as a function of Z. Points are obtained from Deirmendjian's Tables 19-26, $b^2 = 2.3 \times 10^6$, $\gamma = \frac{1}{2}$, $\alpha = 2$. The curve is that of $\bar{P}_1(z)$ with a new $b^2 = 40 \times 10^8$, $\gamma = 1$, $\alpha = 2$.

Figure 5 Equivalence of Haze H to Haze L and Haze M, ($\lambda = .45$).

Figure 6 Equivalence of Haze H to Haze L and Haze M, ($\lambda = 0.7$).

FIGURES

Figure 7 Normalized scattered intensity and degree of polarization for b = 10 and b = 25 as a function of azimuth angle relative to the solar vertical plane.

Figure 8 Normalized scattered intensity and degree of polarization for Mie optical thicknesses of τ_m = .15 and .25 as a function of azimuth angle relative to the solar plane.

Figure 9 Normalized scattered intensity (I) and degree of polarization (P) for aerosol indices of refraction m = 1.34 and 1.54 as a function of azimuth angle (Φ) relative to the solar vertical plane.

Figure 10 Normalized scattered intensity (I) and degree of polarization (P) for various Lambertian ground reflectances A = 0, .2 and .4 as a function of azimuth angle (Φ) relative to the solar vertical plane.

Figure 11 The solid curves are the computed I and P for the aerosol model whose parameters are: b = $25\mu^{-1}$, refractive index = 1.54, Mie optical thickness = 0.25 and ground reflectance = 0.2. The dots are measured values of I and P made at UCLA on 12 August 1973 at 1425 hr. Pacific Daylight Time. The wavelength for this observation was 0.701μ. The zenith angle of observation was 62.8^{o} and the solar zenith angle 27.8^{o}.

Figure 12 The solid curves are the computed I and P for the aerosol model whose parameters are : b = $12.857\mu^{-1}$, refractive index = 1.54; aerosol optical thickness = 0.12 and ground reflectance = 0.2. The dots are measured values of I and P made at UCLA on 12 August 1973 at 1438 hr. Pacific Daylight Time. The wavelength for this observation was .701 μ. The solar and observation zenith angles were 28.3^{0} and 41.3^{0}, respectively.

Figure 13 The solid curves are computed values of I and P for the aerosol model whose parameters are: b = 18 μ^{-1}; refractive index = 1.44; aerosol optical thickness = 0.25 and ground reflectance = 0.2. The dots are measured values of I and P made at UCLA on 12 August 1973 at 1457 hr.,Pacific Daylight Time. The solar and observation zenith angles were 33.3^{0} and 62.3^{0}, respectively.

Figure 14 Normalized haze H size distribution functions obtained by fitting the data (figs. 6, 7, and 8). The mode radii are r_c = .080 μ, 111 μ and .156 μ for the distribution with b = 25, 18 and 12.857, respectively.

Figure 15 Normalized size distribution functions for haze H and the equivalent hazes L and M corresponding to data set #1.

Figure 16 Normalized size distribution functions for haze H and the equivalent hazes L and M corresponding to data set #2.

Figure 17 Normalized size distribution functions for haze H and the equivalent hazes L and M corresponding to data set #3.

TABLE I. OPTICAL PARAMETERS FROM BEST FIT OF DATA

Data Set No.	Time P.D.T.*	Solar Zenith Angle (deg)	Observation Zenith Angle (deg)	Parameters Obtained from best fit			
				b (μ^{-1})	τ total†	m	albedo
1	1425	27.8^0	62.8^0	25	.287	1.54	.2
2	1438	28.3^0	41.3^0	12.857	.156	1.54	.2
3	1457	33.3^0	62.3^0	18	.287	1.44	.2

* Pacific Daylight Time

† $\tau_{total} \equiv \tau_{Rayleigh} + \tau_M$ and $\tau_{Rayleigh} = 0.037$ for $\lambda = 0.7$

TABLE II. EQUIVALENT OPTICAL PARAMETERS

Data Set No.	Haze H (α=2, γ=1)	Haze L (α=2, γ=.5)	Haze M (α=1, γ=.5)
	b	b_L	b_M
1	25	28	25
2	12.857	19	10
3	18	23	20

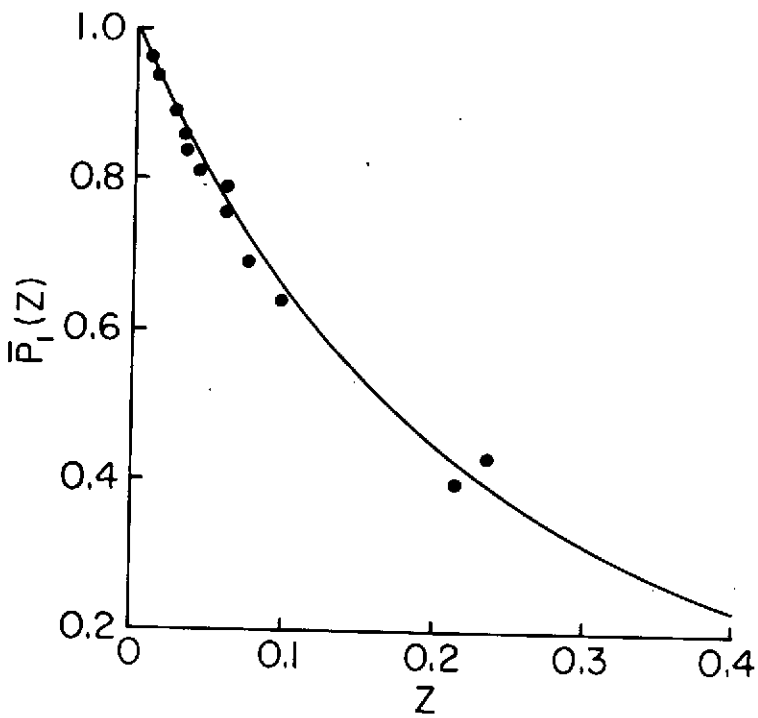

FIGURE 1

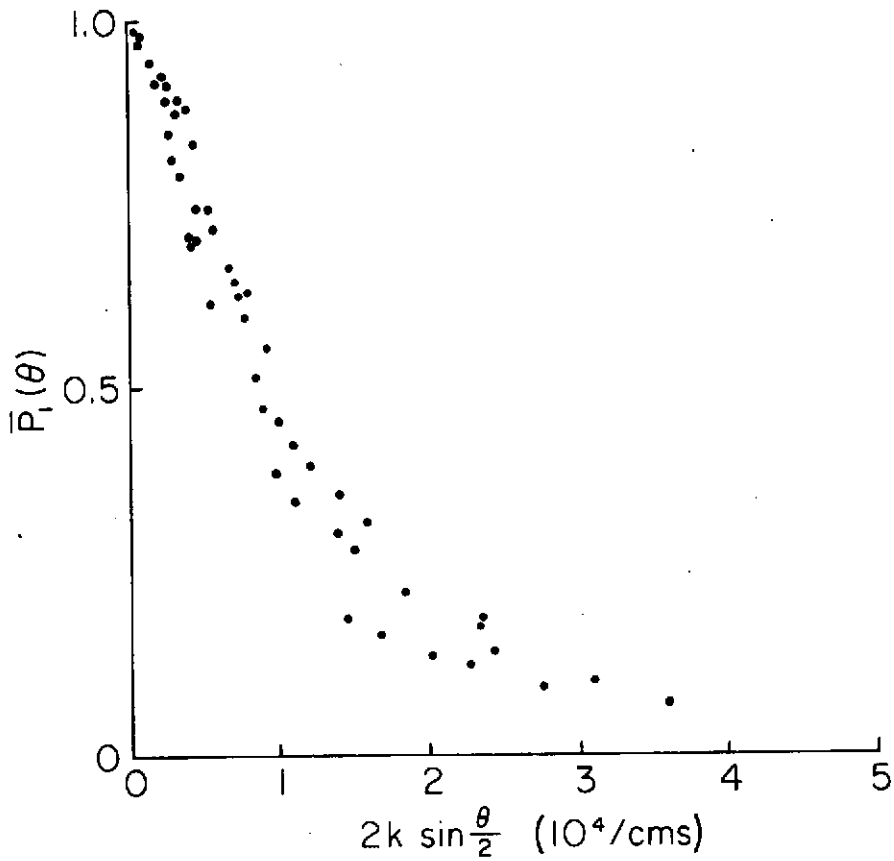

HAZE M (tables 1-15) $0.45\mu \leq \lambda \leq 16.6\mu$

FIGURE 2

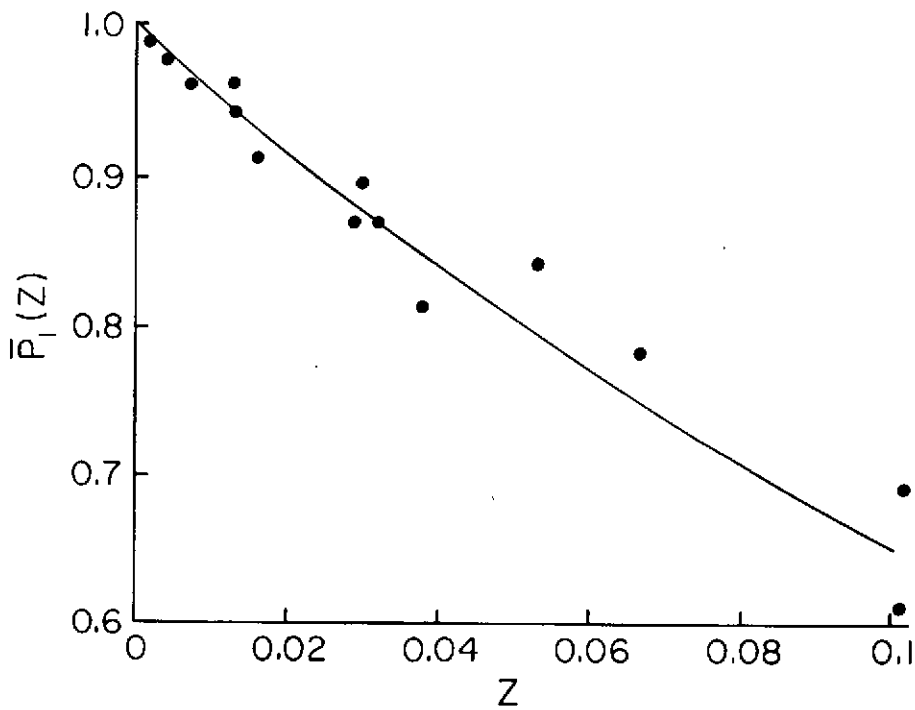

FIGURE 3

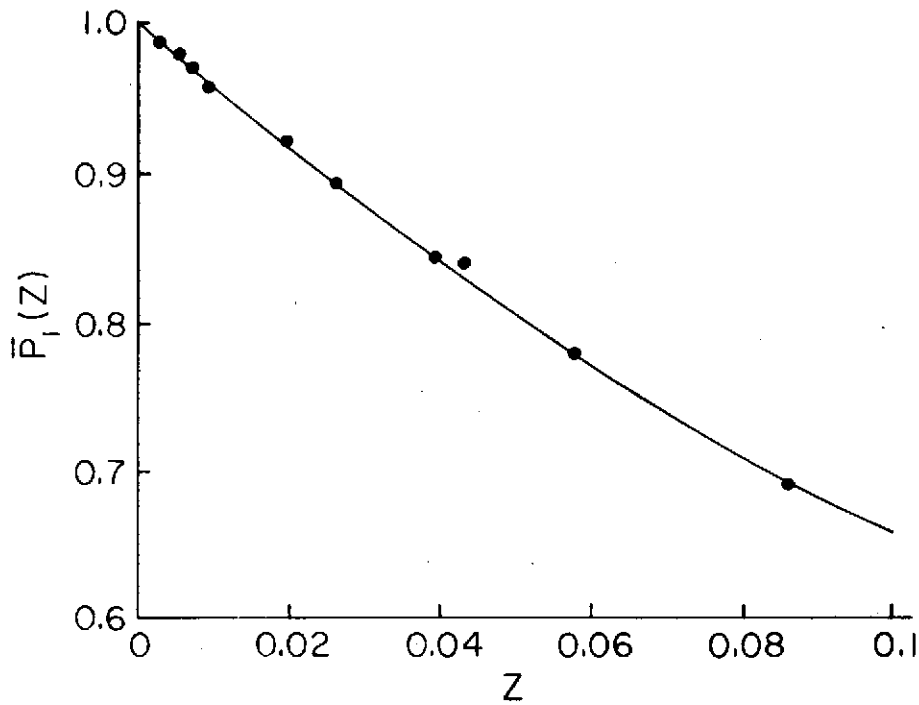

FIGURE 4

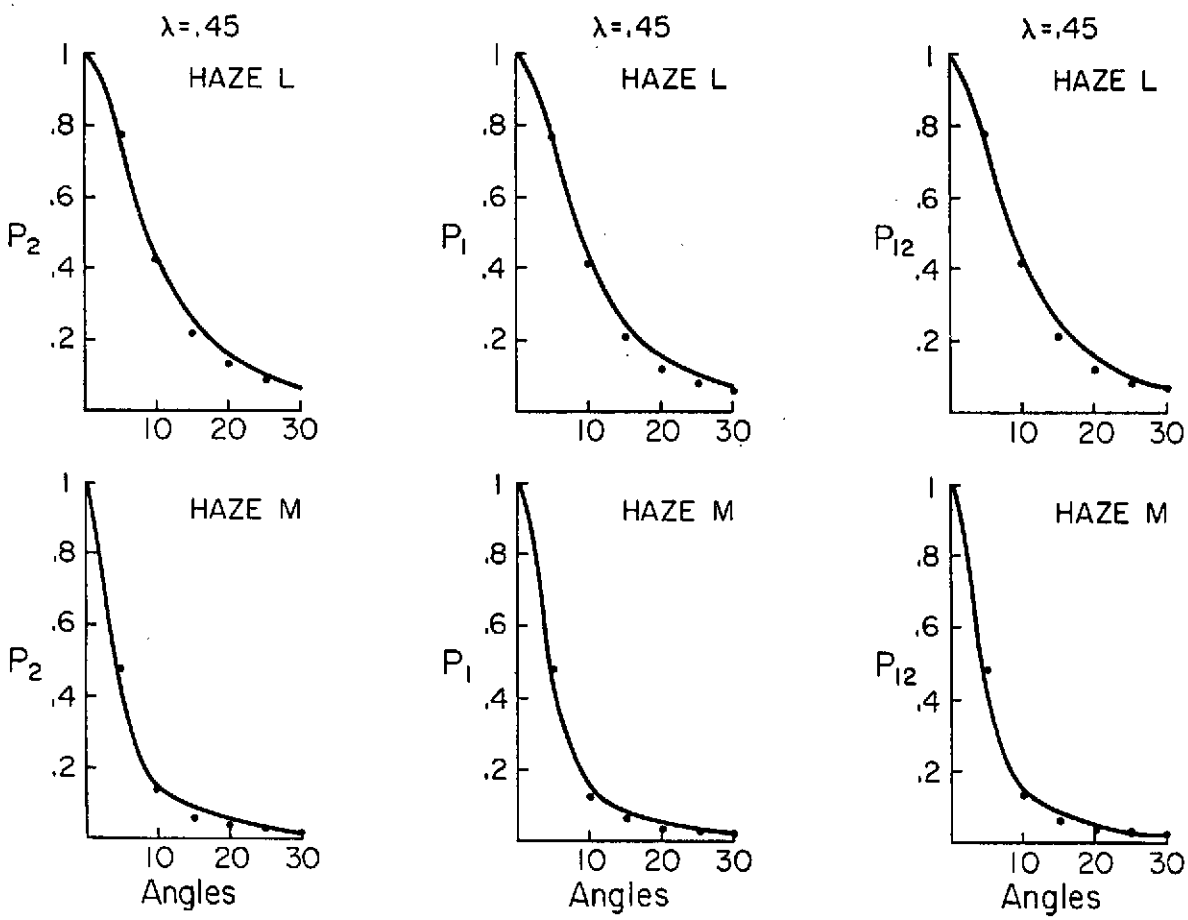

FIGURE 5

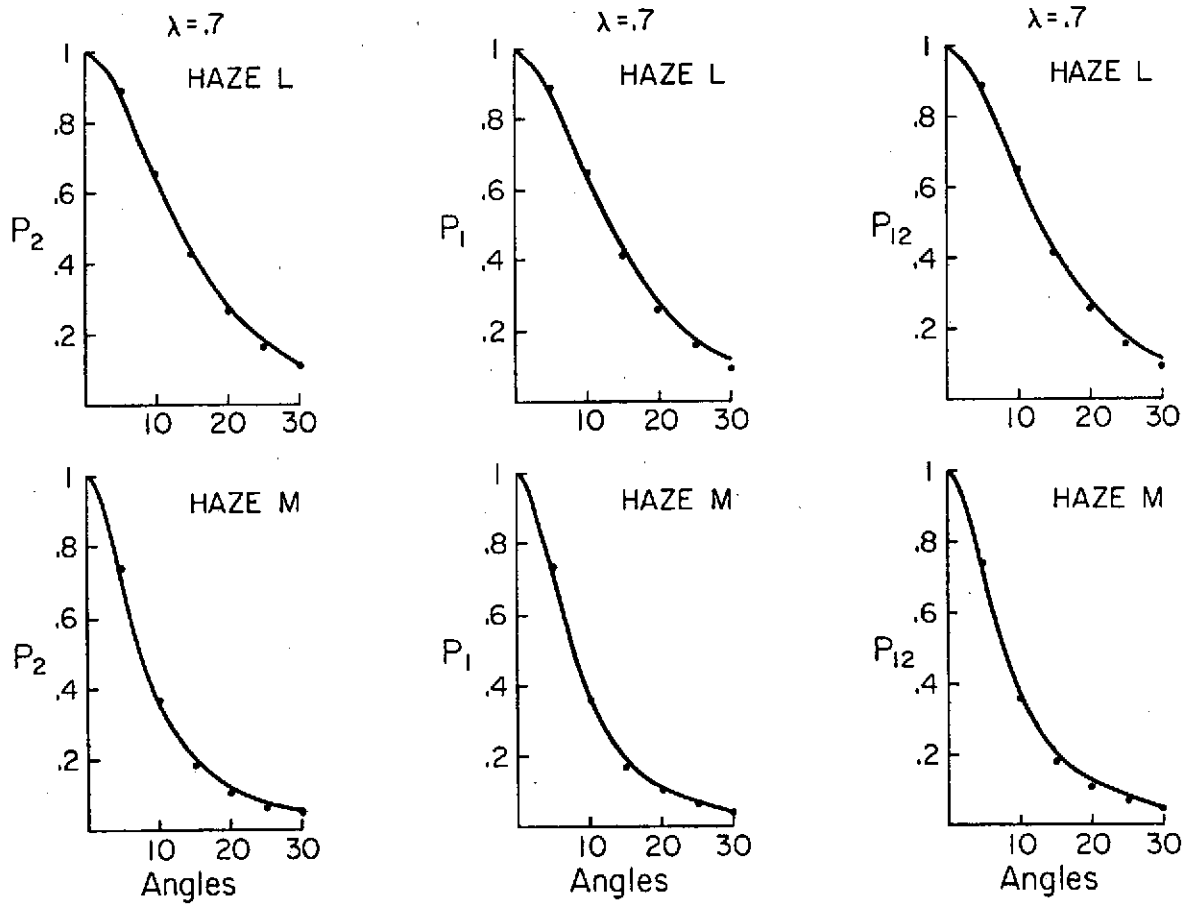

FIGURE 6

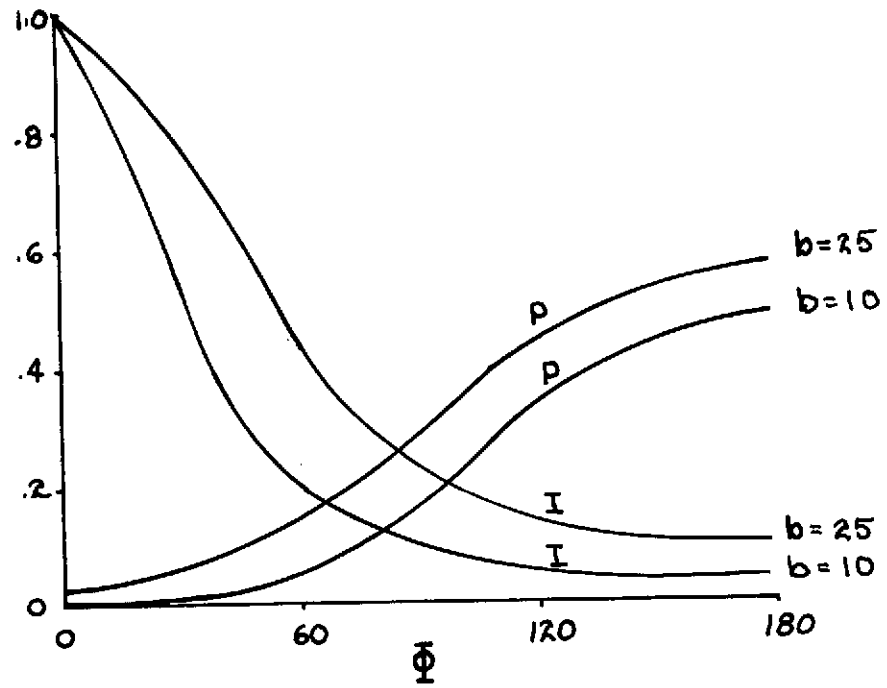

FIGURE 7

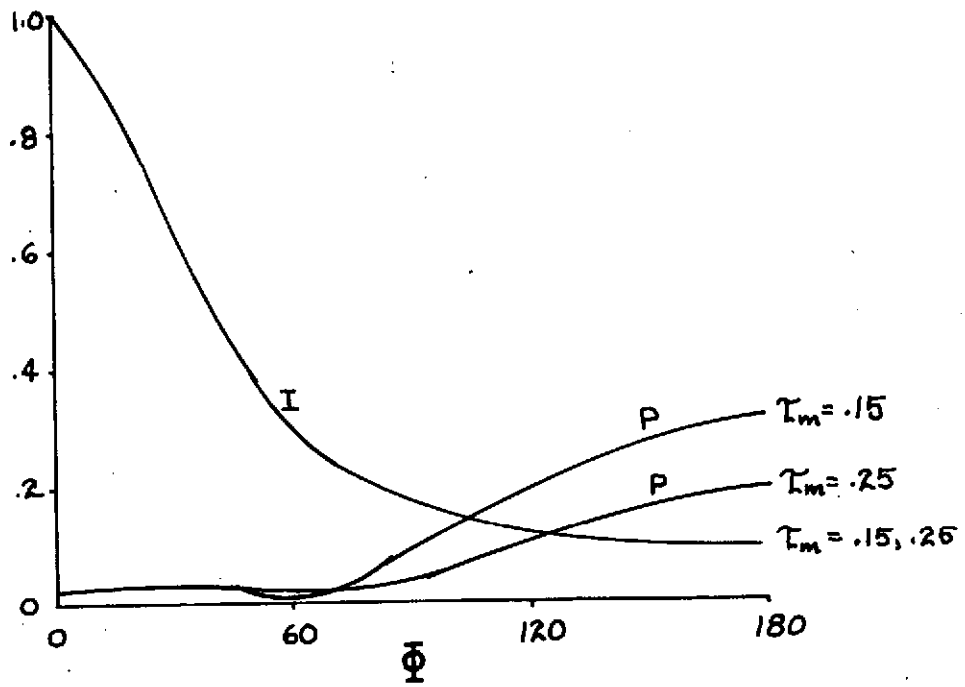

FIGURE 8

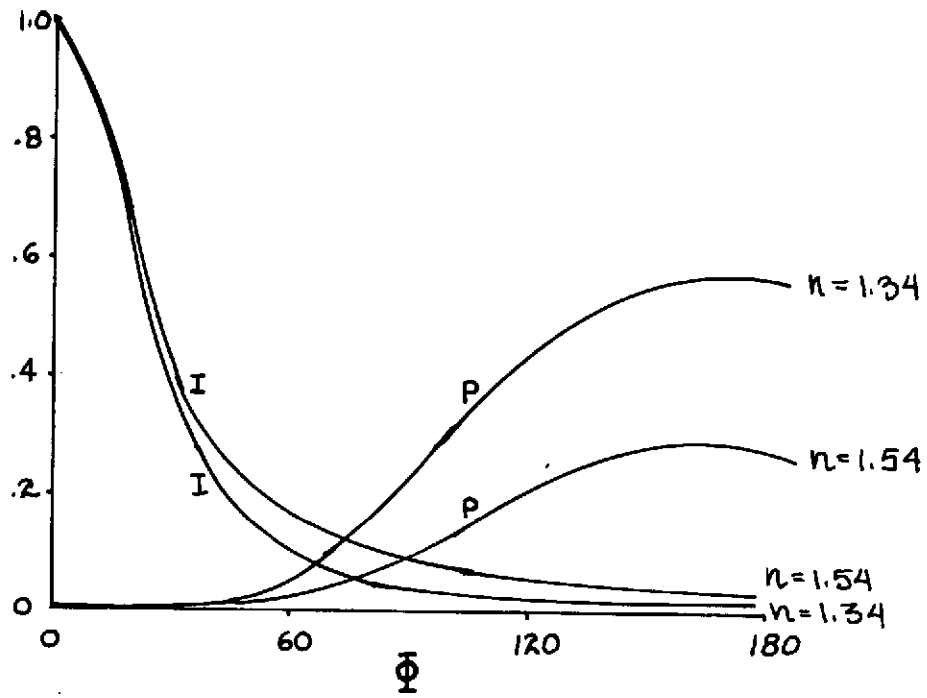

FIGURE 9

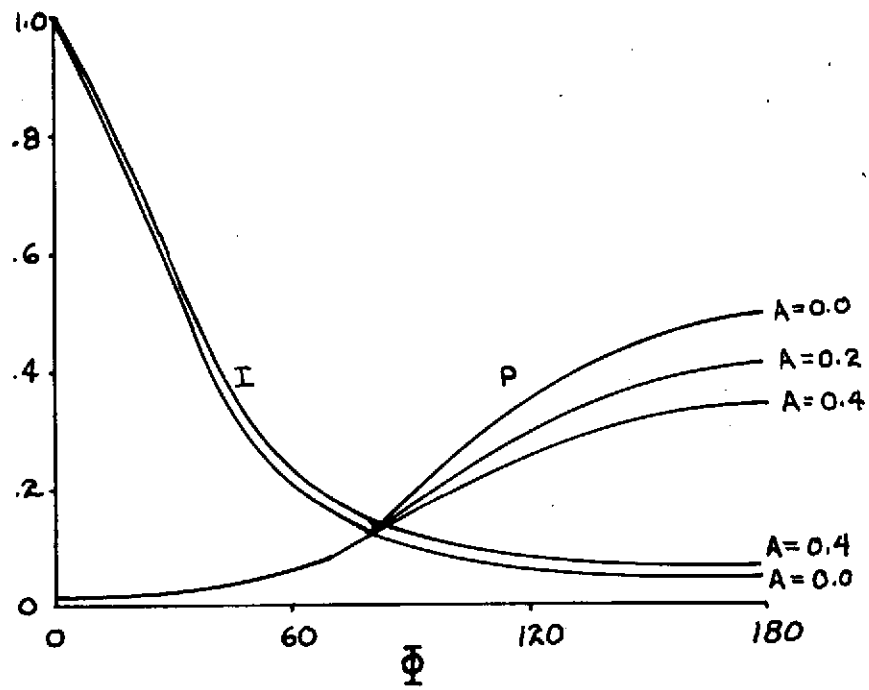

FIGURE 10

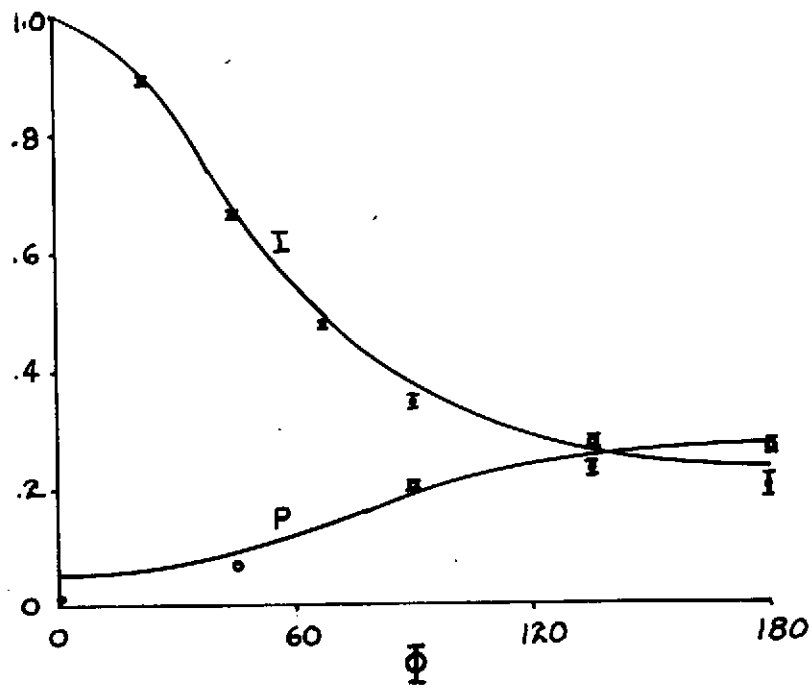

FIGURE 11

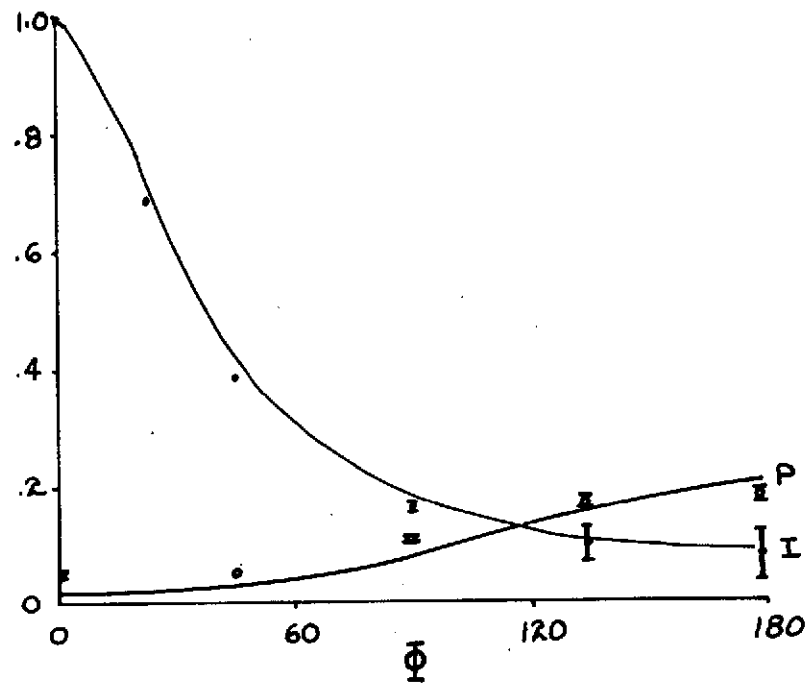

FIGURE 12

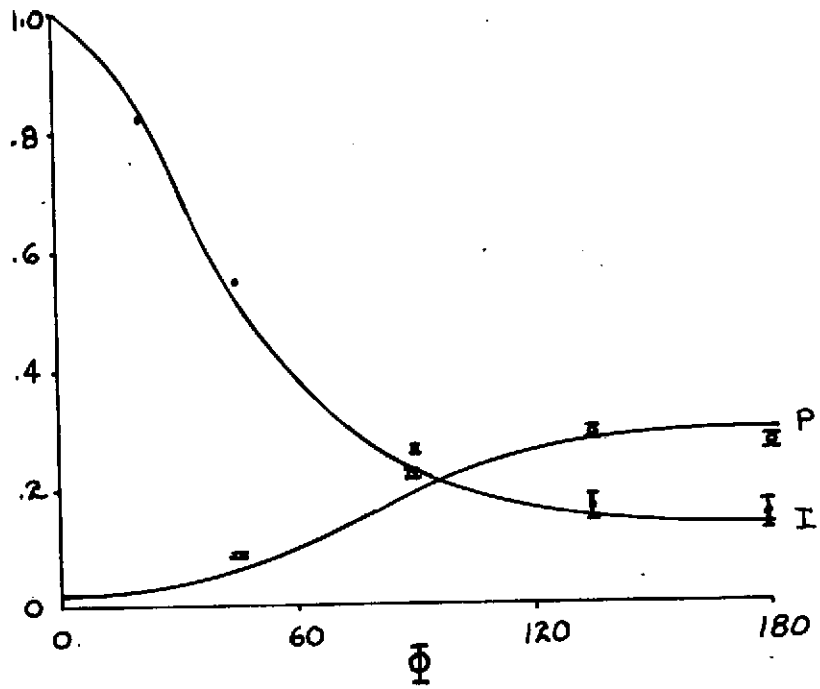

FIGURE 13

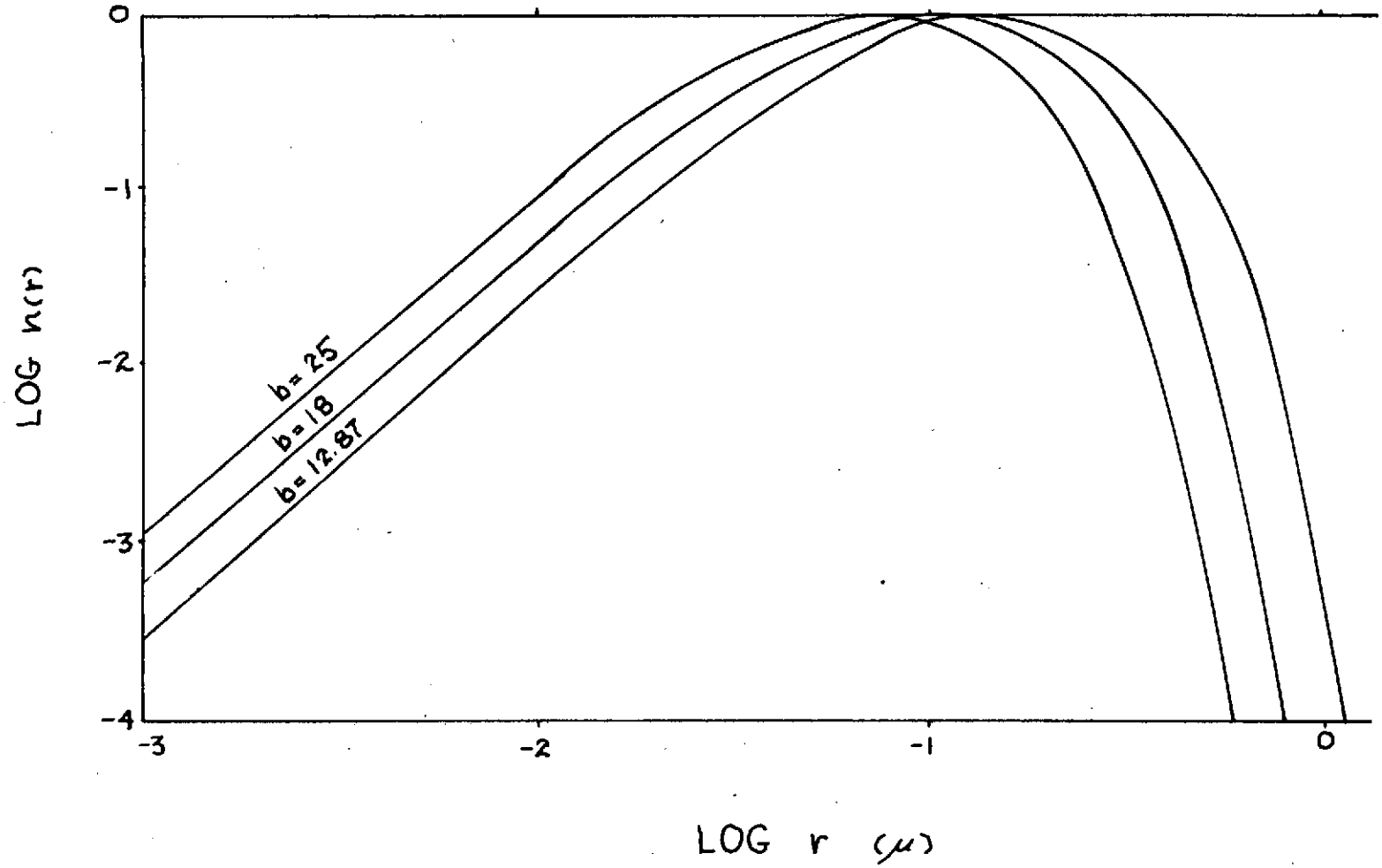

FIGURE 14

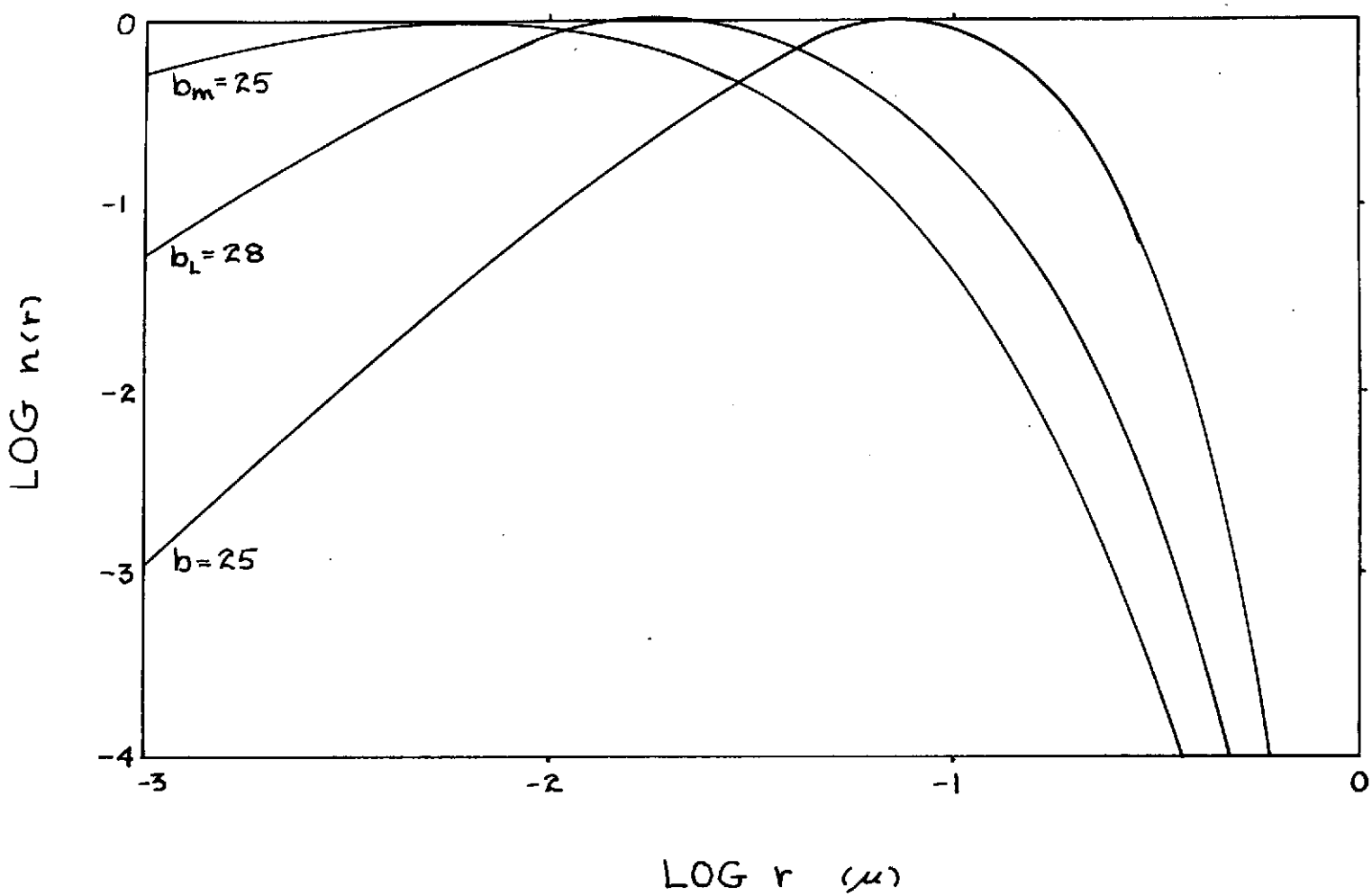

FIGURE 15

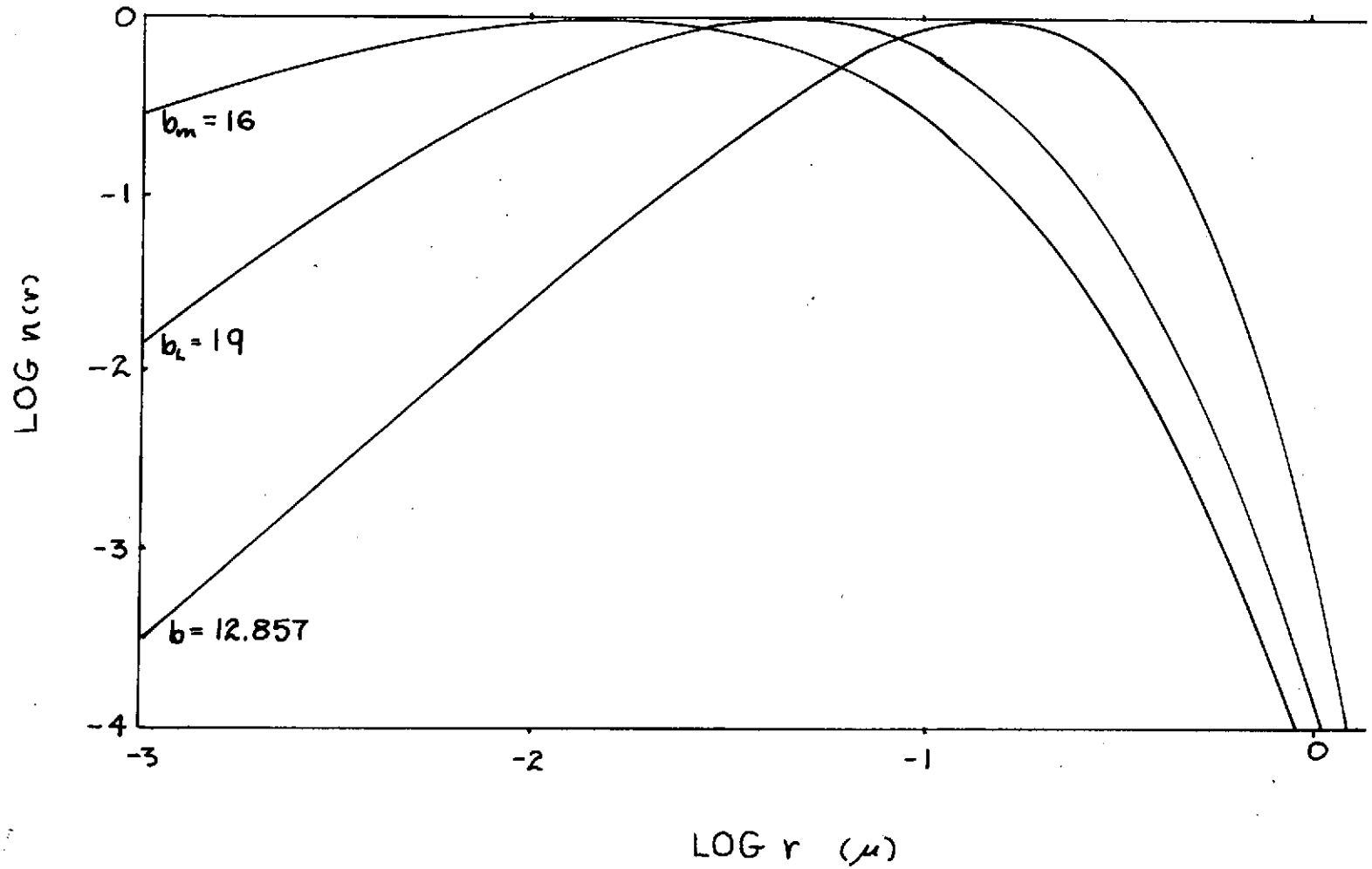

FIGURE 16

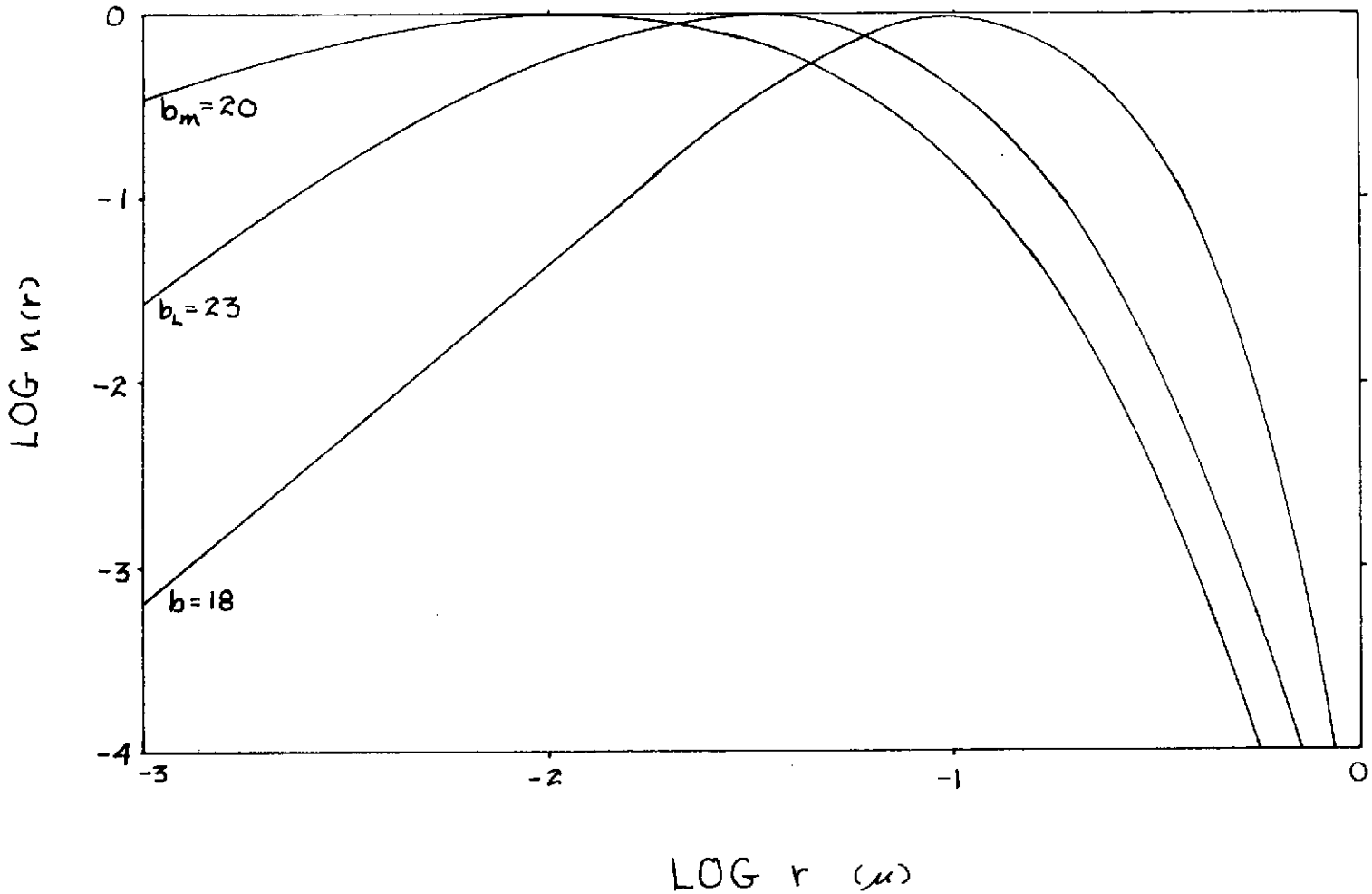

FIGURE 17

LIDAR OBSERVATIONS OF ATMOSPHERIC PARTICULATE CONTENT

R. T. H. Collis, P. B. Russell, E. E. Uthe and W. Viezee
Atmospheric Sciences Laboratory
Stanford Research Institute
Menlo Park, California 94025

1. INTRODUCTION

The lidar, or laser radar technique of atmospheric probing has just celebrated its 10th Anniversary. In the decade since the first observations of elastic backscatter from atmospheric particulates of the "clear air" were made, this basic capability has been applied to a wide range of atmospheric observations and, in addition, a number of sophisticated concepts which exploit the wave and quantum nature of light have received attention, (Collis, 1970). These include the measurement of gaseous species concentration by Raman scattering or by differential absorption techniques; the measurement of turbulence, velocity or temperature by Doppler techniques and the detection of atomic elements in the outer atmosphere by resonance scattering. These applications, however, are for the most part still at an exploratory stage. The basic elastic backscattering approach on the other hand has been extensively used for the observation of cloud and haze, which provides direct information on atmospheric conditions of obvious importance in general meteorology, and for mapping and tracking aerosol concentrations in various research applications--such as those concerned with the transport and diffusion of pollutants. One of the most exciting and valuable contributions of lidar, however, has been to extend our knowledge of the "transparency" of the clear air.

A description and discussion of lidar in this role is very pertinent in the context of this conference, concerned as it is with both radiative energy transfer and remote sensing techniques.

Before proceeding to this, however, we briefly review the basic lidar concept and identify the nature of lidar observations in this context.

2. LIDAR OBSERVATIONS

a) Basic Concepts

Lidar, as discussed here, is the application of the pulsed radar technique at visible or near IR frequencies using high powered, very short pulse, lasers as the energy source. Such energy, backscattered by the molecular and particulate phases of the atmospheric aerosol provides a signal, the intensity of which varies with time from the transmission of the pulse, in accordance with the following single-scattering lidar equation:

$$P_r(R) = P_t\, L\, \beta(R)\, A\, R^{-2} \exp\left\{-2\int_0^R \sigma(r)dr\right\} \qquad (1)$$

where

P_r is instantaneous received power;

P_t is transmitted power at time t_0;

L is effective pulse length (ℓ);

($L = c\tau/2$ where c is the velocity of light and τ is pulse duration; it is the range interval from which signals are simultaneously received at time t).

β is the volume backscattering coefficient of the atmosphere ($ster^{-1}\ell^{-1}$);

R is range ($R = c(t-t_0)/2$ where t_0 is the time of transmission of pulse;

σ is the volume extinction coefficient, (ℓ^{-1}); and

A is the effective receiver aperture.

The magnitudes of β and σ depend upon the wavelength of the incident energy, and the number, size, shape and refractive properties of the illumination particles per unit volume, in a complicated manner (with the exception of the case of Rayleigh scattering, which occurs when the scattering particles are small compared to the laser wavelength). The physics of elastic light scattering by particles is thoroughly described by a number of texts, including van de Hulst (1957), Deirmendjian (1969), and Kerker (1969).

The relation of the optical parameters β and σ to each other, and their relation to such physical parameters as number or mass concentration, even to a meaningful degree of approximation, are problems of considerable difficulty. Nevertheless useful solutions of the lidar equation have been accomplished. (See Section 2c below).

Essentially the current capabilities of lidar lie in three areas:

1) providing analog representations of the variability of atmospheric particulate concentration, which, especially in two dimensional cross-section form, reveal the presence and geometry of significant structure--such as layering, with indications of at least relative concentration;

2) providing quantitative data on the observed optical parameters (β and σ) and their temporal and spatial variation (as in vertical profiles) for the wavelength used (limited in present technology to the visible and and near IR);

3) providing, to a limited degree, quantitative information on physical parameters that can be derived from the optical data of 2), given certain additional data or assumptions.

b) Evaluation of the Lidar Equation

A number of solution techniques have been proposed to evaluate the lidar equation (1) for quantitative purposes (Barrett and Ben-Dov, 1967; Fernald et al., 1972). The general approach followed by SRI is typical (Johnson and Uthe, 1971; Davis, 1969) and is described below.

The returned signal in logarithmic form is range normalized and corrected for instrumentation transfer anomalies and any pulse-to-pulse variations in lidar performance. The resulting S-values, defined as

$$S(R) \equiv 10 \log \frac{P_r(R)\, R^2}{P_r(R_0)\, R_0^2} \tag{2}$$

$$= 10 \log \frac{\beta(R)\, T^2(R)}{\beta(R_0)\, T^2(R_0)} \tag{3}$$

evaluate, in relative terms, the atmospheric dependent parameters of the lidar equation, viz: $\beta \exp -2\int\sigma dr$ or βT^2, where T is the path transmittance. (R_0 is a reference range--normally that at which β is measured or can be assumed to be constant).

In differential form:

$$\frac{dS}{dR} = 4.34 \frac{1}{\beta} \frac{d\beta}{dR} - 8.7\sigma \tag{4}$$

and from this, given i) an assumption or data on the relationship between σ and β, and ii) a boundary value of an appropriate parameter, we can derive evaluations of the optical parameters, or, given additional relationships, certain physical parameters. By a linearization transformation, Equation 4 can be expressed in the general form from which various solutions may be derived, according to the input parameters used as illustrated in Table I.

$$\Phi(R) = \frac{\exp C_1\, S(R)}{\Phi^{-1}(R_0) - C_2 \int_{R_0}^{R} \exp(C_1\, S(r))dr} \tag{5}$$

In the case of turbid atmospheres, certainly for example in fog or cloud, multiple scattering occurs and the solutions proposed above are invalid. In such cases, more sophisticated formulations of the lidar equation must be used (Liou and Schotland, 1971; Weinman, 1972; and Eloranta, 1972), although useful evaluations of lidar observations in fog have been made by Viezee, et al. (1973b) using a semi-empirical approach.

However, in less turbid atmospheres and certainly in what is commonly thought of as "clear" air, the assumption of single scattering appears to be wholly acceptable for lidar data where we are concerned with evaluations of backscattering within a narrow beam (of the order of 0.01°). In fact, in such conditions, useful quantitative data may often be derived on the assumption that attenuation is negligible or given by certain model values. (See Section 3 below).

Table 1

Some Solution Possibilities for Given Input Parameters (See Eq. 5)

Solution for	Basic relationship measured or assumed	C_1	C_2
β	$\beta = k_1 \sigma$	$\frac{1}{4.34}$	$\frac{2}{k_1}$
σ	$\frac{d\ell n\beta}{d\ell n\sigma} = k_2$	$\frac{1}{4.34}$	$\frac{2}{k_2}$
C (concentration)	Relative size distribution, n_r, invariant with range.	$\frac{1}{4.34}$	$2\int_0^\infty \pi r^2 Q_e n_r dr$
($n = C n_r$; Q_e = Mie efficiency factor; r = particle radius)			
M (mass concentration)	$\S_e = \frac{\sigma}{M}$ and β/M is invariant with range	$\frac{1}{4.34}$	$2 \S_e$ See Johnson & Uthe, 1971

c) Polarization Measurements

Mention should also be made of the possibility of exploiting depolarization effects to acquire further information from lidar backscattering observations, especially in studies of clouds. With only one angle of view (π), it is only possible to make limited inferences from such observations. Most usefully the presence of non-spherical particles (e.g. ice crystals) can be determined by comparing the magnitude of lidar returns measured under various combinations of transmitter and receiver polarization. Since spherical particles will return incident energy with no change in polarization, the observation of significant depolarization will indicate the presence of non-spherical scatterers (Zuev, et al., 1973; Schotland, et al., 1971). Note however that with high concentrations of spherical particles--as in fog or cloud, multiple scattering will also contribute to depolarization effects (Liou and Schotland, 1971; Eloranta, 1972). Distinguishing between the depolarization effects of non-spherical particles and those of multiple scattering by spheres is a subject of current investigation at several laboratories (Carswell, et al., 1973).

d) Discussion of the Validity of Lidar Observations

As noted above, the interpretation of lidar signals in physically significant terms is open to some uncertainty due to the fundamental difficulties of deriving absolute information from such signals alone. For example, an increase of signal intensity with range could be ascribed either to an increase in the number of scatterers present, given that their size distribution, shape, and refractive properties is unchanged or to a change in one or other of these characteristics without an increase of number concentration. While this concept is strictly correct, in practice it is wholly possible to assess the lidar signal on the basis of certain assumptions regarding the nature of the aerosols observed or of the possible changes therein, provided that the interpretation based upon such assumptions is not carried beyond reasonable bounds. Thus, for example, if the returned signal from a certain atmospheric layer shows an enhancement by a factor of 10 over that from the atmosphere immediately below it, it is reasonable to infer that the layer comprises an increased number concentration of particles, if reasons exist for believing that the aerosol present in both layers is from a common source. This inference becomes more certain if it can be shown that any change of refractive properties and/or change of particle size distribution that can reasonably be expected, would result in a change in backscatter coefficient by a factor less than 10. The accuracy with which the change of particulate number concentration can be specified, however, will obviously depend upon the degree to which the other variables (and their relationship) are known.

These concepts are basic to the faith of those familiar with the use of lidar, but warrant further examination in the present context, where we are concerned with relatively small variations in the returned signals from, or the characteristics of, the "clear" air.

A complete analysis of all possible combinations of the variables involved in relating the optical and physical parameters of an aerosol is not possible in this review. In order to indicate the degree of uncertainty inherent in lidar observations, or in inferences of their physical significance, that might result from such variables, however, Table II (by no means exhaustive) summarizes the results of a number of investigations in this area. Table II is necessarily in very abbreviated form. To illustrate its use, consider the first entries relating to changes in particle size distribution (Grams, 1966). In column i, we indicate the nature of the changes from an initial state where (as noted

in column vii, in a Junge distribution with an upper particle radius, R_2 = 3.3 μ, and a wavelength of 0.6943 μ), ν = 3.5 and R_1 = .275 μ. We first consider changes within a "reasonable" range, to

$$\nu = 4.0 \text{ and } R_1 = 0.3\ \mu, \text{ or to } \nu = 3.0 \text{ and } R_1 = .1\ \mu$$

and then changes to extreme values treated by Grams, - viz. to

$$\nu = 4.0 \text{ and } R_1 = .5\ \mu, \text{ or to } \nu = 2.0 \text{ and } R_1 = .03\ \mu$$

The effects of such changes on the number concentration N required to maintain the same backscattering coefficient as that resulting from the initial state, are shown in column ii where, for example, "x 1.4" indicates that the changes shown in column i would require an increased number concentration equal to 1.4 times that given by the initial state.

Conversely, to show the effect of such changes in terms of the sensivity of lidar backscattering measurements, column v indicates what happens to a scattering ratio (i.e., $\beta_{total}/\beta_{molecular}$, see Section 3e) of 1.1, when different parameters are used to derive this ratio from the number concentration giving a ratio of 1.1 under the assumption of the initial state parameters.

For the most part the effects noted represent extreme ranges, in practice the uncertainty might be expected to be must less.

As Table II shows, considerable caution must be applied in drawing inferences regarding other optical or physical parameters from lidar measurements of backscatter coefficient on the basis of theoretical assumptions alone. Although not excessive, the dependence of relationships between the various parameters on specific characteristics of an aerosol is significant, certainly where Mie theory applies. However, there are strong grounds for believing that in practice, probably because of the non-sphericity of the particles involved and/or the complexity of their refractive properties, Mie theory is inappropriate for specifying the scattering characteristics of some natural aerosols in simple terms.

The inapplicability of Mie theory in these cases is manifest in two important ways. Firstly, predictions of the relationship between the optical and physical characteristics, derived by Mie theory, can be inaccurate. Secondly, empirically derived relationships are evidently more consistent and less dependent upon critical values of individual parameters than would be expected on the basis of Mie computations. Some examples of these considerations are given in Table III. This leads to two important conclusions: firstly, that lidar observations of natural aerosols are likely to be less affected by minor changes in the detailed characteristics of an aerosol than is suggested by theoretical considerations; secondly, that independently derived information can be used most effectively, to provide useful and consistent interpretations of lidar data.

3. THE USE OF LIDAR DERIVED INFORMATION

a) General

With due recognition of the foregoing reservations, lidar can provide better understanding of the nature of the real atmosphere--the form particulate concentrations and layers take--and, more quantitatively, the detailed variation of the optical properties, particularly with height.

Table II Various Aspects of the Interrelation of Physical and Optical Parameters of Atmospheric Aerosols (Theoretically Derived)

(i)	(ii)	(iii)	(iv)	(v)	(vi)	(vii)
Particulate characteristic and change therein	For given backscattering coefficient β, change in:			For given N,M,σ or σ_s a scattering ratio R = 1.1 becomes:	Ref.	NOTES $N = \int_0^\infty n(r)dr$ $R = \beta_{total}/\beta_{molecular}$, (see Sect. IIIe)
	number concentration N	mass concentration M	extinction coefficient σ, or total scattering coefficient σ_s			
SIZE DISTRIBUTION						
$\nu = 3.5$ $R_1 = 0.275\ \mu$ ($m = 1.5$)					Grams (1966)	Based on Junge distribution: $n(r) = Cr^{-(\nu+1)}$, $R_1 \leq r \leq R_2$ where $n(r)dr$ = number of particles with radii between r and r + dr ($\lambda = 0.6943\ \mu$) $R_2 = 3.3\ \mu$
to $\nu = 4.0$ $R_1 = .3\ \mu$	x 1.4			1.07		
to $\nu = 3.0$ $R_1 = .1\ \mu$ (reasonable range)	x .6			1.17		
to $\nu = 4.0$ $R_1 = .5\ \mu$	x 2.0			1.05		
$\nu = 2.0$ $R_1 = .03\ \mu$ (extreme range)	x .3			1.30		
Haze Model L to Haze Model H (with m = 1.33)	x 3.7			1.03	Viezee, et al. (1973a)	Based on Deirmendjian's (1969) haze models ($\lambda = 0.6943\ \mu$)
$\nu = 2.5$ $R_1 = 0.04\ \mu$ $R_2 = 10\ \mu$ to $\nu = 4.0$ $R_1 = 0.08$ $R_2 = 3\ \mu$ (extreme range) (m = 1.5)			x .6	1.17	Harrison et al (1972)	Based on Junge distribution ($\lambda = 0.6943\ \mu$)
$\nu = 2.0$ to $\nu = 3.75$ (m = 1.5) (extreme range)			x .6	1.17	Gambling and Bartusek (1972)	Based on Junge distribution ($\lambda = 0.6943\ \mu$)
to $\nu = 3$ (m = 1.33) (widest range for m = 1.33)			x .75	1.13		
$\nu = 3$, $R_1 = 0.08\ \mu$, $R_2 = 3.0\ \mu$ to $\nu = 4$, $R_1 = 0.04\ \mu$, $R_2 = 10.0\ \mu$ (extreme range) (m = 1.5)		x 2.01		1.05	Russell et al (1973b)	Based on Junge distribution
Haze Model L to Haze Model H when m = 1.45		1.35		1.07	Russell et al (1973b)	Based on Deirmendjian's (1969) haze models
when m = 1.33		.99		1.1		

Table II Various Aspects of the Interrelation of Physical and Optical Parameters of Atmospheric Aerosols (Theoretically Derived)

(i)	(ii)	(iii)	(iv)	(v)	(vi)	(vii)
Particulate characteristic and change therein	For given backscattering coefficient β, change in:			For given N, M, σ or σ_s a scattering ratio R = 1.1 becomes:	Ref.	NOTES $N = \int_0^\infty n(r)dr$ $R = \beta_{total}/\beta_{molecular}$, (see Sect. IIIe)
	number concentration N	mass concentration M	extinction coefficient σ, or total scattering coefficient σ_s			
REFRACTIVE INDEX						
m = 1.5 - 0i to m 1.33 - 0i	x 3			1.03	Grams (1966)	(λ = 0.6943 μ) see note in row 1 above
n_{im} = 0 to n_{im} = 0.01 (reasonable range)	x 2.9			1.03	Grams et al. (1972)	(λ = 0.694 μ) n_{rs} = 1.55 empirical size distribution
n_{im} = 0.01 to n_{im} = 0.1 (extreme range)	x 10			1.01		
m = 1.7 - 1.84i to m = 1.33 - 0i					Viezee et al. (1973a)	(λ = 0.6943 μ)
for Haze Model L	x 1.5			1.07		
for Haze Model H	x 3.7			1.03		
n_{im} = 0 to n_{im} = 0.025			x 2.3	1.04	Harrison et al. (1972)	Effect on total scatter coefficient σ_s (λ = 0.6943)
m = 1.6 - 0i to m = 1.33 - 0i			x 3	1.03		Based on Junge distribution
m = 1.5 - 0i to m = 1.33 - 0i			x 2.3	1.04	Gambling and Bartusek 1972	- do -
m = 1.33 - 0i to m = 1.54 - 0i for Haze Model H		x 3.5		1.03	Russell et al (1973b)	Based on Deirmendjian's (1969) haze models

Table II Various Aspects of the Interrelation of Physical and Optical Parameters of Atmospheric Aerosols (Theoretically Derived)

(i)	(ii)	(iii)	(iv)	(v)	(vi)	(vii)
Particulate characteristic and change therein	For given backscattering coefficient β, change in:			For given N,M,σ or σ_s a scattering ratio R = 1.1 becomes:	Ref.	NOTES $N = \int_0^\infty n(r)dr$ $R = \beta_{total}/\beta_{molecular}$, (see Sect. IIIe)
	number concentration N	mass concentration M	extinction coefficient σ, or total scattering coefficient σ_s			
SHAPE						
Sphere to "onion shaped artifact"			x 1.5	1.07	Harrison et al (1972)	- do -
Sphere to plate			x 10 see note	1.01	Holland and Gagne (1970)	Laboratory measurement Differences of as large as order of magnitude noted at near backscatter angle, but not at 180° (λ = .4860 μ and λ = .5460 μ) Authors caution against generalization from their limited results, but stress importance of shape

TABLE III

Some Determinations of the Interrelation of Optical and Physical Properties of Aerosols

Reference	Results	Notes
BACKSCATTER/EXTINCTION ($A = 4\pi\beta/\sigma$)		
McCormick, et al. (1968)	A = 0.4-0.6	Theoretical derivation on basis of several size distributions and m = 1.5-0i
Waggoner, et al. (1972)	0.15	Comparison of ruby (λ = .6943μ) lidar and nephelometer measurements in urban atmosphere with variable relative humidity below 70%
Davis, (1969) (1971)	0.40	For cirrus cloud, derived from ground (1969) and airborne (1971) ruby lidar observations
Hamilton, (1969)	0.3-0.5	Both β and σ derived from lidar observations of boundary layer urban aerosol (ruby lidar)
BACKSCATTER/NUMBER OR MASS CONCENTRATION		
Johnson and Uthe, (1971)	Assessment of mass concentration of fly ash in smoke stack plume--good agreement with estimates based upon quite independent data.	Fly ash material of known refractive index and density (ruby lidar)
Uthe and Lapple, (1972) (see Collis and Uthe, 1972)	Series of comparisons of lidar observations of β and σ (at λ = 0.6943μ and λ = 1.06μ) with known concentrations of virtually mono-disperse aerosols in test chamber, gave good agreement with Mie theory predictions.	Fly ash material of known refractive index and density, ruby and neodymium lidars (comparison also made with σ for broad band light)
Uthe and Johnson, (1971) (see Collis and Uthe, 1972)	Lidar observed backscatter profiles consistently related to profiles of particle concentration independently obtained by in-situ sampling.	See Section IIId, below. Observation made over sea below 3 kms.
Dynatrend, (1973)	Comparison of lidar observed backscatter profiles of stratospheric layers show close correspondence, with height and relative magnitude. to particle count profiles derived by in-situ balloon sampling.	NCAR and NASA Langley, ruby lidars

TABLE III (Continued)

Reference	Results	Notes
BACKSCATTER/NUMBER OR MASS CONCENTRATION		
Russell, et al. (1973b)	Comparison of ruby lidar observation of stratospheric layer with mass concentration (filter sample) obtained by aircraft shows very close agreement.	Using Mie theory computation based on measured refractive index, shape and density, and assumed size distribution (Deirmendjian Haze Model H)-- in-situ measurement: $9.8 \pm 1.8 \times 10^{-14} gcm^{-3}$ ambient Lidar derived measurement: $9.6 \pm 2.3 \times 10^{-14} gcm^{-3}$ ambient

In some cases, of course, this sort of information has direct, specific value for its own sake--as for example in providing knowledge of the range of variation of the stratospheric aerosol concentration. It certainly can be of great assistance in the interpretation of other measurements--particularly from passive sensors.

In a more general sense, such information can provide a basis for advancing our understanding of the physical processes of the atmosphere. Both points bear on the topics of this meeting. In studying and modelling radiative transfer processes, more realistic inputs on the effects of particulates are badly needed. In any form of remote sensing, either of the earth's surface or of the atmosphere itself, modern techniques have reached such a level of sophistication and precision that the effects of particulates can no longer be neglected as being insignificant factors.

These concepts are now illustrated.

b) Aerosol Distribution in the Urban Atmosphere

The first example shows how lidar can contribute in radiative transfer studies. With NSF sponsorship, we have been participating in the METROMEX project in St. Louis. There, in addition to making observations in support of research into the effect of urban pollution on precipitation, we are also studying the modifying role of the boundary layer aerosol in energy transfer and atmospheric energetics. Associated with this effort, with internal funding, we are also attempting to develop a capability for modelling climatic change due to changes in the aerosol content of the atmosphere. In both these cases, our aim is to use lidar observations in <u>support</u> of radiometric observations and to extend the scope of measurements obtained by the passive techniques.

To amplify: current attempts to model climate changes induced by aerosols range between the simple single layer approach and recent much more extensive numerical integrations of the equations of radiative transfer in more realistic model atmospheres (e.g., Yamamoto and Tanaka, 1972, and elsewhere in these proceedings; Braslau and Dave, 1973). The simple models in one way or another consider a simple geometry in which a single layer is introduced at some level in an otherwise transparent atmosphere. While this approach fulfills a useful role in conceptualizing, and to a certain extent in quantifying, the possible climatic consequences of changes in atmospheric aerosol content is inadequate in a great many realistic situations such as those revealed by the lidar observations shown in Figures 1 and 2.

The first feature that is apparent from these figures is that typically there is not just one aerosol layer, but many, and their geometric and optical properties vary continuously as solar heating proceeds. In addition, of course, clouds are frequently present which have a profound effect on radiative transfer.

The more complex models which have been recently developed represent a major advance over the simple models, but have two difficulties in practical application:

- They depend upon detailed and accurate input parameters for which measurement data are generally not available.
- They require exceedingly large amounts of computer time.

It is thus clear that practical studies of the climatic consequences of aerosol pollution in realistic atmospheres would benefit from a model that lies somewhere in the middle ground between the simple single-layer models and the complex numerical approaches. An example of such a "middle ground" model is that of Atwater (1971), which describes the infrared and solar effects of polluted layers in an urban environment. The present internal research program at SRI includes our attempt to develop a similar multi-layer model based upon that of Shettle and Weinman (1970) which employs a more complete treatment of solar radiative transfer and which draws upon available experimental data for appropriate input parameters. The structure of this model produces a system of linear equations, which describe the continuity conditions at layer interfaces. The project includes the development of novel matrix techniques for the efficient solution of this system. Fundamental data for such models, which treat the problem on a multi-layered basis, can be provided by lidar observations, which yield, in a unique manner, height, geometrical thickness, and, given a solution of the lidar equation by one or any other of the techniques noted earlier, an estimate of the optical thickness of each layer.

It should be noted in passing that, as illustrated in Figure 2, the changes in layer height and shape with time reveal dynamic aspects, such as convective lifting, which can be directly related to surface heating, in studying the role of energy transfer in the boundary layer.

c) Cirrus Cloud

In addition to monitoring aerosols in the boundary layer, lidar can also monitor particulate concentrations at higher levels. For example, Figure 3 shows an observation of tenuous cirrus cloud layers--made in daylight in what appeared to be a clear sky. The presence of such cirrus clouds--and they are often present in depths of as much as 1 or 2 km in very tenuous form unsuspected by a visual observer--has as obvious a significance in considering radiative transfer processes as do the aerosols of the boundary layer. Further, the presence of ice crystal clouds or water clouds, for that matter, is certainly significant to the interpretation and evaluation of many types of remote sensing observations, as for example from satellites (Davis, 1969 and 1971).

d) Dust Layers over the Ocean

The capability of lidar for observing aerosol layers in the clear air is further illustrated in Figure 4 which shows data acquired by a lidar operated in an aircraft flying over the sea in the Barbados Oceanographic and Meteorological Experiment (BOMEX) in 1969 (Uthe and Johnson, 1971). The figure shows a computer-generated representation of positive and negative departures of the lidar-observed S-value profiles relative to a best-fit exponential curve. To the extent that particle size variations and attenuation can be neglected, this cross-section thus shows concentrations of particles in layers, notably that at about 1.8 km altitude. This layer is interpreted as being caused by the stream of dust carried by the north-east tradewinds to the Caribbean area from the Sahara Desert. The assumption that attenuation is negligible in such conditions, and the relationship of the lidar data to absolute volume concentrations was investigated with the help of particle size distributions that were made available from an independent aircraft sampling program. Using these data and Mie theory, expected lidar signal returns were computed. These are shown for three occasions in Figure 5.

The light short dashed lines represent simulated relative lidar returns, ignoring the effect of atmospheric attenuation of the energy pulse. The corresponding light solid lines represent another set of simulated relative lidar returns obtained after taking into account the attenuation of the laser energy. A lidar altitude of 3 km is assumed. By comparing the dashed and solid profiles, which show only 1 dB difference at the surface for the two hazy days, it is seen that the neglect of atmospheric attenuation does not significantly affect the return signal profile. In such conditions of low or moderate turbidity, lidar observations over short path lengths can be interpreted directly without the need for rigorous solution of the lidar equation.

The lidar system constant in this experiment may be inferred by comparing the computed lidar returns. The relative signals from three lidar traces each recorded during the aerosol sampling period are shown in Figure 5 as heavy lines. The three computed and three observed profiles were first plotted on two separate graphs and the horizontal displacement between these graphs was adjusted for the best overall fit of computed and observed data. The abscissa values represent the observed lidar signals in relative logarithmic units.

Good agreement exists between computed and observed relative lidar return signals in terms of both day-to-day and altitude variations. The result indicates that the absolute aerosol densities could be inferred from the lidar backscatter signatures, subject to errors due to non-linear variations between particulate density and the volume backscatter coefficient.

e) Stratospheric Particulate Layers

In an ongoing program, we are making lidar observations of the variability of particulates in the stratosphere between 10 km and 30 km. These observations are part of the program of the CIAP Office of the Department of Transportation to assess the impact of climatic changes that may result from perturbation of the upper atmosphere by the propulsion effluents of high-altitude supersonic aircraft.

The objective of the SRI lidar experiment is to provide information on particulate material in the natural (unperturbed) stratosphere, by observing the spatial and temporal variations in a series of periodic nighttime measurements over Menlo Park, California. A ground-based lidar containing both a pulsed ruby laser and a tunable dye laser is being used to obtain data over an 18-month period to extend earlier observations of a similar type (Grams and Fiocco, 1967; Kent and Wright, 1970; Hirono, et al., 1972) and complement other current programs (Dynatrend, 1973; Schuster, et al., 1973; Melfi, et al., 1973).

Beginning in October 1972, the results of each observation are present as vertical profiles (with a resolution of 250 m to 500 m in altitude z) of two quantities indicative of stratospheric aerosol content.

- The "scattering ratio," R(z), equal to the ratio of total (molecular plus particulate) atmospheric backscattering coefficient to molecular backscattering coefficient.
- The particulate backscattering coefficient, $\beta_A(z)$ (per meter per steradian).

The lidar backscattering data for a single observation period are obtained by integrating the return signals from up to 1000 single-pulse transmissions. This signal integration extends for a period of approximately 1 hour .

Figure 6 shows the three principal steps in the analysis of the recorded backscatter data. The first step [Figure 6(a)] consists of matching the measured (range-corrected) vertical profile of lidar backscatter signals (indicated by the solid curve) with a computed vertical profile of molecular backscatter (indicated by the dashed curve). The measured profile of backscatter data has an observational error estimated to be only 1 to 2 percent. The profile of molecular (Rayleigh) backscatter is computed by using an assumed vertical profile of atmospheric attenuation [Elterman, 1968], and a measured vertical distribution of molecular number density corresponding to the Oakland radiosonde data nearest in time to the lidar observation period. (Oakland is approximately 20 miles north of Menlo Park). The matching of the two profiles clearly shows a large bulge in the measured profile near 20 km, and it must be attributed to a significant contribution to the atmospheric backscatter from particulate matter.

Matching is accomplished objectively and relates the lidar observations to the backscattering coefficient of the atmosphere at levels at which minimum ratio values suggest that aerosol concentrations are non-existent. This relationship is the basis for the derivation of the scattering ratio profile, R(z), illustrated in Figure 6B. The validity of the assumption that the reference layer is in fact purely gaseous is clearly critical to a determination of the absolute magnitudes of the aerosol backscatter. This commonly used approach has been widely discussed in the literature (e.g. Grams and Fiocco, 1967; Kent and Wright, 1970). It is generally believed that any errors due to the presence of aerosols in the supposedly clear layer will be small--smaller in fact than those due to measurement uncertainties. In-situ observations (Davis, 1971; Newkirk and Eddy, 1964; Bigg, et al., 1970) tend to confirm the presence of clear, gaseous layers, but it must be pointed out that the experimental methods employed in in-situ sensing have themselves limited sensitivity to detect extremely small concentrations of particulate material.

At the very least, there appears to be ample ground for claiming these lidar evaluations of scattering ratio profiles based upon the assumption of a clear layer are not in error by more than 1% or 2%, and that any error in this assumption must lead to the conclusion that the aerosol backscatter cross section, derived from the profiles of scattering ratios, (see Figure 6C, for example), are too small rather than too large. It should, of course, be noted that the uncertainties noted in no way affect the relative variations of scattering ratio or aerosol backscatter cross sections as a function of height.

Both the scattering ratio and the aerosol backscattering coefficient are integrated optical quantities, and as noted earlier they cannot be converted to unambiguous values of total scattering coefficient (extinction), particle number, or mass concentration without auxiliary information on particle size distribution, shape, index of refraction and mass density. This auxiliary information may be obtained concurrently with the lidar measurements by means of direct sampling equipment on aircraft or balloon platforms. Alternatively, typical values of these auxiliary data as inferred from a representative direct sampling program may be used to convert the lidar data. The advantage of the lidar over the direct sampling techniques lies, of course, in its ability to rapidly observe stratospheric regions of large vertical extent, in the fact that it does not alter the quantities that it is sampling, and its significantly lower cost per observation.

Even without the auxiliary data or assumptions necessary to convert them to extinction coefficients, abosolute number or mass concentrations, the lidar data provide direct information on stratospheric aerosol content given the reasonable assumption that particle size distributions and refractive properties (as discussed in Section IIc above) do not vary in a capricious manner over large ranges from height to height, or within continuous layers from observation to observation. The profiles of scattering ratio and aerosol backscattering coefficient thus immediately reveal the presence, altitude, and variability (in space and time) of stratospheric aerosol layers. As such, they can provide a valuable phenomenological basis for modeling and other studies that attempt to describe the dynamic, radiative, physical, and chemical processes responsible for natural and man-made changes in the stratosphere. For example, on the basis of the lidar observations already carried out in this program, the following can be concluded:

- The level of the tropopause (12 to 15 km at Menlo Park, California) appears to be a level of relative minimum aerosol content.

- The presence of a layer of relative maximum aerosol content near 20 km is evident in all the observations. The ruby lidar data for this layer show a particulate contribution to the atmospheric backscatter that is 10 to 15 percent of the assumed molecular contribution. This may be compared with particulate contributions that were 50 to 100 percent of the assumed molecular contribution during 1964 and 1965 when the Agung volcanic material was present in the stratosphere (Grams and Fiocco, 1967).

  Although not direct evidence of atmospheric transmission, lidar observations of atmospheric backscatter coefficient may be used to infer atmospheric extinction coefficients to a useful degree as discussed in Section IIc above. The reduction in the stratospheric aerosol since 1964, has of course led to a reduction in atmospheric attenuation. This has been noted among others by Elterman et al (1973) who in the reference cited, gives data on his latest searchlight determinations of atmospheric turbidity obtained in New Mexico in 1970. The values given there approximate conditions believed to obtain in the pre-Agung period in early 1963. However, our current lidar observations (Russell, et al., 1973a, b) indicate that present (1973) stratospheric particulate extinction is considerably lower than even the 1970 values.

  The lidar data show large differences in the vertical distribution of the stratospheric aerosol from one monthly observation period to the next.

  Sequential ruby (λ = 0.6943 μm) and dye (λ 0.5890 μm) lidar observations on the same night produced scattering ratio profiles having the same shape; however, the scattering ratios R(z) at the shorter dye wavelength were consistently

lower than those at the longer ruby wavelength. This confirms that the enhanced return from the 20 to 25 km layer is of a particulate origin rather than from an anomalously molecular layer, since the variation in scattering ratios observed indicates the presence of non-Rayleigh scattering. Differences between the particulate backscattering coefficient $\beta_A(z)$ at the two wavelengths are nearly within the uncertainty of the measurements, but the possible wavelength dependence suggested by this observation is consistent with size distributions for the stratospheric aerosol that other investigators have measured and suggested.

- The lidar observations reveal a slight increase in the aerosol backscattering coefficient of the 20-km layer from 2×10^{-9} per meter per steradian in October 1972 to 6×10^{-9} per meter per steradian in May and June 1973. On the assumption that the refractive properties, shape, and size distribution of the particulates in this layer remained constant, the observed increase indicates that the particle number density increased by a factor of 3.

- As shown in Figure 7, which compares the change in layer mean aerosol backscatter coefficient ($\overline{\beta}_A$) as a function of height by month, the largest variability in particulate backscatter was observed between 22.5 and 27.5 km.

  In the 25 to 27.5 km layer, the lidar-observed aerosol backscattering coefficient showed a decrease by a factor of about 10 from December 1972 to mid-January to April. Whether this variability was caused by a change in aerosol number density, an influx of large particulates, or a significant change in the nature of the particulates cannot be determined at this time. However, it is most interesting to note that the decrease of backscattering in this layer (and the corresponding but smaller decrease in the 22.5 to 25.0-km layer) coincides with a change in the zonal wind (which is also plotted in Figure 7) from a westerly to an easterly direction at those altitudes. This reversal from westerly to easterly flow at the levels in question occurred at the time of the seasonal sudden stratospheric warming. The subsequent increase in backscattering in those layers coincides with a return of the wind direction from easterly to westerly. It is suggested that the preceding change from westerly to easterly wind direction aloft brought a relatively "cleaner" air mass overhead. Nevertheless, caution must be applied in interpreting this coincidence of wind and particulate variability, because a subsequent change in zonal winds from westerly to easterly during April, May, and June was evidently <u>not</u> accompanied by a corresponding decrease in particulate backscatter. (It should also be noted that the wind data is acquired by daytime rocket sounding at a site some 200 miles SSE of Menlo Park where the lidar observations are made at night). We will continue to observe the relationship os stratospheric winds and particulate backscatter to determine if significant correlations are present over a long period of time.

- On the basis of the lidar observations made during the past eight months, the conclusion is that large natural variations in the aerosol can be expected in the stratosphere. For example, if routine measurements of particulate mass loading were made between 25 and 30 km, variations by a factor as large as 10 could be attributed to natural changes--at least when the concentrations are as low as those currently observed.

4. CONCLUSIONS

To summarize, we view the role of lidar in atmospheric studies concerned with radiative energy transfer and remote sensing, not as an end in itself, but as a valuable supporting or complementary capability, that can greatly enhance data obtained by other (passive) techniques.

At the very least, it can contribute greatly to a more realistic understanding of the nature of the real atmosphere and its variability. For example, it can show both in general terms and for particular circumstances, the sort of problems an effective radiative energy transfer model must be able to cope with in treating aerosol layers. Further, it can provide quantitative data on the thickness and heights of such layers for use in modelling studies. This information is also significant for remote sensing techniques, that are affected by the particulate material in the atmosphere even although they are concerned with measurements of the gaseous state (e.g., temperature, humidity, etc.) or with the condition of the surface of the earth seen through the atmosphere. And finally, as illustrated by the CIAP Project, the technique can provide most useful direct information (and more economically than in situ sensing) on the stratospheric aerosol for a specific purpose. Here again, apart from characterizing the natural variability of the particulate content of the upper atmosphere, lidar observations can provide inputs to the modellers as well as raising important new questions--such as the reason for the parallelism noted between zonal wind direction and particulate loading in the lower stratosphere.

In the field of atmospheric radiation studies, particularly in connection with such pertinent questions as possible climatic change, there appears to be an increasing realization that the need to obtain a better understanding of the nature and scope of the interrelated factors on the natural scale, is greater than the need to probe further into the finer details. It is our hope that lidar observations can, at least in regard to the role of particulates in the atmosphere, provide assistance and stimulation both in formulating the relevant problems and in their solution.

ACKNOWLEDGEMENT

The authors wish to acknowledge the contributions of the remainder of the SRI team engaged in lidar research, whose work is referenced herein, and especially Dr. Paul A. Davis for help in preparation of this paper.

REFERENCES

Atwater, M. A., 1971: Radiative Effects of Pollutants in the Atmospheric Boundary Layer, J. Atmos. Sci., 28, 1367-1373.

Barrett, E. W., and O. Ben-Dov, 1967: Application of Lidar to Air Pollution Measurements, J. Appl. Meteor., 6, 500-515.

Bigg, E. K., A. Ono, and W. J. Thompson, 1970: Aerosols at Altitudes Between 20 and 37 km, Tellus, 22, 550-563.

Braslau, N., and J. V. Dave, 1973: Effect of Aerosols on the Transfer of Solar Energy Through Realistic Model Atmospheres, J. Appl. Meteor., 12, 601-619.

Carswell, A. I., J. D. Houston, W. R. McNeil, and S. R. Pal, Lidar Scattering in the Troposphere. Fifth Conference on Laser Radar Studies of the Atmosphere, Williamsburg, VA, 4-6 June 1973, Conference Abstracts, pp. 74-75.

Collis, R. T. H., 1970: Lidar, Appl. Opt., 9, 1782-1788.

Collis, R. T. H., and E. E. Uthe, 1972: Mie Scattering Techniques for Air Pollution Measurement with Lasers, Opto-electronics, 4, 87-99.

Davis, P. A., 1969: The Analysis of Lidar Signatures of Cirrus Clouds, Appl. Opt., 8, 2099-2102.

Davis, P. A., 1971: Applications of an Airborne Ruby Lidar During a BOMEX Program of Cirrus Observations, Appl. Opt., 10, 1314-1323.

Deirmendjian, D., 1969: Electromagnetic Scattering on Spherical Polydispersions, American Elsevier Publishing Co., Inc., New York.

Dynatrend, 1973: Laramie Comparative Experiment, Data Report and Preliminary Report of Conclusions. Report CIAP, DOT, Edited by Dynatrend Inc., March 15, 1973.

Eloranta, E. W., 1972: The Calculation of Doubly Scattered Lidar Returns from Homogeneous Clouds, Presented at 4th Conference on Laser Radar Studies of the Atmosphere, Tucson, January 1972.

Elterman, L., 1968: UV, Visible and IR Attenuation for Altitudes to 50 km, AFCRL-68-0153, Environmental Research Papers No. 285.

Elterman, L., R. B. Toolin, and J. D. Essex, 1973: Stratospheric Aerosol Measurements with Implications for Global Climate, Appl. Opt., 12, 330-337.

Fernald, F. G., B. M. Herman, and J. A. Reagan, 1972: Determination of Aerosol Height Distributions by Lidar, J. Appl. Meteor., 11, 482-489.

Gambling, D. J., and K. Bartusek, 1972: Lidar Observations of Tropospheric Aerosols, Atmos. Environ., 6, 181-190 and 6, 869-870.

Grams, G. W., 1966: Optical Radar Studies of Stratospheric Aerosols, Ph. D. Thesis, May 1966, MIT.

Grams, G., and G. Fiocco, 1967: Stratospheric Aerosol Layer During 1964 and 1965, J. Geophys. Res., 72, 3523-3542.

Grams, G. W., I. H. Blifford, Jr., B. G. Schuster, and J. J. DeLuisi, 1972: Complex Index of Refraction of Airborne Fly Ash Determined by Laser Radar and Collection of Particles at 13 km, J. Atmos. Sci. 29, 900-905.

Hamilton, P. M., 1969: Lidar Measurement of Backscatter and Attenuation of Atmospheric Aerosol, Atmos. Environ., 3, 221-223.

Harrison, H., J. Herbert, and A. P. Waggoner, 1972: Mie-Theory Computations of Lidar and Nephelometrics Scattering Parameters for Power Aerosols, Appl. Opts., 11, 2880-2885.

Hirono, M., M. Fujiwara, O. Uchino, and J. Itabe, 1972: Observations of Aerosol Layers in the Upper Atmosphere by Laser Radar, Report of Ionospheric and Space Research in Japan, 26, 237-244.

Holland, A. C., and G. Gagne, 1970: The Scattering of Polarized Light by Polydisperse Systems of Irregular Particles, Appl. Opt., 9, 1113-1121.

Johnson, W. B., and E. E. Uthe, 1971: Lidar Study of the Keystone Stack Plume, Atmos. Environ. 5, 703-724.

Kent, G. S., and R. W. Wright, 1970: A Review of Laser Radar Measurements of Atmospheric Properties, J. Atmos. Terrest. Phys., 32, 917-943.

Kerker, M., 1969: The Scattering of Light and Other Electromagnetic Radiation, Academic Press, New York.

Liou, K. N., and R. M. Schotland, 1971: Multiple Backscattering from Water Clouds for a Pulsed Lidar System, J. Atmos. Sci., 28, 772-784.

McCormick, M. P., J. D. Lawrence, and F. R. Crownfield, 1968: Mie Total and Differential Backscattering Cross Section at Laser Wavelengths for Junge Aerosol Models, Appl. Opt., 7, 2424-2425.

Melfi, S. H., G. B. Northam, and M. P. McCormick, 1973: Comparison of Lidar and In-situ Measurements of Stratospheric Aerosols. Presented at 5th Conference on Laser Radar Studies of the Atmosphere, Williamsburg, Virginia, 1973.

Newkirk, G., and J. A. Eddy, 1964: Light Scattering by Particles in the Upper Atmosphere, J. Atmos. Sci., 21, 25-60.

Russell, P. B., W. Viezee, and R. D. Hake, 1973a: Lidar Measurements of the Variability of Stratospheric Particulates, SRI Report CIAP DOT Contract NAS2-7261, July 1973.

Russell, P. B., W. Viezee, and R. D. Hake, 1973b: Lidar Measurements of the Variability of Stratospheric Particulates, SRI Report CIAP DOT Contract NAS2-7261, October 1973.

Shettle, E. P., and J. A. Weinman, 1970: The Transfer of Solar Irradiance Through Inhomogeneous Turbid Atmospheres Evaluated by Eddington's Approximation, J. Atmos. Sci., 27, 1048-1055.

Schotland, R. M., K. Sassen, and R. Stone, 1971: Observations by Lidar of Linear Depolarization Ratios for Hydrometeors, J. Appl. Meteor., 10, 1011-1017.

Schuster, B. G., F. G. Fernald, and C. L. Frush, 1973: Global Reconnaissance of Stratospheric Aerosol by Airborne Lidar. Presented at 5th Conference Laser Radar Studies of the Atmosphere, Williamsburg, June 1973.

Uthe, E. E., and W. B. Johnson, 1971: Lidar Observations of Lower Tropospheric Aerosol Structure during BOMEX, SRI Final Report AEC Contract AT(04-3)115.

Uthe, E. E., 1972: Lidar Observations of the Urban Aerosol Structure, Bull. Am. Met. Soc., 53, 358-360.

Uthe, E. E., and C. E. Lapple, 1972: Study of Laser Backscatter by Particulates in Stack Emissions, SRI Final Report, EPA Contract CPA 70-173.

van de Hulst, H. C., Light Scattering by Small Particles, John Wiley and Sons, Inc., New York.

Viezee, W., R. D. Hake, and P. B. Russell, 1973: Lidar Measurements of Stratospheric Constituents, SRI Report CIAP DOT Contract NAS2-7261, March 1973.

Viezee, W., and R. T. H. Collis, and J. D. Lawrence, 1973c: An Investigation of Mountain Waves with Lidar Observations, J. Appl. Meteor., 12, 140-148.

Viezee, W., J. Oblanas, and R. T. H. Collis, 1973b: Evaluation of the Lidar Technique of Determining Slant Range Visibility for Aircraft Landing Operations, SRI Final Report AFCRL Contract F19628-71-C-0152, November 1973.

Waggoner, A. P., N. C. Ahlquist, and R. J. Charlson, 1972: Measurements of the Aerosol Total Scatter-Backscatter Ratio, Appl. Opt., 11, 2886-2889.

Weinman, J. A., 1972: Effects of Multiple Scattering on Laser Pulses Transmitted Through Clouds. Presented at 4th Conference on Laser Radar Studies of the Atmosphere, Tucson, Arizona, January 1972.

Yamamoto, G., and M. Tanaka, 1972: Increase of Global Albedo Due to Air Pollution, J. Atmos. Sci., 29, 1405-1412.

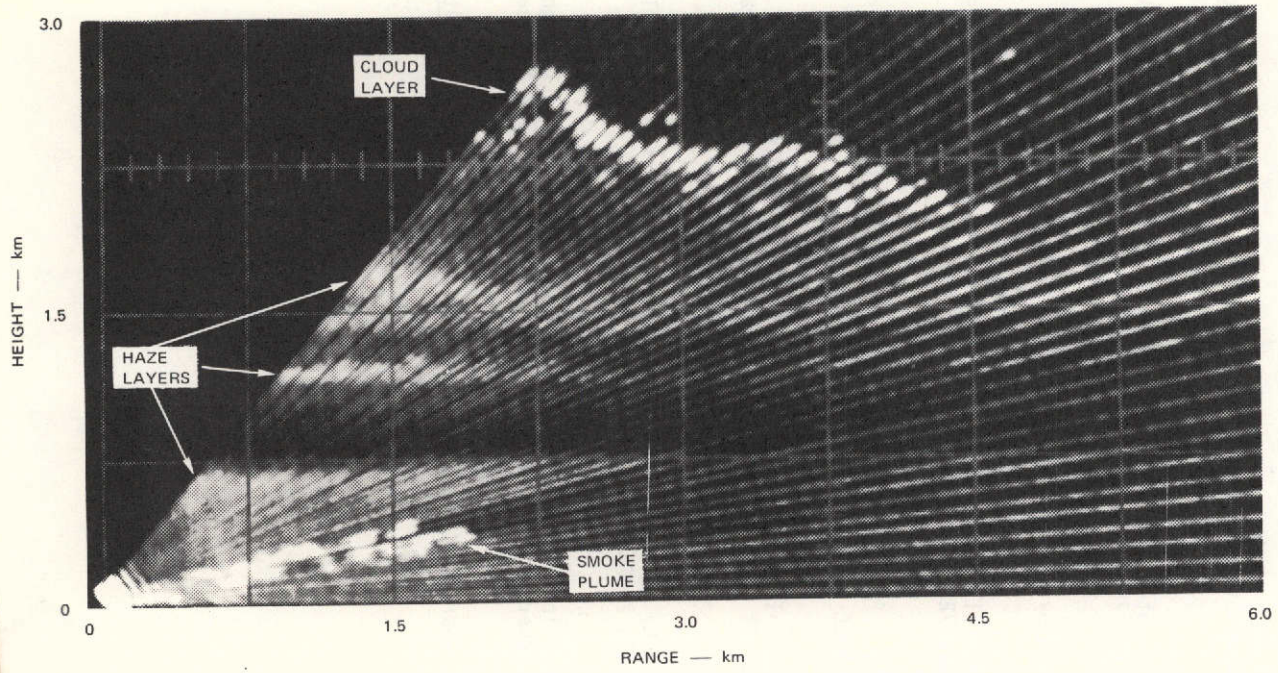

FIGURE 1 VERTICAL CROSS-SECTION THROUGH A SMOKE PLUME 1.5 km DOWNWIND FROM THE 245m STACK AT HOMER CITY POWER PLANT AS DERIVED BY ANALOG LIDAR TECHNIQUES.

The turbid boundary layer extends to 0.75 km altitude, stratification is apparent in the clean air at 1.1 and 1.5 km altitude, and the base of visible cloud is at about 2 km altitude. Attenuation limits penetration into the cloud.

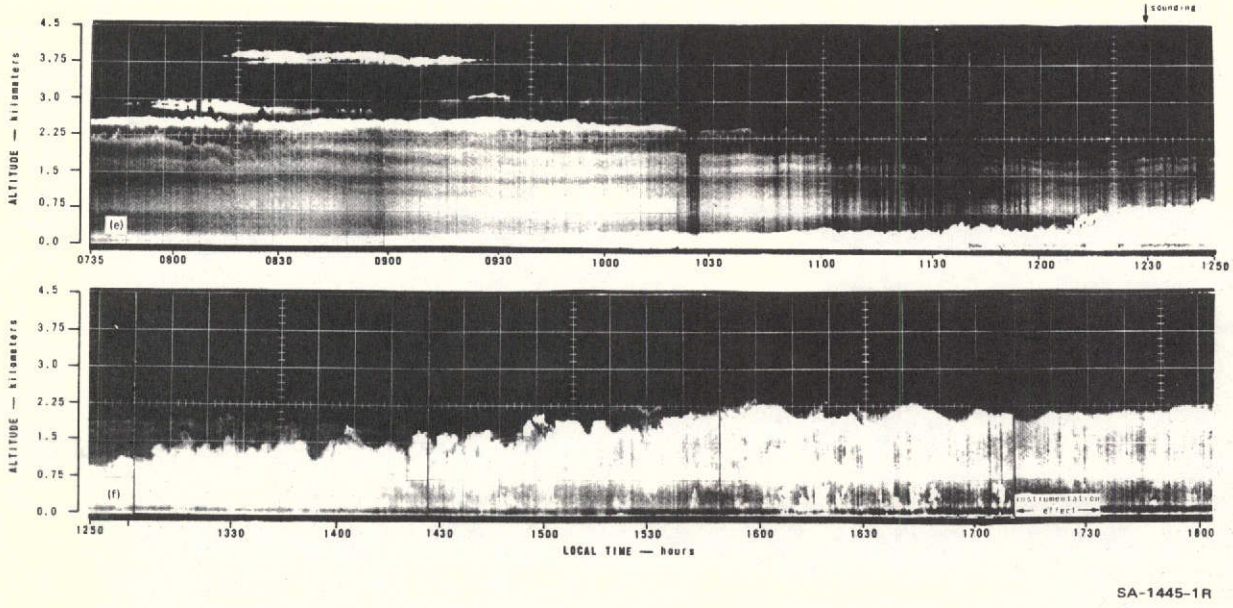

FIGURE 2 HEIGHT/TIME CROSS SECTION OF THE AEROSOL STRUCTURE OVER ST. LOUIS, MISSOURI, ON 13 AUGUST 1971, AS OBSERVED BY THE SRI/EPA MARK VIII LIDAR SYSTEM.

The stratification is associated with temperature inversions at 2.3 km and 0.3 km altitude, the former being capped by visible cloud from 0735 local time to approximately 1000 local time. The build up of a denser aerosol layer at the surface during the period shows the influence of convective mixing from about 1300 local time. The surface layer penetrates earlier strata to become the dominant layer by about 1430 local time (Uthe, 1972).

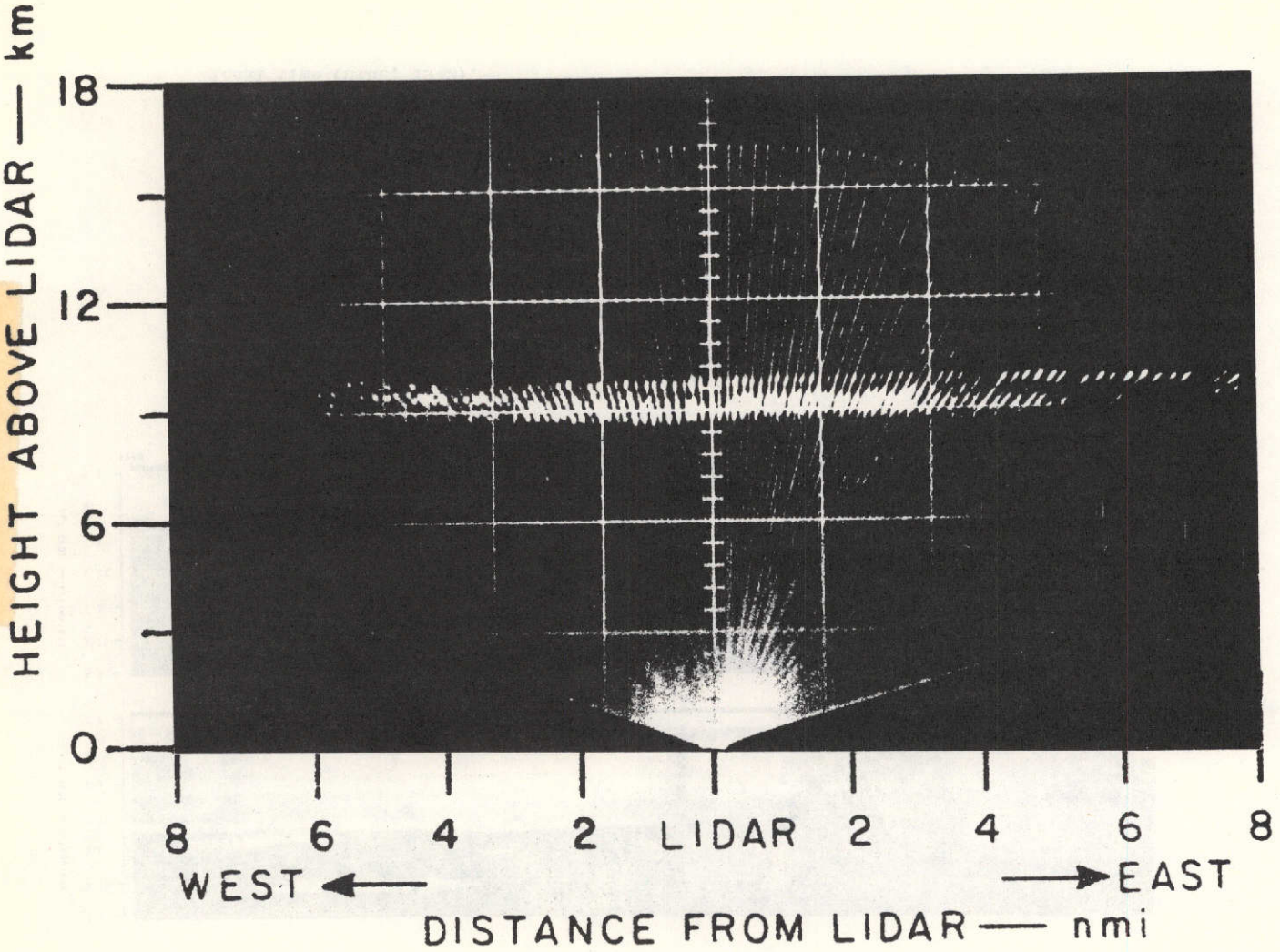

FIGURE 3 TENUOUS CIRRUS CLOUD BARELY PERCEPTIBLE TO THE EYE (Viezee, et al. 1973c)

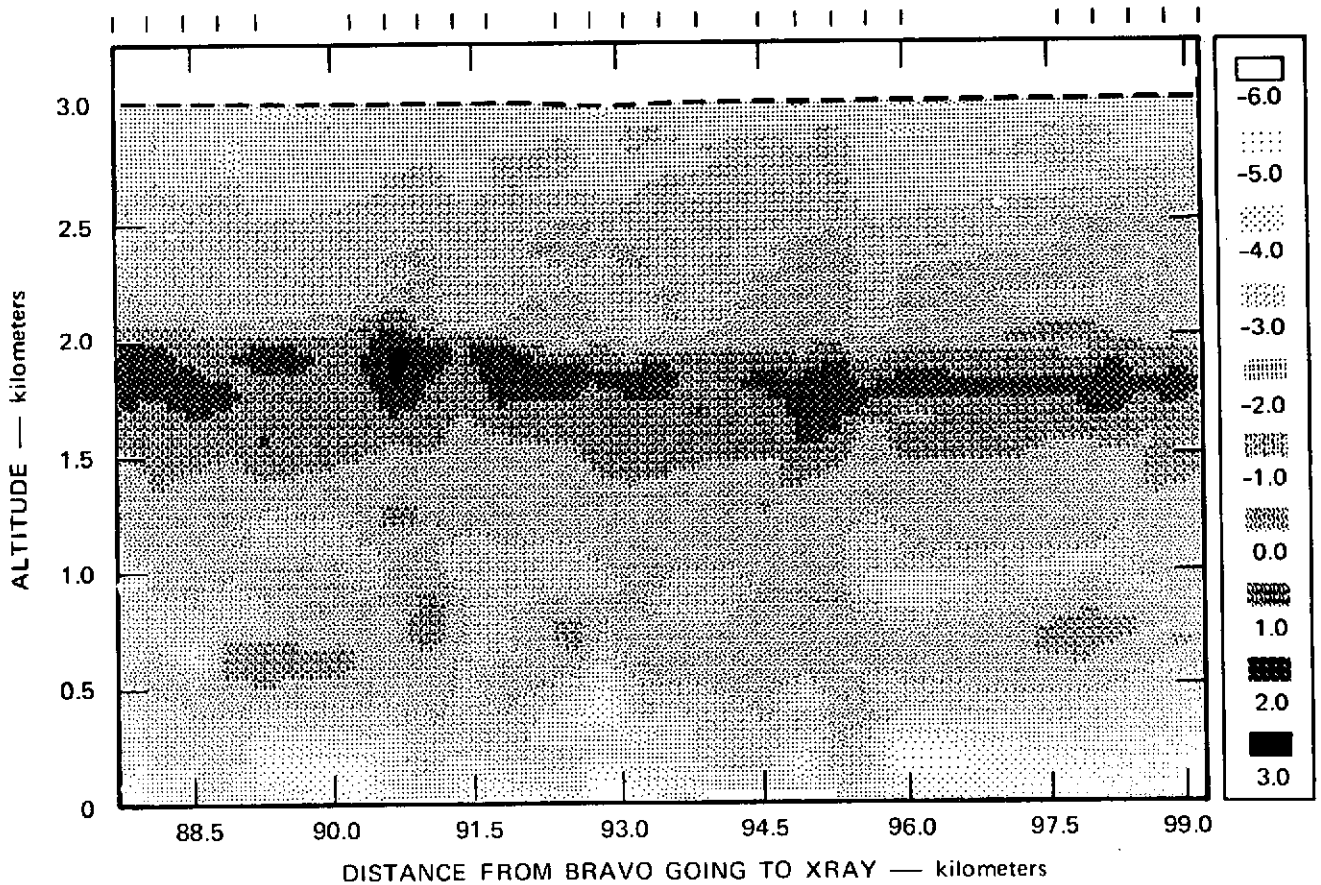

FIGURE 4 DIGITAL PRESENTATION OF LIDAR OBSERVED AEROSOL STRUCTURE DURING BOMEX (30 June 1969 1053-1056 EDT, run 30-7).

(Bravo and X-ray are locations in the experimental area.)
The location of each observation is indicated by vertical marks along the top line of the section. The scale of intensity is given in dB relative to a best fit exponential atmosphere (Collis and Uthe 1972).

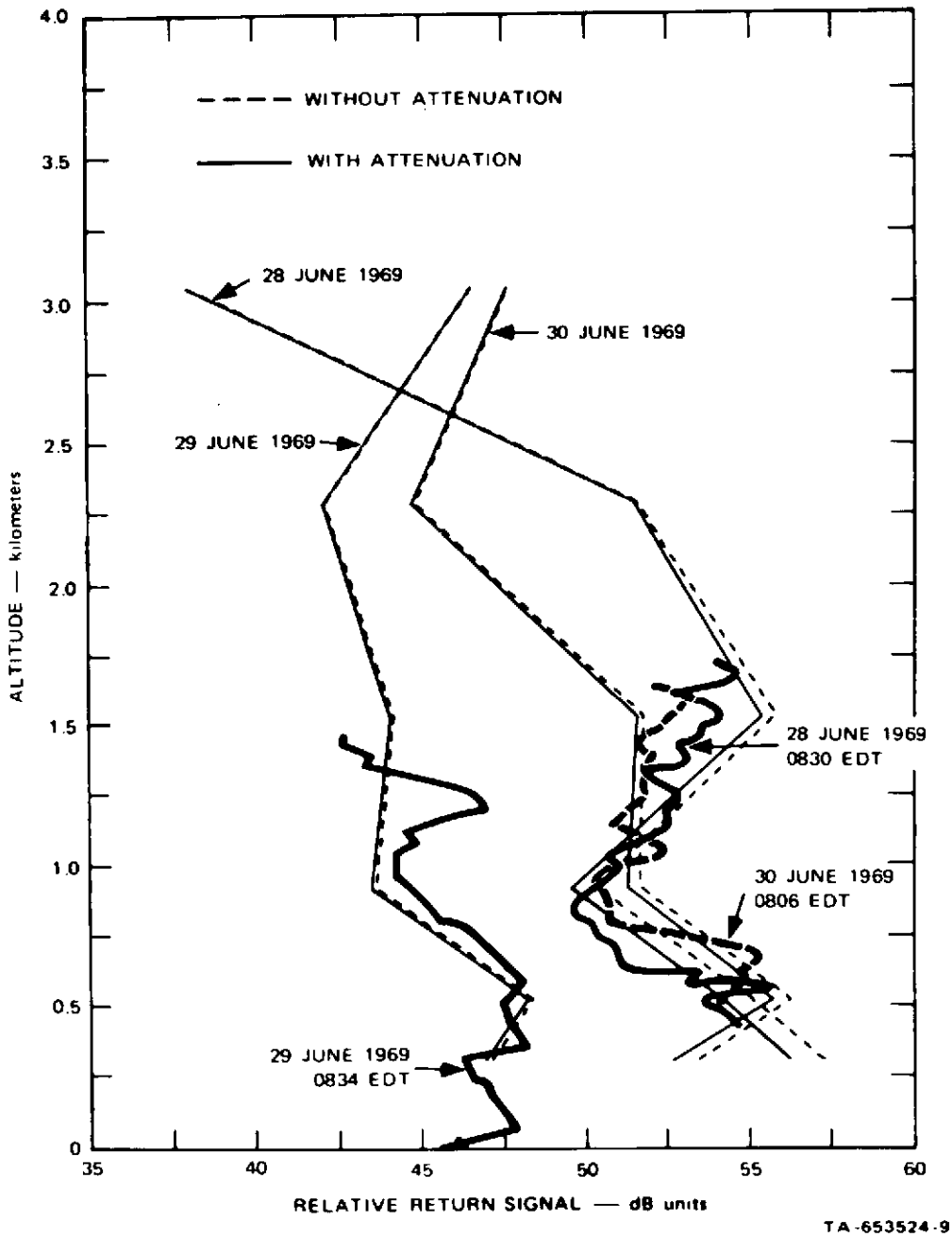

FIGURE 5 DERIVATION OF LIDAR CALIBRATION FROM PARTICLE COUNT DATA (see Fig. 4)

Actual lidar profiles are shown as heavy lines while backscatter profiles evaluated from particle count data are shown as less heavy lines extending from 3.0 km.

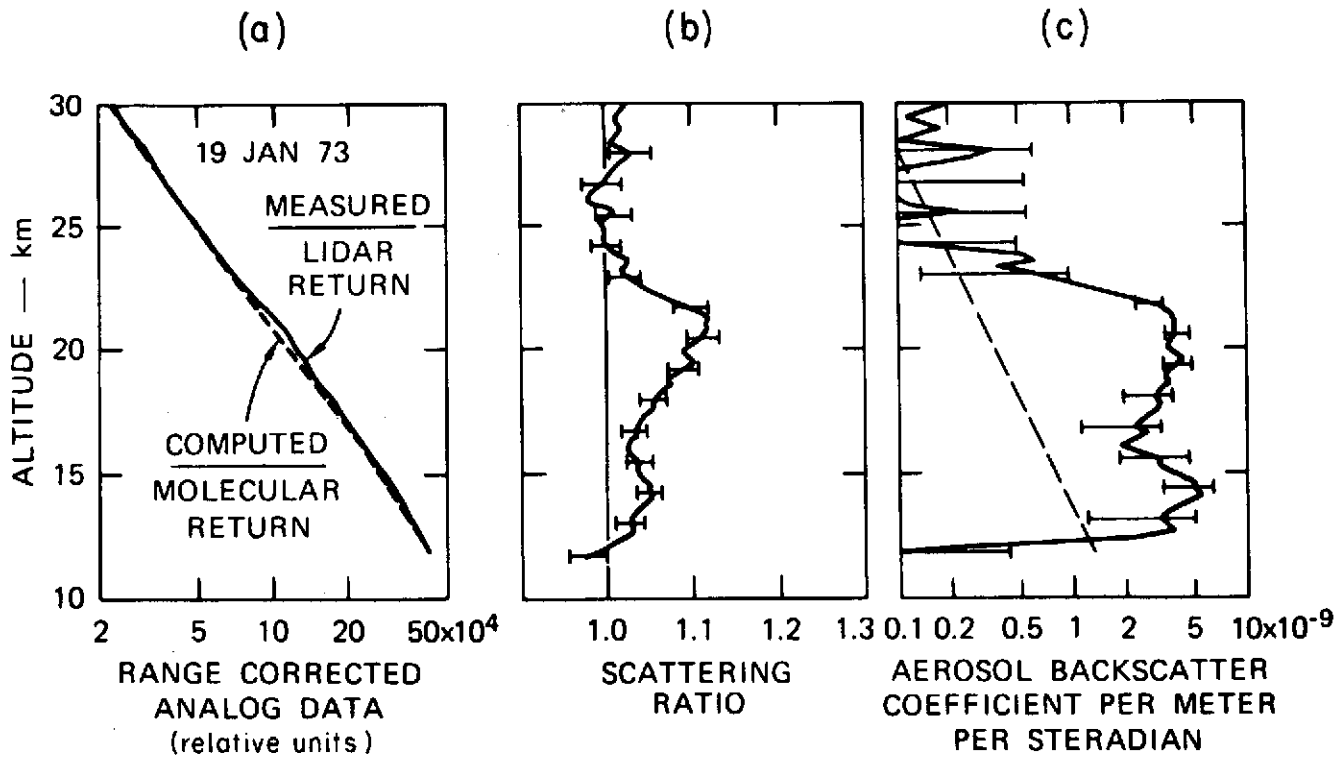

FIGURE 6 LIDAR OBSERVATIONS OF STRATOSPHERIC PARTICULATE LAYERS--ANALYSIS PROCEDURE
(Viezee, et al. 1973a)

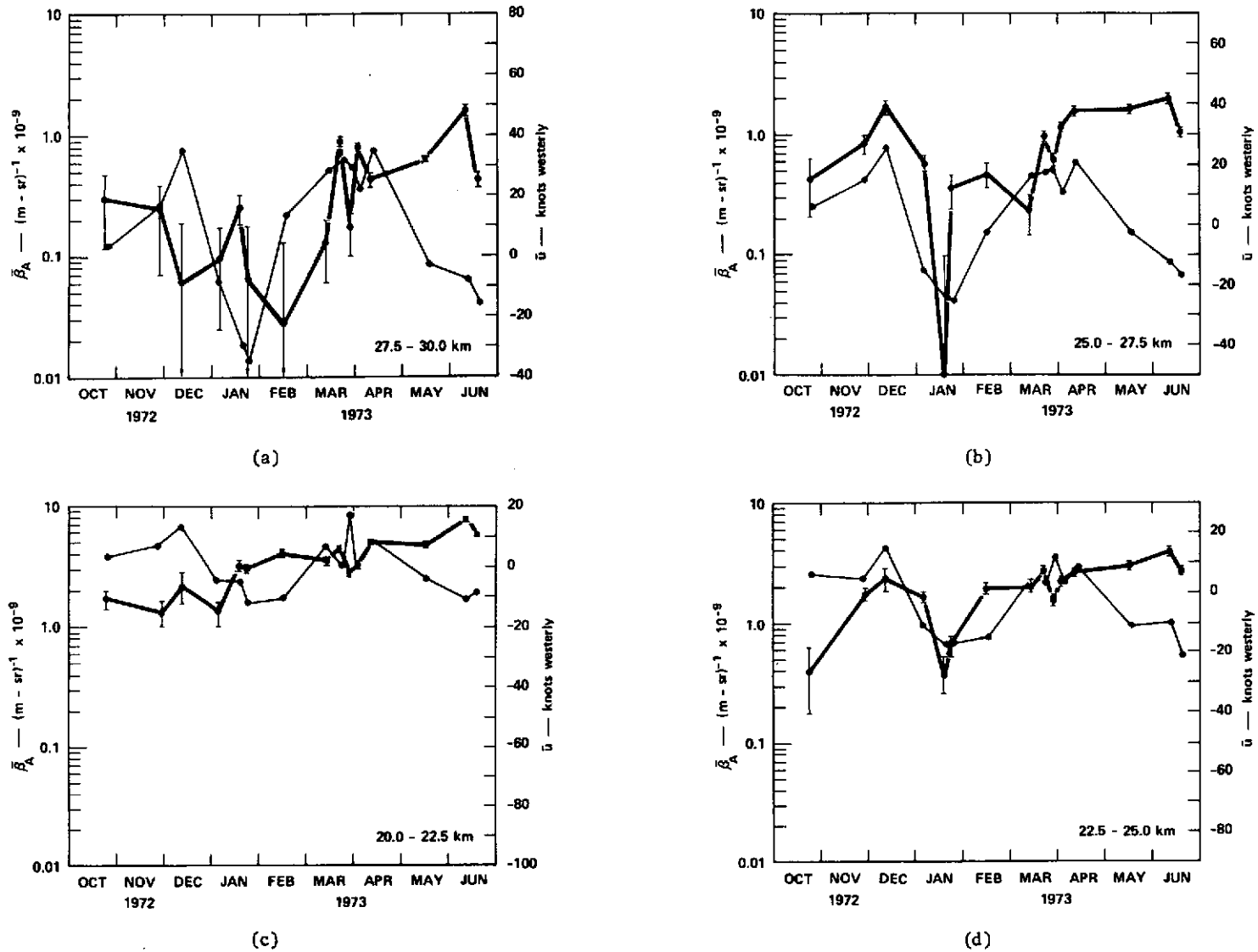

FIGURE 7 TIME VARIABILITY OF LAYER-AVERAGED AEROSOL BACKSCATTERING COEFFICIENT ($\overline{\beta}_A$) (HEAVY LINE) AND ZONAL WIND (LIGHT LINE) FOR FOUR ALTITUDE LAYERS [Note relationship between $\overline{\beta}_A$ and zonal wind in layers 22.5 - 25.0 km (d) and 25.0 - 27.5 km (b)]

METHODS OF CALCULATING INFRARED TRANSFER - A REVIEW

John C. Gille

National Center for Atmospheric Research*

Boulder, Colorado 80303

* The National Center for Atmospheric Research is sponsored by the National Science Foundation.

1. INTRODUCTION

This paper will very briefly summarize recent work on methods for calculating the transfer of infrared radiation in planetary atmospheres. Because several volumes, notably those by Kondratyev (1965) and especially by Goody (1964a) have reviewed this field up to about a decade ago, the emphasis will be on developments since that time. It should also be noted at the outset that this review will emphasize results published in the U. S. and Western Europe, while directing less attention to work done elsewhere, notably in the U.S.S.R.

There are two principal reasons for making calculations of infrared transfer. The first is for the study of the radiative terms in the atmosphere's energy budget, which must be known for making predictions of weather and climate. The second is to infer information about atmospheric structure by comparing such calculations with measurements.

Three developments have strongly influenced the improvement of computational methods. The ability to make better measurements has led to requirements for more accurate calculations. Much better parameters for radiative transfer calculations have been obtained, often in the form of lists of spectral line parameters. Since these are described elsewhere in this volume by McClatchey, nothing more needs to be said except to note their availability. The ready access to large, fast computers now makes possible very detailed and exact calculations, either routinely or, more usually, to check approximate calculational schemes.

Although infrared transfer through cloudy and turbid atmospheres is a very active field at present, this review will treat transfer in molecular atmospheres only, in order to keep within a reasonable length. This is a crucial problem however, for if we cannot make good calculations for clear atmospheres, we are likely to be in a worse position with turbid ones.

The calculations can usually be done in a brute-force way, but one that is quite time consuming, even on the fastest available computers. The problem is often to select a method that possesses enough of the basic physics to have sufficient (and verified) accuracy for a specific use. With the assumption of a non-scattering atmosphere in thermodynamic equilibrium, the equation of transfer may be written

$$I_i(s, \mu)\Delta\nu_i = \int_{\Delta\nu_i} I_\nu(s, \mu)\, d\nu$$

$$= \int_{\Delta\nu_i} I_\nu (0, \mu)\, e^{\frac{-\int_0^s k_\nu(p(z'), T(z'))\rho(z')\, dz'}{\mu}}\, d\nu$$

$$+ \int_{\Delta\nu_i} \int_{s'=0}^{s'=s} B_\nu(s') \, e^{-\frac{\int_{s'}^{s} k_\nu(p(z'), T(z'))\rho(z')\, dz'}{\mu}} \left[k_\nu(p(s'), T(s'))\rho(s') \, \frac{ds'}{\mu} \, d\nu \right] \tag{1}$$

where $I(s,\mu)$ is the intensity of the radiation at s, proceeding in a direction which makes an angle $\theta = \cos^{-1}\mu$ with the outward normal,

i subscript denotes an average value over the i^{th} finite spectral interval, $\Delta\nu_i$ wide

ν subscript denotes a monochromatic value at frequency

0 indicates a point (almost invariably on a boundary) at which I_ν may be conveniently calculated

$k_\nu(p, T)$ is an absorption coefficient, which depends on the local pressure and temperature

ρ is absorber density

B is the Planck black body radiance.

ν subscript denotes a monochromatic value at frequency ν

The problem may be elucidated by considering the spectral variation of the quantities on the right hand side of (1).

The Planck function, B, is a very slowly varying function, with a scale of approximately $1000cm^{-1}$. The absorption coefficient k_ν varies on three scales, however. An individual vibration-rotation band may be $100\text{-}200\ cm^{-1}$ wide, with lines spaced $1\text{-}2\ cm^{-1}$ apart. The lines have half widths varying from $0.1\ cm^{-1}$ at the surface to $0.001\ cm^{-1}$ in the stratosphere. The interval over which the transmission T through a mass a of absorber may be regarded as obeying Beer's law

$$T(\nu) = e^{-k_\nu a} \tag{2}$$

is considerably smaller than the smallest of these, which could lead to the order of $10^5\text{-}10^6$ separate points per band. Clearly something more clever must be done.

In Section 2 the most exact technique, detailed spectral integration, or line-by-line calculation is described. Section 3 describes recent developments in band modeling, treatments of inhomogeneous paths are described in Section 4, while flux and heating rate calculations are described in Section 5.

2. DETAILED SPECTRAL INTEGRATIONS (LINE-BY-LINE CALCULATIONS)

Detailed spectral integrations or line-byline calculations, as they are more commonly known, rely on a direct integration over frequency. Direct integration requires that monochromatic transmittances be calculated at a number of points, sufficiently closely spaced to represent the rapid variation with frequency. A quadrature formula is then applied to obtain an integral over a finite spectral band. This method was first used by Hitschfeld and Houghton (1961) for narrow intervals in the 9.6 μ m band of ozone. The approach was subsequently used by Gates (1962), but Drayson (1966) popularized its use for calculations of atmospheric transmittance. In addition to allowing detailed integrations over frequency, it is possible to allow for the variation of parameters such as line half-widths and intensities with altitude. The atmosphere may be broken into thin slabs which may be assumed isothermal, and over which an analytical integration over pressure may be made. In addition, the line shape changes from a pressure broadened Lorentz shape near the surface to Doppler shape at high altitudes. This variation was also easily included in his calculations.

To indicate the kind of procedure required, Drayson's method will be described. The spectrum was divided into intervals 0.01 cm^{-1} wide, and spectral lines were located at the nearest hundredth of a wave number. If a line was present on a particular point, the region near the center was divided into intervals from 0.001 to 0.004 cm^{-1} wide, and a four point Gaussian quadrature mesh was applied over those narrow intervals. If there was no line, larger intervals up to 0.01 cm^{-1} were taken as the minimum interval, over which a four point Gaussian quadrature mesh was extended. In these calculations, all lines within an interval above 10 cm^{-1} wide were included exactly.

The wings of all lines more distant than 10 cm^{-1} were calculated separately. These data were stored every .5 cm^{-1} and values interpolated to the quadrature points.

Once the total absorption coefficient was known at a particular frequency, it was multiplied by the absorber amount to give the optical depth. Taking the negative exponential of the optical depth gave the monochromatic transmission. The frequency quadrature was performed on the transmission, using the mesh points established above.

When a number of lines are close together, or a line falls at the end of an interval, slightly more complicated expressions are used. The results were averaged to give values over every 0.1 cm^{-1} interval.

A more recent calculational scheme has been described by Kunde and McGuire (1974). Details of their spectral mesh are shown in Fig. 1. Fig. 1a indicates spacing of up to four Gaussian quadrature points when no spectral lines fall within a 0.1 cm^{-1} interval. If there is only one line as in Fig. 1b, two subintervals of width $d_1 = 0.01$ cm^{-1} are formed on either side flanked by subintervals of width d_2 and d_3 going to the ends of the 0.1 cm^{-1} interval. Gaussian quadrature is preformed over each d_1, d_2, d_3 subinterval. The use of these subintervals results in two to three significant figure accuracy. When more than one line is present in the interval, the division is as shown in Fig. 1c. This scheme leads to between four and eighty quadrature points in an interval.

In order to compare the detailed spectral integration calculation with measurements, the calculated transmittance or radiance over the 0.1 cm^{-1} intervals must be convolved with an instrument response function. This has usually been done in a straightforward way; these authors used a fast Fourier transform approach to perform the convolution.

Results of such a calculation by Drayson, et al. (1968) for a homogeneous path (constant pressure and temperature) are shown in Fig. 2, where transmission through a cell of carbon dioxide is compared with experimental data by Burch. It can easily be seen that there is good quantitative agreement between the two, deviations being generally less than 5-10%. Discrepancies are in the main Q branch, where calculated transmittance is considerable lower than the measured value, and also in the Q branches at 640 and 720 wave numbers. One difficulty in these regions is that the true instrument function must be known very accurately to give accurate values.

An additional use of such calcualtions is apparent in the figure, in which the results using two different line half-widths for all lines of a band are compared with values using the half-widths varying with rotational quantum numbers. While it is hard to draw conclusions from a cursory inspection of the diagram of the figure, it is clear that the half-widths must be greater than 0.06 cm^{-1} near the band center.

A similar calculation for the 701 cm^{-1} (14 micrometers) band of ozone is shown in Fig. 3. Here a line-by-line calculation of Kunde and McGuire is compared with experimental data of McCaa and Shaw (1968). Again, overall accuracy is 5-10%.

Before showing results of detailed integration through the atmosphere, mention should be made of an ingenious suggestion by Kyle (1968) that a much faster integration could be done with a uniform, coarse mesh. This scheme is illustrated in Fig. 4. Here numbers on the abscissa indicate the location of quadrature points for a net centered on a spectral line. This would lead to the result shown by the dotted lines. However, if the quadrature net is offset from the line center by Δ, the dashed lines would result. Alpha is the line half-width.

Kyle showed that normalization of the area under a line gives Δ (delta) as an unique function of D/α, where D is the spacing of the quadrature points. For the atmosphere, delta is approximately 1/6 D. The total absorbance was calculated as a function of the dimensionless parameter $SU/2\pi\alpha$, which is one-half of the optical depth at the line center, and parametrically as a function of D/α. The results in Fig. 5 show that to minimize the maximum error, D/α should be approximately one; thus quadrature points could be spread approximately .05 cm^{-1} apart at the surface. For paths going through the stratosphere, however, the quadrature points should be spaced 10^{-3} cm^{-1} apart. Since this is of the order of the spacing for Drayson or Kunde and McGuire, there is not much difference in fact. Kyle's scheme has the disadvantage of requiring closely spaced calculations even when there are no lines. Additionally the error is somewhat larger than one would like.

The results that can be obtained by line-by-line integration through the atmosphere are illustrated in Fig. 6, from Kunde, et. al. (1974). They compared interferometer spectra taken from the Nimbus-4 satellite with calculations between 425-1415 cm^{-1}. The computations, were based on a 0.1 km vertical interval. The transmission was computed in this fine spacing by calculating transmission at a coarser vertical mesh, 0.5-4 km spacing, and then interpolating to finer vertical spacing. Not all spectral lines need to be included. Lines having intensities less than 10^{-6} cm^{-2} $atms.^{-1}$ were omitted (giving a total range of seven orders of magnitude of line intensity). This still resulted in over 8,000 lines of carbon dioxide in the interval 300 to about 1100 cm^{-1}.

The departures of actual line shape from the Lorentz line shape are easily included in a detailed spectral integration. The wings of the carbon dioxide band at 667 cm^{-1} (15μm) have been found experimentally (Burch, 1970) to be one percent of their Lorentzian value. Kunde and McGuire applied this correction to their line wings. In addition, they employed the Bignell (1970) scheme of self broadening for water vapor in the 1000 cm^{-1} window region.

A number of familiar spectral features are immediately seen, including the water vapor rotation band between 425 and 580 cm^{-1}, the carbon dioxide band between 580 and 800 cm^{-1}, the 1040 cm^{-1} ozone bands (on the observation only), and the water vapor band centered at 1600 cm^{-1}. Not as apparent are the contributions by methane and nitrous oxide near 1300 wave numbers.

The accuracy achieved by these authors is indicated in Fig. 7, where percentage error is plotted as a function of wave number. Note that the errors in the rotational water vapor band and water vapor continuum are generally less than 5%. Because of lack of data on ozone distribution, the ozone bands at 1040 and 701 cm^{-1} were not included, contributing to larger errors in those regions. The N_2O band at 588 wave number was not included, while the N_2O band near 1200 cm^{-1} and a methane band near 1300 cm^{-1} were included only crudely. Surprisingly large errors, 10 to 15%, are seen in the 667 cm^{-1} band of carbon dioxide. These are rather surprising, and important in view of the widespread use of this band for temperature determination. However, the authors believe much of this error is due to inadequate temperature measurement in the atmosphere.

The conclusion that we may draw from these results are that the line-by-line calculation scheme, in conjunction with good spectral data for atmospheric gases, gives results in good agreement with measurements made by carefully calibrated satellite borne spectrometers. Differences still exist, of course, which may be traced in part to the absolute calibration of the satellite instrument and to inadequacies in the in-situ measurements. As the authors note, the outgoing radiance is more sensitive to Planck radiance (temperature) than to details of the transmittance model. Therefore, this is not a good way of improving knowledge of atmospheric transmittance.

Based on these calculations, we may regard the adequacy of the line-by-line calculations as established; however, they are obviously quite elaborate, and require a great deal of time on a fast digital computer. They provide information with high spectral detail, but this is not required for many applications. Let us next look at simpler schemes for calculating transfer through the atmosphere.

3. BAND MODELS

Band models provide means of calculating transmission across finite spectral intervals. They are based on analytical deductions from plausible assumptions about line positions, intensities and half-widths. They may be used to treat an entire band, or some fraction of it. Goody (1964a) discusses a number of band models in detail.

Elasser (1942) proposed the first band model, an infinite array of lines of constant intensity and half-widths spaced uniformly in frequency. This is often referred to as the regular band model. At the other extreme, Goody (1952) described a model in which the lines in the array were randomly positioned in frequency, and the line intensities were prescribed by a probability distribution function. Three distributions were reviewed by Goody (1964a), i.e. a delta function (all lines having the same intensity) and probability falling off exponentially with line intensity, and probability inversely proportional to line intensity. (A fourth, newer distribution is discussed below). The random model was originally developed for water vapor, the spectrum of which exhibits a random appearance to the eye. One surprising result has been the discovery that carbon dioxide, which appears to be a relatively regular band, and also ozone can be parameterized reasonably well with the random model.

Fig. 8 taken from Goldman and Kyle (1968) shows a comparison of detailed lin-by-line calculations of ozone transmission in a random band model with exponential line intensity distribution. A close agreement can be seen. This finding is at odds with earlier results which suggested that ozone transmission could not be well represented by a random model.

Random band models can also be fit to experimental or computational results (Goody, 1964a; Rodgers and Walshaw, 1966). One requires agreement in the weak line limit and the strong line limit; the behavior in between is determined by the band model. One must investigate the agreement between the band model prediction in the intermediate region and the data to assess its usefulness for a particular purpose.

An example of such a fit is shown in Fig. 9 (Gille, unpublished). Here the plot is of - ln T/p as a function of the ratio a/p, where T equals transmission, p is pressure, and a is the amount of absorbing material in the path. For the random bands, this plot yields a universal curve for each distribution of line intensities. The line of slope 1 at the lower left side of the figure is the weak line region, while the line of slope 1/2 at the upper right side is the strong line limit. Here agreement has been forced at the two ends, and a reasonable fit is obtained over nine orders of magnitude. The calculated points, taken from CO_2 transmission values calculated by Yamamoto, Wark et al (1963) fall below the line in the transition region. For a distribution in which all lines have constant intensity, the transition region is sharper and higher; (Fig. 11) for a probability distribution with a S^{-1} distribution, the line would lie lower, and in better agreement with the data. This indicates the need to include more weak lines than the exponential distribution will allow. Nonetheless, carbon dioxide transmission in this interval fits a random exponential model reasonably well. Maximum transmission errors are ~15%. The random-exponential model does not fit data for spectral regions containing the 667 cm^{-1} Q-branch at all well.

This inability of the random-exponential model to fit data because of a lack of weak lines appears to be a common occurrence. Gille and Goody (1964) found that it was necessary to add weak lines to obtain agreement between crude NH_3 spectral data and emissitivity measurements. Lee (1973, unpublished) using much better spectral data, again found better agreement with the S^{-1} distribution. This indicates that transmittances calculated from theoretical spectral line data must be tested whereever possible against experimental observations, since the total number of weak lines may not be adequately calculated.

The effect of large numbers of weak lines was also explored by Plass (1964). He noted that, with the addition of a large number of lines 10^{-4} as strong as the strongest line in an interval, the intermediate region between the strong and weak lined asymptotes became longer and more irregular. This point was considered further by Malkmus (1967). Fig. 10, from his paper, shows plots of probability distribution functions for the exponential distribution of line intensity (Curve C) and two curves (A, B) having an S^{-1} distribution. Curves A and B differ in the range over which the distribution holds. Malkmus considered adding exponential tails on the high and low value ends of the S^{-1} distribution, and showed that a simpler expression for the transmittance results. Fig. 11 shows the plot of $-\ln T/p$ versus a/p for four distributions of line intensities. The f distribution is for all lines at the same intensity; e is for the exponential distribution; g is for the S^{-1} distribution, and h is Malkmus exponential tailed S^{-1} distribution. The addition of more weak lines in the Malkmus' model leads to a broader transition region. Advantages of this distribution are a more realistic distribution of higher intensities, and a simpler algebraic representation. Rodgers (1968) derived this model from somewhat different considerations, and showed that two bands of this form give a good representation of Walshaw's (1957) data on the 1040 cm^{-1} bands of ozone.

All band models to this point have been based on two parameters, (S/δ and α/δ). Zachor (1968) has generalized this by pointing out that

$$\left(-\frac{1}{\ln T}\right)^2 = \left(\frac{1}{\ln T_W}\right)^2 + \left(\frac{1}{\ln T_S}\right)^2 - \frac{M}{\ln T_W \ln T_S}$$

is a representation of a random band model if $M = 0$. Here T_W, T_S represent the transmittance in the weak and strong line regions, respectively. Addition of the final term can lead to a slower or more rapid approach to the asymptotes, depending on whether M is greater or less than zero. He showed that this expression is also a very good approximation to the random, regular, or Curtis model (random distribution of lines of equal intensities) if M is determined from a single point on the curve.

Zachor also noted that King (1967) proposed a two parameter fit to the strong line region, given by

$$T_S = 1 - P\left\{ n, \left[n\Gamma(n)\ (2\ Cap/\pi)^{1/2} \right]^{1/n} \right\}$$

where n is an adjustable parameter depending upon the ratio of the variance (δ^2) of the line spacing to the square of the mean line spacing (δ^2) and $P(a, x)$ is the incomplete gamma function.

$$P(a, x) = \left[\Gamma(a)\right]^{-1} \int_0^x t^{a-1} e^{-t} \, dt.$$

This expression for T_S provides a continuous set of trial functions, including the regular model (n=0.5) and the random model (n=1). Clustering of the lines leads to values of n greater than one. The transmission may now be written in terms of the four parameters S/δ, M, n and C for each wavelength interval.

Gibson and Pierluissi (1971) have extended the model slightly further, while getting closer to the concept of a model as a (complex) curve fit, by noting that

$$T_W = Sa/\delta = B_W^{-1/2} a$$

and writing

$$\left(-\frac{1}{\ln T}\right)^2 = \frac{B_W}{a^2} + \frac{B_S^2}{\ln \tau_S^2} + \frac{B_{WS}}{a \ln \tau_S}$$

where $B_W, B_S > 0$, $B_{WS} < B_W B_S$.

With Kings expression for the strong line limit, this is now a five parameter model. Applying this formulation to calculated CO_2 transmittances at 300K averaged over 50 cm^{-1}, they found rms deviations of 18.2×10^{-3}, $3 \cdot 7 \times 10^{-3}$ and 2.3×10^{-3} for the Goody random model, the Zachor model, and the five parameter models, respectively. Pierliussi (1973) found similar results for 5 cm^{-1} experimental data on a CO_2 band at 4853.6 cm^{-1}.

By comparison, Smith (1969) used a straightforward fit of $\ln(-\ln T)$ to a, p, θ, ap, $a\theta$, a^2 and in some cases higher terms still, where T came from experimental results and θ is temperature. The rms errors are of the order of 1%, which suggests that the 5-parameter model is more economical.

In a somewhat similar vein, McClatchey, et al. (1972) have presented nomograms for obtaining empirical transmittances. A program is now available to compute these (Selby and McClatchey, 1972). Accuracies are stated to be of the order of 10%.

The final example of a band model is the quasi-random model, described by Wyatt, et al. (1962), although the idea is implicit in Goody's (1964a) discussion of general random models. This is physically motivated, but relies much more heavily on computer handling of data than other band models, and therefore in some ways falls between the simple band models, and line-by-line calculations. It is motivated by the realization that line positions in real bands are neither completely regular nor

completely random, and that line intensities are not simply characterized nor uncorrelated with line positions. The approach is as follows:

1. The spectrum is divided into small intervals, e.g. 5, 50, or 100 cm^{-1}. Spectral lines are located within the correct small interval, but are assumed to be randomly located within it;
2. The spectral line intensities in the interval are characterized by a histogram of actual line intensities;
3. An analytical expression is used for the absorption by the spectral lines in the interval, and the actual number of lines are used;
4. The transmission for each group of lines in the intensity histogram is calculated, and these transmissions are multiplied to give the effect of all local lines;
5. The transmission by the wings of lines in other intervals is calculated, and multiplied by the effects of local lines to give the total transmission by the interval.

Obviously, this requires a computer to do, but is far less time consuming than a detailed frequency integration. An example of some transmittances calculated by Stull et al. (1964) according to the quasi-random model and their comparison with laboratory measurements is shown in Fig. 12. The agreement is seen to be generally quite good, although there are problems near the Q branches.

Another quite different approach has been recently explored by Arking and Grossman (1972), although the idea, mentioned by Kondratyev (1965, 1969) goes back at least to Lebedinsky (1939). In this method, rigorously applicable only to a homogeneous atmosphere, the absorption coefficient $k(\nu)$ is transformed into a k distribution function, giving the frequency of occurrence of absorption coefficient k within a wavenumber interval. The authors point out the advantages of such an approach - exact and relatively simple treatment of integrals over frequency and zenith angle. They have also provided considerable insight by showing the distribution functions for single line regular and random band models, as well as an example for a portion of the 15 μm band of CO_2.

In practical application, this generally becomes a histogram of absorption coefficients in a given band, such that

$$T(a) = \sum_{i=1}^{N} b_i e^{-k_i a}$$

where clearly $\sum_{i=1}^{N} b_i = 1$, and both b_i and k_i are functions of the conditions in the homogeneous layer. This approach is often used in heat transfer engineering. Kondratyev (1965, 1969) discusses examples of its use in the USSR. Raschke and Stucke (1973) show the agreement of such fits with experimental data.

4. TRANSMISSION THROUGH INHOMOGENEOUS ATMOSPHERE

Because the variation of pressure and temperature along a ray path may be calculated directly in a line-by-line scheme, the treatment of atmospheric inhomogeneity is a problem only for band model calculations.

The Curtis-Godson (CG) approximation is the standard method of treating radiative transfer through an inhomogeneous atmosphere. Goody (1964) presents a derivation of the required expressions. The goal is to replace the inhomogeneous path by an "equivalent" homogeneous path, for which the results of the preceeding section will be valid. This equivalence is defined by requiring exact agreement in the strong and weak line limits, which would be expected to yield reasonably accurate values over the entire range. Several studies (Kaplan, 1959; Walshaw and Rodgers, 1963; Goody, 1964b; Zdunkowski and Raymond, 1970) have in fact indicated that the CG approximation generally gives very good results, with the exception of situations in which there are small amounts of absorber at high pressure and large amounts at low pressure. The form in which it has been most widely used most recently was developed by Godson and applied by Rodgers and Walshaw (1967).

This has, for the amount of material in the equivalent path

$$\bar{a} = \int \psi(T)\, da$$

and

$$\overline{pa} = \int \phi(T) p\, da$$

where $\psi(T) = \sum S_i(T) / \sum S_{i0}$, $\phi(T) = \sum_i (S_i \alpha_i)^{1/2} / \sum (S_{i0} \alpha_{i0})^{1/2}$, and subscript 0 refers to conditions at standard temperature. The functions ψ and ϕ contain the information on the temperature dependence.

Goody (1964b) has used an early formulation of van de Hulst to develop a higher approximation to obtain more exact results. The algebra is complex, but expressions are given which may be used to correct for the amount of absorbing material.

Armstrong (1968d) considered several improvements to the CG approximation for single lines. The most accurate method evolved from performing the integral over pressure (altitude) by Gaussian quadrature. This is equivalent to dividing the path into two or more sequential homogeneous paths. The labor involved appears to be less than that required by Goody's method.

Following a different approach, Yamamoto and Aida (1970) found excellent results for a uniformly mixed gas in a non-isothermal atmosphere by introducing a suitable mean temperature. Following this approach, Yamamoto et al. (1972) obtained a better approximation for non-uniformly distributed gases by defining a suitable mean half-width $\bar{\alpha}$ from

$$(\overline{\alpha})^{\varepsilon} = \int S\alpha^{\varepsilon}\ du / \int du S.$$

The parameter ε depends upon $\overline{a}^2 / \overline{ap}$ and an exponent n, whose value can be determined from initial calculations which include the vertical distribution.

The percent error of integrated absorption by a single ozone line from the top of the atmosphere to the surface is shown in Fig. 13 as a function of absorber amounts (slant angle). Clearly this approximation provides results more accurate than those given by the Curtis-Godson or Goody approaches.

The simplest method of handling atmospheric inhomogeneity is by the scaling approximation,(Goody, 1964a). This has recently been employed by McClatchey, et al. (1972) by expressing transmittance as a function of ap^n where $n=0.9$ for water vapor, 0.75 for CO_2 and 0.4 for ozone.

A further problem that becomes important in the stratosphere, where the pressure is low is the appearance of Doppler effects on the spectral lines and the emergence of Voigt (combined Doppler-Lorentz) line shapes. Several authors including Young (1967), and Hummer (1964) have written on numerical methods for computing the Voigt profiles for single lines. These have been lucidly discussed by Armstrong (1967). Tabulated values of equivalent widths of single Voigt lines have been prepared by Jansson and Korb (1968).

The effects of Doppler broadening on a random array of lines with exponential distribution of intensities is shown in Fig. 14, from Gille and Ellingson (1968). As $W/\alpha/_L$ is proportional to $-\ln T/p$, and u to a/p, the axis are those seen above. The parameter d is $2\alpha_L/\alpha_D$ where subscripts L, D, V will refer to Lorentz, Doppler and Voigt respectively. For small d, where the Voigt shape is relevant, the weak line region extends to larger values of a/p, followed by a flat region merging eventually into the square root region.

Gille and Ellingson showed that the transmittance of this band may easily be corrected for Doppler effects, since

$$T_L = \exp\ (-A_L)$$

and

$$T_V = \exp\ (-A_V) = \exp\left(-A_L \cdot \frac{A_V}{A_L}\right)$$

$$= T_L^{\,C}$$

where $C = A_V/A_L$ is a function of a/p and d, as shown in Fig. 15. This same correction should give a good first approximation for other random models.

5. FLUX AND HEATING RATE CALCULATIONS

Time does not permit a discussion of all the schemes used for atmospheric calculations. Rodgers and Walshaw (1967) developed a code employing the random-exponential band model based on spectral data and an analytic form of the integration over zenith angle to obtain the flux, defined as

$$F = 2\pi \int \mu I(\mu) \, d\mu$$

for a homogeneous plane parallel atmosphere. They concluded that, to nearly the same accuracy, one could use a diffusivity factor $r = 1.67$. This allows calculation of the flux from a flux transmittance, which is

$$T_F(a) = T(ra) \quad .$$

(The theory of the diffusivity factor has been extensively investigated by Armstrong, 1968b.) They also incorporated the Curtis-Godson approximation, to treat the variation of temperature and pressure along atmospheric paths, and Gaussian quadrature in the vertical direction to minimize errors. Finally, they solved for heating rates instead of fluxes.

Ellingson and Gille (in preparation) have developed a model employing many of the same features. They used newer spectral data. The principal differences between this model and the Rodgers-Walshaw (RW) model are that this model has 100 spectral intervals, about ten times more than RW, in order to follow the rapid variation of atmospheric absorption with frequency more closely. Other important differences lie in the atmospheric absorbers included, and the sources of transmission data. The ozone bands at 9.6 and 14 μm were included, along with less detailed treatments of methane (CH_4) and nitrous oxide (N_2O) bands near 7.75 μm. Temperature dependence was included for all bands. Finally, Bignell's (1970) e type continuum was included in the window region.

This model can also be used to compute the upward intensity at the top of the atmosphere which can be compared to satellite measurements. An example is shown in Fig. 16, where the value computed by the Ellingson-Gille model is compared to measurements obtained with the Infrared Interferometer Spectrometer (IRIS) experiment on Nimbus 3 (Conrath, et al., 1970). The agreement is seen to be quite good. Percent differences in individual spectral intervals are less than 5% in individual intervals (except for two beyond 1320 cm^{-1}). The integrated difference is 1.12%. This is typical of five such comparisons under clear conditions. This comparison is significant, as it is one of the first between a calculation scheme designed to give fluxes and heating rates in the atmosphere and precise satellite observations. Comparisons with low, cost, expendable radiometersondes do not yield as good agreement, as the study by Gille and Kuhn (1973) shows.

If no spectral resolution is required, emissivity type calculations may be made. Sasamori (1968) and Manabe and Wetherald (1967) have described traditional calculations of this type for use in general circulation modeling where speed is crucial. Cox (1973) has also developed a model of this type

to study the sensitivity to the e type continuum.

Emissivities may also be thought of simply as parameterizations which can be chosen to give best results. Rodgers (1967) has explored several different formulations for the emissivities, and found that separate emissivities for upward and downward fluxes, obtained by fitting values calculated by more accurate schemes to temperature corrected absorber amounts, gave excellent results.

Another method for calculating cooling rates relies on the fact that above the lower troposphere, most of the cooling is due to loss to space, and may be approximated by Newtonian cooling. Originally used by Murgatroyd and Goody (1958), this has been developed most fully by Dickinson (1972, 1973) for the atmospheres of Venus and Earth.

6. CONCLUSIONS

The comparisons between direct spectral integration and high precision measurements suggest that calculational techniques are sufficient for molecular atmospheres. However, such computations are extremely time-consuming.

A wide range of approximate treatments is available. Traditional band models are much faster, but may introduce undesirably large errors. More sophisticated models and ways of using them, developed over the last 10 years, appear capable of providing quite good results with relatively modest increases in computational effort.

The problem of transfer through turbid atmospheres is now under active investigation in many places.

BIBLIOGRAPHY

Arking, A., and K. Grossman, 1972: The influence of line shape and band structure on temperatures in planetary atmospheres. J. Atmos. Sci., 29, 937-949.

Armstrong, B. H., 1967: Spectrum line profiles: the Voigt function. J. Quant. Spectrosc. Radiat. Transfer, 1, 61-88.

Armstrong, B. H., 1968a: Analysis of the Curtis-Godson approximation and radiation transmission through inhomogeneous atmospheres. J. Atmos. Sci., 25, 312-322.

Armstrong, B. H., 1968b: Theory of the diffusivity factor for atmospheric radiation. J. Quant. Spectros. Radiat. Transfer, 8, 1577-1599.

Bignell, K. J., 1970: The water vapor infra-red continuum. Quart. J. Roy. Meteor. Soc., 96, 390-403.

Burch, D. E., 1970: Investigation of the absorption of infra-red radiation by atmospheric gases. Aeronutronic Division. Publ. V-4784, Philco-Ford, Newport Beach, California.

Burch, D. E., D. Gryunak and D. Williams, 1962: Total absorpance of carbon dioxide in the infrared. Applied Optics, 1, 759-765.

Conrath, B. J., R. A. Hanel, V. G. Kunde, and C. Prabhakara, 1970: The infrared interferometer experiment on Nimbus 3. J. Geophys. Res., 75, 5831-5857.

Cox, S. K., 1973: Infrared heating calculations with a water vapour pressure broadening continuum. Quart. J. Roy. Meteor. Soc., 99, 669-674.

Dickinson, R. E., 1972: Infrared radiative heating and cooling in the Venusian mesosphere, 1. Global mean radiative equilibrium, J. Atmos. Sci., 29, 1531-1556.

Dickinson, R. E., 1973: Method of parameterization for infrared cooling between altitudes of 30 and 70 kilometers. J. Geophys. Res., 78, 4451-4457.

Drayson, S. R., 1966: Atmospheric transmission in the CO_2 bands between 12 μm and 18 μm. Appl. Optics, 5, 385-391.

Drayson, S. R., S. Y. Li and C. Young, 1968: Atmospheric absorption by carbon dioxide, water vapor and oxygen. U. Michigan College of Engineering Report 08183-2-F.

Ellingson, R. G. and J. C. Gille, 1974: A new long wave radiative transfer model: calibration and application (in preparation).

Elsasser, W. L., 1942: Heat transfer by infrared radiation in the atmosphere. Harvard Meteorological Studies No. 6, Cambridge, Harvard Univ. Press. 107 pp.

Gates, D. M., R. F. Calfee and D. W. Hansen, 1963: Computed transmission spectra for 2.7 micron H_2O band. Applied Optics, 2, 1117-1122.

Gibson, G. A. and J. H. Pierluissi, 1971: Accurate formula for gaseous transmittance in the infrared. Appl. Optics, 10, 1509-1518.

Gille, J. C. and R. G. Ellingson, 1968: Correction of random exponential band transmissions for Doppler effects. Appl. Optics 7, 471-474.

Gille, J. C. and R. Goody, 1964: Convection in a radiating gas. J. Fluid Mech. 20, 47-78.

Gille, J. C. and P. M. Kuhn, 1973: The International Radiometersonde Intercomparison Programme (1970-71). Tech. Note No. 128, Geneva, World Meteorological Organization. 127 pp.

Goldman, A. and T. G. Kyle, 1968: A comparison between statistical model and line-by-line calculation with application to the 9.6-mu ozone and the 2.7-mu water vapor bands. Appl. Optics 7, 1167-1177.

Goody, R., 1952: A statistical model for water vapour absorption. Q. J. Roy. Meteor. Soc., 78, 165-169.

Goody, R. M., 1964a: Atmospheric Radiation, I: Theoretical Basis. Oxford, University Press, 436 pp.

Goody, R. 1964b: The transmission of radiation through an inhomogeneous atmosphere. J. Atmos. Sci. 21, 575-581.

Hitschfeld, W. and J. T. Houghton, 1961: Radiative transfer in the lower stratosphere due to the 916 micron band of ozone. Q. J. Roy. Meteor. Soc. 87, 562-577.

Hummer, D. G., 1964: The Voigt function: an eight--significant--figure table and generating procedure. Univ. of Colorado - NBS JILA Report 24.

Jansson, P. A. and C. L. Korb, 1968: A table of the quivalent widths of isolated lines with combined Doppler and collision broadened profiles. J. Quant. Spectrosc. Radiat. Transfer, 8, 1399-1409.

Kaplan, L. D., 1959: A method for calculation of infrared radiative flux for use in numerical models of atmospheric motion, in The atmosphere and the sea in motion. Rockefeller Inst. Press, p. 170.

King, J. I. F., 1964: Band absorption model for arbitrary line variance. J. Quant. Spectros. Radiat. Transfer, 4, 705-711.

Kondratyev, K. Y., 1965: Radiative Heat Exchange in the Atmosphere. Oxford, Pergamon Press, 411 pp.

Kondratyev, K. Ya., 1969: Radiation in the Atmosphere. New York, Pergamon Press, 912 pp.

Kunde, V. G. and W. C. Maguire, 1972: Direct integration transmittance model. NASA Preprint X-622-73-258, Goddard Space Flight Center, Greenbelt, Maryland. (Submitted to J. Quant. Spectrosc. Radiat. Transf.)

Kunde, V. G., B. J. Conrath, R. A. Hanel, W. C. Maguire, C. P. Prabhakara and V. V. Salomonson, 1974: The Nimbus 4 Infrared Spectroscopy Experiment 2. Comparison of Observed and Theoretical radiances from 425-1450 cm^{-1}. J. Geophys. Res., 79, 777-784.

Kyle, T. G., 1968: Net interval for calculating absorption spectra. J. Optical Soc. Amer., 58, 192-195.

Lebedinsky, A. I., 1939: Radiative equilibrium in the earth's atmosphere. Proc. Leningrad Univ., Ser. Math. 3, No. 31.

McCad, D. J. and J. M. Shaw, 1968: The infrared spectrum of ozone. J. Mol. Spectrosc., 25, 374-397.

McClatchey, R. A., R. W. Fenn, J. E. A. Selby, F. E. Volz, and J. S. Garing, 1972: Optical properties of the atmosphere (Third edition). Air Force Cambridge Research Laboratories Environmental Research Paper No. 411, 108 pp.

Malkmus, W., 1967: Random Lorentz band model with exponential-tailed S^{-1} line-intensity distribution function. J. Opt. Soc. Amer., 57, 323-329.

Manabe, S. and R. T. Wetherald, 1967: Thermal equilibrium of the atmosphere with a given distribution of relative humidity. J. Atmos. Sci., 24, 241-259.

Murgatroyd, R. J. and R. Goody, 1958: Sources and sinks of radiative energy from 30-90 km. Quart. J. Roy. Meteor. Soc., 84, 225-234.

Pierluissi, J. H., 1973: Polynomial representation of transmittance models. Appl. Optics, 12, 776-778.

Plass, G. N., 1964: The influence of numerous low-intensity spectral lines on band absorptance. Appl. Optics, 7, 859-866.

Raschke, E. and U. Stucke, 1973: Approximations of band transmission functions by finite sums of exponentials. Beträge Phys. Atmos., 46, 203-212.

Rodgers, C. D., 1967: The use of emissivity in atmospheric radiation calculations. Q. J. Roy. Meteor. Soc., 93, 43-54.

Rodgers, C. D., 1968: Some extensions and applications of the new random model for molecular band transmission. Q. J. Roy. Meteor. Soc., 94, 99-102.

Rodgers, C. D. and C. D. Walshaw, 1966: The computations of infra-red cooling rate in planetary atmospheres. Quart. J. R. Meteor. Soc., 92, 67-92.

Sasamori, T., 1968: The radiative cooling approximation to General circulation experiments. J.Appl. Meteor., 7, 721-729.

Selby, J. E. A., and R. M. McClatchey, 1972: Atmospheric transmittance from 0.25 to 28.5 mm: Computer Code LOWTRAN 2. Air Force Cambridge Research Laboratories Environmental Research Paper No. 427. 77 pp.

Smith, W. L., 1969: A polynomial representation of carbon dioxide and water vapor transmission. ESSA Technical Report NESC 47. National Environmental Satellite Cents, Washington, D. C.

Stull, V. R., P. J. Wyatt and G. N. Plass, 1964: The infrared transmittance of carbon dioxide. Appl. Opt., 3, 243-254.

Walshaw, C. D., 1957: Integrated absorption by the 9.6 μ band of ozone. Q. J. Roy. Meteor. Soc., 83, 315

Walshaw, C. D. and C. D. Rodgers, 1963: The effect of the Curtis-Godson approximation on the accuracy of radiative heating rate calculations. Q. J. Roy. Meteor. Soc., 89, 122

Wark, D. Q., J. Alishouse and G. Yamamoto, 1963: Calculations of the earth's spectral radiance for large zenith angles. U. S. Weather Bureau Meteorological Satellite Laboratory Dept. No. 21, Washington, D. C., 45 pp.

Wyatt, P. J., V. R. Stull and G. N. Plass, 1962: Quasi-random model of band absorption. J. Opt. Soc. America, 52, 1209-1217.

Yamamoto, G. and M. Aida, 1970: Transmission in a non-homogeneous atmosphere with an absorbing gas of constant mixing ratio. J. Quant. Spectrosc. Radiat. Transfer, 10, 593-608.

Yamamoto, G., M. Aida and S. Yamamoto, 1972: Improved Curtis-Godson approximation in a non-homogeneous atmsophere. J. Atmos. Sci., 29, 1150-1155.

Young, C., 1965: Calculation of the Absorption Coefficient for lines with combined Doppler and Lorentz broadening. J. Quant. Spectrosc. Radiat. Transfer, 5, 549-552.

Zachor, A. S., 1968: A general approximation for gaseous absorption. J. Quant. Spectrosc. Radiat. Transfer, 8, 771-781.

Zdunkowski, W. G. and W. H. Raymond, 1970: Exact and approximate transmission calculations for homogeneous and non-homogeneous atmospheres. Beiträge zur Physik der Atmosphäre, 43, 185-201.

FIGURE CAPTIONS

Figure 1. Schematic of spectral mesh used for 0.1 cm^{-1} interval.
a) No spectral lines, one interval, four mesh points;
b) one spectral line, six sub-intervals, 24 mesh points;
c) two spectral lines, 11 sub-intervals, 44 mesh points.
(After Kunde and McGuire, 1973).

Figure 2. Homogeneous path comparison for the 667 cm^{-1} band of carbon dioxide between low resolution laboratory measurements by Burch, et al. (1962) and line-by-line calculations. Experimental conditions: absorber amount, 6.30 atm cm; equivalent pressure, 0.0205 atm; temperature, 300K. (After Drayson, et al., 1968).

Figure 3. Homogeneous path comparison for the 701 cm^{-1} ozone band between laboratory measurements by McCaa and Shaw (1968) and line-by-line calculations. Experimental conditions:
a) absorber amount, 2 atm cm, pressure, 0.0876 atm; room temperature;
b) absorber amount, 9.4 atm cm; pressure, 0.701 atm; room temperature.
(After Kunde and McGuire, 1973).

Figure 4. Illustration of two quadrature nets, with Δ, the offset of the mesh from line center, equal to zero (dotted line) and offset by Δ (dashed line). (After Kyle, 1968).

Figure 5. Percent error of the integrated absorption of an atmospheric line for the step sizes D/α shown above the curves, for optimal Δ. Abscissa is one-half the optical depth at the line center.

Figure 6. Comparison of observed and calculated radiances for a clear atmosphere near Guam at 15.1°N latitude and 215.3°W longitude on April 27, 1970. (After Kunde, et al., 1974).

Figure 7. Percent difference between observed and calculated radiance for the Guam case shown in Fig. 6. (After Kunde, et al., 1974).

Figure 8. Comparison of absorption spectra obtained by line-by-line calculation, (curves 1), and by the statistical model calculation, (curves 2), for the 9.6 μm ozone band. The line-by-line calculations are displaced by 20%. Conditions: A curves, pressure, 0.0197 atm, path length, 97.88 cm. For both calculations, line half width was taken to be 0.08 cm^{-1} atm^{-1}, temperature, 233°K. (After Goldman and Kyle, 1968).

Figure 9. Fit of a portion of the 667 cm^{-1} band of CO_2 to a random band model with exponential distribution of line intensities. (Gille, 1965, unpublished).

Figure 10. Line intensity probability distribution functions. Curve C is the exponential intensity distribution $P(S) = \bar{S}^{-1} \exp(-S/\bar{S})$. The dashed curves A and B are the truncated S^{-1} distributions $P(S) = (S \ln R)^{-1}$ $(S_M/R \leq S \leq S_M)$, $P(S) = 0$ (otherwise). The solid curves A and B are the exponential-tailed S^{-1}distributions $P(S) = S(\ln R)^{-1} [\exp(-S/S_M) - \exp(-RS/S_M)]$. For curves B, R is 10^3, for curves A, R is 10^6. In all cases, P(S) is normalized and $\bar{S}$ denotes the mean intensity: $\bar{S} = \int SP(S)\, dS$. For A and B, $\bar{S}$ is equal to $(R-1)(R \ln R)^{-1} S_M$. The figure demonstrates the greater emphasis placed on weaker lines relative to stronger lines in the distributions proportional to S^{-1}. (After Malkmus, 1967).

Figure 11. Curves of growth for random band models composed of pressure broadened lines for four different intensity distribution functions: $f(x_E)$, all lines of the same intensity; $e(x_E)$, exponential distribution, $P(S) \propto \exp(-4S/\pi S_E)$; $g(x_E)$, ogival distribution, $P(S) \propto S^{-1} (S \leq S_{max})$, $P(S) = 0$ $(S > S_{max})$; $h(x_E)$, exponential tailed ogival distribution, $P(S) \propto S^{-1} \exp(-S/\pi S_E)$. $x_E = ca/p$. Quantities are defined so that asymptotes are the same in all cases. (After Malkmus, 1967).

Figure 12. Homogeneous path comparison for the 667 cm^{-1} band of carbon dioxide between laboratory measurements by Burch, et al. (1962) and quasi-random model calculations. Experimental conditions: absorber amount, 46.4 atm cm; pressure, 0.0205 atm. (After Stull et al., 1964).

Figure 13. Percent error of integrated abosrption of the R(44) line of ozone as a function of absorber amount (slant angle) for paths between the surface and top of the atmosphere, for three treatments of the inhomogeneous atmosphere. The arrow indicates values that actually occur in the spherical, terrestrial atmosphere. (After Yamamoto et al., 1972).

Figure 14. Mean curves of growth for a line in a random band of lines having exponential distribution of line intensities, for several ratios of Lorentz to Doppler half widths. Curves are marked with values of $d = 2\alpha_L/\alpha_D$. Pure pressure broadened (Lorentz lines) correspond to the line $d = \infty$. On this scale, the line $d = 1$ cannot be distinguished from $d = \infty$. (After Gille and Ellingson, 1968).

Figure 15. $C = A_V/A_L$ as a function of $u \propto a/p$ for several values of d. The x- axis (C=1) corresponds to pure Lorentz lines. Plus signs show values calculated according to a modified Curtis approximation (Rodgers and Walshaw, 1966). An improved approximation is available (Rodgers, 1973, private communication.)

Figure 16. Comparison between observed (dotted lines) and calculated (solid line histogram) upward radiances from earth and atmosphere near Barbados, W.I. on June 4, 1969. Observations were made by Infrared Interferometer Spectrometer (IRIS) experiment on Nimbus 3 (Conrath, et al., 1970). The smooth curves give values of the Planck function for the indicated temperatures. Calculations are from Ellingson and Gille, 1974.

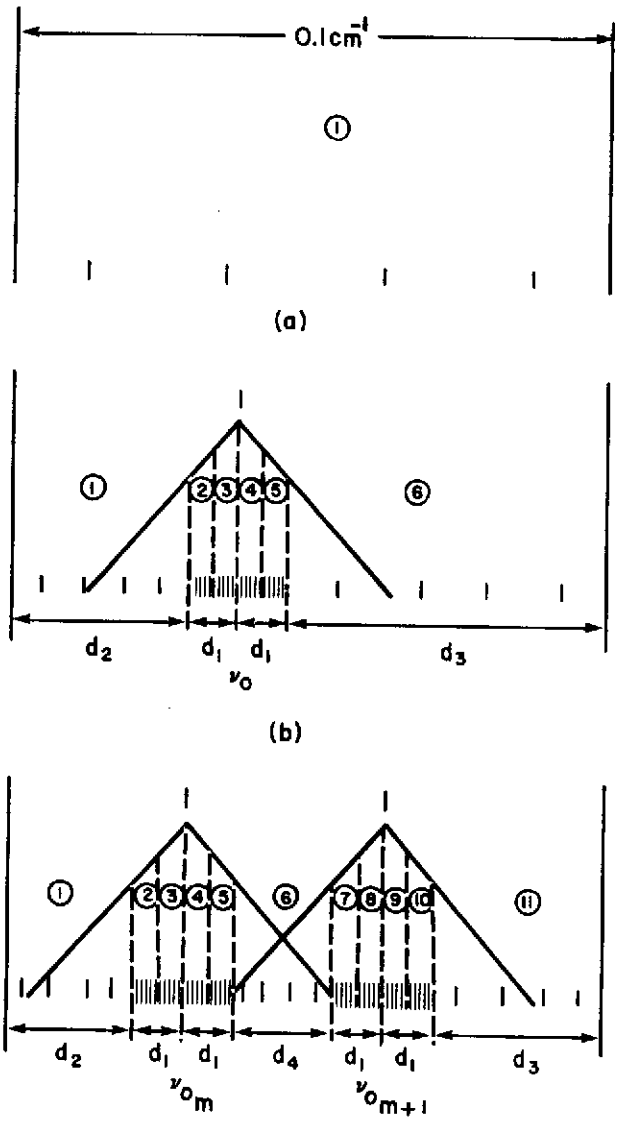
0.1cm⁻¹
①
(a)
①
2 3 4 5
⑥
d2
d1
d1
d3
νo
(b)
①
2 3 4 5
⑥
7 8 9 10
⑪
d2
d1
d1
d4
d1
d1
d3
νom
νom+1

FIGURE 1

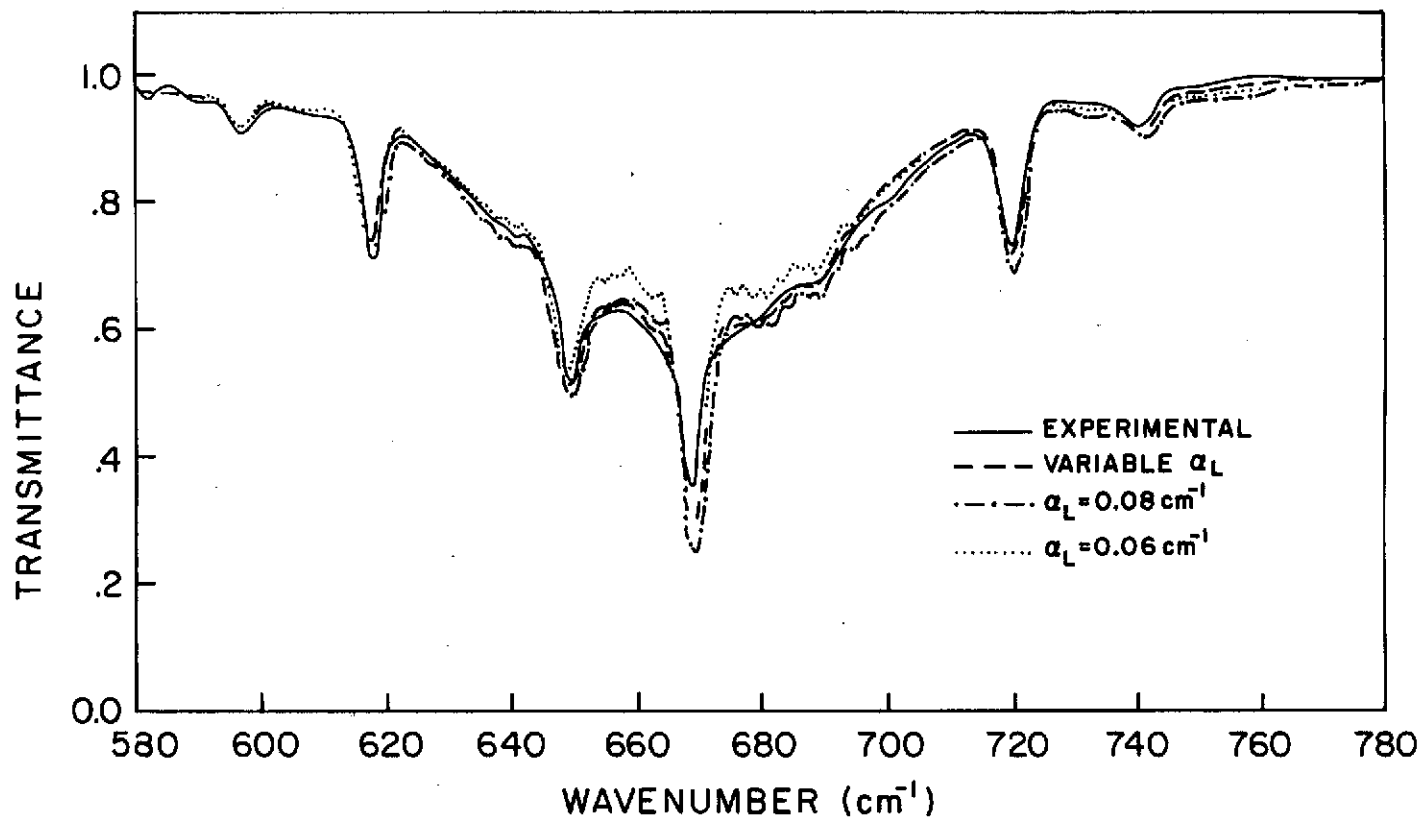
TRANSMITTANCE
1.0
.8
.6
.4
.2
0.0
580
600
620
640
660
680
700
720
740
760
780
WAVENUMBER (cm⁻¹)
EXPERIMENTAL
VARIABLE α_L
α_L=0.08 cm⁻¹
α_L=0.06 cm⁻¹

FIGURE 2

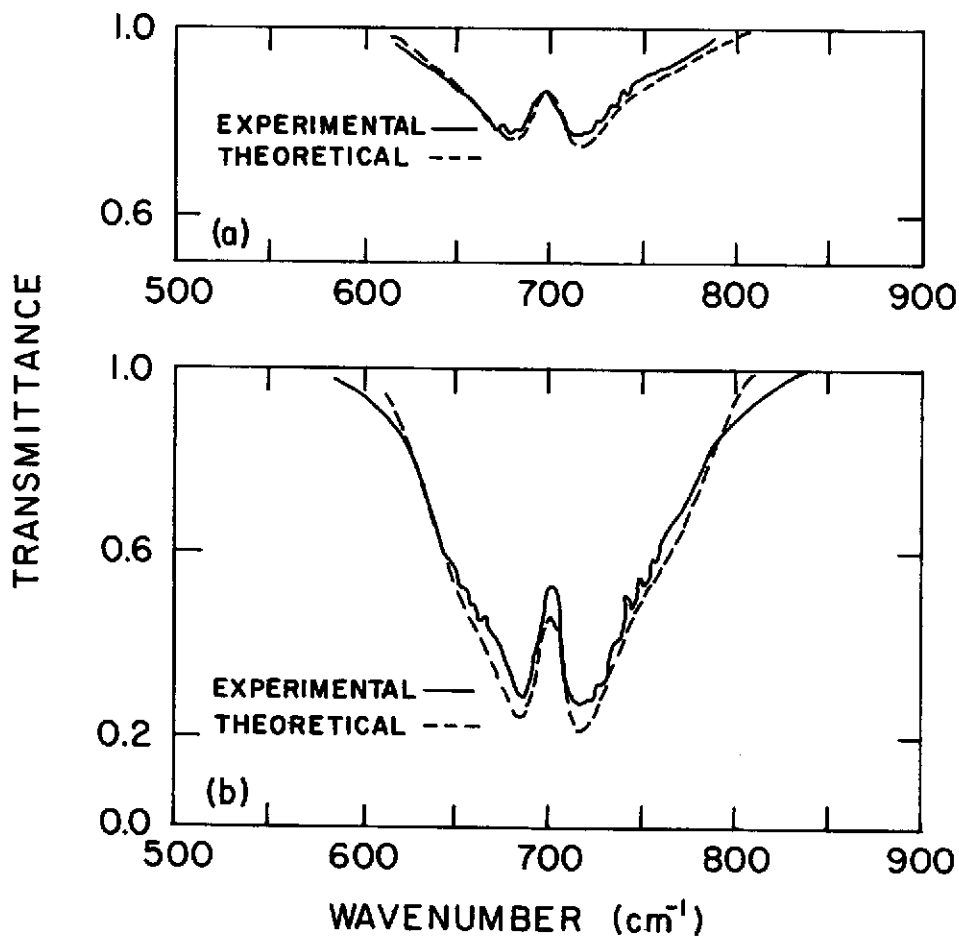
1.0
0.6
EXPERIMENTAL
THEORETICAL
(a)
500
600
700
800
900
TRANSMITTANCE
1.0
0.6
0.2
0.0
EXPERIMENTAL
THEORETICAL
(b)
500
600
700
800
900
WAVENUMBER (cm⁻¹)

FIGURE 3

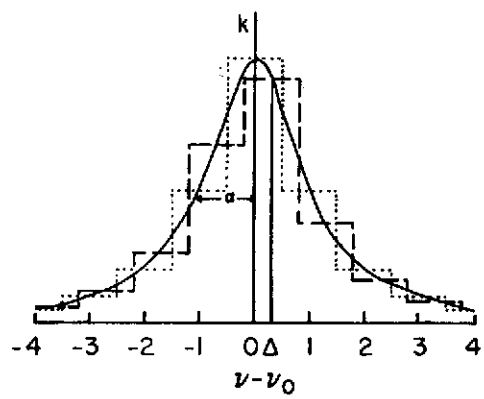

FIGURE 4

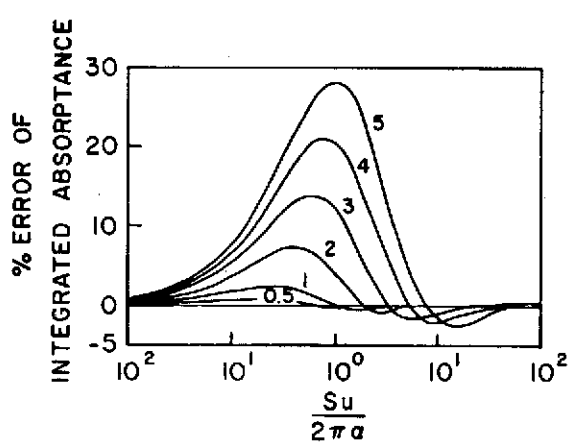

FIGURE 5

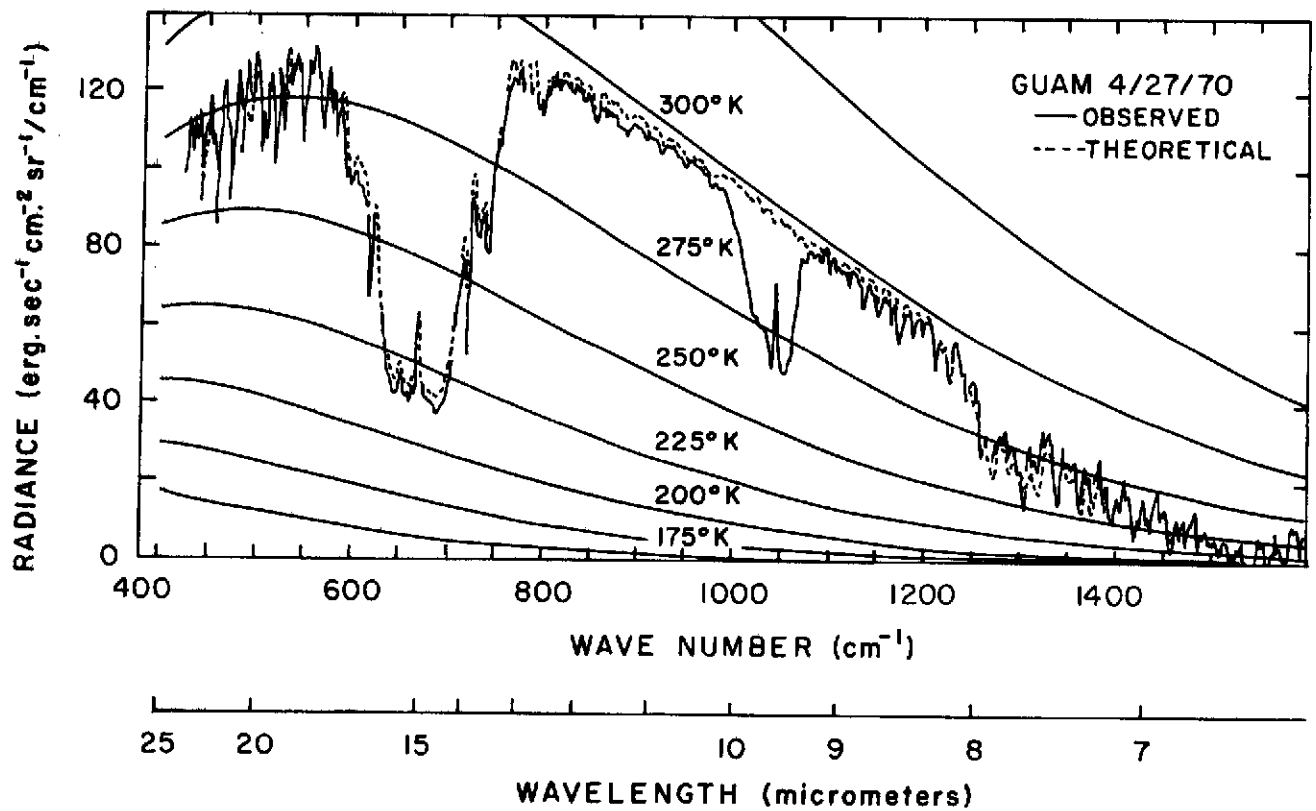
GUAM 4/27/70
—OBSERVED
----THEORETICAL
300°K
275°K
250°K
225°K
200°K
175°K
RADIANCE (erg.sec⁻¹cm⁻².sr⁻¹/cm⁻¹)
0
40
80
120
400
600
800
1000
1200
1400
WAVE NUMBER (cm⁻¹)
25
20
15
10
9
8
7
WAVELENGTH (micrometers)

FIGURE 6

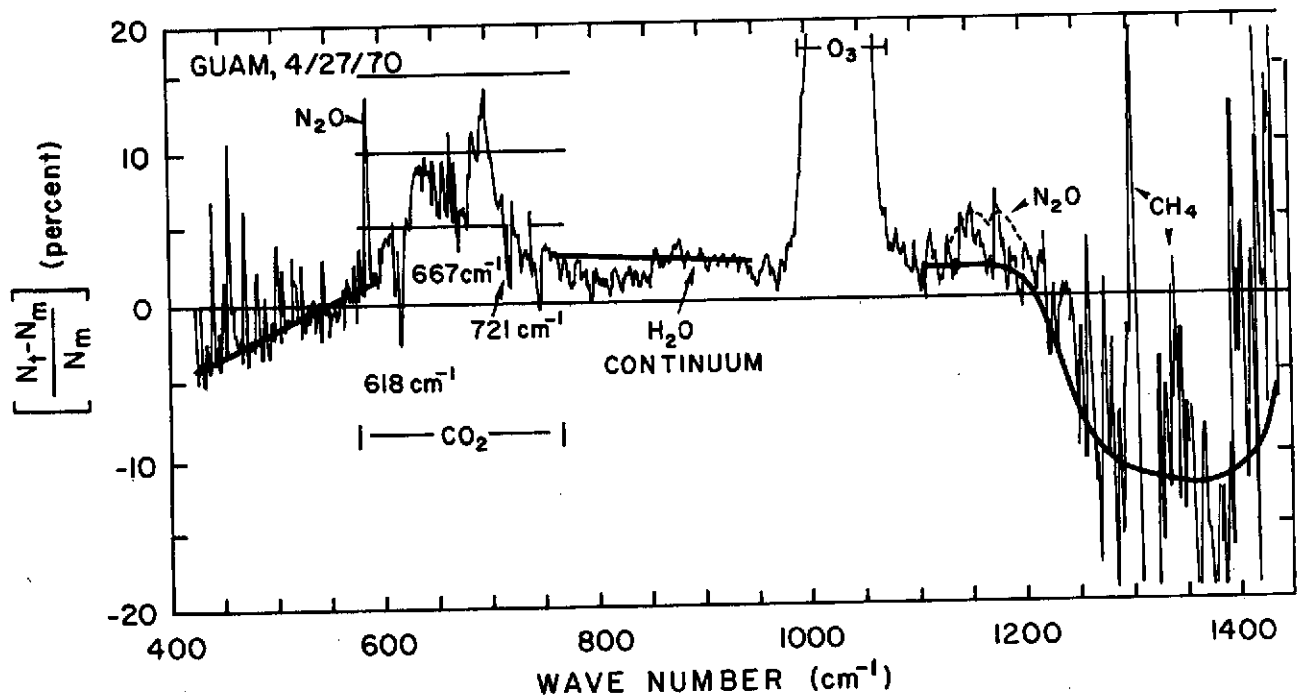
GUAM, 4/27/70
N_2O
667cm^{-1}
721 cm^{-1}
618 cm^{-1}
CO_2
H_2O CONTINUUM
O_3
N_2O
CH_4
$\left[\frac{N_t-N_m}{N_m}\right]$ (percent)
20
10
0
-10
-20
400
600
800
1000
1200
1400
WAVE NUMBER (cm^{-1})

FIGURE 7

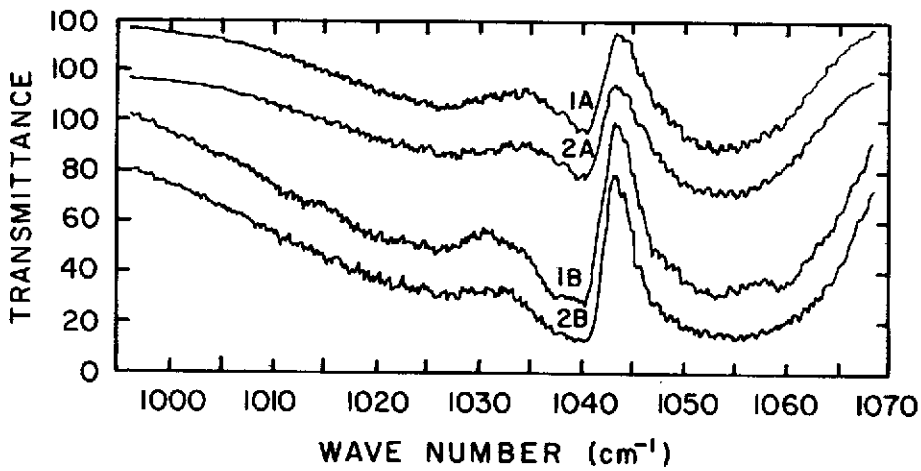
100
100
100
80
60
40
20
0
TRANSMITTANCE
1A
2A
1B
2B
1000
1010
1020
1030
1040
1050
1060
1070
WAVE NUMBER (cm⁻¹)

FIGURE 8

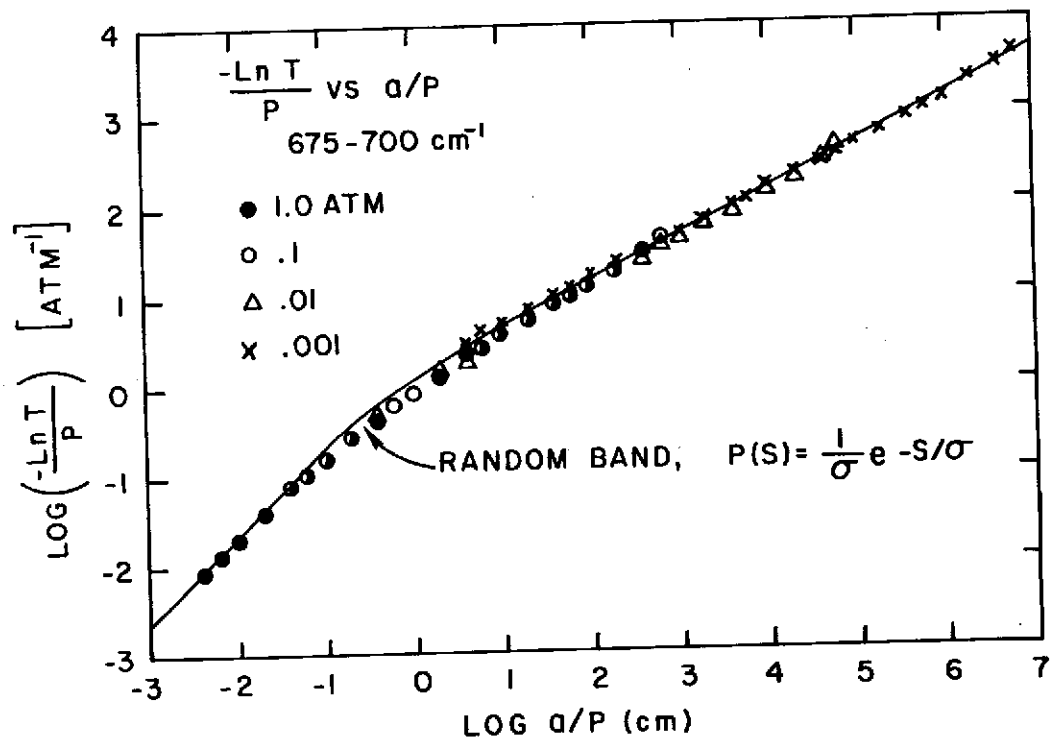
-Ln T / P vs a/P
675-700 cm⁻¹
● 1.0 ATM
o .1
Δ .01
x .001
RANDOM BAND, P(S)= 1/σ e -S/σ
LOG (-Ln T / P) [ATM⁻¹]
LOG a/P (cm)
4
3
2
1
0
-1
-2
-3
-3
-2
-1
0
1
2
3
4
5
6
7

FIGURE 9

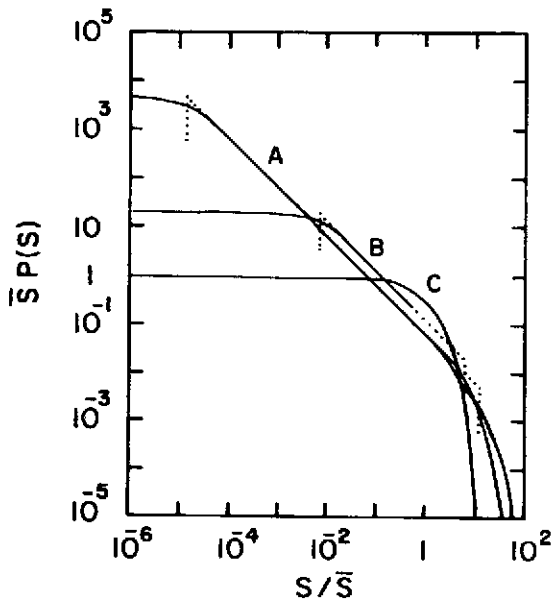

FIGURE 10

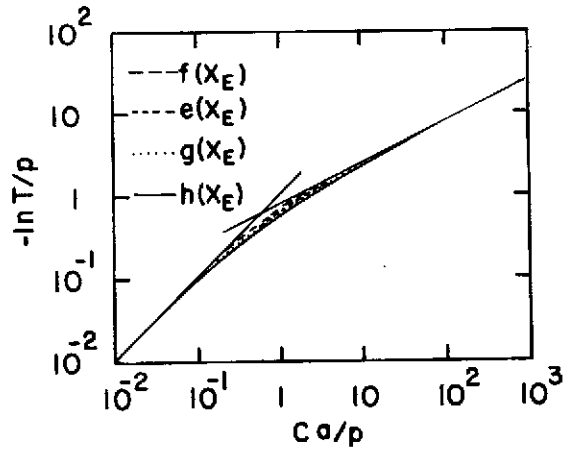

FIGURE 11

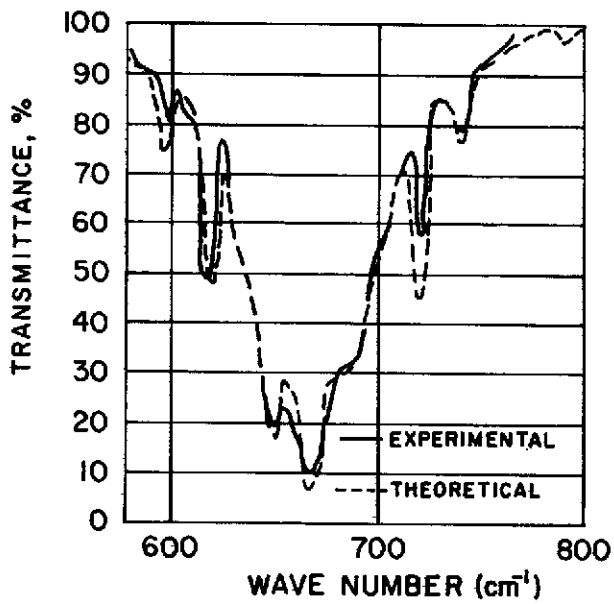
100
90
80
70
60
50
40
30
20
10
0
TRANSMITTANCE, %
600
700
800
WAVE NUMBER (cm⁻¹)
EXPERIMENTAL
THEORETICAL

FIGURE 12

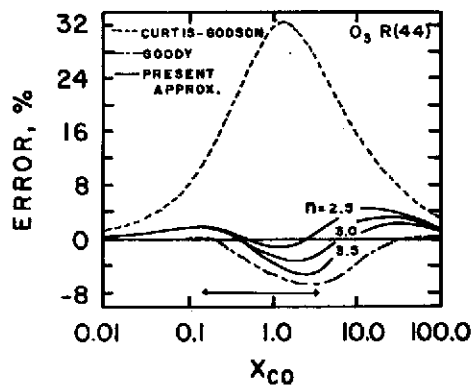
CURTIS-GODSON
GOODY
PRESENT APPROX.
O_3 R(44)
n=2.5
3.0
3.5
ERROR, %
32
24
16
8
0
-8
0.01
0.1
1.0
10.0
100.0
X_{CO}

FIGURE 13

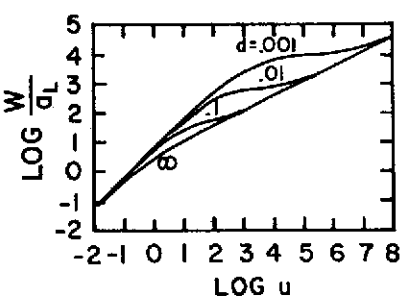

FIGURE 14

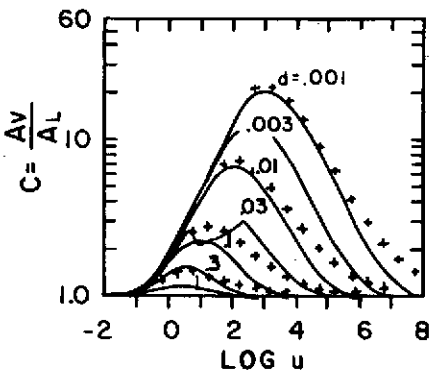

FIGURE 15

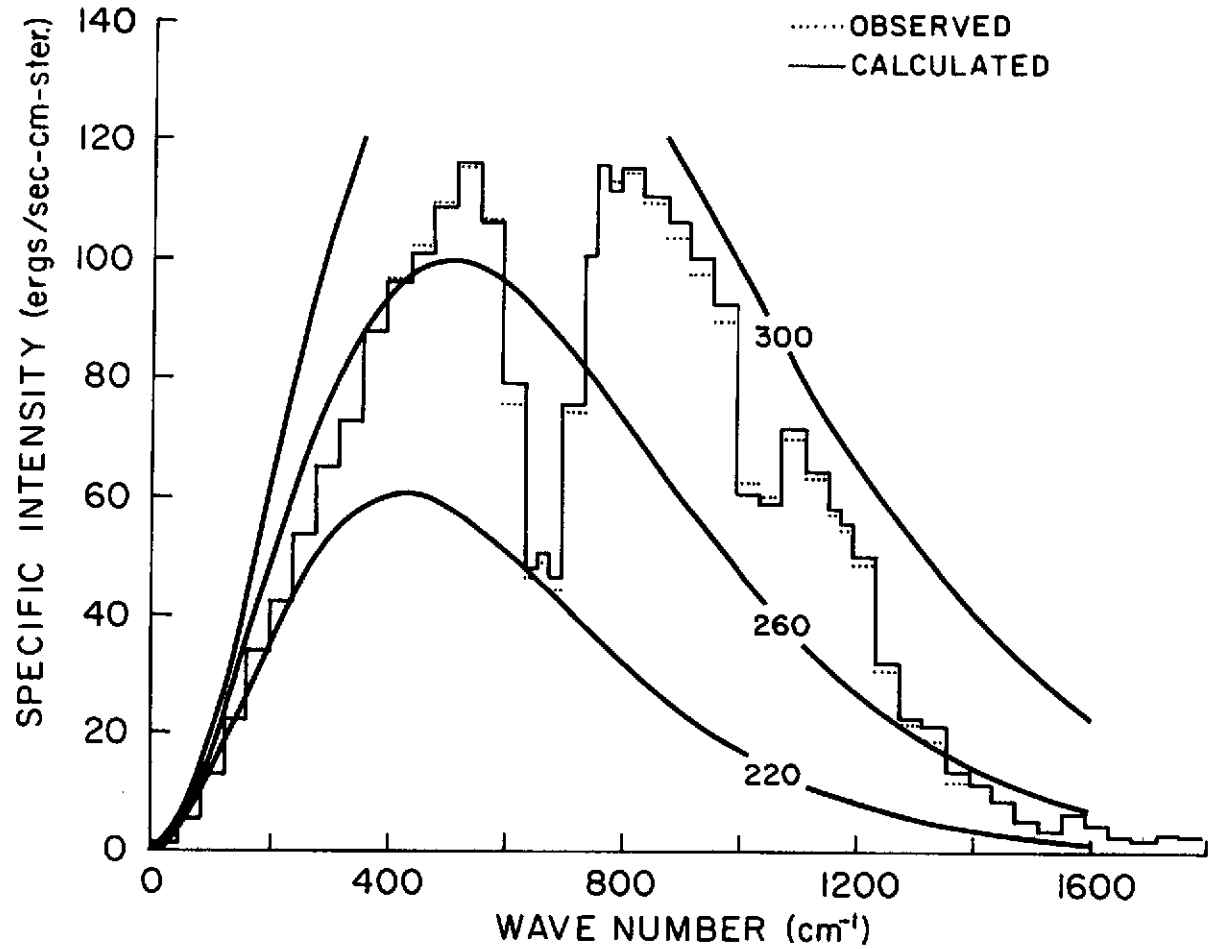
OBSERVED
CALCULATED
SPECIFIC INTENSITY (ergs/sec-cm-ster.)
140
120
100
80
60
40
20
0
0
400
800
1200
1600
WAVE NUMBER (cm⁻¹)
300
260
220

FIGURE 16

MOLECULAR ABSORPTION PARAMETERS IN ATMOSPHERIC MODELLING

Robert A. McClatchey
Air Force Cambridge Research Laboratories (AFSC)
Bedford, Massachusetts

Abstract

The report describes a compilation of the molecular spectroscopic parameters for a number of infrared-active molecules occurring naturally in the terrestrial atmosphere. The following molecules are included in this compilation: water vapor; carbon dioxide; ozone; nitrous oxide; carbon monoxide; methane; and oxygen. The spectral region covered extends from less than 1 μm to the far infrared, and data are presented on more than 100,000 spectral lines. The parameters included in the compilation for each line are: frequency, intensity, half-width, energy of the lower state of the transition, vibrational and rotational identifications of the upper and lower energy states, an isotopic identification, and a molecular identification. Using this data compilation, band model parameters are presented (ΣS_i and $\Sigma(S_i\alpha_i)^{1/2}$) for water vapor, carbon dioxide and ozone averaged over 20 wavenumber intervals between 10 and 2500 cm^{-1}. Using these parameters in a random model formulation, transmittance spectra are provided and compared with both degraded monochromatic calculations and laboratory data.

1. INTRODUCTION

The molecular data described and used in this discussion are part of an extensive compilation of molecular spectroscopic data for atmospheric molecules compiled by McClatchey, Benedict, et al, 1973.

About ten years ago a program was initiated to compile spectroscopic data on individual vibration-rotation lines of water vapor in the 2.7 μm region (Gates, et al, 1964). This work continued resulting in a publication on the 1.9 and 6.3 μm bands of water vapor (Benedict and Calfee, 1967). Other workers have published similar results on the 15 μm bands of CO_2 (Drayson and Young, 1967), the 9.6 μm bands of O_3 (Clough and Kneizys, 1965), the CO bands whose fundamental is near 5 μm (Kunde, 1967), the CH_4 bands near 3 and 7.5 μm (Kyle, 1968) and the unpublished rotational water data calculated by Benedict and Kaplan in 1959 (see Goody, 1964, p. 184).

About five years ago an effort was initiated at AFCRL to continue this work with the aim of providing a complete set of data for all vibration-rotation lines of all naturally occurring molecules of significance in the terrestrial atmosphere. With such data at hand, it would be possible to compute the transmittance appropriate for atmospheric paths by first computing the monochromatic transmittance many times in a finely spaced frequency grid and then degrading the results to any appropriate spectral resolution. Up to now the molecules shown in Table 1 have been included in this compilation.

All of these molecules except oxygen are minor constituents of the atmosphere, but nonetheless represent most of the absorption lines in the visible and infrared. Although there is some evidence for decreasing concentration with height of N_2O, CO, and CH_4, it is probably reasonable for most purposes to assume that all of these gases except H_2O and O_3 are uniformly mixed by volume in the atmosphere unless other specific information is available. Table 1 provides concentrations for these uniformly mixed gases. Water vapor and ozone are, of course, not uniformly mixed and an appropriate set of models useful in considering the radiation effects of these gases is provided by McClatchey, et al, 1972. The number of entries of each molecular species covered is also given in Table 1.

2. DESCRIPTION OF COMPILATION

In order to compute the transmittance due to a given spectral line in the atmosphere, it is necessary to describe the absorption coefficient as a function of frequency for each line. The four essential line parameters for each line included in Table 2 are the resonant frequency, $\nu_0(cm^{-1})$, the intensity per absorbing molecule, $S(cm^{-1}/molecule\ cm^{-2})$ the Lorentz line width parameter, $\alpha_0(cm^{-1}/atm)$, and the energy of the lower state, $E''(cm^{-1})$. The frequency, ν_0 , is independent of both temperature and pressure (except for possibly very small pressure effects of less than 0.01 cm^{-1} atm, which have been ignored here). The intensity, S, is pressure-independent, and, as discussed below, its temperature dependence can be calculated from E" and ν.

The line half-width at half maximum, α, is by definition proportional to the pressure, p, and its temperature dependence can be estimated as discussed below.

The precise line shape is a matter of some uncertainty, but in the derivation of line parameters from laboratory measurements, it is customary to start from the Lorentz shape (see Goody, 1964) given in Eq. (1).

$$k(\nu) = \frac{S\alpha}{\pi(\nu - \nu_0)^2 + \alpha^2} \tag{1}$$

$$S = \int k(\nu)\, d\nu$$

The validity of Eq. (1) to describe the true line shape is subject to two limitations. The first, which can be precisely estimated and corrected for by the use of the Voigt shape, occurs when $\alpha_0\, P/\alpha_D < 1.0$ where α_D is the doppler line width which varies with frequency, temperature and molecular mass as given in Eq. (2).

$$\alpha_D = \frac{\nu}{c}\left(\frac{2kT\ \ell n\ 2}{m}\right)^{1/2} = 4.298 \times 10^{-7}\ \nu(T/M)^{1/2} \tag{2}$$

where M = molecular weight and here k = Boltzmann's constant and m = mass of a molecule.

For atmospheric molecules and infrared frequencies, modifications of the Lorentz shape begin to be required at pressures below 10 to 100 mb.

The second limitation concerns possible inadequacies of the Lorentz shape, especially in the distant wings of a line ($|\nu - \nu_0| >> \alpha$) (see Winters et al, 1964, and Burch, et al, 1969) or when the long range intermolecular forces responsible for collision broadening are dipole-quadrupole, leading to an exponent 1.75 rather than 2.0 for $(\nu - \nu_0)$, (Varanasi, 1972). Throughout this compilation we assume the validity of the Lorentz exponent.

The line intensity is temperature dependent through the Boltzmann factor and the partition function as indicated in Eq. (3) (the induced emission term has intentionally been omitted here),

$$S(T) = \frac{S(T_s)Q_v(T_s)\,Q_r(T_s)}{Q_v(T)\,Q_r(T)} \exp + \left| \frac{1.439E''(T-T_s)}{T\,T_s} \right| \qquad (3)$$

where E" (in cm^{-1}) is the energy of the lower state of the transition and where Q_v and Q_r are the vibrational and rotational partition functions. The vibrational partition functions for the most abundant isotopes are given in Table 3. Partition functions for the other isotopes are similar. The temperature dependence of the rotational partition function is given by $(T/T_s)^j$ where j is also provided in Table 3 (T_s is taken to be 296°K).

It is also necessary to know the temperature variation of α. In the absence of specific indications discussed under each molecule, the equation $\alpha(T)/\alpha(T_s) = (T/T_s)^{-n}$, with n = 1/2, corresponding to the assumption of temperature-independent collision diameters, may be made. The validity of the assumption is more uncertain, the larger the dependence of the diameter on the particular rotation-vibration transition (that is, it is most unrealistic for H_2O and the low-J transitions of the other molecules). The theory of Tsao and Curnutte (1954) when applied to the determination of line width for H_2O lines gives a wide variation of n about the mean value of 0.62 (Benedict and Kaplan, 1959). Measurements made with a CO_2 laser (Ely and McCubbin, 1970) indicate a value of n = 1.0 for the P20 line of the 10.4 μm CO_2 band.

An examination of Eqs. (1) and (3) indicates that it is necessary to know the ν_0, $S(T_s)$, $\alpha(P_0,T_s)$ and E" value for each line in order to compute a spectrum. The data compilation described here contains these four quantities for each of the more than 100,000 lines between 1 μm and the far infrared belonging to the seven molecular species listed in Table 4.

In order to establish the "Criterion Intensity Minimum" values given in Table 4, an extreme atmospheric path was considered, assuming the gas concentrations specified in Table 1 and maximum concentrations over the path of 3×10^{24} molecules/cm^2 for water vapor and 1×10^{20} molecules/cm^2 for ozone. This extreme radiation path was the atmospheric path tangent to the earth's surface, and extending from space to space. Using this criterion, lines yielding less than 10 percent absorption at the line center would normally be omitted.

Although this absolute line intensity cutoff was established, it has not always been possible to achieve. In some cases it would have been unrealistic to push calculations to this limit when experimental confirmation fell far short. There are two specific areas in which this absolute cutoff has been violated: (1) In regions of very strong absorption, very weak lines above this absolute limit have been neglected; (2) Q-branch lines below this limit have occasionally been included where it is felt that the accumulation of many weak, closely spaced lines would still produce an appreciable absorption under some atmospheric circumstances. In some cases, (for example, CO_2), sufficient laboratory measurements and theoretical work were available so that this limit was exceeded throughout the infrared.

In the past, line intensities have been defined in various units, different for each molecular species. It was common to define water vapor concentration in precipitable cm, or g/cm^2, in the path in question. On the other hand, the amount of CO_2 and the other uniformly mixed gases in a path were often given in cm-atm of gas at STP. In order to unify the units and ultimately to lead to less confusion, we decided to use the more fundamental quantity, $molecules/cm^2$ as a measure of absorbing gas abundance along the path. The appropriate conversion factors are:

$$1\ (\text{cm-atm})_{STP} = 2.69 \times 10^{19}\ \text{molecules/cm}^2$$

$$1\ \text{g/cm}^2\ \text{of}\ H_2O = 3.34 \times 10^{22}\ \text{molecules/cm}^2$$

It was also decided, as indicated in Table 4, to define line (and band) intensities at 296°K, the normal room temperature at which most measurements are made. Intensities of all bands are based on the total number of molecules of a given species of all isotopes in their normal abundance, not on the number of the particular isotope responsible for a given band.

Half-widths of lines have been added where available. Details are discussed in the report by McClatchey, Benedict, et al (1973). In some cases, it is felt that insufficient data exist to warrant the inclusion of a variable half-width. In these cases, a mean, constant value has been inserted for each molecular species and values are given in Table 5.

In Table 6, I have provided some information concerning the accuracy of the data contained in the compilation. As can be seen, it is difficult to simply specify accuracy because it is different from molecule to molecule, from band to band, and is also a function of the line intensity, there being much more experimental confirmation available for strong lines than weak lines. The reader is referred to McClatchey, et al (1973) for a more complete discussion of accuracy.

3. TRANSMITTANCE MODELS

The compilation of molecular spectroscopic data pertinent to atmospheric absorption has had as its objective from the beginning the straight-forward calculation of atmospheric transmittance by line-by-line or degraded monochromatic techniques. In principle the availability of such a compilation removes the need for band models, Curtis-Godson approximations, etc. In practice, low resolution calculations (spectral resolution lower than about 1 or 2 cm^{-1}) performed by line-by-line techniques cannot be done in connection with the reduction of field measurements except on an occasional basis due to computer time and storage limitations. This is particularly a problem in connection with remote sensing

measurements because of the necessity to iterate the solution of the remotely sensed variable with a recomputation of the transmittance.

Thus, it is recommended here that this molecular data compilation be used to generate synthetic spectra for a range of conditions which can then serve as a basis of comparison of various models. It can further serve as a basic source of the fundamental parameters required in various band models. Although I have sounded pessimistic about the use of line-by-line calculations in routine analysis of field measurements, it should be recognized that very high spectral resolution measurements and laser measurements require this calculation technique and in those cases, there can be no band model shortcuts. Such high resolution measurements of atmospheric transmittance and emission are being made and lidar is being used as a remote probing tool. Figures 1 and 2 show measurements of both transmittance (solar spectra) and emission made from a balloon platform. Figure 2 shows a comparison of a calculated and measured emission spectrum in the 20 μm region. These measurements were used by A. Goldman, et al (1972) to infer the stratospheric distribution of water vapor. Figure 3 is a comparison of solar spectral measurements in the 15 μm region with calculations of the 15 μm CO_2 band. These kinds of calculations depend on the availability of the molecular data compilation. Another important application of these data is the comparison of high resolution synthetic spectra with measured spectra in order to detect additional trace gases (natural and pollutant). The previously shown Figure 2 is an indication of this in the case of HNO_3. Figures 4-6 show calculations of transmittance through a vertical path at various spectral resolutions. Figures 7-9 show sample high resolution spectra for horizontal paths and are samples of curves covering most of the infrared provided by McClatchey (1971), McClatchey and Selby (1972a and 1972b).

As indicated above, an important use of the molecular data compilation is the generation of band model parameters and the subsequent checking of band models against degraded monochromatic calculations. To this end I am providing here in Figures 10 to 13 curves of $\sum_i S_i$ and $\sum_i S_i \alpha_i$ for the spectral region from 10-2500 cm^{-1} where S_i is a line intensity in the units of cm^{-1}/molecule-cm^{-2} and α_i is the half-width at half maximum in units of cm^{-1}/atmosphere. Curves are provided separately for the water vapor, CO_2, and ozone data included on the data tape. Sums have been computed for overlapping 20 wavenumber intervals so that results are provided every 5 cm^{-1}.

Various researchers have applied the Goody random model to the calculation of atmospheric transmittance with varying degrees of success. Rogers and Walshaw (1966) applied it to the 6.3 μm and rotational water vapor bands with apparent success. They felt less comfortable applying it to the 15 μm CO_2 band and they felt that its application to the 9.6 μm band of ozone presented "difficulties". Goldman and Kyle (1968), on the other hand, found that the statistical model agreed with line-by-line calculations for the 2.7 μm H_2O band and 9.6 μm O_3 band to a level exceeding the agreement between either one and experimental data. Following the example of Goldman and Kyle, we have used our data compilation to generate appropriate band model parameters for water vapor, CO_2 and ozone summed over 5 cm^{-1} increments and spaced 1 cm^{-1} apart. Figures 14 though 16 show the results of using these parameters in a Goody random model formulation and then comparing these calculations with the line-by-line technique. The results are also compared with experimental data for the 6.3 μm water vapor band, the 15 μm CO_2 band and the 9.6 μm ozone band. Table 7 summarizes the results of calculations made for each of these band complexes for a number of different conditions.

4. CONTINUOUS ABSORPTION BY ATMOSPHERIC GASES

Although notpart of the data tape of primary concern in this report, a few words should be said about the relatively continuous regions of absorption of particular interest in the atmospheric "windows" near 2500 cm^{-1} (4 μm), from approximately 1250 cm^{-1} to 700 cm^{-1} (8 μm - 14 μm), and near 450 cm^{-1} (22 μm). In other spectral regions the contribution by nearby absorption lines is much greater than that by the continuum absorption, so that for practical purposes the continuum effect can be neglected, although it may be greater than in the windows.

This continuous absorption is caused by one or more of the following processes: (1) extreme wings of strong collision-broadened absorption lines centered more than 10-20 cm^{-1} away; (2) pressure-induced absorption resulting from transitions that are forbidden for unperturbed molecules; and (3) the possible existence of the water dimer ($H_2O;H_2O$) in the case of the 8 to 14 μm region.

The absorption coefficient due to continuum absorption can be expressed as

$$k = C_s P + C_b P_b \tag{4}$$

where C_s is the self-broadened coefficient and C_b is the foreign gas broadening coefficient, P is the total pressure and P_b is the foreign gas pressure.

Figure 17 gives the spectral dependence of C_s for water vapor absorption in the 8 to 14 μm region for three temperatures (Burch, 1970). The C_b value has been most reliably measured by McCoy et al, 1969, and is found for nitrogen to be $C_b = 0.005C_s$ at room temperature.

Figure 16 gives the spectral dependence of C_s for the water vapor absorption in the region near 4 μm for four different temperatures (Burch et al, 1971a). Note that the T = 296°K curve is an extrapolation based on the measurements at higher temperature. These same workers found the ratio C_b/C_s for nitrogen broadening to be 0.12 ± 0.03.

Figure 19 gives the spectral dependence of the absorption coefficient due to the pressure-induced nitrogen absorption centered near 2330 cm^{-1} (Burch et al, 1971a). Measurements have also been made by Shapiro and Gush, 1966, and Farmer and Houghton, 1966. Since the foreign gas broadening in this case results from a gas (oxygen) having a constant mixing ratio in the atmosphere, Eq. (4) reduces to

$$K = \text{Const.} \times P \tag{5}$$

Since the nitrogen abundance in the atmosphere is also directly proportional to P, the absorption depends on P^2 and Figure 19 has as ordinate the absorption expressed in the units, $atm^{-2}\ Km^{-1}$.

Since line wings as given by the Lorentz shape, Eq. (1), have been found to be in error in the extreme wings, an appropriate rule to follow for the truncation of line wings and the introduction of continuum absorption coefficients in accordance with Figures 17 through 19 is difficult to state. It is recommended that the user familiarize himself with this problem (see, for example, Burch et al, 1969) and in any case the use of the Lorentz shape beyond 20 or 30 wavenumbers of line centers is inappropriate. A suggested line shape modification for CO_2 lines is given in Table 8 taken from Burch (1970). Recent laboratory experimental work by Long, et al (1973) and confirmed by Burch (1972) indicates a

super-Lorentz nature of water line wings in the 6 μm H_2O band. Monochromatic (laser) errors of about a factor of two in the absorption coefficient would be made if the Lorentz shape were assumed to extend 10 cm^{-1} from the center of a strong line.

REFERENCES

1. Benedict, W. S. and L. D. Kaplan, 1959: J. Chem. Phys., 30, 2, 388.

2. Benedict, W. S. and R. F. Calfee, 1967: Line parameters for the 1.9 and 6.3 micron water vapor bands. ESSA Professional Paper 2 (June 1967), U. S. Government Printing Office.

3. Bouanick, J. and C. Haeusler, 1972: J. Q. S. R. T., 12, 695.

4. Burch, C. B., D. A. Gryvnak, R. R. Patty, and C. F. Bartky, 1969: J. Opt. Soc. Am., 59, 3, 267.

5. Burch, D. E. and D. A. Gryvnak, 1969: Appl. Opt., 8, 1489.

6. Burch, D. E., 1970: Semi-Annual Technical Report: Investigation of the absorption of infrared radiation by atmospheric gases. Aeronutronic Report U-4784 (31 Jan 1970).

7. Burch, D. E., D. A. Gryvnak, and J. D. Pembrook, 1971a: Philco-Ford Corporation, Aeronutronic Division, Contract No. F-19628-69-C-0263, U-4897, ASTIA AD882876.

8. Burch, D. 1972: Private Communication.

9. Calfee, R. F. and W. S. Benedict, 1966: Carbon dioxide spectral line positions and intensities calculation for the 2.05 and 2.7 micron regions. NBS Technical Note 332 (15 March 1966), U. S. Government Printing Office.

10. Clough, S. A. and F. X. Kneizys, 1965: Ozone absorption in the 9.0 micron region. AFCRL-65-862.

11. Drayson, S. R. and C. Young, 1967: The frequencies and intensities of carbon dioxide absorption lines between 12 and 18 microns. Univ. of Michigan Technical Report 08183-1-T, Nov. 1967.

12. Ely, R. and T. K. McCubbin, 1970: Appl. Opt., 9, 5, 1230.

13. Farmer, C. B. and J. T. Houghton, 1966: Nature, 209, 1341 and 5030.

14. Gates, D. M., R. F. Calfee, D. W. Hanson, and W. W. Benedict, 1964: Line parameters and computed spectra for water vaport bands at 2.7 μm. NBS Monograph 71, Aug. 3, 1964, U. S. Government Printing Office.

15. Goldman, A. and T. G. Kyle, 1968: Appl. Opt., 7, 1167.

16. Goldman, A. D., G. Murcray, F. H. Murcray, W. J. Williams, and J. N. Brooks, 1972: Distribution of water vapor in the stratosphere as determined from balloon measurements of atmospheric emission spectra in the 24-29 μm region. AFCRL-72-0077, Feb. 1972.

17. Goody, R. M., 1964: Atmospheric Radiation I, Theoretical Basis. Clarendon Press.

18. Kunde, V. G., 1967: Tables of theoretical line positions and intensities for the $\Delta V = 1$, $\Delta V = 2$, and $\Delta V = 3$ vibration - rotation bands of $C^{12}O^{16}$, NASA TMX-63183.

19. Kyle, T. G., 1968: Line parameters of the infrared methane bands, AFCRL-68-0521, October 1968.

20. Lichtenstein, M., J. J. Gallagher, and S. A. Clough, 1971: J. Mol. Spec., 40, 10.

21. Long, R. K., F. S. Mills, and G. L. Trusty, 1973: Experimental absorption coefficients for eleven CO laser lines, RADC-TR-73-126, March 1973.

22. McClatchey, R. A., W. S. Benedict, S. A. Clough, D. E. Burch, R. F. Calfee, K. Fox, L. S. Rothman, and J. S. Garing, 1973: AFCRL atmospheric absorption line parameters compilation, AFCRL-TR-73-0096, January 1973.

23. McClatchey, R. A. and J. E. A. Selby, 1972: Atmospheric transmittance, 7-30 μm: Attenuation of CO_2 laser radiation, AFCRL-72-0611, 12 Oct 72.

24. McClatchey, R. A., R. W. Fenn, J. E. A. Selby, F. E. Volz, J. S. Garing, 1972: Optical properties of the atmosphere, Third Edition, AFCRL-72-0497, Aug 1972.

25. McClatchey, R. A., and J. E. A. Selby, 1972: Atmospheric attenuation of HF and DF laser radiation, AFCRL-72-0312, 23 May 1972.

26. McClatchey, R. A., 1971: Atmospheric attenuation of CO laser radiation, AFCRL-71-0370, 1 July 1971

27. McCoy, J. H., D. B. Rensch, and R. K. Long, 1969: Appl. Opt., 8, 1471.

28. Rodgers, C. D. and C. D. Walshaw, 1966: Q. J. R. M. S., 92, 67.

29. Shapiro, M. M., and H. P. Gush, 1966: Canad. J. Phys., 44, 949.

30. Toth, R. A., 1971a: J. Mol. Spectry., 40, 588.

31. Toth, R. A., 1971b: J. Mol. Spectry., 40, 605.

32. Varanasi, P., 1971: J. Q. S. R. T., 11, 1711.

33. Varanasi, P., and G. D. T. Tejwani, 1972: J. Q. S. R. T., 12, 849.

34. Winters, B. H., S. Silverman, and W. S. Benedict, 1964: J. Q. S. R. T., 4, 527.

35. Yamamoto, G., M. Tanaka, and T. Aoki, 1969: J. Q. R. S. T., 9, 371.

TABLE AND FIGURE CAPTIONS

Table I

MOLECULES INCLUDED IN COMPILATION

Molecule	Abundance (ppm)	No. Entries
H_2O	Variable (3×10^{24} molecules/cm^2)	38, 145
CO_2	330	32, 839
O_3	Variable (1×10^{20} molecules/cm^2)	19, 328
N_2O	0. 28	14, 969
CO	0. 075	354
CH_4	1. 6	1, 741
O_2	2.1×10^5	490

Table 2

PARAMETERS INCLUDED IN COMPILATION

ν	Line Frequency
S	Line Intensity
α	Line Half-Width
E''	Energy of the Lower State
Q(v)	Quantum Numbers of Upper and Lower State
ISOT	Isotopic Identification
MOL	Molecular Identification

TABLE 3

Vibrational Partition Functions

Molecule	j	Temperature	175	200	225	250	275	296	325
H_2O	1.5		1.000	1.000	1.000	1.000	1.000	1.000	1.001
CO_2	1.0		1.0095	1.0192	1.0327	1.0502	1.0719	1.0931	1.1269
O_3	1.5		1.004	1.007	1.013	1.022	1.033	1.046	1.066
N_2O	1.0		1.017	1.030	1.048	1.072	1.100	1.127	1.170
CO	1.0		1.000	1.000	1.000	1.000	1.000	1.000	1.000
CH_4	1.5		1.000	1.000	1.001	1.002	1.004	1.007	1.011
O_2	1.0		1.000	1.000	1.000	1.000	1.000	1.000	1.001

TABLE 4

Intensity Criteria for Lines Included in Compilation

Molecule	Identification No.	Criterion Intensity* Minimum at T=296K	Existing Intensity Minimum at T=296K
H_2O	1	3×10^{-27}	3×10^{-27}
CO_2	2	2.2×10^{-26}	3.7×10^{-27}
O_3	3	3.5×10^{-24}	3.5×10^{-24}
N_2O	4	3.0×10^{-23}	4.0×10^{-23}
CO	5	8.3×10^{-23}	1.9×10^{-23}
CH_4	6	3.3×10^{-24}	3.3×10^{-24}
O_2	7	3.7×10^{-30}	3.7×10^{-30}

*Units are $cm^{-1}/(molecule\text{-}cm^{-2})$

TABLE 5

Mean Half-width Values

Molecule	Half-width (cm^{-1}/atm)	References
CO_2	0.07	Yamamoto et al (1969)
O_3	0.11	Lichtenstein et al (1971)
N_2O	0.08	Toth (1971)
CO	0.06	Bouanich and Haeusler (1972)
CH_4	0.055	Varanasi (1971) (see Section 6.3)
O_2	0.060	Burch and Gryvnak (1969)

TABLE 6

ACCURACY OF DATA

	ν (cm^{-1})	S	α
H_2O	$\pm$ 0.00001-0.05	1-10% Rotat. 10%-X2 others	$\pm$ 10%→X3
CO_2	$\pm$ 0.01	$\pm$ 5%	$\pm$ 10%
O_3	$\pm$ 0.01→1.0	$\pm$ 10%	Constant Value
N_2O	$\pm$ 0.01	$\pm$ 5%	Constant Value
CO	$\pm$ 0.001→0.01	$\pm$ 2%→$\pm$ 10%	$\pm$ 10%
CH_4	$\pm$ 0.01	$\pm$ 20%	Constant Value
O_2	$\pm$ 0.01	$\pm$ 10%	Constant Value

TABLE 7

COMPARISON OF INTEGRATED ABSORPTION RESULTS

H_2O

P(mb)	W(mol./cm^2)	W(LBL)	W_5(RANDOM)	W_{20}(RANDOM)
1079.64	3.41×10^{20}	320	273	339
800.00	2.0×10^{22}	665	592	673
400.00	8.0×10^{20}	321	275	334
139.95	1.50×10^{20}	112	102	121

CO_2

P(mb)	W(mol./cm^2)	W(LBL)	W_5(RANDOM)
1024	2.60×10^{21}	164	164
500	7.00×10^{21}	179	178
100	1.40×10^{20}	55.8	60.0
100 (T=250K)	1.40×10^{20}	47.4	51.0
10	1.40×10^{19}	8.45	9.77

O_3

P(mb)	W(mol./cm^2)	W(LBL)	W_5(RANDOM)
399.87	1.83×10^{19}	70.3	70.5
66.65	7.53×10^{19}	91.3	92.4
66.65	1.722×10^{19}	55.2	59.7
19.96	2.69×10^{19}	50.8	53.4
19.96	1.21×10^{19}	35.9	38.2

TABLE 8

MODIFICATION FACTOR FOR ATMOSPHERIC CO_2 LINES

$\lvert\nu-\nu_0\rvert$ cm^{-1}	χ
0	1.00
0.5	1.00
0.6	0.96
0.7	0.89
0.8	0.82
0.9	0.77
1.0	0.70
1.2	0.60
1.5	0.50
2.0	0.41
2.5	0.34
3.0	0.31
5.0	0.29
8.0	0.23
10.0	0.19

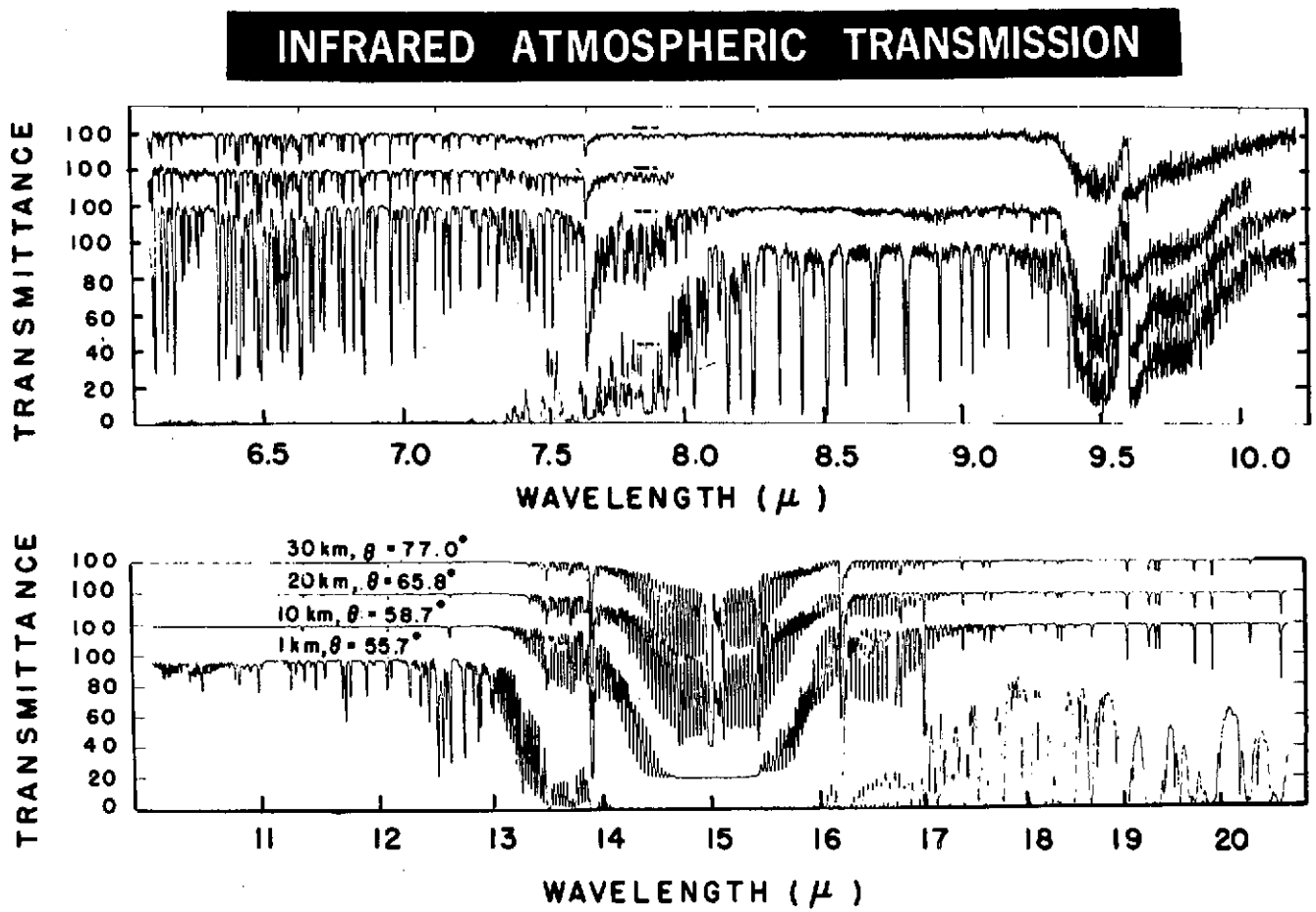
INFRARED ATMOSPHERIC TRANSMISSION
TRANSMITTANCE
100
100
100
100
80
60
40
20
0
6.5
7.0
7.5
8.0
8.5
9.0
9.5
10.0
WAVELENGTH (μ)
TRANSMITTANCE
30 km, θ = 77.0°
20 km, θ = 65.8°
10 km, θ = 58.7°
1 km, θ = 55.7°
100
100
100
100
80
60
40
20
0
11
12
13
14
15
16
17
18
19
20
WAVELENGTH (μ)

FIGURE 1

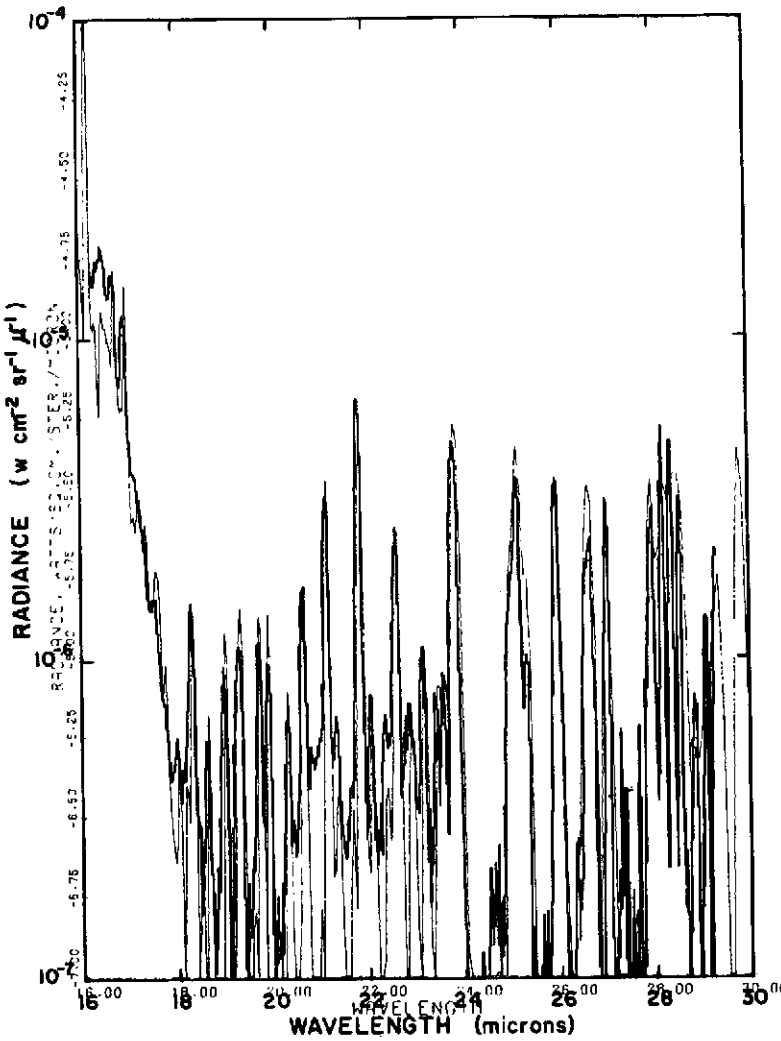

Radiance vs Wavelength at 70.2 kft and 0607 MST.

FIGURE 2

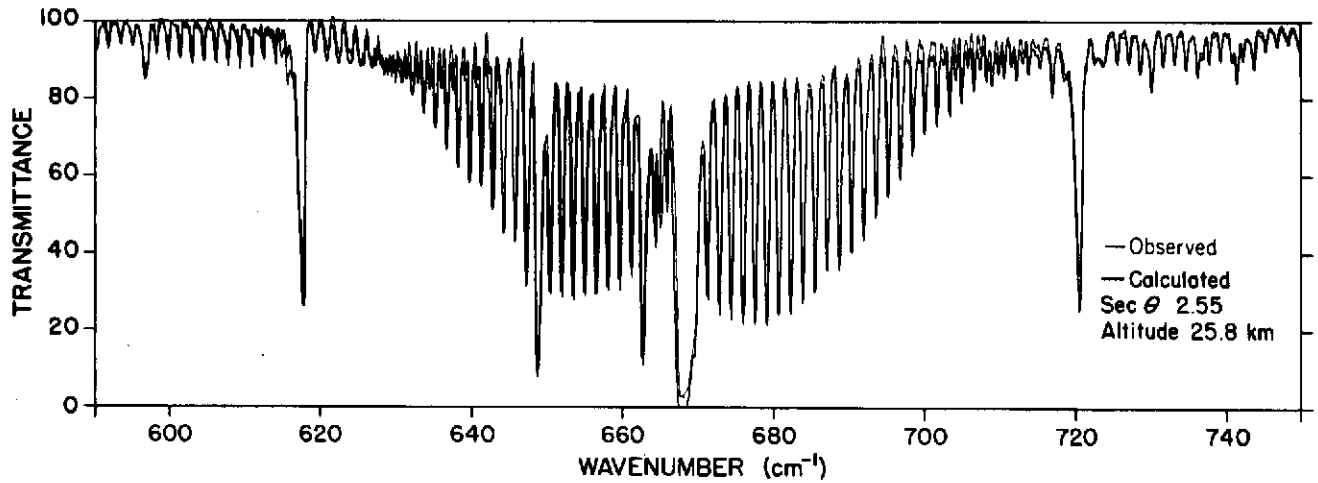
100
80
60
40
20
0
TRANSMITTANCE
600
620
640
660
680
700
720
740
WAVENUMBER (cm⁻¹)
—Observed
—Calculated
Sec θ 2.55
Altitude 25.8 km

FIGURE 3

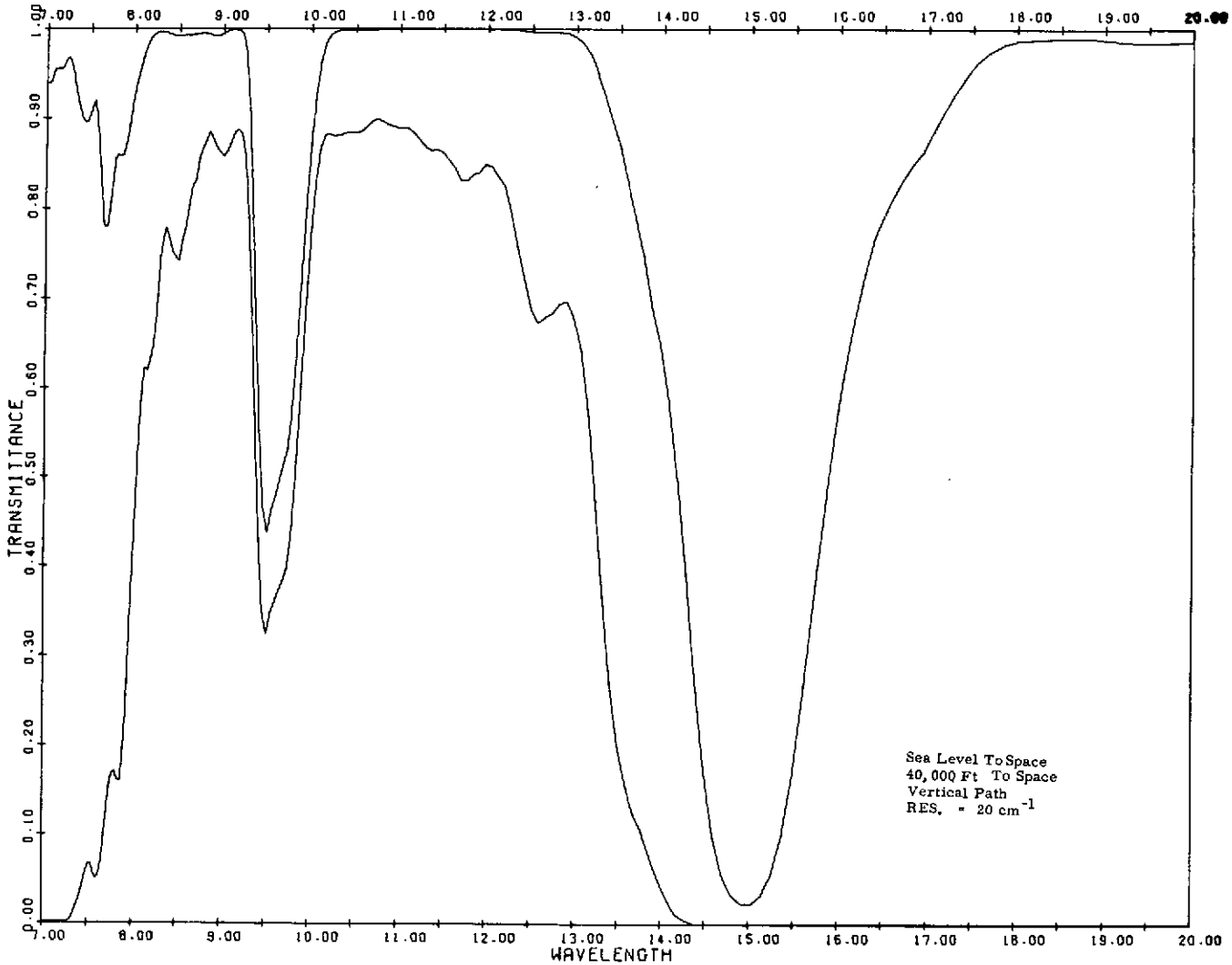
TRANSMITTANCE
WAVELENGTH
7.00
8.00
9.00
10.00
11.00
12.00
13.00
14.00
15.00
16.00
17.00
18.00
19.00
20.00
0.00
0.10
0.20
0.30
0.40
0.50
0.60
0.70
0.80
0.90
1.00
Sea Level To Space
40,000 Ft To Space
Vertical Path
RES. = 20 cm-1

FIGURE 4

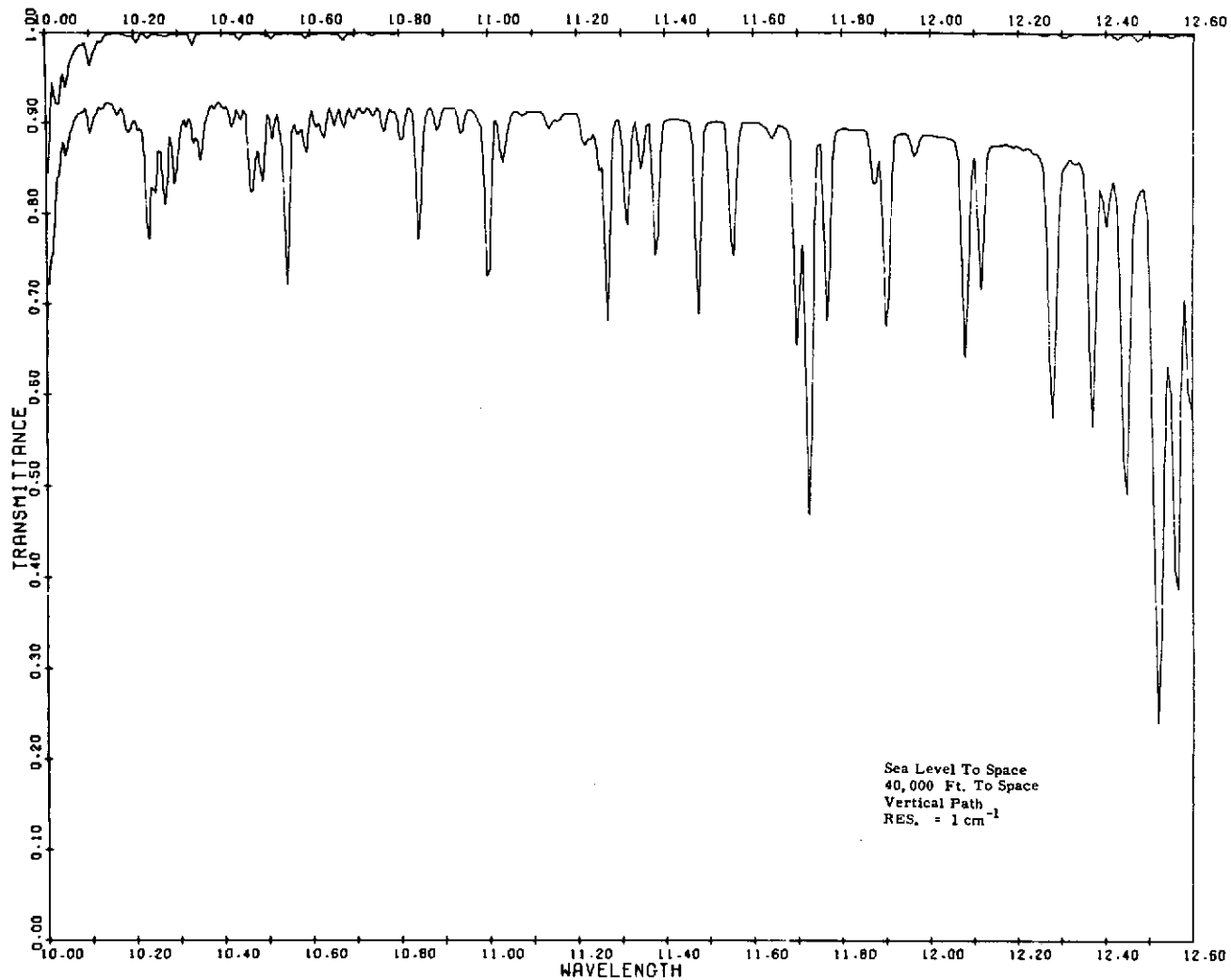
10.00
10.20
10.40
10.60
10.80
11.00
11.20
11.40
11.60
11.80
12.00
12.20
12.40
12.60
1.00
0.90
0.80
0.70
0.60
0.50
0.40
0.30
0.20
0.10
0.00
TRANSMITTANCE
WAVELENGTH
Sea Level To Space
40,000 Ft. To Space
Vertical Path
RES. = 1 cm-1

FIGURE 5

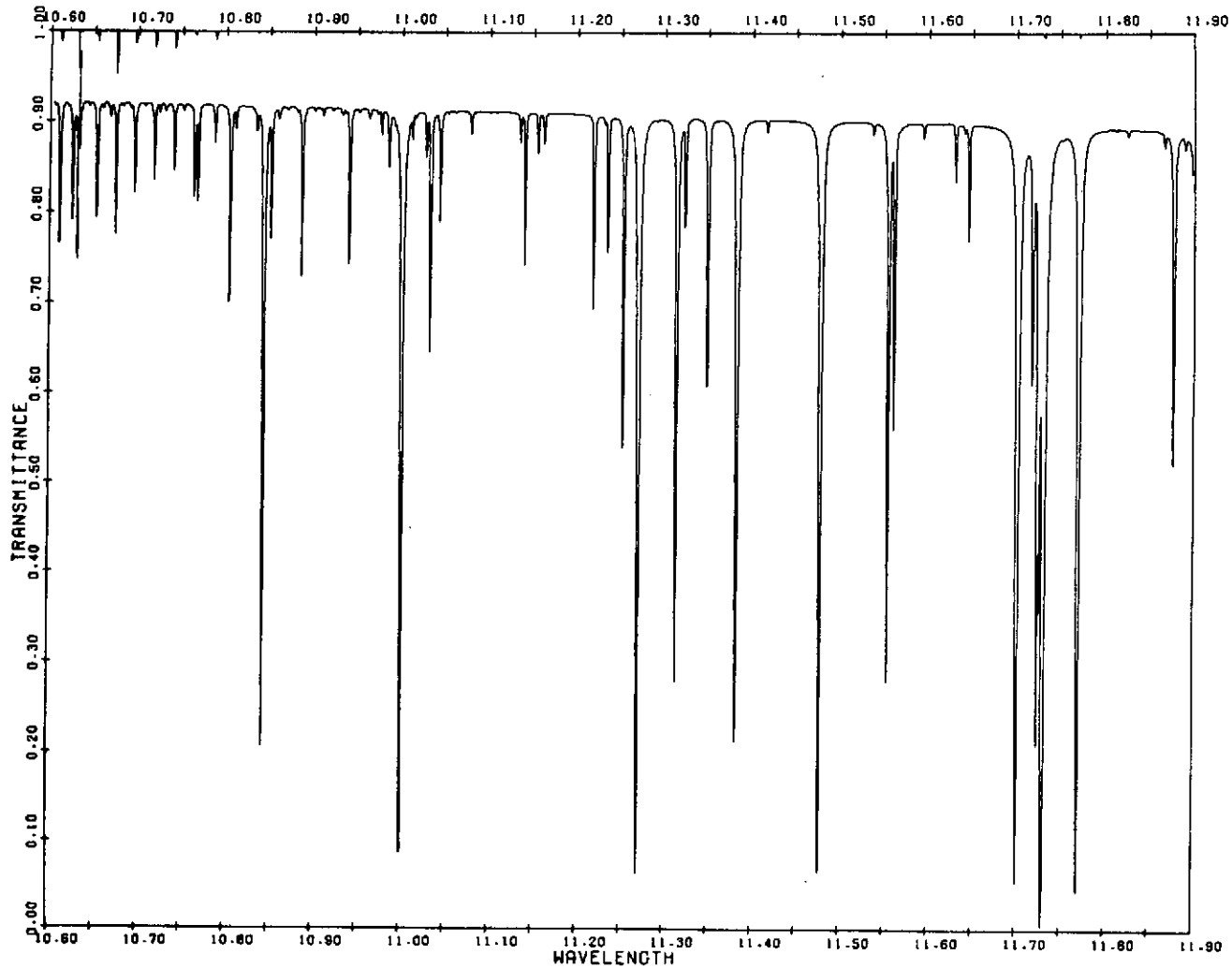
10.60
10.70
10.80
10.90
11.00
11.10
11.20
11.30
11.40
11.50
11.60
11.70
11.80
11.90
1.00
0.90
0.80
0.70
0.60
0.50
0.40
0.30
0.20
0.10
0.00
TRANSMITTANCE
WAVELENGTH

FIGURE 6

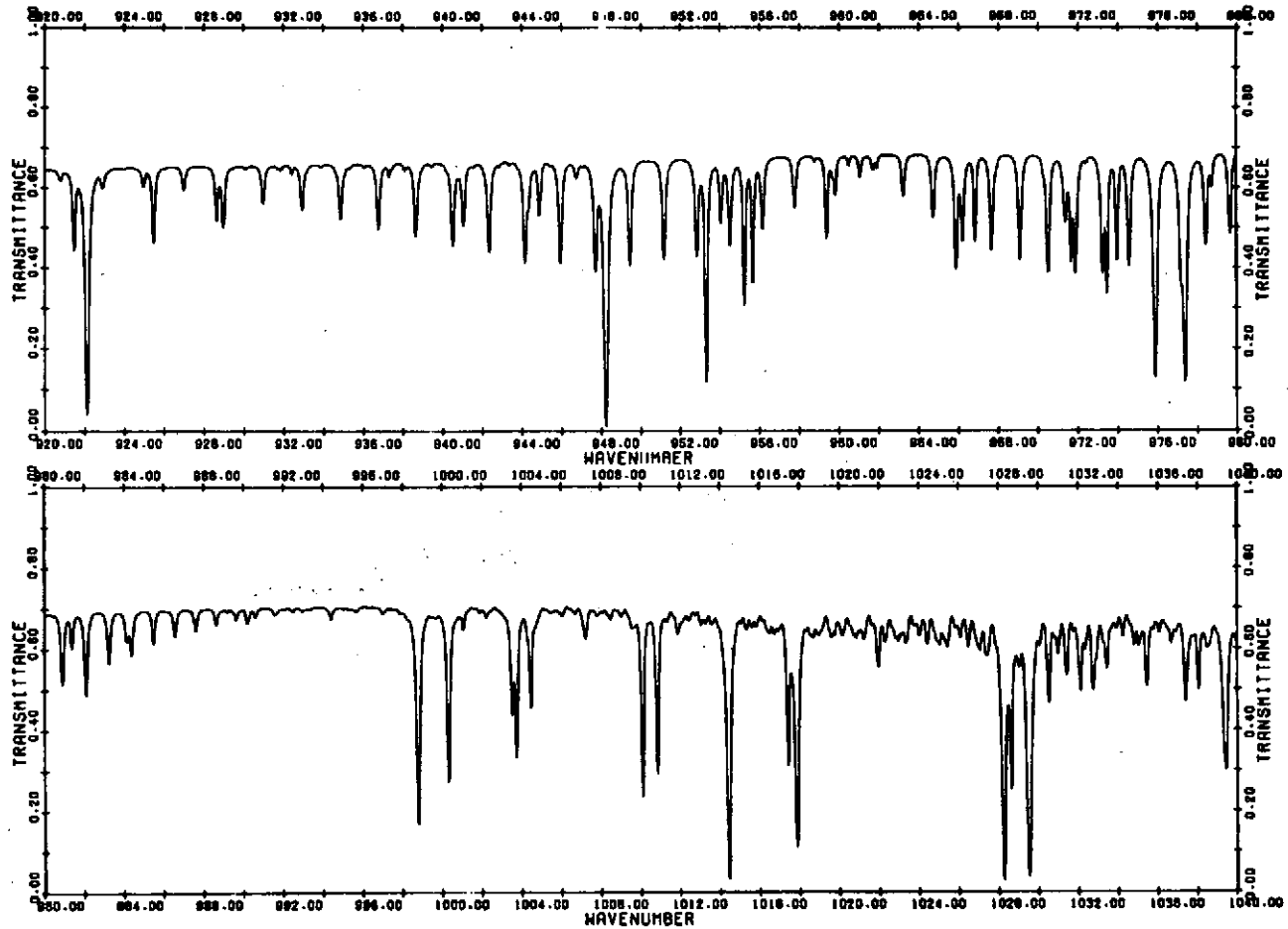

Atmospheric Transmittance due to Molecular Absorption Through a 10-km Horizontal Path at Sea Level

FIGURE 7

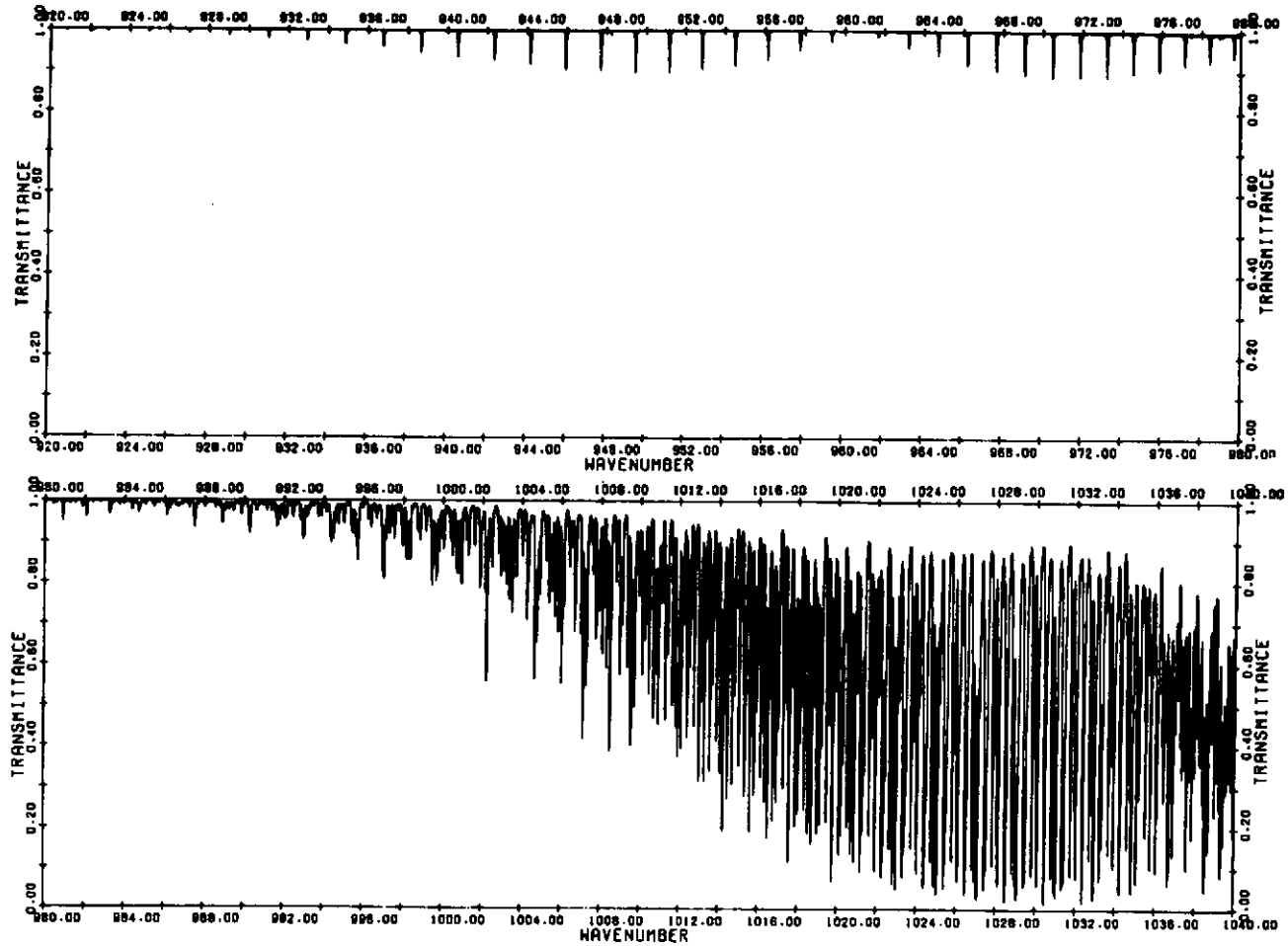

Atmospheric Transmittance due to Molecular Absorption Through a 10-km Horizontal Path at an Elevation of 12 km

FIGURE 8

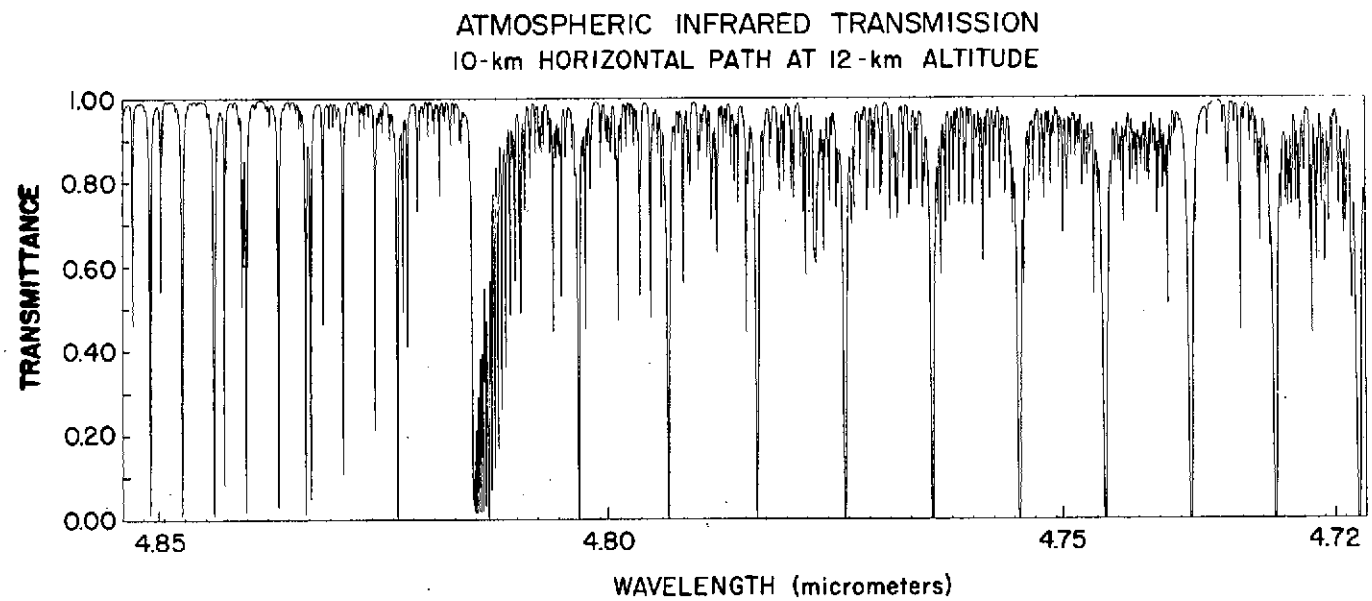
ATMOSPHERIC INFRARED TRANSMISSION
10-km HORIZONTAL PATH AT 12-km ALTITUDE
TRANSMITTANCE
1.00
0.80
0.60
0.40
0.20
0.00
4.85
4.80
4.75
4.72
WAVELENGTH (micrometers)

FIGURE 9

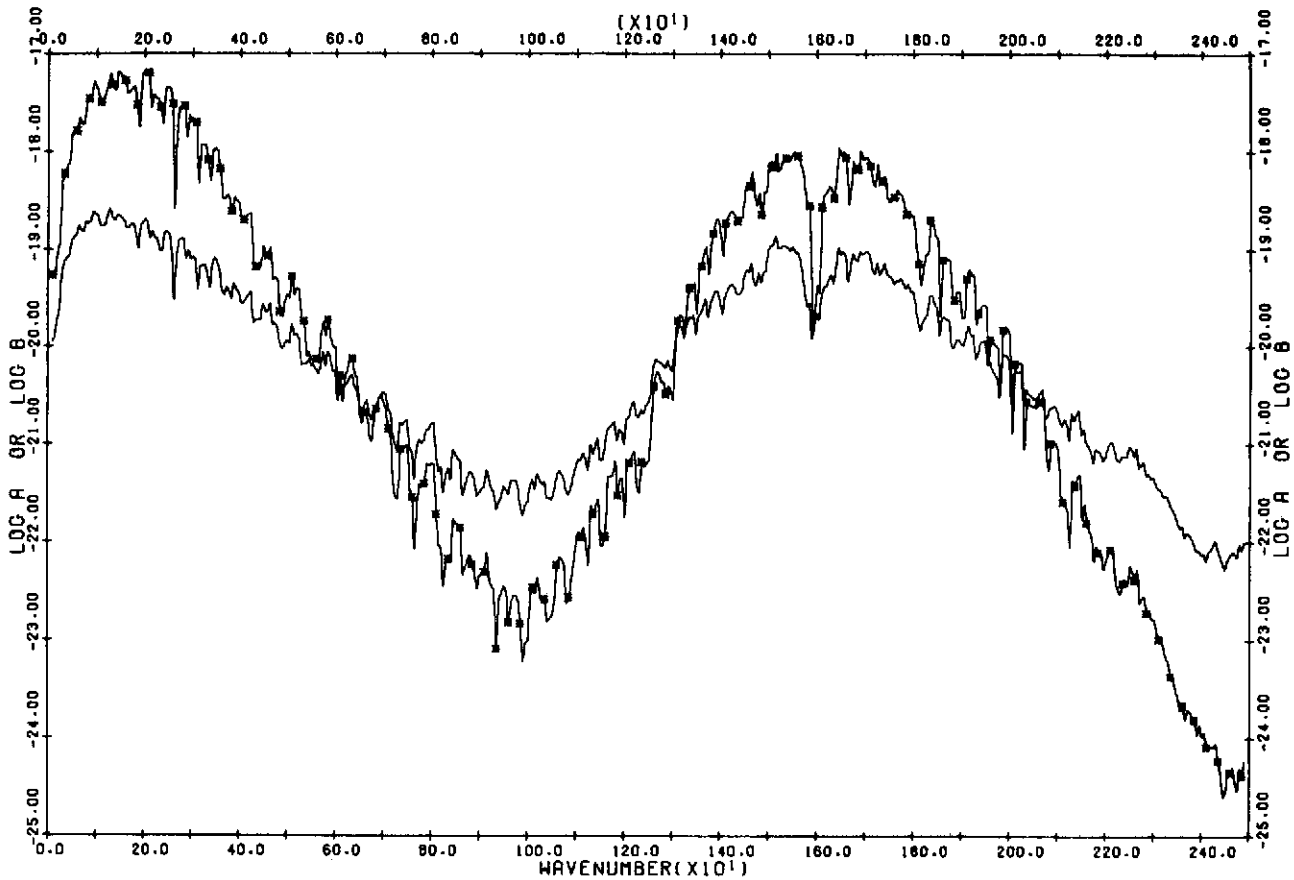
(X10¹)
0.0
20.0
40.0
60.0
80.0
100.0
120.0
140.0
160.0
180.0
200.0
220.0
240.0
-17.00
-18.00
-19.00
-20.00
-21.00
-22.00
-23.00
-24.00
-25.00
LOG A OR LOG B
WAVENUMBER(X10¹)

FIGURE 10

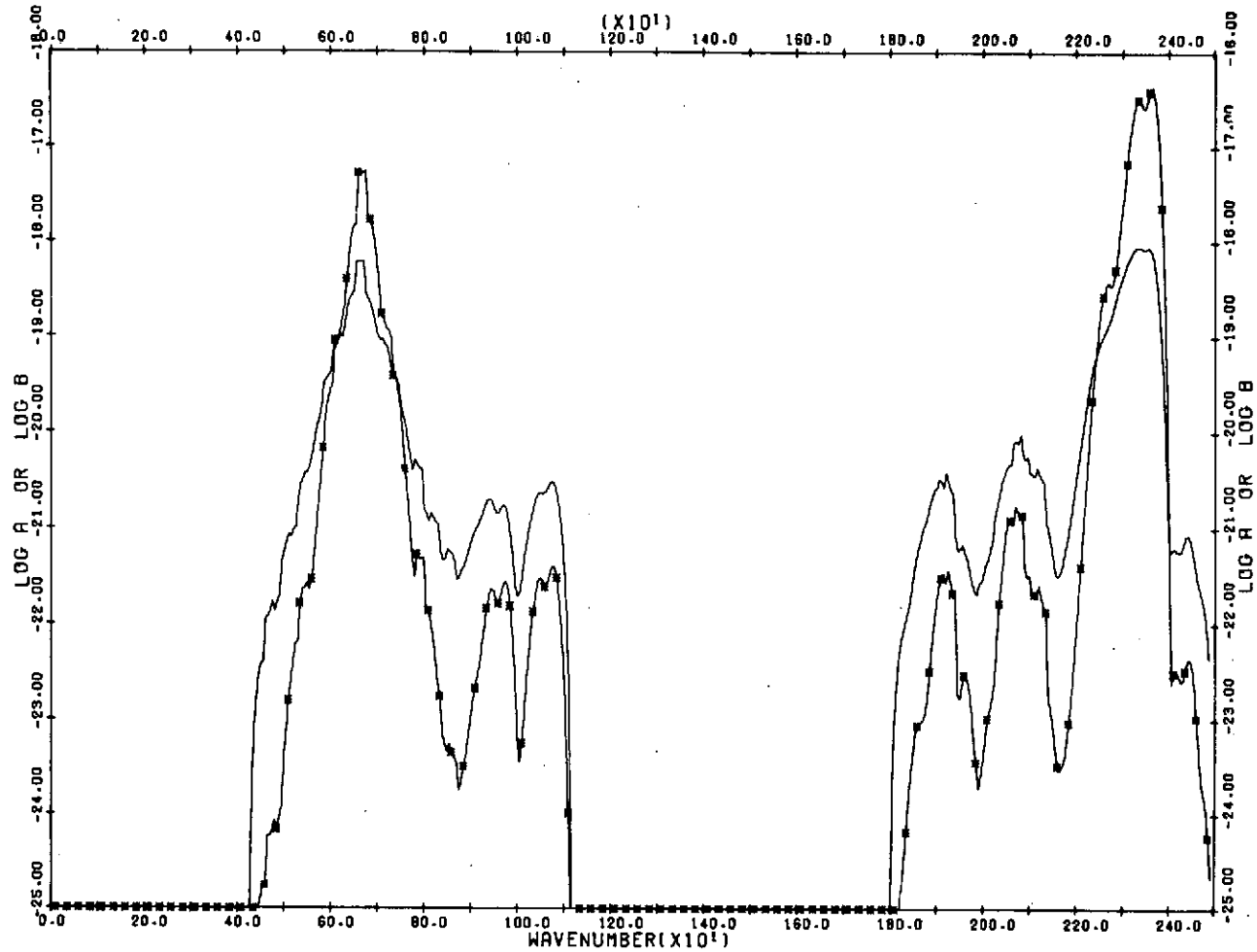
(X10¹)
0.0
20.0
40.0
60.0
80.0
100.0
120.0
140.0
160.0
180.0
200.0
220.0
240.0
-16.00
-17.00
-18.00
-19.00
-20.00
-21.00
-22.00
-23.00
-24.00
-25.00
LOG A OR LOG B
WAVENUMBER(X10¹)

FIGURE 11

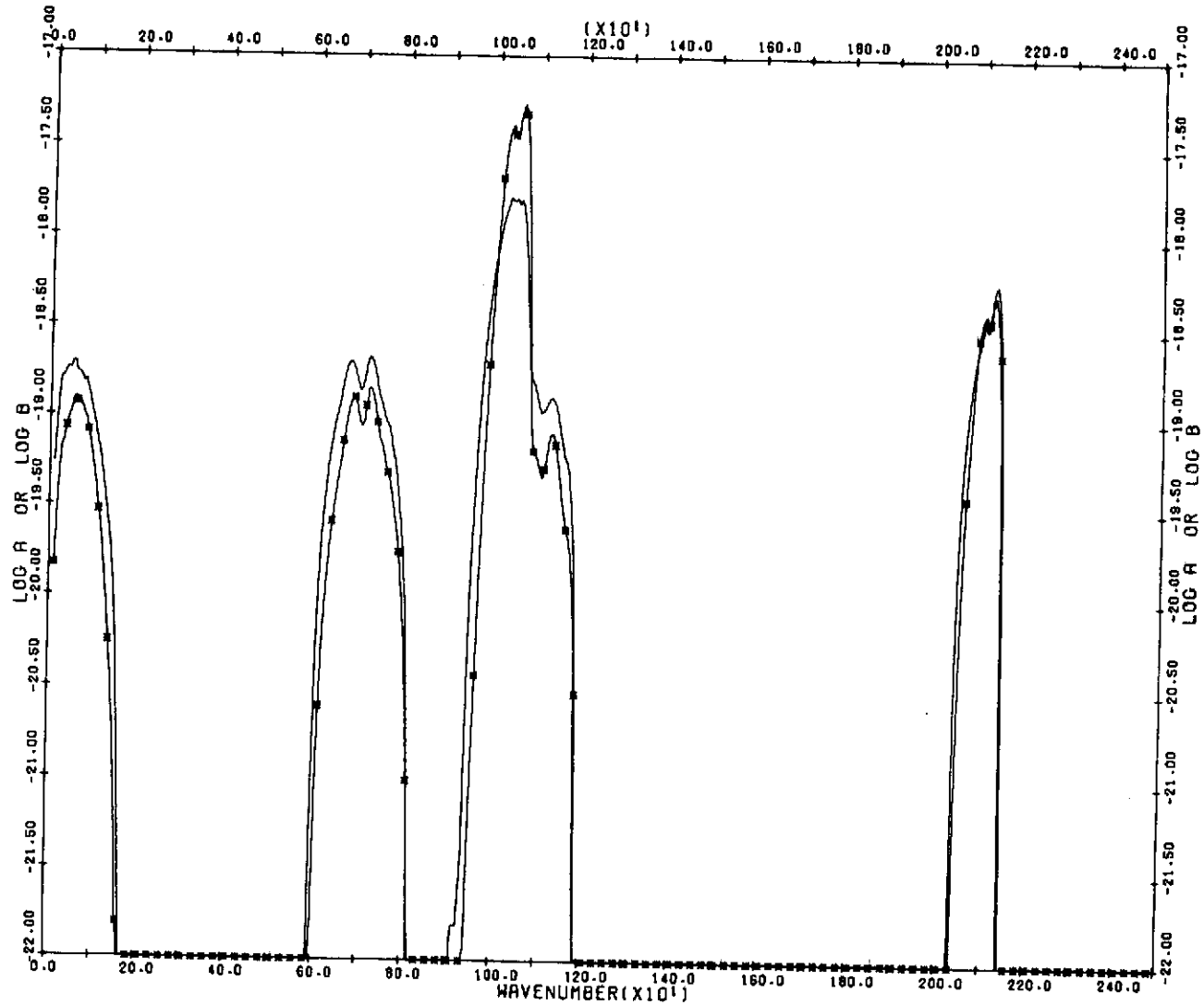
(X10¹)
LOG A OR LOG B
WAVENUMBER(X10¹)
-17.00
-17.50
-18.00
-18.50
-19.00
-19.50
-20.00
-20.50
-21.00
-21.50
-22.00
0.0
20.0
40.0
60.0
80.0
100.0
120.0
140.0
160.0
180.0
200.0
220.0
240.0

FIGURE 12

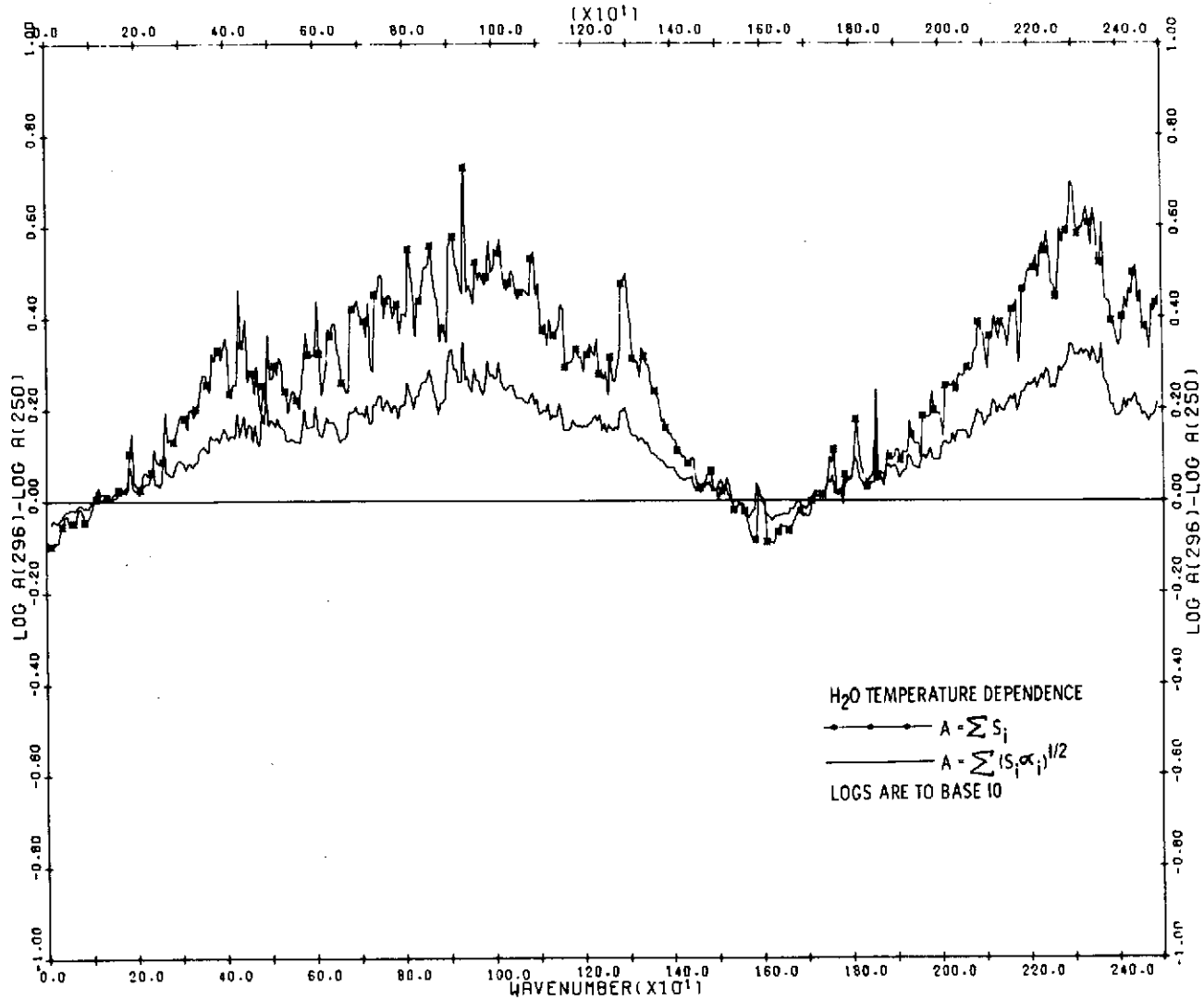

AFCRL PHOTO 103-446

FIGURE 13 a

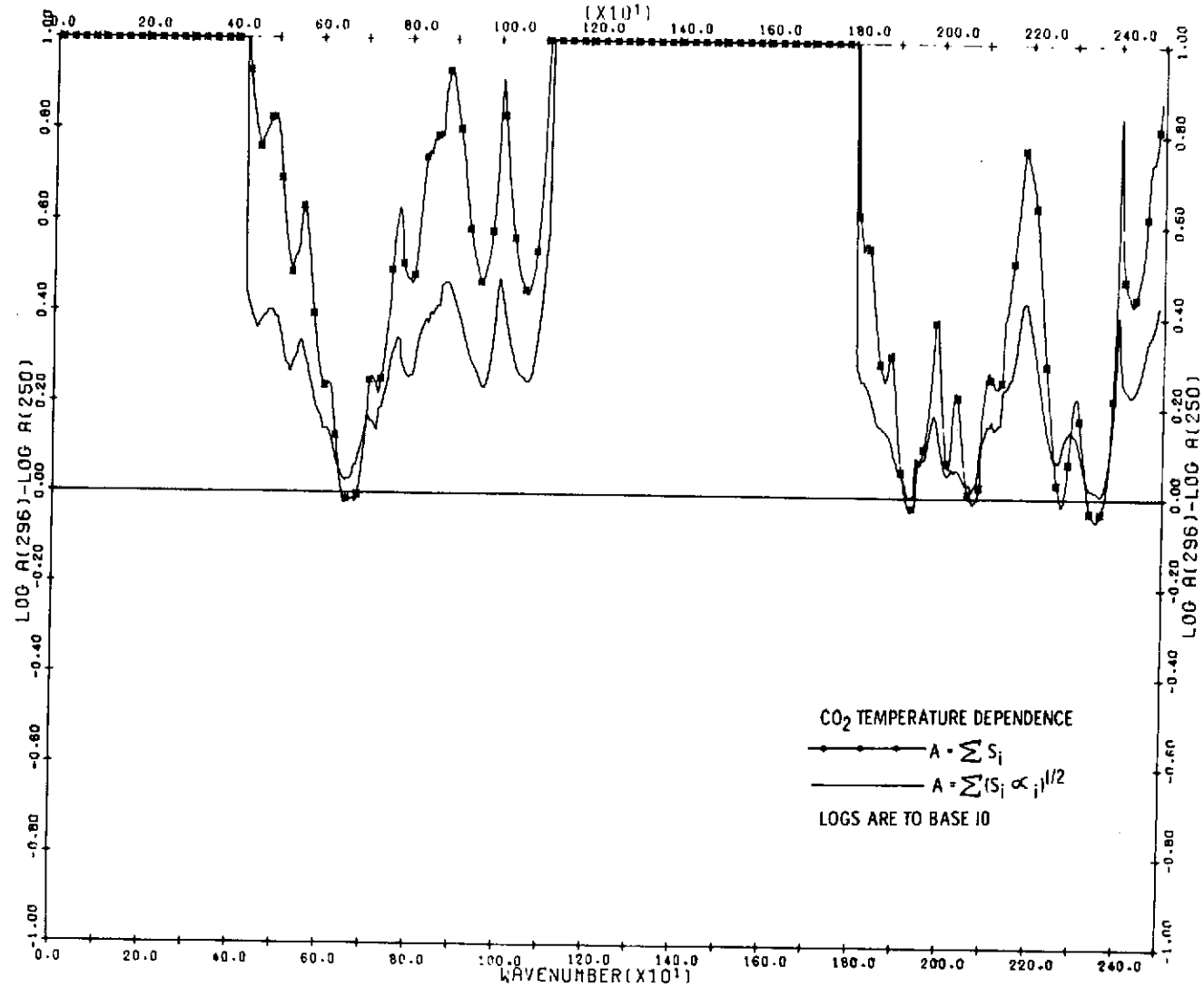

AFCRL PHOTO 103-444

FIGURE 13 b

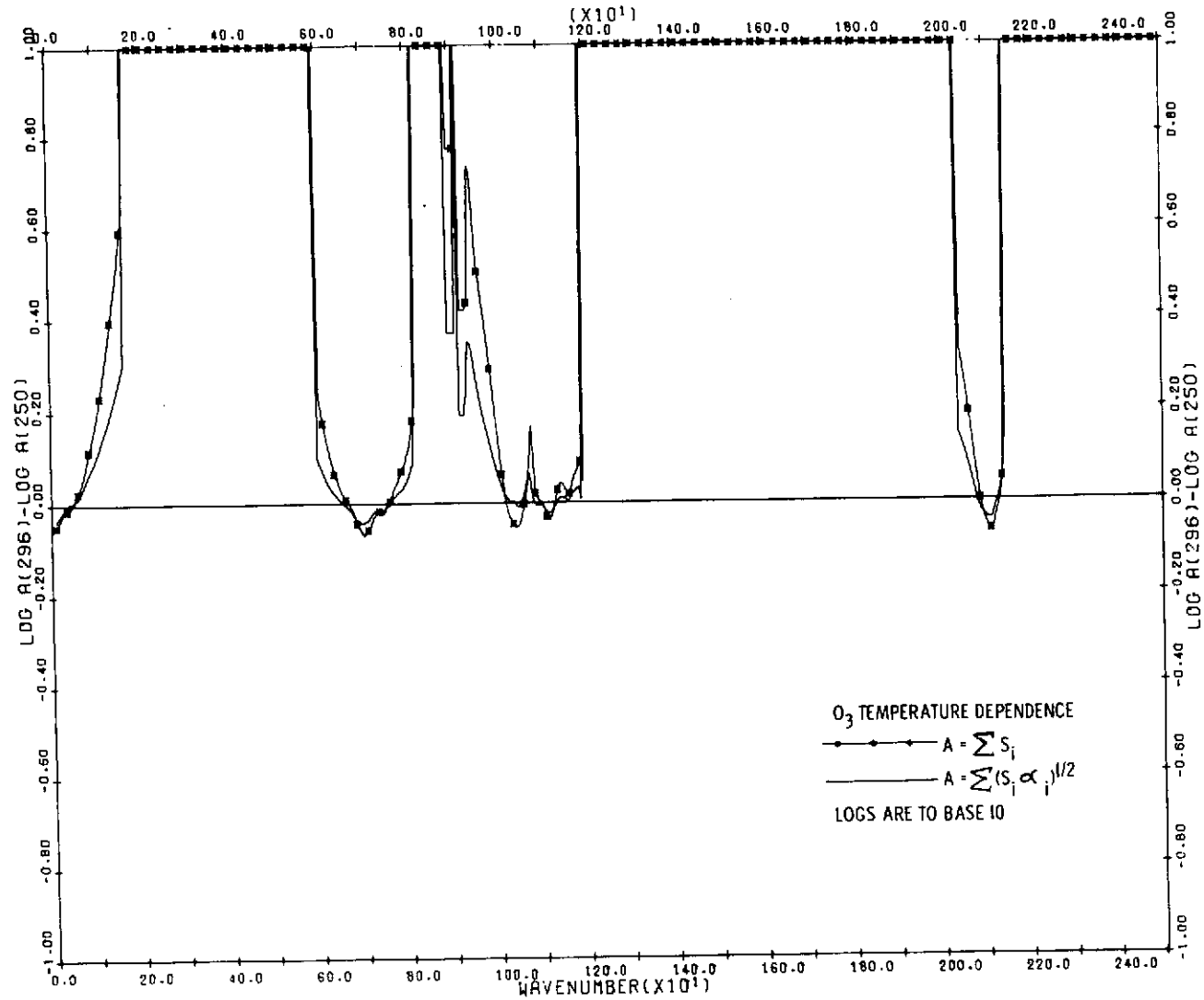

AFCRL PHOTO 103-442

FIGURE 13 c

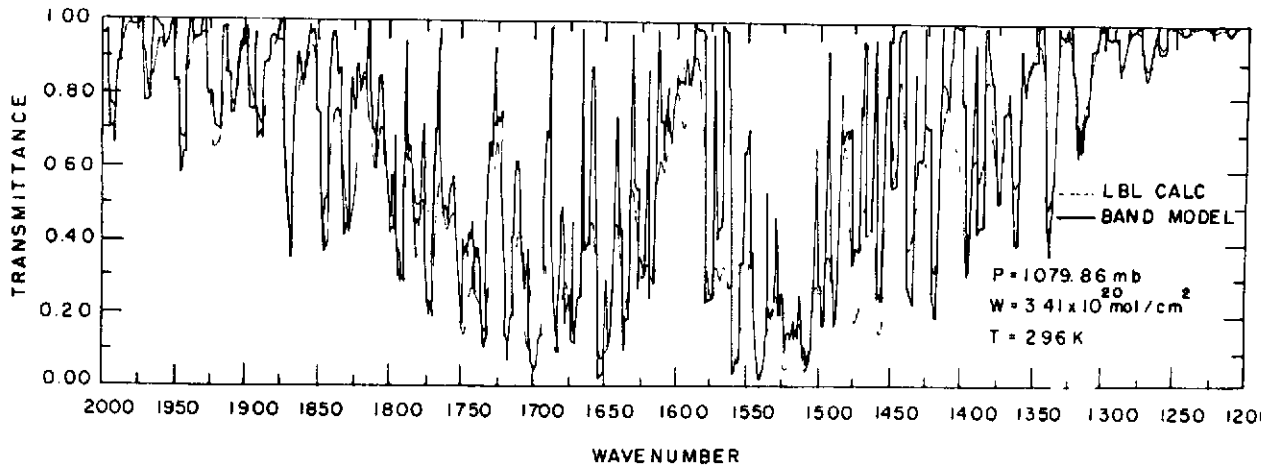

AFCRL PHOTO [illegible]

FIGURE 14

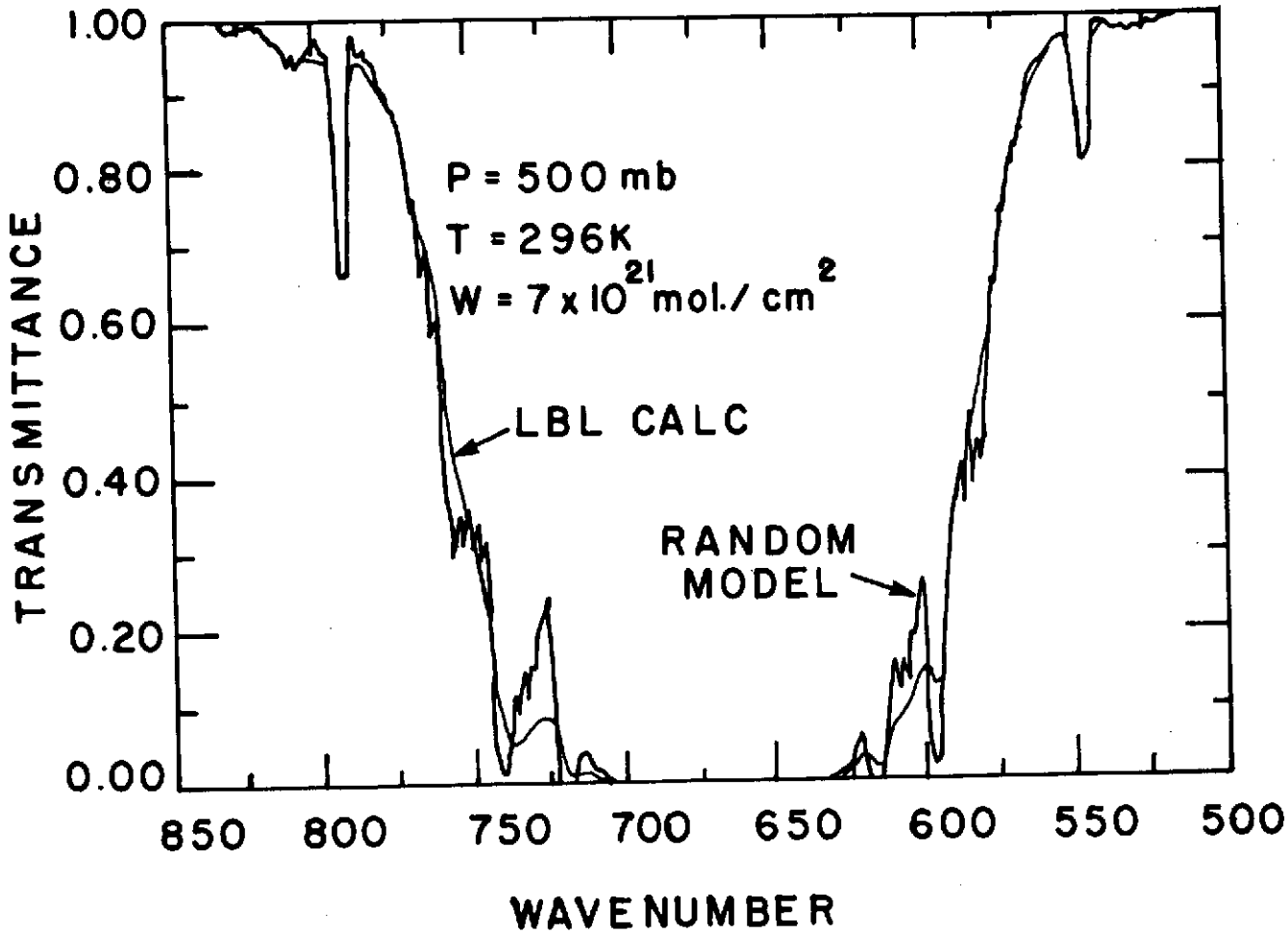
1.00
0.80
0.60
0.40
0.20
0.00
TRANSMITTANCE
P = 500 mb
T = 296K
W = 7 x 10^21 mol./ cm^2
LBL CALC
RANDOM
MODEL
850
800
750
700
650
600
550
500
WAVENUMBER

FIGURE 15

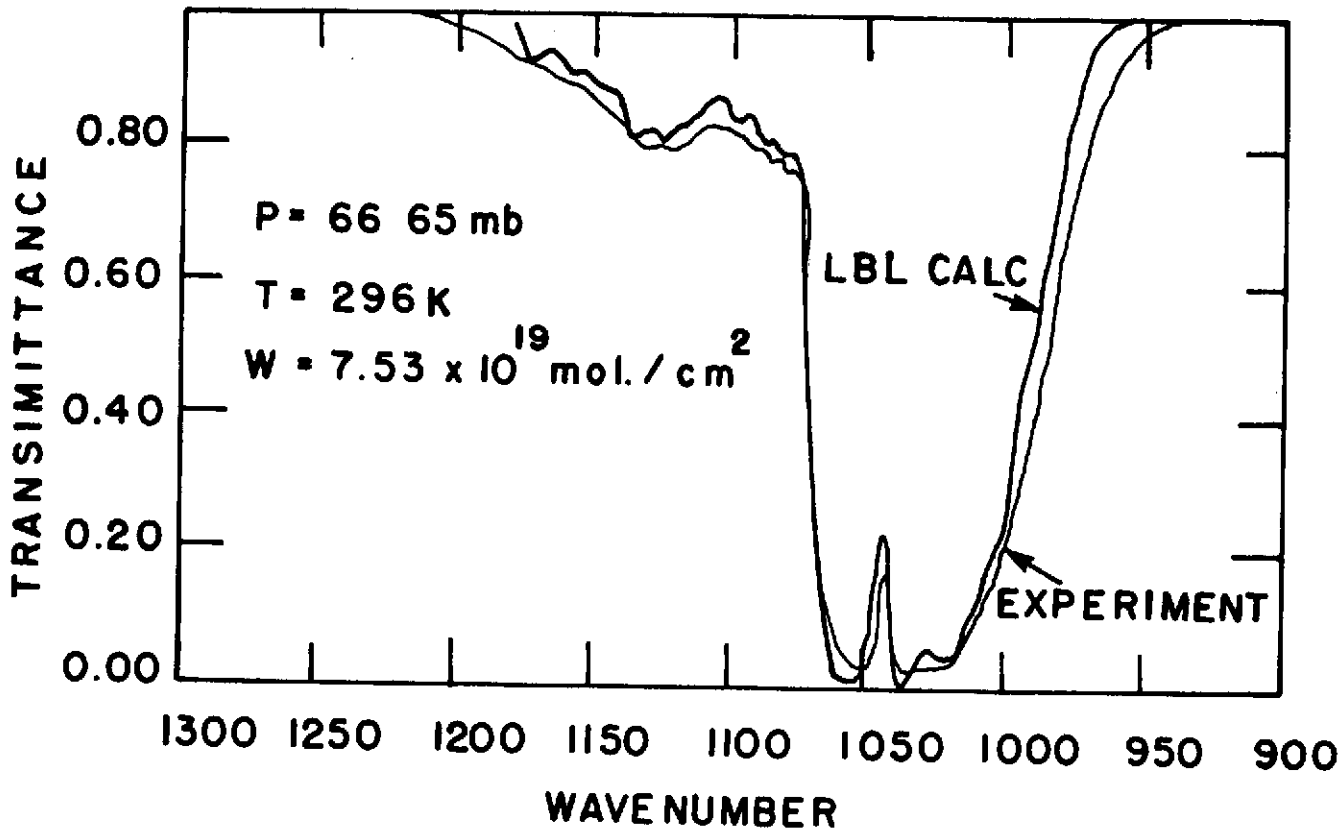
TRANSIMITTANCE
0.80
0.60
0.40
0.20
0.00
P = 66 65 mb
T = 296 K
W = 7.53 x 10^19 mol./cm^2
LBL CALC
EXPERIMENT
1300 1250 1200 1150 1100 1050 1000 950 900
WAVE NUMBER

FIGURE 16-A

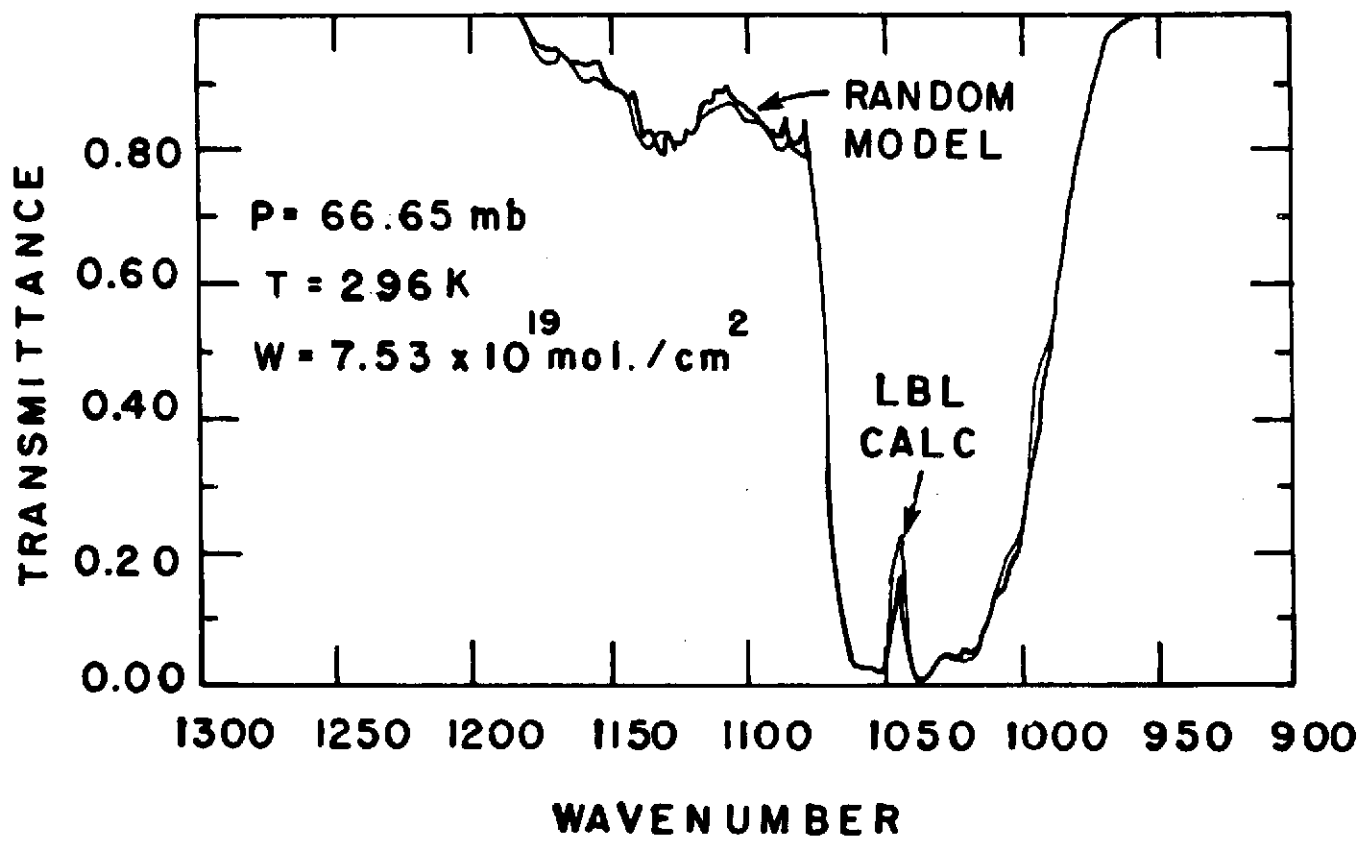
TRANSMITTANCE
0.80
0.60
0.40
0.20
0.00
P= 66.65 mb
T = 296 K
W = 7.53 x 10^19 mol./cm^2
RANDOM
MODEL
LBL
CALC
1300 1250 1200 1150 1100 1050 1000 950 900
WAVENUMBER

FIGURE 16-B

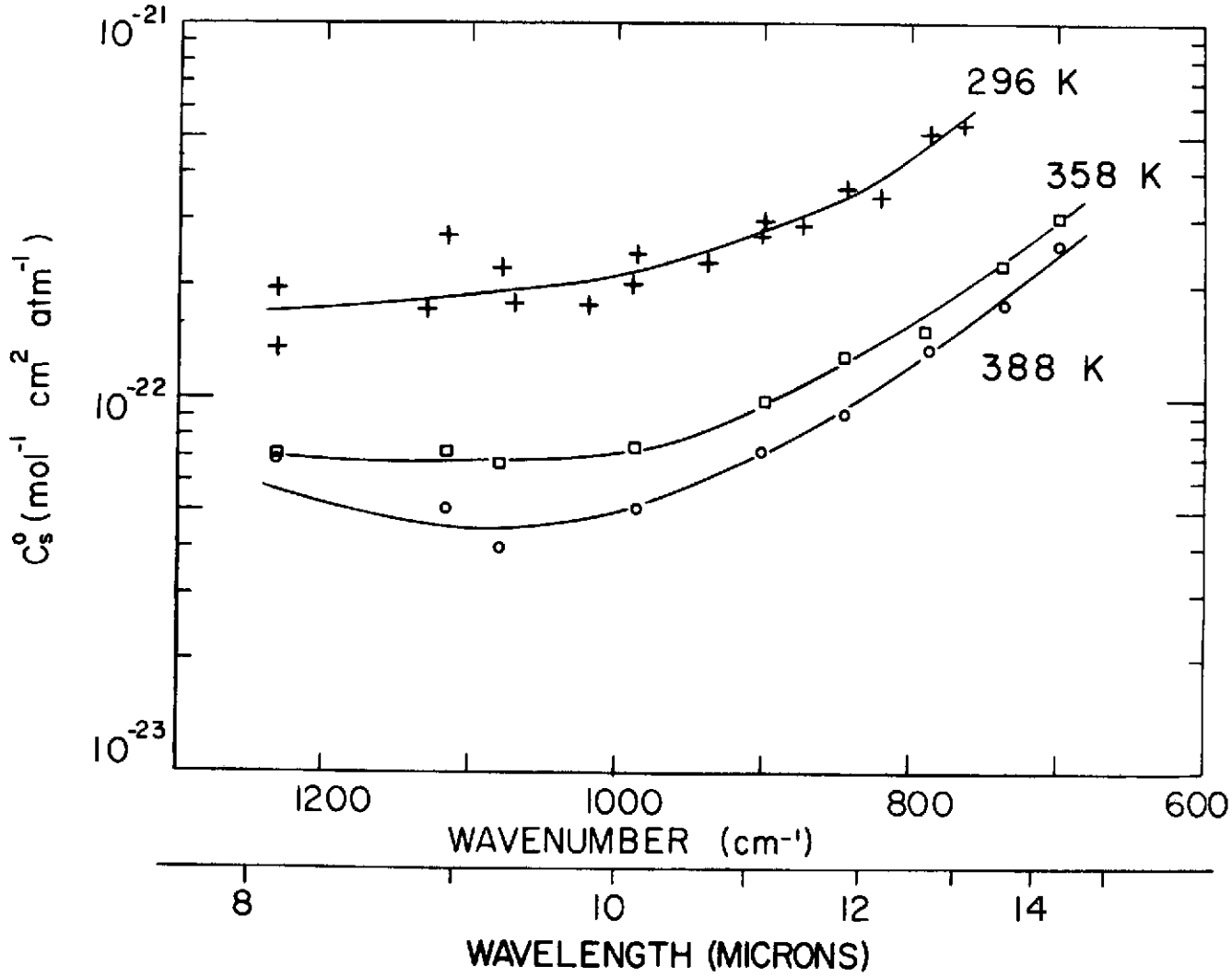
10^{-21}
10^{-22}
10^{-23}
C_s^o (mol^{-1} cm^2 atm^{-1})
296 K
358 K
388 K
1200
1000
800
600
WAVENUMBER (cm^{-1})
8
10
12
14
WAVELENGTH (MICRONS)

FIGURE 17

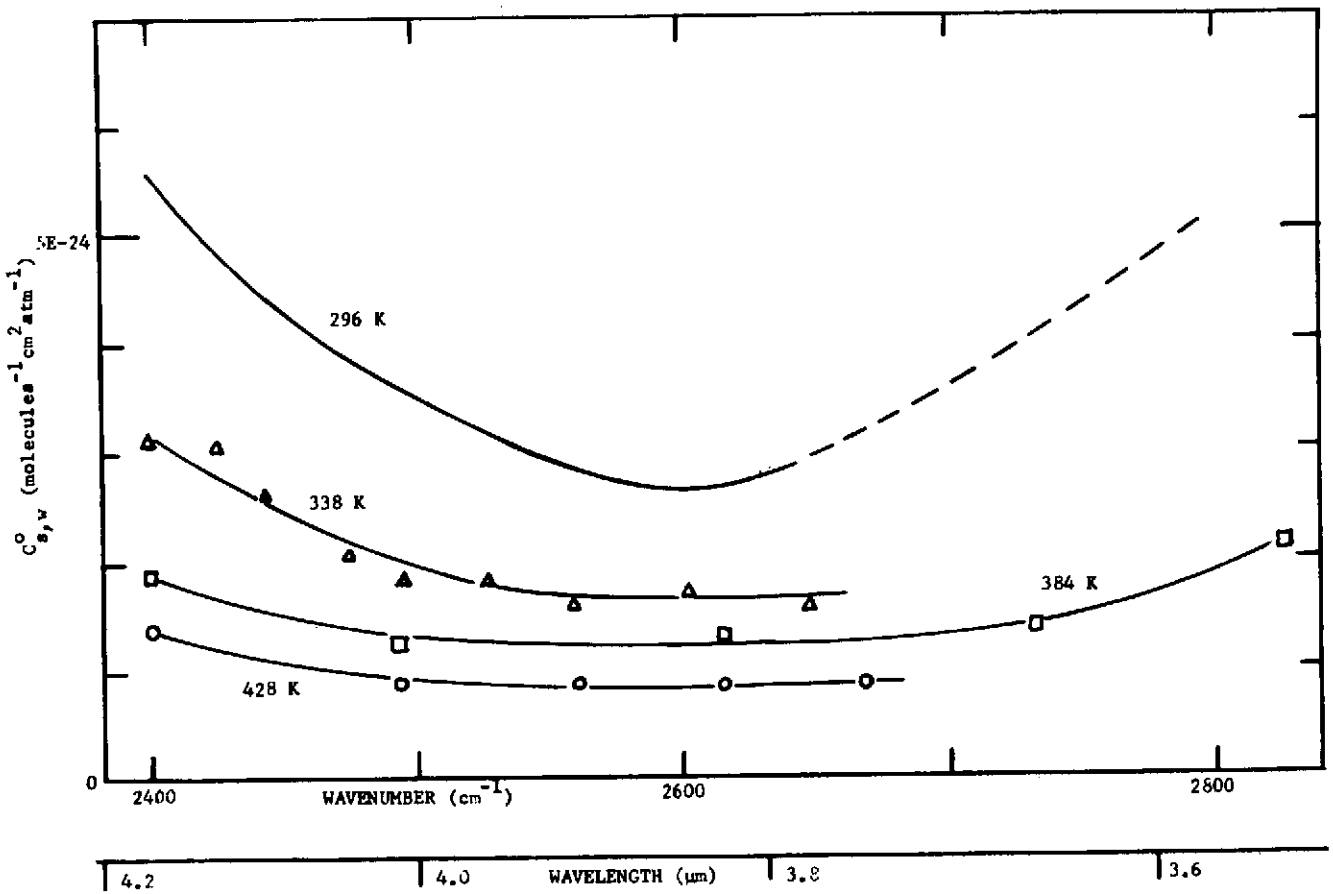
5E-24
0
$C^{\circ}_{s,w}$ (molecules^{-1}cm^{2}atm^{-1})
296 K
338 K
384 K
428 K
2400
2600
2800
WAVENUMBER (cm^{-1})
4.2
4.0
3.8
3.6
WAVELENGTH (μm)

FIGURE 18

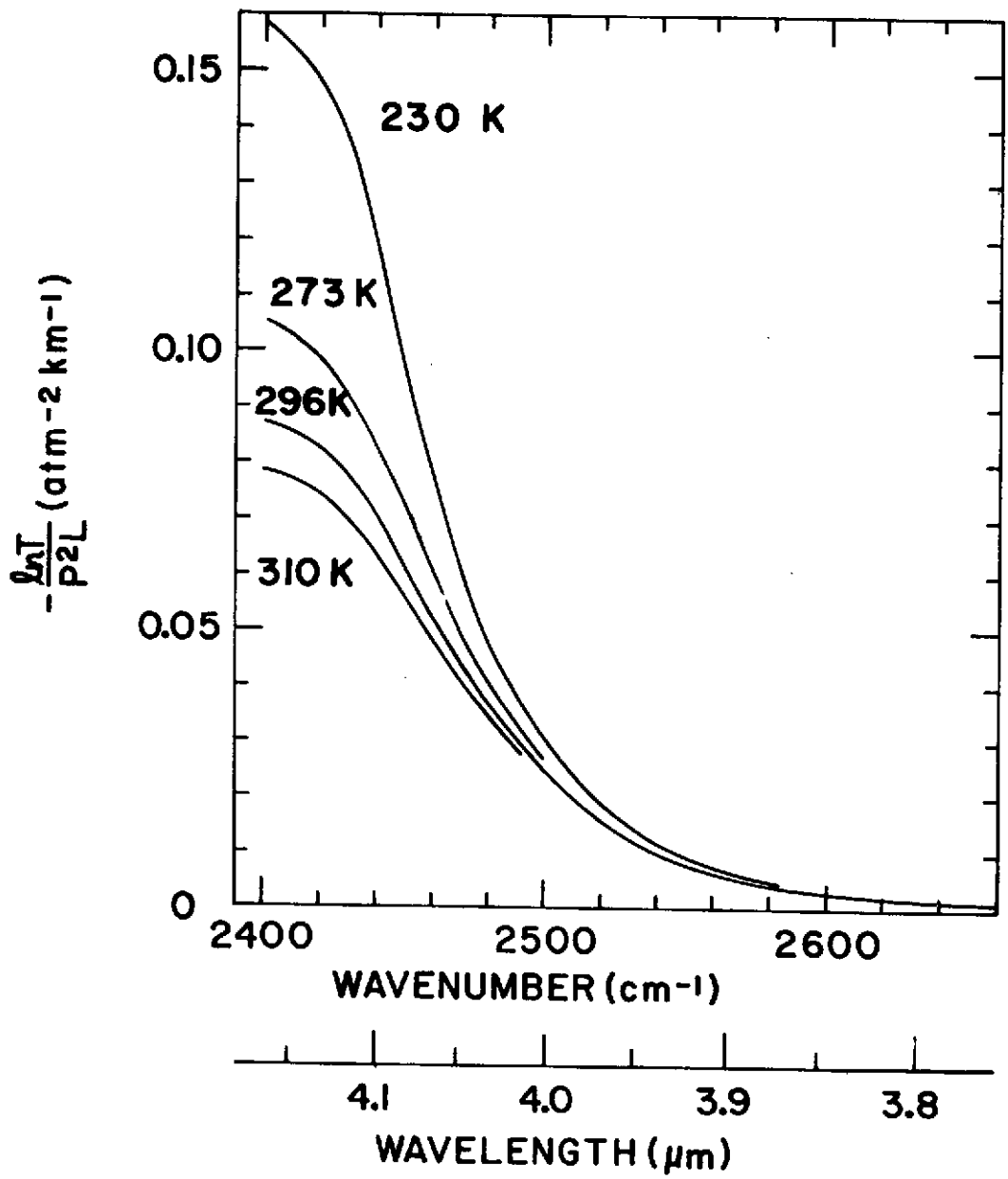
0.15
0.10
0.05
0
230 K
273 K
296K
310 K
$-\frac{\ln T}{P^2 L}$ (atm^{-2} km^{-1})
2400
2500
2600
WAVENUMBER (cm^{-1})
4.1
4.0
3.9
3.8
WAVELENGTH (μm)

FIGURE 19

INFRARED REMOTE SOUNDING

C. D. Rodgers, Clarendon Laboratory
Oxford, England

INTRODUCTION

The potentialities of artificial earth satellites for remote sounding of the earth's atmosphere were first realised towards the end of the 1950's, at about the time the first satellites were launched. Kaplan (1959) pointed out that the thermal radiation emitted by the atmosphere depends on the distribution of temperature and absorbing gases, and proposed a practical method whereby the temperature distribution could be sounded using the absorption band of CO_2 at 15 μ.

Of course it is not only temperature that can be observed. Any quantity that affects the emitted radiation can in principle be measured. Fig. 1 shows two typical spectra of the earth's atmosphere measured from a satellite using the IRIS instrument (Hanel et al 1971). We can clearly see features due to thermal emission by carbon dioxide (667 cm^{-1}), water vapour (everywhere) and ozone (1040 cm^{-1}). With a little care, emission due to methane and nitrous oxide (1300 cm^{-1}) can also be distinguished. In window regions, the nature of the surface affects the spectrum. Information about the atmosphere can also be obtained from reflected solar radiation. However as the theory and techniques are different from those for thermal radiation, this paper will be restricted to thermal sounding in the infrared and microwave regions. The spectra of Fig. 1 are of relatively low resolution. Many of the broad scale features actually consist of thousands of spectral lines. To illustrate this, Fig.2 shows an absorption spectrum of carbon dioxide in a 0.7 cm^{-1} interval in the Q branch at 15 μ. This calculated spectrum shows the scale of wavelength on which there is information. No satellite instrument could hope to measure the emission by the atmosphere at this resolution. Still less could we hope to make use of all the information that there is in the spectrum. We must be selective. So far we have only mentioned wavelength as one of the variables. There is also information in the way the spectrum varies with position and angle, for example we may use imaging and limbscanning techniques. This gives us an even wider choice of possibilities.

The radiation emitted by the atmosphere may be measured as a function of:

* wavelength (wavenumber)
* position (of the observer or the emitting element)
* angle
* time

It is determined by the distribution of:

* temperature
* cloud, aerosol
* composition - CO_2, H_2O, O_3, CH_4, N_2O, etc.
* surface emissivity and height.

In principle it should be possible to determine all these quantities by remote sounding. In practice some quantities are more easily sounded than others. Temperature distribution is the simplest, and is that which has received most attention. Of the possibilities, it is probably the most important meteorologically. The only gases whose distribution has been measured so far are water vapour and ozone, but instruments are being designed for future spacecraft which will measure the distribution of other atmospheric trace gases such as CH_4, CO, N_2O, NO, NO_2. Fig. 3 gives a general indication of the composition of the atmosphere in terms of trace gases and Fig. 4 shows some of the spectral features that can be used for measuring them.

THEORY OF RADIATIVE TRANSFER

Much has been said elsewhere in the proceedings of this conference about the direct problem, i.e. the dependence of thermal radiation upon the state of the atmosphere, so that derivation of the equations is hardly required here (e.g. Gille 1974). The intensity I of thermal radiation emitted at the top of the atmosphere can be written as

$$I(\nu, \phi) = B(\nu, \theta(z)) \frac{dT(\nu, z, \phi)}{dz} dz + B(\nu, \theta(g)) T(\nu, g, \phi) \qquad (1)$$

where ν is wavenumber, ϕ is angle of emergence, B is the Planck function, $\theta(z)$ is the temperature at height z, and g is the ground. $T(\nu, z, \phi)$ is the transmission of the atmosphere from height z to the spacecraft. This is a function of the distribution of those absorbers which have significant absorption at wavenumber ν. We note that $T(\nu, z, \phi) \to 1$ as $z \to \infty$, and $\to 0$ as $z \to -\infty$. Thus dT/dz must have a peak of some shape at some value of z. The height and shape of this peak depend on the absorber distribution and absorption coefficient. Thus the measured intensity is a weighted mean value of the Planck function profile, with dT/dz as the weighting function. A typical set of such weighting functions is shown in Fig. 5. These are for the vertical sounding of temperature in a cloudless atmosphere using the 15 μ band of CO_2 by the SIRS instrument on Nimbus 4.

Qualitatively we can see that it should be possible to measure the temperature profile with a vertical resolution of about 10 km using radiation emitted by CO_2. However, to reach great heights, line centres where k_ν is large must be used, but this requires very high spectral resolution. Low spectral resolution allows a range of k_ν to be seen, and this smears out the weighting function giving poorer resolution.

We can obtain higher vertical resolution by using limbscanning methods as illustrated in Fig. 6. The weighting function as a function of distance along the line of sight is still very broad, but when the geometry is transformed so that it is expressed in terms of absolute heights the weighting function is very narrow (Fig. 7).

Distribution of absorbing gas is less straightforward to sound than temperature. It affects the measured intensity through the shape and height of the weighting function, and therefore enters the equation in a grossly non-linear manner. Qualitatively we can say that if the absorber amount is increased then the height of the emitting layer (peak of the weighting function) rises, and the emitted radiation changes because the temperature of the emitting layer changes. Thus we measure the distribution of absorber as a function of atmospheric temperature. If the temperature profile is measured independently, it should then be possible to relate the distribution of absorber to height.

Clouds may be regarded as absorbers throughout most of the thermal infrared, but normally the absorption is so great that they can be treated as black bodies. Their irregular distribution in both the horizontal and the vertical, and their effect of masking radiation originating in lower layers, makes them the most important and difficult problem in retrieving atmospheric information from measurements of infrared radiation. The only way of bypassing this problem is to use microwave sounding, when clouds are largely transparent.

RETRIEVAL METHODS

The problem of finding the best value of a quantity given measurements of related quantities is shared by many disciplines. In the particular case of remote sounding the problem is unusually difficult because the observables are related in such a complex way to the required quantities.

There are two aspects of the retrieval problem that can, in one sense, be treated separately. The obvious aspect is the problem of inverting the equation of transfer so that the atmospheric state is expressed as a function of the observed radiation. The less obvious aspect is the question of the information content of the observations. This second aspect involves such questions as the vertical resolution of the derived profiles of temperature and composition, the accuracy of the solution, and just which components can be measured and which cannot.

We will discuss the "information content" problem first, before dealing with the more practical problem of inverting the equation of transfer. To do this, we will use a simplified version of the equation of transfer:

$$I_i = \sum_{z=1}^{M} K_{iz} B_z + \varepsilon_i \qquad i = 1.....N \tag{2}$$

where I_i is the measured radiance in spectral interval i, B_z is the atmospheric state vector, K_{iz} is the transformation applied to B_z by the instrument (the weighting function), and ε_i is the experimental error. The integral in equation 1 has been replaced by a summation. This equation is a good approximation for some types of observation (e.g. microwave sounding for temperature), or it may be regarded as a step in an iterative process for the solution of more complicated problems (see below).

The first question is whether a unique solution of this equation is possible at all. The answer must be no, on two counts. The presence of the term $\underset{\sim}{\varepsilon}$ implies that we only know $\underset{\sim}{I}$ within certain limits. Thus even if we could solve the equation for $\underset{\sim}{B}$ if $\underset{\sim}{\varepsilon} = 0$, we find that there is uncertainty due to $\underset{\sim}{\varepsilon}$. The second count hinges on the relative sizes of N and M. The number of spectral intervals used for a particular observation is necessarily finite. The height co-ordinate is continuous. Thus M should be infinite. Therefore the problem is underconstrained, and there must be an infinite number of solutions consistent with the observations even in the absence of noise.

The question of retrieval must now be restated as "Given the observations $\underset{\sim}{I}$, the statistics of experimental error $\underset{\sim}{\varepsilon}$, and the instrumental function $\underset{\sim}{K}$, what can we say in a physically meaningful way about $\underset{\sim}{B}$?" There are several ways of looking at this:

* Deduce a 'good' approximation to $\underset{\sim}{B}$, and estimate the statistics of its error.
* Deduce a 'good' approximation to some specified (linear) function of $\underset{\sim}{B}$, (e.g. total water amount, thickness between pressure surfaces), and estimate the statistics of its error.
* Find a physically meaningful linear function of $\underset{\sim}{B}$ which could be deduced exactly from the observation in the absence of noise.

If we are going to try to solve for $\underset{\sim}{B}$, we must impose some constraint so that we obtain a unique solution. Examples of such constraints are:

* Make $\underset{\sim}{B}$ a function of N variables. One must then investigate how well the real atmosphere may be represented by the particular form chosen
* Choose the 'most likely' solution consistent with the observations. This requires a knowledge of the statistics of $\underset{\sim}{B}$
* Choose the 'expected' value of $\underset{\sim}{B}$. This is the average value of all $\underset{\sim}{B}$'s weighted with their probabilities of being a solution.
* Constrain the solution to be 'near' a first guess of some kind, and within experimental error of the observations.
* Choose the solution which is 'smoothest' within experimental error of the observations.

Another aspect of the information problem that must be clearly understood is that of independence of observations. Typically the weighting functions overlap considerably, so that different spectral intervals measure contributions from the same part of the atmosphere. The instrument scrambles information about the profile $\underset{\sim}{B}$ by the transformation $\underset{\sim}{K}$, before presenting it to the observer as radiance $\underset{\sim}{I}$. One question in trying to unscramble it again to discover how many independent measurements we have of a particular profile, given N non-independent measurements I_1 to I_N. To do this, we must find a linear transformation $(\underset{\sim}{L})$ of $\underset{\sim}{K}$, $\underset{\sim}{M} = \underset{\sim}{L} \cdot \underset{\sim}{K}$, such that the transformed weighting functions $\underset{\sim}{M}$ are independent. We can then regard $\underset{\sim}{M}$ as a set of independent windows through which we view the atmosphere. Independence requires $\underset{\sim}{M}\underset{\sim}{M}^T = \underset{\sim}{\Lambda}$, a diagonal matrix. Thus

$$\underset{\sim}{L}\underset{\sim}{K}\underset{\sim}{K}^T\underset{\sim}{L} = \underset{\sim}{\Lambda}$$

If we also require that the transformation $\underset{\sim}{L}$ be orthogonal, i.e. $\underset{\sim\sim}{L}\underset{\sim\sim}{L}^T = \underset{\sim}{U}$, the unit matrix, we see that $\underset{\sim}{L}$ is the matrix of eigenvectors of $\underset{\sim\sim}{K}\underset{\sim\sim}{K}^T$, with eigenvalues Λ_i. The transformed observations are $\underset{\sim}{I}' = \underset{\sim}{M} \cdot \underset{\sim}{B} = \underset{\sim}{L} \cdot \underset{\sim}{K}\,\underset{\sim}{B} = \underset{\sim}{L} \cdot \underset{\sim}{I}$. It can easily be shown that if the $\underset{\sim}{B}$'s are regarded as independent quantities of equal variance then the variances of the elements of $\underset{\sim}{I}'$, the transformed observations, are proportional to the corresponding eigenvalues Λ_i. It is found that some of these eigenvalues are very small, implying that there is little information in the corresponding observation. In fact the number of independent observations that one can make with a given set of $\underset{\sim}{K}$'s is the number of eigenvalues of $\underset{\sim\sim}{K}\underset{\sim\sim}{K}^T$ which are greater than the square of the experimental noise/signal.

This analysis tells us about the nature of the instrument. However, the atmosphere itself has correlations between its properties, so that the number of statistically independent quantities that can be measured is smaller than the above analysis shows. A statistical analysis requires us to diagonalise the covariance matrix of the observations themselves, and compare the eigenvalues with $(\text{noise/signal})^2$ (Rodgers 1971).

INVERSION OF THE EQUATION OF TRANSFER

The precise details of how the equation is inverted depend to some extent on the constraints applied.

If the equation is linear, and quadratic form constraints are used, i.e. we minimise

$$(\underset{\sim}{I} - \underset{\sim\sim}{K}\underset{\sim}{B})^T \underset{\sim}{E}^{-1} (\underset{\sim}{I} - \underset{\sim\sim}{K}\underset{\sim}{B}) + (\underset{\sim}{B} - \overline{\underset{\sim}{B}})^T \underset{\sim}{H}^{-1} (\underset{\sim}{B} - \overline{\underset{\sim}{B}})$$

where $\underset{\sim}{H}$ is the inverse of the constraint matrix, and $\underset{\sim}{E}$ is the covariance of the experimental error, then we can solve the equation to give

$$\underset{\sim}{B} = \underset{\sim\sim}{H}\underset{\sim\sim}{K}^T (\underset{\sim}{E} + \underset{\sim\sim\sim}{K}\underset{\sim\sim}{H}\underset{\sim\sim}{K}^T)^{-1} (\underset{\sim}{I} - \overline{\underset{\sim}{I}}) + \overline{\underset{\sim}{B}} \qquad (3)$$

Unfortunately in most cases the equation is not linear. However we can use the same basic principle of a quadratic form constraint, and minimise

$$(\underset{\sim}{I} - \underset{\sim}{I}(\underset{\sim}{B}))^T \underset{\sim}{E}^{-1} (\underset{\sim}{I} - \underset{\sim}{I}(\underset{\sim}{B})) + (\underset{\sim}{B} - \overline{\underset{\sim}{B}})^T H^{-1}(B - \overline{B})$$

where $I(B)$ is the appropriate direct model. The minimisation can be carried out by a general minimising process (e.g. Powell 1964), but this may be inefficient in a particular case. A Newton-Raphson process may be used if the direct equation is not too nonlinear. This requires linearising the equations about the current iteration, and solving it as a linear problem using equation (3) to find the next iteration.

For some problems particular features of the equation of transfer and the instrument design may be used to advantage.

For example, the ITPR instrument on Nimbus 5 uses a scanning arrangement (Fig. 11) which enables independent measurements to be made close together in space. If it is assumed that adjacent observations are of the same temperature and humidity profile, and cloud height, but differ only in cloud amount, then it is possible to eliminate the cloud mathematically, and estimate what the radiances would have been in the absence of cloud.

The relaxation method of Chahine (1968) is of value when the equation of transfer is too non-linear for the Newton-Raphson approach to work efficiently. For example, when the sounding frequencies are widely spaced. However it does require a set of weighting functions with distinct peaks. The iteration is of the form:

$$B(T_j^{(n)}, \nu_j) = B(T_j^{(n-1)}, \nu_j) \cdot I_{obs}(\nu_j)/I_{calc}^{(n-1)}(\nu_j)$$

where $T_j^{(n)}$ is the nth iteration for the temperature at a height defined by the peak of the weighting function for the spectral interval at ν_j, $I_{obs}(\nu_j)$ is the observed radiance, and $I_{calc}^{(n-1)}(\nu_j)$ is the calculated radiance for an atmospheric profile defined by the (n-1)th iteration values $T_j^{(n-1)}$.

Backus and Gilbert (1970) have developed a quite distinct approach to retrieval methods. Their particular problem is sounding the solid earth using seismological information, but mathematically the equation to be solved is similar to our equation of transfer. In their case the kernels do not have peaks at various depths, they all peak at the surface. This is akin to the atmospheric remote sounding problem for an observer at the surface. Backus and Gilbert investigated the question of taking linear combinations of kernels so that the result has a peak at a specified position. The same linear combination of their observations would then correspond to the function sounded at the position of the peak. They found it possible to do this, but in constructing the narrowest possible peak (i.e. best resolution) the noise in the observations was amplified so that the result could in some cases be useless. Their next step was to jointly minimize the width of the peak and the noise in the solution, thus producing a "trade off" between noise and resolution. One of the results of their analysis is a set of "trade off curves" showing how the noise is amplified as resolution gets better. Thus it is possible to say just what the vertical resolution is for any particular accuracy in the estimation.

This approach has been applied to the IRIS instrument by Conrath (1972). Fig. 8 shows some of his trade off curves. In this diagram σ_T is the error in the temperature measurement, and σ_E is the noise equivalent temperature in the radiometer. 'Spread' is a measure of vertical resolution. Curves A are for a measurement of the temperature at 780 mb, and curves B are for 50 mb. The dotted lines are for 7 spectral regions, and the full lines are for 16 regions. These curves show how rapidly noise goes up if it is attempted to improve the vertical resolution beyond a certain point.

EXPERIMENTAL TECHNIQUES

Infrared remote sounding techniques have been widely used from earth satellites, and one planetary probe (Mariner 9) has used thermal radiation to sound the Martian atmosphere. Several different types of instrument have been used. These can be classified broadly as:

1. Michelson Interferometer
2. Grating Spectrometers
3. Filter Radiometers
4. Microwave detectors

The Michelson Interferometer has the advantage in an experimental situation that it records the whole spectrum of the atmosphere. This means that the interesting spectral regions can be chosen after the instrument is launched, and unexpected features of the thermal emission are not lost. However, very high resolution cannot be used, as this leads to a problem of data storage and telemetry because of the high data rate required. The IRIS experiments on Nimbus 3 and 4 and on Mariner 9 have been of great value. A typical spectrum has already been seen in Fig. 1.

Grating Spectrometers have been flown on Nimbus 3 and 4. The instrument (SIRS) is a spectrometer of fairly conventional design using an array of detectors or a set of fixed exit slits. This produced radiance measurements in specified spectral regions, rather than a continuous spectrum, as did the IRIS. SIRS 3 had seven channels in the 15 μ band of carbon dioxide, and one window channel. SIRS 4 included further channels for water vapour sounding.

Many instruments have used the rather simple basic design of a filter radiometer. This consists of a set of optics to condense the incoming radiation onto a detector, with a filter at the appropriate place in the system to select the required spectral region. The first instrument to measure atmospheric temperatures from a satellite was of this type. This was MRIR on TIROS G, which had a filter covering the whole 15 μ band, thus measuring the mean temperature for the whole stratosphere.

An improvement on this basic design came with the introduction of Selective Chopping and Selective Absorption in the SCR instruments on Nimbus 4 and 5. The height of the peak of the weighting function depends on the absorption coefficient. If this varies widely within the spectral pass band of the instrument, then the weighting function will have contributions from a variety of heights, and will be broadened compared with the monochromatic case. This problem occurs when using molecular vibration rotation bands, as can be seen from Fig. 9. Selective absorption requires an absorbing cell at CO_2 to be included in the instrument to remove radiation from line centres. Thus the detector only sees radiation from the troughs between lines, where the absorption coefficient is much less variable. The improvement in the shape of the weighting functions is shown in Fig. 9. Selective chopping is in a sense the reverse of selective absorption. By one of a variety of techniques the difference is measured between the total radiation reaching the detector, and that reaching the detector after selective absorption. This difference signal is proportional to the radiation in the centres of the CO_2 lines, where the absorption is high, and results in a weighting function which is high in the atmosphere (Fig. 10). Alternatively, the difference signal may be

measured between two paths containing different amounts of CO_2. This gives weighting functions of intermediate heights.

Another filter radiometer is the ITPR which is flying on Nimbus 5. This instrument has seven channels specifically designed for tropospheric sounding. It uses a narrow field of view which is scanned over a grid of 140 elements, as described above (Fig. 11).

An entirely different approach to the problem of cloud is the use of microwave sounding. Thermal radiation is easily measureable in the microwave region to very high spectral resolution using conventional though carefully designed microwave receivers. One such instrument is NEMS on Nimbus 5. The spectral region used is the 5 mm O_2 band, together with a window channel, and a water vapour channel. The major advantage is that most clouds are transparent in this region, so that the retrieval is straightforward. Only in the case of large precipitating clouds is there any problem, (Staelin 1969).

For future spacecraft there are more basic designs under development.

A limb scanning radiometer (L.R.I.R.) is to be flown on Nimbus F, (Gille 1972). This instrument will provide soundings of the stratosphere with a much higher vertical resolution than has been available until now, although its horizontal resolution is relatively low. It comprises a radiometer measuring emission from the 15 μ band of carbon dioxide through a very narrow angular field of view which is scanned over the limb by means of a moving mirror.

A further development of the selective chopping principle is the Pressure Modulator Radiometer (PMR) which is due to be flown on Nimbus F (Taylor et al 1972). In this instrument only one cell of carbon dioxide is used, but its pressure is modulated by means of a piston. The detector measures radiation at the modulation frequency; this originates in the line centres. The use of a single cell eliminates the problems of balancing between two halves of an optical system, and simplifies the optical design, thus allowing more energy to reach the detector. The Nimbus F PMR should measure temperature from 40 km to 85 km.

A limb scanning PMR is being desinged for Nimbus G, in order to measure both the temperature profile, and the distribution of trace gases. The gas to be measured is used in the modulator cell, and acts as a filter to detect its own presence in the atmosphere.

SOME APPLICATIONS OF REMOTE SOUNDING

One of the most important applications of remote sounding is, of course, in monitoring the temperature profile in the troposphere and lower stratosphere on a global scale as basic information for weather forecasting. Remote sounders on Nimbus 3, 4 and 5 have been used for this purpose, and now there is a remote sounding package (VTPR) for the ITOS series of operational satellites. This aspect of remote sounding has been widely discussed in the literature. Here we will discuss some of the scientific and research applications.

Remote sounding provides basic data sets for study of the atmosphere on a global scale. The data is global in coverage and uniform in quality, thus removing many of the problems of patching together data from irregularly placed and often incompatible instruments. A typical example of this is shown in Fig. 12, which gives the global distribution of ozone for one particular day, based on IRIS measurements. The high concentrations of ozone can all be related to low pressure areas. This map could never have been produced by conventional means (Prabhakara and Conrath 1971).

Fig. 13 shows how satellite measurements can contribute to climatology. Here we have a sequence of zonal mean temperature cross sections based on Nimbus 4 SCR data. The cross section for 13 December 1970 shows a typical early winter situation with an extensive cold area over the winter pole, and the strong horizontal temperature gradient at a height of 30-50 km in the latitude region 40-60^{o} N. By 8 January there has been a midwinter warming, and this temperature gradient has reversed, making the temperature at 45 km over the north pole similar to that over the south pole. The original situation is re-established by mid February, but by mid March the cross section shows the south polar region cooling and the north polar region warming up. The June 1971 situation is approximately the reverse of that in December 1970, except that the south polar stratosphere is 10^{o} cooler than the corresponding north polar stratosphere. This is probably due to the ellipticity of the earth's orbit; we are further from the sun in June than in December. By 21 September 1971 there has been a warming in the southern hemisphere showing general similarities to the January 1971 case, but there are marked differences in the 50^{o} S region.

The details of these warming events can be very clearly seen from remote sounders (Barnett J.J. 1973). Figs 14-17 show one such event. Fig. 14 gives the temperature seen by the highest channel of the Nimbus 5 SCR (at about 45 km) on 24 January 1973. A warm area has begun to develop over Western Europe. Four days later (Fig. 15) this warm area has grown considerably, and the pattern has developed into a typical "wavenumber one warming". The temperature field has one maximum around latitude circles, and the longitude of the maximum is more easterly at higher latitudes. Fig. 16 shows the temperature field lower in the atmosphere (at about 30 km). A comparison of Figs. 15 and 16 shows that the maxima and minima of temperature slope westward with height. Fig. 17 shows that the southern hemisphere is hardly affected by these massive perturbations in the Northern hemisphere. The westward slope with height of the temperature extreme is clearly seen in Fig. 18. This is a cross section around a latitude circle of deviations of temperature from the zonal mean. A similar plot is also shown for geopotential height. The event is a similar one to the above, but two years earlier. It is a much more intense warming; notice that the temperature contrast around the latitude circle at 3 mb is about 100^{o} K.

Wave number two is often present in the temperature field, and on some occasions dominates the event. Fig. 19 shows such an occasion, the southern hemisphere winter of 1971. The units in this figure are radiance rather than temperature. Channel A is at about 40 km, showing a hot area over the pole, flanked by two cold areas. Channel D is at about 20 km, showing a cold area over the pole, flanked by two warm areas. The deviations from the zonal mean showed the same westward tilt in this case as in the northern hemisphere. This pattern remained essentially unchanged, except that it rotated about the pole, for a period of 30 days. The track of the cold centre of channel A is shown in Fig. 20. The rate of progression was fairly uniform at about 360^{o} in 25 days, as can be seen from Fig. 21.

Wave motions in the atmosphere can be studied in general by means of Fourier Analysis of the measurements. A typical example is shown in Fig. 22, which shows more stratospheric wave sctivity in higher latitudes than at the equator, and more activity in the winter hemisphere than the summer hemisphere. In all cases the amplitude decreases with increasing wavenumber, this effect being most marked for the high latitude winter case.

Fig. 23 illustrates an entirely different application of remote sounding, this time to ozone photochemistry. There are a large number of chemical reactions involved in the maintenance and production of ozone in the stratosphere, and it is not yet clear which reactions dominate at various levels in the atmosphere, because some reaction rates are not known sufficiently accurately. Each set of reaction rates will, however, lead to a particular temperature dependence of the equilibrium ozone concentration. A measurement of this temperature dependence will provide constraints on possible reaction rates. Fig. 23, plot (a), shows ozone concentration at 1.9 mb measured by the B.U.V. (Backscattered Ultra Violet) instrument on Nimbus 4 plotted against SCR channel A (about 2 mb) temperatures on a log-reciprocal scale, giving a clear measurement of the temperature dependence. Plot (b) shows less correlation, because the two instruments are not seeing the same part of the atmosphere, but this may be improved by using the westward slope with height of temperature disturbances, and plotting the temperature from the previous orbit (plot (c)).

CONCLUSIONS

This survey of remote sounding in the infrared has necessarily been brief, and somewhat selective. The field is very large and is growing rapidly, and it is not possible to cover all aspects and describe all the experiments and their applications in the time and space allotted. A comprehensive review of this and other aspects of remote sounding may be found in Houghton and Taylor (1973).

The immediate future for infrared remote sounding is clear: microwave techniques will be further developed and used operationally for tropospheric soundings, limb scanning will improve vertical resolution in the stratosphere and mesosphere, and the distribution of more trace constituents will be measured. After this, I hesitate to predict.

FIGURES

Fig. 1 Spectra of thermal radiation emitted from the earths atmosphere (Hanel et al 1971)

Fig. 2 A calculated spectrum of carbon dioxide in the Q branch at 15 microns.

Fig. 3 Typical mixing ratios of atmospheric trace gases in the stratosphere and mesosphere.

Fig. 4 Spectral features that may be used to measure distribution of atmospheric trace gases (J. H. Shaw)

Fig. 5 Weighting functions for remote sounding of atmospheric temperature by the SIRS instrument (Smith et al 1970)

Fig. 6 Geometry for Limb sounding

Fig. 7 Weighting functions for a limb sounding instrument.

Fig. 8 Trade off curves for the IRIS instrument (see text for details) (Conrath 1972)

Fig. 9
a. Weighting function for an Elsasser band model, i.e. a spectral interval containing several spectral lines
b. Weighting function for an Elsasser band model after selective absorption.
c. Monochromatic weighting function.

Fig. 10 Illustrating Selective Chopping
A. 15 micron Q branch weighting function
B. 15 micron Q branch weighting function, after absorption by CO_2 in the instrument
C. Difference between A and B.

Fig. 11 The ITPR scanning arrangements

Fig. 12 Global distribution of ozone determined from IRIS data for 22 April 1969 (from Prabhakara and Conrath 1971)

Fig. 13 Global zonal mean temperature cross sections from Nimbus 4 SCR measurements.

Fig. 14 Equivalent temperature channel B1B2 Nimbus 5 SCR. Northern Hemisphere 24 January 1973.

Fig. 15 Equivalent temperature channel B1B2 Nimbus 5 SCR. Northern Hemisphere 28 January 1973.

Fig. 16 Equivalent temperature channel B3B4 Nimbus 5 SCR. Northern Hemisphere 28 January 1973.

Fig. 17 Equivalent temperature channel B3B4 Nimbus 5 SCR. Southern Hemisphere 28 January 1973.

Fig. 18 Deviations of temperature and geopotential height from the zonal mean for 64^{0} N 5 January 1971

Fig. 19 Channel A and D radiances from Nimbus 4 SCR. Southern Hemisphere 26 September 1971.

Fig. 20 Track of the cold centre of channel A. Southern Hemisphere 7 September - 7 October 1971.

Fig. 21 Progression of wave number two pattern around the south pole. 7 September - 7 October 1971.

Fig. 22 Spectrum of Planetary Waves. Average amplitudes of zonal wave numbers 1 to 6 during the period 21 November 1971 to 6 March 1972 (Barnett 1973)

Fig. 23 Ozone mixing ratio at 1.9 and 0.9 mb plotted against the Nimbus 4 S. C. R. channel A temperature.

REFERENCES

Backus, G. and Gilbert, F., 1970: Uniqueness in the inversion of inaccurate gross Earth data. Phil. Trans. R. Soc. A266, 123-192.

Barnett, J. J., 1973: Analysis of stratospheric measurements by the Nimbus IV and V Selective Chopper Radiometers. Meteorological Satellites, International Conference 1973, C.N.E.S. Paris. 173-185.

Chahine, M. T., 1968: Determination of the Temperature profile in an atmosphere from its outgoing radiance. J. Opt. Soc. Am. 58, 1634-1637.

Conrath, B. J., 1972: Vertical Resolution of Temperature Profiles obtained from Remote Measurements. J. Atmos. Sci. 29, 1262-71.

Gille, J. C., 1972: Temperature, its Measurement and Control in Science and Industry, Vo. 4, (N. Y. American Inst. of Physics).

Gille, J. C., 1974: This conference

Hanel, R. A., Schlachman, B., Rodgers, D. and Vanons, D., 1971: The Nimbus 4 Michelson Interferometer. Appl. Opt. 10, 1376-82.

Houghton, J. T. and Taylor, F. W., 1973: Remote sounding from artificial satellites and space probes of the atmospheres of the earth and the planets. Rep. Prog. Phys. 36, 827-919.

Kaplan, L. D., 1959: Inference of atmospheric structure from remote radiation measurements. J. Opt. Soc. Am. 49, 1004-7.

Powell, M. J. D., 1964: An efficient method for finding the minimum of a function of several variables without evaluating derivatives. Computer Journal 7, 155-162.

Rodgers, C. D., 1971: Some Theoretical aspects of remote sounding in the Earth's atmosphere. J. Quant. Spec. Rad. Transfer 11, 767-777.

Smith, W. L., Woolf, H. M. and Jacob, W. J., 1970: A regression method for obtaining real time temperature and geopotential height profiles from satellite spectrometer measurements and its application to Nimbus 3 SIRS observations. Mon. Weath. Rev. 98, 582-603.

Staelin, D. H., 1969: Passive Remote sensing at microwave wavelengths. Proc. IEEE 57, 427-439.

Taylor, F. W. et al, 1972: Radiometer for Remote Sounding of the Upper Atmosphere. Appl. Opt. 11, 135.

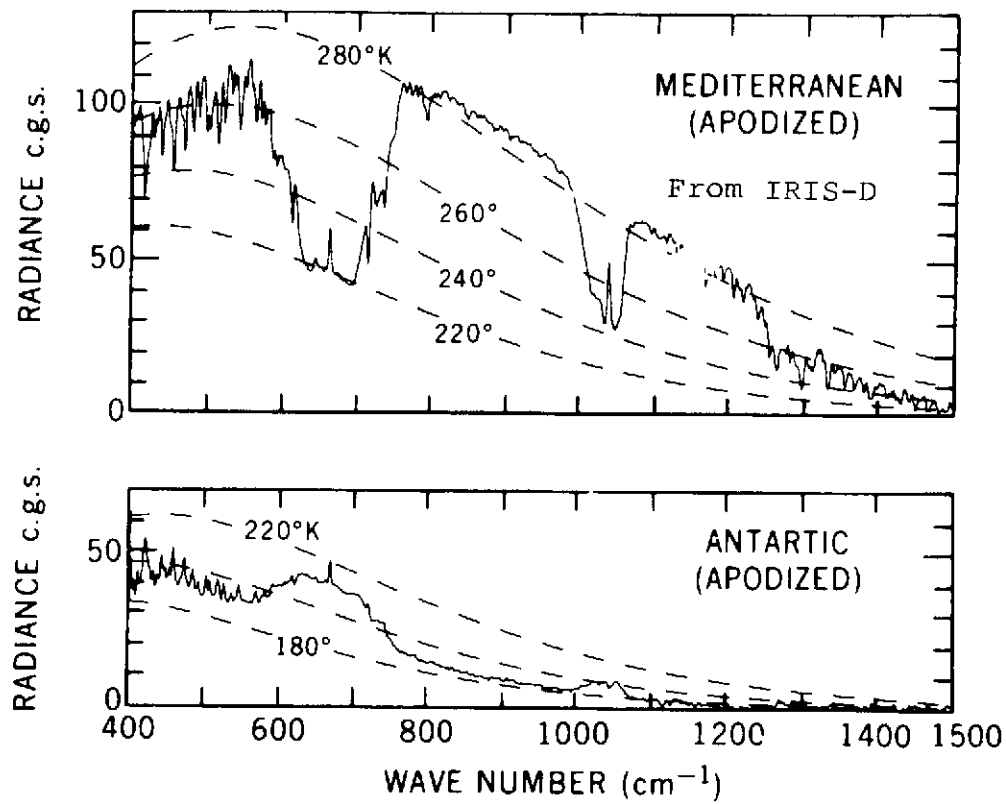
RADIANCE c.g.s.
100
50
0
280°K
260°
240°
220°
MEDITERRANEAN
(APODIZED)
From IRIS-D
RADIANCE c.g.s.
50
0
220°K
180°
ANTARTIC
(APODIZED)
400
600
800
1000
1200
1400
1500
WAVE NUMBER (cm^{-1})

FIGURE 1

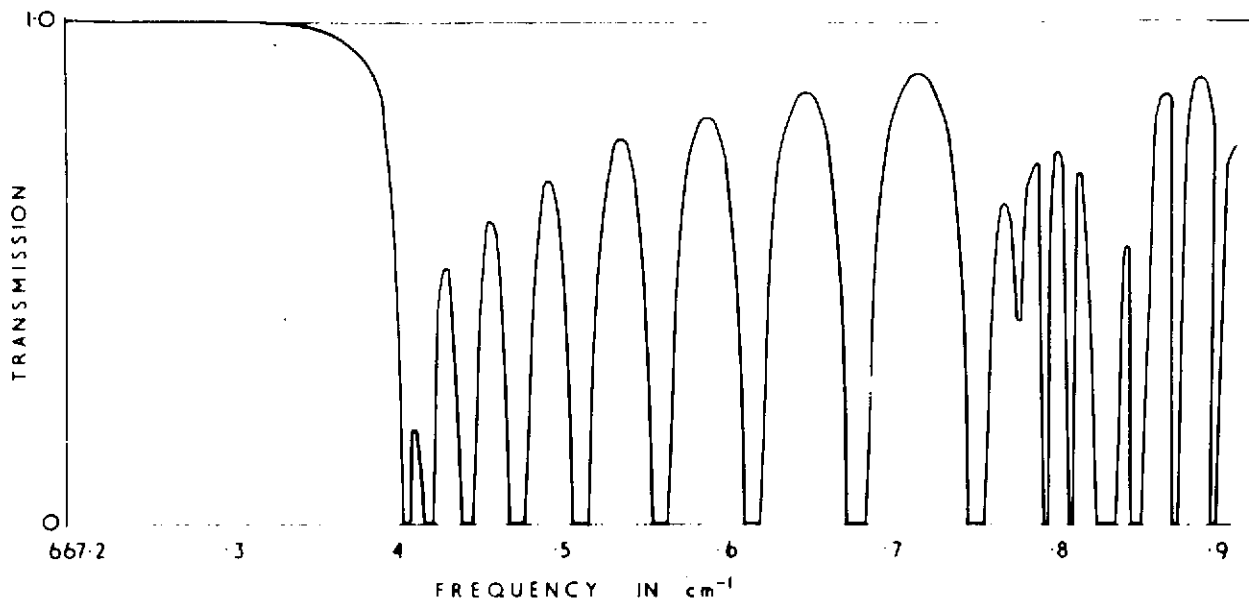

FIGURE 2

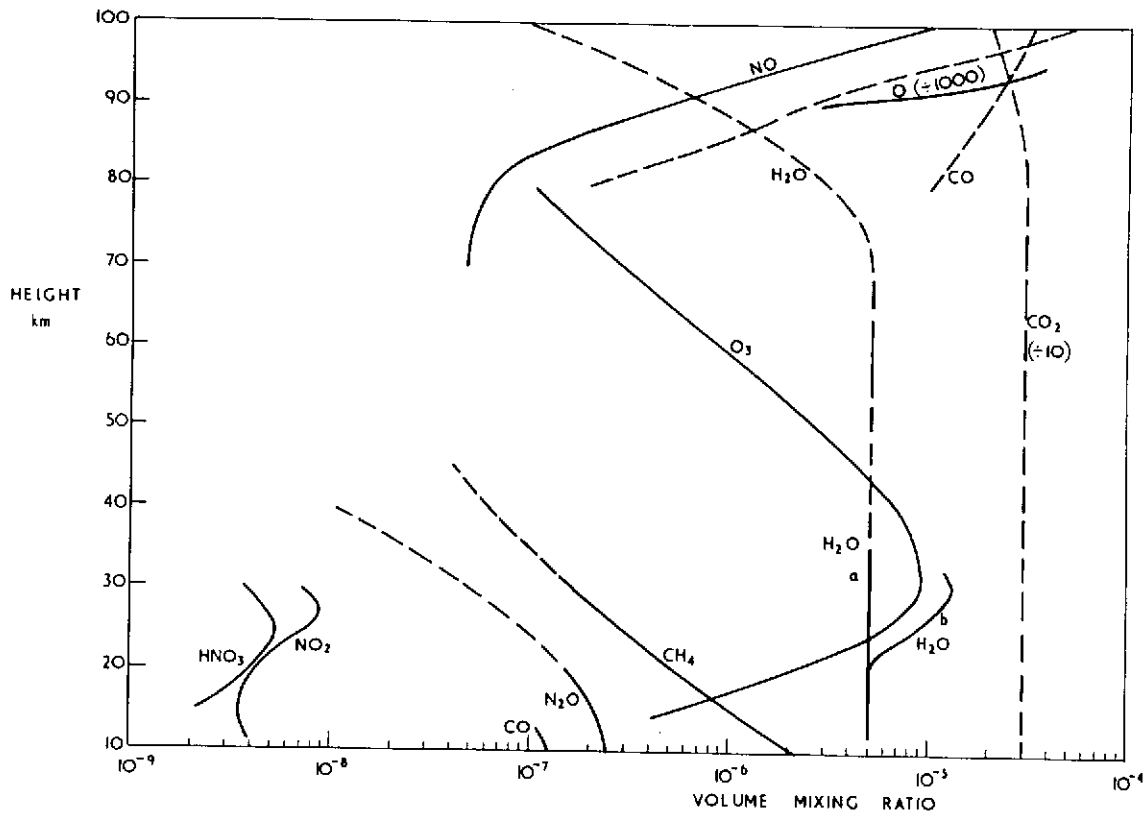
HEIGHT
km
100
90
80
70
60
50
40
30
20
10
NO
O (÷1000)
H2O
CO
CO2
(÷10)
O3
H2O
a
b
H2O
CH4
HNO3
NO2
N2O
CO
10-9
10-8
10-7
10-6
10-5
10-4
VOLUME MIXING RATIO

FIGURE 3

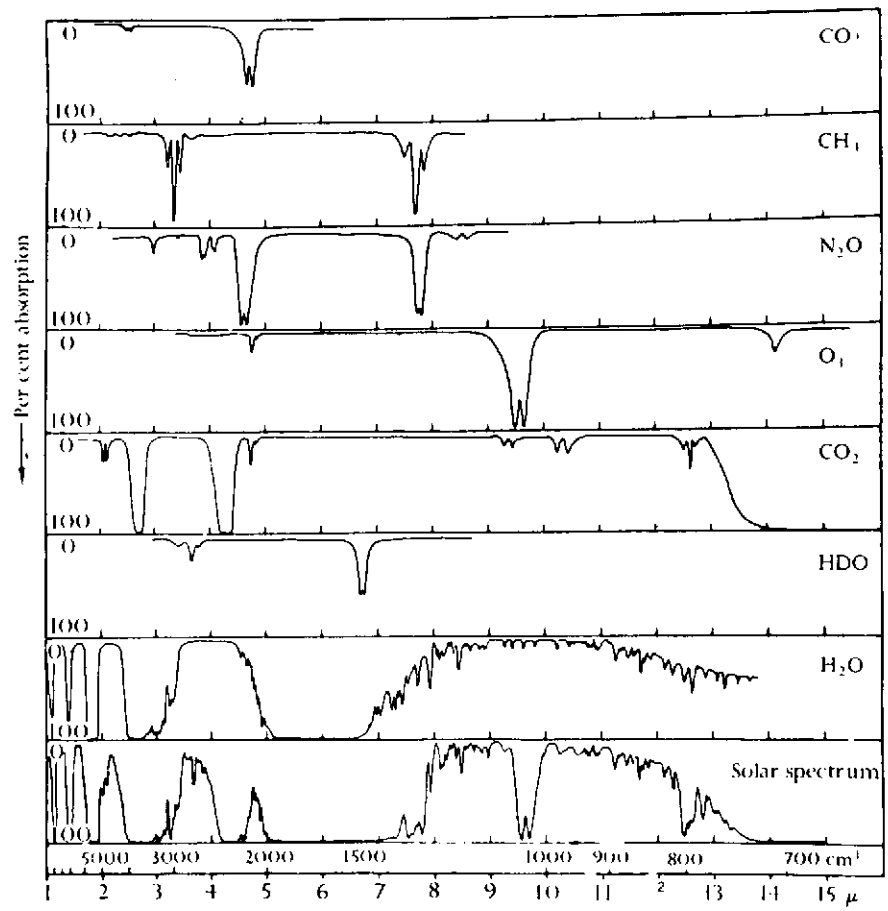
Per cent absorption
0
100
CO
CH4
N2O
O3
CO2
HDO
H2O
Solar spectrum
5000
3000
2000
1500
1000
900
800
700 cm-1
1
2
3
4
5
6
7
8
9
10
11
12
13
14
15 μ

FIGURE 4

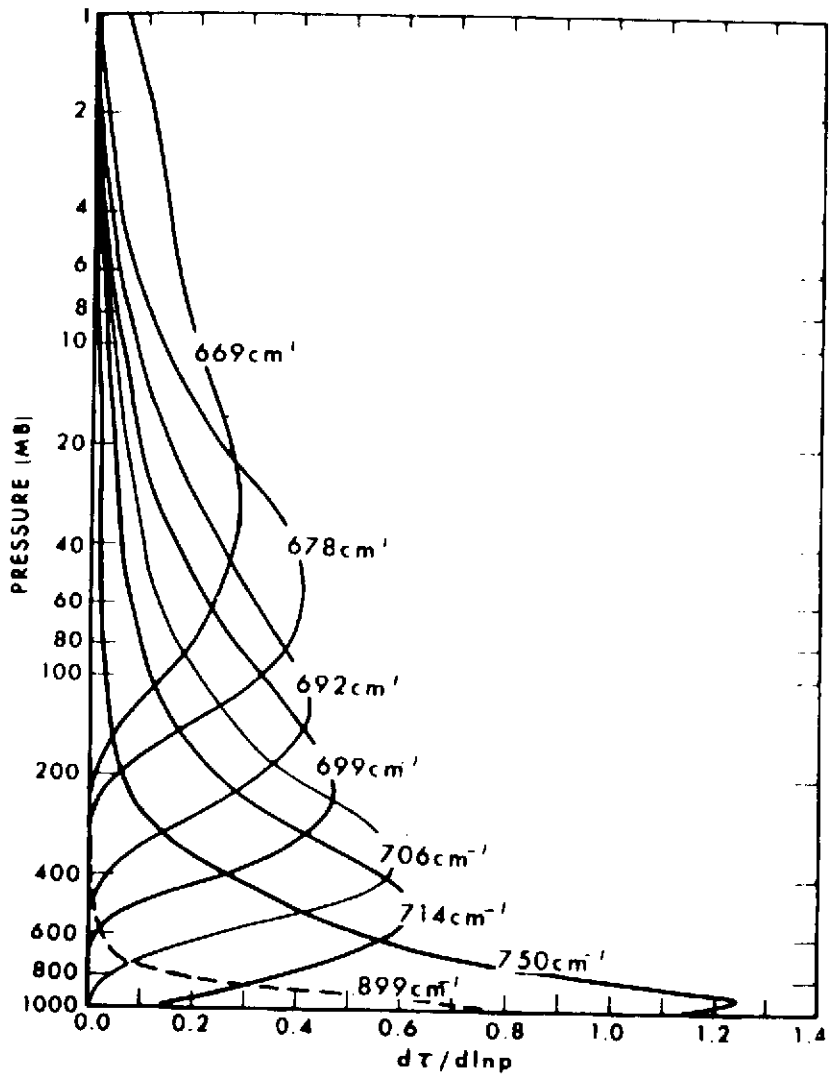
PRESSURE (MB)
1
2
4
6
8
10
20
40
60
80
100
200
400
600
800
1000
669cm⁻¹
678cm⁻¹
692cm⁻¹
699cm⁻¹
706cm⁻¹
714cm⁻¹
750cm⁻¹
899cm⁻¹
0.0
0.2
0.4
0.6
0.8
1.0
1.2
dτ/dlnp

FIGURE 5

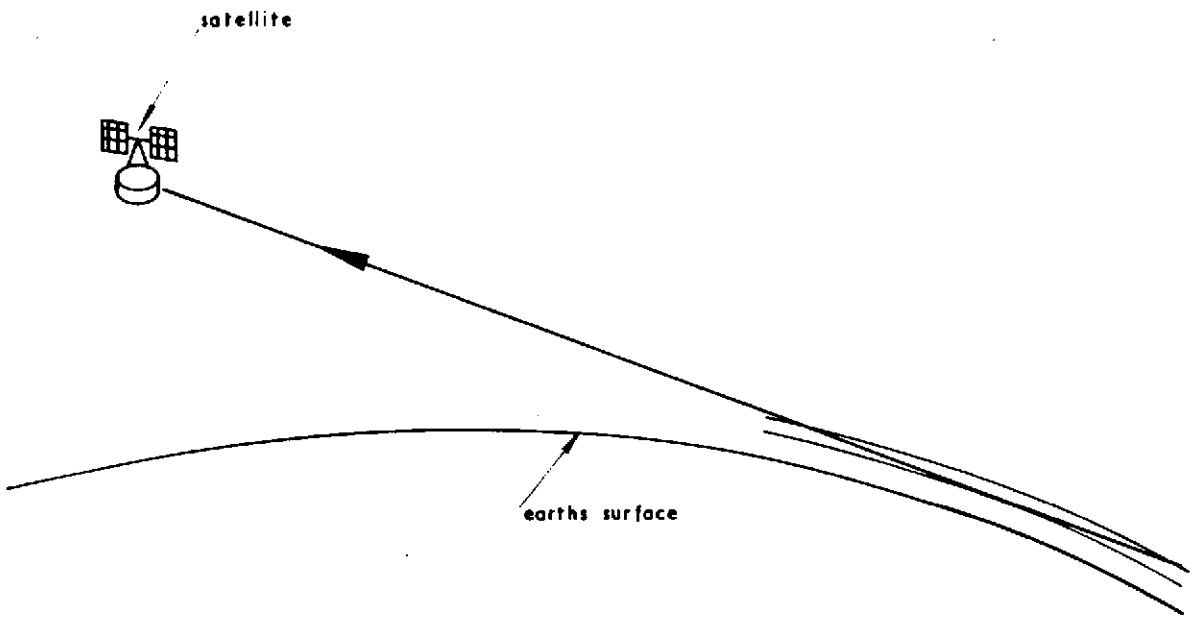

Illustrating limb — sounding.

FIGURE 6

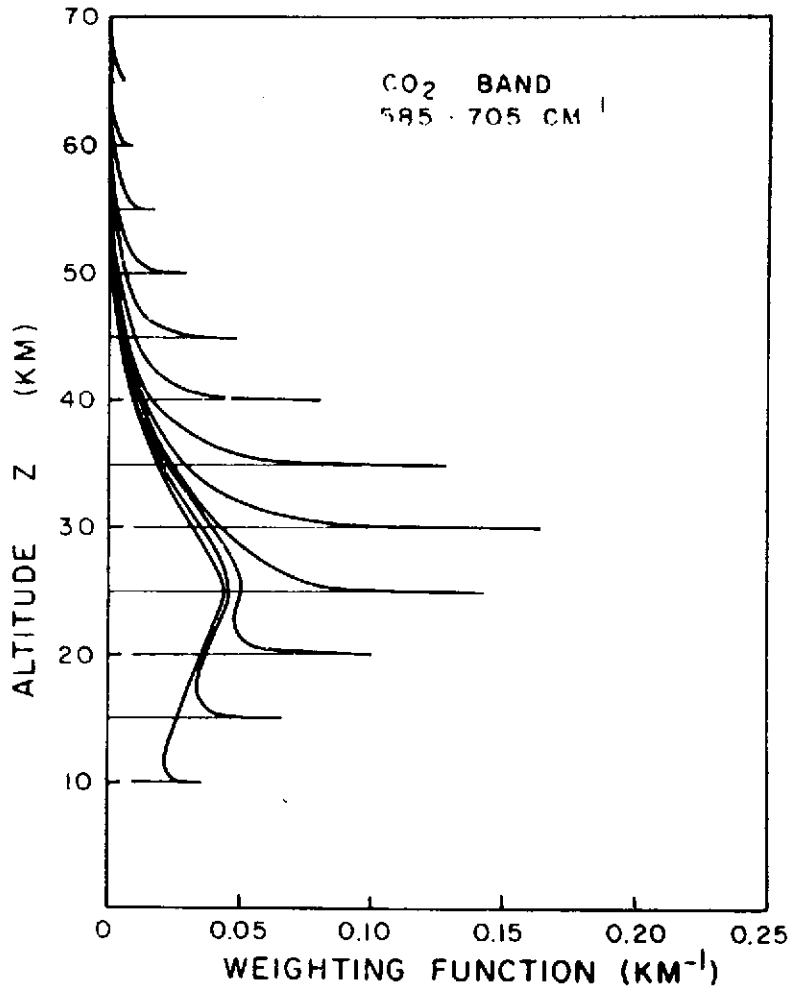
CO_2 BAND
585 - 705 CM^{-1}
ALTITUDE Z (KM)
70
60
50
40
30
20
10
0
0.05
0.10
0.15
0.20
0.25
WEIGHTING FUNCTION (KM^{-1})

FIGURE 7

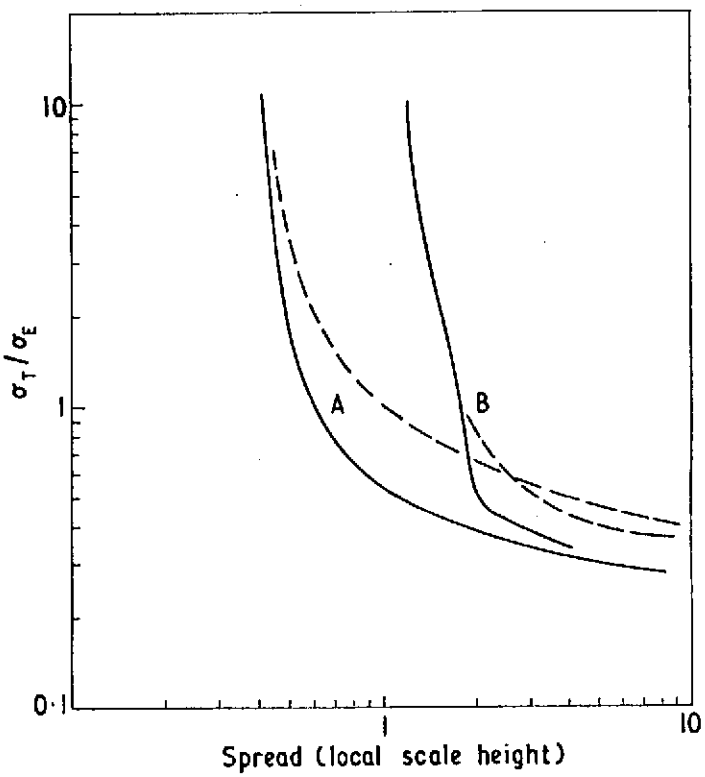

FIGURE 8

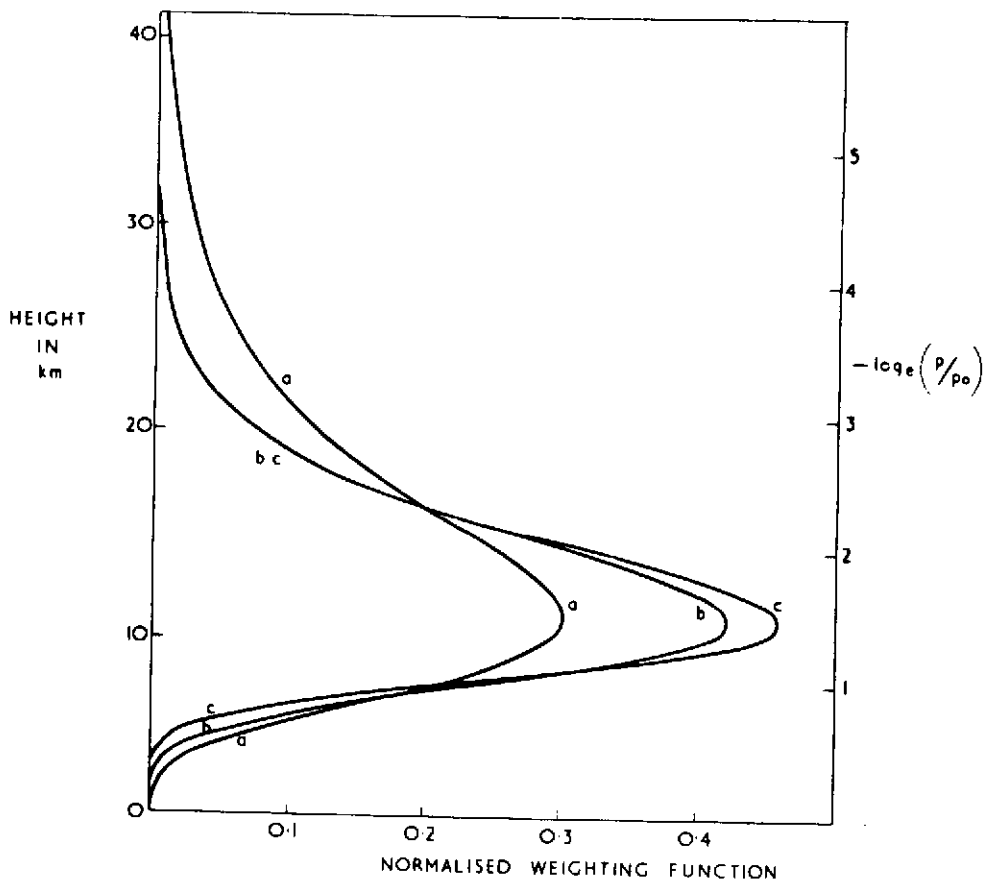
HEIGHT
IN
km
40
30
20
10
0
5
4
3
2
1
$-\log_e\left(p/p_0\right)$
a
b c
a
b
c
c
b
a
0·1
0·2
0·3
0·4
NORMALISED WEIGHTING FUNCTION

FIGURE 9

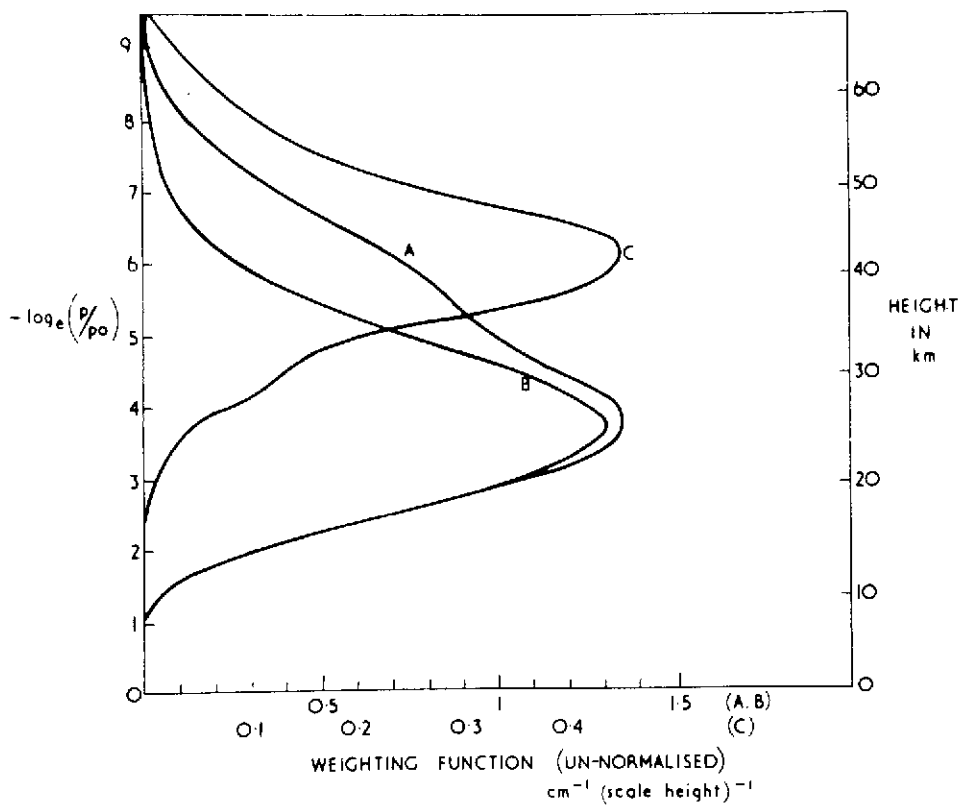
$-\log_e\left(\frac{p}{p_0}\right)$
HEIGHT IN km
A
B
C
0·1
0·2
0·3
0·4
0·5
1
1·5
(A, B)
(C)
WEIGHTING FUNCTION (UN-NORMALISED)
cm^{-1} (scale height)$^{-1}$

FIGURE 10

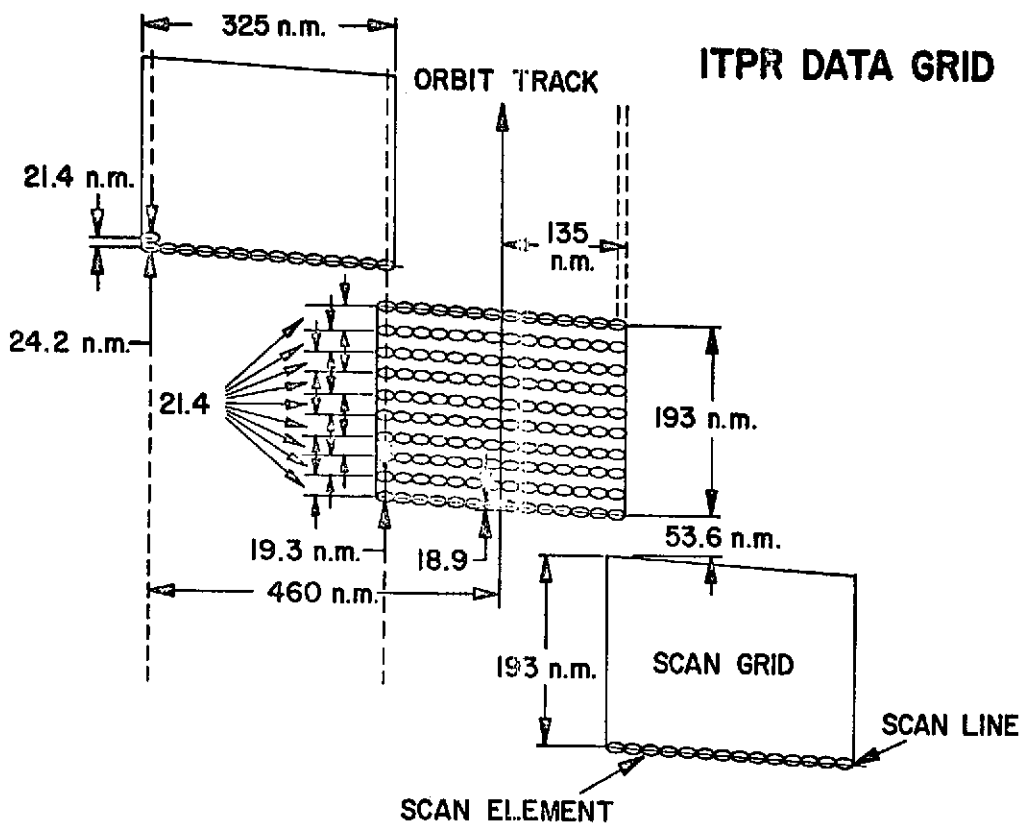
325 n.m.
ORBIT TRACK
ITPR DATA GRID
21.4 n.m.
135 n.m.
24.2 n.m.
21.4
193 n.m.
53.6 n.m.
19.3 n.m.
18.9
460 n.m.
193 n.m.
SCAN GRID
SCAN LINE
SCAN ELEMENT

FIGURE 11

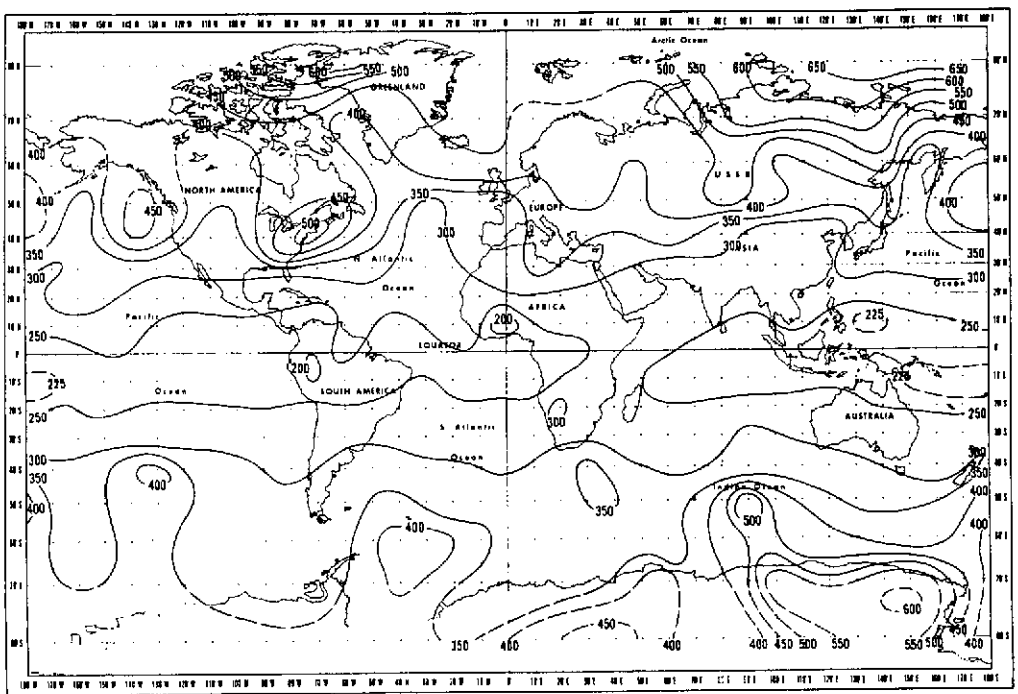

Global distribution of ozone determined from IRIS data for 22 April 1969.

FIGURE 12

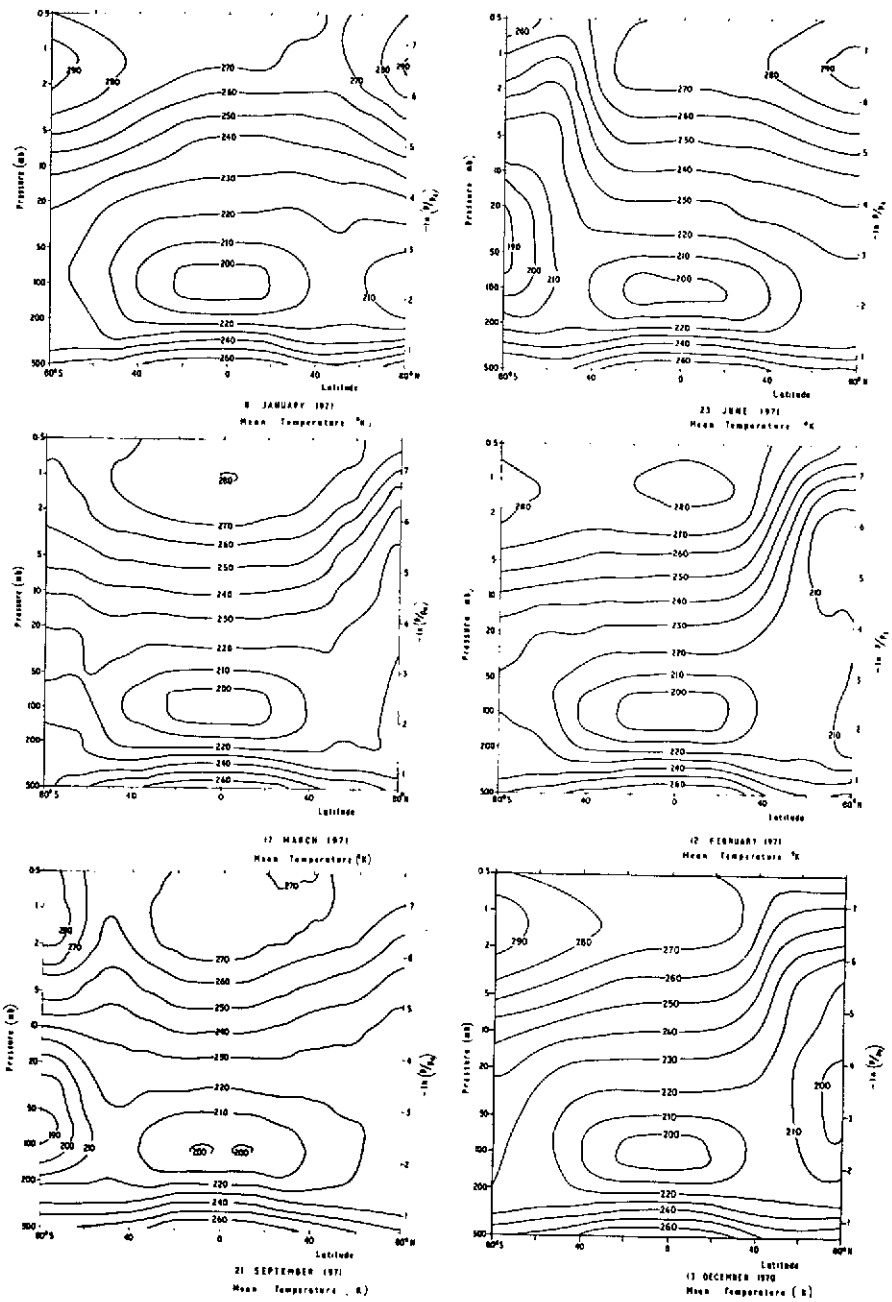

FIGURE 13

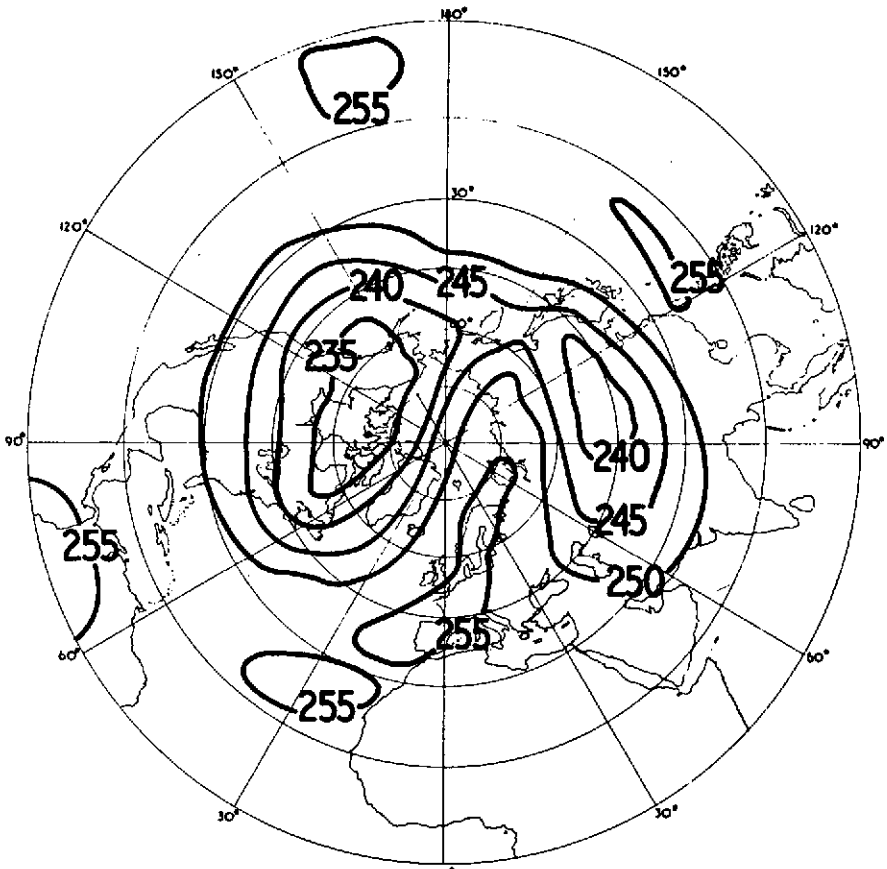

Equivalent temperature (K) channel BIB2 Nimbus V SCR
Northern Hemisphere 24 January 1973

FIGURE 14

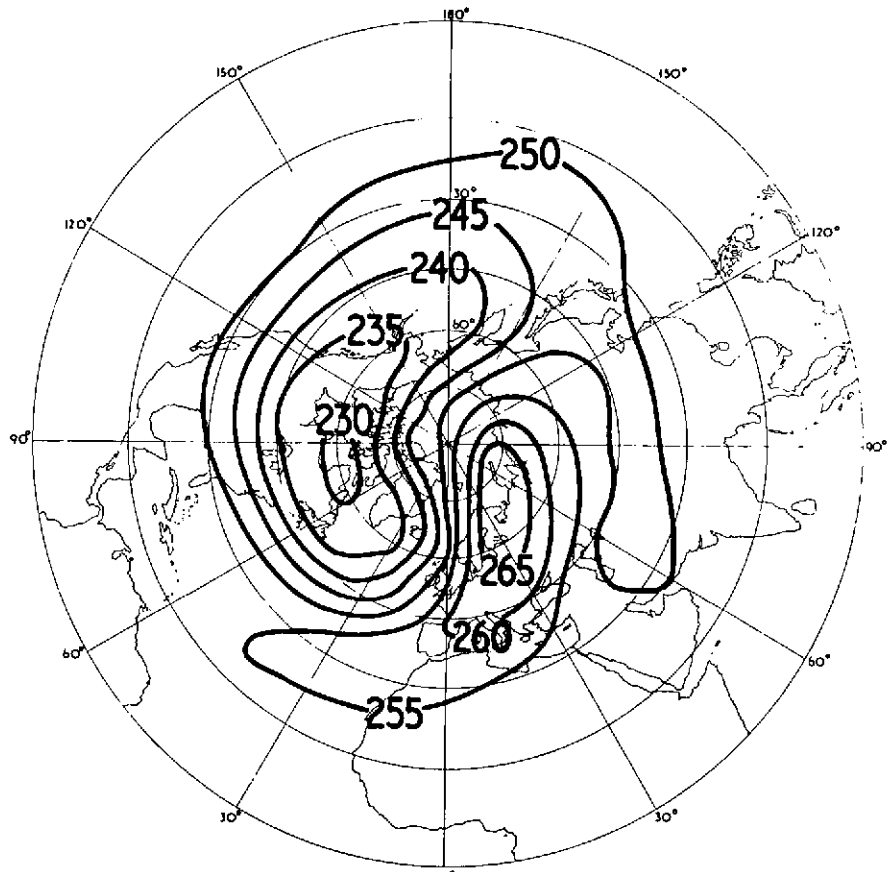

Equivalent temperature(K) channel BIB2 Nimbus V SCR
Northern Hemisphere 28 January 1973

FIGURE 15

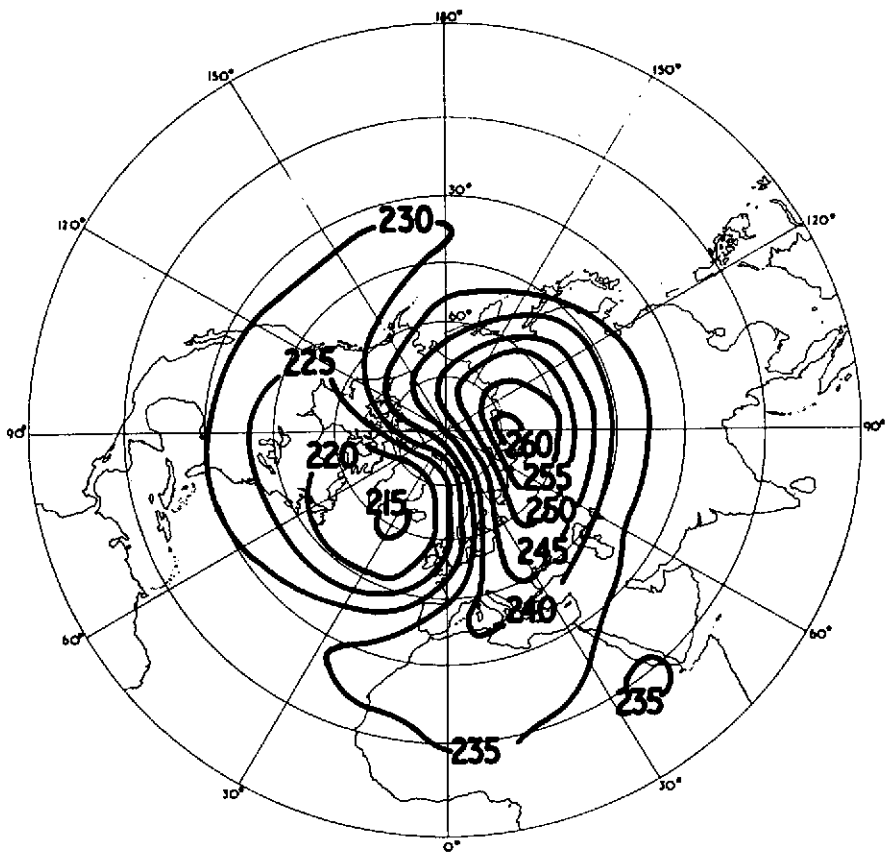

Equivalent temperature (K) channel B3B4 Nimbus V SCR
Northern Hemisphere 28 January 1973

FIGURE 16

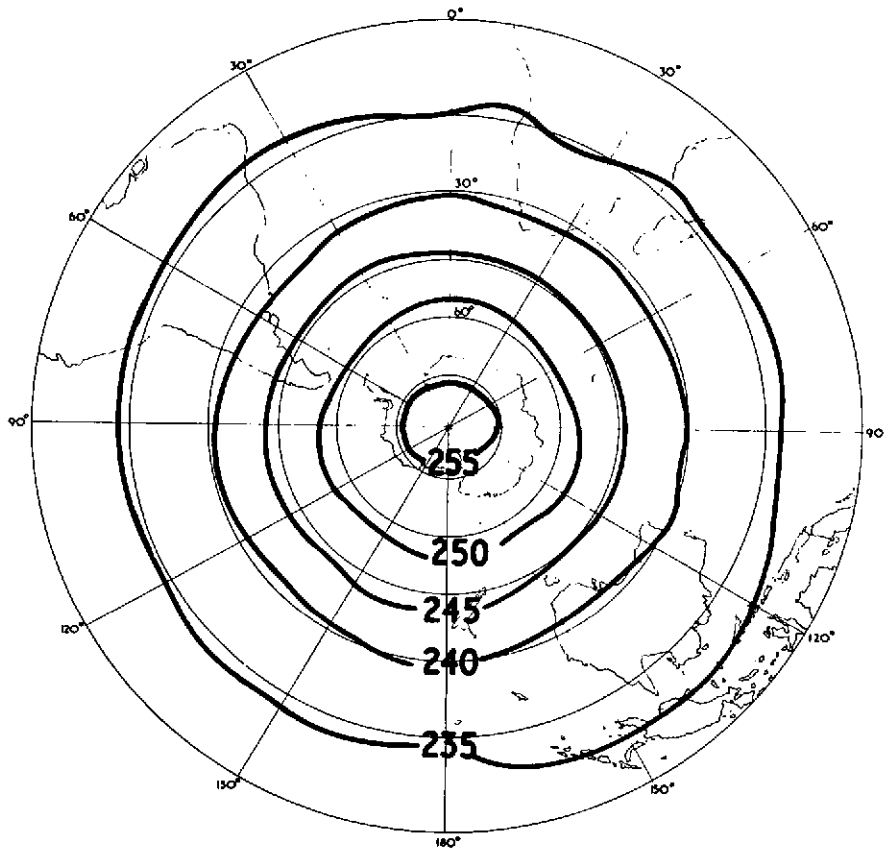

Equivalent temperature (K) channel B3B4 Nimbus V SCR
Southern Hemisphere 28 January 1973

FIGURE 17

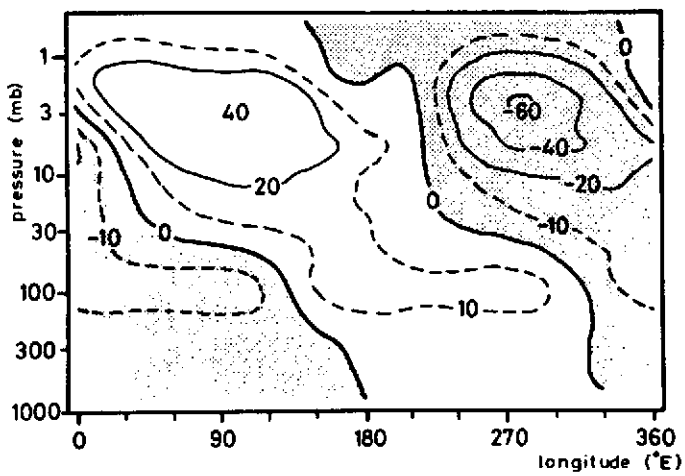

Deviation of temperature (K) from zonal mean.
64°N 5 January 1971.

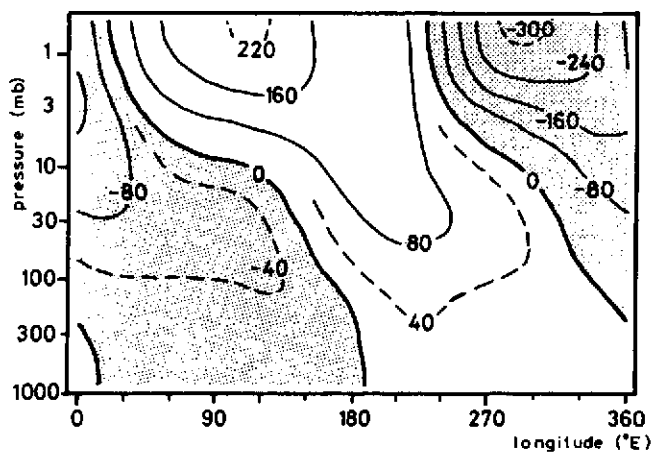

Deviation of geopotential height (dm) from the zonal mean.
64 N 5 January 1971.

FIGURE 18

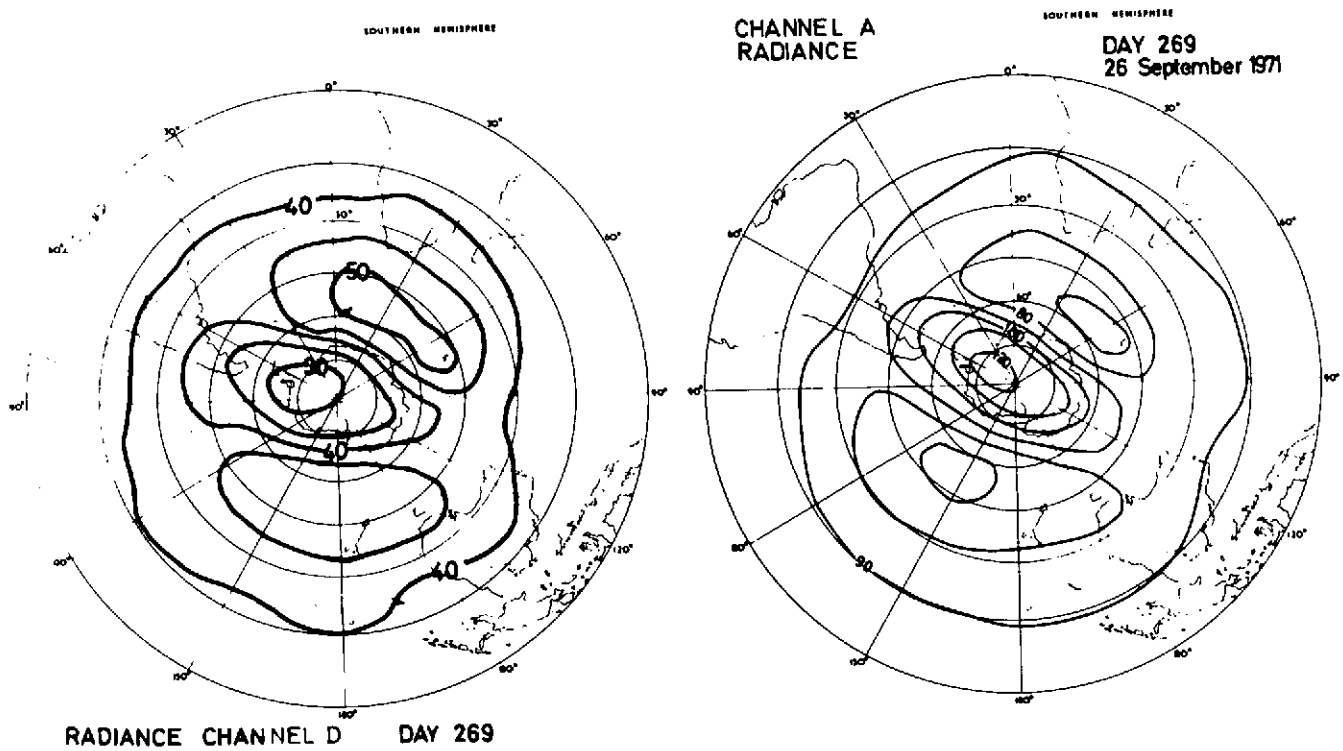
SOUTHERN HEMISPHERE
40
50
40
40
RADIANCE CHANNEL D DAY 269
CHANNEL A
RADIANCE
SOUTHERN HEMISPHERE
DAY 269
26 September 1971
90

FIGURE 19

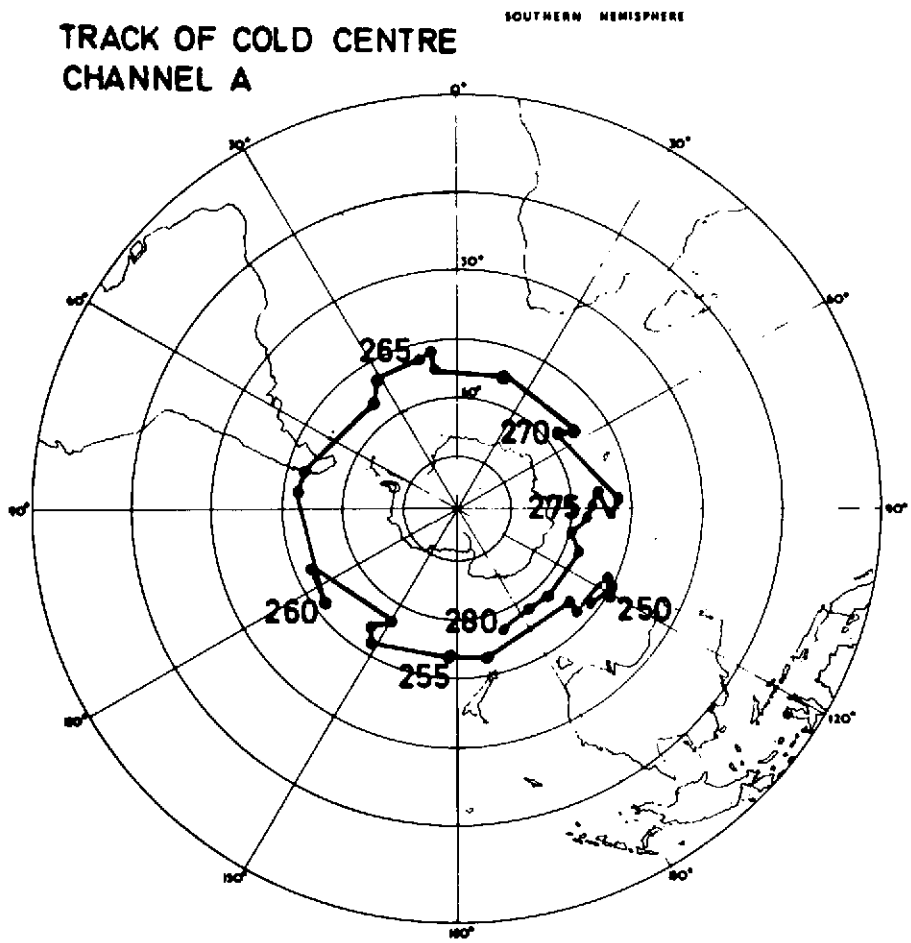
TRACK OF COLD CENTRE
CHANNEL A
SOUTHERN HEMISPHERE
265
270
275
250
260
280
255

FIGURE 20

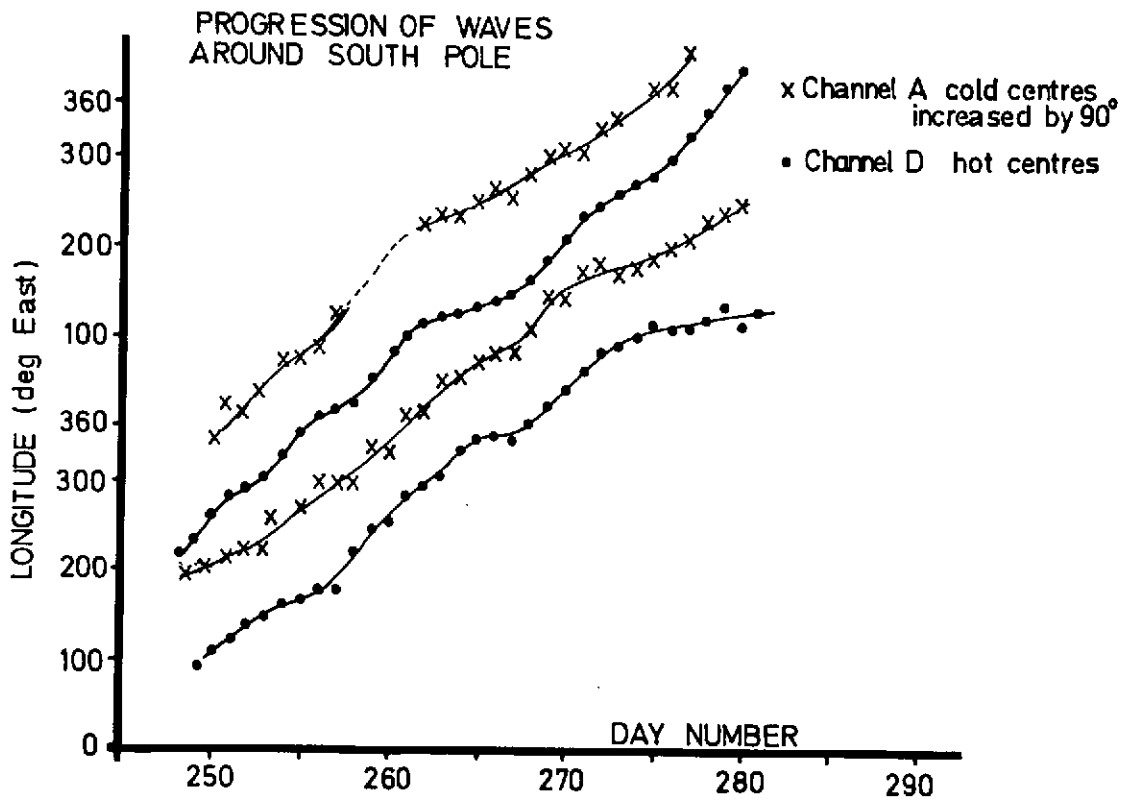
PROGRESSION OF WAVES
AROUND SOUTH POLE
x Channel A cold centres increased by 90°
• Channel D hot centres
LONGITUDE (deg East)
360
300
200
100
360
300
200
100
0
DAY NUMBER
250
260
270
280
290

FIGURE 21

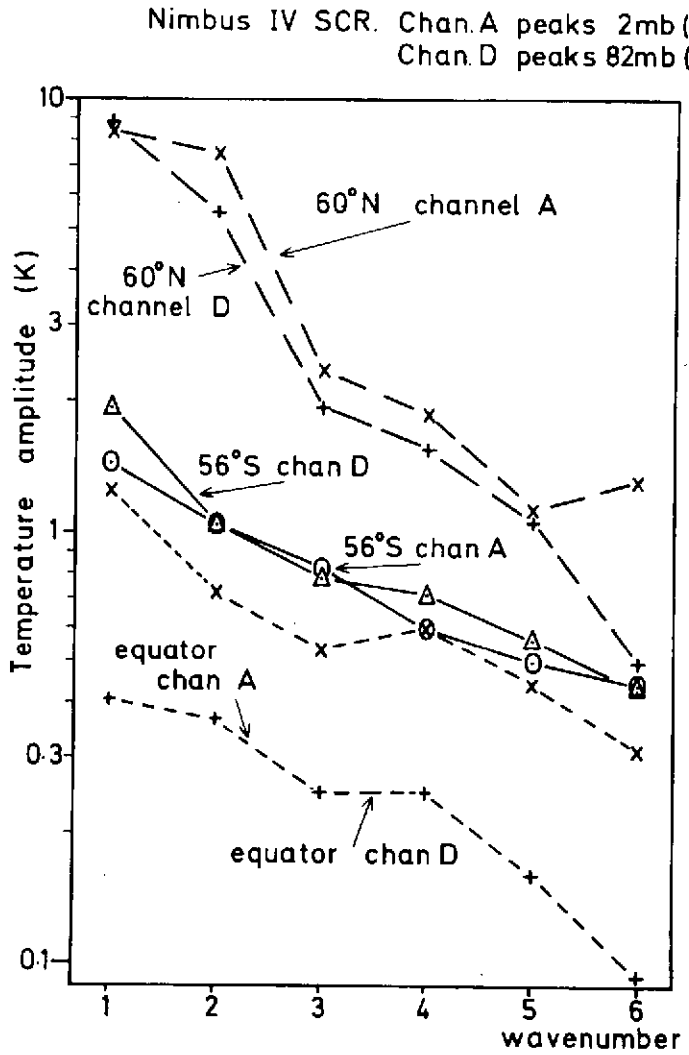

Spectrum of planetary waves: average amplitudes of zonal wavenumbers 1-6 during period 21 November 1971 to 6 March 1972

FIGURE 22

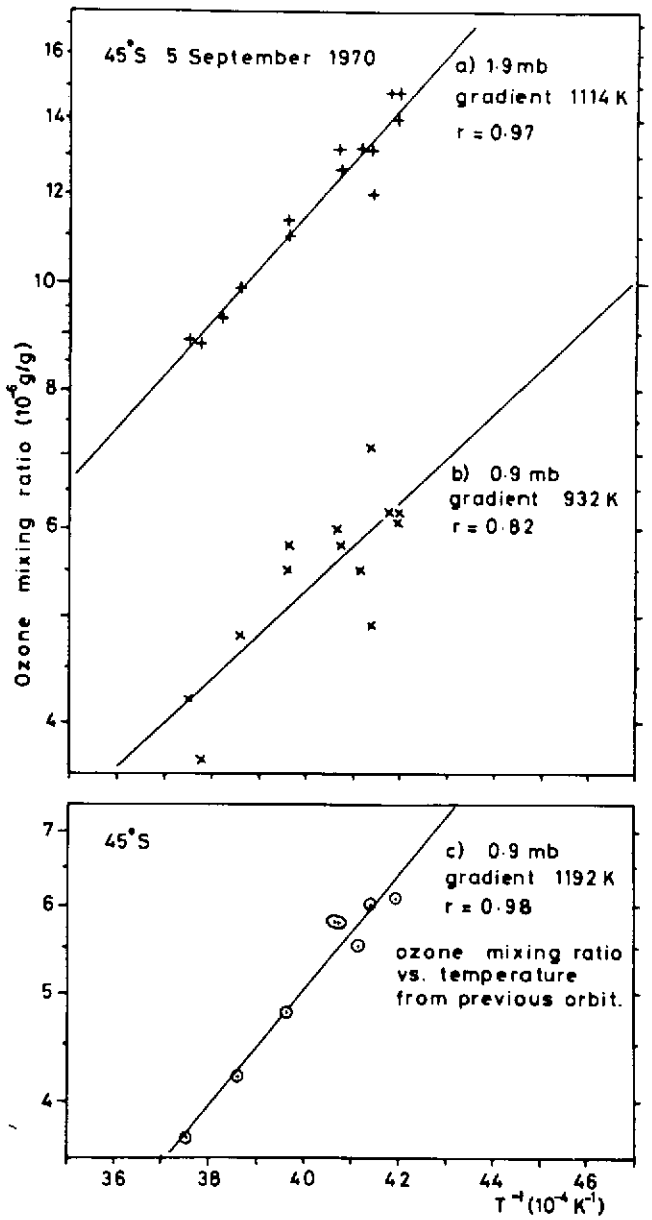
45°S 5 September 1970
a) 1·9 mb
gradient 1114 K
r = 0·97
b) 0·9 mb
gradient 932 K
r = 0·82
Ozone mixing ratio (10^{-6} g/g)
45°S
c) 0·9 mb
gradient 1192 K
r = 0·98
ozone mixing ratio
vs. temperature
from previous orbit.
T^{-1} (10^{-4} K^{-1})

FIGURE 23

THE FOLLOWING PAGES ARE DUPLICATES OF ILLUSTRATIONS APPEARING ELSEWHERE IN THIS REPORT. THEY HAVE BEEN REPRODUCED HERE BY A DIFFERENT METHOD TO PROVIDE BETTER DETAIL